

Sonochemistry and Sonoluminescence

Edited by

Lawrence A. Crum, Timothy J. Mason,
Jacques L. Reisse and Kenneth S. Suslick

NATO ASI Series

Series C: Mathematical and Physical Sciences – Vol. 524

Sonochemistry and Sonoluminescence

NATO ASI Series

Advanced Science Institute Series

A Series presenting the results of activities sponsored by the NATO Science Committee, which aims at the dissemination of advanced scientific and technological knowledge, with a view to strengthening links between scientific communities.

The Series is published by an international board of publishers in conjunction with the NATO Scientific Affairs Division

A Life Sciences

B Physics

Plenum Publishing Corporation

London and New York

C Mathematical and Physical Sciences

D Behavioural and Social Sciences

E Applied Sciences

Kluwer Academic Publishers

Dordrecht, Boston and London

F Computer and Systems Sciences

G Ecological Sciences

H Cell Biology

I Global Environment Change

Springer-Verlag

Berlin, Heidelberg, New York, London,

Paris and Tokyo

PARTNERSHIP SUB-SERIES

1. Disarmament Technologies

Kluwer Academic Publishers

2. Environment

Springer-Verlag / Kluwer Academic Publishers

3. High Technology

Kluwer Academic Publishers

4. Science and Technology Policy

Kluwer Academic Publishers

5. Computer Networking

Kluwer Academic Publishers

The Partnership Sub-Series incorporates activities undertaken in collaboration with NATO's Cooperation Partners, the countries of the CIS and Central and Eastern Europe, in Priority Areas of concern to those countries.

NATO-PCO-DATA BASE

The electronic index to the NATO ASI Series provides full bibliographical references (with keywords and/or abstracts) to about 50,000 contributions from international scientists published in all sections of the NATO ASI Series. Access to the NATO-PCO-DATA BASE is possible via a CD-ROM "NATO Science and Technology Disk" with user-friendly retrieval software in English, French, and German (©WTV GmbH and DATAWARE Technologies, Inc. 1989). The CD-ROM contains the AGARD Aerospace Database.

The CD-ROM can be ordered through any member of the Board of Publishers or through NATO-PCO, Overijse, Belgium.



Series C: Mathematical and Physical Sciences – Vol. 524

Sonochemistry and Sonoluminescence

edited by

Lawrence A. Crum

Applied Physics Laboratory,
University of Washington,
Seattle, Washington, U.S.A.

Timothy J. Mason

School of Natural and Environmental Sciences,
Coventry University,
Coventry, U.K.

Jacques L. Reisse

Service de Chimie Organique,
Université Libre de Bruxelles,
Bruxelles, Belgium

and

Kenneth S. Suslick

School of Chemical Sciences,
University of Illinois at Urbana-Champaign,
Urbana, Illinois, U.S.A.



Springer-Science+Business Media, B.V.

Proceedings of the NATO Advanced Study Institute on
Sonochemistry and Sonoluminescence
Leavenworth, Washington, U.S.A.
18–29 August 1997

Library of Congress Cataloging-in-Publication Data

** This work relates to Department of the Navy grant N00014-97-1-0149 issued by the Office of Naval Research. The United States Government has a royalty-free license throughout the world in all copyrightable material contained in the publication.*

ISBN 978-90-481-5162-2 ISBN 978-94-015-9215-4 (eBook)
DOI 10.1007/978-94-015-9215-4

Printed on acid-free paper

All Rights Reserved
© 1999 Springer Science+Business Media Dordrecht
Originally published by Kluwer Academic Publishers in 1999
No part of the material protected by this copyright notice may be reproduced or utilized in any form or by any means, electronic or mechanical, including photocopying, recording or by any information storage and retrieval system, without written permission from the copyright owner.

TABLE OF CONTENTS

PREFACE	ix
ACKNOWLEDGEMENTS	xi
FUNDAMENTALS OF CAVITATION	
<i>Sonic Effervescence: A Tutorial on Acoustic Cavitation</i>	1
R.E. Apfel	
<i>Cavitation Sonophysics</i>	25
R.A. Roy	
<i>Old-fashioned Bubble Dynamics</i>	39
A. Prosperetti	
<i>Nonlinear Bubble Dynamics: Response Curves and More</i>	63
W. Lauterborn and R. Mettin	
<i>Light Scattering by Bubbles in Liquids and Applications to Physical Acoustics</i>	73
P.L. Marston	
CAVITATION BUBBLE DYNAMICS	
<i>The Interaction of a Cavitation Bubble with a Rigid Boundary</i>	87
J.R. Blake, R.P. Tong, G.S. Keen and Y. Tomita	
<i>Acoustic Cavitation and Multi Bubble Sonoluminescence</i>	97
W. Lauterborn and C.D. Ohl	
<i>Particle Drift Near an Oscillating Cavity: A New Approach to Sonoluminescence</i>	105
M. Longuet-Higgins	
<i>Viscous Streaming Near an Oscillating and Pulsating Spherical Cavity</i>	117
M. Longuet-Higgins	
<i>Hydrodynamics, Acoustics and Transport Phenomena in Sonoluminescence</i>	127
R.I. Nigmatulin, I.Sh. Akhatov, N.K. Vakhitova and R.T. Lahey, Jr.	
<i>Particle Approach to Structure Formation in Acoustic Cavitation</i>	139
R. Mettin, C.D. Ohl and W. Lauterborn	
SINGLE-BUBBLE SONOLUMINESCENCE	
<i>Single-Bubble Sonoluminescence: Some Recent Experiments</i>	145
T.J. Matula and L.A. Crum	

<i>Star in a Jar</i>	159
W.C. Moss, D.B. Clarke and D.A. Young	
<i>The Hydrodynamical/chemical Approach to Sonoluminescence: A Detailed Comparison to Experiment</i>	165
M.P. Brenner, S. Hilgenfeldt and D. Lohse	
<i>Aspherical Bubble Collapse and Sonoluminescence</i>	183
C.D. Ohl, O. Lindau and W. Lauterborn	
SONOCHEMISTRY FUNDAMENTALS	
<i>Hot Spot Conditions During Multi-Bubble Cavitation</i>	191
K.S. Suslick, W.B. McNamara III and Y. Didenko	
<i>Some Physico-chemical Aspects of So-called "Homogeneous Sonochemistry"</i>	205
J. Reisse, T. Caulier, C. Dekkerckheer, Y. Kegelaers, N. Segebarth and K. Bartik	
<i>Detection of Primary Free Radical Species in Aqueous Sonochemistry by EPR Spectroscopy</i>	225
V. Mišík and P. Riesz	
<i>Acoustic Dosimetry for Sonochemistry</i>	237
S.I. Madanshetty	
<i>Laboratory Equipment and Usage Considerations</i>	245
T.J. Mason	
<i>High Power Ultrasonic Transducers</i>	259
J.A. Gallego-Juárez	
APPLICATIONS OF SONOCHEMISTRY	
<i>Elements of Organic Chemistry of Interest to Sonochemists</i>	271
T.J. Mason	
<i>Single-Bubble Sonochemistry</i>	285
T. Lepoint, F. Lepoint-Mullie and A. Henglein	
<i>Applications of Sonochemistry to Materials Synthesis</i>	291
K.S. Suslick, M.M. Fang, T. Hyeon and M.M. Midleleni	
<i>Polymer Sonochemistry: Controlling the Structure and Properties of Macromolecules</i>	321
G.J. Price	
<i>Sonochemistry and Sonoluminescence in Colloidal Systems</i>	345
F. Grieser, M. Ashokkumar and J.Z. Sostaric	

<i>Sonochemical Environmental Remediation</i>	363
T.J. Mason	
<i>Cavitational Environmental Remediation</i>	371
J.P. Russell	
<i>Industrial Applications of Sonochemistry and Power Ultrasonics</i>	377
T.J. Mason	
SUBJECT INDEX	391
LIST OF CONTRIBUTORS	397

PREFACE

This volume is an outgrowth of the NATO Advanced Study Institute (ASI) on Sonochemistry and Sonoluminescence that was held at the Sleeping Lady Conference Center in Leavenworth, Washington, USA, 18–29 August 1997. The purpose of this meeting, which is also the focus of this volume, was to bridge the gap between the expertise of physicists and chemists involved in sonoluminescence and sonochemistry research. This goal attracted 73 participants from 19 countries to attend 10 days of intensive tutorials and lectures combined with lively informal discussions and debates.

The end result of the Institute was a significant advancement in knowledge of all participants and an increased potential for unraveling the mysteries of these two scientifically interesting and topical phenomena. This volume captures the best of the Institute, providing a tutorial textbook that will be useful both to those approaching these topics for the first time, as well as to seasoned researchers in the field.

The genesis of the Institute lay in the widespread interest in the scientific community in sonochemistry and sonoluminescence. Although the scientific content of these two topics is closely related, the professional disciplines within the community studying these phenomena have been distinctly different. Sonochemistry is being studied primarily by the chemistry community and sonoluminescence by the physics community, although a single physical phenomenon, acoustic cavitation, unites the two topics.

The knowledge gap addressed by this volume exists because the physics of cavitation bubble collapse is relatively well understood by acoustical physicists but has been practically unknown to chemists. On the other hand, the chemistry that gives rise to electromagnetic emissions and the acceleration of chemical reactions has been relatively well known to chemists but practically unknown to acoustical physicists. Forcing these two groups together in an isolated retreat for ten days provided just the right environment for each of us to gain more than five percent from the other's lecture. Indeed, it was refreshing to see chemists and physicists arguing with each other over the *same* topic.

Included here are contributions from many of the world's experts in the fields of sonoluminescence and sonochemistry. In the first section, the fundamentals of cavitation are addressed, including excellent tutorials by Apfel and by Roy. Also in this section are more detailed background papers on acoustic cavitation by Prosperetti and by Lauterborn and Mettin. This section concludes with a detailed article by Marston on the basic principles of light scattering from bubbles, a technique that has extensive applications in single bubble sonoluminescence (SBSL).

In the second section, the essentials of cavitation bubble dynamics are discussed in more detail. An article by Blake *et al.* discusses the important interaction of a cavitation bubble with a rigid boundary, and articles by Lauterborn and Ohl, Nigmatulin *et al.*, and Mettin *et al.* delve into the phenomena of acoustic cavitation and bubble dynamics in considerable depth. In this section also are two important papers by Longuet-Higgins on the streaming forces that are involved in cavitation bubble oscillations.

A section on single bubble sonoluminescence follows. The paper by Matula and Crum can serve as an introduction to the topic; the following article by Moss *et al.* considers the potential of cavitation-induced nuclear fusion. Two additional papers by Brenner *et al.* and by Ohl *et al.* consider the details of SBSL in considerable depth and offer explanations for many of the interesting attributes of this phenomenon.

In the next two sections, the new scientific discipline of sonochemistry is discussed. The first section again introduces the topic by a series of introductory tutorials. The papers by Suslick and by Reisse *et al.* are tutorial in nature, but quickly bring the interested and educated reader to the forefront of knowledge in this subject. Also included in this section is a relatively specialized paper by Misik and Riesz that deals with the important role of free radical species in sonochemistry. Important treatments of dosimetry by Madanshetty and of the transducers utilized in this discipline by Gallego-Juárez are also included. In addition, a broad review of the laboratory equipment and usage considerations is given by one of the pioneers in the field of sonochemistry, Tim Mason.

The volume concludes with a section on a detailed description of the applications of sonochemistry. An introductory article by Mason heads this section, with more details on applications to materials synthesis provided by Suslick, to macromolecules by Price, and to colloidal systems by Grieser *et al.* A paper by LePoint *et al.* on the discovery of single bubble sonochemistry is an important addition to this section. Finally, the topic of toxic waste remediation and other environmental applications of sonochemistry are treated with papers by Mason and by Russell.

This volume is not only a collection of scientific papers, it is also a physical representation of the collective spirit of scientific curiosity and exchange that grew from the people who participated in this ASI. The Sleeping Lady Conference Center venue itself was yet another important participant in this process. Although readers will not be able to smell the fragrance of the ponderosa pines nor hear the voice of Icicle Creek as it runs by the main lodge, they will hopefully reap the benefits of the calming and reflective atmosphere up there in the mountains of the North Cascades that fostered our ability to focus on our science for those two weeks in the summer of 1997. If you missed those two weeks at Sleeping Lady, you missed something special; hopefully, this volume will provide some useful information and capture a bit of the spirit of that conference.

ACKNOWLEDGEMENTS

First of all, I would like to acknowledge the NATO Scientific and Environmental Affairs Division for providing the principal support for the Advanced Study Institute that led to this volume. In addition, I offer a special thanks to Logan Hargrove, Program Manager for Physical Acoustics at the Office of Naval Research^{*} for providing supplemental funding that was extremely helpful in addressing costs that were not covered by NATO allocations. Finally, I wish to express my appreciation to Robert Spindel, Director of the Applied Physics Laboratory at the University of Washington, for permitting various members of the APL staff, including myself, to devote time and attention to the coordination and management of the Institute and the editing of the book.

One of the most important aspects of the conference was the remarkably pleasant environment in which we found ourselves at the Sleeping Lady Conference Center in Leavenworth, Washington. A special thanks goes to Harriet Bullitt and her staff at Sleeping Lady for providing a wide variety of accommodations, especially the food, that made this conference one of the best that many of us have ever attended.

The idea for this conference arose at a meeting of the European Society of Sonochemistry, in a discussion with Jacques Reisse, who together with Ken Suslick and Tim Mason, soon outlined a plan for a proposal to NATO. I wish to express my sincere appreciation to Jacques, Ken, and Tim who were always available when I asked their assistance and who always offered wise counsel and enthusiastic encouragement.

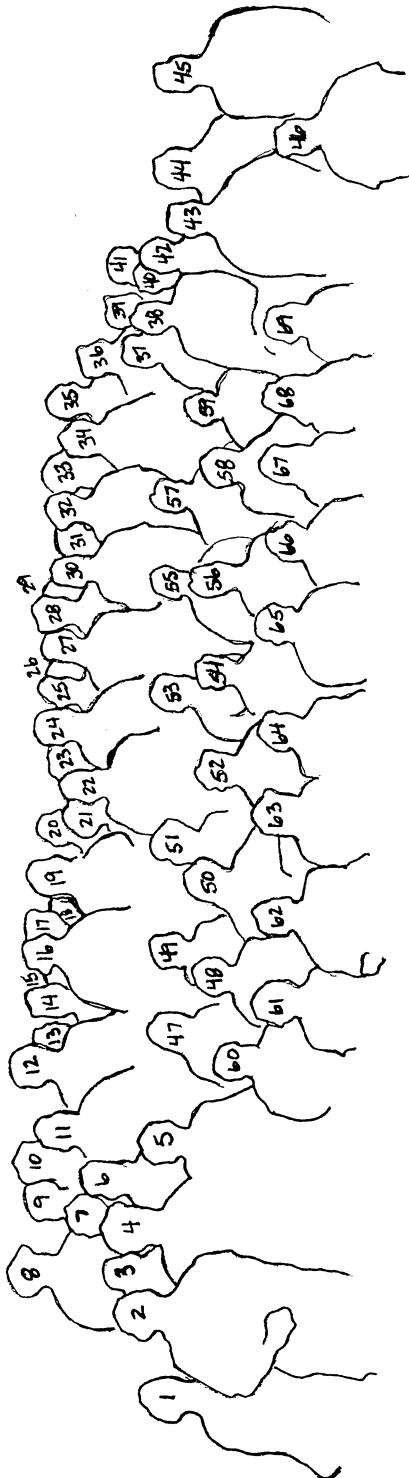
Finally, a great deal of credit for the success of the conference and for the completion of this volume must go to Nancy Penrose and Jennifer Clesceri, who engaged themselves in the administration and coordination of both the conference and this volume with a level of detail and an enthusiasm that was simply incredible. I join the attendees at the conference, the authors of this volume, and my fellow editors in offering them our most sincere thanks.

Lawrence A. Crum

Applied Physics Laboratory
University of Washington
1013 NE 40th Street
Seattle, Washington 98105
USA

1 October 1998





1. C. Mason
2. T. Mason
3. S. Madanshetty
4. R. Nigmatulin
5. Y. Koltynin
6. V. Abramov
7. R. Godwin
8. P. Marston
9. A. Voskoboinikov
10. J. Dion
11. I. Akhatov
12. D. Cheeke
13. J. Blake
14. G. Keen
15. V. Misik
16. M. Germano
17. M. Vanni
18. W. Moss
19. G. Muzio
20. T. Matula
21. T. Riesz
22. J. Gallego-Juarez
23. I. Mazzarino
24. P. Riesz
25. M. Hodnett
26. N. Penrose
27. Z. Lazar
28. G. Diebold
29. Y. Didenko
30. A. Tuulmet
31. S. Nikitenko
32. N. Segebarth
33. D. Lohse
34. K. Bartik
35. L. Kondic
36. T. Chou
37. M. Ozyar
38. J. Reisse
39. C. Ohl
40. C. Frenstey
41. R. Mettin
42. S. Kalem
43. K. Sustick
44. G. Price
45. D. Hunicke
46. L. Crum
47. A. Frost
48. A. Lopes
49. J. Ding
50. R. Roy
51. M. Moreno
52. M. Dan
53. S. Hayashi
54. S. Hilgenfeldt
55. D. Peters
56. M. Ashokkumar
57. J. Debus
58. F. Grieser
59. W. Lauterborn
60. M. Salomaa
61. M. Eral
62. P. Werner
63. F. Machityre
64. M. Longuet-Higgins
65. N. Garcia
66. R. Gupta
67. A. Sarkilahti
68. L. Weavers
69. N. Miyoshi

SONIC EFFERVESCENCE: A TUTORIAL ON ACOUSTIC CAVITATION*

ROBERT E. APFEL
Yale University
New Haven, CT 06520-8286

1. Introduction

The objective of this tutorial article is to give the reader a semi-quantitative appreciation for the physical phenomena and many applications that fall under the term: acoustic cavitation. Because of the required brevity of this effort, much is left out, and, therefore, the reader is asked to forgive omissions of content and attribution which are found, instead, in the comprehensive review articles and books found in the bibliography.

Cavitation can be defined as any stimulated bubble activity. The stimulation may be due to flow, decompression, acoustic waves, sudden deposition of electromagnetic or ionizing radiation, or heat. The activity can refer to bubble inception or dynamics.

Acoustic cavitation is just acoustically induced bubble activity. In general, we should assume that the activity is observable to the extent that we can measure the activity or the effect of that activity. When the collapse of a bubble is capable of producing high fluid velocities, shock waves, and/or jetting phenomena, the cavitation is called "inertial," because the kinetic energy stored in the liquid is imparted to the bubble, and dominates the motion. This designation is typical of bubbles that grow to more than twice their original size in one or two acoustic cycles. For a more gentle cavitation in which the size changes in each acoustic cycle are relatively small, the term "noninertial" cavitation has been deemed appropriate. Here, the restoring force of the internal gas is important in the cycle-to-cycle motion. These designations, inertial and noninertial, are considered more appropriate than the terms "transient" and "stable" cavitation, which have been used to describe the same phenomena.¹

1.1. CAVITATION AS THE GREAT ENERGY CONCENTRATOR

Sound waves are, in general, of relatively low energy density. For instance, even a progressive sound wave in water of pressure amplitude of five atmospheres (0.5 MPa) has an energy density of only about 50 Joules per cubic meter, which, on a per molecule basis is about six orders of magnitude below the thermal energy per molecule of water at room temperature. But that same five atmosphere sound wave at a frequency of 3 MHz (typical of diagnostic ultrasound) can cause a bubble with an initial radius of one micron to grow to a radius of about three microns. This nearly empty gas bubble will collapse in about 0.3 microseconds depositing into a fraction of a cubic micron about 3 ten-thousandths of an erg, which, for purposes of comparison with ionizing radiation, is over 100 million electron volts. The nearly adiabatic bubble collapse will lead to almost nine orders of magnitude of enhancement in the energy per molecule, producing internal gas pressures of hundreds to thousands of atmospheres and temperatures of thousands of degrees Kelvin. It is no wonder that sound and ultrasound can be used to catalyze chemical reactions, in a process called sonochemistry. An example of the energy concentrating effects of acoustic cavitation is given in Table 1.

TABLE I. Example of energy concentration (3-MHz sound wave, 5-atmosphere pressure amplitude).

	Initial	Final
Radius	1 micron	3 microns, max size to 0.14 microns, min. size
Internal pressure	1 atmosphere	4140 atmospheres
Internal temperature	20 °C	2900 °C
Energy density	1 MeV/micron ³	383 MeV/micron ³

1.2. CONTEXT OF RELATED BUBBLE PHENOMENA

Acoustic cavitation shares much with other bubble phenomena. Inception mechanisms and the role of impurities (cavitation "nuclei") are similar, and dynamical effects can be similar. The early work of Harvey is noteworthy in this context.² Consider the factors that can influence the growth or collapse of a spherical bubble in a fluid:

1.2.1. Boiling

When the temperature of a liquid is high enough that the vapor pressure exceeds the ambient pressure, then boiling may take place. But if no pre-existing nuclei are present and if there is no free surface (one in contact with a gas or vapor), then bubbles must originate at the submicroscopic scale; at this scale, one can see from the bubble equilibrium equation that the inward stress due to surface tension can be large. Liquids will "superheat" significantly before boiling occurs. For instance, we have shown that water drops moving slowing in hot oil can be superheated at atmospheric pressure to 279.5°C before bursting into the vapor phase.³

This superheat limit will not be achieved in the presence of sufficiently energetic ionizing radiation, as Donald Glaser demonstrated in 1952 in his invention of the "bubble chamber," an instrument that has played a major role in the advancement of elementary particle physics. Apfel has shown that certain liquid drop materials, chosen to be superheated at room temperature, could be immersed in a gel in order to form a sensitive radiation detector composition, with applications in radiation safety and medicine.

1.2.2. Bends

As with boiling, the pressure on the inside of the bubble plays an essential role in bubble formation in gas-supersaturated liquids. The "bends" refers to the effects of gas bubble formation in living systems. These bubbles usually form when a gas-saturated tissue is decompressed. The growth of gas bubbles is, in general, much slower than vapor bubble growth in boiling for the same pressure differential, because in the

latter case one is dealing with evaporation from the bubble wall interface, whereas in case of the motion of non-condensable gases, such as air, gas diffusion through the liquid controls rate processes.

A human diver saturated at 2.5 atmospheres gauge pressure, corresponding to a water depth of about 25 meters, could face fatal consequences if decompressed to the surface without adequate time for dissolved gas to come out of tissues. It appears that there are numerous sites for bubble nucleation in moderately supersaturated tissue.

1.2.3. Beer

The opening of a beer or a soft drink can often lead to the formation of bubbles, in much the same way as bubbles form in a rapidly decompressed diver. Pouring a soft drink or beer into a glass or plastic container with or without ice can result in quite different behavior. With a plastic cup, ice, or a dirty glass surface, bubbles will be nucleated on the available surfaces. With a clean glass, the water will tend to wet the glass, and the smooth surface is less likely to produce bubbles. Do you think it is better from the point of view of not nucleating too many bubbles, to add the ice before or after the drink is in the glass?

1.2.4. Bark

How does water get from the roots of a tree to the leaves? With some redwoods, that distance is 365 feet. Transpiration of water at the leaves leads to a capillary action that works to lift the water. But this is a pump that is lifting water that is atmospheric pressure at the base of the tree. With a redwood, that might imply that the xylem path for carrying water and nutrients near the top of the tree is subjected to a negative pressure (positive tension) of about 11 atmospheres (Figure 1). Bubbles may be nucleated by disease or even cosmic rays. A tension of 11 atmospheres on a bubble nuclei of radius $0.15\mu\text{m}$ will cause the nuclei to grow.

Some of the highly redundant xylem paths can be blocked by bubbles. But with disease and/or serious freezing, it is possible that too many paths can be interrupted, and a tree can die.

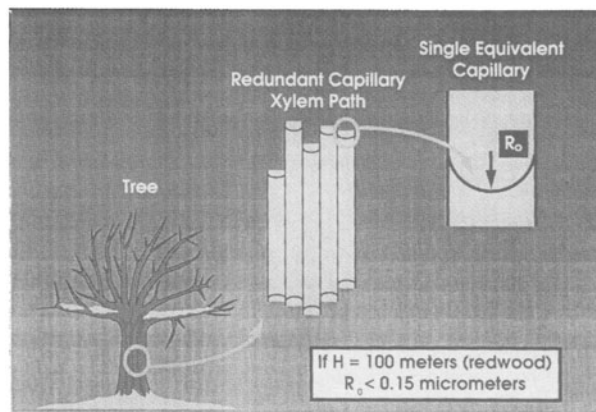


FIG. 1. Transpiration of water from the pores of leaves atop a redwood tree can, by capillary action, draw water from the roots. A negative pressure of up to 11 atmospheres must be sustained in the xylem path, and the pores at the point of transpiration must have a radius of less than $0.15 \mu\text{m}$.

1.2.5. "Boats" (hydrodynamic)

Hydrodynamic cavitation occurs when the flow past an object leads to a pressure reduction, according to Bernoulli's law, that is measured by the product of one half the liquid density and the square of the flow velocity. For water, for example, a pressure reduction of one atmosphere corresponds to a velocity of about 14 meters per second (31 miles per hour). Hydrodynamic cavitation is common on ship propellers, sometimes leading to the erosion of propeller edges and surfaces and substantial cavitation noise (Figure 2).⁴ Special shaping and materials can ameliorate these effects.

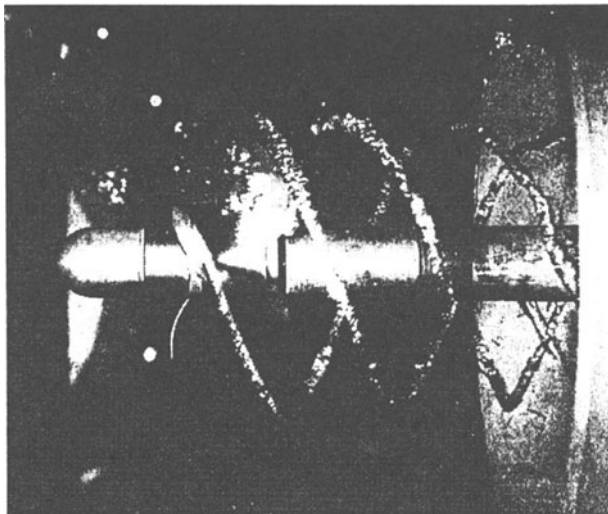


FIG. 2. Bubble generation on a propeller tip, from Strasberg, Ref. 4.

1.3. HISTORY AND LITERATURE

Bubbles attract and amuse. It is no wonder that this subject has a long and revered history. The books and chapters on cavitation listed in the references are a rich source of information on the historical development of this ever-intriguing field of interest to both experimentalists and theorist. It is also no surprise why theoreticians have tackled the problem of bubble dynamics; for what could be a better starting point than the spherical symmetry that bubbles (at least small ones) afford.

We have already provided one result that follows quickly from the equations describing the motion of a spherical void in an incompressible, inviscid liquid. That was the collapse time for a bubble of a given initial size (e.g. 3 μs for a bubble reaching a maximum radius of 3 μm). We also estimated the energy of collapse as the product of the bubble volume and the ambient pressure, leaving out the contribution due to surface tension, which is okay for bubbles that are a few microns in radius or larger.

2. Relevant Parameters

In trying to summarize the vast amount of literature on acoustic cavitation, we can categorize bubble dynamics by the relative amplitude of bubble motion (low, medium, and high) and by the importance of certain fluid parameters which will influence bubble motion. The following parameters come into our computations.

2.1. LIQUID AND GAS (AND NOT ONLY WATER)

Density, viscosity, compressibility, diffusion constant, surface tension (and other surface properties if surfactants or contaminants are present), vapor pressure, expansivity, thermal conductivity, specific heat, inner gas properties, dissolved gases and impurities.

2.2 THERMODYNAMIC VARIABLES

External pressure, temperature, heat balance.

2.3 ACOUSTIC VARIABLES

Acoustic pressure, frequency or waveform (spectrum), duty cycle, pulse shape and width.

The processes involved in cavitation involve bubble inception, bubble activity, and the effects due to bubble motion, as illustrated in the schematic of Figure 3.

Bubble Evolution

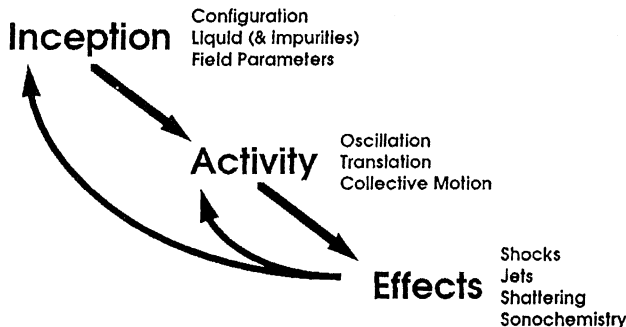


FIG. 3. Bubbles evolve in an acoustic field through stages of inception, bubble activity, and effects due to bubble motion. Each phase may affect the others.

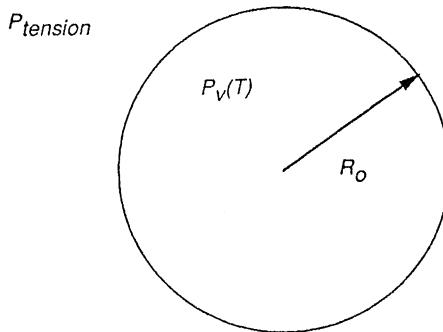
3. Inception

3.1. INTRODUCTION

Cavitation inception or nucleation refers to the threshold conditions to initiate observable bubble activity. That activity refers to the motion or dynamics of the bubble or bubbles in a particular environment (e.g. near or far from solid surfaces). That activity can produce observable effects, such as radiation forces, acoustic streaming, shock waves, fluid jetting, enhanced chemical reactions, thermal effects (fusing), surface erosion, etc.

3.2. HOMOGENEOUS NUCLEATION THRESHOLDS--TENSILE STRENGTH OF LIQUIDS

When no pre-existing bubbles or pockets of gas are present in a liquid, it may be necessary to create a bubble *ab initio* in order to cavitate a liquid. Theory predicts, for instance, that a tension of over 1000 atmospheres may be necessary to initiate a bubble in pure, nuclei-free, room temperature water.⁵ Figure 4 illustrates the use of the Kelvin equation to estimate the initial bubble size for nucleation at a negative pressure of 1000 atmospheres. Experiments are difficult to perform, not only because it is difficult to produce such a pure sample, but also because it is difficult to produce such large tensile stresses in a liquid. Clever approaches which examine the melting of ice inclusions in solids have produced tensions comparable to the theoretical prediction,⁶ and Greenspan and Tschiegg have demonstrated acoustic cavitation thresholds in pure water in excess of 250 atmospheres.⁷ This is remarkable given that slightly impure water may only withstand acoustic tensile stresses of a few atmospheres.



$$P_{tension} = P_V(T) - 2\gamma(T) / R_0$$

$$\text{If } R_0 = 1.44 \text{ nm, } P_{tension} = 1000 \text{ atm.}$$

FIG. 4. For a negative pressure of 1000 atmospheres in water, the spontaneous formation of a bubble of radius 1.44 nm is required according to the Kelvin equation.

Acoustic levitation of a drop in an immiscible host liquid allows one to examine the strength of very small samples, many of which may be free of gaseous nuclei. In this way, Apfel has measured tensile strengths of organic liquids in good agreement with predictions of homogeneous nucleation theory.⁸

3.3 HETEROGENEOUS NUCLEATION THRESHOLDS

When there are pre-existing nuclei, thresholds for bubble inception can be much lower, even approaching the vapor pressure of the liquid. Blake predicted the minimum acoustic pressure to cause a free, spherical gas bubble to overcome surface tension stresses and to grow unstably.⁹ His results assume low acoustic frequencies and negligible viscosity. When the frequency is sufficiently high, the liquid inertia can delay the bubble growth for a long enough duration as to exceed the tensile phase. Thus, the acoustic pressure must be greater in order to overcome these inertial forces during the tensile phase. These inertial effects are especially important in raising thresholds at megahertz frequencies associated with diagnostic ultrasound. Figure 5 illustrates the calculations of Apfel and Holland showing the heterogeneous threshold vs. bubble size.¹⁰ For small sizes the Blake mechanism dominates. For larger bubbles, liquid inertia dominates.

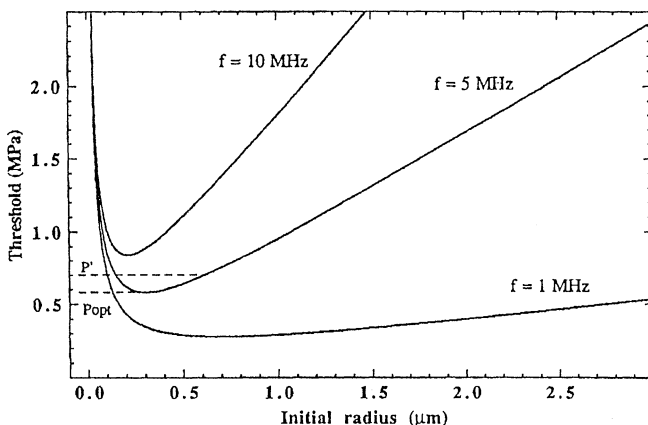


FIG. 5. Calculations of the threshold for inertial cavitation in water at three frequencies, after Apfel and Holland, Ref. 10.

3.4. MOTE-INDUCED CAVITATION; CAVITATION NUCLEI

Since free gas bubbles in pure liquids are inherently unstable (they will either dissolve or, if the liquid is supersaturated with gas, they will grow), free bubbles are unlikely to act as nuclei in liquids that have been given time to "settle down." Gas can, however, be trapped in the crevices of solid particles (Figure 6). Depending on the size of these particles and the wettability of the liquid, it will take a certain minimum

acoustic pressure to induce these gas pockets to grow. For sufficiently small crevices (10 micron or less), surface tension remains a dominant factor. For larger crevices, gas saturation and prior history of the liquid are most important.

In the body, crevices may not be the only mechanism for bubble stabilization. Semi-impermeable organic skins can coat bubbles. Injectable bubbles based on this stabilization principle are used as bubble contrast agents for ultrasound imaging¹¹ and may also be used as cavitation seeds in therapeutic uses of ultrasound.

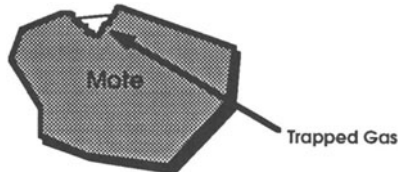


FIG. 6 Schematic of gas particles trapped in a crevice of a hydrophobic particle (mote). Tap water containing 50,000 motes/ml corresponds to one mote for each drop of 1/3 mm diameter.

3.5. RADIATION-INDUCED

As with superheated liquids used in bubble chambers to follow the paths of elementary particles, tensilely stressed liquids will also form bubbles initiated by radiation of the right type and of sufficient energy. Greenspan and Tschiegg performed a comprehensive set of measurements of thresholds for radiation-induced cavitation in organic liquids and water. Fast neutrons, for example will reduce the threshold to a few atmospheres for some organic liquids, but, for water, the threshold drops only to about 50 atmospheres.¹²

Superheated drop detectors are a new class of bubble chamber in which drops of a volatile liquid are immersed in a gel. For instance, Freon®-12 drops in an aqueous gel at room temperature are superheated by over 50 degrees Celsius. These will "pop" when exposed to neutrons. Since superheat and tension both produce the metastable state, it is not unexpected to find that acoustic waves can increase the sensitivity of these superheated drop suspensions.¹³

4. Regimes of Dynamics

4.1. INTRODUCTION

Depending on the conditions of the liquid, the size of initial bubbles, and the acoustical conditions, bubbles can experience a wide range of phenomena, including a) radial motion ranging from small to high amplitude (with the consequent radiation of waves ranging from pure sin waves, to shock waves to broad band noise),

b) shape oscillations ranging from steady state quadrupole oscillations, to high amplitude jetting and bubble fission, c) single bubble translation due to radiation forces, and d) multiple bubble effects due to secondary wave scattering.

4.2. LOW AMPLITUDE (FREE AND FORCED)

The resonance frequency of a symmetrically pulsating bubble (called volume pulsations) is attributed to the stiffness of the internal non-condensable gas resonating against the effective inertia of the surrounding liquid. For bubbles that are more than 10 micron in diameter, one can get the resonance frequency of a bubble at atmospheric pressure in water (in Hz) by dividing 326 by the bubble radius in centimeters. Different resonance frequencies for different size bubbles are shown in Figure 7

Bubbles are damped by three primary mechanisms: Thermal losses, viscous losses, acoustic radiation. Over different frequency regimes, each of these can be more or less important.

Bubble Diameter	Resonance Frequency	Relevance
1 mm	3 kHz	Underwater Propagation, Noise in the Ocean, Ultrasonic Cleaning
Human Hair (80 μm)	40 kHz	
Red Blood Cell (4 μm)	1 MHz	Diagnostic and Therapeutic Ultrasound
Cell Nucleus x 10	30 MHz	

FIG. 7. The resonance size of bubbles at an ambient pressure of one atmosphere for a given frequency, with typical occurrences.

4.3. HIGH AMPLITUDE (NONLINEAR ACOUSTICS ALL THE WAY TO CHAOS)

But bubble motion is not entirely linear. One reason is that the gas "spring" is only linear for small amplitude motion. As the amplitude increases, harmonics ($2f_0$, $3f_0$, etc.), subharmonics ($f_0/2$, $f_0/3$, etc.), and ultraharmonics (e.g. $3f_0/2$) can be observed,¹⁴ as seen in Figure 8.

One can interpret some of this behavior in terms of the general approach of nonlinear dynamics. That is, one can find a threshold for bifurcations and the approach to chaos in bubble dynamics when the pressure amplitude of this nonlinear oscillator is increased to greater values as illustrated in the predictions of Kamath and Prosperetti (Figure 9).¹⁵

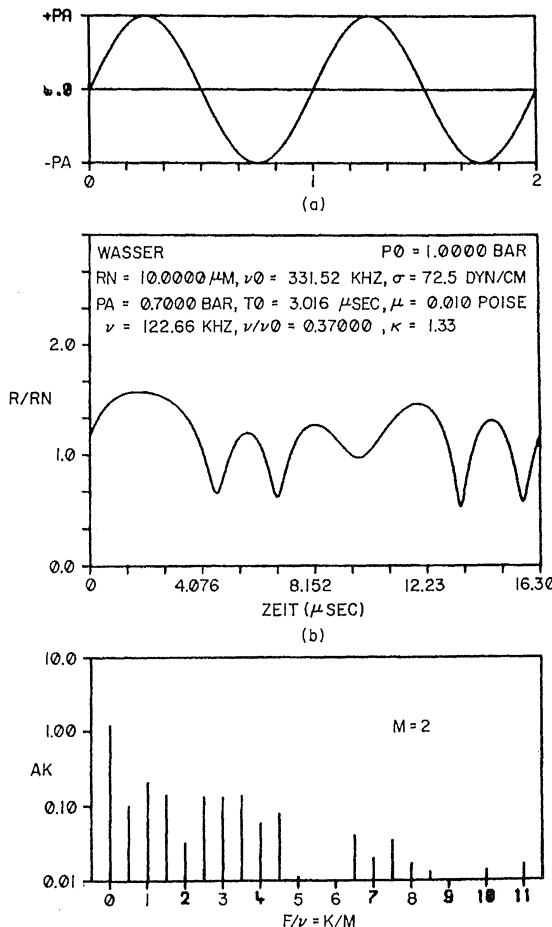


FIG. 8. Predicted nonlinear oscillations of bubbles showing radius versus time and spectral content, after Lauterborn, Ref. 14.

For bubbles that do not oscillate about an equilibrium position but rather grow in a cycle or two to a much larger size, the collapse is violent and impulsive in character. If the viscosity is sufficiently high or the bubble is sufficiently small so that surface tension is important, then the collapse can retain a nearly spherical shape, and bubble rebound is expected. During the rebound, as much as 70% of the energy can radiate away as sound. Since most of the action takes place in a very small fraction of the acoustic cycle, the acoustic spectrum of the radiated sound energy tends to be very broad; that is, there is a white noise spectrum.

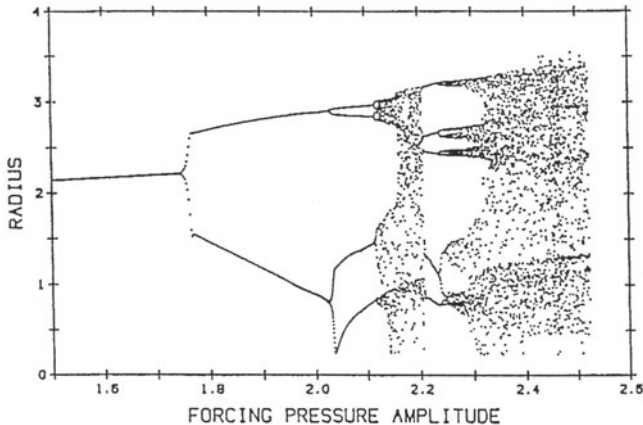


FIG. 9. Nonlinear dynamics of bubbles, after Kamath and Prosperetti, Ref. 15.

4.4. RADIALLY SYMMETRIC (AND SHOCK WAVES)

From the simple analysis by Rayleigh of the collapse of a void in an incompressible liquid, we know that the bubble wall achieves sonic velocity when the bubble has collapsed to about 1/30 of its original diameter.¹⁶ Of course, this does not take into account surface tension, which will be important when bubbles are in the micron size range or smaller, or the compressibility of either the inner gas or outer liquid. When sonic velocities are approached, compressibility becomes more important. A rarefaction wave will be launched. More importantly, when the wall motion is suddenly decelerated by the trapped gas, a strong pressure wave is launched. If this is strong enough, shock waves will be generated. But with spherical spreading, these shock waves do not retain their strength very far from the bubble. The biggest effect, therefore, may be in bubble-bubble interactions, in which bubble shattering sometimes occurs.

There is good evidence that suggests that there is also a shock wave that is radiated into the bubble when the speed of sound in the gas is exceeded. This situation is discussed later when effects such as sonoluminescence are discussed.

4.5. SHAPE DEFORMATION AND JETS

Normally, if effects are to be felt, surfaces must be in the near vicinity. And if a bubble collapses in the vicinity of these surfaces, whether they be solid, another liquid, or gas (free surface or another bubble), then the bubble collapse will not remain symmetrical. From simple hydrodynamic arguments, one can see that fluid rushing inward during the rapid collapse of a bubble will be forced from an initial radial direction if the bubble is near a solid surface. This asymmetric flow deforms the bubble, which then further distorts the flow. A powerful jetting can ensue, as shown on the accompanying photographic sequence of a bubble collapsing near a solid surface (Figure 10).¹⁷ The role of these jets in effects is discussed later.

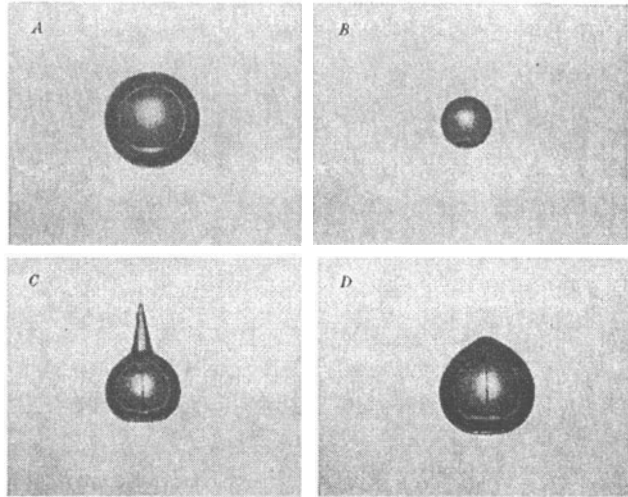


FIG. 10. Photo of jet formation from bubble collapse near a solid boundary, after Benjamin and Ellis, Ref. 17.

4.6. SURFACE INSTABILITIES

A surface that continues to grow in size tends to reduce the irregularities in the surface shape. A surface that is forced to decrease in size, tends to buckle like a compressed beam. In the case of a growing bubble, spherical symmetry is encouraged. In the case of a collapsing bubble, small perturbations in the shape may grow. Moreover, surface perturbations grow when a gas-liquid interface accelerates in the direction of the liquid, which is common in bubble collapse. This is called the Rayleigh-Taylor instability, and is related to flow and surface parameters.

The photographic sequence of Figure 11 shows the explosive growth of a vapor bubble (originating from a superheated drop), and its subsequent collapse. Notice that the growth is a smoothing process, and the collapse leads to instabilities. Surface tension works against these perturbations, because the greater the radius of curvature of the surface, the greater the acoustic stress working to eliminate the perturbations.¹⁸

Surface waves of wavelength λ , propagate around a bubble with a velocity of $V = (2\pi\sigma/\rho\lambda)^{1/2}$. Note that these waves are dispersive (depending on frequency). For a spherical bubble of radius R , if one trip around the sphere corresponds to the acoustic period, we have a shape resonance of the lowest order (the quadrupole mode). For instance for a 1 mm diameter bubble, the quadrupole resonance frequency associated with alternating oblate and prolate shapes is 342 Hz, whereas for a 1 cm diameter bubble, the result is 11 Hz (i.e. this resonance frequency goes inversely as the 3/2 power of the diameter).

A different type of surface instability occurs when a surface (whether curved or flat) is subjected to a high intensity sound field. In this case, the sound field itself interacts with the perturbed surface; at a

given threshold intensity, instabilities will grow, and the surface will shatter into small pieces (mixing gas and liquid). This principle can be used for emulsification, as discussed in Section VII having to do with applications of cavitation.

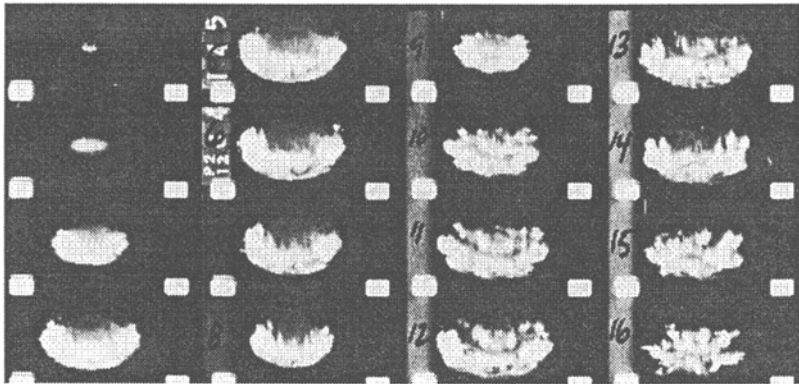


FIG. 11. Oscillations of a vapor bubble after the nucleation of a superheated drop, showing surface instabilities. (Harbison and Apfel, ref. 18)

4.7. EFFECTS INSIDE THE BUBBLE

When heat conduction cannot keep up with the increase of temperature in a rapidly collapsing bubble, then the motion can be modeled as adiabatic, with pressure increasing as the 3γ power of the inverse bubble radius, and with temperature increasing to the $3(\gamma-1)$ power. (γ is the ratio of specific heats.) An example of this energy concentration is given in Table 1.

4.8. EFFECTS OUTSIDE THE BUBBLE (RADIATION: SOUND AND LIGHT)

One can learn something about the cavitation process based on the sound and light that emanates from cavitating bubbles. As we have seen, harmonics, subharmonics and ultraharmonics give some evidence of the nonlinear nature of the phenomena and the amplitude of bubble motion. White noise in the spectrum indicates violent collapse. The three sound spectra given in Figure 12 indicate growing broadband emission with increasing acoustic amplitude.¹⁹

When light is emitted, there is strong evidence for high internal bubble temperatures, and chemical processes are possible, at least internally. Additional discussion of this phenomenon is given below.

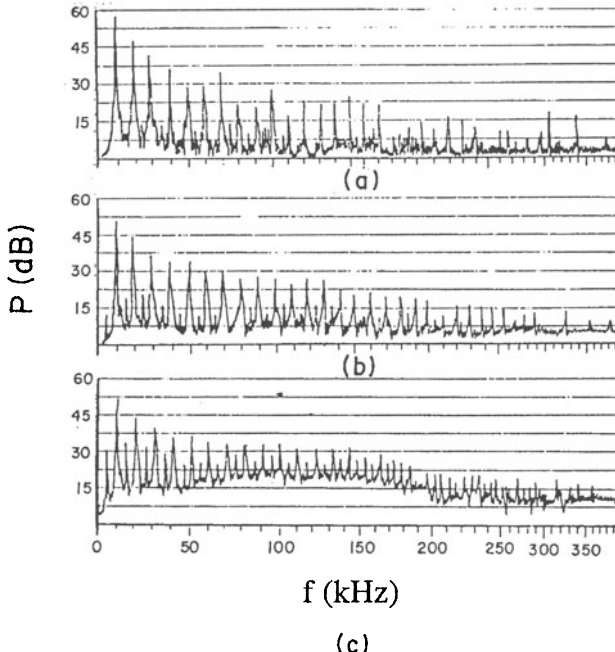


FIG. 12. Sound emissions from radiating bubbles. Discrete frequencies (corresponding to bubble modes) in the spectrum are apparent even for low-pressure amplitudes. At higher pressures, broad band radiation from inertial cavitation becomes more apparent (after Rosenberg, Ref. 19).

5. Bubble Translation and Other Motions in a Sound Field: Introduction

A sound wave can exert a force on a bubble or other inclusion in a fluid due to the fact that the fundamental fluid equations from which the linearized sound wave equation is derived are essentially nonlinear. The force is just the integral of the pressure over an area. This is equivalent to the time average of the product of bubble volume (which is time varying) and the acoustic pressure gradient. $[F = \langle V(t) \text{grad}P \rangle]$. Notice that since both the volume and pressure gradient are time varying, the time average of their product may have a non-zero component. Physically, the bubble moves in pressure and particle velocity gradients while at the same time the bubble size is changing. This combination leads to a rectified effect that forces the bubble to move in a given direction.

5.1. MOTION IN PROGRESSIVE WAVE FIELD: PRIMARY FORCES

When a bubble finds itself in a plane progressive wave sound field, it will move in the direction of the progressive wave. A pulsating bubble produces a pressure field that varies as the inverse of the distance from the bubble. In such a diverging field, particles will be attracted to the bubble. For example, red blood cells have been observed to gather around resonating bubbles trapped in the pores of hydrophobic, Nucleopore™, membranes, as schematically illustrated in Figure 13.

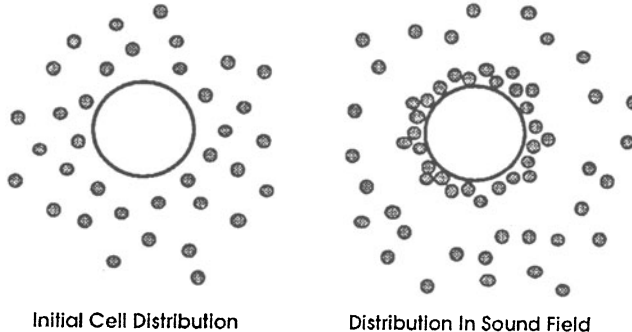


FIG. 13. Schematic illustrating how a radiating bubble will draw particles (e.g., blood cells) toward it due to acoustic radiation forces.

5.2. MOTION IN A STANDING WAVE FIELD

In a standing wave field, the motion of a bubble will depend on the size of the bubble in relation its resonance size. For a bubble smaller than resonance size, the bubble size decreases as the acoustic pressure increases; in this case, bubbles move toward a position of spatial pressure maximum (velocity node) in the standing wave field. For bubbles greater than resonance size, the bubble is growing as the pressure increases (in the same way as a mass moves in opposite phase to the forcing in a spring-mass system driven above resonance); here, the bubble moves away from the pressure maximum and toward a velocity maximum.

For particles or liquid drops, the motion depends on the compressibility and density contrasts of the inclusion as compared to the host medium. For bubbles of smaller than resonance size and for drops that are far more compressible than the surrounding medium's compressibility (e.g. oil drops), there is migration toward the pressure maximum in the field, with the inclusion ending up at a position above or below that

position depending on its density assuming the field variation is vertical (in the earth's gravitational field.) For solid particles with lower compressibility than the surrounding medium, and for bubbles larger than resonance size, migration is toward the acoustic pressure minimum in the standing wave. This potential differentiation based on these factors makes possible separation of materials in a standing wave field.

5.3. SECONDARY FIELDS AND FORCES: E.G. BUBBLE-BUBBLE EFFECTS

When two bubbles in a sound field are within a few diameters of each other, then they may attract each other. During the rarefaction part of cycle, bubbles expand; flow between bubbles causes a pressure reduction (Bernoulli principle), and bubbles move toward each other. During compression phase, bubbles contract, and fluid that was forced out from between bubbles now flows back. This too induces Bernoulli effect, since pressure is reduced no matter what the direction of the flow. Thus, the net effect averaged over one complete cycle is bubble attraction.

The form of attracting force for two bubbles of volume V_1 and V_2 separated by R is, for the case of wavelength long compared to the separation, $F = A V_1 V_2 / R^2$. This, of course, reminds us of gravitational and electrostatic forces, which are yet to be unified by physicists in any Grand Unified Theory. Is this just a coincidence, or is there some deeper reason for the same form for the force?²⁰

5.4. RADIATION PRESSURE AND THE RESONANCE SIZE OF BUBBLES

This difference in behavior of bubbles above and below resonance size in a sound field produces interesting cavitation phenomena. When observing cavitation from a continuous wave source with a frequency under 100 kHz, one sees darting, comet-like cavities moving away from a particular spot (see Figure 14 from Crum²¹). Hissing and pinging sounds are often heard. What is happening is that very small bubbles, below resonance size, are growing by rectified diffusion (that is, more gas passes into the bubble in expansion than leaves during contraction, leading to a net gas increase each cycle); simultaneously, they move toward pressure maxima in the sound field due to acoustic radiation forces, as discussed above; at the pressure maxima, they continue to grow and perhaps coalesce with other bubbles until a bubble of resonance size is reached. Very high amplitude motion ensues, accompanied by short broad band "clicks" and some additional growth, at which point the bubble's phase relative to the sound field is reversed and the bubble is driven away from the sound pressure maximum. It continues, however, to grow and collapse as it translates toward a region of low acoustic pressure. With each collapse, the bubble may shatter, and then reform as it grows again, giving a comet like appearance. If this bubble hits a container surface, a pinging sound may be heard. Bubbles, larger than resonance size adhering to wall or transducer surfaces may oscillate with relative large amplitude, radiating both pure and broad band emissions.

In the steady state, this procession of inward-moving small bubbles and of outward-moving comets is referred to as "streamers". Sometimes, the process has a period quality to it, which is called cyclic cavitation.

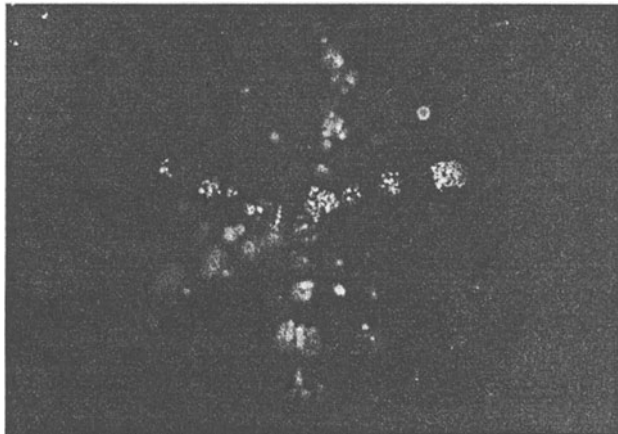


FIG. 14. Stroboscopic image, after Crum, Ref. 21, of bubble "comets" moving radially from an acoustic pressure maximum in an acoustic standing wave field.

6. Bubble Detection

To detect cavitation one can employ direct or indirect measures. Direct measures refer, for example, to optical or acoustic observations that allow one to determine, or at least infer, the dynamic character of the bubble motion in real time (with only a delay for the interrogating wave to reach the receiver). For instance, a shadow image of a bubble can be picked up with a photo diode. For extremely fast phenomena, such as cyclic sonoluminescence, high speed photomultiplier tubes have been used. Commonly, hydrophones monitor the acoustic pressure in a given region due to bubble activity in another region, giving information on amplitude, phase, and frequency content of bubble emissions. Such information can provide data on the amplitude and scale of bubble activity.

There are a wide variety of indirect measures for cavitation, including erosion of solid surfaces, chemical assays (e.g. iodine release), histological analysis of tissues, etc. Since these methods are indirect, often involving the effects of cavitation on systems, one must infer the kind of bubble activity that created the effect. Sometimes one cannot be sure that the effect was due to bubbles; for instance, thermal effects can also produce bioeffects in tissue that can, in some instances, be confused with mechanically induced effects.

7. Essentials of Applications of Acoustic Cavitation

7.1. INTRODUCTION

Acoustic cavitation may be a desirable or undesirable effect of the use of high intensity sonic or ultrasonic waves. In the ocean, for instance, it may be a limiting factor in the range of long range sonar applications.

7.2. MACROSONICS (CLEANING, SONOCHEMISTRY, ETC.)

Bubbles driven into activity by acoustic waves act as sources of pressure variation and fluid motion. For instance, a bubble driven at its resonance frequency will lead to high oscillatory fluid velocities. Such fluid motion can increase heat, momentum, and mass transport. Gas diffusion, for example, will increase so that an evacuated liquid can be outgassed more quickly in the presence of an intense sound field. A chemical reaction that depends on the surface area of a solid material in a fluid, will be aided by oscillatory fluid motion which will convect away unfavorable gradients of chemical reactants.

High fluid velocities occur at cavitation centers that also are the places where dirt and other impurities form on surfaces. This situation is, of course, favorable for ultrasonic cleaning. Whether in large scale industrial cleaning at 20 kHz, or in the fine scale cleaning required of microchips at 1 MHz, the type of cavitation must produce fluid velocities for scrubbing the surface without powerful inertial cavitation, which might actually pit or otherwise damage the surface below the dirt. The addition of solvents and surfactants, in appropriate amounts, can aid the process. For instance, adding a solvent of high vapor pressure can soften cavitation, since the pressure inside the bubble is cushioned by the vapor of the solvent; at the same time, the surface tension lowering characteristic of surfactants aids in wetting solids and helps the acoustically induced fluid motion to clean effectively.

When flow and macrosonics are combined, one can achieve a variety of phenomena. For instance, flow itself over an edge can produce broadband sound. If the edge is part of a resonant chamber (as with a flute), then particular frequencies are enhanced. In a liquid flow over an edge, one can also get a pressure reduction. Combine this with an orifice, and one can produce a sonic or ultrasonic atomizer of liquids. Or the acoustics in such systems can be produced by a standard piezoelectric transducer. In any event, dc flow (which can produce hydrostatic pressure reduction via Bernoulli's principle) coupled with ac pressure variation enables a wide range of possibilities when cavitation is produced.

7.3. BUBBLES IN THE OCEAN

Bubbles in the ocean act as sources of sound. Some of these bubbles come from wave motion, some from rain drops entraining gas as they enter the water surface, and some from cool, gas-saturated water becoming supersaturated as it warms. These bubbles contribute to the overall sound level in the oceans. Sound encountering these bubbles is attenuated and is slowed because the effective elasticity modulus of the medium is reduced. Since sound refracts toward regions of lower sound velocity, it will bend toward the ocean surface where bubbles are most prevalent.

Underwater explosions not only generate shock waves from the immediate chemical explosion but also from a large amplitude acoustic wave that follows the oscillation period of the bubble that accompanies the explosion. Also, when the initial positive pressure pulse of the explosion hits the free ocean surface, it will reflect as a rarefaction, often leading to a high amplitude, long-duration tension that creates a large bubble just beneath the surface; these bubbles will rise due to their buoyancy and burst at the surface.

Surface reflected rarefactions also can occur in the body from high intensity sources of therapeutic or diagnostic ultrasound, as discussed below.

Long range sonar transmission requires high acoustic pressures of low frequency. The deeper the sound source, the higher the acoustic pressure attainable without cavitation. Pressurized sonar domes can

produce an analogous effect near the surface, but their limited size and pressure means that cavitation represents an ultimate limitation on long range sonar propagation.

7.4. BUBBLES AND BIOACOUSTICS

Ultrasound in the body is used for diagnostic and therapeutic applications. Diagnostically, the primary applications are imaging and flow assessment (the latter through doppler modalities); the frequency range is typically from 2 to 15 MHz, the lower frequencies for deeper penetration as in fetal examination and the higher frequencies for shallow penetration with high resolution, such as in the eye.

Current clinical diagnostic ultrasound equipment produces peak acoustic pressure amplitudes of 10 to 50 atmospheres (1 to 5 MPa). These have been shown to produce cavitation *in vitro*, and recently tests suggest that bubbles can be produced *in vivo*, as well. The problem in such observations is that the bubbles that are produced are on the scale of one micrometer, and they survive for about a microsecond. Given the large number of scattering objects in the body (e.g. millions of blood cells of 4 micron diameter), finding the bubble in the body is akin to finding a needle in a haystack.

But even if bubbles did form and collapse in the body, would there be any reason for concern? Here, the issue is the amount of bubble activity and its consequences. For instance, bubble activity in rat lung tissue insonified at diagnostic levels produces extravasation of blood vessels and visible damage on the lung surface.²² Could bubble activity at the submicron level induce mutation of dividing fetal cells? As we have shown earlier, bubbles of this size deposit an energy comparable to ionizing radiation. Yet, there is no evidence for diagnostically induced mutation of fetal cells.

Therapeutic applications of ultrasound usually are in the frequency range of 0.1 to 5 MHz, and employ continuous waves or long pulses with duty cycles in excess of 25%, although for shock-wave lithotripsy, a sequence of single cycle pulses is used. At duty cycles above 10 or 20%, acoustic absorption with the consequent rise in temperature is possible, and applications for producing hypothermia exist. (This is useful in some cancer treatment therapies.) In such a regime, bubbles produced by the ultrasound can undergo a non-inertial cavitation in which a bubble will continue to oscillate about its equilibrium radius.

Unconstrained bubbles may grow by rectified diffusion to resonant size and then may undergo much stronger oscillations, in effect turning into inertial cavitation. If constrained or damaged near or at resonance, the amplitudes of relatively stable cavitation bubbles can be great enough to induce fluid flow and to promote radiation forces on nearby particles. Elder²³, for example, observed such bubble induced effects, plotting the nature of the acoustically-induced radiation pressure and fluid "microstreaming" (Figure 15). At low frequencies, in the 10s of kilohertz range, such streaming can produce shear stresses sufficient to cause the breaking of cell membranes, which has found use in ultrasonic cell disrupters. Nyborg and colleagues have observed the attraction of blood cells to resonantly driven bubbles in hydrophobic Nucleopore membranes (Figure 13). The implications of this work to separation science are obvious, though practical, cost-effective applications in this area have yet to be developed.

Recently, new applications in medicine for high amplitude ultrasound have been proposed. For instance, an ultrasonic horn that is terminated with a long, ball-tipped wire and driven at about 20 kHz can be introduced into blood vessels, and the cavitation created at the ball tip can remove plaque from clogged arteries. At the same frequency, high molecular weight drugs have been driven through the skin, aided by acoustic cavitation, in a process called transdermal drug delivery.²⁴ A continuous wave, 4 MHz transmitter can be inserted in the male rectum and placed so that it disrupts prostate tissue; this "debulking" can relieve urinary flow insufficiency. And extracorporeal lithotripter pulses of 10s to 100s of MPa positive pressure and perhaps 10 MPa rarefaction pressures, normally used to shatter kidney stones as an alternative to surgery, are being tested to see if they can enhance the effectiveness of drug take-up in the body.

In addition, micron scale bubbles have been stabilized with semi-permeable lipid skins.¹⁰ When injected in the body, these bubbles can act as ultrasound contrast agents or as the seeds for inducing cavitation in order to promote some therapeutic effect.

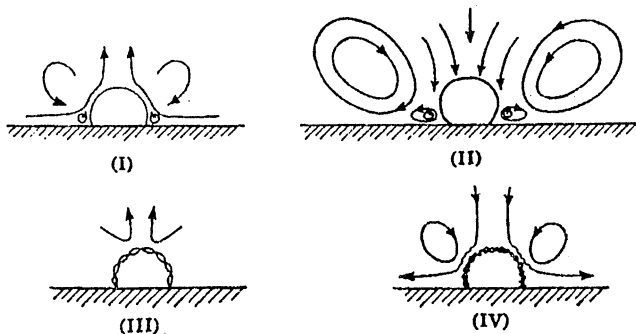


FIG. 15. Streaming (flow) patterns near oscillating bubble, after Elder, Ref. 23.

7.5. INVESTIGATIVE TOOL

7.5.1. Sonoluminescence

Because inertial collapse of bubbles is associated with high internal pressures, exceeding hundreds of atmospheres, and high temperatures of several thousand degrees Kelvin, it is not surprising to expect light emission from this hot, dissociated gas. Prior to 1990, this "sono-luminescence" was examined as a function of several variables to determine its physical origin. Most of the evidence pointed to a thermal mechanism. For instance, it was found that dissolved gases of lower thermal conductivity led to greater sonoluminescence, all other things being equal. It was also found that if the liquid had a higher vapor pressure (which could be achieved by adding some alcohol to water), then the light emissions were diminished, presumably because the bubble collapse was cushioned by the higher internal gas pressure.

Some experimenters added chemicals, such as Luminol^{®25}, which produced a chemically induced luminescence in the presence of intense sound. But in all of these chemi- and sono-luminescence experiments, control of the position and regularity of the phenomena was limited.

Then, in 1989, University of Mississippi graduate student Felipe Gaitan, working under the supervision of Lawrence Crum, reported that he had found a unique regime of parameters for his cavitation experiments that permitted a bubble to emit a single pulse of light synchronously with each acoustic cycle, as illustrated in Figure 16.²⁶ Key elements of this discovery were using a liquid of low gas concentration, so that the collapsing vapor bubble would achieve a sufficient collapse velocity to cause the residual dissolved gas to heat to luminescing temperatures. Also, to maintain the bubble cycle after cycle, without shattering, the initial bubble had to be small enough (on the scale of microns) so that surface tension stresses could

maintain the bubble's spherical shape for a significant part of the collapse phase. The acoustic pressure also had to be chosen carefully. The acoustic field plays the role both of holding the bubble against buoyancy forces and of driving it sufficiently hard to produce the repetitive sonoluminescence pulses. The frequency of these early experiments was between 21 and 25 kHz. Subsequent experiments by others have extended this frequency range up to about 60 kHz and down to about 10 kHz.

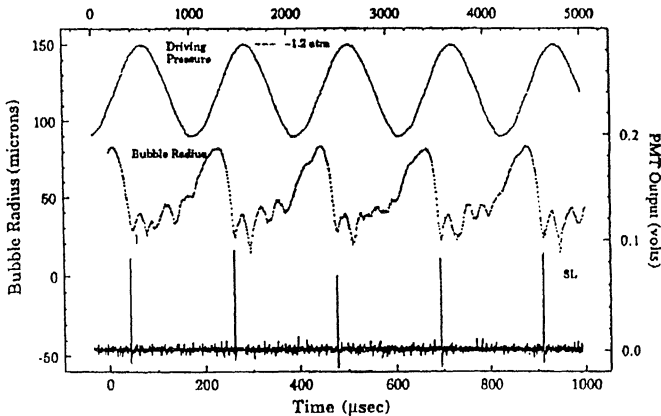


FIG. 16. Bubble radius and light output vs time for a sonoluminescing bubble, after Gaitan and Crum, Ref. 26.

Seth Putterman of UCLA visited Gaitan and Crum and recognized that some extremely interesting physics might be going on inside the collapsing bubble. Putterman's research team then performed some ground-breaking experiments in which the time history and spectra of the light pulses, the dynamics of the bubbles, and the sensitivity of the phenomena to a wide variation of experimental parameters were examined. They determined, for instance, that the light pulses had a duration of less than 50 picoseconds, that the pulse synchronicity was steady to within 50 ps, that the efficiency of light emission is high, and that the light emission was broad band, with no distinct spectral lines.²⁶

Current work by several groups suggests that a shock wave inside the bubble is responsible for the time history of luminescence, although there are almost as many theories of light generation as there are theorists. Much work continues not only on understanding this fascinating field of sonophysics, but also determining whether there are practical applications of this new knowledge.

7.5.2. Sonochemistry

One well-established application of inertial cavitation is called sonochemistry. The field has spanned the first observations of sonically induced chemical changes dating back to the 1920s, to the first substantial practical applications of this effect beginning in the 70s and 80s. Suslick and his colleagues have examined

both the underlying phenomena and the practical applications of sonochemistry.²⁸ For instance, they have measured light spectra to determine internal temperatures of cavitating bubbles in excess of 5000°K. These temperatures are sufficient, for example, to melt metal. At much lower temperatures this cavitation can accelerate chemical reactions (which require from tenths to tens of electron volts per molecule). Common in this regime is the production of free radicals which can catalyze reactions. Intense fields can, through shock waves and jetting, break long chain polymers as part of a process to synthesize block co-polymers.

Increases in heterogeneous chemical reaction rates of 10 fold are not unusual, with reactions with metals such as magnesium, lithium and zinc being common. One remarkable observation by Suslick and his colleagues was the sonochemical deposition of volatile organometallics to produce amorphous iron powder. It is assumed that the process requires cooling rates on the order of one million degrees Kelvin per second, which is only possible in a dynamic process that involves sufficiently low thermal inertia, which is possible with fine particles.²⁹

Sonochemistry for producing and enhancing chemical processes is still at an early stage/ The benefits of high energy concentration (up to 12 orders of magnitude) is both a benefit and a limitation. For when sound energy is focused in one small region, it is not able to process the rest of the material. That is, its effect is felt at points in the medium. One solution is to raise the energy of application and to use flow and scanning to distribute these hot spots. But there is a limit here because the fluid heats up as well. The thermal effects may not be desirable, or if they are, can be achieved without ultrasound. Therefore, it appears that sonochemistry may offer its best opportunities in "high value added" processes.

8. Concluding Remarks

Acoustic cavitation is an enormously broad area of study of relevance in a wide variety of practical processes; it can be a tool for fundamental scientific studies spanning enormous scales of size and energy. This tutorial exercise, which strives to give a broad overview and provide enough numbers to put the reader in the right ballpark of the phenomena associated with cavitation, has only scratched the surface. Major reviews of work on cavitation, in general, and acoustic cavitation, in particular, complement the present work.^{30 31 32 33³⁴ 35 36} In these reviews, one can find listed primary references to many of the topics discussed in this brief tutorial (and also to many not mentioned!)

9. References

* This article is reprinted (and reformatted) with permission of The Acoustical Society of America.
R. APFEL, SONIC EFFERVESCENCE: A TUTORIAL ON ACOUSTIC CAVITATION J. ACoust. SOC. AM. 101 (3), 1227-1237(1997)., COPYRIGHT 1997, ALL RIGHTS RESERVED.

¹ National Council on Radiation Protection, NCRP Report #66, draft report, W. Nyborg

² See, for example, E.N. Harvey, D. Barnes, W. McElroy, A. Whitely, D. Pease, and K. Cooper, "Bubble formation in animals," J. Cellular & Comp. Physiol. 24, 1-34 (1944).

³R.E. Apfel, "Water superheated to 279.5°C at atmospheric pressure," Nature 238, 63-64(1972).

- ⁴ M. Strasberg, "Propeller cavitation noise after 35 years of study," ASME Symposium on "Noise and Fluids Engineering," Nov. 1977, pp. 89-99.
- ⁵ M. Volmer and A. Weber, Z. Phys. Chem. 119, 277 (1926); W. Doring, Z. Phys. Chem. 36, 371 (1937).
- ⁶ E. Roedder, Science 155, 1413-1417 (1967).
- ⁷ M. Greenspan and C.E. Tschiegg, Radiation-induced acoustic cavitation; apparatus and some results. J Res Natl Bur Stand Sect C 71: 299-311 (1967).
- ⁸ R. Apfel, Scientific American, 227, 58-71 (Dec. 1972).
- ⁹ F.G. Blake Technical Memo 12, Acoustics Research Laboratory, Harvard University, Cambridge, Massachusetts, USA, (Sept. 1949).
- ¹⁰ R.E. Apfel and C.K. Holland, "Gauging the likelihood of cavitation from short-pulse, low-duty cycle diagnostic ultrasound," Ultrasound in Med. and Biol. 17, 179-185 (1991).
- ¹¹ H.J. Bleeker, K.K. Shung, and J.L. Barnhart, Ultrasonic characterization of AlbunexTM, a new contrast agent. J. Acoust Soc Am, 87: 1792-1797 (1990).
- ¹² M. Greenspan and C.E. Tschiegg, J. Res. Nat. Bur. Stand. 71C, 299 (1967).
- ¹³ R. Apfel, Nucl. Instrum. Methods 162, 603 (1979).
- ¹⁴ W. Lauterborn, J. Acoust Soc Am, 59 283 (1976).
- ¹⁵ V. Kamath and A. Prosperetti, Numerical integration methods in gas-bubble dynamics. J. Acoust Soc Am, 85: 1538-1548 (1989).
- ¹⁶ Rayleigh Lord. On the pressure developed in a liquid during the collapse of a spherical cavity. Phil Mag, 34: 94-98 (1917).
- ¹⁷ T.B. Benjamin and A.T. Ellis, Philos. Trans. R. Soc. London Sect. A, 260, 221 (1966).
- ¹⁸ J. Harbison and R. Apfel, J. Acoust. Soc. Am. 57, 1371-1373 (1975).
- ¹⁹ L. Rosenberg, High Intensity Ultrasonic Fields, p. 248, Plenum, New York (1971).
- ²⁰ R. Apfel, Am. J. Phys. 53, 66 (1985).
- ²¹ L. A. Crum and D. A. Nordling, J. Acoust. Soc. Am. 52, 294 (1972).
- ²² C. Holland, X. Zheng, R. Apfel, J. Alderman, L. Fernandez, and K. Taylor, Ultrasound in Med and Biol., in press.

- ²³ S.A. Elder, Cavitation microstreaming, *J. Acoust Soc Am*, 31, 54-64 (1958).
- ²⁴ S. Mitragotri, D. Blankschtein, and R. Langer, "Ultrasound-mediated transdermal protein delivery," *Science* 269, 850-853 (1995).
- ²⁵ K. Negishi, Experimental studies on sonoluminescence and ultrasonic cavitation. *J. Phys Soc Japan*, 16, 1450-1465 (1961)
- ²⁶ D.F. Gaitan, L.A. Crum, C.C. Church, and R.A. Roy, "Sonoluminescence and bubble dynamics from a single, stable cavitation bubble," *J. Acoust. Soc. Am.* 91, 3166-3183 (1992).
- ²⁷ B.P. Barber and S. J. Puttermann, *Nature*, 352, 318 (1991).
- ²⁸ K.S. Suslick , *Science*, 247, 1430-1445 (1990).
- ²⁹ K.S. Suslick , *Science*, 247, 1067-1069 (1990).
- ³⁰ H.G. Flynn, "Physics of Acoustic Cavitation in Liquids," in *Physical Acoustics*, Vol. 1 Part B (W.P. Mason, ed., Academic Press, New York, 1964) pp.57-172.
- ³¹ E.A. Neppiras, "Acoustic Cavitation," *Physics Reports* 61, 159-251(1980).
- ³² R.E. Apfel, "Acoustic Cavitation" in Ultrasonics (ed. P. Edmonds), Vol. 19 of Methods of Experimental Physics series (Academic Press, New York, 1981).
- ³³ A. Prosperetti, "Bubble dynamics: A review and some results," *Appl. Sci. Res.*, 38, 145-164(1982).
- ³⁴ F. Ronald Young, Acoustic Cavitation (McGraw Hill Book C., London, 1989).
- ³⁵ T.G. Leighton, The Acoustic Bubble (Academic Press, London, 1994).
- ³⁶ NCRP Report 74 (on exposure criteria and biological effects of ultrasound), prepared by committee headed by W. Nyborg (National Center for Radiological Protection, Bethesda, MD, 1983).

CAVITATION SONOPHYSICS

RONALD A. ROY

*Boston University, Department of Aerospace and Mechanical Engineering
110 Cummington Street, Boston, MA 02215*

1. Abstract

When a sound wave interacts with a bubble or a collection of bubbles present in a fluid, there is a conversion of acoustical to mechanical energy through a process known as acoustic cavitation. The resulting physical effects include cavitation microstreaming, collapse microjets, shock waves, elevated pressures and temperatures, and excess acoustic attenuation. It is possible to influence, and in some cases control, these processes through careful manipulation of the relevant physical parameters. The article provides a brief overview of the basics of cavitation nucleation and dynamics, followed by capsule descriptions of various physical effects that result from acoustic cavitation activity.

2. Introduction

It is widely known that many of the physical effects leading to sonochemical activity are due, either wholly or in part, to the action of acoustic cavitation. The term "acoustic cavitation" is very broad and includes a host of bubble-related physical processes ranging from the production of free radicals [1,2] to the generation of microscopic fluid streaming [3,4] to the shielding and channeling of acoustic energy [5]. Which processes prove dominant depend to a large extent on the nature of the cavitation field and on the consequences that these mechanical actions have on a desired chemical reaction or process. For example, if one seeks to promote chemistry using a catalyst which is isolated by an oxide surface layer, then those cavitation effects that promote surface cleaning (microstreaming, microjets, etc.) are desirable.

In order to optimally achieve a desired cavitation environment, one must understand the physics of the cavitation process and use that knowledge to "tailor" the cavitation field in an appropriate manner. It is not the goal of this paper to discuss the many ways in which bubbles can promote sonochemistry. Rather, we shall focus on the cavitation process itself. This includes a discussion of the nucleation process followed by description of the various "species" of cavitation, the relationship between fluid and acoustic properties on cavitation activity, and the resulting physical effects. The treatment is tutorial and broadly based; interested readers are directed to the cite references

for more detail. In particular, the book by Leighton [6] covers all of these topics in detail and offers an extensive list of references to guide further study.

3. Cavitation Nucleation

The term acoustic cavitation generally refers to the driven response of a gas bubble or a field of bubbles exposed to periodic acoustic stress. However, in order for a cavitation field to form, one must first have a population of free gas bodies for the acoustic field to act upon. These gaseous inclusions are the “seeds” of cavitation activity and are commonly called cavitation nuclei.

Unless there is a mechanism for sustained gas injection (such as sparging), it is unreasonable to assume that free gas bubbles will be present to serve as nucleation sites. Such bubbles will either rise to a free surface due to buoyancy [7], or dissolve due to the forces of surface tension [8]. Clearly, some mechanism is required to stabilize small gas bodies against dissolution. Of the several models that have been proposed [9], the one that seems to most viable in the widest range of applications is the *crevice model*.

In the crevice model, gas pockets adhere to small hydrophobic particles that have a density that is greater than that of the surrounding fluid. In a similar manner, gas bodies can adhere to any hydrophobic surface within a container, including the container walls. The affinity between the gas body and the solid object is the result of imperfections on the surface of the solid. When a gas pocket resides in a crevice of an imperfectly wetted solid, its radius of curvature is concave outward. Thus, the force of surface tension that normally drives gas out of a bubble is now directed toward the liquid phase. This results in a reduction in the pressure inside the gas pocket, which permits it to retain stability against dissolution even in undersaturated liquids.

When exposed to a sufficient level of tensile stress, the bubble wall advances up to the mouth of the crevice, at which point a free bubble can be produced. This nucleation mechanism, first proposed by Harvey *et al.* [10] has received considerable attention [11-14] and is commonly regarded as the dominant nucleation mechanism for systems involving liquids exposed to the atmosphere (dust motes serve as nuclei) and otherwise physically “dirty” systems.

Another mechanism for nucleation is called the *variably permeable skin model*. First proposed by Fox and Hertzfeld [15] this model exploits the presence of organic impurities present in most water samples. These impurities can accumulate on the wall of a microscopic bubble, resulting in a surface skin that is impermeable to gas transfer. Yount [16,17] extended the concept to include a *semi-permeable skin* which inhibited gas transfer during the acoustic compression phase but allowed for the influx of gas into the bubble during the acoustic rarefaction phase due to the expansion of the bubble surface.

There have been several other methods for bubble stabilization and cavitation nucleation. These include *homogeneous nucleation* [9], nucleation from *cosmic rays* [9], and *tribonucleation* [18] and stabilization via surface active polar molecules [19] and ionic charges [20]. It suffices at this point to assert that, by some means, most liquids support large numbers of cavitation nuclei. What happens from here on depends on

several factors, such as the acoustic pressure amplitude, the size of the bubble and the properties (mainly temperature and dissolved gas concentration) of the host liquid

4. The Bubble Equation of Motion: Small Amplitude Behavior

Over the years there has been a significant amount of activity directed at the modeling of spherically symmetric bubble pulsations in a sound field; see Section 4.2 in [6]. Although several models exist, a particularly useful one can be attributed to the cumulative efforts of Rayleigh, Plesset, Noltingk & Neppiras, and Poritsky (see [6] and [21] for summaries). This model considers the radial pulsation of a single bubble in an infinite, incompressible liquid of density ρ . It assumes uniform acoustic forcing, a uniform internal pressure, constant vapor pressure, P_V , and no mass diffusion across the bubble wall. The physics is embodied in the well known *Rayleigh Plesset Equation*:

$$\rho \left(R \ddot{R} + \frac{3\dot{R}^2}{2} \right) = \left[\left\{ P_o + \frac{2\sigma}{R_o} - P_V \right\} \left\{ \frac{R_o}{R} \right\}^{3\kappa} + P_V \right] - \left[\frac{2\sigma}{R_o} + \frac{4\eta\dot{R}}{R} + P_o + p(t) \right]. \quad (1)$$

<i>Inertial Terms</i>	<i>Total Internal Pressure</i>	<i>Total External Pressure</i>
-----------------------	--------------------------------	--------------------------------

Here R is the instantaneous bubble radius, R_o is the equilibrium bubble radius, σ is the surface tension, η is the shear viscosity of the liquid, P_o is the ambient pressure, κ is the polytropic exponent for the gas, and $p(t)$ is the time-varying acoustic pressure. Note that the equation is essentially a force balance, where the inertial terms on the left hand side are equal to the net force across the bubble wall. This equation can be greatly simplified if one assumes time harmonic, small-amplitude motion:

$$p(t) = P_o e^{i\omega t} \quad R(t) = R_o + \zeta \quad \zeta \ll R_o. \quad (2)$$

Equation (1) reduces to the following simple harmonic oscillator equation:

$$\ddot{\zeta} + \omega_{res}^2 \zeta = \frac{p(t)}{\rho R_o} e^{i\omega t} \quad \omega_{res}^2 = \frac{1}{\rho R_o^2} \left[3\kappa \left\{ P_o + \frac{2\sigma}{R_o} \right\} - \frac{2\sigma}{R_o} \right]. \quad (3)$$

For sufficiently large bubbles (larger than 5-10 μm in water):

$$P_o \gg \frac{2\sigma}{R_o} \quad \text{and} \quad f_{res} = \frac{1}{2\pi R_o} \sqrt{\frac{3\kappa P_o}{\rho}} \quad \text{or} \quad R_o = \frac{1}{2\pi f_{res}} \sqrt{\frac{3\kappa P_o}{\rho}}. \quad (4)$$

Equation 4 gives the *resonance frequency* of a bubble of equilibrium radius R_o or, equivalently, the *resonance radius* associated with a frequency f_{res} . The concepts of resonance radius and resonance frequency are interchangeable. Indeed, the product of the two quantities is a constant. For an air bubble in water at STP:

$$f_{res} R_o = 3.26 \text{ Hz} - \text{m} . \quad (5)$$

Thus, a 1-mm bubble resonates at 3.26 kHz, or the resonance radius at 1 kHz is 3.26 mm. As one increases the frequency, the resonance radius decreases proportionally. Since the response of a bubble is maximum when driven at its resonance frequency, the sizes of acoustically relevant bubbles decrease linearly with increasing frequency. Reactors operating in the low kHz frequency range will employ bubbles with radii on the order of a millimeter. Devices operating in the MHz range utilize bubbles with sub-micron sizes.

The low-amplitude response of bubbles is relevant to sonochemistry primarily through their action on the sound field. Bubbles of resonance size will maximally scatter and absorb sound; see Section 4.1.2 in [6]). Thus they can serve as barriers to sound propagation. When designing reactors, it is important that the acoustic coupling path between the sound source and the reaction zone is as free of bubbles as possible, otherwise most of the sound energy will either redirected or lost in transit.

5. Large Amplitude Bubble Behavior: Stable and Inertial Cavitation

As the amplitude of acoustic forcing increases, the approximations leading to Eqs. 3 are no longer valid. The motion of the bubble becomes nonlinear and unstable in the sense that the equilibrium radius can no longer be assumed to remain constant due to mass transfer across the bubble wall (discussed below). Such behavior is often termed *stable cavitation*, since these bubbles usually will not self destruction in the absence of nearby boundaries. Briefly put, stable cavitation bubbles have the following gross attributes:

- (a) The motion is dominated by the compressibility of the gas in the bubble, thus this activity is often referred to as *gassy cavitation*.
- (b) The bubbles undergo fairly large amplitude pulsations, about an equilibrium radius, without self destructing.
- (c) The equilibrium radius will often change slowly over time due to mass transfer across the bubble wall. The transfer is driven by a process called *rectified diffusion* [22,23].
- (d) The bubble wall motion induces rapid local fluid streaming called *cavitation microstreaming* [3].
- (e) The bubbles are subject to body forces caused by direct radiation pressure from the sound field (the primary Bjerknes force [24-26]) or by bubble-bubble interaction (secondary Bjerknes forces [*ibid.*]).

When the forcing amplitude is again increased above a well-defined threshold pressure, the character of the bubble motion changes abruptly. The bubble experiences explosive growth during which time the pressure in the bubble rapidly drops to the liquid vapor pressure. At that point in time, the bubble is essentially a large vapor cavity filled with a little gas. During the ensuing positive pressure cycle of the sound field, the bubble collapses violently and in a manner reminiscent of the classic Rayleigh cavity [27]. Needless to say, this behavior, which is termed *inertial cavitation*, is very violent, resulting in the concentration of energy over very small length and time scales. Such activity has the following gross attributes:

- (a) The collapse is dominated by the inertia of the in-rushing liquid.
- (b) The bubbles will frequently (not always) self destruct upon collapse. This is especially true of bubbles that collapse near boundaries.
- (c) Very high peak internal temperatures and pressure can be attained, often on the order of thousands of degrees and thousands of atmospheres [2]. This can result in the production of free radicals, but usually does not impact the bulk temperature of the liquid to any great extent. Light emission can result from the relaxation and/or recombination of reactive chemical species, usually excited hydroxyl radicals in the case of water-borne cavitation or diatomic carbon emissions in the case of hydrocarbons. The process is termed *sonoluminescence*.
- (d) Fluid microstreaming accompanies the motion and high-velocity collapse jets will result with the bubbles collapse near boundaries or near each other (see [3] and Section 5.4.1 in [6]).
- (e) Rapid bubble collapse/rebound can result in the production of radiated shock waves.
- (f) Under highly restrictive circumstances, the bubble can experience repetitive, large amplitude excursions leading to the formation of internal shocks, significant adiabatic heating (during compression) and associated extreme conditions in the bubble. This behavior, sometimes referred to as repetitive-transient cavitation, results in the production of light visible to the naked eye [28]. There is a single light flash produced each and every acoustic cycle -- a process which has been termed *single-bubble sonoluminescence*.

6. The Importance of Acoustic and Fluidic Parameters

The type of cavitation produced depends on several factors associated with both the fluid and the sound field. Although there are no hard and fast rules to go by, in general it is possible to promote specific types of cavitation given proper control the relevant physical properties. We already know that a very important factor is the degree of cleanliness of the liquid. Without cavitation nucleation sites, the likelihood of initiating acoustic

cavitation is very small. In addition there are several other acoustic and fluidic properties that one can manipulate to good effect. Many of these are listed below, along with a brief description of their respective roles in dictating the cavitation dynamics.

6.1. ACOUSTIC PRESSURE

Increasing the acoustic pressure will take you from linear to nonlinear-stable to nonlinear-inertial bubble motion. Each transition occurs at a more or less predictable threshold pressure, and the value of this threshold depends on the other physical parameters, most notably the equilibrium bubble size. (For a more detailed description of threshold phenomenon in acoustic cavitation, see [7] and [9].) In general, the greater the pressure amplitude, the more energetic the cavitation.

Now, at this point it is important to recognize that, with regards to predicting or controlling cavitation dynamics, knowledge of the instantaneous acoustic pressure is more important than the time-average acoustic intensity or power. Of course, if one employs continuous-wave sound sources, then these quantities are closely related. However, when working with pulsed acoustic systems, it is possible to have very large peak acoustic pressures while maintaining relatively low average acoustic intensities. This situation would correspond to the case of short pulse durations with long inter-pulse periods.

A excellent example of this effect is the extracorporeal shock wave lithotripter (29), where very large amplitude (order 10 MPa), very short duration (order 5 μ sec) shock waves are used to pulverize kidney stones. The resulting cavitation field is *highly* inertial in nature, however, since the repetition rate of the device is so low (order 1 second) the time average intensity, and by extension the acoustic power, is in fact quite small!

6.2. ACOUSTIC FREQUENCY

In general, the higher the frequency the more difficult it is to produce energetic inertial cavitation, for it takes time to make a bubble grow explosively. For frequencies below 500 kHz or so, the frequency dependence of the inertial cavitation threshold is relatively weak. For MHz frequencies in water that is populated with a broad range of free-bubble nucleation sites, the relationship between the threshold pressure and the frequency follows approximately the following power law (this applies primarily for single-cycle forcing):

$$P_{\text{thresh}} \propto f^{-1/2} \quad (6)$$

This relationship is widely used to model the frequency dependence of inertial-cavitation bioeffects *in vivo* and *in vitro*. It has led to the adoption of an output display standard used in the diagnostic ultrasound industry called the *mechanical index* (M.I.) [30]. The M.I. is defined as

$$\text{M.I.} \equiv \frac{p^*}{\sqrt{f^*}} \quad (7)$$

where p^* is the derated (to account for sound absorption in tissue) peak rarefaction pressure in MPa, and f^* is the frequency in MHz. Experiments indicate that when the M.I. is greater than about 1, the acoustical conditions are such that inertial cavitation becomes possible. However, this assumes the *a priori* presence of viable cavitation nuclei. When no nucleation sites are present, all cavitation is suppressed, even for pressures well in excess of M.I. = 1. For more details regarding the M.I. and its use, see [30].

6.3. ACOUSTIC PULSE DURATION AND DUTY CYCLE

As indicated above, by pulsing the sound field it is possible to generate large-amplitude pressure waves with relatively low time-average intensity. The type of cavitation you generate will depend on the instantaneous pressure, however, there is another important effect that occurs when you have long-duration pulses or higher duty cycles.

As the bubble pulsates gas is transferred across the bubble wall. During expansion, this transfer is into the bubble because the partial pressure of dissolved gas is greater than the internal pressure of the expanding cavity. During collapse, gas travels out of the bubble because the internal pressure is now large, forcing free gas into solution. Since the surface area of the bubble is larger during expansion, than it is during compression, more gas diffuses in than out. This process is superimposed on the normal process of surface tension-driven bubble dissolution. If the dynamic gas transfer effect is large enough, the equilibrium size of the bubble can actually increase over time. This process is called *rectified diffusion* [22,23] and it occurs only so long as the sound field is turned on (thus the importance of duty cycle or pulse duration) and the peak pressure exceeds a minimum value (another threshold pressure to consider!).

Now, why is this important? Briefly put, the equilibrium size of the bubble relative to the resonance size is almost as important as the instantaneous pressure in determining the subsequent bubbles dynamics (more on this below).

6.4. EQUILIBRIUM BUBBLE SIZE

The equilibrium size of a bubble is the size it attains in the absence of acoustic forcing (ignoring dissolution, of course). The critical quantity is the bubble size relative to the resonance size, for that determines to a large extent the characteristics of the driven bubble motion. If a bubble is larger than equilibrium size, then it is very difficult to induce explosive growth during the rarefaction phase of the acoustic cycle, for the loading of the surrounding liquid serves to inhibit the rate at which the bubble can expand. Conversely, if the bubble is very small, then the pressure of surface tension, often called the *Laplace pressure*, inhibits bubble growth. There is an optimum size range which leads to inertial cavitation at the lowest possible acoustic pressure. In general, this “optimum nuclei size” is on the order of $R_o/3$, where R_o is the resonance radius associated with the acoustic frequency (see Eq. 4). If one endeavors to generate highly energetic inertial cavitation, then bubbles in this size range are desirable. If one desires to produce stable cavitation, then larger bubbles are called for. Unfortunately, it is usually difficult or impossible to directly control bubble sizes in a cavitation field. This is normally achieved by

controlling the mass transfer process through the acoustic pressure, the acoustic duty cycle and the dissolved gas concentration.

6.5. DISSOLVED GAS CONCENTRATION

The threshold pressure for rectified diffusion (and the subsequent bubble growth rate) is influenced by the concentration of gas dissolved in the liquid. The more dissolved gas you have, the more likely you are to induce rectified diffusion, ultimately resulting in larger equilibrium bubble sizes. As indicated earlier, the term “gassy cavitation” often refers to the stable pulsations of these larger, gas-filled bubbles. If one desires inertial cavitation, then a good strategy is to degas the liquid. That way, when a small bubble grows explosively, you will have less gas diffusion into the cavity, resulting in a more energetic collapse (gas serves to cushion the collapse) and less long-term bubble growth.

6.6. SURFACE TENSION

The impact of surface tension on bubble dynamics can be quite complex, however, a good rule of thumb exists for assessing when surface tension matters. As mentioned earlier, the curvature of the gas-liquid interface results in a surface tension pressure, often called the Laplace pressure which is directed radially inward. The magnitude of this force is given in terms of the bubble radius and the surface tension by:

$$P_{LAPLACE} \equiv \frac{2\sigma}{R} \quad (8)$$

and it serves to increase the internal pressure of the bubble. If this increase in pressure is small compared to the ambient pressure, then surface tension can be ignored. (This approximation was used in deriving Eq. 4.) However, when R is of order $2\sigma/P_0$, the Laplace and ambient pressure are comparable. In such a case the contributions of surface tension must be formally considered when assessing the bubble dynamics. For an air bubble in clean water at 1 ATM, this size is about 1.5 μm , thus one can argue that from bubble on the order of about 7 μm and smaller, the impact of surface tension must be considered. If you assume that this corresponds roughly to a range of bubble resonance radii, then the corresponding frequencies are 500 kHz and above. Thus, for most applications involving biomedically relevant frequencies, accurate assessment of the relevant bubble dynamics requires consideration of surface tension in the model.

6.7. OTHER FACTORS

There are several other factors that can contribute to bubble dynamics. These include the vapor pressure, the liquid temperature, the gas thermodynamics, the liquid viscosity, surface active contaminants, etc. Although each of these quantities can be quite important given the right circumstances that are, in general, less significant than the parameters listed above. The interested reader is directed to [6] for a detailed description of the

relationship between cavitation inception, cavitation dynamics, and the whole range of acoustic and material properties.

7. Physical Effects

The range of physical effects associated with cavitation phenomena is as broad as the range of bubble activity itself. They can be roughly broken down into three categories: acoustic, fluidic and thermal/chemical. Capsule descriptions of some of the more important effects follow below.

7.1. CAVITATION MICROSTREAMING

When a bubble pulsates, it moves fluid back and forth. The fluid motion eventually manifests itself as a steady flow called *cavitation microstreaming*. The velocity of this flow can be quite high, sometimes on the order of several m/s. Moreover, the transition for high velocities (along the bubble surface) to low velocities away from the bubble tends to occur in a minute region called the viscous boundary layer, given by [31]:

$$\delta = \sqrt{\frac{2\eta}{\rho\omega}}. \quad (9)$$

For a bubble with equilibrium radius R_o and surface displacement amplitude ζ , the tangential velocity near the bubble surface is given approximately by [32]:

$$U_t \approx \frac{\omega\zeta^2 R_o^4}{r^5} \Rightarrow \frac{\omega\zeta^2}{R_o}. \quad (10)$$

The resulting shear stress induced by the velocity gradient is:

$$\psi = \eta \frac{\partial U_t}{\partial r} \approx \frac{\eta\omega\zeta^2}{R_o\delta}. \quad (11)$$

Since both R_o and δ tend to be small, the shearing forces can be quite large. For example, for a 5 μm bubble driven at 1 MHz with a displacement amplitude of $\zeta = 0.5 \mu\text{m}$, the boundary layer thickness, velocity gradient and shear stress are 0.6 μm , $5.5 \times 10^5 \text{ sec}^{-1}$, and $550 \text{ N}\cdot\text{m}^{-2}$ respectively [32]. Such velocities and shearing forces can clean surfaces, disrupt biological cells, break down boundary layers, transport mass, and so on. Normally associated with stable cavitation, cavitation microstreaming is most pronounced when the bubbles are of resonance size and positioned near a boundary. It is considered to be a critical process in ultrasonic cleaning applications.

7.2. COLLAPSE MICROJETS

When a bubble undergoes inertial collapse near a boundary, the imposed asymmetry in the liquid flow field results in a jet of water that traverses the bubble and impacts the boundary (in the case of a rigid boundary). Tomita and Shima [33] have shown that the magnitude of the effect scales with the ratio of the distance from the wall, L_w , to the maximum radius of the bubble, R_M . For L_w/R_M greater than about 0.9, the jet is cushioned by a thin film of water, thereby reducing the pressure upon impact. Vogel *et al.* [34] observed velocities on the order of 100 m/sec for laser generated bubbles collapsing near a wall in which L_w/R_M was of order 1. For bubbles closer to the wall, the absence of this film results in some rather dramatic effects. Vogel *et al.* [34] calculated the pressure at the boundary to be 250 MPa for a 3.5 μm bubble (maximum radius) essentially sitting on a solid wall ($L_w/R_M = 0.2$). The potential for erosive damage is obvious. It is believed that this is the process that is responsible for the pitting of propellers. Cavitation microjets can play a role in processes ranging from ultrasonic cleaning to the destruction of kidney stones using high-intensity acoustic shock waves [35]. It is associated with inertial cavitation, thus the effects tend to be discrete in space and time.

7.3. ACOUSTIC EMISSIONS FROM CAVITATION

Cavitation is a noisy process. As bubbles pulsate, they displace fluid volume and are very efficient sources of sound [6]. For stable cavitation, this noise possesses both harmonics and subharmonics of the fundamental driving frequency [36]. As the forcing amplitude is increased, and depending on the equilibrium bubble sizes and the liquid properties, the bubbles can be made to pulsate inertially. At this point, the emissions become more broad band and can be temporally discrete. The sudden initiation of sizzling/popping noise is sometimes used as a marker for the onset of violent, inertial cavitation [37].

When an inertial cavity collapses, it can generate an outgoing shock wave [38] which offers some potential for mechanical effect. The outgoing shock wave can have pressure amplitudes as high as 1 GPa, however, the waveform is spherically diverging and therefore weakens rapidly with distance from the bubble. It is generally believed that only surfaces and objects existing within a few bubble radii are susceptible to damage from these shocks [39].

7.4. CONVERSION OF ACOUSTIC ENERGY TO HEAT

When a sound wave passes through a bubbly region, some of the energy is scattered and some of the energy goes into driving the bubbles. Both of these processes ultimately lead to the generation of excess heat in the bulk. There are many processes that contribute to this conversion. The scattered sound “rattles around” in the bubble field (i.e. multiple scattering), resulting in an increased path length and correspondingly greater viscous attenuation loss. The surfaces of the bubbles possess viscous boundary layers that leads to the conversion of mechanical energy to heat. The driven pulsations of the bubbles

result in pressure and temperature fluctuations inside the bubble that can lead to modest heating of the liquid surrounding the bubble. All of these factors (and more) add up to enhanced heating of the medium when bubbles are present. This effect has been documented by Watmough et al. [40] for continuous-wave therapeutic ultrasound. In hyperthermia experiments using pulsed, high-intensity focused ultrasound, Holt *et al.* [41] observed marked increases in heating rates associated with the onset of cavitation activity. The effect is more likely to be significant when dealing with biomedical frequencies (MHz) and energetic cavitation fields.

7.5. BUBBLE SHIELDING

In addition to heating, another important effect of bubbly media is its impact on the propagating field itself. The bubbles greatly attenuate the wave due to large amounts of both scattering and absorption. Thus, too many bubbles in the propagation path can be detrimental for in such a case one cannot deliver the sound to the target, be it a chemical reaction zone, a surface to be cleaned, or a region or human tissue. This is often called *bubble shielding* and it must be avoided if one wishes to get reliable results from a cavitation-driven process. One way to limit the number of bubbles present is to reduce the dissolved gas concentration, therefore forcing more bubbles into solution. Another way is to briefly turn off the sound field, which gives free bubbles a chance to either dissolve or rise out of the propagation path. This may be one reason why some investigators [42-44] have observed enhanced yields when insonifying reactors with pulses rather than continuous wave -- an effect that is often called *pulse enhancement*. This is the interplay between bubble production/growth while the sound is on versus dissolution while the sound is off. Pulse enhancement represents an optimization process in which a tradeoff exists between the desire to limit bubble-related acoustic attenuation and the recognition that an adequate level of cavitation activity is required to produce acceptable sonochemical yields.

7.6. INTERNAL THERMODYNAMICS

One of the more notable physical effects accompanying bubble activity takes place within the contents of the cavity. As the bubble pulsates, the internal gas and vapor experiences pressure and temperature fluctuations determined by the equation of state. For gentle pulsations, the fluctuations are modest. As the pulsation amplitude increases, the pressures and temperatures attained upon collapse increase dramatically. This is due largely to the fact that, as the bubbles begins to behave inertially, the collapse occurs so quickly that the resulting compression is approximately adiabatic. The extreme temperatures achieved within the bubble can dissociate molecules, which recombine radiatively, producing light. This is the well known process of sonoluminescence.

By analyzing the characteristics of the light emissions, it is possible to gain an estimate of the temperature achieved within the cavity. Estimates range from about 5,000K for a cavitation field in hydrocarbon liquids [45] to well over 20,000K for a single bubble pulsating in an acoustic standing wave. (The unique and interesting physics of

single-bubble sonoluminescence is addressed at length in several publications and will not be discussed here. The reader is referred to the excellent survey article by Crum [46].

It seems reasonable to consider that such extreme conditions can result in many sonochemical effects. It is important to note, however, that these effect will be limited largely to the contents of the bubble. The level of heating generated in the bulk is quite modest [2] and any free radicals produced tend to recombine quickly once they leave the confines of the hot cavity. Nevertheless, the notion that a bubble can serve as a microscopic chemical reactor is quite intriguing, and it is a well accepted fact that hot chemistry results from intense, inertial acoustic cavitation.

8. Conclusions & Closing Remarks

When an intense sound wave interacts with a bubble, there is a conversion of acoustical to mechanical energy, with the latter being concentrated on small scales. The specific nature of the bubble activity depends on the amplitude of forcing and on the size of the bubble relative to the acoustic wavelength. The resulting physical effects are broad in scope. Microstreaming, collapse microjets, shock waves, elevated pressures and temperatures, and excess attenuation are but a few of the many phenomena that can accompany this activity. These effects can be desirable, as in the case of sonochemistry and ultrasonic cleaning, or detrimental, as in the case of unwanted surface erosion or deleterious biological affects. Fortunately, it is possible to control the process through careful manipulation of acoustic and fluidic parameters.

It is important to note that there are yet several facets of cavitation activity that have not been addressed in this article. The translational dynamics of bubbles in standing waves [5], the organizing of bubbles in standing waves through secondary Bjerknes forces [5] and the effect of bubbles frequency-dependent sound speed [47] are all effects of import to many sonochemical processes. The acoustic cavitation zone is a truly complex system, where several interdependent processes occur simultaneously. Moreover, the relationship between cavitation cause and physical effect can be quite ambiguous. Consistent, predictable performance from a cavitating system requires careful attention to detail, both in terms of the acoustics as well as the fluidics.

9. Acknowledgments

The author would like to thank the Workshop Organizer, Larry Crum, for his exquisite patience and infectious enthusiasm as well as the financial support of the Defense Advanced Projects Agency, and the Office of Naval Research.

10. References

1. Suslick, K.S., Doktycz, S.J., and Flint, E.B. (1990) On the origin of sonoluminescence and sonochemistry, *Ultrasonics* **28**, 280-290.

2. Kamath, V., Prosperetti, A. and Egolofopoulos, F.N. (1993) A theoretical study of sonoluminescence, *J. Acoust. Soc. Am.* **94**, 248-260.
3. Elder, S.A. (1958) Cavitation microstreaming, *J. Acoust. Soc. Am.* **31**, 54-64.
4. Nyborg, W.L. (1958) Acoustic streaming near a boundary, *J. Acoust. Soc. Am.* **30**, 329-339.
5. Leighton, T.G. (1995) Bubble population phenomena in acoustic cavitation, *Ultrasonics Sonochemistry* **2**, S123-S136.
6. Leighton, T.G. (1994) *The Acoustic Bubble*, Academic Press, London.
7. Flynn, H.G. (1964) Physics of acoustic cavitation in liquids, in W.P. Mason (ed.), *Physical Acoustics, Vol. I, Part B*, Academic Press, New York, pp. 57-172.
8. Epstein, P.S. and Plesset, M.S. (1950) On the stability of gas bubbles in liquid-gas solutions, *J. Chem. Phys.* **18**, 1505-1509.
9. Apfel, R.E. (1981) Acoustic Cavitation, in P.D. Edmonds (ed.), *Methods in Experimental Physics, Vol. 19*, Academic Press, New York, pp. 355-413.
10. Harvey, E.N., Barnes, D.K., McElroy, W.D., Whiteley, A.H., Pease, D.C., and Cooper, K.W. (1944) Bubble formation in animals, *J. Cell. Comp. Physiol.* **24**, 1-22.
11. Strasberg, M. (1959) Onset of ultrasonic cavitation in tap water, *J. Acoust. Soc. Am.* **31**, 163-176.
12. Apfel, R.E. (1970) The role of impurities in cavitation threshold determination, *J. Acoust. Soc. Am.* **48**, 1179-1186.
13. Crum, L.A. (1979) The tensile strength of water, *Nature* **278**, 148-149.
14. Atchley, A.A. and Prosperetti, A. (1989) The crevice model of bubble nucleation, *J. Acoust. Soc. Am.* **86**, 1065-1084.
15. Fox, F.E. and Hertzfeld, K.F. (1954) Gas bubbles with organic skin as cavitation nuclei, *J. Acoust. Soc. Am.* **26**, 984-989.
16. Yount, D.E. (1979) Skins of varying permeability: a stabilization mechanism for gas cavitation nuclei, *J. Acoust. Soc. Am.* **65**, 1429-1439.
17. Yount, D.E. (1982) On the evolution, generation, and regeneration of gas cavitation nuclei, *J. Acoust. Soc. Am.* **71**, 1473-1481.
18. Hayward, A.T.J. (1967) Tribonucleation of bubbles, *Brit. J. Appl. Phys.* **18**, 641-644.
19. Sirotyuk, M.G. (1970) Stabilisation of gas bubbles in water, *Sov. Phys. Acoust.* **16**, 237-240.
20. Akulichev, V.A. (1966) Hydration of ions and the cavitation resistance of water, *Sov. Phys. Acoust.* **12**, 144-149.
21. Lauterborn, W. (1976) Numerical investigation of nonlinear oscillations of gas bubbles in liquids, *J. Acoust. Soc. Am.* **59**, 283-293.
22. Eller, A.I. and Flynn, H.G. (1965) Rectified diffusion through nonlinear pulsations of gas bubbles, *J. Acoust. Soc. Am.* **37**, 493-503.
23. Crum, L.A. and Hanson, G.M. (1984) Rectified diffusion, *Ultrasonics* **22**, 15-223.
24. Bjerknes, V.F.J. (1906) *Fields of Force*, Columbia University Press, New York.
25. Blake, F.G. (1949) Bjerknes forces in stationary sound fields, *J. Acoust. Soc. Am.* **21**, 551.
26. Crum, L.A. and Eller, A.I. (1969) Motion of bubbles in a stationary sound field, *J. Acoust. Soc. Am.* **48**, 181-189.
27. Rayleigh, Lord (1917) On the pressure developed in a liquid during the collapse of a spherical cavity, *Phil. Mag.* **34**, 94-98.
28. Gaitan, D.F., Crum, L.A., Church, C.C. and Roy, R.A. (1992) Sonoluminescence and bubble dynamics for a single, stable, cavitation bubble, *J. Acoust. Soc. Am.* **91**, 3166-3183.
29. Sturtevant, B. (1989) The physics of shock wave focusing in the context of extracorporeal shock wave lithotripsy, *Proc. Intl. Workshop on Shock Wave Focusing*, Sendai, Japan, pp. 39-64.
30. Holland, C.K. and Apfel, R.E. (1989) An improved theory for the prediction of microcavitation thresholds, *IEEE Trans. Ultrasonics Ferroelectrics Freq. Control* **36**, 204-208.
31. Morse, P.M. and Ingard, K.U. (1968) *Theoretical Acoustics*, Princeton Univ. Press, Princeton, pg. 286.
32. Coakley, W.T. and Nyborg, W.L. (1978) Chapter II: cavitation; dynamics of gas bubbles; applications in F. Fry (ed.), *Ultrasound: its Applications in Medicine and Biology*, Elsevier, Amsterdam, pp. 77-159.
33. Tomita, Y. and Shima, A. (1886) Mechanisms of impulsive pressure generation and damage pit formation by bubble collapse, *J. Fluid Mech.* **169**, 535-564.
34. Vogel, A., Lauterborn, W. and Timm, R. (1989) Optical and acoustic investigations of the dynamics of laser-produced cavitation bubbles near a solid boundary, *J. Fluid Mech.* **206**, 299-338.
35. Crum, L.A. (1989) Cavitation microjets as a contributory mechanism for renal calculi disintegration in ESWL, *J. Urol.* **85**, 1518-1522.
36. Neppiras, E.A. (1980) Acoustic cavitation, *Phys. Rep.* **61**, 159-251.
37. Roy, R.A., Atchley, A.A., Crum, L.A., Fowlkes, J.B. and Reidy, J.J. (1985) A precise technique for the measurement of acoustic cavitation thresholds and some preliminary results, *J. Acoust. Soc. Am.* **78**, 1799-1805.
38. Plesset, M.S. and Prosperetti, A. (1977) Bubble dynamics and cavitation, *Ann. Rev. Fluid Mech.* **9**, 145-185.
39. Hickling, R. and Plesset, M.S. (1964) Collapse and rebound of a spherical bubble in water, *Phys. Fluids* **7**, 7-14.
40. Watmough *et al.* (1993) *Ultrasound in Med. and Biol.* **19**, 231.

41. Holt, R.G., Cleveland, R.O. and Roy, R.A. (1998) Optimal acoustic parameters for induced hyperthermia from focused MHz ultrasound: phantom measurements with fluid flow and bubble activity, in *Proceedings of the 16th International Congress on Acoustics and the 135th Meeting of the Acoustical Society of America, Vol. II*, American Institute of Physics, pp. 1057-1058.
42. Henglein, A. and Gutierrez, M. (1986) Chemical reactions by pulsed ultrasound: memory effects in the formation of NO_2^- and NO_3^- in aerated water, *Int. J. Radiat. Biol.* **50**, 527-533.
43. Ciaravino, V., Flynn, H.G., Miller, M.W. and Carstensen, E.L. (1981) Pulsed enhancement of acoustic cavitation: a postulated model, *Ultrasound Med. Biol.* **7**, 159-166.
44. Flynn, H.G. and Church, C.C. (1984) A mechanism for generating cavitation maxima by pulsed ultrasound, *J. Acoust. Soc. Am.* **76**, 505-512.
45. Flint, E.B. and Suslick, K.S. (1991) *Science* **253**, 1379.
46. Crum, L.A. (1994) Sonoluminescence, *Physics Today* (Sept.) 22-29.
47. Commander, K.W. and Prosperetti, A. (1989) Linear pressure waves in bubbly liquids: comparison between theory and experiments, *J. Acoust. Soc. Am.* **85**, 732-746.

OLD-FASHIONED BUBBLE DYNAMICS

ANDREA PROSPERETTI

*Department of Mechanical Engineering
The Johns Hopkins University
Baltimore MD 21218 U.S.A.*

Abstract. This chapter reviews some basic aspects of the dynamics of gas bubbles in liquids: the effect of liquid compressibility, thermal processes inside the bubble, the stability of the spherical shape, and acoustic radiation forces. Some remarks on sonoluminescence are also included.

The laws of nature are widely believed to be invariant under a time translation. One of the consequences of this property is that a paper published 50 or 100 years ago is not necessarily irrelevant or wrong. The purpose of the present work is to review some basic results in the theory of bubble dynamics in the belief that they may benefit newcomers to the field.

1. The liquid

From the point of view of classical fluid mechanics, a bubble in a liquid is a free-boundary problem in which the mechanical and thermal behavior of the fluids – liquid and gas – is described by the usual conservation equations coupled by suitable conditions at the gas-liquid interface. The position of this interface is itself unknown *a priori* and is determined in the process of applying the interface conditions. In its generality the problem is therefore complex and only amenable to numerical calculations. Much progress can however be made analytically with the introduction of suitable approximations, first and foremost of which is the assumption of a spherical shape of the interface. Physically, sphericity is promoted by two agents: surface tension which, in general, is quite weak in comparison with inertia forces and other disturbances, and the dynamics of stretching of the interface, that is only at work during the expansion of the bubble (see section 3 below). Hence, while extremely useful, sphericity is an assumption the validity of

which needs to be closely examined in each case. For the time being we proceed with this assumption that, even when not entirely justified, is useful to shed light on the important physics of the various processes.

When coupled with the other assumption, discussed in the next section, that the liquid at the interface remains essentially isothermal, sphericity enables one to decouple the thermo-fluid-dynamic processes in the liquid and in the gas, which represents a major simplification. Since the liquid is assumed to be isothermal and in radial motion, its behavior is governed by the equation of continuity

$$\frac{1}{\rho} \left(\frac{\partial \rho}{\partial t} + u \frac{\partial \rho}{\partial r} \right) + \nabla \cdot \mathbf{u} = 0, \quad (1)$$

and momentum

$$\frac{\partial u}{\partial t} + u \frac{\partial u}{\partial r} = - \frac{1}{\rho} \frac{\partial p}{\partial r}. \quad (2)$$

Here the symbols have the usual meaning: t is time and r the radial coordinate measured from the center of the bubble. The velocity \mathbf{u} consists of only one component, u , along the radial direction; p is the pressure, and ρ is the density. For an irrotational motion like the present one, viscous effects only affect a term proportional to $\nabla \cdot \mathbf{u}$. For slightly viscous, slightly compressible liquids this effect is therefore negligible.

Let us now introduce the velocity potential ϕ , the enthalpy h , and the speed of sound c through the relations:

$$u = \frac{\partial \phi}{\partial r}, \quad d\rho = c^{-2} dp, \quad dh = \rho^{-1} dp. \quad (3)$$

In principle, in the presence of shock waves, the liquid cannot remain strictly isentropic. A consideration of the energy equation and the introduction of a second thermodynamic variable to express the differentials of ρ and h would therefore be necessary. However, it is well known that weak shocks cause a negligibly small increase of the fluid entropy (Ref. 1, section 83). To establish a scale against which to judge the magnitude of shock waves in the liquid it is useful to quote the widely used (modified) Tait equation of state for the liquid:

$$\frac{p + B}{p_\infty + B} = \left(\frac{\rho}{\rho_\infty} \right)^n \quad (4)$$

where $\rho_\infty = \rho(p_\infty)$. The values $B = 3.047$ kbars, $n = 7.15$ are a good fit to the isentropic pressure-density relation for water up to 25 kbars [2].

With the relations (3), the continuity equation (1) becomes

$$\nabla^2 \phi + \frac{1}{c^2} \left(\frac{\partial h}{\partial t} + u \frac{\partial h}{\partial r} \right) = 0, \quad (5)$$

while the momentum equation (2) is reduced to a total differential from which, upon integration, we have

$$\frac{\partial \phi}{\partial t} + \frac{1}{2} u^2 + h = 0. \quad (6)$$

We define the reference state of the enthalpy as the undisturbed pressure of the liquid p_∞ so that, from (3) and (4),

$$h = \frac{c^2 - c_\infty^2}{n-1}, \quad c^2 = n \frac{p+B}{\rho}, \quad (7)$$

where $c_\infty = c(p_\infty)$. The integration constant in (6) has been set to 0 by suitably adjusting the arbitrary function of time included in the potential (see e.g. Ref. 3, section 6.2).

Upon eliminating h between the continuity equation (5) and the Bernoulli integral (6) we have

$$\nabla^2 \phi - \frac{1}{c^2} \frac{\partial^2 \phi}{\partial t^2} = \frac{u}{c^2} \left(\frac{\partial u}{\partial t} - \frac{\partial h}{\partial r} \right). \quad (8)$$

It is a simple matter to see that the terms in the right-hand side are small in many circumstances, as is already indicated by the presence of the factor u/c – the Mach number – in front of the parentheses. Consider the region near the bubble first. Here the relevant length scale is the bubble radius R , the velocity is of the order of \dot{R} , and the potential is therefore of the order of $R\dot{R}$. (Here and in the following dots denote time derivatives.) The ratio between the first term in the right-hand and left-hand side of (8) is

$$\frac{(u/c^2)\partial u/\partial t}{\nabla^2 \phi} \simeq \frac{\omega}{c^2} \frac{\dot{R}^2}{R\dot{R}/R^2} \simeq \frac{R}{\lambda} \frac{\dot{R}}{c}. \quad (9)$$

Here ω and $\lambda = 2\pi c/\omega$ are the characteristic (angular) frequency and wavelength of the sound driving the bubble motion. In order for the bubble to remain spherical, the applied external pressure cannot vary appreciably over its surface, which implies that $R \ll \lambda$. The effect of the term considered will thus be small in the near field even if the radial velocity were to become sonic. Proceeding similarly for the second term in the right-hand side of (8), and using (3) to estimate h , we find

$$\frac{(u/c^2)\partial h/\partial r}{\nabla^2 \phi} \simeq \frac{\dot{R}}{c^2} \frac{\Delta p/\rho R}{R\dot{R}/R^2} \simeq \frac{\Delta p/\rho}{c^2}. \quad (10)$$

From (7) it is evident that, unless Δp , the magnitude of a typical pressure perturbation, is comparable with the constant B in the equation of state

(4), this ratio will also be small in the near field. A similar argument can be followed to show that the second term in the right-hand side of (8) is small in comparison with the first one near the bubble:

$$\frac{(1/c^2) \partial^2 \phi / \partial t^2}{\nabla^2 \phi} \simeq \frac{(\omega^2/c^2) \phi}{\phi/R^2} \simeq \frac{R^2}{\lambda^2}. \quad (11)$$

We conclude that, in the near field of the bubble, the exact equation (8) can simply be approximated by the Laplace equation

$$\nabla^2 \phi = 0, \quad (12)$$

the solution of which, satisfying the kinematic boundary condition $u = \dot{R}$ at the bubble surface, is

$$\phi = -\dot{R} \frac{R^2}{r} + g(t). \quad (13)$$

The function $g(t)$ cannot be determined by imposing boundary conditions at infinity as (12) is only valid near the bubble.

The previous arguments need to be modified in the far field as there the pertinent length scale is λ . Nevertheless, even without a formal argument, we can simply appeal to the smallness of the perturbation induced by the bubble in this region to linearize Eq. (8), thus effectively setting the right-hand side to zero and $c = c_\infty$ in the left-hand side. Of course, in addition to the bubble-induced disturbance, we should also consider the incident sound field, but this can certainly be treated in the acoustic approximation provided its amplitude is not comparable with the constant B in Tait's equation of state. In the far field, therefore, a valid approximation to (8) is

$$\nabla^2 \phi - \frac{1}{c_\infty^2} \frac{\partial^2 \phi}{\partial t^2} = 0. \quad (14)$$

In the region surrounding the bubble, the field consists of the sound incident on, and reflected by the bubble and of the wave radiated by the bubble itself. Let us neglect the latter component for the time being. Then the relevant solution of Eq. (14) must have the structure

$$\phi = \frac{c_\infty}{2r} \left[-G \left(t - \frac{r}{c_\infty} \right) + G \left(t + \frac{r}{c_\infty} \right) \right]. \quad (15)$$

This form is the consequence of assuming spherical symmetry and of noting that the wave must be regular in the neighborhood of $r = 0$. The factor $\frac{1}{2}c_\infty$ has been introduced for later convenience. The pressure field p_s associated to the potential (15) is given by $p_s = -\rho_\infty \partial \phi / \partial t$, or

$$p_s = \frac{c_\infty \rho_\infty}{2r} \left[\dot{G} \left(t - \frac{r}{c_\infty} \right) - \dot{G} \left(t + \frac{r}{c_\infty} \right) \right]. \quad (16)$$

Note that the relations (15), (16) do not necessarily hold near the bubble, but they certainly do outside the near field provided $\lambda \gg R$. The scale of spatial variation of ϕ and p_s given by (15), (16) is λ and therefore, at the edge of the near field, the argument r is small and one can expand in Taylor series to find

$$\phi \simeq \dot{G}(t) + O\left(\frac{r^2}{c_\infty^2} \ddot{G}\right), \quad p_s \simeq -\rho_\infty \ddot{G}(t). \quad (17)$$

When measured on the scale of R , the region where these expressions hold is far from the bubble where the near field potential (13) is approximately given by

$$\phi \simeq g(t). \quad (18)$$

The two expressions (17) and (18) are only compatible if $g(t) = \dot{G}(t)$, which determines the unknown function g in terms of the incident wave field G .

At this point we can impose conservation of the normal momentum across the interface:

$$p_B = p_i - \frac{2\sigma}{R} - 4\mu \frac{\dot{R}}{R}, \quad (19)$$

where $p_B \equiv p(R(t), t)$, the liquid pressure at the interface, can be found from the Bernoulli integral (6) and p_i is the bubble internal pressure, discussed in the next section; σ and μ denote the surface tension coefficient and the liquid viscosity. By using the equation of state (7), one can find the value h_B of the enthalpy corresponding to p_B .

Upon evaluating the Bernoulli integral (6) at $r = R(t)$, with the previous results for the near-field potential, we have

$$-\frac{1}{R} \frac{d}{dt} (R^2 \dot{R}) + \ddot{G} + \frac{1}{2} \dot{R}^2 + h_B = 0. \quad (20)$$

In order to reduce this expression to a well-known form it is useful to assume the liquid to be incompressible so that

$$h \simeq \frac{p - p_\infty}{\rho_\infty}. \quad (21)$$

Then, by (17), the previous result becomes

$$R \ddot{R} + \frac{3}{2} \dot{R}^2 = \frac{1}{\rho_\infty} [p_B - (p_\infty + p_s)]. \quad (22)$$

This is of course the Rayleigh-Plesset equation describing the radial motion of a bubble in an incompressible liquid. The manner of its derivation should make clear the meaning of the liquid “ambient pressure” $p_\infty + p_s(t)$ that

appears here: it is the *pressure in the liquid at the location of the bubble neglecting the response of the bubble*. For certain applications it is also useful to rewrite this equation identically in the form of an energy integral:

$$\frac{d}{dt} \left[\frac{1}{2} \left(\frac{4}{3} \pi \rho R^3 \rho_\infty \right) \dot{R}^2 \right] = 4\pi R^2 [p_B - (p_\infty + p_s)]. \quad (23)$$

The term in parentheses in the left-hand side can be identified with the added (or virtual) mass of the bubble.

It should be noted that the previous derivation shows that the Rayleigh-Plesset equation can be obtained from the complete formulation by ignoring terms of order $1/c_\infty$. It may therefore be said that this is an approximation valid to zero order in the Mach number of the liquid. In order to correct the result for the effect of the compressibility of the liquid, we must refine the expression (15) of the far-field potential including the wave radiated by the bubble. We therefore write

$$\phi = \frac{c_\infty}{2r} \left[-G \left(t - \frac{r}{c_\infty} \right) + G \left(t + \frac{r}{c_\infty} \right) \right] - \frac{1}{r} F \left(t - \frac{r}{c_\infty} \right). \quad (24)$$

Proceeding as before, we note that in the near field this reduces to

$$\phi \simeq \dot{G}(t) + \frac{1}{c_\infty} \dot{F}(t) - \frac{1}{r} F(t). \quad (25)$$

Upon comparing with the near-field potential (13) we thus find

$$g(t) = \dot{G}(t) + \frac{1}{c_\infty} F'(t), \quad F(t) = R^2 \dot{R}. \quad (26)$$

When these results are substituted into the Bernoulli integral evaluated at the interface as before, one finds

$$R \ddot{R} + \frac{3}{2} \dot{R}^2 - \frac{1}{c_\infty} \frac{d^2}{dt^2} (R^2 \dot{R}) + \ddot{G} = h_B. \quad (27)$$

This result can be cast in a variety of equivalent forms that have caused a certain confusion in the literature (for a complete discussion see Refs. 4 to 6). The key to the following discussion is the fact that the incompressible Rayleigh-Plesset equation (22) and the equation (27) should be considered asymptotic approximations to a hypothetical “exact” radial equation with errors of order $1/c_\infty$ and $1/c_\infty^2$ respectively. In this connection it is useful to note that the enthalpy can be approximated in a Taylor series as

$$h = \frac{p - p_\infty}{\rho_\infty} \left(1 - \frac{1}{2} \frac{p - p_\infty}{\rho_\infty c_\infty^2} + \dots \right). \quad (28)$$

The use of the incompressible approximation (21) is therefore consistent with the order of accuracy of both the Rayleigh-Plesset equation (22) and the first-order correction (27). We adopt this approximation for the time being, again to bring the results in the form found by earlier investigators.

In the first place, by executing the double time differentiation indicated in (29) and recalling (17), one finds

$$R\ddot{R} + \frac{3}{2}\dot{R}^2 - \frac{1}{c_\infty} \left(R^2 \frac{d\ddot{R}}{dt} + 6R\dot{R}\ddot{R} + 2\dot{R}^3 \right) = \frac{1}{\rho_\infty} [p_B - (p_\infty + p_s)]. \quad (29)$$

The term in parentheses will be recognized as the third time derivative of the bubble volume V divided by 4π . In spite of the presence of the third-order derivative of the radius, in principle this is a perfectly legitimate form of the first compressibility correction to the Rayleigh-Plesset equation. There is, however, a serious practical problem similar to one well known in the Abraham-Lorentz theory of the classical electron (see e.g. Refs. 7 to 10), namely the presence of a highly unstable spurious solution diverging approximately as $\exp c_\infty t/R$. The way to tackle this problem would be to set the initial condition on \ddot{R} so that this spurious solution is not excited. I doubt however that such an approach would be robust enough to withstand the numerical errors inherent in any computation. A more appealing alternative is to use the Rayleigh-Plesset equation (22) to express the $O(1/c_\infty)$ correction. This can be done in different ways as follows. Start by writing

$$\frac{d^2}{dt^2} (R^2 \dot{R}) = \theta \frac{d^2}{dt^2} (R^2 \dot{R}) + (1 - \theta) \frac{d^2}{dt^2} (R^2 \dot{R}), \quad (30)$$

where θ is an arbitrary parameter of order 1. Then use (20) to calculate the first derivative in the right-hand side, and (22) to calculate the third derivative of R arising by expanding the second term in the right-hand side. The result is

$$\begin{aligned} \frac{d^2}{dt^2} (R^2 \dot{R}) &= (1 + \theta) R \dot{R} \ddot{R} + \frac{1}{2} (1 + 3\theta) \dot{R}^3 + (1 - \theta) \dot{R} (h_B + \ddot{G}) \\ &+ R \frac{d}{dt} (h_B + \ddot{G}) + O(c_\infty^{-1}). \end{aligned} \quad (31)$$

This expression can then be used in (29) to find an entire *one-parameter family* of equations that we write omitting the subscript ∞ from ρ and c :

$$\begin{aligned} \left[1 - (\theta + 1) \frac{\dot{R}}{c} \right] R \ddot{R} + \frac{3}{2} \left[1 - \frac{1}{3} (3\theta + 1) \frac{\dot{R}}{c} \right] \dot{R}^2 \\ = \frac{1}{\rho} \left[1 - (\theta - 1) \frac{\dot{R}}{c} + \frac{R}{c} \frac{d}{dt} \right] [p_B - p_\infty - p_s(t)] \\ + O(c^{-2}). \end{aligned} \quad (32)$$

The form obtained from this equation by setting $\theta = 0$ has been given by Keller and co-workers [11,12]; the form corresponding to $\theta = 1$ is instead essentially that found by Herring and Gilmore (see e.g. [13]).

The previous derivation, patterned after the more rigorous one presented in Refs. 4 and 5, clearly shows that there is no unique form of the equation of motion incorporating first-order compressibility effects other than (29) with the third-order derivative.

As the previous derivation shows, the correct form of the equation includes a term proportional to \dot{p}_s in the right-hand side. While the effect of this term is probably small, it has been missed by some researchers who have extended Gilmore's equation simply by analogy. A related point is that, to the same order of accuracy, one may use the relation

$$\left(1 + \frac{R}{c} \frac{d}{dt}\right) p_s(t) \simeq p_s \left(t + \frac{R}{c}\right) \quad (33)$$

in the right-hand side of (32). In Ref. 4 it was also shown numerically that the accuracy of (32) can be significantly enhanced by using h_B in the right-hand side, in place of the expansion (21).

Over the years, many papers have been devoted to the problem of correcting the Rayleigh-Plesset equation for compressibility, even in the last decade during which the situation could have been regarded as clarified [14-17]. A plethora of equations has been proposed. The previous analysis shows that all of them are equivalent if they fall in the class (32), while they are either inconsistent or incorrect otherwise.

2. The gas

A bubble is generally filled with a mixture of vapor and incondensable gases. Once more, therefore, a detailed description of the phenomena taking place in the bubble interior is complex: in addition to the phase change at the bubble surface, one needs to take into account the mutual diffusion among the different gas species, the heat balance at the interface, mass diffusion in the liquid etc. Theories making an attempt to include many of these processes are necessarily complicated [18-20] and only shed limited light on their complex interplay. We again proceed with the help of some approximations.

In the first place, upon integrating the momentum equation in the gas:

$$\frac{\partial}{\partial t}(\rho v) + \frac{\partial}{\partial r}(\rho v^2) = -\frac{\partial p}{\partial r} \quad (34)$$

between two points separated by a distance $\sim R$ we readily find the following estimate for the pressure difference between them:

$$\frac{\Delta p}{p} \simeq O\left(\frac{\dot{R}^2}{c^2}, \frac{\omega R \dot{R}}{c^2}\right) \simeq O\left(\frac{\dot{R}^2}{c^2}, \frac{R}{\lambda} \frac{\dot{R}}{c}\right). \quad (35)$$

In deriving these estimates we have set $p/\rho \sim c^2$, $c/\omega \sim \lambda$. The bubble radius is usually much smaller than the wavelength in the gas. Therefore, whenever the radial velocity is small compared with the speed of sound in the gas, this estimate shows that $p \simeq \text{const}$. In considering the accuracy of this approximation it should be kept in mind that the speed of sound in the gas increases with temperature, and that the radial velocity tends to be large chiefly during the compression phase when the gas temperature is also large.

Another simplification occurs when the density of the vapor is small, so that the liquid temperature drop necessary to keep the bubble full of vapor at the appropriate partial pressure is negligible. In this case most of the liquid surface temperature change is due to the heating and cooling of the gas, and its magnitude can easily be estimated as follows. If the bubble is not too small, most of the drop from the temperature T_C at the bubble center to the value T_S at its surface occurs in a boundary layer with a thickness δ_G of the order of $\sqrt{D_G/\omega}$ where $D_G = k_G/\rho c_{pG}$ is the gas thermal diffusivity expressed in terms of its thermal conductivity k_G and constant-pressure specific heat c_{pG} . The conduction heat flux from the center to the surface is then of the order of

$$q_G \simeq k_G \frac{T_C - T_S}{\delta_G}. \quad (36)$$

A similar argument applies to the liquid, where the drop from the surface temperature to the undisturbed temperature T_∞ occurs in a boundary layer of thickness δ_L analogously defined. Upon equating the two conduction heat fluxes (which, of course, is the proper expression of conservation of energy across the bubble surface) gives

$$\frac{T_S - T_\infty}{T_C - T_S} \simeq \left(\frac{k_G c_{pG} \rho_G}{k_L c_{pL} \rho_L} \right)^{1/2}. \quad (37)$$

The term in the right-hand side is typically of the order of 10^{-3} to 10^{-2} , which implies that the temperature rise of the bubble surface is but a minute fraction of the temperature rise of the gas. Detailed calculations [21] indicate, for example, that the center of a 26 μm -radius argon bubble driven at 21 kHz by a sound field with a pressure amplitude of 0.93 bars

reaches a temperature of the order of 3000 K, while the temperature rise of the surface is about 35 K. Even if the temperature rise of the liquid may be small compared with that of the gas, it must be kept in mind that the saturation vapor density is a rapidly increasing function of the liquid temperature. At very high acoustic pressures, phase change effects may thus become significant during brief fractions of the sound period even though the heating of the liquid is but a small fraction of that of the gas. These statements of course are dependent on the prevailing of the spherical shape of the bubble during the oscillations, a crucial point on which we return below.

The approximation of a spatially uniform gas pressure permits a great simplification of the analysis that has been presented in detail in earlier papers. The reader is referred to those studies for details [18,21-24]. Here we wish to stress another very significant effect of thermal conduction in the bubble uncovered in Ref. 21 namely that, during the fraction of the pressure cycle during which the bubble is in an expanded state, there may be sufficient time for the gas – cooled by the expansion – to heat up again to a temperature close to that of the liquid. Hence the commonly held belief that the adiabatic relation of perfect gases gives an upper bound for the temperature of pulsating bubbles may not always be justified. A true upper bound can be found by assuming an isothermal expansion followed by adiabatic collapse, and this is indeed the route followed by Putterman and co-workers in their recent work on sonoluminescence [25, 26].

In [21] the calculated temperature at the bubble center was used together with a chemical kinetics model to calculate the production of radicals and chemical species in a pulsating argon bubble. The reaction rates were found to be significant and, in particular, a significant amount of hydroxyl radicals and hydrogen peroxide was predicted. These results are compatible with the observation of hydrogen-peroxide-induced reactions and of a hydroxyl spectral line in conventional sonoluminescence experiments [27]. The maximum temperature at the bubble center was found to be around 3000 K, to be compared with the typical value of 5000 K deduced from spectroscopic studies of cavitation [28, 29]. These experiments are typically conducted at a much higher pressure amplitude than the calculations mentioned before which, with the assumption of a spherical bubble, would give far higher temperatures. The discrepancy between this prediction and the measurements indicates that the spherical model is inappropriate at large driving. Most likely, the bubbles break up during the collapse phase and the kinetic energy stored in the liquid is dissipated in the resulting microconvection instead of compressing the gas.

The calculation of the gas pressure in the bubble requires that of the temperature and thus, even within the framework of the approximate model

mentioned before, it is a matter of some complexity. It is therefore interesting to inquire about possible simplified models. Historically the oldest one, which is still widely used, is the so-called polytropic approximation:

$$p = p_0 \left(\frac{R_0}{R} \right)^{3\kappa}, \quad (38)$$

where κ is the polytropic index expected to take values between 1 (isothermal behavior) and γ (adiabatic behavior). This concept was originally introduced in applied thermodynamics to approximate the behavior of systems in which heat transfer is neither negligible nor perfect. Since in thermodynamics time enters only as a parameter with no dynamical significance, the polytropic relation makes no attempt to capture the timing between pressure, temperature, and volume changes, which in some cases can be very important. For example, if (38) is used to calculate the mechanical energy absorbed by the gas in one cycle, the result vanishes because $p dV$ becomes a perfect differential. Energy dissipation due to thermal processes is therefore completely missed by the polytropic relation (38). As another example, for shock waves in bubbly liquids, (38) gives grossly incorrect results, not only quantitatively but even qualitatively [30].

Given the relative crudeness of this approximation, it is somewhat surprising that the radius-time curves calculated with it in connection with the recent work on single-bubble sonoluminescence are supported by the data (see e.g. Refs. [25, 26, 31]). The reason is probably that, at these very large amplitudes of oscillation, the hybrid isothermal-adiabatic model mentioned before is fairly accurate as the bubble lasts very long in its expanded phase, while the collapse is extremely brief. The effect of the internal pressure is of course essential to reverse the motion of the bubble at the end of the collapse, but the entire process lasts a very short time and it is extremely sensitive to the last few instants before the minimum radius. Here, indeed, a difference between prediction and data is probably present (Ref. 25, Fig. 3). This is also the phase of the motion where energy loss by compressibility effects is very strong, which is another aspect poorly resolved by the theory in the extreme conditions of these experiments. As a consequence, it is difficult to pinpoint the cause of the discrepancies between observed and predicted “afterbounces” that, in any event, occur around the equilibrium radius, information about which is correctly contained in (38). The approximation therefore works only because the amplitude of oscillation is very large. Indeed, calculations at smaller amplitudes [23] show big differences between (38) and the more precise theory.

The most convincing experimental confirmation of the formulation described above comes from the study of shock waves in bubbly liquids (see e.g. Refs. 30, 32, 33). For some unknown – and possibly important – reason,

the direct study of levitating bubbles at small to moderate pressure amplitudes gives results with the right trends, but not in precise quantitative agreement with the theory (see e.g. Refs. 34, 35). It is possible that trapping of the bubble in the sound field is in itself responsible for these discrepancies. A hypothesis on the possible underlying mechanism is suggested in section 4 below.

The general theory of thermal processes in the bubble can be simplified in the case of small and large bubbles (with respect to the thermal penetration length in the gas). In the former case, it can be shown that the internal pressure is approximately given by [24]

$$\frac{p}{p_0} \left(\frac{R}{R_0} \right)^3 = 1 - \frac{\gamma - 1}{5\gamma} \frac{R_0^3}{D_G} \frac{\dot{R}}{R^2}. \quad (39)$$

For large bubbles instead a nearly adiabatic behavior prevails and [24, 36, 37]

$$\frac{p}{p_0} \left(\frac{R}{R_0} \right)^{3\gamma} = 1 + \frac{3\gamma}{4\pi} \sqrt{\frac{D_G}{\pi\omega R_0^2}} \int_0^\tau \left[\left(\frac{R}{R_0} \right)^{3(\gamma-1)} (\tau - s) - 1 \right] \frac{ds}{\sqrt{s}}, \quad (40)$$

where the dimensionless time τ is given by

$$\tau(t) = (4\pi)^2 \int_0^t \left(\frac{R}{R_0} \right)^{4-3\gamma} (t') dt'. \quad (41)$$

The result (40) shows that the pressure develops according to its past history, which is expected from a diffusion-dominated process. This form must be used with caution however as the error starts accumulating after a few cycles and spurious results can be found [37].

Some results of a calculation of the gas temperature in the course of non-spherical bubble collapse have recently been reported [38]. The situation considered was that of a gas bubble collapsing near a solid wall under the action of a stepwise increase in the ambient pressure, and is therefore different from that prevailing during acoustic cavitation. Nevertheless, the wall-directed jet has some similarity with the jets that very likely develop in the cavitating bubble and eventually lead to its destruction. Hence, some of the conclusions of this study may be relevant to cavitation, at least in a broad sense. It was found that the heat flux into the jet tip as it progresses through the bubble core reaches, for brief times, extreme values, about 200 MW/m² for a 1 mm-radius bubble subjected to a 10 atm overpressure. The liquid surface temperature was calculated to reach 600 - 700 K. This result is not realistic because no phase change was allowed in the study (recall that the critical temperature of water is 647 K). One may speculate

that violent surface evaporation would occur, capable perhaps of tearing off clusters of molecules from the liquid exposing them to the hot bubble interior. This might be a pathway to the hot bubble interior for substances with negligible vapor pressure dissolved in the liquid.

3. Spherical stability

There are two agents – one static and one dynamic – that tend to promote sphericity of a bubble but many more that, on the contrary, tend to destroy it. A spherical bubble should therefore be considered more the exception than the rule.

The static agent is surface tension that induces, across the interface, a pressure jump given by

$$p_i - p_B + \tau_v = \sigma \mathcal{C}, \quad (42)$$

where τ_v represents the normal viscous stresses on the liquid side of the interface and \mathcal{C} the local curvature. For a spherical bubble in radial motion this relation reduces to (19). Since, as was argued before, the gas pressure is uniform to a close approximation, any variation of the liquid pressure or of the normal viscous stresses must be balanced by a variation of the curvature which, evidently, implies a loss of sphericity. To appreciate the weakness of surface tension it is useful to compare it with the hydrostatic pressure difference across the bubble diameter, $2R\rho g$. The two are of equal magnitude for

$$R = \sqrt{\frac{\sigma}{\rho g}}, \quad (43)$$

which is about 2.7 mm for water. In other words, a column of water with a height of a few mm is sufficient to cause an appreciable deformation of the bubble. Only bubbles with a radius much smaller than the value given by this formula can remain nearly spherical at normal gravity. If the surface tension overpressure corresponding to the radius (43) is converted to a stagnation pressure, the corresponding velocity is about 0.3 m/sec, which happens to be quite close to the terminal velocity of mm-size bubbles. This is of course the origin of the flattening of rising bubbles in a quiescent liquid as soon as their size approaches 1 mm. For a bubble moving 5 times as fast (not an unrealistic velocity for bubbles in a large-amplitude sound field, see e.g. Ref. 39), the bubble radius has to be much smaller than 100 μm for surface tension to be able to counter the deformation induced by the motion.

The dynamic effect tending to restore sphericity is conservation of momentum. The momentum (or, more precisely, the impulse) of the motion associated with one spatial period of a standing wave on the surface of

the bubble varies in proportion to the virtual mass of the mode, which is itself proportional to R^3 , as immediately follows from dimensional arguments. In the absence of forces this momentum must be conserved, which implies that the surface velocity is inversely proportional to R^3 . Mathematically, this conclusion follows from the well-known equation governing the amplitude a_n of a single spherical harmonic deformation in the linear approximation [40]:

$$\ddot{a}_n + 3 \frac{\dot{R}}{R} \dot{a}_n + (n-1) \left[-\frac{\ddot{R}}{R} + (n+1)(n+2) \frac{\sigma}{\rho R^3} \right] a_n = 0. \quad (44)$$

The coefficient of the \dot{a}_n is positive when the bubble expands, and therefore qualitatively the effect is that of a damping action, as suggested by the previous argument. The equation can be identically rewritten as

$$\frac{d}{dt} \left(R^3 \dot{a}_n \right) + (n-1) \left[-R^2 \ddot{R} + (n+1)(n+2) \frac{\sigma}{\rho} \right] a_n = 0, \quad (45)$$

from which indeed one sees that, when the radial acceleration and surface tension are negligible, $\dot{a}_n \propto R^{-3}$. The rate of growth of the disturbance therefore rapidly decays as the bubble expands. The role played by geometry in establishing this result is confirmed by the corresponding equation for a cylindrical bubble, which is

$$\ddot{a}_n + 2 \frac{\dot{R}}{R} \dot{a}_n + (n-1) \left[-\frac{\ddot{R}}{R} + n(n+1) \frac{\sigma}{\rho R^3} \right] a_n = 0, \quad (46)$$

so that $\dot{a}_n \propto R^{-2}$ in this case.

From (45) one sees that the result $R^3 \dot{a}_n = \text{constant}$ is exact for $n = 1$, which corresponds to translation of the bubble with velocity $U = \dot{a}_1$. Restoring some constants, we thus find the well-known statement of the conservation of the impulse I of the liquid-bubble system:

$$I = \frac{2}{3} \pi R^3 \rho U, \quad (47)$$

expressed as the product of U with the added mass of a translating sphere. It should be expressly noted that, in the absence of external forces such as buoyancy, I is conserved not only for small a_1 , but actually for translations of arbitrary magnitude of a sphere with a constant or variable radius. In particular, for the latter case, we have

$$U = \left(\frac{R_0}{R} \right)^3 U_0, \quad (48)$$

where the index 0 denotes initial values. This relation implies that U tends to grow as $R \rightarrow 0$. The physical mechanism that counteracts this singularity may have important consequences as will be discussed below.

Another point worth noting in this connection has to do with the coupling between spherical distortions and the translatory motion of the bubble. Due to the complexity of the problem, only incomplete results (recently reviewed in Ref. 41) are available, and these are restricted to somewhat idealized situations. Nevertheless it is clear not only that translation induces surface deformation but also that, conversely, surface deformations can induce translation [42 - 44]. Again, the point here is the extreme fragility of the sphericity of a bubble, particularly in those situations of violent motion where it is least observable. The appearance of surface deformations is therefore not only dependent on an intrinsic instability as described by (44) but, due to mechanisms not included in this equation – chiefly translation, but possibly also volume-shape resonance [45] – is likely even in situations in which (44) predicts stability.

Once surface modes – for whatever reason – appear, (44) approximately describes their interaction with the radial motion and therefore plays a central role in their subsequent development. It has become customary in the literature (see e.g. Ref. 46) to refer to a parametric and a Rayleigh-Taylor instability, both described by Eq. (44). The former is the modulated growth of the disturbance over several cycles of the radial motion. The latter is a more violent growth during times in which the radial acceleration is positive and large i.e., typically, near the point of minimum volume of the bubble. In a certain sense this distinction is artificial as the instability is, in all cases, essentially due to the \ddot{R} term in (44).

For wavelengths short compared to the radius, it is possible to show that the stability equation (44) becomes identical to that of the usual plane Rayleigh-Taylor instability for waves of amplitude a and wavenumber $k \simeq n/R$:

$$\ddot{a} - \left(k\ddot{R} - \frac{\sigma}{\rho}k^3 \right) a = 0. \quad (49)$$

For constant \ddot{R} , the fastest growing mode corresponds to $k = \sqrt{\rho\ddot{R}/3\sigma}$ with a growth rate given by $(4\rho\ddot{R}^3/27\sigma)^{1/4}$. With accelerations of the order of $10^{11}g$ quoted in some work on sonoluminescence (see e.g. Ref. 47), this formula gives a characteristic time for the growth of the instability of the order of 100 psec. The corresponding wavenumber is of the order of 10^6 cm^{-1} which, for $R \sim 1 \mu\text{m}$, suggests that the dominant instability is that of a low-order mode. While there are many reasons why these results cannot be taken literally, one would expect the general orders of magnitude indicated to be representative.

4. Bubble levitation

The total force exerted by a fluid on a body is the integral of the fluid stress over the body surface S . If viscous effects are unimportant, as often happens near a free surface (see e.g. Ref. 3, p. 364), it is only necessary to consider pressure forces and the fluid-dynamic force on the body is

$$\mathbf{F} = - \oint p \mathbf{n} dS \quad (50)$$

where unit normal \mathbf{n} is directed out of the body. In the special case of a spherical bubble pulsating in an external sound field, the pressure has a component p_s due to the driving, and one due to the pressure radiated by the bubble. Pressures much smaller than the scale B appearing in Tait's equation of state (4) combine linearly and therefore the two contributions to the integral can be considered separately. The wave radiated by the bubble is spherically symmetric, and therefore its contribution to the integral vanishes. In common applications the wavelength of the sound is much greater than the bubble radius, so that a two-term Taylor series expansion is adequate to represent the integrand over the bubble surface. By using the divergence theorem, it is therefore immediate to find from (50)

$$\mathbf{F} = -V \nabla p_s + O\left(\frac{R}{\lambda}\right)^2, \quad (51)$$

where V is the volume of the bubble and the sound pressure gradient is evaluated at a point actually inside the bubble, e.g. at its center. This quantity should be interpreted as the pressure at the position of the bubble if the bubble were not there.

Upon balancing buoyancy and the pressure force with the effect of added mass and drag, one may write the following approximate equation of motion for a spherical bubble:

$$\frac{d}{dt} \left(\frac{2}{3} \rho R^3 \mathbf{U} \right) = -V \nabla p_s(\mathbf{Z}, t) - V \rho \mathbf{g} - D \mathbf{U}. \quad (52)$$

Here $\mathbf{Z}(t)$ is the position of the bubble center, $\mathbf{U} = \dot{\mathbf{Z}}$, D is a constant representing drag forces, and \mathbf{g} is the acceleration of gravity. The very small liquid velocity due to the sound wave has been disregarded in this equation. Strictly speaking, all the terms in this equation, including buoyancy, derive from the integral of the liquid stress over the bubble surface; the present derivation of the force due to the sound field therefore may be fast, but also somewhat "dirty"! The equation is, nevertheless, correct with the possible exception of drag effects.

For steady conditions, upon averaging over a sound cycle and neglecting viscosity, the previous equation gives

$$-\langle V \nabla p_s \rangle = \rho g \langle V \rangle . \quad (53)$$

If this equation is satisfied (which, among others, implies that the pressure gradient is parallel to gravity), the bubble will execute an up-down translatory motion around a mean position of equilibrium. This is the mechanism of acoustic levitation widely used in experiments on bubbles and, in particular, in the recent work on sonoluminescence. Although this translatory motion may have a small amplitude, and therefore be difficult to detect by the naked eye, it is nevertheless present and causes surface deformations of the bubble that – unlike deformations due to instability – are quite deterministic and reproducible.

It was already mentioned before that a translating bubble tends to flatten in the direction normal to its velocity as a consequence of the Bernoulli effect. If, in addition to translating, the bubble is also collapsing, there is another effect that can be understood as follows. Suppose the velocity of collapse is equal to that of translation. Then the front stagnation point of the bubble will not move and the pressure there will be the same as the ambient pressure. On the other hand, the bubble is still translating and the liquid that streams past it comes to rest at the rear stagnation point where the pressure is therefore higher. This state of affairs is obviously in conflict with the requirement of constancy of the pressure in the bubble and leads to the development of a jet of liquid directed from the rear toward the front stagnation point. If the collapse proceeds long enough, this jet will eventually reach the front stagnation point thus rendering the space occupied by the gas doubly connected. Since, at the moment at which the two opposing liquid surfaces touch, they carry different values of the velocity potential, circulation is set up in the doubly connected liquid and a toroidal vortex forms around a gaseous core. This process resolves the paradox mentioned before in connection with (48) that, in order to conserve the system's impulse, the translational velocity of the bubble would have to become infinite if its volume were to shrink to zero. The initial impulse of the translating bubble is transformed into the impulse of the vortex ring. Support for this scenario is provided by the beautiful experiments and elegant theory given in Benjamin and Ellis's 1966 paper [48]. More recently, Blake and co-workers have used the notion of impulse to derive in a simple fashion several results on bubble jetting (see e.g. Refs. 49, 50).

If, instead of translating in an unidirectional fashion as in the previous argument, the bubble executes translational oscillations (e.g. due to acoustic levitation), the degree of penetration of the jet into the bubble during the collapse half-cycle will of course depend on several factors including the

bubble size and pressure amplitude. It has been proposed that this process may play an important role in single-bubble sonoluminescence [51].

It goes without saying that the previous derivation of the expression Eq. (51) for the acoustic radiation force is also applicable to the case in which the pressure field in which the bubble is immersed is caused by the pulsations of another neighboring bubble. The mean attractive or repulsive force between the bubbles that arises in these conditions is the well-known secondary Bjerknes force.

5. Sonoluminescence

Sonoluminescence has attracted considerable attention in the past few years. While an explanation of the phenomenon is still unavailable, the recent observation of light emission by bubbles attached to [52] or near [53] a solid boundary – which cannot possibly be spherical – has at least served to lay to rest some extravagant theories critically dependent on sphericity. It may be hoped that energies can now be channeled in more productive and physically plausible directions.

One essential aspect of the phenomenon – that has become clear only relatively recently – is that there are two kinds of sonoluminescence that, for lack of better terminology, are referred to as single-bubble and multi-bubble sonoluminescence. The former type is the one that has recently attracted the greatest attention after its discovery by Gaitan and Crum [54,55] and is characterized by a continuous spectrum with no discernible spectral lines. The other type was discovered in the 30's and exhibits a spectrum with many spectral lines dependent on the liquid and gases present in the cavitation cell. The relation between the two types is unclear. While the single-bubble variety can be observed by itself, it is probable that in the other type the same mechanism responsible for single-bubble luminescence coexists with a different one – perhaps thermal – responsible for the spectral lines. There is also the possibility that the lines are – at least in part – a by-product of the same mechanism responsible for the other type of emission.

The fact that the essential difference between the two types of sonoluminescence is a recent discovery makes the interpretation of earlier experiments ambiguous. Nevertheless if, alongside the multi-bubble mechanism, the single-bubble process is a significant component of the light emission, some of the observations reported by these investigators may have a bearing on the latter. In an early study, Chambers [56] observed that the light emission from several liquids (with the notable exception of water) correlated with the product of the viscosity and the molecular electric dipole moment. From this fact he deduced that light emission was due to the “frac-

ture" of the liquid when a bubble was created. At the time this hypothesis was justifiable as the crucial role of impurities in determining the heterogeneous nucleation of bubbles had not yet been established. When this fact was clarified, and it was proven that light emission correlated with bubble collapse rather than growth, Chambers's hypothesis was quickly forgotten but, with it, out went his observation of a correlation with liquid properties. Nevertheless, there is no reason to discard this fact even if, as Jarman pointed out, Chambers's liquids belonged to a particular homologous series of alcohols. A possible physical interpretation is that sonoluminescence is favored by a large dipole moment that cannot readily reorient itself in the presence of strong viscous effects.

Another indication that the liquid structure may be important is given by the difference between single-bubble light emission from normal and heavy water [57], as the two liquids have extremely similar physical properties and only differ significantly in the liquid structure.

A third, possibly related observation is due to Flint and Suslick [58] who found that, while the intensity of the emission was dependent on factors expected to affect the bubble temperature, "the observed line width and peak position [were] independent of cavitation conditions." From this they concluded that the light emission occurred from atoms in the liquid phase and postulated that the mechanism consists of energetic radicals that form in the bubble and migrate to the liquid surface where they excite the alkali atoms. This hypothesis could perhaps be tested by a precise measurement of the time interval between the instants at which a pressure pulse and light are emitted by a collapsing bubble, since presumably the diffusion of radicals from the hot core to the surface would take some time. Interestingly, from the width of the potassium lines, the authors estimate a local density of the surrounding matter of the order of 1.5 g/cm^3 . Upon using this value in the Tait equation (4) for water, one finds a corresponding pressure of the order of 50,000 bars. This result is very crude and highly sensitive to the density estimation but, if indeed light emission occurs in the liquid phase, the liquid must be under extremely high pressures at that moment. In the previously quoted pressure value is converted to a stagnation pressure, the corresponding velocity would be about 3,000 m/sec, i.e. about twice the speed of sound in water.

These observations seem to point to a role of the liquid structure, as distinct from composition and physical properties in the emission of light. A mechanism in which structure would be a factor has been suggested in a recent paper [51]. The hypothesis is that the levitated bubble deforms non-spherically, as suggested before, with a high-speed jet striking the opposite side. Due to the time scale of the impact, the liquid does not have time to flow and cracks emitting light according to the well-known – if not

understood – process of fractoluminescence (see e.g. Refs. 59 to 61).

In conclusion, I would like to mention some other observations that do not seem to have made their way into the current literature on sonoluminescence, namely the fact that luminescence can be observed in flow cavitation. The first report of this fact, by Konstantinov, dates from 1947 (cited in Refs. 62 and 63). Extensive observations were later reported by Peterson and Anderson [64] and, more recently, by van der Meulen [65]. Peterson and Anderson's observations match in several respects features of single-bubble sonoluminescence. The presence of small amounts of xenon in water substantially increased the light output, which was instead decreased by a temperature increase. The rise time of the light flash was of the order of hundreds of psec (note that these bubbles were much larger than the acoustic cavitation ones), and the spectrum continuous, if somewhat different from those recently reported. In flow cavitation collapsing bubbles are essentially never spherical. The mere fact that luminescence is observed in these conditions therefore concurs with the recent observation mentioned at the beginning of this section in disproving the role of any mechanism relying on bubble sphericity.

6. Conclusions

Bubble dynamics is a complex field. While much progress has been made in both theory and experiment, our understanding remains limited, particularly in the conditions of large-amplitude motion and high pressures that are the most interesting scientifically and technologically. Even computational tools are insufficient to deal with this regime due to a variety of difficulties – free surfaces, compressibility, numerical stability, and mathematical modelling, for example of liquid-liquid contact – that stretch current resources and knowledge.

In the light of these limitations, the subject has been plagued by a history of crude modeling and unjustifiable extrapolations. Unfortunately, given that the bubble is essentially a singularity, it is extremely easy to generate astounding results that are only an amplification of incorrect hypotheses. In this case, the famous dictum “garbage in, garbage out” should be modified by a large amplification factor in front of the output. An amusing example is the “rocket effect”, proposed in the early 70's, based on an extrapolation to $R \rightarrow 0$ in Eq. (48) with the bubble – of course! – remaining spherical. More recent examples can also be quoted.

It is my impression that the community would be well served by a skeptical view of the notion of sphericity. This seems to be another instance to which S.J. Gould's famous quote is applicable: “Often the greatest obstacle to scientific progress is conceptual lock, rather than factual lack.” If this

“paradigmatic shift” moves cavitation studies out of Acoustics and into the neighboring field of Fluid Mechanics, so be it. We will learn more and have more fun in the process.

Acknowledgments

This chapter is based in part on work with several students and colleagues (who appear as co-authors in my papers cited in the references) to all of whom I would like to express my gratitude.

Past and present financial support by NSF, ONR, AFOSR, and NASA is also gratefully acknowledged.

References

1. Landau, L.D. and Lifshitz, E.M. (1959) *Fluid Mechanics*, Pergamon.
2. Cole, R.H. (1948) *Underwater explosions*, Princeton U.P., Princeton. Reprinted by Dover, 1965.
3. Batchelor, G.K. (1967) An Introduction to Fluid Dynamics, Cambridge U.P., Cambridge.
4. Prosperetti, A. and Lezzi, A. (1986) Bubble dynamics in a compressible liquid. Part 1. First-order theory, *J. Fluid Mech.* **168**, 457-478.
5. Lezzi, A. and Prosperetti, A. (1987) Bubble dynamics in a compressible liquid. Part 2. Second-order theory, *J. Fluid Mech.* **185**, 289-321.
6. Prosperetti, A. (1987) The equation of bubble dynamics in a compressible liquid, *Phys. Fluids* **30**, 3626-3628.
7. Rohrlich, F. (1965) *Classical Charged Particles*, Addison-Wesley, Reading.
8. Burke, W.L. (1970) Runaway solutions: remarks on the asymptotic theory of radiation damping, *Phys. Rev. A* **2**, 1501-1505.
9. Jackson, J.D. (1975) *Classical Electrodynamics*, 2nd Ed., Wiley, New York.
10. Prosperetti, A. (1980) The motion of a charged particle in a uniform magnetic field, *Nuovo Cimento* **57B**, 253-268.
11. Keller, J.B. and Kolodner, I.I. (1956) Damping of underwater explosion bubble oscillations, *J. Appl. Phys.* **27**, 1152-1161.
12. Keller, J.B. and Miksis, M.J. (1980) Bubble oscillations of large amplitude, *J. Acoust. Soc. Am.* **68**, 628-633.
13. Trilling, L. (1952) The collapse and rebound of a gas bubble, *J. Appl. Phys.* **23**, 14-17.
14. Pollman, U. (1989) Extension of the improved Gilmore equation of Lastman and Wentzell for a vapor bubble with respect to the mass-transfer at the bubble-wall, *Acustica* **68**, 241-250.
15. Aymé-Bellgarda, E.J. (1990) Collapse and rebound of a gas-filled spherical bubble immersed in a diagnostic sound field, *J. Acoust. Soc. Am.* **88**, 1054-1060.
16. Barbone, P.E., Nadim, A., and Goldman, D. (1994) Compressibility in bubble dynamics and scattering, *J. Acoust. Soc. Am.* **96**, 3253.
17. Moss, W.C. (1997) Understanding the periodic driving pressure in the Rayleigh-Plesset equation, *J. Acoust. Soc. Am.* **101**, 1187-1190.
18. Nigmatulin, R.I., Khabeev, N.S., and Nagiev, F.B. (1981) Dynamics, heat, and mass transfer of vapour-gas bubbles in a liquid, *Int. J. Heat Mass Transfer* **24**, 1033-1044.
19. Fanelli, M., Prosperetti, A., and Reali, M. (1981) Radial oscillations of gas-vapor bubbles in liquids. Part I. Mathematical formulation, *Acustica* **47**, 253-265.
20. Fanelli, M., Prosperetti, A., and Reali, M. (1981) Radial oscillations of gas-vapor bubbles in liquids. Part II. Numerical examples, *Acustica* **49**, 98-109.
21. Kamath, V., Prosperetti, A., and Egolfopoulos, F. (1993) A theoretical study of sonoluminescence, *J. Acoust. Soc. Am.* **93**, 248-260.
22. Nigmatulin, R.I. and Khabeev, N.S. (1974) Heat exchange between a gas bubble and a liquid, *Fluid Dyn.* **9**, 759-764.
23. Prosperetti, A., Crum, L.A., and Commander, K.W. (1988) Nonlinear bubble dynamics, *J. Acoust. Soc. Am.* **83**, 502-514.
24. Prosperetti, A. (1991) The thermal behaviour of oscillating gas bubbles, *J. Fluid Mech.* **222**, 587-616.
25. Löfstedt, R., Barber, B.P., and Puttermann, S.J. (1993) Toward a hydrodynamic theory of sonoluminescence, *Phys. Fluids* **A5**, 2911-2928.
26. Barber, B.P., Hiller, R.A., Löfstedt, R., Puttermann, S.J. and Weninger, K.R. (1997) Defining the unknowns of sonoluminescence, *Phys. Rep.* **281**, 66-143.
27. Verrall, R.E. and Sehgal, C.M. (1988) Sonoluminescence, in Suslick, K.S. (ed.), *Ultrasound: its Chemical, Physical, and Biological Effects*, VCH, New York, pp. 227-286.

28. Suslick, K.S. (1990) Sonochemistry, *Science* **247**, 1439–1445.
29. Flint, E.B. and Suslick, K.S. (1991) The temperature of cavitation, *Science* **253**, 1397–1399.
30. Watanabe, M. and Prosperetti, A. (1994) Shock waves in dilute bubbly liquids, *J. Fluid Mech.* **274**, 349–381.
31. Löfstedt, R., Weninger, K., Puttermann, S., and Barber, B.P. (1995) Sonoluminescing bubbles and mass diffusion, *Phys. Rev. E* **51**, 4400–4410.
32. Kameda, M. and Matsumoto, Y. (1996) Shock waves in a liquid containing small gas bubbles, *Phys. Fluids* **8**, 322–335.
33. Kameda, M., Shimaura, N., Higashino, F., and Matsumoto, Y. (1997) Shock waves in a uniform bubbly flow, *Phys. Fluids*, submitted.
34. Crum, L.A. and Prosperetti, A. (1983) Erratum and comments on “Nonlinear oscillations of gas bubbles in liquids: An interpretation of some experimental results”, *J. Acoust. Soc. Am.* **75**, 1910–1912.
35. Holt, R.G. and Crum, L.A. (1992) Acoustically forced oscillations of air bubbles in water: Experimental results, *J. Acoust. Soc. Am.* **91**, 1924–1932.
36. Miksis, M.J. and Ting, L. (1984) Nonlinear radial oscillations of a gas bubble including thermal effects, *J. Acoust. Soc. Am.* **76**, 897–905; Miksis, M.J. and Ting, L. (1987) A numerical study of thermal effects on nonlinear bubble oscillations, *J. Acoust. Soc. Am.* **81**, 1331–1340.
37. Kamath, V., Oğuz, H.N., and Prosperetti, A. (1992) Bubble oscillations in the nearly adiabatic limit, *J. Acoust. Soc. Am.* **92**, 2016–2023.
38. Yuan, H. and Prosperetti, A. (1997) Gas-liquid heat transfer in a bubble collapsing near a wall, *Phys. Fluids* **9**, 127–142.
39. Crum, L.A. and Nordling, D.A. (1972) Velocity of transient cavities in an acoustic stationary wave, *J. Acoust. Soc. Am.* **52**, 294–301.
40. Plesset, M.S. (1954) On the stability of fluid flows with spherical symmetry, *J. Appl. Phys.* **25**, 96–98.
41. Feng, Z.C. and Leal, L.G. (1997) Nonlinear bubble dynamics, *Ann. Rev. Fluid Mech.* **29**, 201–243.
42. Strasberg, M. and Benjamin, T.B. (1958) Excitation of oscillations in the shape of pulsating bubbles - experimental work, *J. Acoust. Soc. Am.* **30**, 697.
43. Eller, A.I. Crum, L.A. (1970) Instability of the motion of a pulsating bubble in a sound field, *J. Acoust. Soc. Am.* **47**, 762–767.
44. Benjamin, T.B. and Ellis, A.T. (1990) Self-propulsion of asymmetrically vibrating bubbles, *J. Fluid Mech.* **212**, 65–80.
45. Longuet-Higgins, M.S. (1989) Monopole emission of sound by asymmetric bubble oscillations. part i. normal modes, *J. Fluid Mech.* **201**, 543–565.
46. Brenner, M.P., Lohse, D., and Dupont, T.F. (1995) Bubble shape oscillations and the onset of sonoluminescence, *Phys. Rev. Lett.* **75**, 954–957.
47. Weninger, K.R., Barber, B.P., and Puttermann, S.J. (1997) Pulsed Mie scattering measurements of the collapse of a sonoluminescing bubble, *Phys. Rev. Lett.* **78**, 1799–1802.
48. Benjamin, T.B. and Ellis, A.T. (1966) The collapse of cavitation bubbles and the pressures thereby produced against solid boundaries, *Philos. Trans. R. Soc. London A* **260**, 221–240.
49. Blake, J.R. and Gibson, D.C. (1987) Cavitation bubbles near boundaries, *Ann. Rev. Fluid Mech.* **19**, 99–123.
50. Best, J.P. and Blake, J.R. (1994) An estimate of the Kelvin impulse of a transient cavity, *J. Fluid Mech.* **261**, 75–93.
51. Prosperetti, A. (1997) A new mechanism for sonoluminescence, *J. Acoust. Soc. Am.* **101**, 2003–2007.
52. Weninger, K.R., Barber, B.P., and Puttermann, S.J. (1997), UCLA preprint.
53. Ohl, C.D. and Lindau, O. and Lauterborn, W. (1997) Luminescence from spherically

- and aspherically collapsing laser-induced bubbles, University of Göttingen preprint.
- 54. Gaitan, D.F. and Crum, L.A. (1990) Observation of sonoluminescence from a single, stable cavitation bubble in a water/glycerine mixture, in Hamilton, M. & Blackstock, D.T. (eds.), *Frontiers in Nonlinear Acoustics*, New York, Elsevier, pp. 459–463.
 - 55. Gaitan, D.F., Crum, L.A., Church, C.C., and Roy, R.A. (1992) Sonoluminescence and bubble dynamics from a single, stable, cavitation bubble, *J. Acoust. Soc. Am.* **91**, 3166–3183.
 - 56. Chambers, L.A. (1937) The emission of visible light from cavitated liquids, *J. Chem. Phys.* **5**, 290–292.
 - 57. Hiller, R.A. and Puttermann, S.J. (1995) Observation of isotope effects in sonoluminescence, *Phys. Rev. Lett.* **75**, 3549–3551. Erratum ibid., vol. 77, p. 2345, 1996.
 - 58. Flint, E.B. and Suslick, K.S. (1991) Sonoluminescence from alkali-metal salt solutions, *J. Phys. Chem.* **95**, 1484–1488.
 - 59. Walton, A.J. (1977) Triboluminescence, *Adv. Phys.* **26**, 887–948.
 - 60. Chapman, G.N. and Walton, A.J. (1983) Triboluminescence of glasses and quartz, *J. Appl. Phys.* **54**, 5961–5965.
 - 61. Sweeting, L.M., Rheingold, A.L., Gingerich, J.M., Rutter, A.W., Spence, R.A., Cox, C.D., and Kim, T.J. (1997) Crystal structure and triboluminescence 2. 9-Anthracenecarboxylic acid and its ethers, *Chem. Mater.* **9**, 1103–1115.
 - 62. Jarman, P. (1960) Sonoluminescence: A discussion, *J. Acoust. Soc. Am.* **32**, 1459–1462.
 - 63. Finch, R.D. (1963) Sonoluminescence, *Ultrasonics April-June*, 87–98.
 - 64. Peterson, F.B. and Anderson, T.P. (1967) Light emission from hydrodynamic cavitation, *Phys. Fluids* **10**, 874–879.
 - 65. van der Meulen, J.H.J. (1985) The relation between noise and luminescence from cavitation on a hydrofoil, in *Proceedings of the ASME Symposium on Cavitation in Hydraulic Structures and Turbomachinery* A.S.M.E., New York, 149–159.

NONLINEAR BUBBLE DYNAMICS

Response Curves and More

W. LAUTERBORN AND R. METTIN

Drittes Physikalisches Institut

Bürgerstr. 42-44, D-37073 Göttingen

Germany

1. Introduction

A spherical bubble in a liquid can be viewed as a nonlinear oscillator that can be set into radial oscillations by a sound field. At larger oscillation amplitudes this oscillation must become nonlinear because the bubble can be elongated from its equilibrium radius to arbitrarily large radius values, but can be compressed only down to near zero radius. Bubbles of different radius at rest R_n respond differently to the same sound field. This study reports on numerical investigations of this response for bubbles of $1 \mu\text{m} \leq R_n \leq 500 \mu\text{m}$ for sound field frequencies in the near ultrasonic range and sound pressure amplitudes up to 150 kPa. Special attention is paid to the giant resonance at small radii [1].

2. The Bubble model

In the course of time several mathematical models of different sophistication for the oscillation of a spherical bubble in a liquid have been developed. Here we use the Gilmore model [2] that incorporates sound radiation into the liquid augmented by a van der Waals hard core [3] to account for a noncompressible volume of the gas inside the bubble. The bubble model reads:

$$\left(1 - \frac{\dot{R}}{C}\right) R \ddot{R} + \frac{3}{2} \left(1 - \frac{\dot{R}}{3C}\right) \dot{R}^2 = \left(1 + \frac{\dot{R}}{C}\right) H + \frac{\dot{R}}{C} \left(1 - \frac{\dot{R}}{C}\right) R \frac{dH}{dR} \quad (1)$$

$$H = \int_{p|_{r \rightarrow \infty}}^{p|_{r=R}} \frac{dp(\rho)}{\rho} \quad (2)$$

$$p(\rho) = A \left(\frac{\rho}{\rho_0} \right)^n - B \quad (3)$$

$$p|_{r=R} = \left(p_{stat} + \frac{2\sigma}{R_n} \right) \left(\frac{R_n^3 - bR_n^3}{R^3 - bR_n^3} \right)^\kappa - \frac{2\sigma}{R} - \frac{4\mu}{R} \dot{R} \quad (4)$$

$$p|_{r \rightarrow \infty} = p_{stat} + p(t) \quad (5)$$

$$C = \sqrt{c_0^2 + (n-1)H} \quad (6)$$

where the variables and constants appearing in the equation have the following meaning: R is the bubble radius, R_n is the bubble radius at rest, an overdot means differentiation with respect to time, ρ is the liquid density, ρ_0 is the liquid density at normal conditions (998 kg/m^3), p is the pressure in the liquid, $\sigma =$ surface tension (0.0725 N/m for water), μ is the viscosity of the liquid (0.001 Ns/m^2 for water), c_0 is the sound velocity in the liquid at normal conditions (1500 m/s), C is the sound velocity in the liquid at the wall of the bubble, p_{stat} is the static ambient pressure (100 kPa), κ is the polytropic exponent (chosen as $5/3$ for a monoatomic gas), b is the van der Waals constant (taken as 0.0016 to model some artificial gas), A of the Tait equation (3) is 300.1 MPa , B is 300.0 MPa , n is 7 . This set of equations is solved for a sinusoidal sound field $p(t) = \hat{p}_a \sin 2\pi\nu t$ with $\nu = 20 \text{ kHz}$ for several sound pressure amplitudes \hat{p}_a up to 150 kPa . At 150 kPa a comparison of bubble response is done for several driving frequencies.

3. Response Curves at Low Driving

When bubbles of different sizes are subject to only a very small acoustic pressure amplitude, they will respond with small oscillations about their equilibrium radius. Going up in the driving amplitude will bring out the effects of nonlinearity manifesting themselves in the occurrence of several resonances. Figure 1 shows this regime that for a driving frequency of 20 kHz reaches up to a sound pressure amplitude of 70 kPa . The resonances can be labeled with two numbers [4]. Two sets of resonances are to be seen. The large peaks that fall off towards lower radii, labeled with a ‘1’ in the denominator, and the smaller ones in between, labeled with a ‘2’ in the denominator. The first set constitutes the main resonance (resonance of order $1/1$) and the harmonic resonances of order $n/1$ with $n = 2, 3, \dots$. The second set belongs to the set of subharmonic resonances, starting with the main subharmonic resonance, $1/2$, to the right of the main resonance, and going on with the $3/2, 5/2, 7/2$ resonances (also called ultrasubharmonic resonances), where the last two resonances in Fig. 1 only occur with a driving pressure amplitude of 70 kPa . There appear straight vertical dotted lines in the diagram. At these radii the steady state oscillation behaves nonmonotonously with the bubble radius at rest. The reason is the over-

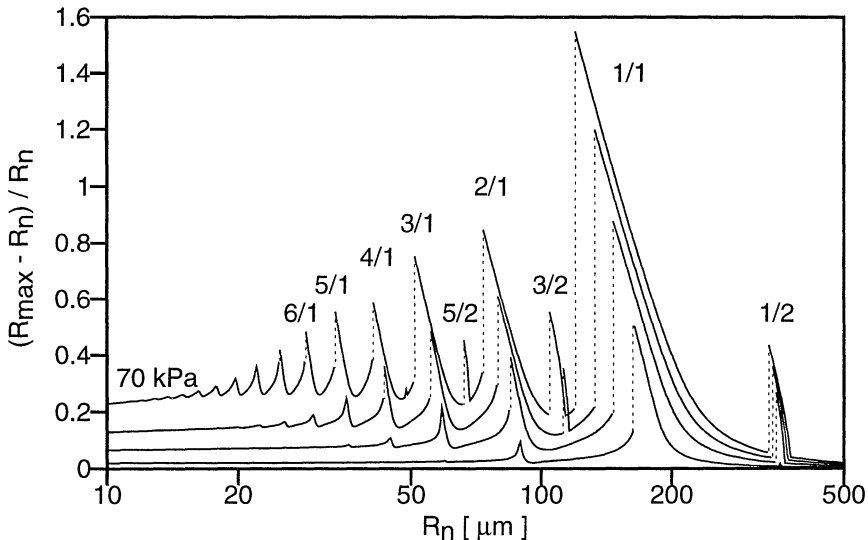


Figure 1. Resonance curves for bubbles of different sizes subject to a fixed frequency of 20 kHz. Driving amplitudes are 10 (bottom curve), 30, 50 and 70 kPa (upper curve). Initial condition is the respective bubble at rest.

turning of the resonances leading to a small or a large amplitude oscillation depending on the initial condition chosen. In the language of nonlinear dynamical systems theory [5] there are two coexisting attractors. They span a region of hysteresis made up of the region where both attractors are stable. Each of the attractors then has a set of initial conditions leading to them: their basin of attraction. The diagram was calculated with the respective bubble starting from its rest position ($R = R_n, \dot{R} = 0$). Then just one attractor will be reached and the jump occurs when the boundary between the two basins of attraction sweeps over the rest position.

In Fig. 2, for $\hat{p}_a = 80$ kPa, two attractors are obtained in hysteresis regions by the following computing technique. The curve is started at a small bubble radius at rest R_n (here 10 μm) and increased in small steps (here 600 steps) to a final R_n (here 200 μm), whereby the initial condition at the next R_n is taken from the final condition at the previous R_n . That way an attractor can be followed until its basin shrinks to zero or is destroyed otherwise. Subsequently the same procedure is repeated, but going backwards, i. e. decreasing R_n with the last final condition again being the new initial condition. We see that the high amplitude oscillation of the main resonance leans over to lower bubble radii so strongly that it does not stop until beyond the 3/2 ultrasubharmonic resonance. Similarly the 2/1 harmonic resonance shadows the 5/2 resonance and so forth, in the case of the 80 kPa curve up to the 9/2 resonance.

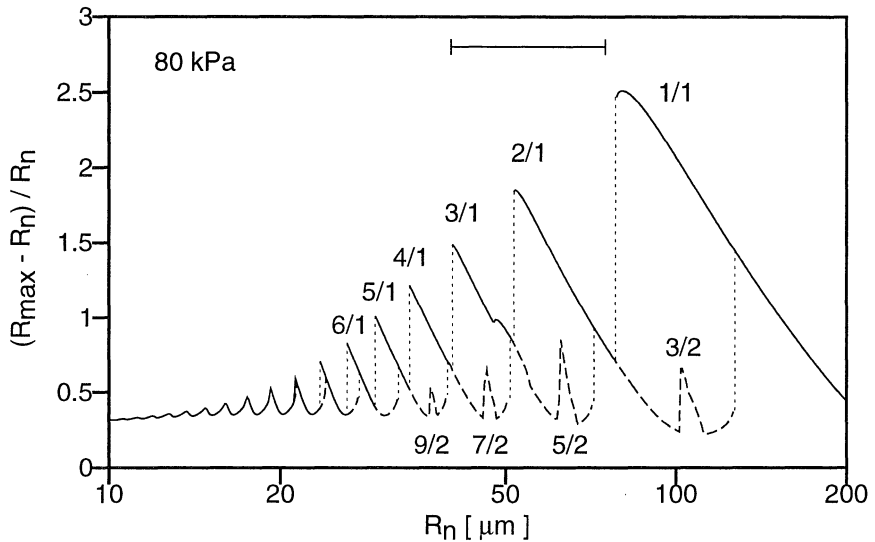


Figure 2. Resonance curves for bubbles of different sizes subject to a fixed frequency of 20 kHz. Driving amplitude is 80 kPa. The two curves belong to calculations with stepwise decreasing bubble radius (solid line) and stepwise increasing bubble radius (dashed line) using 600 steps.

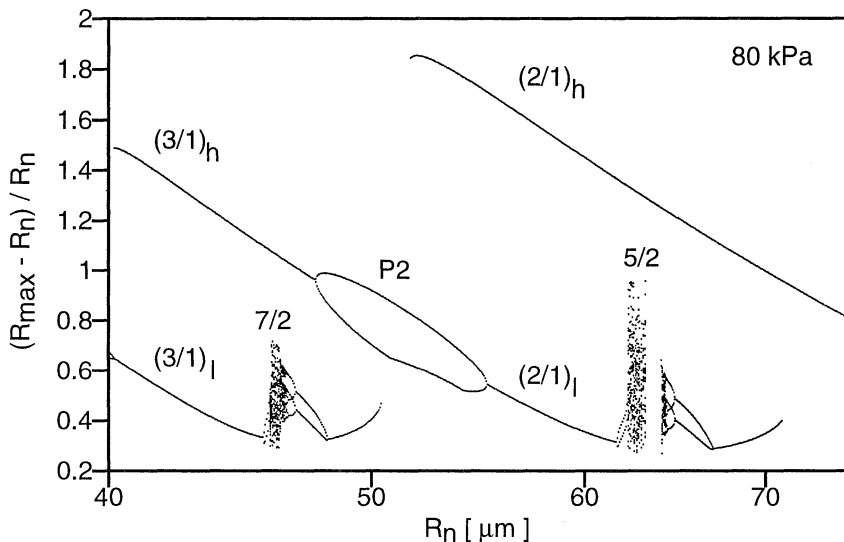


Figure 3. Response between the harmonic resonances of order 3/1 and 2/1 for $p_a = 80$ kPa and $\nu = 20$ kHz.

Between the harmonic resonances of order 3/1 and 2/1 some additional features appear as given on an expanded scale in Fig. 3. On the shoulder

of the 3/1 resonance leading down to the low amplitude branch of the 2/1 resonance a period doubling has taken place, i. e. the bubble oscillation only repeats after two oscillations of the driving (see P2 in Fig. 3). The two maxima then encountered are plotted in the diagram. In the same region further attractors other than the low amplitude [(2/1)_l and (3/1)_l] and high amplitude [(2/1)_h and (3/1)_h] harmonic resonances appear. The pure ultrasubharmonic resonances of order 5/2 and 7/2 also show period doubling that even reaches out to chaotic dynamics. Furthermore, there is a period-3 attractor (not shown) that can be reached only with special initial conditions, not with those going up and down with the bubble radius taking the previous ones. These attractors mark the beginning of complex behavior in the response of bubbles at higher driving the detailed investigation of which is beyond the scope of the present paper.

The resonances cease towards lower bubble radii. This is not due to surface tension effects. Even with zero surface tension this is the case; the respective curves are just shifted slightly to higher elongations for small bubbles. It is the effect of being far below the main resonance in an oscillatory system with small damping. We now turn to higher driving.

4. Response Curves at Intermediate High Driving

When the sound pressure amplitude is increased to $\hat{p}_a = 90$ kPa (Fig. 4) the overall response gets more involved due to ever more coexisting attractors appearing in extended regions of R_n . The diagram of Fig. 4 has been calculated by plotting the maxima of the bubble oscillation in several consecutive periods of the driving sound field taking the main maximum in each period. A period 1 solution has one main maximum and thus gets one dot, a period 2 solution gets two dots, etc, and a chaotic solution gets as many dots as periods calculated for plotting. It is seen that the large bubbles in the diagram tend to period-doubled and even chaotic oscillations. This behavior is very similar to the response curves in dependence on the driving frequency [6] instead of on the bubble radius at rest as considered here.

When only looking at small bubble radii (below about 20 μm) the situation simplifies again. The response is then similar to that for 80 kPa below about 50 μm . This is a general feature in the region of low and intermediate high driving that the same general features shift to lower bubble radii with higher driving. This behavior persists to about $\hat{p}_a = 110$ kPa as seen in Fig. 5 where the response in the region $4 \mu\text{m} \leq R_n \leq 10 \mu\text{m}$ is given for $\hat{p}_a = 100$ kPa, 105 kPa and 110 kPa. At 110 kPa we observe that the now high harmonic resonances acquire a high response level down to low bubble radii until they start to cease. The concave decay turns to a convex decay

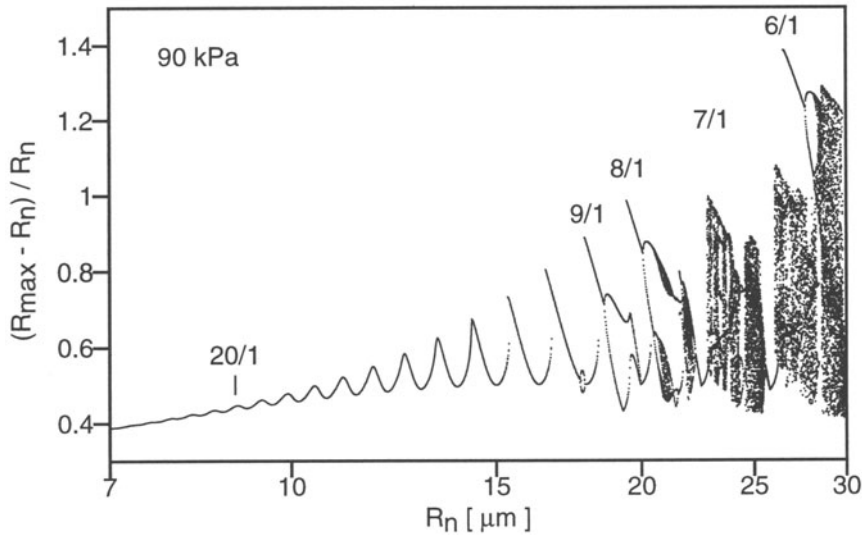


Figure 4. Response curves for bubbles of different sizes subject to a fixed frequency of 20 kHz. Driving amplitude is 90 kPa.

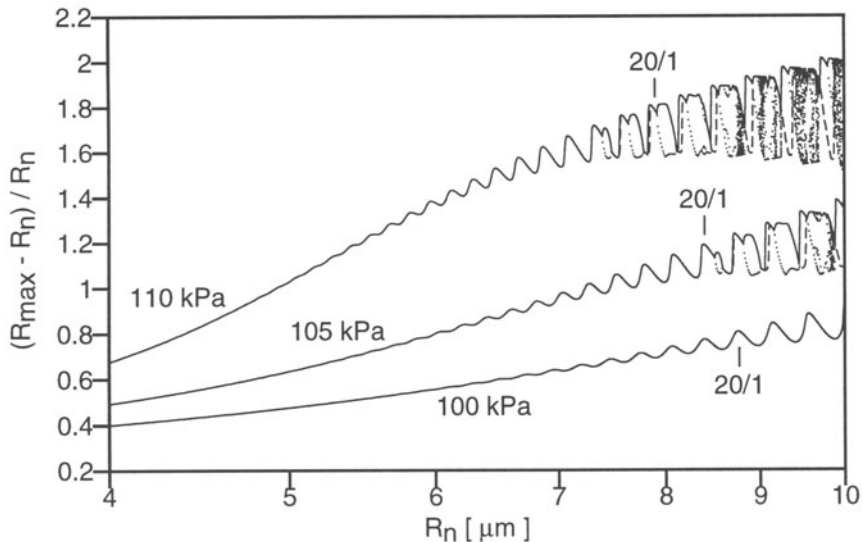


Figure 5. Response curves for bubbles of different sizes subject to a fixed frequency of 20 kHz. Driving amplitudes are 100 kPa, 105 kPa and 110 kPa.

between 100 kPa and 110 kPa indicating a new feature of bubble response only occurring for high driving and small bubbles and described next.

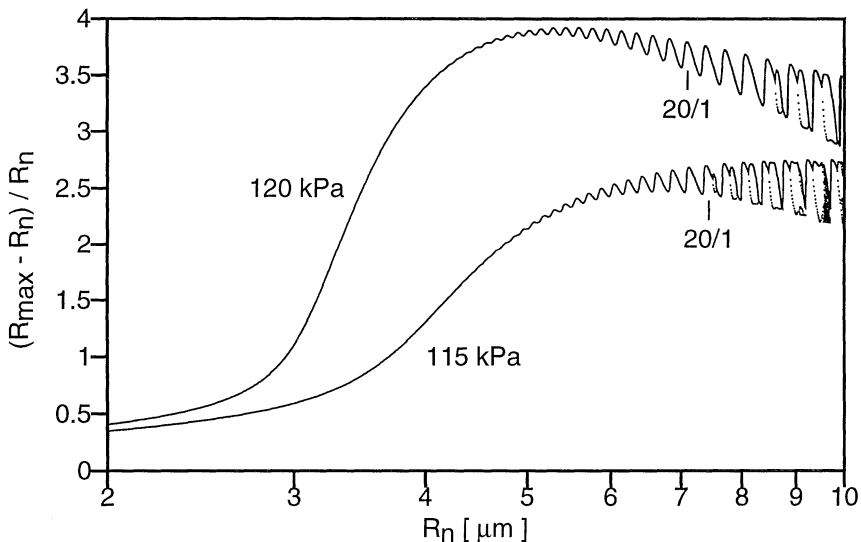


Figure 6. Response curves for bubbles of different sizes subject to a fixed frequency of 20 kHz. Driving amplitudes are 115 and 120 kPa.

5. Response Curves at High Driving

Going on in increasing the driving level to $\hat{p}_a = 120$ kPa a dramatic increase in the response of small bubbles is observed (Fig. 6). The response gets higher than even that of the main resonance and quite suddenly drops down to low values towards small R_n . The harmonic resonances of high order are still present and still decay to smaller bubbles. But they ride on what may be called a giant resonance. Physically this giant resonance comes about through the instability of the bubble, when the static pressure p_{stat} is overcome by the sound pressure during part of the sound cycle (actually an overall tension then). It is also connected with the surface tension via the pressure $2\sigma/R$ that comes with a bubble of radius R in a liquid with surface tension σ . Because the surface tension pressure $2\sigma/R_n$ increases with lowering R_n for fixed σ , there exists a radius R_n where a given driving pressure is no longer strong enough to overcome it and the bubble oscillation drops to small values. This resonance gets more pronounced at driving pressures beyond 120 kPa. In Fig. 7 the response curves are given for $\hat{p}_a = 130$, 140 and 150 kPa. The curves are remarkably smooth. The harmonic resonances are damped out below 5 μm . Comparison of the 20/1 and 10/1 resonances for different pressures \hat{p}_a (Figs. 4 - 7) shows that their complexity first increases (period doubling and chaos), but then reduces for higher driving.

Surface tension has a strong influence in this region through forcing

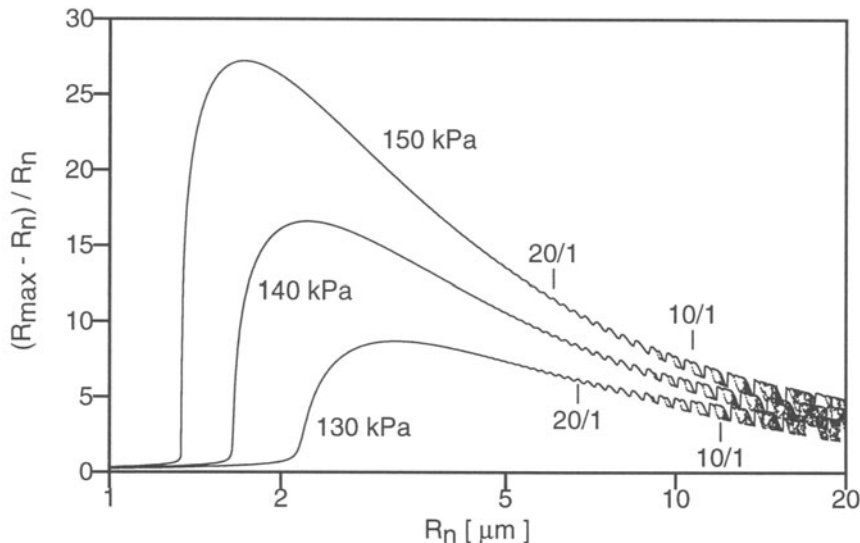


Figure 7. Response curves for bubbles of different sizes subject to a fixed frequency of 20 kHz. Driving amplitudes are 130, 140 and 150 kPa.

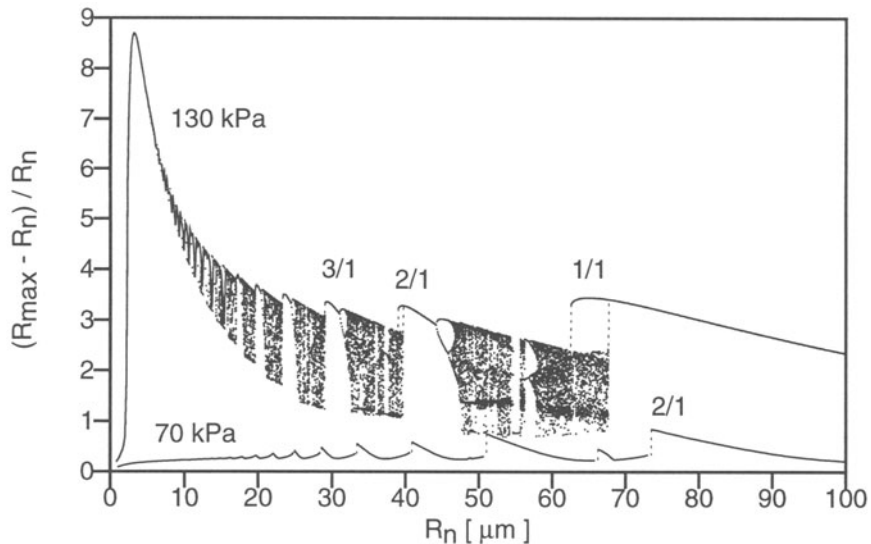


Figure 8. Complete view of the response for bubbles of different sizes subject to a fixed frequency of 20 kHz. Driving amplitude is 130 kPa. For comparison the response for 70 kPa is given.

the sudden, but smooth, decay that occurs at lower bubble radii. Without surface tension this decay would be missing.

To put the giant resonance at small bubble radii into perspective Fig. 8

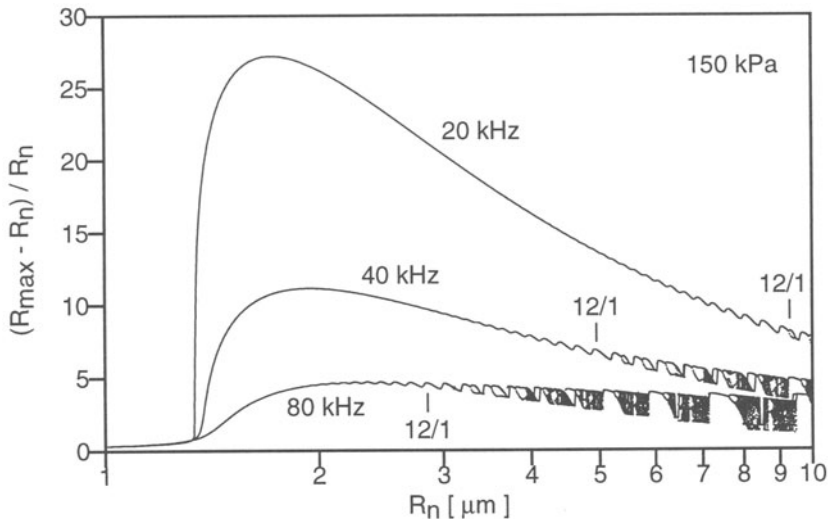


Figure 9. Response for bubbles of different sizes subject to different frequencies of 20, 40 and 80 kHz. Driving amplitude is 150 kPa.

gives the response for $\hat{p}_a = 130$ kPa and 70 kPa at 20 kHz for bubbles from 1 μm to 100 μm on a linear radius scale. The by far greater relative amplitude of the giant resonance with respect to the main resonance now can easily be noticed. The relation gets even more pronounced at higher driving amplitudes.

6. Discussion

The response of bubbles to periodic acoustic driving shows a very complex behavior even in the case of just spherical oscillations. Small bubbles develop a giant resonance much larger than the main resonance at fixed frequency through inertial instability during part of the acoustic cycle. Surface tension stops the resonance towards smaller bubble sizes. The giant resonance strongly depends on frequency (Fig. 9). The peak reduces with increasing frequency as expected because the duration of the inertial instability gets smaller in proportion to the smaller period of the driving. High frequencies can thus suppress the giant resonance. This may be of importance in sonoluminescence and sonochemical experiments for finding the optimal operating conditions. Low frequencies more easily lead to strong collapse, high frequencies to more collapses in a fixed amount of time.

Attention has been paid neither to the spherical stability of the bubble [7,8] nor to diffusive stability [8,9]. But intuitively it is clear that the spherical stability is the higher the smaller the bubble because of surface tension and is high for the small bubbles in the giant resonance. Diffusive stabil-

ity can be expected on the right shoulder of the giant resonance, because surface tension wants to dissolve the bubble, but rectified diffusion then increases due to increasing oscillation strength of the bubble. Depending on the gas concentration the bubble settles down at a point on the right shoulder being a stable attractor with a large basin of attraction around it ranging from left of the maximum to the ripples of the harmonic resonances or even further. This is the reason for the ease of getting the right bubble size for sonoluminescence experiments. Only the large basin of attraction needs to be hit, then the bubble adjusts its size automatically to the only one compatible with the giant resonance, the gas concentration and the pressure amplitude.

7. Acknowledgments

We thank the Nonlinear Dynamics Group at the Drittes Physikalisches Institut, Universität Göttingen, for help in various matters and the Ministerium für Wissenschaft und Kultur, Niedersachsen, for investments that made this study possible.

8. References

1. Lauterborn, W. (1968) On the dependence of erosion and luminescence on the sound pressure amplitude in cavitation (in German), *Acustica* **20**, 105-108.
2. Gilmore, F. R. (1952) The growth or collapse of a spherical bubble in a viscous compressible liquid, Report No. 26-4, Hydrodynamics Laboratory, California Institute of Technology, Pasadena, California, USA.
3. Löfstedt, R., Barber, B. P. and Puttermann, S. J. (1993) Toward a hydrodynamic theory of sonoluminescence, *Phys. Fluids A5*, 2911-2928.
4. Lauterborn, W. (1976) Investigation of nonlinear oscillations of gas bubbles in liquids, *J. Acoust. Soc. Am.* **59**, 283-293.
5. Lauterborn, W. and Parlitz, U. (1988) Methods of chaos physics and their applications to acoustics, *J. Acoust. Soc. Am.* **84**, 1975-1993.
6. Parlitz, U., Englisch, V., Scheffczyk, C. and Lauterborn, W. (1990) Bifurcation structure of bubble oscillators, *J. Acoust. Soc. Am.* **88**, 1061-1077.
7. Strube, H. W. (1971) Numerical investigations on the stability of bubbles oscillating non-spherically (in German), *Acustica* **25**, 289-301.
8. Hilgenfeldt, S., Lohse, D. and Brenner M. P. (1996) Phase diagrams for sonoluminescing bubbles, *Phys. Fluids* **8**, 2808-2826.
9. Akhatov, I., Gumerov, N., Ohl, C. D., Parlitz, U. and Lauterborn, W. (1997) The role of surface tension in stable single-bubble sonoluminescence, *Phys. Rev. Lett.* **78**, 227-230.

LIGHT SCATTERING BY BUBBLES IN LIQUIDS AND APPLICATIONS TO PHYSICAL ACOUSTICS

P. L. MARSTON

*Department of Physics
Washington State University
Pullman, WA 99164-2814*

1. Introduction

This paper is concerned with the basic optical properties of bubbles in liquids. An understanding of the scattering of light by bubbles is important for the proper application of optical methods for monitoring the dynamics of bubbles and also for the use and interpretation of high speed imaging technologies. Furthermore, various optical methods are feasible for modifying the dynamics of bubbles. The approach taken in the present paper may appear to be somewhat "introductory" or "old fashion" to some readers since at least in the case of spherical bubbles, the results of Mie theory may be trivially numerically evaluated using modern algorithms [1]. The needed understanding of scattering processes, however, involves different lines of reasoning than the numerical evaluation of Mie's partial-wave series for the range of sizes typically encountered in bubble dynamics research. In motivating a related review of scattering processes, Nussenzveig [2] gives the following quote attributed to E. P. Wigner "It is nice to know that the computer understands the problem, but I would like to understand it too." It seems also appropriate to note that van de Hulst's highly influential monograph on light scattering [3] draws heavily on reasoning worked out without significant computational aids in his thesis.

In the present review important scattering properties computed for bubbles in water are compared with those for drops of water in air. Some physical and geometrical lines of reasoning are summarized for distinguishing between the bubble and drop cases. Some relevant analytical, computational, and experimental studies are cited. Several relevant papers have been reprinted in a single volume [4]. The most complete earlier review appeared in 1989 [5] and there have been numerous developments since then some of which will be summarized here though specific experimental results applied to single bubble sonoluminescence (SBSL) [6] will be left to other authors of the present volume. A few results are presented here for the first time.

The scattering calculations shown for spherical bubbles and drops are given for the purpose of introducing certain features whereas real bubbles can be distorted and can have coated surfaces. Some of the resulting modifications to the scattering are noted in Sec. 7. Unless otherwise indicated, the relative refractive index of water and air is approximated as 4/3 which corresponds roughly to the case of blue light and the refractive index is approximated as purely real so that absorption is neglected. The illumination is taken to be a linearly polarized plane wave.

2. Mie Theory for Scattering by Spherical Bubbles and Drops

Figure 1 shows the scattering calculated using Wiscombe's algorithm [1] for a bubble (a) and a drop (b), each having a dimensionless size parameter $ka = 100$ where a is the sphere radius and $k = 2\pi/\lambda$ with λ being the wavelength in the outer medium respectively of (a) water and (b) air. Thus for green light with $\lambda_{\text{air}} = 514 \text{ nm}$, a is $8.2 \mu\text{m}$ for the drop but for the bubble $k = (4/3)(2\pi/514 \text{ nm})$ so that $a = 6.1 \mu\text{m}$. In each case the scattering is expressed in terms of a dimensionless "gain" or scattered irradiance I_j which is related to the true scattered irradiance i_{sj} and the incident irradiance i_{inc} by

$$i_{sj} = i_{\text{inc}} I_j a^2 / (4R^2), \quad j = 1, 2, \quad (1)$$

where $R \gg ka^2$ denotes the radius of the observer from the bubble and j is a polarization index. The normalization is such that $I_j = 1$ for geometric reflection from a perfectly reflecting sphere. The I_j are related to the dimensionless complex scattering amplitudes S_j of Mie theory [1-3] by $I_j = |S_j|^2(2/ka)^2$. The polarization convention is such that $j = 1$ if the E field is perpendicular to the scattering plane defined by the incident and scattered wave-vectors while $j = 2$ in the parallel case. For unpolarized illumination I_j is replaced by $(I_1 + I_2)/2$ and other polarization cases are discussed in [3].

Comparison of Figs. 1 (a) and (b) shows that even for the relatively small value of ka under consideration that there are significant differences in the drop and bubble scattering patterns away from each forward diffraction peak. The scattering is shown to depend on polarization. Figure 2 shows ray diagrams that are helpful in explaining some of the scattering contributions. For example, Fig. 1(b) shows for the drop a broad peak in I_1 near the Descartes rainbow scattering angle $\theta_D \approx 138^\circ$ which is where the scattering angle of the 2-chord ray has an extreme value in Fig. 2(a). The peak is suppressed in I_2 because the internal reflection within the drop happens to lie close to the Brewster condition and is suppressed [2-4]. Since the rainbow maximum is associated with a caustic, simple geometrical optics (based on flux conservation) is unable to describe the scattering. As reviewed here, there are similarly several regions in scattering by bubbles where "diffraction" or physical-optics corrections are essential [7-18] though

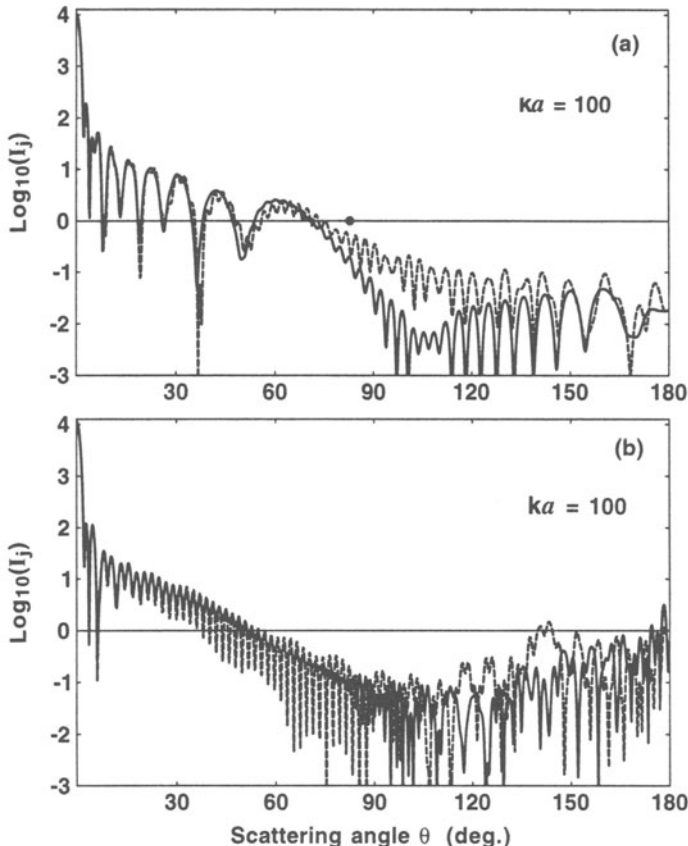


Figure 1. Normalized irradiance I_j from Mie theory for scattering (a) by a bubble in water and (b) by a drop of water in air; $j = 1$ is dashed, and $j = 2$ is solid.

they are interpreted using the ray diagrams shown in Fig. 2(a)-(c).

It is also instructive to contrast the "efficiency factors" for scattering by drops [1-4] with those for bubbles [19,20] computed from Mie theory. These are defined as the following ratios: $Q_{\text{ext}} = \sigma_{\text{ext}}/\pi a^2$, $Q_{\text{sca}} = \sigma_{\text{sca}}/\pi a^2$, $Q_{\text{pr}} = Q_{\text{sca}}(1 - g)$ for optical extinction, scattering, and radiation pressure where σ_{ext} and σ_{sca} are the extinction and total scattering cross sections and g denotes an asymmetry factor in the average directivity of the scattering. The radiation force on a sphere is [3,20] $i_{\text{inc}} v^{-1} \pi a^2 Q_{\text{pr}}$ where v denotes the velocity of light in the medium surrounding the sphere. The absorption efficiency is defined as $Q_{\text{abs}} = Q_{\text{ext}} - Q_{\text{sca}}$ and is proportional to the absorbed power; Q_{abs} vanishes for the lossless examples shown in Figs. 3 and 4. For large values of ka , Q_{ext} is known to lie close to 2 for both drops and bubbles [3,19]. For the range of ka considered in Fig. 3, van de Hulst [3,21] has shown that the deviation from 2 largely depends on the relative phase of

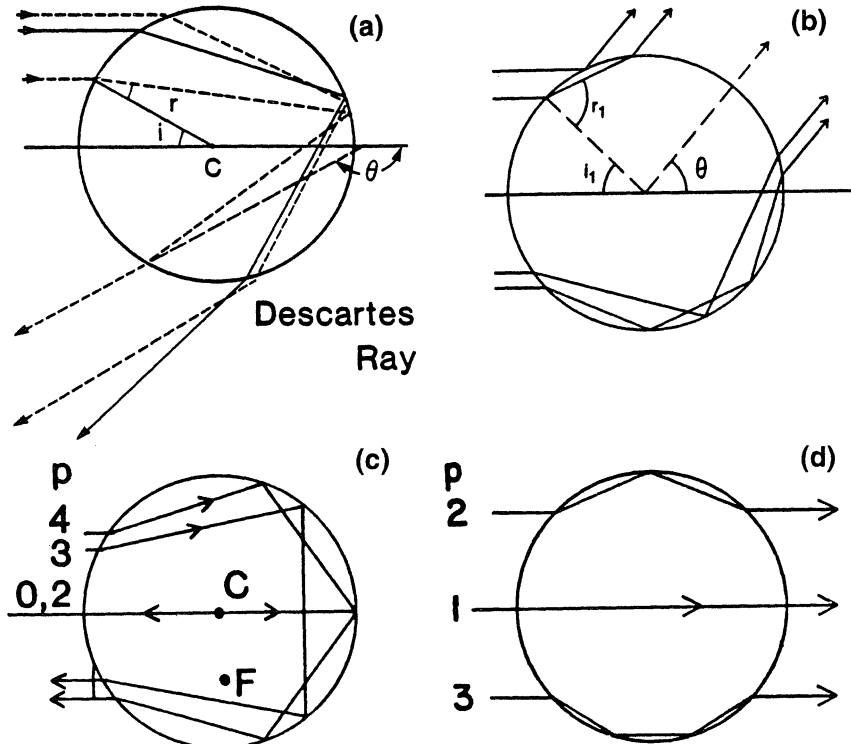


Figure 2. Some ray diagrams for scattering: (a) by a drop, and (b), (c) and (d) by a bubble. The numbers indicate the number p of internal chords.

the axial ray through the center of the drop or bubble which is given by $2\pi ka(m - 1)$ where m is the relative refractive index of the scatterer. Hence, the abscissa for the drop case in Fig. 3(a) is stretched so that for a given distance $(ka)_{\text{drop}} = (3/4)(ka)_{\text{bubble}}$ and comparison of the plots confirms that van de Hulst's reasoning pertains to the broad structure. Figure 3 shows that the bubble lacks the "ripple" structure in the Q_{ext} and Q_{pr} of drops which is due to resonances. This is also true for the much larger drop and bubble cases shown in Fig. 4. The presence of sharp resonances for the drop-like scatterer is attributable to the trapping (via total internal reflection) of energy within the drop [2]. The resonances are narrow and may not be easily resolved in the plots shown. Similar examples for drops are given by Irvine [22]. Energy is not trapped within the bubble and hence there are no sharp resonances. This also applies to the normalized backscattering amplitude $I_B = I_1 = I_2$ which from symmetry does not depend on polarization.

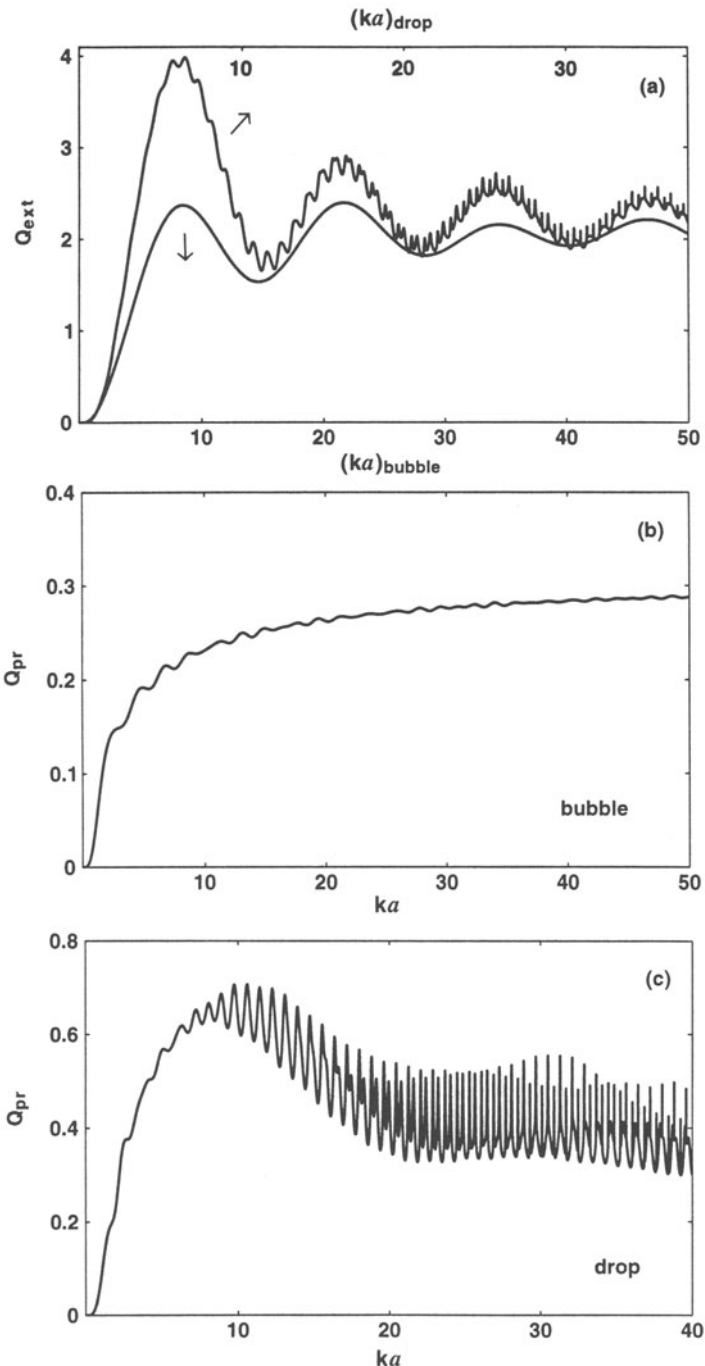


Figure 3. (a) Extinction efficiency for a water drop (upper scale) and a bubble in water (lower scale). Radiation pressure efficiency factor (b) for a bubble and (c) for a drop.

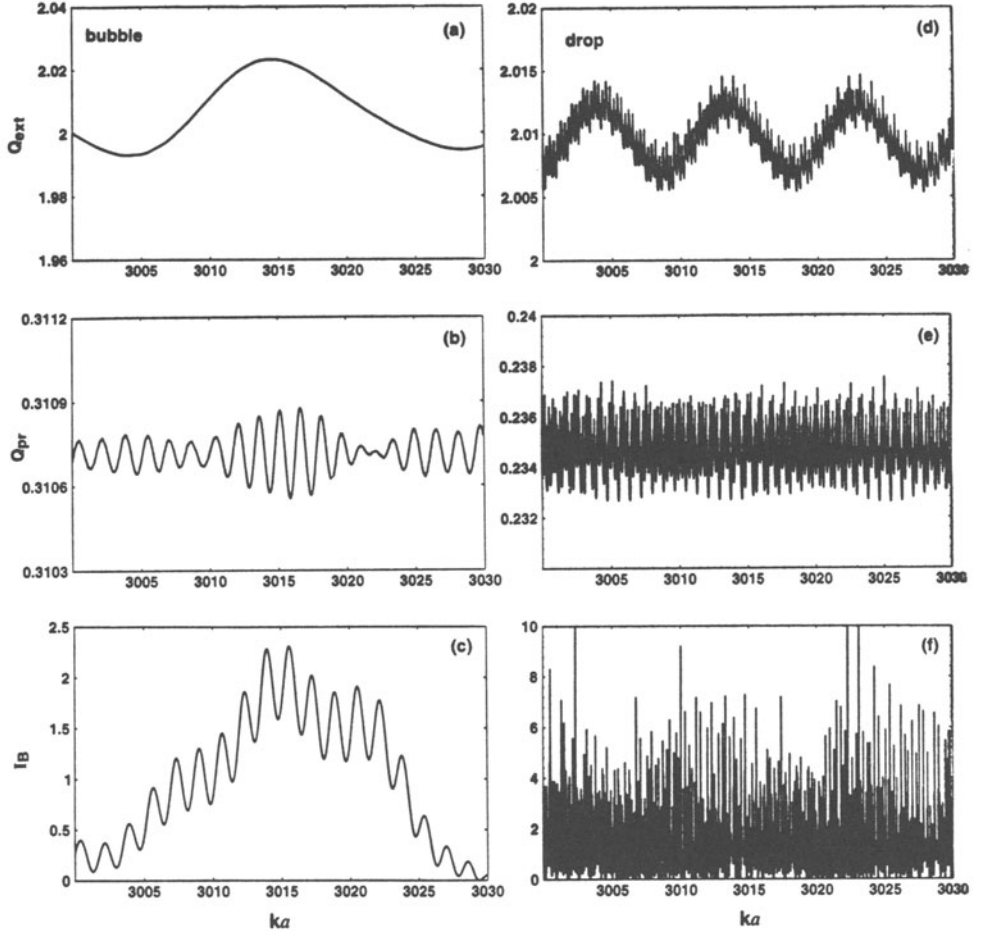


Figure 4. The column on the left is computed for a spherical bubble in water and the one on the right is for a water drop: (a) and (d) extinction efficiency; (b) and (e) radiation pressure efficiency factor; (c) and (f) backscattering I_B normalized as in Eq. (1).

3. Critical and Brewster Angle Scattering and Application to Sizing

Inspection of Fig. 1(a) reveals a broad peak followed by a general decrease in the scattering in the region near 80° . This feature is associated with the critical scattering angle at $\theta_c = 180^\circ - 2i_c \approx 82.8^\circ$. Here $i_c = \sin^{-1}(m) \approx 48.6^\circ$ is the critical angle of incidence; see Fig. 2(b). For angles of incidence $i \geq i_c$, the scattering is total (if tunneling [8] is neglected) so that the reflection would be total for scattering angles $\theta \leq \theta_c$. The existence of this transition was known by 1888 from the work of Pulfrich (translated and quoted in

[10]) and more recently from a geometrical analysis by Davis [23]. Quantitative measurements and physical-optics corrections and Mie computation were given by Marston et al. [7-11]. In addition to the broad structure near θ_c , Fig. 1(a) shows the presence of a fine structure which is associated with interference with weaker two and three chord ray contributions refracted at the far side of the bubble, Fig. 2(b).

If the only scattering contribution present at θ_c were the external reflection and if that contribution could be geometrically approximated then $I_j(\theta_c) = 1$, $j = 1$ and 2, which is shown as the point in Fig. 1(a). The actual irradiance is depressed below unity and both a detailed asymptotic analysis [2,12,13] and Fresnel zone properties [12] show that the leading correction is $O(ka)^{-1/4}$, which makes the convergence to the geometric limit extremely slow. Because this diffractive correction is a slowly varying function of ka , it follows that to good approximation $i_{sj}(\theta_c) \propto a^2$ where \propto denotes "is proportional to" and the weak effects of the far-side ray interference have been neglected. For θ appreciably less than θ_c , the dependence of i_{sj} on the bubble radius is more complicated due to the interference from the one-chord near-side ray, Fig. 2(b). This special attribute of near critical angle scattering [7,8] has been applied to size measurements based on scattered irradiance for static [24] and dynamic [6] bubbles and in many other more recent studies. Instead of smoothing the fine structure with an angular average, a wavelength average may be used [12]. Other approaches to size measurements based on near critical angle scattering include the angular width of the coarse structure, the fine structure spacing, and the detailed phase and amplitude of the interference modulations [11]. Approaches based on comparisons at a few scattering angles have been described [25,26]. While not asymptotically correct at large ka , a simple physical optics approximation recovers the angular dependence of the coarse features over a wide range of bubble sizes typically encountered in research [8,11].

When the E-field is parallel to scattering plane, the external reflection is quenched when the angle of incidence is the Brewster angle $i_B = \tan^{-1}(m)$. Near the corresponding scattering angle of $\theta_B = 180^\circ - 2i_B \approx 106.2^\circ$, I_2 is suppressed in Fig. 1(a) along with the interference oscillations due to the far-side ray. These effects have been experimentally verified [5].

4. Backscattering and Glory Patterns

The power reflection coefficient for normal incidence at a water-air interface is only $[(m - 1)/(m + 1)]^2 \approx 1/49$ though the typical normalized irradiance in Fig. 4(c) is $>> 1$. The reason for this enhancement and the quasi-periodic dependence on ka is that for large spherical bubbles the backscattering is dominated not by axial reflections (or subsequent reverberations along the bubble's axis) but by off-axis rays that are exactly backscattered. Such "glory" rays, Fig. 2(c), produce a type of focusing in the backward direction.

Because of this focusing, the glory contributions to I_B increase in proportion to ka so that the glory ray contributions must dominate axial reflections for spherical bubbles at large ka . Glory backscattering for bubbles in oil [14] and water [16] has been observed and a model of the backscattering pattern has been confirmed and used to determine bubble size. A related backward focusing of scattering by drops was originally suggested by van de Hulst to explain the glory of cloud drops [3]. The ray contributions for drops have important differences with those shown in Fig. 2(c) and an analysis [2] has been able to confirm that this type of focusing contributes to the narrow spikes shown in Fig. 4(f).

For bubbles, the broad feature in Fig. 4(c) tends to be repeated as shown in [19] for a calculation over a wider range of ka . This broad quasi-period is associated with the interference of glory rays having similar optical path lengths. For example, the quasi-period for interference oscillations between the 3 and 4 chord glory rays (labeled $p = 3$ and 4 in Fig. 2(c)) may be shown to be [15]:

$$(\Delta ka)_{bg} \approx \pi / [m(4\cos r_4 - 3\cos r_3) + (\cos i_3 - \cos i_4)] \quad (2)$$

where i_p and r_p denote the angle of incidence and refraction for the glory ray having p chords. Evaluation of Eq. (2) for $m = 3/4$ gives $(\Delta ka)_{bg} \approx 32.2$ in agreement with the width of a typical feature as shown in Fig. 4(c). The closely spaced oscillations are primarily due to the interference between axial reflections and the stronger glory contributions.

5. Forward Scattering, Forward Glory, and Extinction

The near-forward scattering is important not only for certain sizing and imaging modalities but also because the "optical theorem" [2,3] indicates that σ_{ext} may be expressed in terms of the forward scattering amplitude. Except when $|m - 1|$ is small, when ka is large the dominant contribution to the forward scattering amplitude is proportional to ka^2 with the result that $Q_{ext} \approx 2$ and the normalized forward irradiance $I_F \approx (ka)^2$. For large spherical bubbles, the leading-order corrections are due to forward-focused glory rays shown in Fig. 2(d). Neglecting interference between glory rays, those contributions considered separately give [18] $I_{FG} \propto ka$. Accounting for the interference with the ordinary forward diffraction, the resulting corrections to $Q_{ext} = 2$ are $O(ka)^{-1/2}$. It is these glory contributions that cause the oscillations of Q_{ext} in Fig. 4(a) as opposed to the unfocused $O(ka)^{-1}$ axial ray contributions to Q_{ext} that are dominant in Fig. 3(a). The quasi-period of the oscillations is approximated by requiring the phase of the glory amplitude relative to the forward diffraction to evolve by 2π which gives

$$(\Delta ka)_{fg} \approx \pi / (mp\cos r_p - \cos i_p), \quad (3)$$

where i_p and r_p are the angles of incidence and refraction for the pth forward glory ray, $p = 2,3,\dots$. For bubbles in water $m = 3/4$ and the strongest contributor has $p = 2$ and has only one internal reflection. Evaluation of Eq. (3) gives $(\Delta ka)_{fg} \approx 23.6$ which is close to the quasi-period of 24.5 in Fig. 4(a). For comparison, this is significantly different than the quasi-period of the axial ray correction of [3,21] $(\Delta ka)_{ar} = \pi/|m - 1| \approx 12.6$ for $m = 3/4$ that is dominant in Fig. 3(a). Note also that a different type of forward-glory ray is important for drop-like scatterers [2,21] and that the cross-polarized scattering patterns and ring-like focal circles of forward glory rays of bubbles have been observed [18].

6. Radiation Pressure and Optical Trapping of Bubbles in Water

The downward propagation of a laser beam in water has been demonstrated to exert a sufficient radiation force on freely rising bubbles to completely counteract buoyancy [20]. For this method of levitation to be stable it is necessary for there to be a lateral restoring force which is accomplished by using a laser beam with an irradiance minimum on its axis. Even though the illumination is not a plane wave, the evaluation of Q_{pr} from Mie-Debye theory [1-3] is useful for confirming the importance of the momentum transport of reflected light on radiation pressure [20]. In that analysis, only contributions from the total reflection region are considered where the local angle of incidence $i \geq i_c = \sin^{-1}(m)$. The analysis gives $Q_{pr} \approx (\cos i_c)^4 \approx 0.19$. Inspection of Fig. 3(b) shows that Q_{pr} rapidly rises to a somewhat larger value. Figure 4(b) reveals weak modulations of Q_{pr} correlated with those in Q_{ext} . The fine structure appears to be associated with quasi-periodic oscillations of the asymmetry factor g .

In the experiments [20], the optical power required to trap a $22 \mu\text{m}$ radius bubble was 1.0 W, in general agreement with calculations. Unfortunately, the required beam power is estimated to increase in proportion to a^3 , making the power required prohibitively large for large bubbles. It may be advantageous to use a laser beam to reposition an SBSL bubble in the exciting sound field [27]. A numerical integration shows that the average optical power required may be reduced by modulating the light so that the peak power is applied when the bubble is largest. In other work, the radial projection of the radiation stress of modulated light was demonstrated to drive weak monopole bubble oscillations [28].

7. Changes in the Scattering Caused by Nonsphericity and Coatings

Even in the absence of an applied sound field, a freely rising bubble in water is distorted by hydrodynamic stresses. This distortion is sufficiently large to affect the backward glory scattering pattern when the phase shift of a glory

ray is altered by about 1 radian. For a slightly oblate horizontally illuminated bubble, distortions of the backscattering pattern were observable in photographs [17] for bubble radii as small as 155 μm (or $ka \approx 2685$). The axial caustic of each glory ray was shown to unfold into an astroid caustic consisting of four connected cusp caustics and a rainbow caustic [17, 29]. Somewhat larger bubbles produced a spectacular unfolding of the caustic pattern which was used to infer small values of bubble oblateness in general agreement with a hydrodynamic approximation. Thus the calculations shown in Fig. 4(c) are for the purposes of illustration only since a real bubble having $ka \approx 3000$ is expected to be sufficiently nonspherical to modify I_B .

It is anticipated that bubble oblateness will have a much weaker effect on the critical-angle scattering pattern. That is because the critical scattering angle is given by $\theta_c = 180^\circ - 2\sin^{-1}(m)$ independent of bubble shape. This follows because while the local angle of incidence i_0 for the reflected ray is given by $\cos^{-1}(\hat{n} \cdot \hat{k})$, where \hat{k} is the wave vector and \hat{n} the local surface normal; the associated scattering angle remains [29, p. 30] $\theta = 180^\circ - 2i_0$. Changes in shape would alter the spreading factor and the local asymptotic correction [12]. It is noteworthy in this context that a critical angle transition region has been photographed for freely rising sunlit bubbles which were sufficiently large to be distorted [30]. Forward from θ_c , details of the pattern with laser illumination are shifted along with the phases of near-side ($p = 1$ and 2) and far-side ($p = 2$ and 3) rays. Oscillations in the coarse structure from the interference of near-side rays were used to detect shape oscillations as small as 1 μm in amplitude [31].

In addition to shape changes, the scattering patterns of natural bubbles may be altered by the presence of a sufficiently thick surface coating of an oily substance. For uniformly coated spherical bubbles, the scattering patterns may be computed using the partial-wave series of Aden and Kerker [3] and several examples for bubbles in water with thin oil coatings have been investigated [32]. The most important result is that coatings shift the critical angle scattering pattern by an amount that has been geometrically predicted [30]. Furthermore, coatings thicker than about 0.2 μm are predicted to significantly raise the level of I_2 at the Brewster scattering angle θ_B as well as altering the backscattering. Most of the computational investigation [32] was concerned with critical angle scattering.

8. Applications of Optical Extinction to Bubble Dynamics

In closing, it is appropriate to note some examples where measurement of the time-dependent extinction of light provides a viable alternative to critical angle scattering in dynamical studies. Figure 5 illustrates the method [33]. A levitated bubble is illuminated from below by an expanded laser beam. In response to modulated acoustic radiation pressure, the bubble undergoes quadrupole shape oscillations though the bubble profile illuminated by the

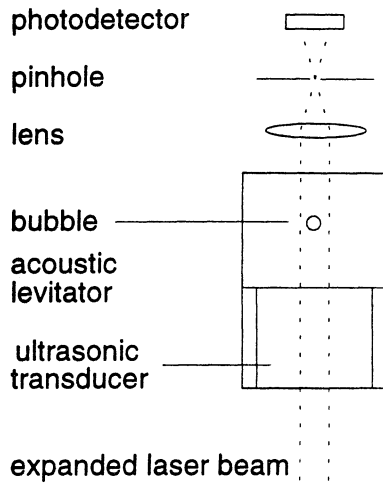


Figure 5. Dynamic bubble profile measurements based on the extinction of light. An increase in the area of the bubble's profile reduces the detected optical power.

beam remains circular with a radius a that varies with time. The total power removed from the beam is $Q_{ext}i_{inc}\pi a^2 \approx 2i_{inc}\pi a^2$. Thus if the radius increases by δa in a true extinction measurement the detected power shifts by $\delta P \approx -4i_{inc}\pi a\delta a$. Here and in related experiments [34,35] it was preferable to make a pseudo-extinction measurement where $\delta P \approx -2i_{inc}\pi a\delta a$. This was achieved by selecting the radius of the pinhole to be sufficiently large that the forward diffraction peak was not blocked; the pinhole radius was somewhat larger than $\lambda f_L/a$ where f_L is the focal length of the lens. This choice was to minimize any variations in the detected power introduced by scattering of light by the sound wave or by other small variations in the refractive index. Oscillations in the detected power were used to monitor the free decay of bubble shape oscillations [33] and the damping introduced by an insoluble surfactant monolayer was measured [34]. It is very important that the noise power of the laser is small since much of the laser power is detected by the photocell. In another application of this method, the transient volume pulsations were measured for bubbles produced by a drop falling on a free surface [35]. The volume pulsations of such bubbles contributes to the underwater noise of rain. In each of these applications, the interpretation of measurements is simplified because the deviations of Q_{ext} from 2 were small for the size range of bubbles studied.

This work was supported in part by the Office of Naval Research. The author is grateful to several former graduate students who contributed to aspects of the work including: D. L. Kingsbury, D. S. Langley, B. T. Unger, S. C. Billette, W. P. Arnott, S. M. Baumer, C. E. Dean, J. S. Stroud, and T. J. Asaki. The author may be reached at marston@wsu.edu.

9. References

1. Wiscombe, W. J. (1980) Improved Mie scattering algorithms, *Appl. Opt.* **19**, 1505-1509.
2. Nussenzveig, H. M. (1992) *Diffraction Effects in Semiclassical Scattering*, Cambridge University Press., Great Britain.
3. van de Hulst, H. C. (1957) *Light Scattering by Small Particles*, John Wiley & Sons, Inc., New York, NY.
4. Marston, P. L. (ed.) (1994) *Selected Papers on Geometrical Aspects of Scattering* in *SPIE Milestone Series*, vol. MS 89, SPIE Optical Engineering Press, Bellingham, WA.
5. Marston, P. L., Arnott, W. P., Baumer, S. M., Dean, C. E., and Unger, B. T. (1989) Optics of bubbles in water scattering properties, coatings, and laser radiation pressure, in T. G. Wang (ed.), *Drops and Bubbles Third International Colloquium*, AIP Proceedings 197, pp. 461-480.
6. Gaitan, D. F. and Crum, L. A. (1990) in M. F. Hamilton and D. T. Blackstock (eds.), *Frontiers of Nonlinear Acoustics*, Elsevier, NY, pp. 459-463.
7. Marston, P. L. (1979) Critical angle scattering by a bubble: Physical-optics Approximation and observations, *J. Opt. Soc. Am.* **69**, 1205-1211; (1980) **70**, 353.
8. Marston, P. L. and Kingsbury, D. L. (1981) Scattering by a bubble in water near the critical angle: interference effects, *J. Opt. Soc. Am.* **71**, 192-196 + 917.
9. Kingsbury, D. L. and Marston, P. L. (1981) Mie scattering near the critical angle of bubbles in water, *J. Opt. Soc. Am.* **71**, 358-361.
10. Marston, P. L., Johnson, J. L., Love, S. P., and Brim, B. L. (1983) Critical angle scattering of white light from a cylindrical bubble in glass: photographs of colors and computations, *J. Opt. Soc. Am.* **73**, 1658-1664 + Plate X.
11. Langley, D. S. and Marston, P. L. (1984) Critical angle scattering of laser light from bubbles in water measurements, models, and application to sizing of bubbles, *Appl. Opt.* **23**, 1044-1054.
12. Dean, C. E. and Marston, P. L. (1991) Critical angle light scattering from bubbles: an asymptotic series approximation, *Appl. Opt.* **30**, 4764-4776.
13. Fiedler-Ferrari, N., Nussenzveig, H. M., and Wiscombe, W. J. (1991) Theory of near-critical-angle scattering from a curved interface, *Phys. Rev. A* **43**, 1005-1038.
14. Langley, D. S. and Marston, P. L. (1981) Glory in optical backscattering from air bubbles, *Phys. Rev. Lett.* **47**, 913-916.

15. Marston, P. L. and Langley, D. S. (1982) Glory in backscattering: Mie and model predictions for bubbles and conditions on refractive index in drops, *J. Opt. Soc. Am.* **72**, 456-459.
16. Arnott, W. P. and Marston, P. L. (1988) Optical glory of small freely-rising gas bubbles in water: Observed and computed cross-polarized backscattering patterns, *J. Opt. Soc. Am. A.* **5**, 496-506.
17. Arnott, W. P. and Marston, P. L. (1991) Unfolded optical glory of spheroids: backscattering of laser light from freely rising spheroidal air bubbles in water, *Appl. Opt.* **30**, 3429-3442.
18. Langley, D. S. and Marston, P. L. (1991) Forward glory scattering from bubbles, *Appl. Opt.* **30**, 3452-3458.
19. Marston, P. L., Langley, D. S., and Kingsbury, D. L. (1982) Light scattering by bubbles in liquids: Mie theory, physical-optics approximations, and experiments, *Appl. Sci. Res.* **38**, 373-383.
20. Unger, B. T. and Marston, P. L. (1988) Optical levitation of bubbles in water by the radiation pressure of laser beam: an acoustically quiet levitator, *J. Acoust. Soc. Am.* **83**, 970-975.
21. van de Hulst, H. C. (1956) The interpretation of numerical results obtained by rigorous diffraction theory for cylinders and spheres, *Transactions of the IRE on Antennas and Propagation*, AP-**4**, 195-202.
22. Irvine, W. M. (1965) Light scattering by spherical particles: radiation pressure, asymmetry factor, and extinction cross section, *J. Opt. Soc. Am.* **55**, 16-21.
23. Davis, G. E. (1955) Scattering of light by an air bubble in water, *J. Opt. Soc. Am.* **45**, 572-581.
24. Hansen, G. M. (1985) Mie scattering as a technique for the sizing of air bubbles, *Applied Optics* **24**, 3214-3220.
25. Marston, P. L. (1986) Light Scattering Theory for Bubbles in Water: Inverse Scattering, coated Bubbles, and Statistics, (available from DTIC as Report No. AD-A174997, Ft. Belvoir, VA).
26. Lentz, W. J., Atchley, A. A., and Gaitan, D. F. (1995) Mie scattering from a sonoluminescing air bubble in water, *Appl. Opt.* **34**, 2648-2654.
27. Thiessen, D. B. and Marston, P. L. (manuscript in preparation).
28. Unger, B. T. and Marston, P. L. (1988) Optically stimulated sound from oil drops and gas bubbles in water: thermal and radiation pressure optoacoustic mechanisms, in M. A. Blizzard (ed.), *Ocean Optics IX*, Proc. SPIE **925**, 326-333.
29. Marston, P. L. (1992) Geometrical and catastrophe optics methods in scattering, in A. D. Pierce and R. N. Thurston (eds.), *Physical Acoustics*, Academic Press, vol. 21, pp. 1-234.

30. Marston, P. L. (1991) Colors observed when sunlight is scattered by bubble clouds in seawater, *Appl. Opt.* **30**, 3479-3484 + p. 3549.
31. Asaki, T. J., Marston, P. L., and Trinh, E. H. (1993) Shape oscillations of bubbles in water driven by modulated ultrasonic radiation pressure: Observations and detection with scattered laser light, *J. Acoust. Soc. Am.* **93**, 706-713.
32. Marston, P. L., Billette, S. C., and Dean, C. E. (1988) Scattering of light by a coated bubble in water near the critical and Brewster scattering angles, in M. A. Blizzard (ed.), *Oceans Optics IX*, Proc. SPIE **925**, 308-316.
33. Asaki, T. J. and Marston, P. L. (1995) Free decay shape oscillations of bubbles acoustically trapped in water and sea water, *J. Fluid Mech.* **300**, 149-167.
34. Asaki, T. J., Thiessen, D. B., and Marston, P. L. (1995) Effect of an insoluble surfactant on capillary oscillations of bubbles in water: observation of maximum in the damping, *Phys. Rev. Lett.* **75**, 2686-2689 + 4336.
35. Stroud, J. S. and Marston, P. L. (1993) Optical detection of transient bubble oscillations associated with the underwater noise of rain, *J. Acoust. Soc. Am.* **94**, 2788-2792.

THE INTERACTION OF A CAVITATION BUBBLE WITH A RIGID BOUNDARY

J. R. BLAKE, R. P. TONG AND G. S. KEEN

*School of Mathematics and Statistics,
The University of Birmingham, Edgbaston, Birmingham, B15
2TT, UK*

AND

Y. TOMITA

*Hakodate College, Hokkaido University of Education, Hakodate,
Japan*

Abstract. This paper presents the results of incompressible flow computations for the collapse of cavitation bubbles close to a rigid boundary, for stand-off distances in the range $0.8\text{--}1.4R_m$, where R_m is the maximum bubble radius. After jet impact on the far side of the bubble, the bubble assumes a toroidal shape with a high velocity outflow along the rigid boundary. This outflow is met by an inflow from the collapsing bubble thence throwing up a vigorous splash into, or around, the bubble. This splash, when coupled with the larger internal gas pressures, may generate higher pressures on the boundary than the original jet impact, although, instead of being on the axis of symmetry, the peak pressures occur on a ring around the axis.

1. Introduction

Data available on the growth and collapse of cavitation bubbles (typically mm sized bubbles) near a rigid boundary is used for comparison and validation of our boundary integral codes [1–6, 8]. The significant feature of this study is that jet impact does not yield the highest pressures on the boundary, but rather a phenomenon we call the ‘splash’ when the outward flow along the rigid boundary, after jet impact, meets the inrushing liquid due to the bubble compression. The peak pressures associated with the splash occur near minimum volume and thence high internal gas pressures, thus

leading to a stagnation pressure on a ring on the boundary which can be an order of magnitude higher than the pressure attributed to jet impact.

There are a number of limitations to our computational study, the most serious being the restriction to incompressible flow, thus limiting our analysis to stand-off parameters between about 0.8 and $1.4R_m$ (the precise values depending on experimental conditions). Outside this range shock pressures would be more important than those developed using incompressible theory.

This paper represents a summary of our current thinking on the modelling of cavitation bubbles near boundaries using integral equation methods, bearing in mind the restrictions mentioned above. We proceed by introducing the dimensionless physical parameters in the next section, followed by a discussion based on a selection of figures that show the principal phenomena.

2. Dimensionless parameters

In this study we suppose the flow is dominated entirely by inertial effects, thus neglecting any role for viscosity. Likewise, surface tension effects do not play an important part in such a violent process, with the possible exception of providing an instability mechanism for spray and droplet formation. Even in the sonoluminescence studies of cavitation bubbles, surface tension only plays a minor role.

We specify two dimensionless parameters as follows. The stand-off,

$$\gamma = \frac{h}{R_m},$$

where h is the distance of bubble initiation from the boundary and R_m is the maximum bubble radius. The second parameter is the strength parameter

$$\alpha = \frac{p_0}{\Delta p}$$

which essentially determines the contribution to the internal bubble pressure due to noncondensable gaseous contents (where Δp , which scales the initial pressure, is the difference between the hydrostatic pressure at the location of bubble inception and the vapour pressure). The ‘gas’ inside is specified by an adiabatic polytropic exponent κ .

The computations follow a number of Lagrangian marker particles on the surface of the bubble in either the axisymmetric or fully 3D codes. For the axisymmetric code we use 31–64 particles on the surface and for the 3D code, 362. The particles give us a clear picture of the bubble shape and, furthermore, allow the calculation of the pressure field anywhere in the fluid or on the rigid boundary.

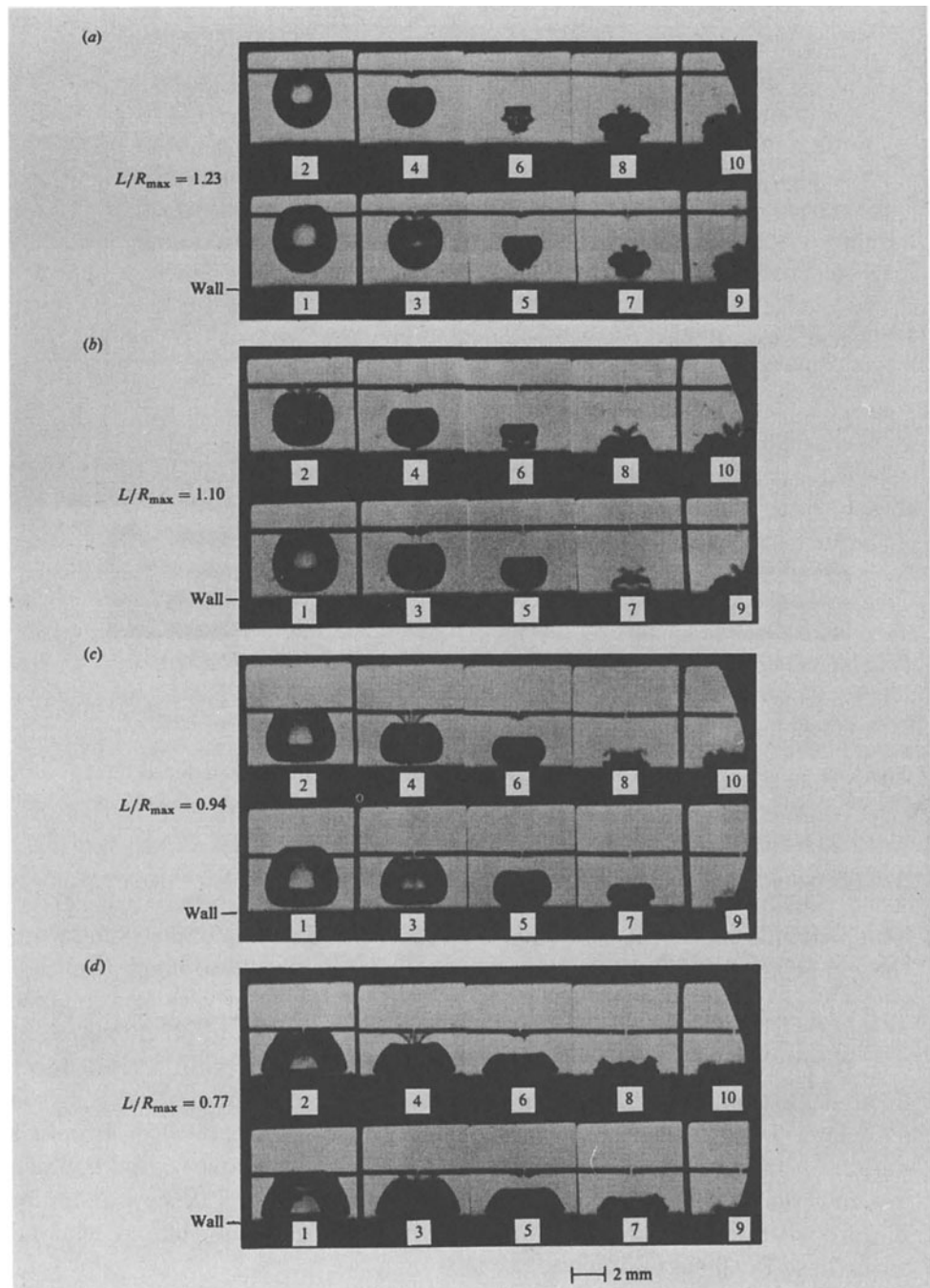


Figure 1. The collapse of spark-induced bubbles for (from top) $\gamma = 1.23, 1.10, 0.94, 0.77$; maximum bubble radius is 3.5 mm, frame interval is $10 \mu\text{s}$.

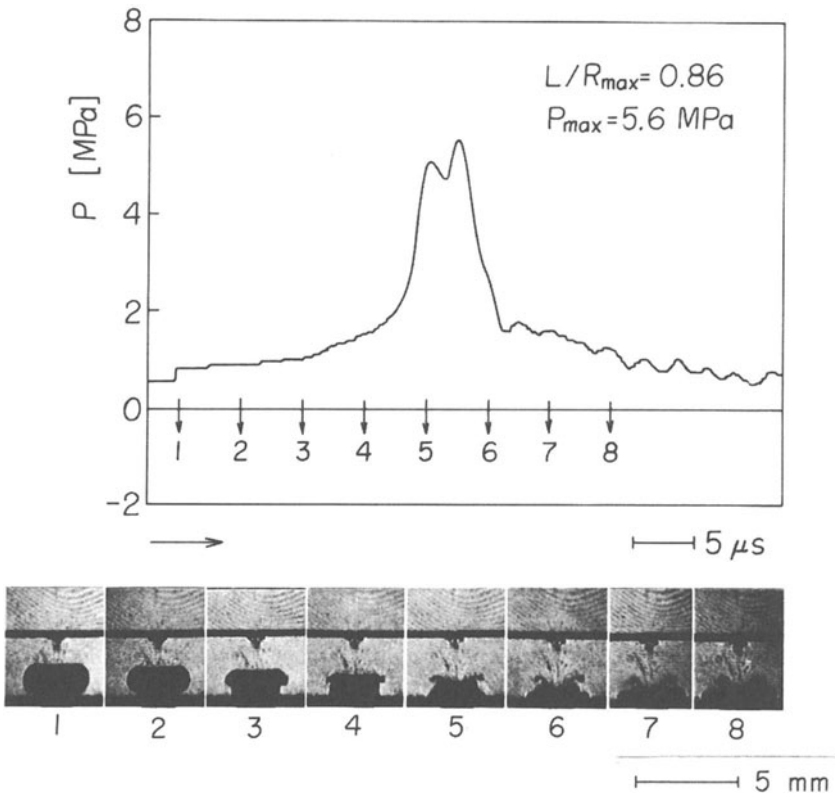


Figure 2. Pressure history on rigid boundary for collapse of spark-induced bubble with shadowgraphs of bubble shape; $\gamma = 0.86$, maximum bubble radius is 3.5 mm.

3. Experimental and computational studies

The principal motivation for the results presented in this paper come from the experiments of Tomita and Shima [7]. In Figure 1 we show the high speed photographic output for a series of studies on the growth and collapse of spark-induced bubbles near a rigid boundary for stand-off distances of $\gamma = 0.77, 0.94, 1.10$ and 1.23 . In Figure 2, the pressures on a transducer located on the axis of symmetry are recorded and compared against the associated bubble shapes for $\gamma = 0.86$. Jet impact occurs between frames 1 and 2, yet maximum pressures are registered between frames 5 and 6 which are an order of magnitude greater. Calculations for $\gamma = 1.0$ show a similar picture with peak pressures associated with bubble shapes that correspond with those in the experiments.

In Figure 3 we show the progressive changes in bubble shape for a collapsing bubble, following impact of the high speed liquid jet which occurs

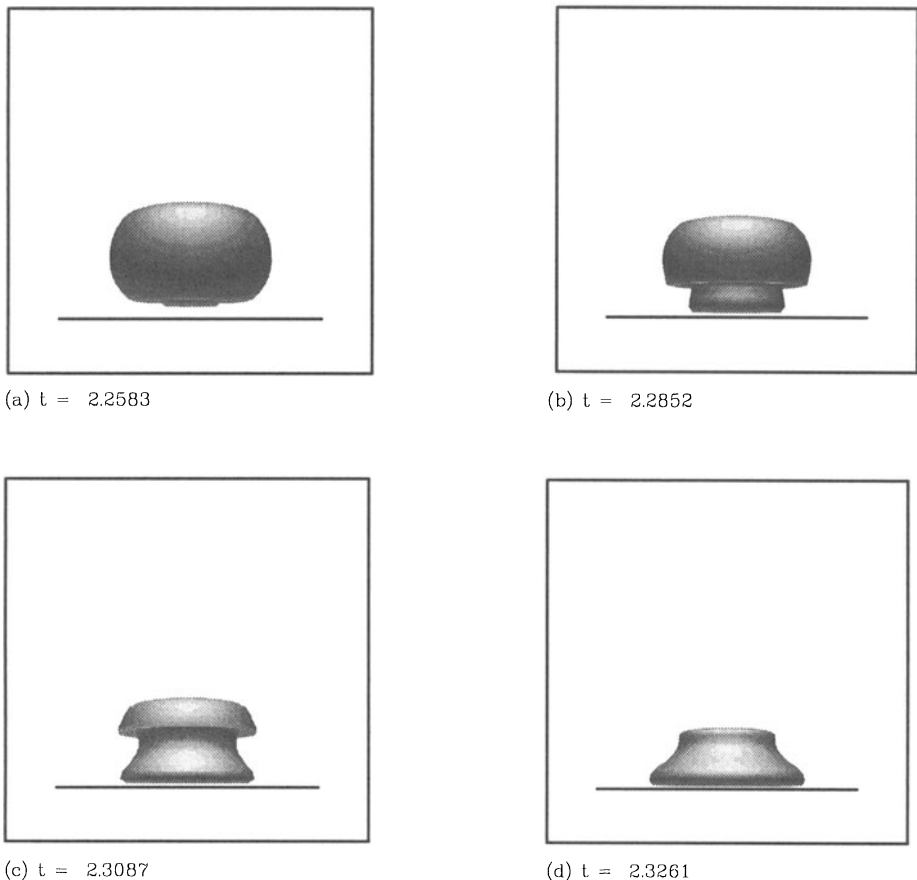


Figure 3. Computed collapse of a bubble near a rigid boundary; $\gamma = 1.0$, $\alpha = 100$, $\kappa = 1.4$.

late in the bubble collapse and through the generation of a toroidal bubble. The bubble minimum volume occurs shortly after frame 4 and the bubble proceeds to re-expand. The formation of a splash produces the ‘mushroom’ shapes in frames (b) and (c).

Figure 4 shows time history calculations for the pressure on the axis of symmetry at the rigid boundary. The key feature of this calculation is the twin-peaked pressure profile at bubble collapse, the first peak associated with the jet impact, the second with the minimum volume of the, by now, toroidal bubble. Clearly, the peak pressures for the toroidal bubble would occur on a ring rather than on the axis of symmetry.

Figures 5 and 6 show comparisons between theory and experiment for the upper and lower surfaces, jet velocity and ‘sideways’ jet velocity (or radial flow outwards from the jet axis along the boundary), for cavitation

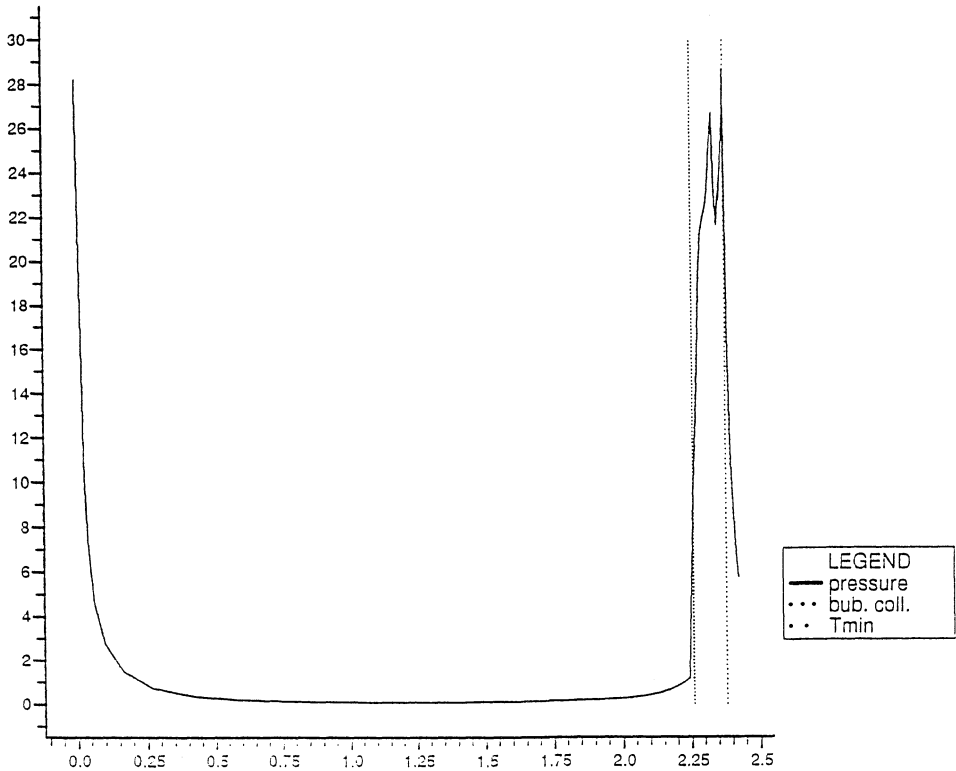


Figure 4. Computed pressures at rigid boundary on axis of symmetry.

bubbles, with stand-off values of $\gamma = 0.86$ and 1.41 [6]. For $\gamma = 0.86$ the bubble is generated by spark discharge and for $\gamma = 1.41$ by laser. The comparisons are remarkably favourable. In Figure 5 the jet velocity is 110 m/s, with sideways jet velocity 37 m/s. The computations produce a higher value for the sideways jet, but there is the possibility that the electrodes may have impeded the jet motion leading to a lower recorded velocity in the experiment. In Figure 6, the liquid jet velocity is observed to be 111 m/s, but because of the greater distance from the boundary there is little sideways motion, but rather a penetration towards the boundary.

Figure 6 attempts to unravel the physical behaviour of the toroidal bubble for a stand-off value of $\gamma = 1.0$ and this matches the experimental observations in Figure 2. Both the left and right hand pictures show the bubble shape, with the left hand one superimposing velocity vectors while the right hand one has pressure contours. The high pressure on the axis can be clearly seen at $t = 2.247$ (which is soon after jet impact) as can

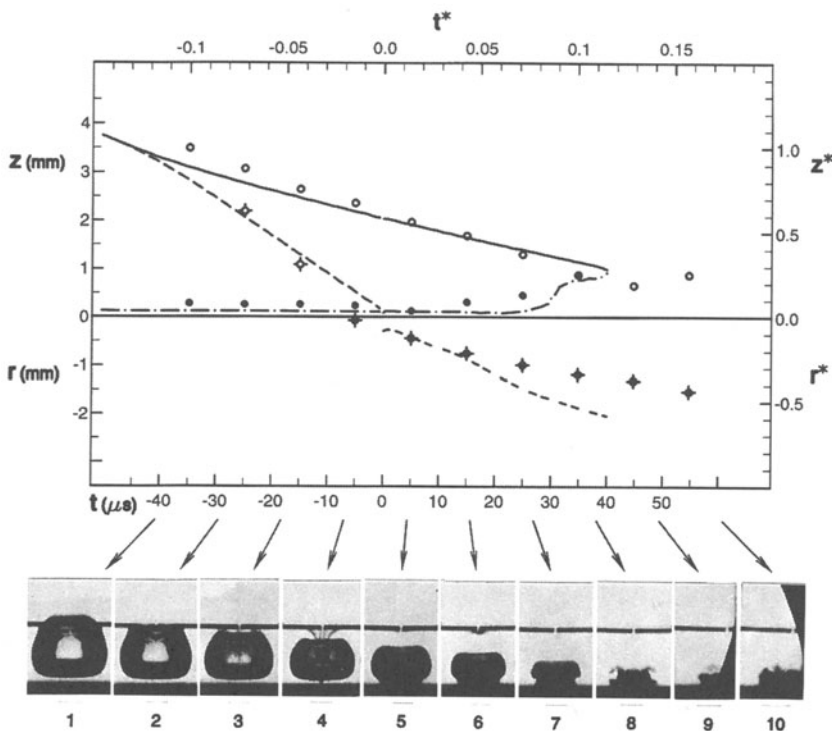


Figure 5. $\gamma = 0.86$; computed surface motion of upper (—) and lower (---) surfaces, jet (- - -) and 'sideways' jet (----) with experimental measurements (○, ●) and corresponding photographs of bubble shapes.

the early development of the splash for times $t = 2.258$ and above. Off-axis high pressures are evident for $t = 2.285$ and beyond, as indeed is the existence of an off-axis stagnation point in all the figures. It should be pointed out, though, that the highest recorded pressures are not on the boundary, but occur as the 'splash' impacts the upper part of the bubble. In some experimental studies, a shock wave appears to emanate from this location [8].

The understanding that has arisen from the calculations is that the vigorous stage of the 'splash' can enhance the pressures associated with the minimum volume. What remains to be done is a more specific analysis of this region in terms of the distribution between potential energy held within the bubble volume and the kinetic energy remaining in the flow, relating this to the internal gas pressure and that due to stagnation point flow.

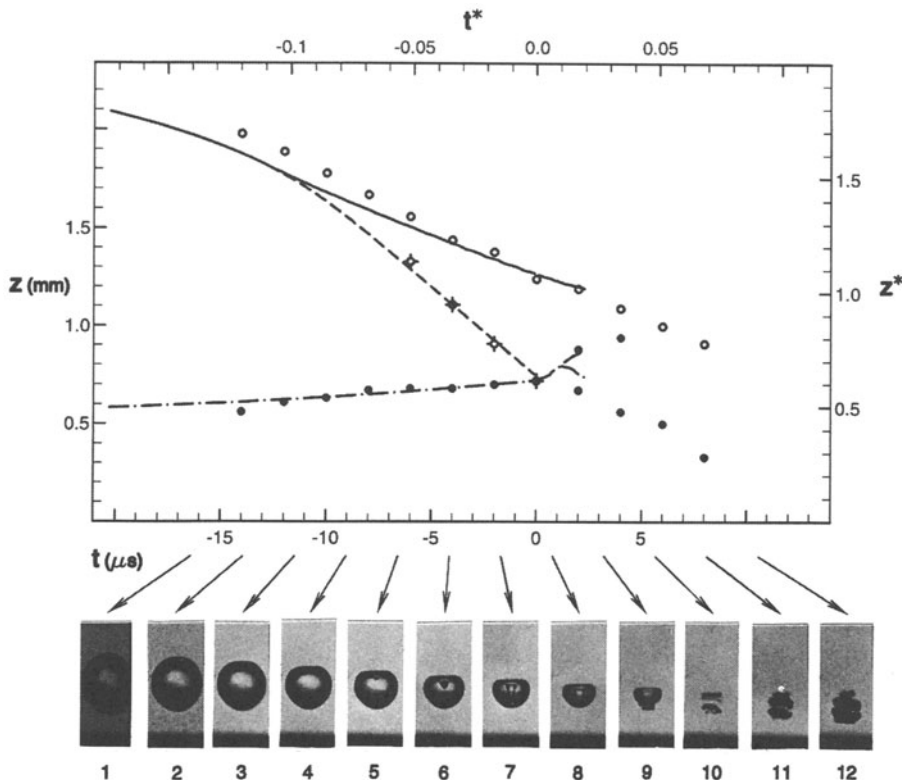


Figure 6. $\gamma = 1.41$; computed surface motion of upper (—) and lower (---) surfaces and jet (- - -) with experimental measurements (\circ , \bullet) and corresponding photographs of bubble shapes.

4. Conclusions

The above represents our preliminary calculations. What we now need is a more detailed experimental study with these or similar parameters to gain a better physical understanding of the relative importance of jet impact, the 'splash' phenomena and minimum volume pressures on the nature of the damage that might be expected due to the localised impact of cavitation bubbles near boundaries. It is hoped that the above representation will assist in the process of conducting further test studies with regard to identifying types of behaviour to be recorded that relate to the bubble phenomena, including jet impact.

Acknowledgements The research presented in this paper has been supported by DRA Dunfermline and DERA Fort Halstead. Professor Tomita is a Royal Society-Japan Society for Promotion of Science Visiting Research Fellow at The University of Birmingham for 1996/97.

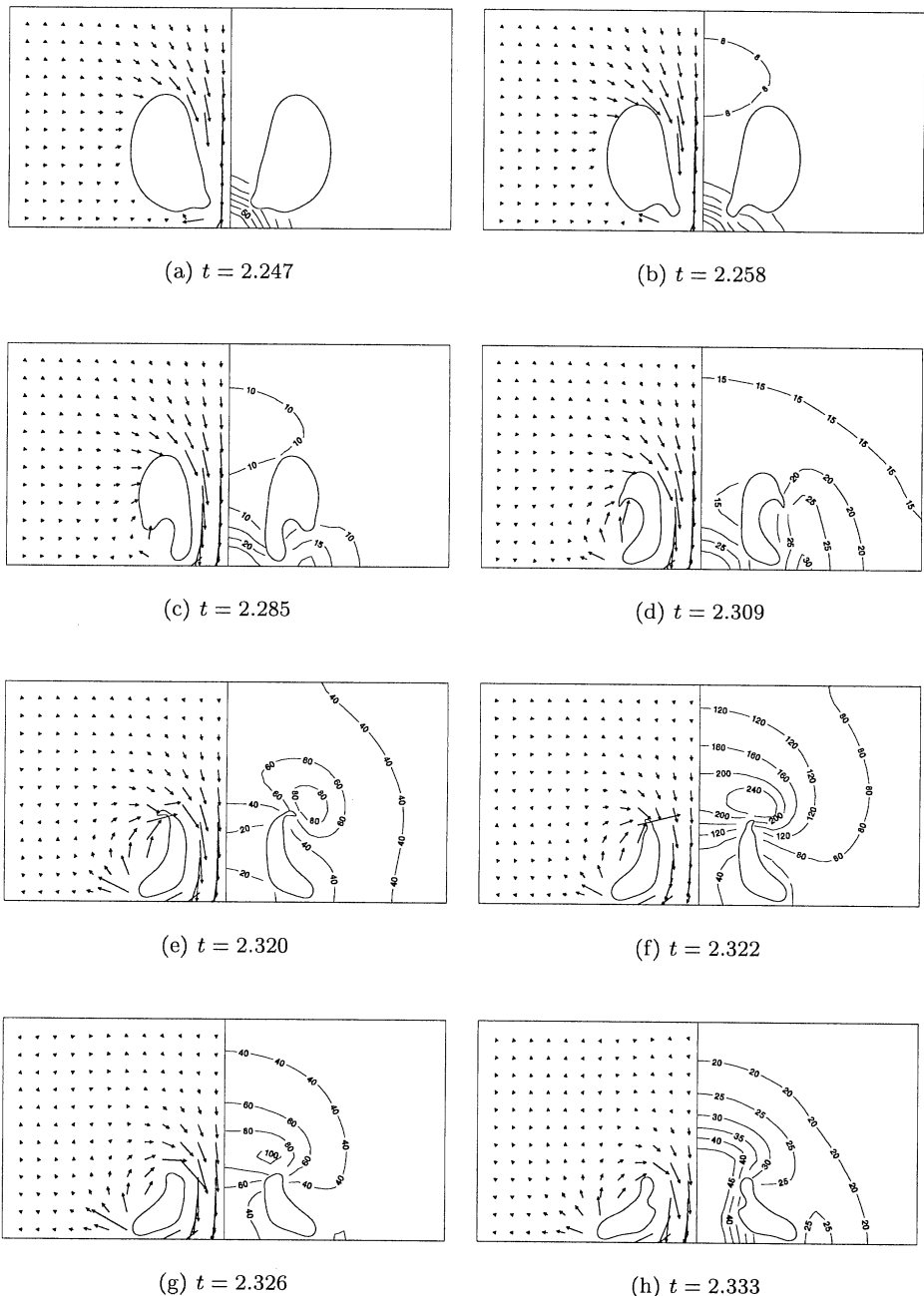


Figure 7. Velocity vectors and pressure contours for toroidal stage of bubble collapse for $\gamma = 1.0$, $\alpha = 100$, $\kappa = 1.4$.

References

1. Best, J. P. (1993) The formation of toroidal bubbles upon the collapse of transient cavities. *J. Fluid Mech.* **251**, 79–107.
2. Blake, J. R., Taib, B. B. and Doherty, G. (1986) Transient cavities near boundaries. Part 1. Rigid boundary. *J. Fluid Mech.* **170**, 479–497.
3. Blake, J. R., Taib, B. B. and Doherty, G. (1987) Transient cavities near boundaries. Part 2. Free surface. *J. Fluid Mech.* **181**, 197–212.
4. Blake, J. R. and Gibson, D. C. (1987) Cavitation bubbles near boundaries. *Ann. Rev. Fluid Mech.* **19**, 99–123.
5. Blake, J. R., Boulton-Stone, J. M. and Tong, R. P. (1995) Boundary integral methods for rising, bursting and collapsing bubbles. In H. Power (ed.) *BE Applications in Fluid Mechanics*, Computational Mechanics Publications, Southampton, pp.31–71.
6. Blake, J. R., Tomita, Y. and Tong, R. P. (1997) The art, craft and science of modelling jet impact in a collapsing cavitation bubble. Submitted to *Appl. Sci. Res.*
7. Tomita, Y. and Shima, A. (1986) Mechanisms of impulsive pressure generation and damage pit formation by bubble collapse. *J. Fluid Mech.* **169**, 535–564.
8. Tong, R. P., Schiffrers, W. P., Shaw, S. J., Blake, J. R. and Emmony, D. C. (1997) The role of ‘splashing’ in the collapse of a laser-generated cavity near a rigid boundary. Submitted to *J. Fluid Mech.*

ACOUSTIC CAVITATION AND MULTI BUBBLE SONOLUMINESCENCE

W. LAUTERBORN AND C. D. OHL

*Drittes Physikalisches Institut
Bürgerstr. 42-44, D-37073 Göttingen
Germany*

1. Introduction

Liquids can be ruptured by sound waves. The cavities thereby formed collect some gas dissolved in the liquid and start to oscillate in the sound field. In space they assemble to a dendritic filamentary pattern. In time this pattern (the set of individual bubbles) shows period doubling to chaotic motion and light emission (multi bubble sonoluminescence). This article reports on measurements pertaining to these topics.

2. Acoustic Cavitation

Acoustic cavitation can be produced in a variety of ways, with a vibrating "horn" dipping into a liquid or by vibrating the walls of a container. We use a hollow cylinder of piezoelectric material submerged in the liquid to be cavitated (Fig. 1). The cylinder has a length of 76 mm, an inner diameter of again 76 mm and a wall thickness of 5 mm. The resonance frequency for half a wavelength across the diameter of the cylinder is about 23 kHz, slightly depending on the container and the water height above the cylinder. When the cylinder is driven at this frequency (fundamental resonance), the maximum sound pressure and tension occur at the center of the cylinder. A second cylinder in use has a length of 45.5 mm and an inner diameter of 57 mm and is coated for cavitation resistance. Besides simply submerging the transducer into water, it also was used closed at both ends with PMMA plates and filled with water. In the latter configuration the water could be cavitated between 8 kHz and 18 kHz. A third cylinder, mostly used in the sonoluminescence studies, has a diameter of 6.5 cm and a length of 13 cm and is driven at 20 kHz.

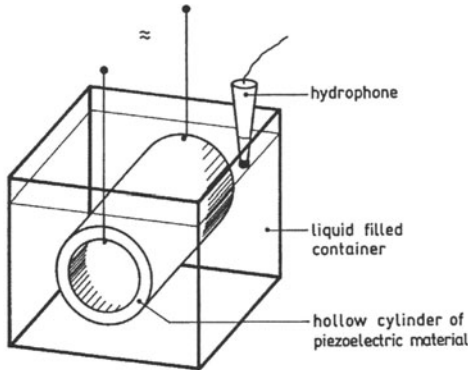


Figure 1. Cylindrical transducer of piezoelectric material to cavitate a liquid.

Beyond a certain threshold of the driving voltage applied to the cylinder a hissing noise is heard and bubbles start dancing around in the liquid. They form a branched structure ("streamers") also called acoustic Lichtenberg

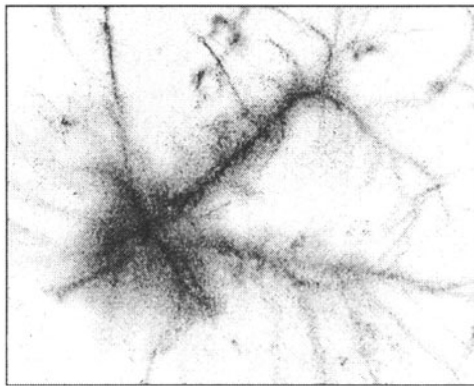


Figure 2. Filamentary structure of bubbles in acoustic cavitation. View along the axis of the cylinder. (Courtesy of A. Billo).

figures by us in reminiscence of the electric Lichtenberg figures. Never a homogeneous cloud of bubbles is observed. The bubbles always organize themselves into filaments. Figure 2 shows an example of this filamentary structure. Obviously a homogeneous distribution of bubbles in the presence of a strong sound field is unstable. This can also be shown theoretically [1]. The pattern formed itself seems to be unstable as it is steadily rearranging on a human time scale although being stable over at least hundreds of cycles of the driving sound field. The processes in the bubble cloud surely are very complex due to competing influences made up of attracting and repelling forces and due to the thousands of tiny interacting bubbles.

3. Period-doubled and Chaotic Bubble Oscillations

Acoustic cavitation bubbles are small and fast moving objects. To capture their dynamics in three-dimensional space a device is needed that records three-dimensional images in rapid succession (holographic cinematography). Such devices are involved, but have been built in the laboratory. Figure 3 shows one of our devices for high speed holographic cinematography. A maximum of 300 000 holograms per second has been reached with a capacity of a few thousand holograms [2]. The series of coherent light

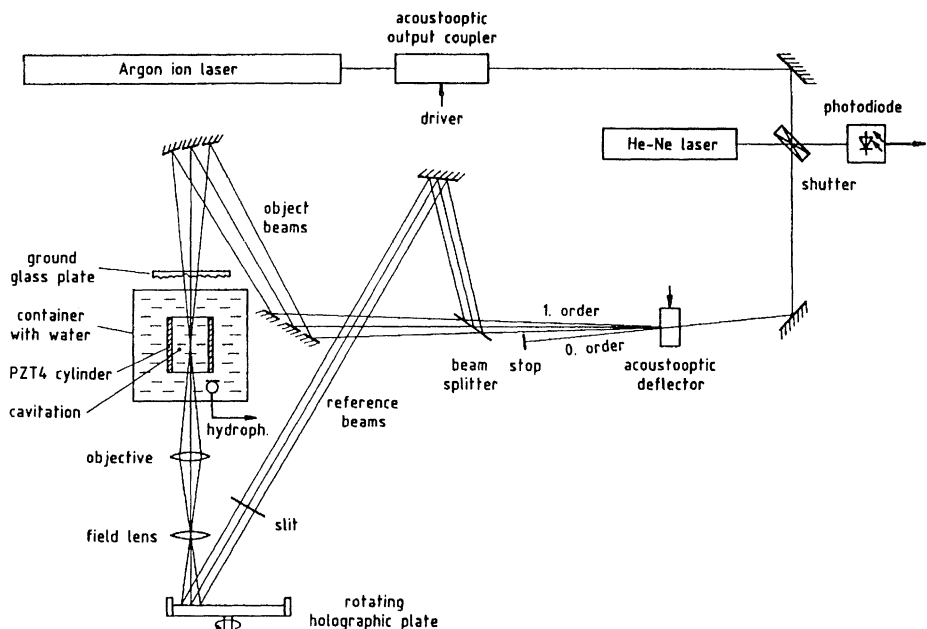


Figure 3. Arrangement for high speed holographic cinematography of acoustic cavitation bubble distributions [4].

pulses needed is delivered by a cavity-dumped argon ion laser. The pulses are deflected by an acoustooptic deflector into three different directions in a cyclic manner. Each pulse is split into object and reference beam and forms a hologram of the bubble distribution transilluminated by the object beam. The holographic plate is rotated at about 250 to 300 revolutions per second. This allows holograms of a few mm^2 in size to be taken at framing rates of about 70 000 holograms per second.

Figure 4 gives an example of a holographic series taken at 23 100 holograms per second of an acoustic cavitation bubble pattern driven at 23.1 kHz. Thus every cycle of the acoustic field a hologram is taken. At low driving the bubbles oscillate with the same period as the driving as shown in Fig. 4.

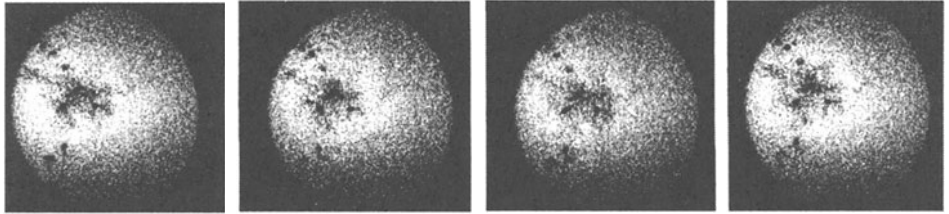


Figure 4. Reconstructed images from a holographic series taken at 23 100 holograms per second. Frequency of the driving sound field is 23.1 kHz. The bubble distribution repeats itself after one period of the driving. (Courtesy of A. Koch).

At higher driving period doubling sets in. Under suitable experimental conditions a period-doubling cascade to chaos is observed both acoustically with a hydrophone in the liquid [3] and optically with high speed holographic cinematography [4]. An example from the cascade is given in Fig. 5. The acoustic output shows period eight via the 1/8 line of the driving frequency in the acoustic Fourier spectrum. The resolution in the images is not high enough to discriminate this step of the period-doubling cascade, but period four is clearly visible. The period-doubling cascade leads to

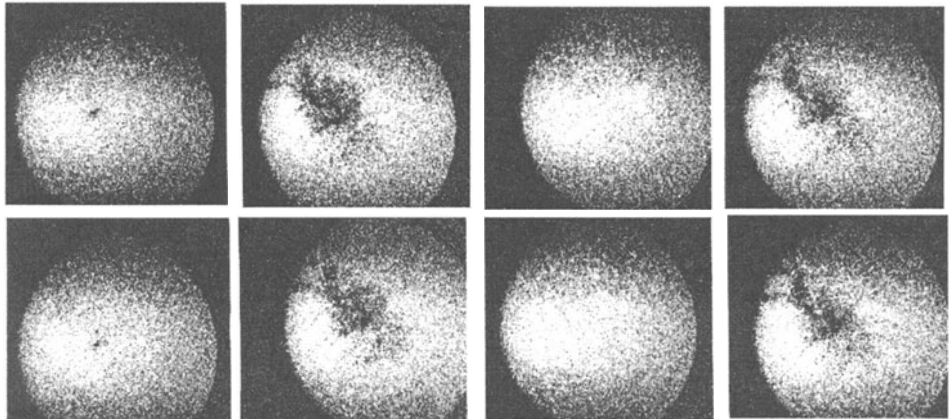


Figure 5. Reconstructed images from a holographic series taken at 69 300 holograms per second, where only every third hologram has been used for reconstructing the images. Frequency of the driving sound field is 23.1 kHz. (Courtesy of A. Koch).

chaos, i. e., aperiodic bubble oscillations despite of periodic driving, when the driving sound field amplitude is increased further. Chaotic bubble oscillations have also been observed holographically. Figure 6 gives an example. This time the images from successive holograms have been reconstructed to also show the intermediate bubble sizes during the oscillation cycle. On one frame a shock wave is seen radiated from a bubble upon strong collapse.

It is nicely captured because of the short duration of the laser illumination pulses of about 30 ns.

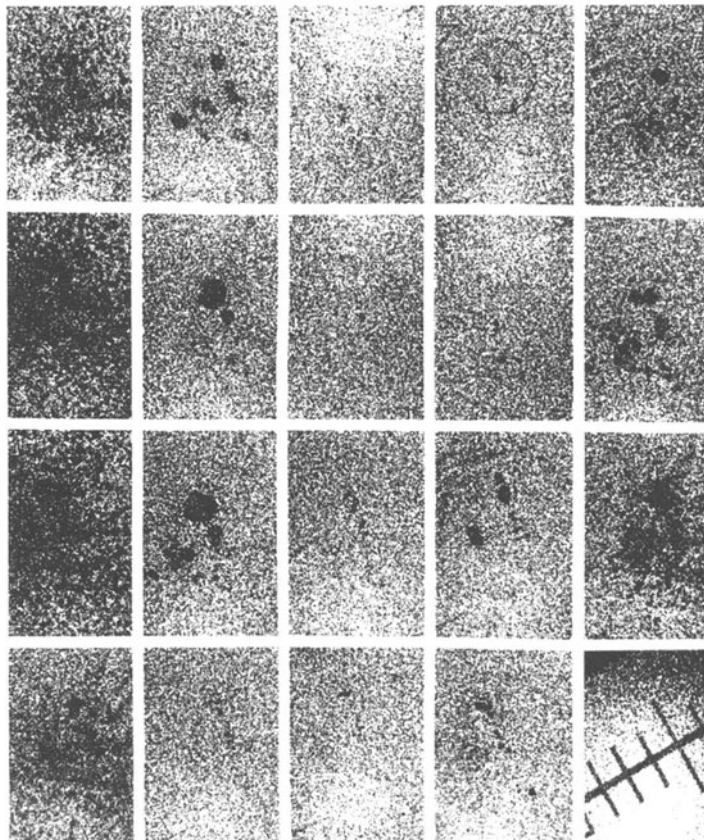


Figure 6. Reconstructed images from a holographic series taken at 69 300 holograms per second. Distance of bars in the scale is 1 mm. Frequency of the driving sound field is 23.1 kHz. (Courtesy of A. Koch).

4. Multi Bubble Sonoluminescence

When the cavitation bubble pattern is observed in total darkness with the dark adapted eye, light can be seen emanating from the liquid (multi bubble sonoluminescence). The faint light emitted can be photographed with a CCD camera equipped with a micro channel plate as "light intensifier" (ICCD = Intensified CCD). Figure 7 shows an image of the interior of a piezoelectric cylinder (this time of diameter 6.5 cm, length 13 cm) driven at 20 kHz as it appears in its own light emitted. Again a filamentary structure is seen. Moreover, it has been found that light is only emitted in a small

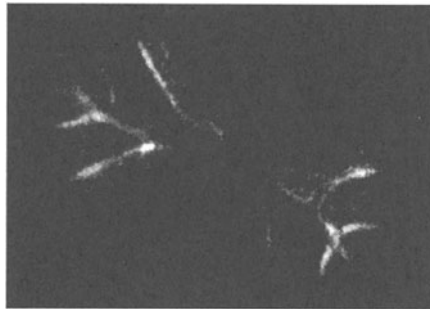


Figure 7. Multi bubble sonoluminescence as seen by an ICCD camera.

window of the driving phase comprising about 1/12th the period of the driving (Fig. 8).

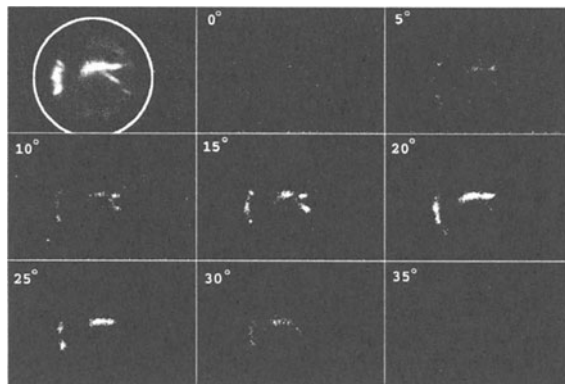


Figure 8. Multi bubble sonoluminescence at 120 kPa and 20 kHz. The first image shows the integrated light emission over 60 seconds. The other images are time gated ones with a gating time of 300 ns at the indicated phases (reference arbitrary).

A certain minimum sound pressure amplitude is needed for the filamentary structure to appear. However, it has been found that there is also an upper threshold where the filaments cease to exist and light is emitted from just one center. Figure 9 shows this bifurcation or phase change in the bubble structure in a sequence of sonoluminescence images that appear at different voltages applied to the cylinder, the light being integrated over many seconds. The luminescence starts localized (here at 180 V). Soon filaments form at higher voltages (190 V, 195 V) and a large area of the liquid is involved in the light emission. At still higher driving the emission shrinks to a single stable emission center (200 V). This center starts to move around in the liquid (210 V) giving the integrated appearance of a large quite unstructured emission region. Below (Fig. 10) time resolved measurements

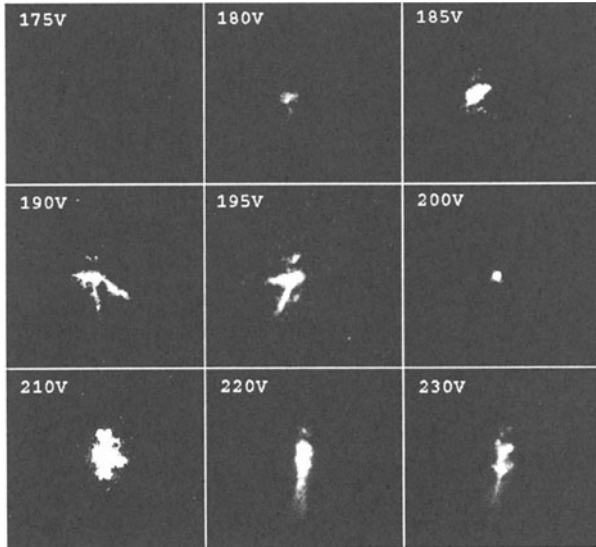


Figure 9. Integrated sonoluminescence images at 20 kHz and different driving voltages. Frame size is 3.4 cm × 3.7 cm.

are given to underpin this interpretation. At still higher driving the emission center splits up into two and again a richer structure appears (220 V, 230 V). This sequence has been obtained reproducibly, whereby changes in the actual values of the voltages may occur.

Noteworthy is the appearance of a single stable emission center and its motion at higher driving. Figure 10 shows time resolved images of the dancing emission center. A possible explanation resorts to the strong non-

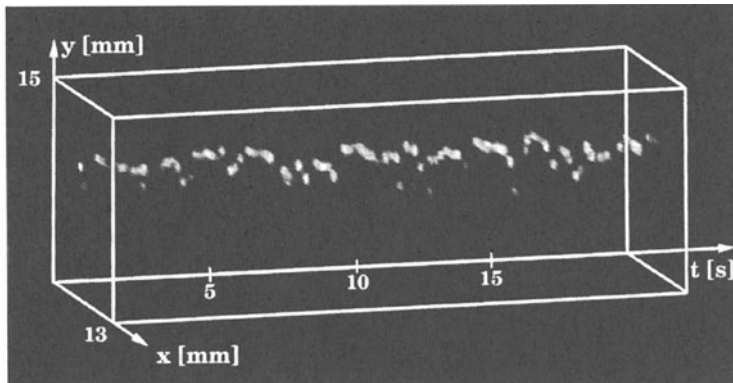


Figure 10. Luminescence images in the course of time in the dancing bubble regime.

linearity of the bubble oscillation. It has been found that a small bubble

can be kept stable in the pressure antinode only in the case of not too large nonlinearity in the oscillation of the bubble [5]. Otherwise the attracting primary Bjerknes force turns repelling and the bubble gets positionally unstable. The bubble thus has to leave the high pressure - high tension region. When it does so, it experiences a lower amplitude of the driving and also lowers its oscillation amplitude. The repelling force then ceases. In a rotationally symmetric system the bubble would settle somewhere away from the maximum sound pressure amplitude on some surface, being free to move along it upon slight additional disturbances. That way the seemingly irregular spatial motion observed in Fig. 10 may be explained.

Irregular motion has also been found by Holt *et al.* [6] in purposely single bubble sonoluminescence experiments by looking at the flash intervals. However, their conjectural explanations do not comprise translational spatial motion as observed here and also in motion studies of nonsonoluminescing bubbles in stationary sound fields [7].

5. Acknowledgments

We thank R. Blatt for loan of and H.-C. Nägerl for help with the ICCD camera to photograph the light emitted by the bubbles and the Cavitation Group at Göttingen for help leading to the level of sophisticated experimentation reported here. The work has been sponsored by the Deutsche Forschungsgemeinschaft, Bonn.

6. References

1. Akhatov, I., Parlitz, U. and Lauterborn, W. (1996) Towards a theory of self-organization phenomena in bubble-liquid mixtures, *Phys. Rev. E* **54**, 4990-5003.
2. Hentschel, W. and Lauterborn, W. (1985) High speed holographic movie camera, *Opt. Eng.* **24**, 687-691.
3. Lauterborn, W. and Cramer, E. (1981) Subharmonic route to chaos observed in acoustics, *Phys. Rev. Lett.* **47**, 1445-1448.
4. Lauterborn, W. and Koch, A. (1987) Holographic observation of period-doubled and chaotic bubble oscillations in acoustic cavitation, *Phys. Rev. A* **35**, 1974-1976.
5. Akhatov, I., Mettin, R., Ohl, C.-D., Parlitz, U. and Lauterborn, W. (1997) Bjerknes force threshold for stable single bubble sonoluminescence, *Phys. Rev. E* **55**, 3747-3750.
6. Holt, R. G., Gaitan, D. F., Atchley, A. A. and Holzfuss, J. (1994) Chaotic sonoluminescence, *Phys. Rev. Lett.* **72**, 1376-1379.
7. Crum, L. A. and Eller, A. I. (1970) Motion of bubbles in a stationary sound field, *J. Acoust. Soc. Am.* **48**, 181-189.

PARTICLE DRIFT NEAR AN OSCILLATING CAVITY

A new approach to sonoluminescence

MICHAEL LONGUET-HIGGINS

Institute for Nonlinear Science

University of California, San Diego

La Jolla, CA 92093-0402

Abstract. Different mechanisms for the generation of light by a sonoluminescent bubble have been proposed, which involve the shape of the bubble near the time of its minimum radius. Since the shape is difficult to observe directly, the author has suggested obtaining further information by studying the drift motions in the fluid surrounding the bubble, which should be observable out to distances of many times the bubble radius. In this paper two theoretical models are considered. In one, a spherical cavity oscillates both radially and laterally, with amplitude comparable to the mean radius of the bubble. This is shown to produce steady drift motions having the form of an axial dipole flow. The strength of the dipole, however, is many times smaller than that seen in recent observations. In the second model the bubble is assumed to collapse asymmetrically, with one wall hitting the opposite wall at high velocity. This again produces a dipole flow in the far field, and the strength of the flow is compatible with that observed.

1. Introduction

Single bubbles stimulated by intense acoustic radiation are of considerable interest on account of their ability, under suitable conditions, to emit regular pulses of light [1]. There is however more than one proposed mechanism. Moss et al. [2] and Wu and Roberts [3] and others have assumed that the bubble remains essentially spherical during collapse, while Prosperetti [4] and Longuet-Higgins [5] have suggested that it may (indeed must) become asymmetric during collapse. At its minimum volume, the shape of the bubble is difficult to observe directly. Accordingly the present author [5] suggested obtaining further information concerning the shape and the type of oscillation of the bubble by observing the drift motions in the water

surrounding the bubble, which should extend outwards to many times the mean radius of the bubble.

Lepoint-Mullie et al. [6] have observed such drift motions, of which an example is shown in Figure 1. In their experiment, conducted in a weak solution of Weissler's reagent, a sonoluminescent bubble suspended near the antinode of a standing sound wave was seen to emit a thin streak of dye extending to distances of the order of 1 cm. How can this be explained? Since the initial motion of the dye was downwards, thermal effects seem unlikely to be the cause.



Figure 1. (from Lepoint-Mullie et al.). Observed stream of dye from an oscillating bubble. Width of frame: 2 cm.

The purpose of the present paper is to construct some simple theoretical models illustrating the phenomenon of streaming, that is to say the steady drift motion associated with an oscillating flow. In the first example (Sections 2 to 3) we consider the streaming induced by a perfect spherical cavity which pulsates radially and simultaneously oscillates vertically, in response to buoyancy forces. Viscosity is entirely neglected. The fluid motion

being very simple, a marked particle of fluid may be tracked by numerical integration of the velocity field. We find that the mean particle paths are similar, in the far field, to the streamlines of a steady, axisymmetric dipole. Even with large-amplitude oscillations, however, the strength of its dipole is many orders of magnitude less than that observed.

In a second calculation (Section 5) the bubble is assumed to collapse asymmetrically, a jet erupting inwards and striking the opposite wall of the bubble. It is shown that each impact produces a dipole displacement in the far field. With reasonable assumptions regarding the impact velocity, the order of magnitude of the mean drift can be estimated, and it is found to be consistent with that observed. Moreover the expected thickness of the dye streak, which is related to the rate of diffusion of the dye near the bubble, is also consistent with observation.

The present paper is essentially an abbreviated version of Ref. [7], to which reference is made for some of the details.

2. Drift motions induced by an oscillating sphere

Consider first a sphere pulsating with purely radial oscillations in an unbounded, uniform fluid. Assuming that no mass is transferred across the surface of the sphere, then by continuity the net radial displacement of a particle must be zero; there is no drift.

Next consider a sphere executing purely lateral oscillations (Figure 2). The flow being irrotational, it is determined uniquely by the normal velocities at the spherical boundary and the motion at infinity. As regards the drift, there will be no difference if we consider the sphere to be at rest and the motion at infinity to be a uniform stream whose direction periodically changes in direction (Figure 3). In this situation it is obvious that a particle will simply travel to and fro along the same streamline and its mean displacement will again be zero.

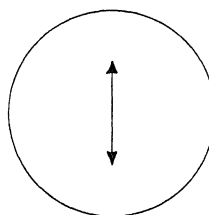


Figure 2. A bubble in purely lateral oscillation, in a stationary reference frame.

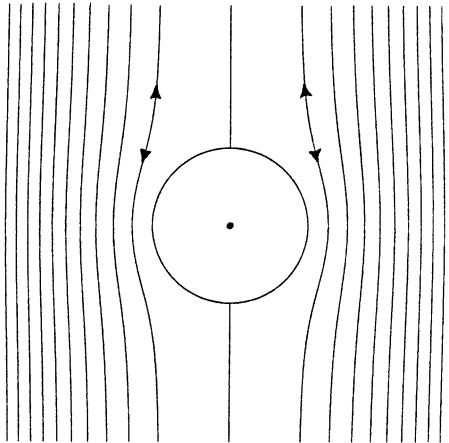


Figure 3. Oscillatory flow around a stationary bubble.

We next enquire what is the outcome if we add a lateral oscillation to a radial oscillation. Does this produce a steady streaming?

Adopting the notation of Figure 4: let us consider the motion induced by a spherical bubble of radius $R(t)$ (t denotes time) whose centre C is at a varying height $h(t)$ above the fixed origin O . ρ and z denote the cylindrical coordinates of a typical point P in the fluid. The sphere is assumed to have two distinct motions: a radial “breathing” oscillation: in which the velocity potential is given by

$$\phi_1 = -\frac{R^2}{r} \frac{dR}{dt} \quad (1)$$

where $r = [\rho^2 + (z - h)^2]^{1/2}$, and a vertical translation given by

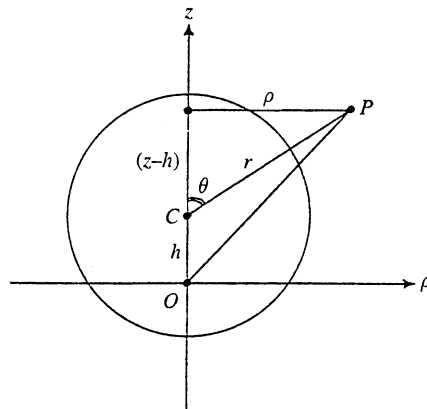


Figure 4. Notation and axes for an oscillating spherical bubble.

$$\phi_2 = -\frac{R^3(z-h)}{2r^3} \frac{dh}{dt}. \quad (2)$$

It can be shown that the combined potential $\phi = \phi_1 + \phi_2$ satisfies the kinematic boundary condition that the normal velocity relative to the surface of the sphere shall vanish. No dynamical boundary condition is imposed.

The path of a given particle can be traced by numerically integrating the two equations

$$\frac{d\rho}{dt} = \frac{\partial\phi}{\partial\rho}, \quad \frac{dz}{dt} = \frac{\partial\phi}{\partial z} \quad (3)$$

with respect to the time t , given the functions $R(t)$ and $h(t)$. For simplicity it is assumed that

$$R(t) = a(1 + \alpha \sin t), \quad h(t) = a\beta \sin(t + \gamma) \quad (4)$$

where a is the mean radius of the sphere and, α , β and γ are constants. The initial coordinates of a particle, at time $t = 0$, are taken to be

$$\rho(0) = a(1 + \delta) \cos \theta_o, \quad z(0) = a(1 + \delta) \sin \theta_o \quad (5)$$

where δ and θ_o are given constants.

A typical trajectory is shown in Figure 5. The two dashed circles indicate the maximum and minimum radii of the sphere. The circular plots mark the position of the particle after an integral number of cycles. Clearly the

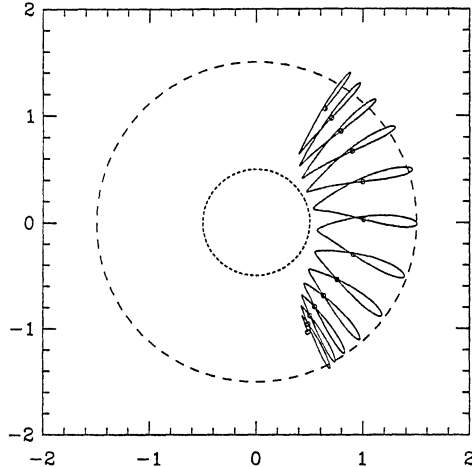


Figure 5. Trajectory of a marked particle when $\alpha = 0.5$, $\beta = 0.2$ and $\gamma = 60^\circ$, with initial starting point given by $\delta = 0.1$, $\theta_o = 20^\circ$.

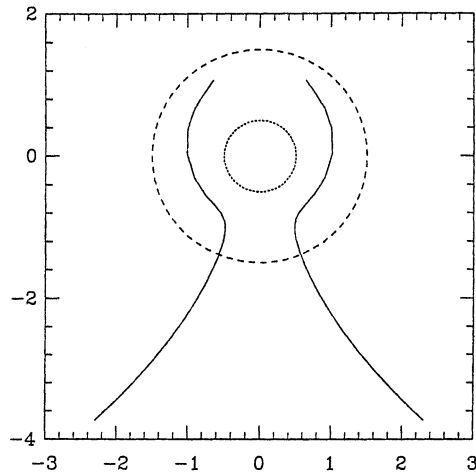


Figure 6. Locus of the circular plots in Figure 5, after 400 complete cycles, and its image in the axes of symmetry.

particle has a net downward drift. The locus of the circular plots after 400 cycles is shown in Figure 6 and a combination of several such trajectories is shown in Figure 7. Particles with initial positions in the upper part of the fluid drift relatively quickly to a corresponding point in the lower part. They then branch outwards, away from the axis of symmetry.

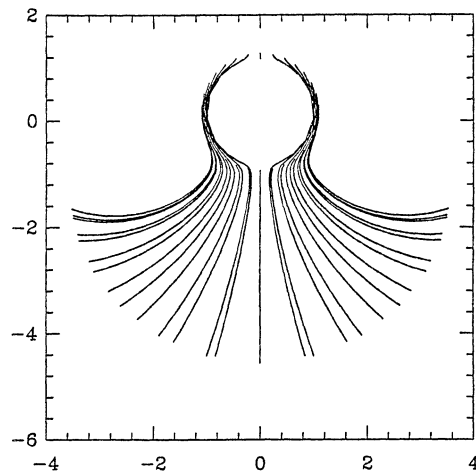


Figure 7. The set of mean trajectories corresponding to Figure 5, having starting points given by $\delta = 0.1$, $\theta_o = 12^\circ$, $m = -15$ to 15 .

3. Comparison to a dipole

It may be verified (Ref. [7]) that the particle trajectories and drift velocities in the outer part of the flow are very close to the streamlines in an axisymmetric dipole, as described by the velocity potential

$$\Phi = \frac{S \cos \theta}{2r^2}. \quad (1)$$

Here S denotes the strength of the dipole. Typical streamlines are shown in Section 7. S will depend on the mean radius a of the dipole, the amplitude αa of the radial pulsation, on the amplitude $b = \beta a$ of the vertical oscillation, and on the relative phase angle γ . As result of many numerical calculations it was found that at relative amplitudes α comparable to unity the effective dipole strength of the drift motion was given approximately by

$$S = 1.5 f a^3 \sin \gamma \quad (2)$$

where f denotes the frequency of oscillation. Note that this expression indicates that S is practically independent of α , the relative amplitude of the radial pulsation, at large amplitudes.

The equation of a typical streamline in Figure 8 is

$$r = L \cos^2 \theta \quad (3)$$

where the constant L equals the maximum horizontal excursion of a particle

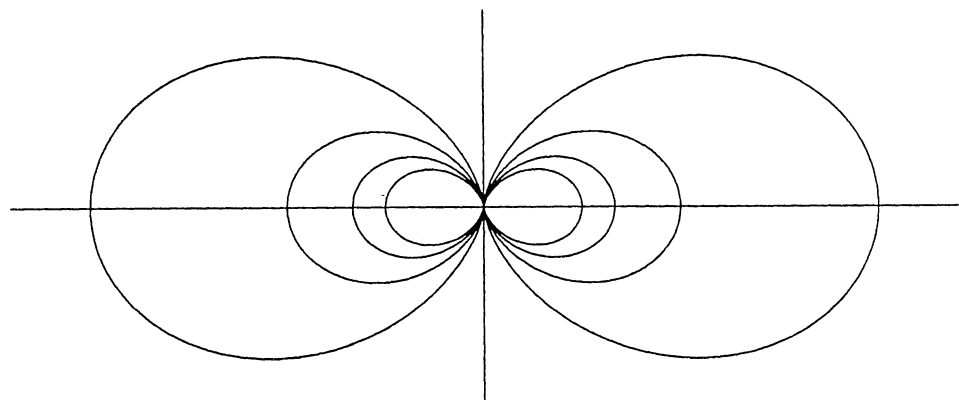


Figure 8. Streamlines in a steady axisymmetric dipole.

from the axis of symmetry, where $\theta = \pi/2$. The time t for a particle to travel from the axis to this point is related to the dipole strength S by

$$t = 0.914 L^4/S \quad (4)$$

(see Section 7 of Ref. [7]).

Note that the streamlines (4.3) are not circles as in a plane dipole, but instead are more elongated in the ρ -direction. Near the origin it can be shown that

$$\rho \sim (z^2/L)^{1/2}, \quad (5)$$

so that the gradient $d\rho/dz$ behaves as $z^{1/2}$. Hence the curvature at the origin is infinite, and any streamline close to the axis of symmetry and not coincident with it tends to bend away sharply at some small distance from the origin.

4. Comparison with observation

In a singly sonoluminescent bubble the minimum radius is only a small fraction of the maximum radius, so that α is approximately unity. The maximum vertical displacement of the center, according to the numerical calculation of Prosperetti [4], is of the order of a tenth of the maximum radius, and hence in equation (2) of Section 4, b is of order $0.1a$ where a is the mean bubble radius. The phase γ appears to be about 160° . In the observations of Lepoint-Mullie et al. [6] the frequency f was 24.1 kHz. The bubble radius was not measured, but a typical value for the mean radius would be $a = 20 \times 10^{-4}$ cm. On substituting these values in equation (2) of Section 4 we obtain

$$S = 2 \times 10^{-8} \text{ cm}^4/\text{s} \quad (1)$$

On the other hand from Figure 1 the lateral dimension L of the observed trajectory is of order 1 cm, and the time t to reach a portion opposite the bubble was less than 10 s. So, if the flow was a dipole we have from equation (4) of Section 3,

$$S > 0.914 L^4/t = 0.09 \text{ cm}^4/\text{s} \quad (2)$$

which is several orders of magnitude greater than (1).

In the next Section we shall consider the possibility that the bubble collapses asymmetrically.

5. Asymmetric collapse

In the typical boundary-integral calculation reported by Prosperetti ([4] Figure 2) a bubble of equilibrium radius 20 μm subjected to an oscillating pressure of frequency 20 kHz and amplitude 1 bar collapsed asymmetrically; the final shape of the bubble before internal contact between the opposite walls is shown in Figure 9.

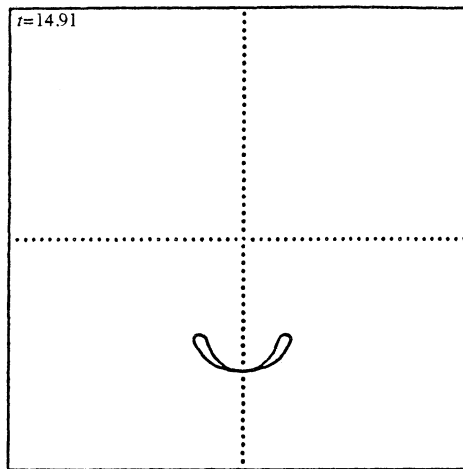


Figure 9. (from Prosperetti 1996). Final shape of a collapsed bubble of equilibrium radius 20 μm subject to an oscillating pressure field of amplitude 1 atm. and frequency 20 kHz.

Let us assume that marked asymmetry first begins when the mean radius a is about 4 μm and that the upward velocity of the lower bubble wall is 400 m/s and that the downward velocity of the jet on impact is three times this value, that is 1,200 m/s. Immediately following impact, the velocity of the jet may be reduced to a value V of about 400 m/s. If the jet continues for some time Δt , then the total momentum injected into the fluid is of order

$$I = \pi a^2 V^2 \Delta t. \quad (1)$$

Now a spherical mass of fluid of radius b travelling with velocity V' induces a dipole flow of strength

$$S = b^3 V' = \frac{3}{4\pi} I' \quad (2)$$

where I' is the total momentum of the spherical mass. If we equate I and

I' in equations (1) and (2) we obtain

$$S = \frac{3}{4}a^2V^2\Delta t. \quad (3)$$

Let us assume that the duration Δt corresponds to the time taken for the toroidal bubble to recover sufficiently to pinch off the axial flow through its center. This time may be taken as some fraction, say one tenth, of the natural period of oscillation of the bubble, which is typically $\frac{1}{50}$ of the period of the applied pressure. Hence we have

$$\Delta t = \eta f^{-1} \quad (4)$$

with η of the order 2×10^{-3} . But the injection of momentum from the jet occurs with frequency f . Therefore if τ denotes the dissipative decay-time for the dipole motion, i.e. each pulse decays like $e^{-t/\tau}$ we shall have for the dipole constant of the sustained motion

$$S = S_1(1 + \lambda + \lambda^2 + \dots) = \frac{S_1}{1 - \lambda} \quad (5)$$

with $\lambda = e^{-t/\tau} = e^{-1/f\tau}$. If $f\tau$ is sufficiently large then (3) can be approximated by $S_1 f \tau$. Hence from equations (3) and (4)

$$S = \frac{3}{4}a^2V^2\eta\tau. \quad (6)$$

Consider the influence of viscosity on the form of the jet. The radial distance r of fluid affected will be of order $(\nu/f)^{1/2}$, where ν denotes the kinematic viscosity. Since ν is about 1.0×10^{-2} , cm²/sec this gives $r = 6 \times 10^{-3}$ cm compared to the initial radius a of the jet, which is 2×10^{-4} cm. Thus the jet will have time to accumulate some mass from the surrounding fluid. During this process, however, the total momentum must be conserved, apart from that convected away by vortex rings; see [5]. Hence the total dipole moment of the exterior flow will not be greatly affected.

A time-constant τ equal to 1.0 sec, say together with the assumed values of a , V and γ , would yield

$$S = 0.10 \text{ cm}^4/\text{sec}, \quad (7)$$

compared to the observed value in equation (2) of Section 4.

To show that our estimate of the time-constant is reasonable, consider the viscous decay-rate of a theoretical dipole. The kinetic energy E of the fluid outside a radius $r = b$ is of order S^2/b^3 , which tends to infinity as $b \rightarrow 0$. We may suppose b to be the radius of the core region strongly affected

by viscosity over a time of order τ , the assumed period of decay. Thus for laminar flow b is of order $(\nu\tau)^{1/2}$. The rate of dissipation D of kinetic energy of the fluid in the region $r > b$, where the motion is irrotational, is of order $\nu S^2/b^5$, so the exterior motion has a decay-rate

$$\tau = E/D = O(b^2/\nu) \quad (8)$$

consistent with our assumption. If we choose $\tau = 1.0$ sec, it implies that the core region has a radius b of order 0.1 cm. This may be compared with the initial distance $V\Delta t$ traveled by the jet which would be 3×10^{-3} cm. Moreover, 0.1 cm is comparable to the thickness of the streak of dye which is seen to emanate from the oscillating bubble.

6. Conclusions

We have discussed two simple models of a sonoluminescent bubble in which the tangential stresses at the surface of the bubble are ignored. By direct numerical integration of the velocity field we have shown that a perfectly spherical bubble undergoing both radial and lateral oscillations produces drift motions given by the velocity potential Φ of Section 3, equations (1) and (2), but when this expression is applied to the case of a typical sonoluminescent bubble it gives results that are less than the observed drift by about seven orders of magnitude.

On the other hand if the bubble is assumed to collapse asymmetrically according to the model of Section 5, then the dipole flow so generated is quite comparable to that observed. Thus the evidence so far favours asymmetric collapse.

In both the above models, however, the generating mechanism for the particle drift is essentially inviscid. Viscous effects will be considered more fully in the paper to follow [8].

References

1. Gaitan, D.F., Crum, L.A., Church, C.C. and Roy, R.J. (1992) Sonoluminescence and bubble dynamics for a single, stable cavitation bubble. *J. Acoust. Soc. Amer.* **91**, 3166-3183.
2. Moss, W.C., Douglas, D.B., White, J.W., and Young, D.A. (1996) Hydrodynamic simulations of bubble collapse and picosecond sonoluminescence. *Phys. Fluids* **6**, 2979-2985.
3. Wu, C.C., and Roberts P.H. (1994) A model of sonoluminescence. *Proc. R. Soc. Lond. A* **445**, 323-349.
4. Prosperetti, A. (1997) A new mechanism for sonoluminescence. *J. Acoust. Soc. Amer.* **101**, 2003-2007.
5. Longuet-Higgins, M.S. (1996) Shedding of vortex rings by collapsing cavities, with application to single bubble sonoluminescence. *J. Acoust. Soc. Amer.* **100**, 2678 (Abstract).

6. LePoint-Mullie, F., LePoint, T., and Henglein, A. (1997) Sonochemistry and sono-luminescence in single bubbles. (personal communication)
7. Longuet-Higgins, M.S. (1997) Particle drift near an oscillating bubble. *Proc. R. Soc. Lond. A* **453**, 1551-1568.
8. Longuet-Higgins, M.S. (1998) Viscous streaming near a pulsating and oscillating spherical cavity. (this volume, pp.117-126)

VISCOUS STREAMING NEAR AN OSCILLATING AND PULSATING SPHERICAL CAVITY

MICHAEL LONGUET-HIGGINS

Institute for Nonlinear Science

University of California, San Diego

La Jolla, CA 92093-0402

Abstract. This paper considers theoretically the viscous streaming from a spherical bubble undergoing small lateral and radial oscillations simultaneously. Assuming the oscillations are of comparable magnitude, it is shown that the radial oscillations greatly enhance the streaming. The form of the flow at large distances is a “Stokeslet”, a steady viscous flow which may however take some time to establish. The sign of the streaming depends on the phase-difference between the two types of oscillation. It should reverse in direction if the phase-difference passes through zero.

1. Introduction

This paper continues the study of the drift motions around an oscillating and pulsating cavity, which was initiated in Refs. [1-3]. For motivation in relation to sonoluminescence, see the preceding paper in this volume.

In the two theoretical models described in Refs. [2] and [3] the amplitude of oscillation was assumed to be fully nonlinear, but the viscosity of the fluid was either neglected, as in the first model, or played a role only in the damping of the drift motion, in the second. In the model to be described here, the viscosity of the water is taken into account fully, but in order to obtain an analytic solution the amplitude of oscillation has to be assumed to be small compared to the bubble radius. Even so, the present results are of some use in showing the nature of the flow and in suggesting certain comparisons with observation.

The mathematical problem of a spherical bubble oscillating laterally and with small motions, in an unbounded, viscous, incompressible fluid, neglecting the inertia of the interior gas, was solved by Davidson and Ri-

ley in a long and difficult paper [4]. There were no radial pulsations; the radius of the sphere was assumed constant. In the present paper we shall simplify their analysis but then add also radial pulsations. We shall show that this gives rise to a qualitatively different type of drift motion, one that is apparently quite similar to that observed experimentally [5].

For the sake of economy the present paper only summarises the method of approach and the results; for further details of the analysis the reader is referred to Ref. [6].

2. Method of approach; lateral oscillations

The assumed situation is as in Figure 1. A spherical cavity of radius a undergoes small lateral oscillations $\epsilon a e^{i\omega t}$, $\epsilon \ll 1$, in the direction of the axis $\theta = 0$, where (r, θ) are polar coordinates. The tangential stress at the boundary is assumed to vanish. In the fluid near the boundary there is a thin oscillatory boundary-layer, with thickness $\delta = (2\nu/\sigma)^{1/2}$, $\delta \ll a$. All the $O(\epsilon)$ vorticity is confined to this layer. Because the fluid is incompressible we may take axes fixed to the sphere, and because it is axisymmetric we may express the radial and tangential components of velocity in terms of a streamfunction ψ :

$$u_r = \frac{1}{r^2 \sin \theta} \frac{\partial \psi}{\partial \theta}, \quad u_\theta = \frac{-1}{r \sin \theta} \frac{\partial \psi}{\partial r}. \quad (1)$$

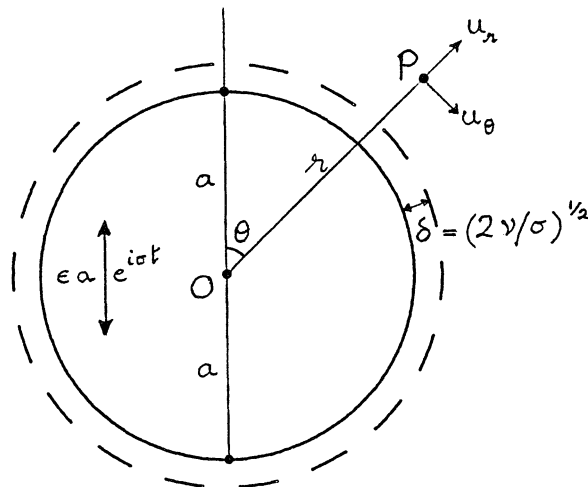


Figure 1. Schematic drawing of a spherical bubble in vertical oscillation. The broken curve indicates the oscillatory boundary-layer.

ψ satisfies a non-linear partial differential equation throughout the fluid (see the Appendix) and a linear boundary condition at $r = a$, expressing the condition that the tangential stress shall vanish there. Because of the nonlinearity, we expand ψ as a power series in ϵ :

$$\psi = \epsilon\psi_1 + \epsilon^2\psi_2 + \dots . \quad (2)$$

We are interested in calculating the Eulerian average $\bar{\psi}_2$ (the time-average at a fixed point) and also the Lagrangian average Ψ (the time-average following a marked particle).

The first approximation ψ_1 can be written down quickly. At infinity ($r \gg a$) it must be a uniform oscillatory flow:

$$\psi_1 \sim \frac{1}{2}a\sigma r^2 \sin^2 \theta e^{i\sigma t} \quad (3)$$

where t is the time, and we find

$$\psi_1 = \sigma a^3 \left[\frac{1}{2} \left(\frac{r^2}{a^2} - \frac{a}{r} \right) + \frac{B}{\alpha^2 r} + \frac{C}{\alpha^2 a} \left(1 + \frac{1}{\alpha r} \right) e^{-\alpha s} \right] \sin^2 \theta e^{i\sigma t} \quad (4)$$

where $s = r - a$ and $\alpha^2 = i\sigma/\nu$, hence $\alpha = (1+i)/\delta$. $B(\alpha)$ and $C(\alpha)$ are constants, and it is understood that on the right the real part is taken. Since the terms in r^2 and r^{-1} represent irrotational motions, all the vorticity is described by the terms multiplying $e^{-\alpha s}$ which vanishes exponentially as s increases; this is the inner, vortical boundary-layer.

In order to determine the mean streaming $\epsilon^2\bar{\psi}_2$, we substitute the form (2) for ψ into the equations and boundary conditions, equate the coefficients of ϵ^2 and take mean values with respect to the time t . Outside the boundary-layer, that is where $e^{-\alpha s} \ll 1$, the mean streamfunction $\bar{\psi}_2$ must have the form

$$\bar{\psi}_2 = (E + Fr^{-2}) \cos \theta \sin^2 \theta \quad (5)$$

in order to satisfy the equation of motion for steady flow and the conditions at infinity (see the Appendix). This solution has to be matched with the boundary-layer solution, and altogether we find for the flow outside the boundary-layer

$$\epsilon^2\bar{\psi}_2 = \frac{27}{40} a^2 \sigma \epsilon^2 \delta \left(\frac{a^2}{r^2} - 1 \right) \cos \theta \sin^2 \theta. \quad (6)$$

to lowest order in δ/a . It turns out that to this order the Lagrangian streamfunction, given by

$$\Psi = \bar{\psi}_2 + \frac{1}{r^2} \overline{\int \frac{\partial \psi_1}{\partial r} dt} \frac{\partial \psi_1}{\partial (\cos \theta)} \quad (7)$$

(see [6]) differs only negligibly from $\bar{\psi}_2$ outside the boundary-layer. Thus

both Ψ and $\bar{\psi}_2$ are given by the streamlines in Figure 2. This shows a drift motion inwards towards the sphere near the equatorial plane, and outwards, away from the sphere, near the axis of symmetry.

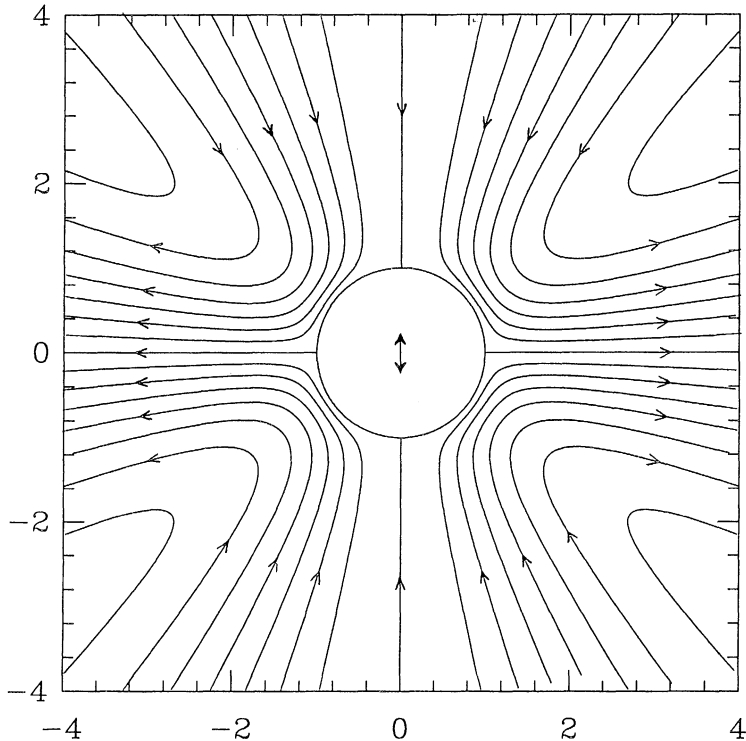


Figure 2. (from Longuet-Higgins 1998a). Streamlines of the steady Lagrangian streaming outside the oscillatory boundary-layer, for a spherical bubble in purely vertical oscillation.

The flow in the boundary-layer itself is not shown, but here there are significant differences between the Eulerian and Lagrangian velocities; see Figure 3 of Ref. [6].

3. Lateral oscillations with radial pulsations

The addition of *radial* pulsations strongly affects the drift motion. We may take as the equation of the free surface

$$r = R(t) \equiv a \left[1 - i\epsilon' e^{i(\sigma t + \phi)} \right] \quad (1)$$

where ϵ' is a small parameter, independent of ϵ , and ϕ is the phase angle between the lateral and radial oscillations. Then the radial velocity at the

free surface is given by

$$\frac{dR}{dt} = \epsilon' a \sigma e^{i(\sigma t + \phi)} \quad (2)$$

corresponding to an axisymmetric streamfunction

$$\epsilon' \psi_{01} = -\epsilon' a^3 \sigma \cos \theta e^{i(\sigma t + \phi)} \quad (3)$$

We now have to expand the total streamfunction ψ as a double series:

$$\psi = (\epsilon \psi_{10} + \epsilon' \psi_{01}) + (\epsilon^2 \psi_{20} + \epsilon \epsilon' \psi_{11} + \epsilon'^2 \psi_{02}) + \dots \quad (4)$$

where ψ_{10} denotes the streamfunction ψ_1 of Section 2, and ψ_{01} is given by equation (3). We are then interested in evaluating the time-averaged streamfunction

$$\bar{\psi} = \epsilon^2 \bar{\psi}_{20} + \epsilon \epsilon' \bar{\psi}_{11} + \epsilon'^2 \bar{\psi}_{02}. \quad (5)$$

But $\bar{\psi}_{20}$ has already been evaluated in Section 2, and $\bar{\psi}_{02}$ clearly vanishes, since by continuity the mean outwards flow from a purely radial pulsation must be zero. It remains to evaluate the interaction term $\bar{\psi}_{11}$.

The analysis can be carried out in a similar way to that in Section 2 (for details, see [6]). It turns out that there is now a significant difference between the Eulerian and the Lagrangian drift velocities. In particular the Lagrangian streamfunction is given by

$$\Psi_{11} = -\epsilon \epsilon' a^3 \sigma \sin \phi \left(\frac{1}{2} \frac{r}{a} - \frac{1}{4} \frac{a}{r} - \frac{1}{4} \frac{a^4}{r^4} \right) \cos^2 \theta \quad (6)$$

to lowest order in δ/a . The streamlines of Ψ_{11} are shown in Figure 3, in the case $\sin \phi > 0$. In contrast to Figure 2, the directions of flow above and below the equatorial plane are either both upwards or both downwards, depending on the sign of the phase ϕ . Moreover the magnitude is greater.

To analyse this result further, consider the velocity components u_r and u_θ . Using equations (1) we find

$$\left. \begin{aligned} u_r &= \epsilon \epsilon' a \sigma \sin \phi \left(-\frac{a}{r} + \frac{1}{2} \frac{a^3}{r^3} + \frac{1}{2} \frac{a^6}{r^6} \right) \cos \theta \\ u_\theta &= \epsilon \epsilon' a \sigma \sin \phi \left(\frac{1}{2} \frac{a}{r} + \frac{1}{4} \frac{a^3}{r^3} + \frac{a^6}{r^6} \right) \sin \theta. \end{aligned} \right\} \quad (7)$$

Note that at large distances the terms in $(a/r)^6$ are much less than those in $(a/r)^3$. The latter correspond to a dipole flow with potential

$$\Phi = -\frac{S \cos \theta}{2r^2} \quad (8)$$

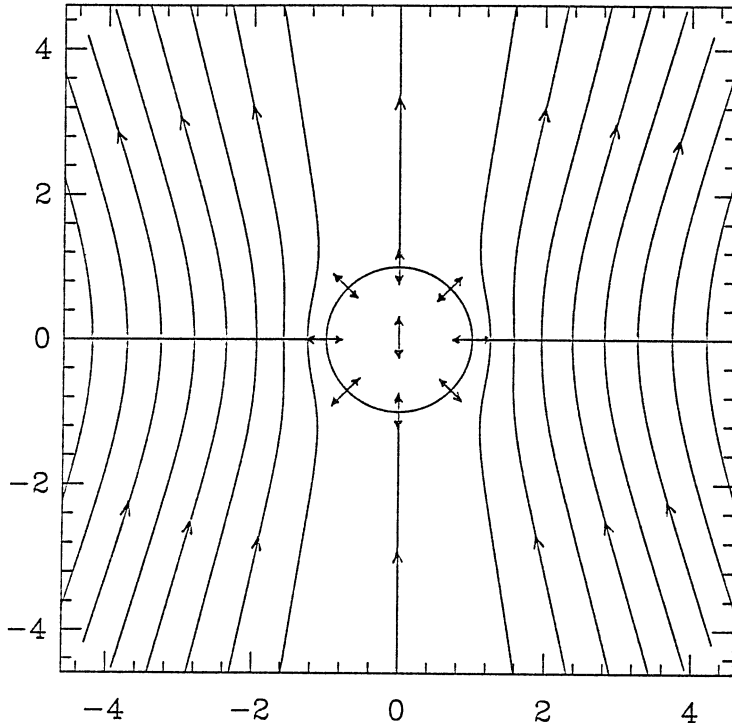


Figure 3. (from Longuet-Higgins 1998a). Streamlines of the steady Lagrangian streaming outside the oscillatory boundary-layer, for a spherical bubble oscillating both radially and vertically.

where S is the dipole strength:

$$S = \frac{1}{2} \epsilon \epsilon' a^4 \sigma \sin \phi. \quad (9)$$

This part of the flow is irrotational, and is similar to the inviscid streaming from an oscillating and pulsating sphere found numerically (see preceding paper) at large amplitudes of pulsation. In that case the dipole strength was found to be

$$S_{\text{inviscid}} = \frac{1.5}{2\pi} \epsilon a^4 \sigma \sin \phi \quad (10)$$

in the present notation, being almost independent of ϵ' at the large amplitudes there considered. If we were to put $\epsilon' = 1$ in equation (9) (which is not permitted under the present assumptions) then S would be comparable to S_{inviscid} and still insufficient to account for the discrepancy of 10^{-7} , between this and the observed streaming.

There remain the terms in (a/r) in equations (8). These represent a

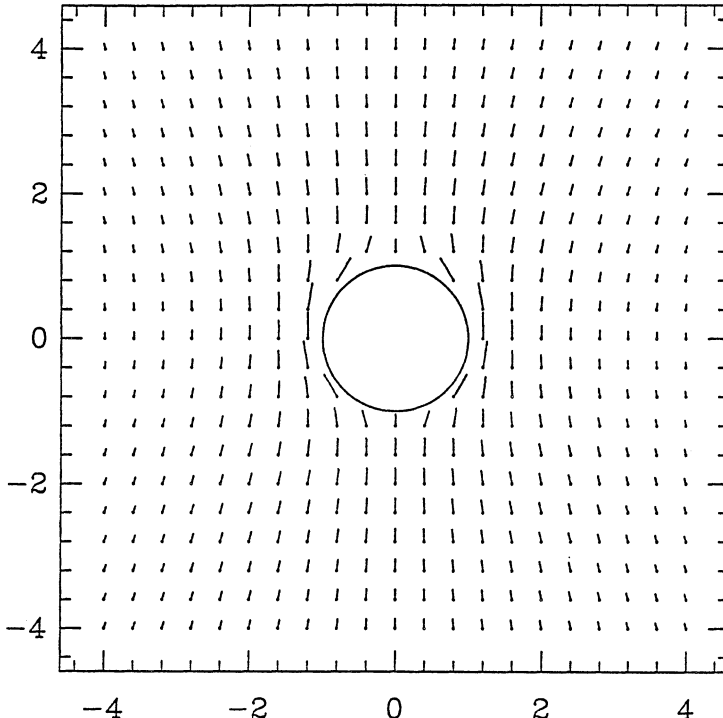


Figure 4. (from Longuet-Higgins 1998a). Velocity vectors in the Lagrangian flow of Figure 3.

viscous (rotational) flow called a “Stokeslet”; see [7]. It is a steady flow which, once established, will extend to greater distances than the dipole flow. Some velocity vectors are shown in Figure 4.

However, being essentially a rotational flow, the vorticity will take time to be propagated from its source at the surface of the sphere to a typical point in the fluid. There are two possible mechanisms for propagation of vorticity: convection and viscous diffusion. Viscous diffusion, which is the dominant mechanism at low Reynolds numbers, would take a time of order r^2/ν to affect a flow region of radius r . In either case, the observed flow at such distances should initially be slowly dependent on the time of observation.

It is notable that the magnitude and size of the streaming in equations (7) depend upon the phase ϕ between the two modes of oscillation. The streaming intensity is greatest when $\phi = (n + \frac{1}{2})\pi$ where n is an integer, and vanishes when $\phi = n\pi$. A similar dependence on the phase was also found in the inviscid case; see [2, 3]. We note that in a sonoluminescent bubble the phase ϕ between the vertical and radial displacements is generally quite small, of the order of 10 degrees, and may change sign, so that in some circumstances the flow may reverse. In this way the direction of the

flow may be a sensitive indicator of the relative phase of the oscillations.

4. Conclusions

We have shown that the acoustical streaming from a bubble undergoing lateral oscillations is enhanced by an order of magnitude when the bubble simultaneously pulsates in a radial sense. The form of the streaming is also different, being more like a dipole than a quadripole. The magnitude of the streaming depends on the phase relation between the lateral and radial oscillations, and is proportional to the product of their amplitudes. The streaming is a maximum when the phase difference is $\pm 90^\circ$, and reverses sign when the phase passes through zero.

The present analysis is strictly valid only for oscillations of the bubble that are small compared to the bubble radius. The oscillations need not be small compared to the thickness of the shear layer. They apply only qualitatively to a sonoluminescent bubble, whose maximum and minimum radius may differ by two orders of magnitude. But they may be used in a quantitative way to check numerical calculations of finite amplitude oscillations as a limiting case.

In the above treatment we have neglected the inertia and viscosity of the gas in the interior of the bubble. Thus the tangential stress at the surface of the bubble was assumed to be zero. In some applications, particularly in collapsed bubbles where the density may increase by two or three orders of magnitude, such an assumption is no longer justified. Nyborg [8] has shown how significant acoustical streaming in a gas may take place at a plane gas-water interface. With gas bubbles in air the effect would be at least as strong.

5. Appendix. Field equations and boundary conditions

It is convenient to write $\cos \theta = \mu$, and define the operators

$$D^2 \equiv \frac{\partial^2}{\partial r^2} + \frac{1 - \mu^2}{r^2} \frac{\partial^2}{\partial \mu^2} \quad (1)$$

and

$$\mathcal{L} \equiv \frac{\mu}{1 - \mu^2} \frac{\partial}{\partial r} + \frac{1}{r} \frac{\partial}{\partial \mu}. \quad (2)$$

The field equation for ψ can then be written (see [9]) as

$$\left(\frac{\partial}{\partial t} - \mu D^2 \right) \Omega + \frac{1}{r^2} \left[\frac{\partial(\psi, \Omega)}{\partial(r, \mu)} + 2\Omega \mathcal{L} \psi \right] = 0 \quad (3)$$

where

$$\Omega = -D^2 \psi. \quad (4)$$

It can be shown that $\Omega = \omega \sin \theta$, where ω denotes the local vorticity. In other words, Ω is proportional to the vorticity integrated around a circle of latitude: the “ring vorticity”.

Vanishing of the tangential stress at the surface of the sphere is expressed by the condition

$$\frac{\partial^2 \psi}{\partial r^2} - \frac{2}{r} \frac{\partial \psi}{\partial r} = 0. \quad (5)$$

Outside the boundary-layer, where the first-order ring vorticity $-\epsilon D^2 \psi_1$ is exponentially small, the second-order mean streamfunction $\epsilon^2 \bar{\psi}_2$ satisfies

$$D^4 \bar{\psi} = 0. \quad (6)$$

Hence if $\bar{\psi} \propto (1 - \mu^2)$, for example, we have from (A1) and (A6)

$$\left(\frac{\partial^2}{\partial r^2} - \frac{2}{r^2} \right)^2 \bar{\psi} = 0. \quad (7)$$

Hence $\bar{\psi}$ can be proportional only r^4 , r^2 , r or r^{-1} , or to a linear combination of such terms. The corresponding radial velocities are proportional to r^2 , 1, r^{-1} and r^{-3} . For large values of r the first two cases are ruled out, leaving only the possibility that $\bar{\psi}$ is of the form

$$\bar{\psi} = (Er + Fr^{-1})(1 - \mu^2) \quad (8)$$

as in Section 3 (Ψ_{11} contains an extra term).

Similarly if $\psi \sim \mu(1 - \mu^2)$, we have

$$\left(\frac{\partial^2}{\partial r^2} - \frac{6}{r^2} \right)^2 \bar{\psi} = 0 \quad (9)$$

then $\bar{\psi}$ can be proportional only to r^5 , r^3 , r^0 or r^{-2} , or to a linear combination of such terms. For large r , the first two possibilities are ruled out; hence equation (5) of Section 2. Hence u_r is proportional to r^{-2} or r^{-4} . It is to be noted that the solution proposed by Wu and Du [10], equation (28), is not of this form, and so must be discounted.

References

1. Longuet-Higgins, M.S. (1996) Shedding of vortex rings by collapsing cavities, with application to single bubble sonoluminescence. *J. Acoust. Soc. Amer.* **100**, pp. 2678 (Abstract).
2. Longuet-Higgins, M.S. (1997) Particle drift near an oscillating bubble. *Proc. R. Soc. Lond. A* **453**, 1551-1568.

3. Longuet-Higgins, M.S. (1998) Particle drift near an oscillating cavity. (This vol., pp .)
4. Davidson, B., and Riley, N. (1971) Cavitation microstreaming. *J. Sound Vib.* **15**, 217-233.
5. Verraes, T., Lepoint-Mullie, F., and LePoint, T. (1998) Experimental study of the liquid flow near a single sonoluminescent bubble. (This vol., pp. .)
6. Longuet-Higgins, M.S. (1998) Viscous streaming from an oscillating spherical bubble. *Proc. R. Soc. Lond. A* (to appear).
7. Batchelor, G.K. (1967) *An introduction to fluid dynamics*. Cambridge Univ. Press, 615 pp.
8. Nyborg, W.L. (1994) *J. Acoust. Soc. Amer.* **96**, 3279.
9. Whitham, G.B. (1963) *Laminar Boundary Layers*, Chapter 3. Oxford University Press.
10. Wu, J., and Du, G., (1997) Streaming generated by a bubble in an ultrasound field. *J. Acoust. Soc. Amer.* **101**, 1899-1907.

HYDRODYNAMICS, ACOUSTICS AND TRANSPORT IN SONOLUMINESCENCE PHENOMENA

R.I. NIGMATULIN, I.SH. AKHATOV AND N.K. VAKHITOVA
*Ufa (Bashkortostan) Branch of Russian Academy of Sciences
K. Marx Str. 6, Ufa, 450000, RUSSIA*

AND

R.T. LAHEY, JR.
*Rensselaer Polytechnic Institute
Troy, NY, 12180-3590, USA*

Abstract.

The spherically-symmetric problem of the oscillations of a gas bubble in the center of a spherical flask filled with a compressible liquid that is excited by pressure oscillations on the flask wall is considered. A generalization of the Rayleigh-Plesset equation for a compressible liquid is given in the form of two ordinary difference-differential equations that take into account the pressure waves which are reflected from the bubble and those that are incident on the bubble from the flask wall. The initial value problem for the initiation of bubble oscillations due to flask wall excitation and for the evolution of these oscillations is considered. Linear and non-linear periodic bubble oscillations are analyzed analytically. Non-linear resonant and near-resonant solutions for the bubble nonharmonic oscillations, which are excited by harmonic pressure oscillations on the flask wall, are obtained. The influence of heat transfer phenomena on the bubble oscillations is analysed.

1. Introduction

Let us consider the spherically-symmetric radial flow of a compressible liquid in a spherical flask (with radius R) around a small spherical gas bubble located at the center of the flask.

If disturbances of the pressure are not large enough to appreciably change the density of the liquid and the length of the pressure wave in the liquid is much more than the bubble radius, then for the mathematical modeling of the process one may use the approximation of an incompressible liquid, for which the momentum equation is the well-known Rayleigh-Plesset (RP) equation ([1],[2],[3]):

$$a \frac{dw_a}{dt} + \frac{3}{2} w_a^2 = \frac{p_a - p_\infty}{\rho}, \quad w_a = \frac{da}{dt}, \quad (1)$$

$$p_a = p_g(a) - \frac{2\sigma}{a} - \frac{4\mu w_a}{a},$$

where a is the bubble radius, ρ, μ, σ are the density, viscosity and surface tension of the liquid, respectively, w_a and p_a are the radial velocity and the pressure of the liquid on the interface of the bubble, p_g is the pressure of the gas in the bubble, and p_∞ is the pressure of the liquid far from the bubble. Sometimes it is assumed that for the case $R \gg a$ the pressure far from the bubble p_∞ , is the pressure on the flask wall $p_R : p_\infty = p_R$.

This is not true for the general case of compressible liquid. Previously the influence of liquid compressibility on volume oscillations of a gas bubble was taken into account within the framework of a so-called acoustical radiation scheme (see [2], [3]); in particular, when using the Herring-Flinn-Gilmore (HFG) equation:

$$a \frac{dw_a}{dt} + \frac{3}{2} w_a^2 = \frac{p_a - p_\infty}{\rho} + \frac{a}{\rho C} \frac{dp_a}{dt}. \quad (2)$$

where C is the speed of sound in the liquid.

An approximate theory has been erected by Prosperetti and Lezzi [4] regarding radial motions of a spherical bubble in an infinite compressible liquid. A whole *family* of equations of bubble oscillations has been obtained including Eq. (2) and other authors' equations ([2], [3]) as specific cases. All these equations are shown to be *equivalent*, as they have one and the same order of accuracy by Mach number. In deriving the equations, the statement is used that bubble oscillations do not affect the outer acoustic field of pressure at infinity. The fact that the fluid is unbounded permits to consider the problem on bubble oscillations separately from the acoustic problem taking into account the outer acoustic field as a definite motive force for the bubble.

The present paper deals with an associated problem on oscillations of a limited liquid volume and of a gas bubble, in which the flask wall is used to excite the liquid. As shown, the problem may be reduced to some equation like the Herring-Flynn-Gilmore one for the evolution of a bubble

radius. Instead of the pressure far from the bubble p_∞ , another pressure p_I appears, which is the incident pressure. The incident pressure differs both from the pressure at local infinity p_∞ , and from the pressure on the flask wall p_R . It must be calculated using a difference-differential equation including the bubble radius a and the pressure on the flask p_R .

2. The system of equations for radius of the bubble

For the low Mach number stage of the process ($M_a = w_a/C \ll 1$) it is shown that the space between the bubble interface and the flask wall consists of three zones:

(1) The external zone, where the weak compressibility of the liquid is essential but convective displacements of the liquid are small. In this region, the non-linear inertia forces due to the convective accelerations are negligibly small and motion of the liquid has an acoustic wave propagation character with a finite and fixed speed of sound in the liquid at the initial state.

(2) The internal zone, near to the bubble interface, where liquid compressibility has negligible influence on the process and the motion occurs only because of the compression and expansion of the bubble, but the non-linear inertia forces in the liquid due to the convective accelerations are essential.

(3) The intermediate zone where both liquid compressibility and non-linear inertia forces (due to the convective accelerations) are important.

In order to obtain an overall solution it is necessary that the asymptotic solutions of the external and internal zones be matched in the intermediate zone by the compatibility conditions for the volume flow and pressure.

Thus, one obtain a long-wave approximation of the equation for bubble oscillations in a compressible liquid ([5]):

$$a\ddot{a} + \frac{3}{2}\dot{a}^2 = \frac{p_a - p_0}{\rho} + \frac{1}{C} [2\ddot{\psi}_2(t) + \ddot{Q}(t)], \quad Q(t) = a^2\dot{a}. \quad (3)$$

where ψ_2 is the velocity potential of the wave incident on the bubble from the flask wall. The pressure on the flask may be expressed by the equation:

$$p_R(t) = p_0 - \frac{\rho}{R} \left[\dot{\psi}_2 \left(t + \frac{R}{C} \right) - \dot{\psi}_2 \left(t - \frac{R}{C} \right) - \dot{Q} \left(t - \frac{R}{C} \right) \right]. \quad (4)$$

From Eq. (3) the expression for the pressure p_∞ at bubble boundary layer infinity (i.e. the local infinity) follows:

$$p_\infty = p_0 - \frac{\rho}{C} [2\ddot{\psi}_2(t) + \ddot{Q}(t)]. \quad (5)$$

It is significant that the solution depends on the third derivative of the bubble radius. This was noted by Prosperetti and Lezzi [4]. However, for the low Mach number and the long wave approximation it is shown that for the term \ddot{Q}/C , which is responsible for the bubble influence on the reflecting wave and for the third derivative, one may use a simple asymptotic solution without the third derivative. Then the bubble radius evolution is described by the following equation:

$$\left(1 - \frac{\dot{a}}{C}\right) a\ddot{a} + \frac{3}{2} \left(1 - \frac{\dot{a}}{3C}\right) \dot{a}^2 = \left(1 - \frac{\dot{a}}{C}\right) \frac{p_a - p_I}{\rho} + \frac{a}{C} \frac{d}{dt} \left[\frac{p_a - p_I}{\rho} \right], \quad (6)$$

$$p_I = p_0 - \frac{2\rho}{C} \ddot{\psi}_2.$$

System (4),(6) of ordinary difference-differential equations having both lagging (retarding) and leading potentials is closed for a given density ρ , sound speed C , surface tension σ , viscosity μ , of the liquid, equation of state for the bubble gas $p_g(a)$, and pressure on the flask wall $p_R(t)$.

It is important that supercompression of the gas and light emission may take place during bubble implosion, when the approximation of an incompressible liquid near the bubble boundary layer is no longer valid. Nevertheless, bubble implosion occupies only a very small part of the oscillation period. For this part of the period it is necessary to take into account the compressibility of the liquid near the bubble, and shock wave formation both in the liquid and in the gas, (i.e. to consider this period using separate numerical codes (Moss *et al.* [6])).

3. Initial value problem

The problem is, to calculate the evolution of the bubble radius $a(t)$ knowing the evolution of the flask's wall pressure $p_R(t)$. In general case the solution of the direct problem may be obtained by the numerical integration of the partial differential equations.

In the paper by Moss *et al.* [6] a numerical hydro-type code was used for the calculation of the bubble behaviour not only for the bubble implosion stage, but for the long wave length and low Mach number stages as well. Needless to say, the computer run time was very large. In the Moss's work, the direct problem was solved for a sinusoidal pressure change on the flask:

$$p_R(t) = \begin{cases} p_0 & , \quad t \leq 0 \\ p_0 - \Delta p_R \sin \omega t & , \quad t > 0 \end{cases} \quad (7)$$

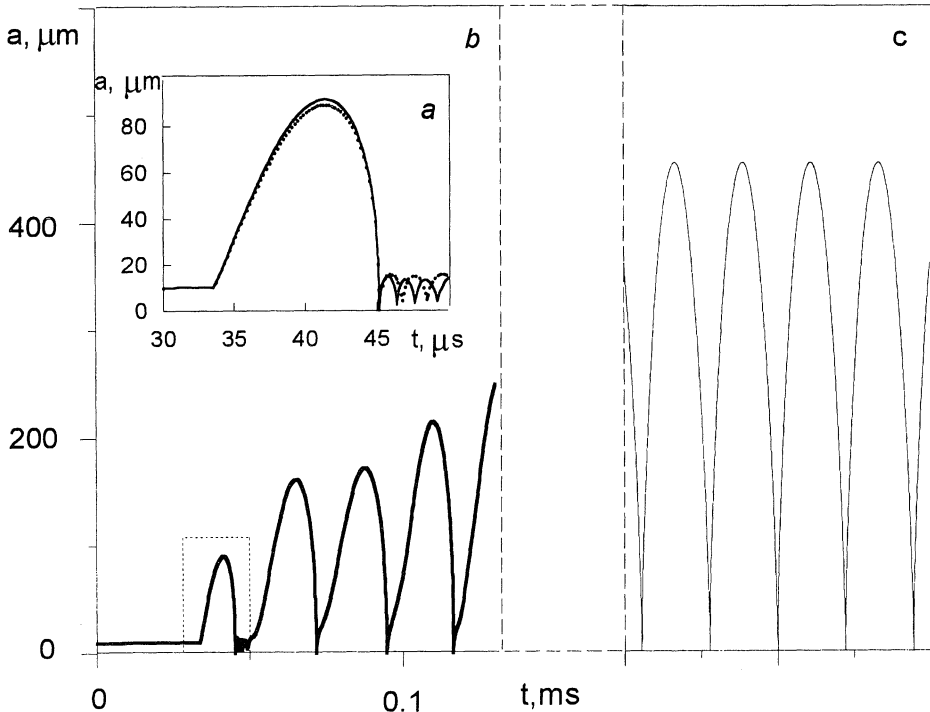


Figure 1. Excitation of bubble ($a_0 = 10\mu\text{m}$) oscillations in a flask ($R = 5\text{cm}$) filled with water ($p_0 = 1 \text{ bar}$, $T_0 = 300 \text{ K}$) when the flask wall produces sinusoidal pressure oscillations (Eq. (7)) with the amplitude, $\Delta p_R = 0.25 \text{ bar}$, and the frequency, $f = f_3 = 45 \text{ kHz}$. On the right side the ideal periodic regime is shown which corresponds to the resonant case ($f = f_3$).

The bubble radius evolution $a(t)$ was calculated but for the first oscillation and not for the periodic regime, which takes place only after many oscillations have concealed the initial conditions. Significantly, this is what is measured in experiments.

In Fig. 1 the results of our calculations are presented. The first oscillation agrees with the Moss *et al.* [6] calculation (dotted line). However, one can see that the second oscillation differs essentially from the first, the third differs from the second, and only after many oscillations ($t \gg \omega^{-1}$) a periodic regime does take place. This is connected with the inertia of the liquid in the flask. In fact, it is the mass of the liquid ($\sim \rho R^3$) that delays the beginning the periodic regime of pressure at local infinity p_∞ . The delay of the periodic regime of bubble oscillation, after the beginning the periodic regime for p_∞ , is much smaller because it is determined by the virtual mass of the liquid round the bubble ($\sim \rho a^3 \ll \rho R^3$).

As follows, the most important and interesting solution is for the peri-

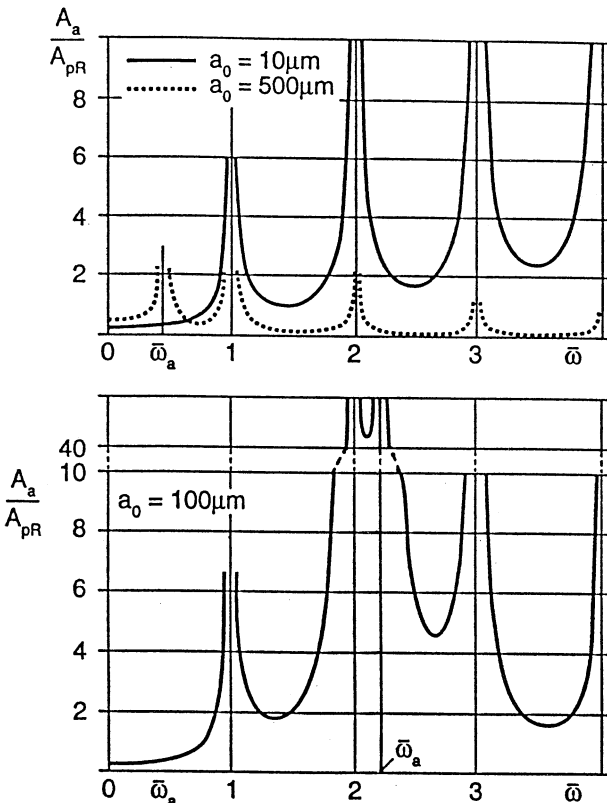


Figure 2. Amplitude-frequency response functions for harmonic oscillations of the bubble ($a_0 = 10 \mu\text{m}$ ($\omega_a = 2160 \text{ kHz}$), $a_0 = 100 \mu\text{m}$ ($\omega_a = 206 \text{ kHz}$), $a_0 = 500 \mu\text{m}$ ($\omega_a = 41.03 \text{ kHz}$)) in a flask ($R = 5 \text{ cm}$, $\omega_R = \omega_1 = 94.2 \text{ kHz}$) filled with water ($p_0 = 1 \text{ bar}$).

odic regime. Direct numerical calculations of the initial value problem for the periodic regime is non-effective and very time-consuming.

4. Linear harmonic forced oscillations

A priori it is clear that the problem has two characteristic frequencies. The first is the flask frequency $\omega_R = \pi C/R$, determined by the time $t_R = 2R/C$, for acoustic wave propagation along the distance $2R$ from the flask wall to its center and back. The second is the bubble free oscillation frequency (i.e. the Minnaert frequency) $\omega_a = \sqrt{3\gamma p_0/a_0^2\rho}$.

Let us consider small amplitude forced steady harmonic oscillations of the form $A \exp i\omega t$, with angular frequency ω . Then the response function, which is the ratio of the relative amplitude of the bubble radius $A_a = \Delta a/a_0$ to the relative amplitude of the flask forcing pressure $A_{pR} = \Delta p_R/p_0$, may be presented as a function of the non-dimensional frequency $\bar{\omega} = \omega [R/\pi C]$.

It is shown that the resonance corresponding to the maximum absolute

value of $|A_a/A_{pR}|$ takes place when $\bar{\omega} \approx 1, 2, 3, \dots$. This is associated with the flask resonance (Fig. 2): $\omega_k = 2\pi f_k = k\pi C/R = k\omega_R$, $k = 1, 2, 3, \dots$; and since the bubble is so small, it does not normally influence the value of the resonant frequencies. For a flask with radius, $R = 5$ cm, filled with water, the first resonance frequency is $f_1 \approx 15$ kHz (i.e. $\omega_1 = 94.2$ kHz).

Influence of the bubble on the resonant frequency takes place only when the frequency of flask excitation is comparable to the Minnaert (resonant) frequency of the bubble ω_a . (e.g., see Fig. 2 for $a_0 = 100$ and $500 \mu\text{m}$).

It is interesting that exterior to the bubble resonance zone the smaller the bubble, the higher is the relative response $|A_a/A_{pR}|$ (compare the curves for $a_0 = 10$ and $500 \mu\text{m}$ in Fig. 2). This explains the fact that sonoluminescence takes place only for tiny bubbles ($a_0 = 4 \dots 10 \mu\text{m}$).

For excitation frequencies close to the resonant frequencies it is necessary to use non-linear analysis when a large amplitude nonharmonic response of the bubble radius occurs $\Delta a \sim a$. This may take place even for small sinusoidal oscillations of the pressure on the flask $\Delta p_R \ll p_0$, such as in experiments in which sonoluminescence occurs.

5. Non-linear analysis for resonant frequencies

Non-linear periodic solutions for the flask resonance: $\omega = \omega_k = k\pi C/R$ ($k = 1, 2, 3, \dots$), were obtained. For the periodic regime excited by sinusoidal oscillations of the flask wall pressure: $p_R(t) = p_0 - \Delta p_R \sin \omega_k t$, the periodic solution can be shown as:

$$a^3 = a_*^3 \left\{ 1 + c_* + \sin \left[\omega_k \left(t + \frac{R}{C} \right) \right] \right\}, \quad (8)$$

$$a_*^3 = \frac{3R^3 A_{pR} p_0}{\pi^2 k^2 \rho C^2}, \quad 1 \gg c_* > 0, \quad a_{max}^3 \approx 2a_*^3.$$

This solution should be treated as an *ideal periodic regime* because it is derived in the limit case of an ideal weakly compressible liquid and non-compressible boundary layer around a bubble that supplies an absence of any dissipation mechanism.

The exact value of the constant parameter c_* should be calculated numerically for the condition, when the flask wall velocity and displacement are periodic.

There is a non-trivial and important parameter a_* , determining the maximum value of the bubble radius a_{max} , which is practically independent on the initial value the bubble radius a_0 for the ideal resonant regime. In order to have bubble implosion and sonoluminescence in the resonance regime it is necessary that $a_{min} \ll a_0 \ll a_{max} \sim a_*$. But the value of

minimum radius of the bubble a_{min} cannot be considered as a physically reliable value because the implosion period does not satisfy the low Mach number approximation.

The ideal periodic resonant regime is shown on the right side of Fig. 1. This regime corresponds to the third flask resonance $f = f_3 = 45$ kHz with the maximum radius of the bubble being $a_{max} = 454 \mu m$, according to Eq. (8).

For small deviations from the acoustic resonant frequency: $\omega = \omega_k + \Delta\omega$, $\Delta\omega \ll \omega_k$, ($\omega_k = \pi k C / R$, $k = 1, 2, 3, \dots$), the ordinary differential equation for periodic forced oscillations of the bubble is:

$$\left(1 - \frac{a\omega_k}{R\Delta\omega}\right) a\ddot{a} + \left(\frac{3}{2} - 2\frac{a\omega_k}{R\Delta\omega}\right) \dot{a}^2 = \frac{p_a - p_0}{\rho} - \frac{1}{\rho} \frac{\omega_k}{\Delta\omega} \Delta p_R \left(t + \frac{R}{C}\right) + \frac{a}{\rho C} \frac{d}{dt} \left[p_a - p_0 - \frac{\omega_k}{\Delta\omega} \Delta p_R \left(t + \frac{R}{C}\right) \right]. \quad (9)$$

There is an important non-dimensional parameter for this near resonant regime characterizing the influence of the bubble on the near resonant oscillations:

$$A_* = \frac{a_0 \omega_k}{R \Delta\omega}. \quad (10)$$

This parameter is a product of small (a_0/R) and large ($\omega_k/\Delta\omega$) parameters, but Eq. (9) is derived for $A_* \ll 1$. In this case the pressure in the bubble controls the bubble motion as opposed to the resonant case ($\Delta\omega = 0$). For $\Delta\omega \rightarrow 0$ ($A_* \rightarrow \infty$) Eq. (9) tends to Eq. (8) for the resonant case.

The calculations for the typical near resonant regime are shown on Fig. 3 (the high amplitude oscillations on the right side of the figure show the corresponding ideal resonant regime).

The dependence of a_{min} and a_{max} on the frequency shift for the third flask resonance for $a_0 = 4 \mu m$ and different pressure amplitudes is shown on Fig. 4. The resonant case ($\Delta\omega = 0$) is denoted by large dots and circles. In the vicinity of flask resonance the curves are given by dashed lines because Eq. (9) is not valid.

6. Heat transfer effect

Heat transfer inside the bubble and heat exchange between the bubble and liquid may play an important role in the phenomenon. Here we use the model proposed in [7] (see also [3]). It is based on the approximation that, first, gas pressure p_g depends only on time and is spatially uniform (*homobaricity*) and, second, there is a minor difference of liquid temperature from its undisturbed value T_0 . This model includes heat balance equation

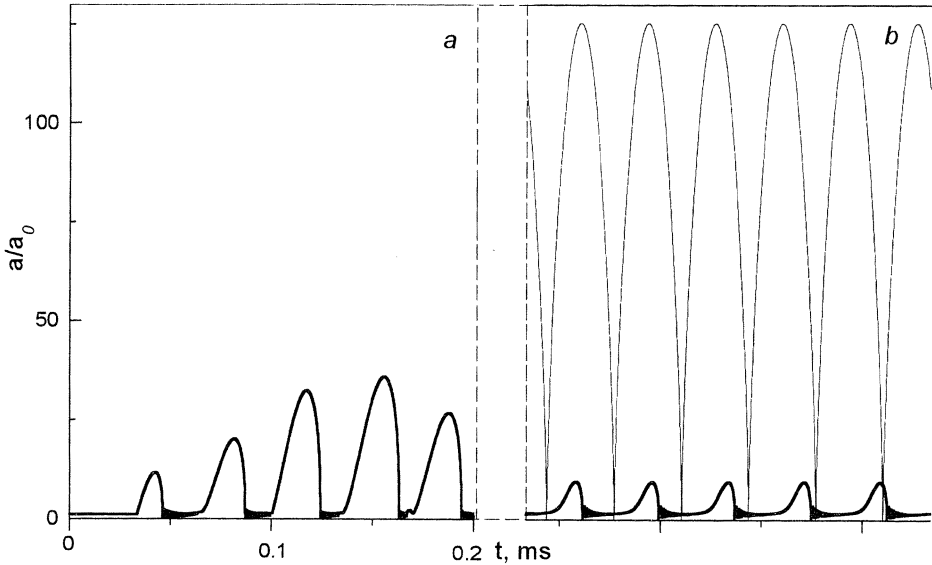


Figure 3. Excitation of bubble ($a_0 = 4 \mu\text{m}$) oscillations in a flask ($R = 5 \text{ cm}$) filled with water ($p_0 = 1 \text{ bar}$, $T_0 = 300 \text{ K}$), when the flask wall produces sinusoidal pressure oscillations (Eq. (7)) with the amplitude, $\Delta p_R = 0.15 \text{ bar}$ and the frequency, $f = 26.5 \text{ kHz}$. On the right side the periodic regime is shown which corresponds to the near resonant case ($f \approx f_2$, $\Delta f = -3.5 \text{ kHz}$, $\Delta\omega = -22 \text{ kHz}$).

in the bubble (Eq. (11)), equation for gas pressure (Eq. (12)), gas velocity distribution in the bubble (Eq. (13)) and boundary conditions (Eq. (14)).

$$c_{pg}\rho_g \left(\frac{\partial T_g}{\partial t} + w_g \frac{\partial T_g}{\partial r} \right) = \frac{1}{r^2} \frac{\partial}{\partial r} \left(\lambda_g r^2 \frac{\partial T_g}{\partial r} \right) + \frac{dp_g}{dt}, \quad (11)$$

$$\frac{dp_g}{dt} = -\frac{3\gamma p_g \dot{a}}{a} + \frac{3(\gamma-1)}{a} \lambda_g \frac{\partial T_g}{\partial r} \Big|_{r=a}, \quad (12)$$

$$w_g = \frac{\gamma-1}{\gamma p_g} \lambda_g \frac{\partial T_g}{\partial r} - \frac{r}{3\gamma p_g} \frac{dp_g}{dt}, \quad (13)$$

$$T_g|_{r=a} = T_0, \quad \frac{\partial T_g}{\partial r} \Big|_{r=0} = 0. \quad (14)$$

This system of equations is connected with Eq. (6) for bubble radius, where $p_a = p_g - 2\sigma/a$. To uncouple the problem from the flask pressure p_R we take $p_I = p_0 - \Delta p_I \sin \omega t$ for simplicity.

Fig. 5 shows the result of computations for $10-\mu\text{m}$ argon bubble oscillating at the driving frequency 21 kHz and $\Delta p_I = 1.5 \text{ bar}$. One cycle of

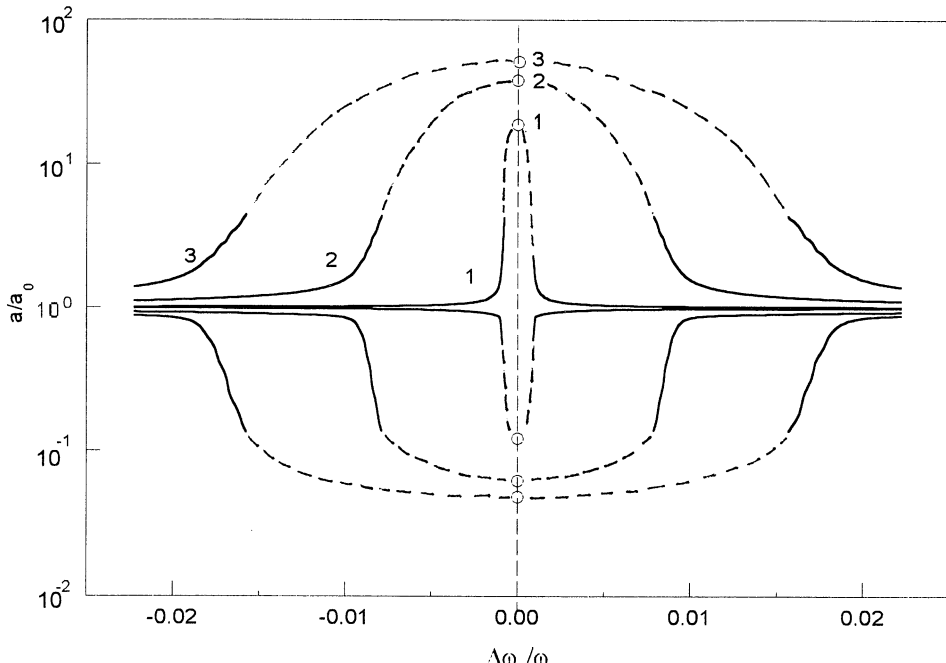


Figure 4. The dependence of a_{min} and a_{max} on frequency shift from the third flask resonance ($\omega = \omega_3 + \Delta\omega$) for $a_0 = 4 \mu m$ and different pressure amplitudes. 1: $\Delta p_R = 0.001$ bar, 2: $\Delta p_R = 0.01$ bar, 3: $\Delta p_R = 0.02$ bar.

driving is presented ($t_f = 2\pi/\omega$). It is clear from the first plot that during long (bubble expansion) time interval of the period bubble remains isothermal ($T_g(0, t) \approx T_0$). For adiabatic gas bubble expansion (the second plot) temperature drops very low (≈ 5 K). During bubble implosion the maximum center temperature is much higher (≈ 68000 K) than in the adiabatic case (≈ 18000 K). To clarify this phenomenon the third plot presents the total heat flux from the liquid to the bubble $\Delta E = \int_0^t 4\pi a^2 \lambda_g (\partial T / \partial r)_a dt$ normalized to the internal thermal energy of undisturbed bubble $E_0 = (4/3)\pi a_0^3 \rho_{g0} c_{gv} T_0$. One can see that during expansion period the bubble pumps out a substantial amount of energy from the liquid (heat pumping). During the set of implosions bubble injects more energy than it has been pumped out. The difference between pumped and injected energies which corresponds to energy losses of the system is shown as $\Delta E_f / E_0$.

This effect has been observed first by Kamath and Prosperetti [8] for larger ($26-\mu m$) bubbles and lower pressure amplitudes (0.93 bar) when bubble expansion and implosion were not so strong as in our case and the difference between maximum center temperatures was much lower (3000 K to 1328 K).

It is expected that the *heat pumping* effect plays a very important role

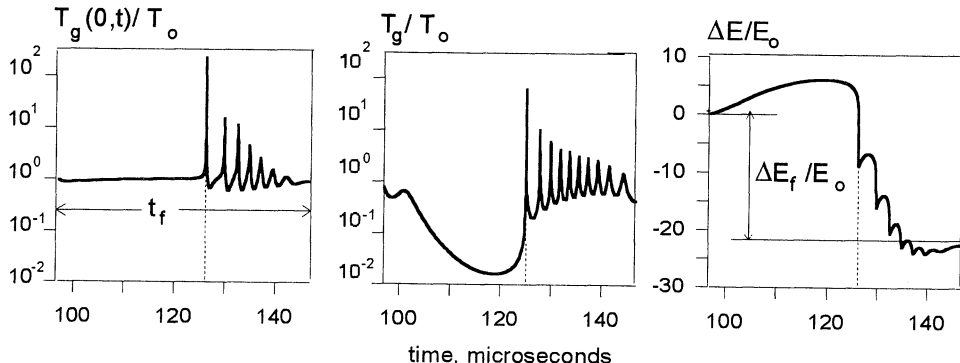


Figure 5. Internal temperature at the bubble center and the total heat flux from liquid to the bubble during one cycle ($a_0=10 \mu\text{m}$, $\Delta p_I=1.5 \text{ bar}$).

in the case of small ($\sim 4 \mu\text{m}$) sonoluminescing bubbles.

7. Summary

(1) There are two stages of the bubble oscillation process.

The first one is a low Mach number stage when the velocity of the bubble interface is small compared with sound speed in the liquid.

The second one, bubble implosion, is a stage corresponding to the collapsing bubble compression and its rebounding expansion, when the velocity of the interface may be comparable to or larger than the local sound speed.

The low Mach number period takes almost all the time of the period ($\sim 10^{-5} \text{ s}$). Implosion occurs only for the flask acoustic resonance, or near resonant excitation, and takes a very short time ($\sim 10^{-8} \text{ s}$). But during this short time period supercompression of the bubble with the extremely high temperature takes place and light emission and even thermonuclear fusion may occur.

(2) Two asymptotic solutions are valid for the low Mach number regime.

The first one is an asymptotic solution for the field far from the bubble, and corresponds to a linear hyperbolic wave equation of the second order.

The second one is an asymptotic solution for the boundary layer near the bubble and corresponds to Laplace equation for an incompressible fluid. For numerical codes the last asymptotic solution gives the possibility to use an economical boundary condition around the bubble during the low Mach number stage that reduces the calculations for this stage by more than three order of magnitude.

(3) The low Mach number stage of the forced oscillations of a bubble in a compressible liquid may be described by the Rayleigh-Plesset equation or Herring-Flynn-Gilmore equation. However, the driving pressures in these equations, namely, the pressure in the local infinity around the bubble p_∞ in the first equation, and the incident pressure p_I in the second one, are different from each other and from the pressure on the flask $p_R(t)$. These two driving pressures, p_∞ and p_I , may be calculated by the flask pressure from the ordinary difference-differential equation presented in this paper.

(4) The amplitude of the pressure at the local infinity of the bubble Δp_∞ , and incident pressure Δp_I , may be much larger than the amplitude of the pressure on the flask Δp_R . This is an effect of amplification of acoustic waves from the flask due to their spherical convergence and this amplification is fully or partly compensated by the expansion and compression of the bubble. This compensation is especially strong at the resonant frequencies.

References

1. Rayleigh, Lord (1917) The pressure developed in a liquid on the collapse of a spherical cavity, *Philos. Mag.*, Vol. 34, pp. 94-98.
2. Knapp, R.T., Daily, J.W., and Hammit, F.G. (1970) *Cavitation*. McGraw-Hill Book Co.
3. Nigmatulin, R.I. (1991) *Dynamics of multiphase systems*, Vol. 1. Hemisphere, Washington.
4. Prosperetti, A., and Lezzi, A. (1986) Bubble dynamics in a compressible liquid. Part 1. First order theory *J. Fluid Mech.*, Vol. 168, pp. 457-478.
5. Nigmatulin, R.I., Akhatov, I.Sh., and Vakhitova, N.K. (1996) The effect of fluid compressibility on the dynamics of the gas bubble, *Physics/Doklady (translated from Russian)*, Vol. 41 no 6, pp.276-279.
6. Moss, W.C., Clarke, D.B., White, J.W., and Young D.A.(1994) Hydrodynamic simulation of bubble collapse and picosecond sonoluminescence, *Phys. Fluids*, Vol. 6 no 9, pp. 2979-2985.
7. Nigmatulin, R.I. and Khabeev, N.S. (1974) Heat exchange between a gas bubble and a liquid, *Fluid Dyn.*, Vol. 9, pp. 759-764.
8. Kamath, V. and Prosperetti, A. (1993) A theoretical study of sonoluminescence, *J. Acoust. Soc. Am.*, Vol. 94 no 1, pp. 248-260.

PARTICLE APPROACH TO STRUCTURE FORMATION IN ACOUSTIC CAVITATION

R. METTIN, C.-D. OHL AND W. LAUTERBORN

Drittes Physikalisches Institut

Bürgerstr. 42-44, D-37073 Göttingen

Germany

1. Introduction

Many gas bubbles emerge when a liquid is strongly sonicated [1]. At least some of them represent the active sites in sonochemistry and multibubble sonoluminescence. Each bubble shows an individual fast dynamics by volume and shape oscillations that are responsible for the specific chemical or luminescent process. However, a bubble field shows a collective dynamics on a slower time scale as well: nucleation, drift, diffusion, coalescence and destruction picture a bubble's life, and many of such histories determine the bubble distribution in space and time. Experiments reveal that this distribution in typical applications is far from homogeneous. On the contrary, the bubbles tend to organize themselves in filaments ("streamers") that can form complex tree-like structures (in analogy to electrical discharge patterns we call them "Acoustic Lichtenberg Figures" or ALFs; see Fig. 1). The inhomogeneous bubble population in strong sound fields is a major complication for the investigation, modeling and enhancement of sonochemical processes, and more insight in the underlying mechanisms are of high demand. Here we report a first step towards a simulation of bubble structure formation by a many particle approach. The basis are recent calculations of Bjerknes forces in strong acoustic fields that govern the bubble motion [2,3].

2. Experiment

The simulation models the following experimental setup: A piezoceramic cylinder (height: 10 cm; radius: 3 cm), filled with tap water, is driven at a frequency near 20 kHz and oscillates in the first radial and first vertical

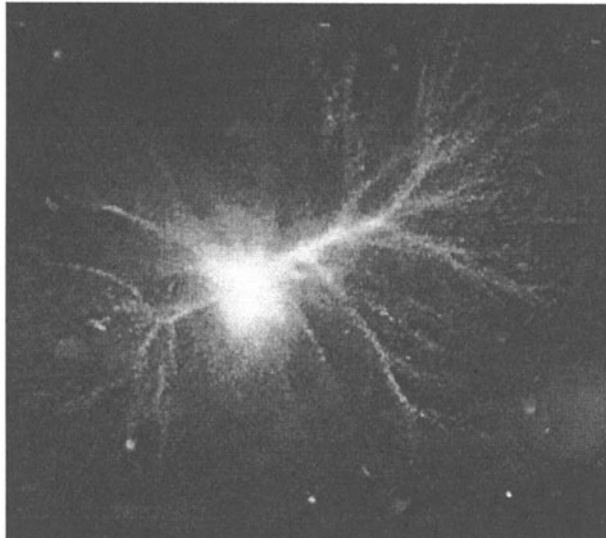


Figure 1. Photograph of a filamentary structure of strong streamers (Acoustic Lichtenberg Figure) arising in the standing wave sound field inside a waterfilled driven piezoceramic cylinder.

mode. Increasing the driving voltage raises the central pressure in the liquid which can reach up to a few bar. Slightly above 1 bar the first very thin (“weak”) streamers appear. They fuse in one center (or node) that is near the geometrical center of the cylinder. Increase of the driving pressure leads to a splitting of the nodes into two, one above and one below the geometrical center. Further increase of the excitation leads to more splitting, and several drifting streamer nodes appear that group on an annulus around the geometrical center. For even stronger driving, above approx. 2 bar, thicker (“strong”) streamers form that unite again in one large centered diffuse node (Fig. 1 shows such an ALF from top). In this regime an intense retroaction of the bubbles on the sound field seems to exist which is not part of our model so far. Therefore, only the transition from one central weak streamer node to many off-centered weak streamer nodes was tried to simulate. Here the bubble density is assumed to be small and without a large disturbing effect on the driving pressure.

ALFs consist of the diffuse node and the filaments (streamers) that contain instreaming bubbles. Experiments with high speed holographic devices revealed that most bubbles in such a structure are sized in the range of a few micron and that their velocities can reach 1 m/s [4]. These investigations are the basis for our bubble size assumptions.

3. Model

The many particle approach calculates the motion in three dimensions of a few hundred bubbles. All are assumed to be spherically symmetric and of the same equilibrium radius $R_0 = 5\mu\text{m}$. Each bubble has a position \mathbf{x}_i and a velocity \mathbf{v}_i that are updated in discrete time steps Δt according to the law of motion. We take into account the following forces on the i -th bubble: induced mass force $(2\pi\rho R_0^3/3)\dot{\mathbf{v}}_i$, primary Bjerknes force \mathbf{F}_{B1}^i , secondary Bjerknes force \mathbf{F}_{B2}^i and a drag force $-\mathbf{v}_i(\beta + \gamma|\mathbf{v}_i|)$ which is fitted to Crum's [5] experimental formula ($\beta = 1.5 \times 10^{-7} \text{ Ns/m}$, $\gamma = 0.25 \times 10^{-7} \text{ Ns}^2/\text{m}^2$). We further assume that the bubbles nucleate near 25 random sites at the resonator wall and vanish after a limited lifetime. By this a permanent in-flow of bubbles is sustained. In clusters, bubbles disappear by a chance of 50% if more than 3 bubbles are closer than $50 \mu\text{m}$, which mimics coalescence. Each time a bubble is destructed, a new one is nucleated. Therefore, the total bubble number stays constant in time. The sound field distribution in the cylindrical resonator is modeled by the first eigenmodes, which is in good correspondence to the measured experimental field:

$$p_a(r, z; t) = \hat{p}_a J_0(k_r r) \cos(k_z z) \cos(2\pi f t),$$

where $f = 20565 \text{ Hz}$ and the boundary conditions determine $k_r = 80.2 \text{ m}^{-1}$ and $k_z = 31.4 \text{ m}^{-1}$. The pressure amplitude depends on the location in space, and consequently also the resulting radial bubble oscillations $R_i(t) = R_i(p_a(r_i, z_i; t))$. This in turn determines direction and magnitude of the Bjerknes forces on bubble i that are computed as follows:

$$\mathbf{F}_{B1}^i = -\langle \nabla p_a(r_i, z_i; t) V_i(t) \rangle = f_{B1}^i \nabla [J_0(k_r r_i) \cos(k_z z_i)],$$

$$f_{B1}^i = \langle V_i(t) \hat{p}_a \cos(2\pi f t) \rangle,$$

$$\mathbf{F}_{B2}^i = \sum_{j \neq i} \frac{\rho}{4\pi} \langle \dot{V}_i(t) \dot{V}_j(t) \rangle \frac{\mathbf{d}_{ij}}{|\mathbf{d}_{ij}|^3} \approx \sum_{j \neq i} f_{B2}^i \frac{\mathbf{d}_{ij}}{|\mathbf{d}_{ij}|^3}, \quad f_{B2}^i = \frac{\rho}{4\pi} \langle \dot{V}_i^2(t) \rangle.$$

Here, $V_i(t) = (4\pi/3)R_i^3(p_a(r_i, z_i; t))$ denotes the volume of the i -th bubble, ρ the liquid density, \mathbf{d}_{ij} the distance vector from bubble i in direction to bubble j , and $\langle \dots \rangle$ means a time average. To speed up computation, the Bjerknes force coefficients f_{B1} and f_{B2} have been tabulated on a spatial grid in (r, z) . The oscillations $R(p_a(r, z; t))$ have been calculated by the Keller-Miksis model from [6] for water under normal conditions. Figure 2 shows the coefficients vs. the radial displacement from the pressure antinode $(r, z) = (0, 0)$ in the $(z=0)$ -plane and for maximum pressure amplitudes $\hat{p}_a = 1.1, 1.3, 1.5$, and 1.8 bar . Positive f_{B1} indicate an attraction towards the pressure antinode, positive f_{B2} indicate attraction between bubbles.

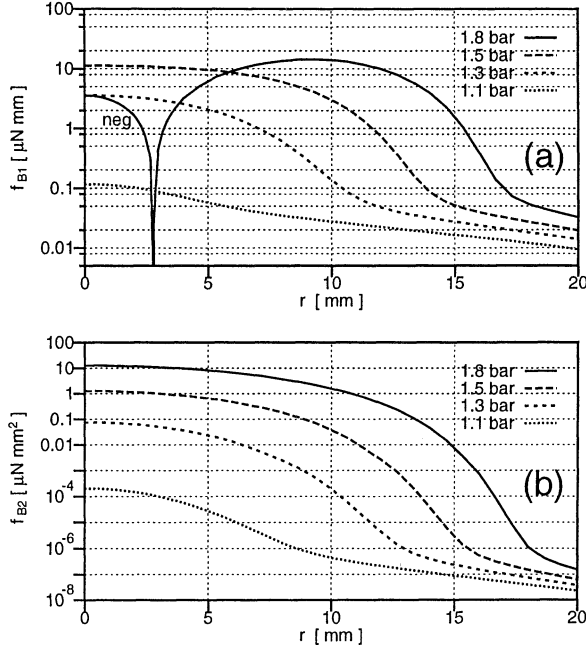


Figure 2. Bjerknes force coefficients f_{B1} (a) and f_{B2} (b) vs. the radial coordinate r in the cylindrical resonator ($z = 0$, $R_0 = 5 \mu\text{m}$) for different maximum pressure amplitudes $\hat{p}_a = 1.1$ to 1.8 bar. The left part of the 1.8 bar curve up to $r \approx 3$ mm labelled with “neg” has negative sign, indicating a repelling antinode.

The strength of the Bjerknes forces varies over several orders of magnitude at different locations and for different values of \hat{p}_a . Note that the pressure antinode becomes repelling for high enough driving (negative values of f_{B1} for $\hat{p}_a = 1.8$ bar below $r \approx 3$ mm in Fig. 2a). The coefficient f_{B2} behaves monotonously with the pressure amplitude. A comparison between the acting Bjerknes forces shows that, for instance, at $\hat{p}_a = 1.3$ bar the primary Bjerknes force at $(r, z) = (1\text{cm}, 0)$ is balanced by the secondary Bjerknes force of a neighboring bubble in a distance of approx. 0.2 mm. At $\hat{p}_a = 1.8$ bar this distance increases to approx. 2 mm. Thus, the bubble-bubble interaction becomes more and more important for higher driving pressure.

4. Results and Discussion

The numerical simulations show collective bubble tracks that can be interpreted as streamers. They fuse in one or more nodes that may drift on a slower timescale. This is similar to the experiment. The number and positions of streamer nodes appear to result from a sensitive interplay of the primary and secondary Bjerknes forces, and they show dependence

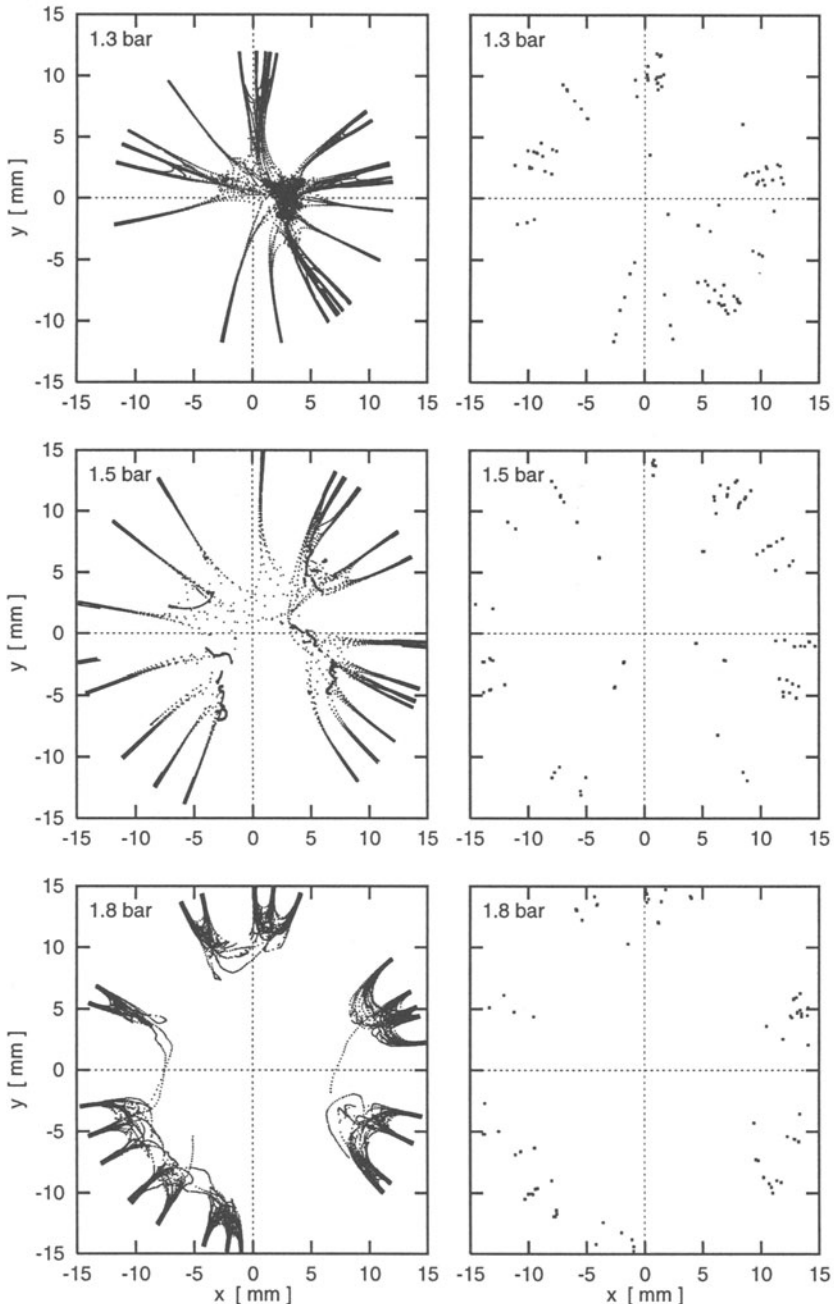


Figure 3. Typical examples of the calculated bubble motion for 100 bubbles and different maximum pressure amplitudes (from the top $\hat{p}_a = 1.3, 1.5$, and 1.8 bar respectively). The left pictures show a superposition of 500 subsequent time steps, the right pictures give a single frame. The view is from the top of the cylinder.

on the quantity, lifetime, and size of the simulated bubbles. However, as a quite robust feature a transition from just one central node to multiple off-centered nodes can be seen for increased pressure. The steps from $\hat{p}_a = 1.1$ bar via 1.3 bar to 1.5 bar are illustrated in Fig. 3 from top to bottom. The left pictures show 500 subsequent frames with respective time steps $\Delta t = 1$ ms (1.3 bar), 0.6 ms (1.5 bar), and 0.1 ms (1.8 bar). The pictures on the right show respective snap shots. The views from the top reveal that the center population decreases and that bubbles group on a ring. On the one hand this is due to the more and more prevailing secondary Bjerknes forces leading to strong attraction of bubble clusters. On the other hand the pressure antinode becomes repelling for nearby bubbles and for large enough \hat{p}_a . The pictured simulated scenario might be identified with the experimentally observed transition of weak streamers from a centered node to many nodes grouped on a ring that takes place between approx. 1 and 2 bar.

The proposed model can only be a first step towards more realistic simulations of collective bubble motion. The ultimate goal of a detailed prediction of the bubble distribution in size and position for a given resonator setup has to take into account many additional effects. Besides efforts to refine the particle approach stands the evolution of a continuous model that has also made progress in recent time [7]. A connection of both models may eventually lead to a satisfactory description of structure formation in acoustic cavitation.

5. References

1. T. G. Leighton (1994) *The Acoustic Bubble* (Academic Press, London).
2. I. Akhatov, R. Mettin, C.D. Ohl, U. Parlitz, and W. Lauterborn (1997) Bjerknes force threshold for stable single bubble sonoluminescence, *Phys. Rev. E* **55**, 3747.
3. R. Mettin, I. Akhatov, U. Parlitz, C.D. Ohl, and W. Lauterborn (1997) Bjerknes forces between small cavitation bubbles in a strong acoustic field, *Phys. Rev. E* **56**, 2924.
4. A. Billo (1996) *Holographische Partikelfeldanalyse am Beispiel Akustischer Lichtenberg-Figuren*, PhD thesis, TH Darmstadt, Germany.
5. L. A. Crum (1975) Bjerknes forces in a stationary sound field, *J. Acoust. Soc. Am.* **57**, 1363.
6. U. Parlitz, V. Englisch, C. Scheffczyk, and W. Lauterborn (1990) Bifurcation structure of bubble oscillators, *J. Acoust. Soc. Am.* **88**, 1061.
7. I. Akhatov, U. Parlitz, and W. Lauterborn (1996) Towards a theory of self-organizing phenomena in bubble-liquid mixtures, *Phys. Rev. E* **54**, 4990.

SINGLE-BUBBLE SONOLUMINESCENCE: SOME RECENT EXPERIMENTS

THOMAS J. MATULA AND LAWRENCE A. CRUM

*Applied Physics Laboratory
University of Washington
1013 NE 40th St.
Seattle WA 98105*

Key words: Sonoluminescence / single-bubble sonoluminescence / bubble levitation / cavitation / bubbles

Abstract. Sonoluminescence refers to the transduction of sound energy into light energy, mediated through the presence of bubbles within the liquid supporting the sound field. The recent discovery that a single air bubble, acoustically levitated in a standing wave in water, can generate sonoluminescence in a stable and repeatable fashion, has led to many remarkable discoveries. Experimentally, single-bubble sonoluminescence is divided by two pressure threshold regions; the luminescence threshold, below which the bubble does not emit light; and the extinction threshold, above which the bubble exists only in a transient fashion. Experimental observations of single cavitation bubbles in the various regions will be described.

1. Introduction

The discovery of single-bubble sonoluminescence by Felipe Gaitan [1], then a graduate student, has led to an explosion of experiments and theoretical models designed to explore and understand this intriguing phenomenon. Felipe showed for the first time that a single bubble, levitated in a sound field, could emit repeatable flashes of light, and using a light scattering technique, showed that the light emission occurred near the minimum of the bubble collapse. These first discoveries solved some of the controversies involving sonoluminescence, but with these new measurements, other questions arose. How can a single bubble, oscillating with such a large dis-

placement amplitude, remain stable, apparently indefinitely? What is the mechanism for converting acoustic energy into electromagnetic energy?

The search for answers to these questions led Seth Putterman at UCLA to explore the details more closely. Instead of finding answers to these questions, his group discovered very interesting phenomena, leading to even more questions. They found that the pulse width was extremely short[2] (later measurements, to be discussed, were able to refine these pulse width measurements). They also found that the spectra of single-bubble sonoluminescence appeared featureless [3] (to the resolution of their system). When they added minute quantities of various gases to their system, strange and inexplicable results were noted. These initial results are described in the references[4].

Although the phenomenon of sonoluminescence from cavitation fields has been known for about 65 years[5], the ability of experimentalists to study sonoluminescence from an individual bubble has led to a much greater understanding of the principles involved. In this paper we discuss some recent experimental findings that offer some answers, but also generate more questions, about this intriguing phenomenon.

2. Single-bubble levitation

In order to study single-bubble sonoluminescence (hereafter called SBSL, for simplicity), one must be able to acoustically levitate the bubble in some vessel or container. Physically, the acoustic radiation force required to levitate a bubble in a standing wave field arises from a pressure difference (gradient) across the bubble. Figure 1 illustrates this effect for the case of *small* driving pressures (and for drive frequencies below the bubble's natural resonance frequency). During the negative portion of the sound field, the bubble grows. There is a pressure force on the bubble due to a slight difference in pressure exerted on either side of the bubble's surface. This force directs the bubble towards the pressure antinode. During the compressive phase of the sound field, the bubble is small, and the force is directed away from the pressure antinode. However, since the corresponding volume is smaller, this force is smaller, and hence, over an acoustic cycle the average (or Bjerknes) force directs the bubble towards the antinode. This argument on the direction of the force applies only to a bubble that is driven below its natural resonance frequency. For bubbles driven above their natural resonance frequency, a different phase response requires them to be forced away from the pressure antinode and toward a node.

Though valid at lower drive pressure amplitudes, the results of this description of the Bjerknes force must be modified at higher driving pressures, where inertial effects become important. In fact, at driving pressures above

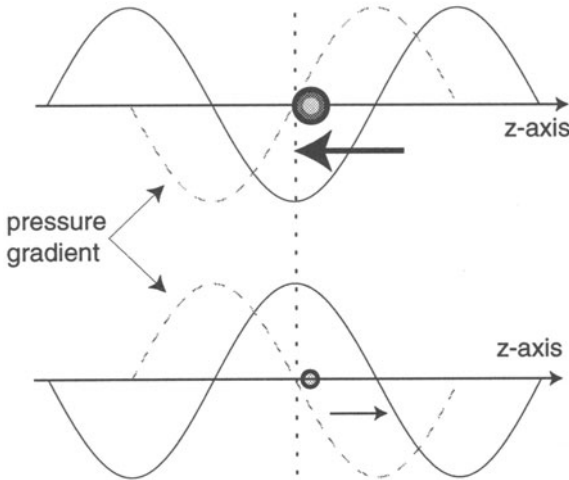


Figure 1. Small bubbles (below resonance size) are levitated at the pressure (velocity) antinode (node). For sonoluminescence bubbles, the highly nonlinear motion of the bubble limits the drive pressure amplitude that can stably levitate the bubble. (From Matula, et al.[6])

about 1.7 atm. the acoustic radiation force pushes the bubble *away* from the pressure antinode, precluding levitation at these relatively high pressure amplitudes[6].

Also important is the effect of buoyancy (and to a lesser extent, the particle velocity, since the bubble is not positioned exactly at the pressure antinode). Thus the *average* buoyancy and acoustic radiation forces balance in order to levitate a bubble. These forces can be expressed as

$$\frac{\rho g}{T} \int_0^T V(t) dt = \frac{\omega k_z P_a}{T} \sin(k_z z) \int_0^T V(t) \sin(\omega t) dt. \quad (1)$$

where ρ is the fluid density, g is the gravitational acceleration, $V(t) = 4/3\pi R(t)^3$ is the bubble volume, $k_z = 2\pi/\lambda_z$ is the vertical wavenumber, T is the acoustic period, and P_a is the applied drive pressure amplitude.

A simple expression for the equilibrium levitation position of the bubble can be obtained, provided one assumes the bubble is near the pressure antinode. Then $\sin(k_z z) \approx k_z z$, and

$$z \approx \frac{\rho g}{\omega k_z^2 P_a} \frac{\Lambda_1}{\Lambda_2}, \quad (2)$$

where $\Lambda_1 = \int_0^T V(t) dt$ and $\Lambda_2 = \int_0^T V(t) \sin(\omega t) dt$.

Figure 2 shows the equilibrium bubble position, (using Eq. 2), above the antinode as a function of the applied pressure amplitude.[7] For small

drive pressures, the equilibrium position of the bubble is nearly inversely related to the drive pressure, as seen in Eq. 2. However, as the drive pressure is increased further, the bubble position begins to shift *away* from the antinode (see Fig. 2, the slope of the curve changing signs). Beyond about 1.78 atm. the bubble can no longer be levitated, since the Bjerknes force now pushes the bubble away from the antinode (due to the highly nonlinear oscillations of the bubble).

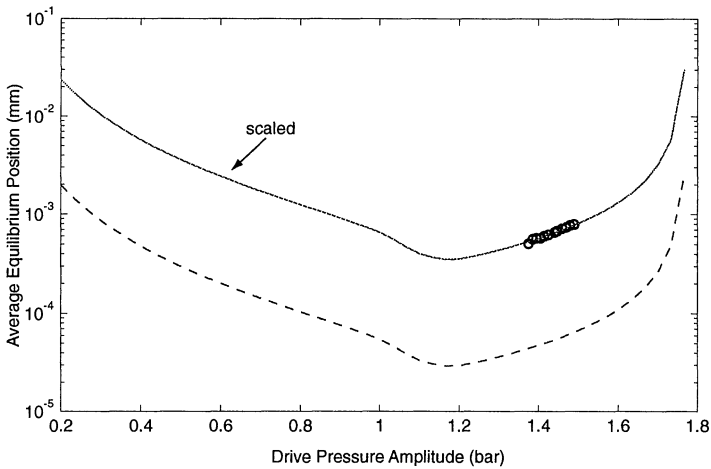


Figure 2. The solution of Eq. 2 results in the dashed line shown above. For acoustic pressure amplitudes below about 1.2 bars, the bubble is drawn toward the antinode; above this value, the bubble, *although still levitated*, is positioned away from the antinode. The calculation agrees qualitatively with experimental measurements, shown as circles, however, quantitative agreement requires a scaling factor (shown as a solid line). (From Matula, *et al.*[6])

Also shown in the figure is experimental measurements of the equilibrium position, as determined using a microscope. Note that the qualitative features of the calculation agree well with experiment, however, there appears to be a scaling discrepancy. The mechanism for the observed discrepancy may involve the interaction of the bubble with the sound field, or even microstreaming around the bubble[6].

It is interesting to note that in the absence of gravity, there is no buoyancy force, and thus the bubble should be levitated almost exactly at the pressure antinode, instead of slightly above the antinode. Under such conditions, one should be able to drive the bubble to a larger volume expansion, and achieve greater light output during the collapse. Of course, this assumes that observed surface instabilities[8] do not limit the collapse energy. If these observed instabilities are due to the translational motion of the bubble (due to periodic variations in the buoyancy and acoustic radiation forces), then

increasing the energetical collapse of SBSL bubbles should be achievable in a microgravity environment. There is some preliminary evidence that this is indeed the case[9], although more studies need to be undertaken.

3. Stability regions

SBSL is found to occur over a relatively small region of drive pressure amplitudes. Figure 3 illustrates the various regions in acoustic pressure amplitude space over which SBSL occurs for an air bubble in water (these regions are defined assuming 1 atm. of ambient pressure). At low driving pressures, the bubble oscillates in a spherical manner, but dissolves due to the low gas concentration in the fluid. At higher drive pressures, the bubble grows by rectified diffusion[10], and eventually fragments and reforms; micro-jetting and dancing behavior appear to occur. As the drive pressure amplitude is increased further, one notices that the bubble appears to “lock” in place. This stability is typically coincidental with light emissions; i.e., the luminescence threshold (≈ 1.2 atm.) has been crossed. Above the luminescence threshold, the light emission intensity is proportional to the drive pressure amplitude[11], until the extinction threshold is reached (≈ 1.4 atm.) above which the bubble self-destructs.

It is worth noting that there is a hysteresis effect; the drive pressure amplitude for the luminescence threshold is lower if approached from above the threshold, rather than approaching from below the threshold. On the other hand, the extinction threshold apparently depends on the *rate* at which the threshold is approached (from below only, since the bubble cannot exist above the extinction threshold). Experimental measurements around these thresholds can be found in the references[8].

4. Transient response of SBSL - Evidence for gas exchange

One of the more interesting hypotheses that have recently come forth is the hypothesis that SBSL with air bubbles results in chemical dissociation of the diatomic species Nitrogen and Oxygen, which are irreversibly removed from the bubble, leaving only argon inside. Thus a sonoluminescing “air” bubble actually becomes an argon bubble. This hypothesis explains why noble gas doping is so influential in SBSL. We tested this hypothesis in a novel way by performing the following experiment[12]:

We begin with a bubble levitated below the luminescence threshold, and then rapidly *increase* the drive pressure amplitude to a level such that the bubble is in a steady sonoluminescing state. By monitoring the light emission intensity, we find that the light emission occurs immediately after the drive pressure is increased [see Fig. 4(a)], and continues to grow in

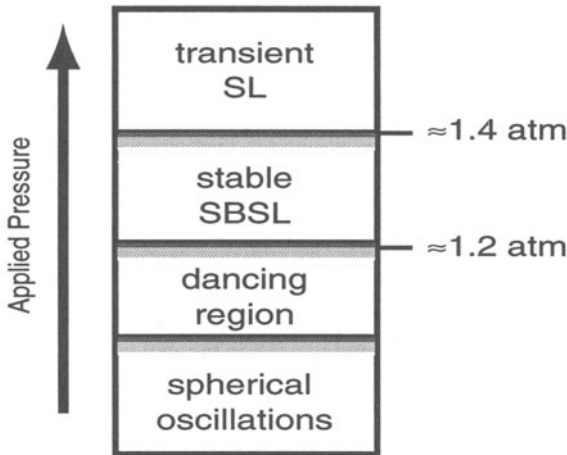


Figure 3. SBSL is bounded by two thresholds in the drive pressure parameter space. Below the lower (incipient, or luminescence) threshold (≈ 1.2 atm.) bubble levitation is possible, but no light is emitted. Above the upper (or extinction) threshold (≈ 1.4 atm.) the bubble exists only transiently, becoming unstable and self-destructs. Stable SBSL occurs between these two thresholds.

intensity, reaching a maximum intensity over several seconds (only the first several milliseconds are shown in the figure).

After the bubble reaches an equilibrium in the steady sonoluminescing state, we rapidly *reduce* the drive pressure to its original value (below the luminescence threshold). Then, after the bubble is subjected to a pressure amplitude below the luminescence threshold for a fixed (short) interval of time, we rapidly *increase* the drive pressure amplitude back up the its value above the luminescence threshold. Figure 4(b) shows that, after the final increase in drive pressure, the light emission intensity is near a maximum, and does not change over time, as it would if the bubble started out below the luminescence threshold [Fig. 4(a)]. If the bubble is held below the luminescence threshold for several seconds before the drive pressure amplitude is increased, one finds that the light emission intensity is diminished, and subsequently grows to its maximum over time scales lasting seconds. The longer one stays below the luminescence threshold before returning the bubble to a luminescing state (after starting out above the threshold), the dimmer the initial emission intensity, and the longer the time required to reach its maximum intensity.

These series of experiments were then compared to similar experiments using either pure nitrogen, hydrogen, argon, helium, or neon. In all cases, the light emission occurred immediately after the drive pressure was increased; however, the diatomic gases showed steady, but diminished intensity, while the noble gases showed steady, but much brighter intensity.

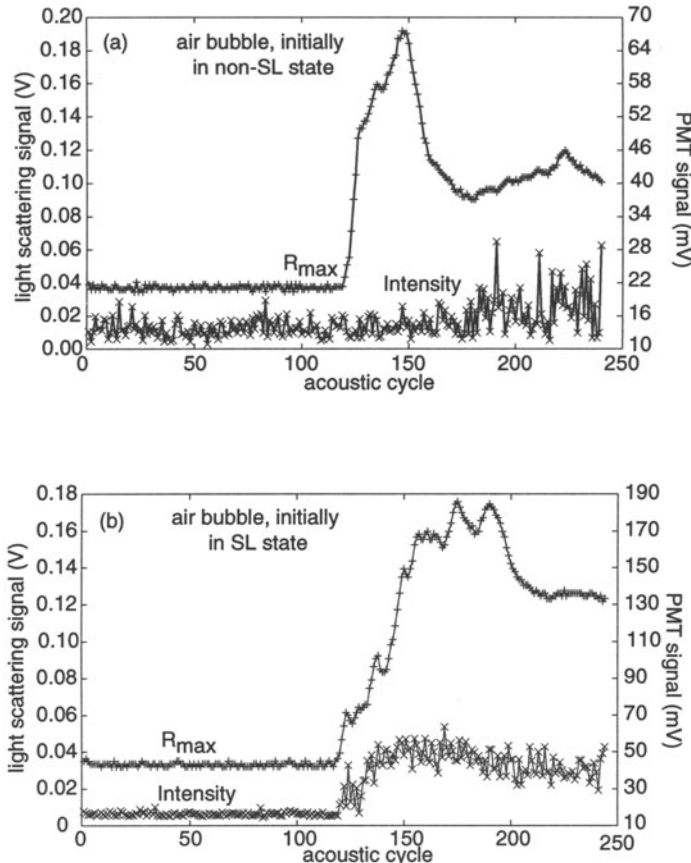


Figure 4. The intensity and temporal evolution of SBSL depend on whether the bubble has previously existed in a state of sonoluminescence. In (a), an air bubble is brought above the luminescence threshold for the first time. Note that the sonoluminescence flashes (labeled ‘intensity’) are dim. In (b), the same bubble is brought above the luminescence threshold after having been in a sonoluminescing state for about 10 seconds. Note how strong the light emission is, compared to (a). If the bubble is allowed to stay below the luminescence threshold for several seconds, and is then brought back to a state above the threshold, it again appears as in (a), suggesting that argon rectification is occurring. The curves labeled R_{max} actually correspond to the maximum scattered light level from our apparatus (From Matula and Crum[12])

That is, experiments using noble gases resulted in observations similar to Fig. 4(b), while experiments with diatomic gases resulted in observations similar to Fig. 4(a). We believe that these series of experiments are strong evidence that support the argon-rectification hypothesis[13].

5. Acoustic emission from SBSL

Although most work involves measurements of the emitted light, a cavitating bubble also generates an acoustic pulse that can be easily detected by most hydrophones. Figure 5 shows the temporal profile of an acoustic pulse generated by an SBSL bubble, as observed using a small PVDF hydrophone placed 1 mm from the bubble. The rise time of this pulse, ≈ 5.2 ns, nearly

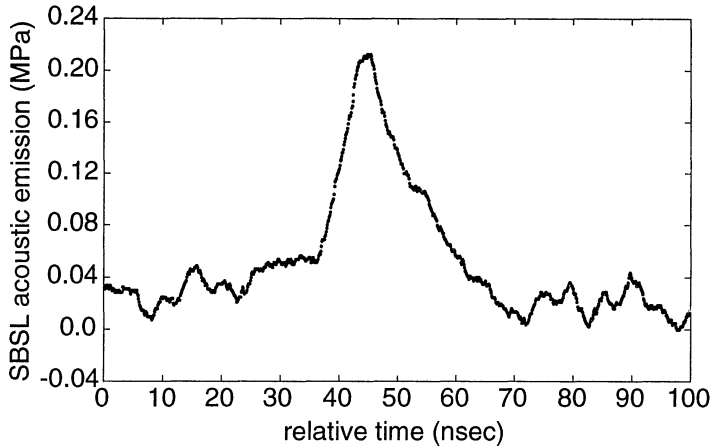


Figure 5. SBSL gives rise to a strong acoustic pulse that can easily be observed using a needle hydrophone or focused transducer. Acoustic pulses from the bubble below the luminescence threshold can also be detected. (From Matula, *et al.*[14])

corresponds to the bandwidth limitations of our system, and may even be broadened by the finite size of the hydrophone[14]. The pulse has a rather large amplitude, even at 1 mm from the bubble. Assuming only spherical spreading, the pulse amplitude near the bubble when the pulse is emitted (assumed to be near 1 μm) is in excess of 1,700 atm. Such a strong pulse can result in damage to tissue or other objects located nearby.

Figure 6 shows that the acoustic pulses are emitted at discrete intervals during the bubble oscillatory cycle, as determined by simultaneous light scattering (discussed later) and hydrophone measurements. In this case, a focused transducer is used to observe not only the main acoustic pulse originating from the main collapse of the bubble, but also those occurring after each consecutive rebound, or afterbounce. The origin of the acoustic pulse may be from internal shock waves, or bubble wall motion, or both.

6. Pulse duration of SBSL

Initial measurements of the pulse duration (or pulse width) claimed that the duration was less than 50 ps[2]. These initial measurements utilized a

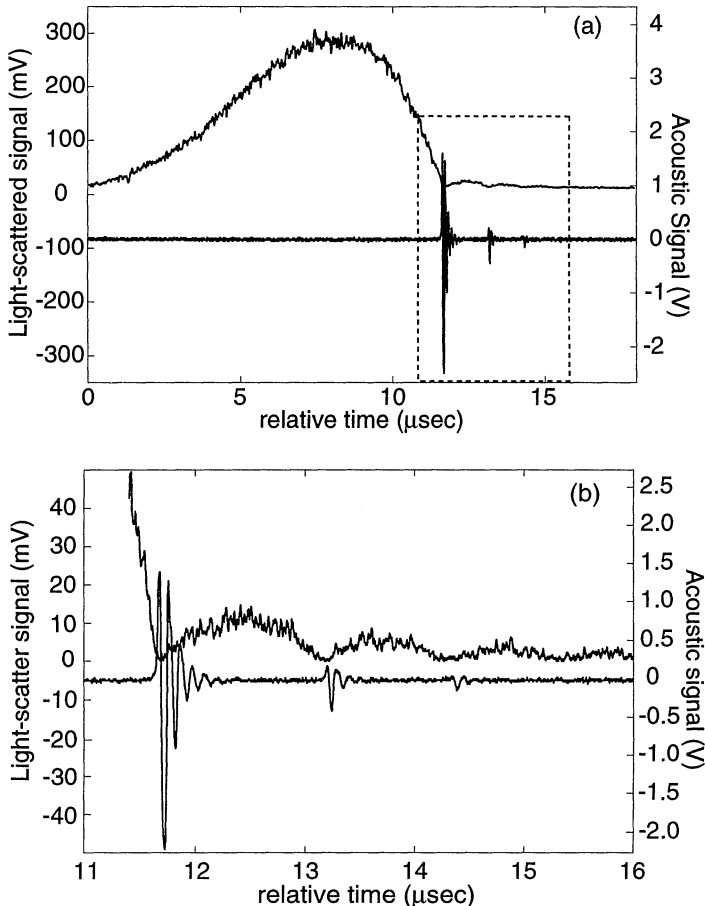


Figure 6. Using a focused transducer as a hydrophone, and correlating the acoustic emissions with the scattered light intensity, we find that the observed acoustic pulses are correlated with each rebound, or afterbounce. (From Matula, *et al.*[14])

photomultiplier tube (PMT) as a direct measure of the pulse shape. Unfortunately, the pulse duration appeared to be near, or less than the impulse response of the PMT. A subsequent measurement using a streak camera also appeared to confirm the early PMT measurements[15]; however, the early streak camera measurements may to be faulty to some extent[16]. Recently, a new method has been employed for measuring the pulse width[17]. Figure 7 illustrates the technique. Two PMT's are positioned such that they each collect photons from the *same* pulse. A histogram of the delay between the arrival times of the photons gives rise to a pulse shape, as shown in Fig. 8. Using this technique, pulse widths have been measured to be between about 35-350 ps.[18] Preliminary streak camera measurements

confirm these results[19].

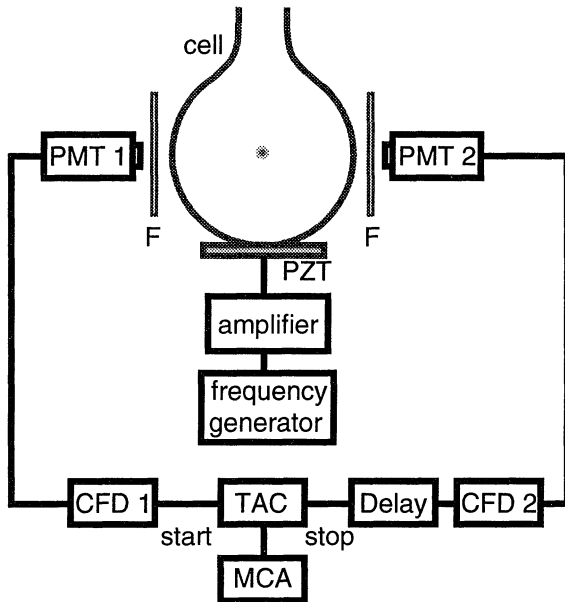


Figure 7. Schematic diagram illustrating the technique used to measure the pulse width from SBSL. This technique involves building a histogram of time intervals between photons observed during each individual pulse. The addition of filters in front of the PMTs allows one to perform time-correlated spectroscopy as well.

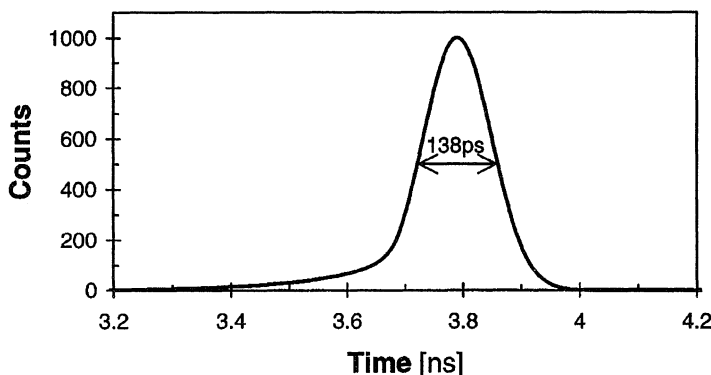


Figure 8. The observed pulse with lasts from ≈ 35 – 350 ps. There is also some asymmetry to the pulse shape, although the technique cannot be used to determine if the asymmetry occurs as a ‘preglow’, or ‘afterglow’. (From Gompf, *et al.*[17])

7. Single-bubble versus Multi-bubble sonoluminescence

Multi-bubble sonoluminescence (MBSL) refers to sonoluminescence from a field of cavitating bubbles. These bubbles presumably are influenced, not only by the large acoustic pressure amplitudes, but also by other nearby bubbles, as well as the vessel walls. It is probable that bubbles in a cavitation field cannot survive more than a few acoustic cycles, and thus, probably do not show evidence for gas exchange, as discussed in a previous section. Nevertheless, some useful comparisons can be made. For instance, if one examines the pulse duration from MBSL using fast optics and digitizers, the duration (or pulse width) is found to be less than about 1 ns (see Fig. 9), which agrees well with the pulse duration of SBSL[20].

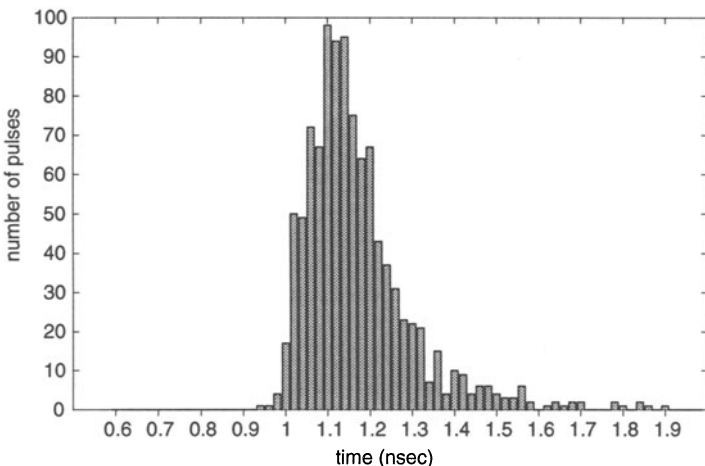


Figure 9. A histogram of pulse widths from MBSL. Our system is limited to about 1.1 ns, as measured with single photon pulse widths, suggesting that MBSL pulses are significantly shorter than 1 ns. (From Matula, *et al.*[20])

Another area of comparison between MBSL and SBSL that has recently been explored is the spectral characteristics of the light emission. In a study comparing the spectral characteristics from an aqueous solution containing sodium chloride, it was found that the sodium doublet, which is prominent in MBSL, is completely absent in SBSL[21] (see Fig. 10). One possible explanation for this difference is in the dynamics of the bubble(s). SBSL bubbles appear to be spherical through most of the acoustic cycle. There is no mechanism for sodium, which is nonvolatile, to enter the bubble's interior, where it can be heated to incandescence. MSBL bubbles, on the other hand, are subject to intense pressures and pressure gradients that result in non-spherical pulsations; thus, there are several mechanisms for

sodium to become entrained within these bubbles, resulting in a sodium emission after the collapse.

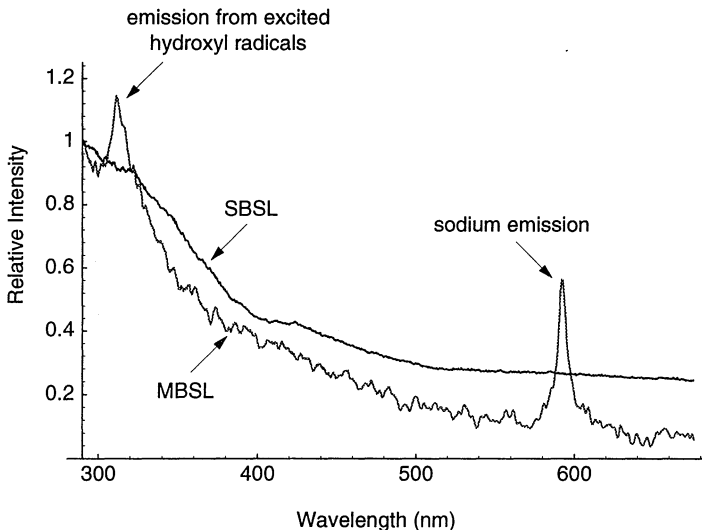


Figure 10. A comparison between MBSL and SBSL shows several differences and similarities. (From Matula, et al.[21])

Although the differences in the spectra are prominent, note that there is a similarity in the underlying continuum. This similarity may be interpreted by assuming some MBSL bubbles act like SBSL bubbles, giving rise to the continuum, while other bubbles are much cooler, and give rise to line and band emissions. Previous interpretations have described the continuum as a series of overlapping band emissions, with some experimental evidence to support that hypothesis[22]; however, recent experiments have cast some doubt on the older experimental results[23]. *It is apparent that the commonality of cause (acoustic cavitation) and effect (light emission) for both types of sonoluminescence suggests some association of the underlying physics.*

8. Conclusion

Although each new experiment still results in many new questions, there has been significant progress in the field of single-bubble sonoluminescence. The pulse width of SBSL can now be measured in many cases. Similarly, the effect of noble gas doping appears to have an explanation involving chemical activity of the bubble constituents, although no one has yet to measure chemical activity from within a luminescing bubble[24]. Experimentalists are still trying to obtain line or band emission from SBSL, which should give scientists clues as to the temperature inside SBSL bubbles. It is still

unknown whether an SBSL bubble can be made to collapse with enough violence so that neutrons can be emitted. Finally, in this paper we have only explored a small portion of the experiments (and *none* of the theories) that have recently been published. This intriguing phenomenon should command our attention for many more years. It's our belief that there are still many new and exciting features of sonoluminescence are yet to be discovered.

9. Acknowledgments

This research is supported by NSF and DOE.

References

1. D. F. Gaitan, (1990) "An experimental investigation of acoustic cavitation in gaseous liquids," Ph.D. Thesis, Univ. of Miss.; D. F. Gaitan, L. A. Crum, C. C. Church, and R. A. Roy, (1992) "Sonoluminescence and bubble dynamics for a single, stable, cavitation bubble, *J. Acoust. Soc. Am.*, **91**, 3166–3183.
2. B. P. Barber and S. J. Putterman, (1991) "Observation of synchronous picosecond sonoluminescence," *Nature*, **352**, 318–320.
3. R. Hiller, S. Putterman, B. P. Barber, (1992) "Spectrum of Synchronous Picosecond Sonoluminescence," *Phys. Rev. Lett.*, **69**, 1182–1184.
4. See e.g., B. P. Barber, R. A. Hiller, R. Löfstedt, S. J. Putterman, K. R. Weninger, (1997) "Defining the unknowns of sonoluminescence," *Physics Reports* **281** 65–143.
5. For a review of sonoluminescence research prior to 1984, see A. J. Walton and G. T. Reynolds, (1984) "Sonoluminescence," *Advances in Physics* **33** 595.
6. T. J. Matula, S. M. Cordry, R. A. Roy, and L. A. Crum, (1997) "Bjerknes force and bubble levitation under single-bubble sonoluminescence conditions," *J. Acoust. Soc. Am.*, **102**, 1522–1527.
7. This calculation was for a 5 μm equilibrium radius bubble, driven at 19.5 kHz. It should be pointed out that at the drive pressure changes, the bubble's equilibrium radius will also change; however, the set of curves generated for different radii appear similar, and differ only slightly from that shown here.
8. R. G. Holt and D. F. Gaitan, (1996) "Observation of stability boundaries in the parameter space of single bubble sonoluminescence," *Phys. Rev. Lett.*, **77**, 3791–3794.
9. T. J. Matula, R. A. Ry, L. A. Crum, and D. L. Kuhns, (1996) "Preliminary experimental observations of the effects of buoyancy on single-bubble sonoluminescence in microgravity and hypergravity," *J. Acoust. Soc. Am.*, **100**, 2717; T. J. Matula, J. E. Swalwell, V. Bezzerezides, P. Hilmo, M. Chittick, L. A. Crum, D. L. Kuhns, and R. A. Roy, (1997) "Single-bubble sonoluminescence in microgravity," *J. Acoust. Soc. Am.*, **102**, 3185;
10. See e.g., L. A. Crum, (1980) "Measurements of the growth of air bubbles by rectified diffusion," *J. Acoust. Soc. Am.*, **68**, 203–211.
11. T. J. Matula, private communication.
12. T. J. Matula and L. A. Crum, (1998) "Evidence for gas exchange in single-bubble sonoluminescence," *Phys. Rev. Lett.*, **80**, 865.
13. M. P. Brenner, S. Hilgenfeldt, and D. Lohse, (1996) "Why air bubbles in water glow so easily," in *Nonlinear Physics of Complex Systems—Current Status and Future Trends* (edited by Parisi, Mueller, and Zimmermann, Springer Lecture Notes in Physics), pg 79–97; (1996) D. Lohse, et al., Sonoluminescing air bubbles rectify argon, *Phys. Rev. Lett.* **78**, 1359.
14. T. J. Matula, I. Hallaj, R. O. Cleveland, R. A. Roy, and L. A. Crum, (1998) "The acoustic emissions from single-bubble sonoluminescence," to appear in *J. Acoust. Soc. Am.*

15. M. J. Moran and R. E. Haigh and M. E. Lowry and D. R. Sweider and G. R. Abel and J. T. Carlson and S. D. Lewia and A. A. Atchley and D. F. Gaitan and X. K. Maruyama, (1995) "Direct observations of single sonoluminescence pulses," Nucl. Instr. and Meth. in Phys. Res. B," **96**, 651–656.
16. The published results that show streak camera measurements of a few picoseconds may simply be noise pulses, and not actual light emissions from SBSL; M. Moran (private communication).
17. B. Gompf, R. G'unther, G. Nick, R. Pecha, and W. Eisenmenger, (1997) "Resolving sonoluminescence pulse width with time-correlated single photon counting," Phys. Rev. Lett., **79** 1405–1408.
18. The lower bound pulse width of 35 ps has recently been measured at UCLA.
19. P. Young, LLNL, private communication.
20. T. J. Matula, R. A. Roy, and P. D. Mourad, (1996) "Pulse width of sonoluminescence from cavitation fields," J. Acoust. Soc. Am.
21. T. J. Matula and R. A. Roy and P. D. Mourad and W. B. McNamara and K. S. Suslick, (1995) "Comparison of multibubble and single-bubble sonoluminescence spectra," Phys. Rev. Lett. **75**, 2602–2605.
22. C. Sehgal, R. G. Sutherland, and R. E. Verrall, (1980) "Selective quenching of species that produce sonoluminescence," J. Phys. Chem., **84**, 529–531.
23. W. B. Mcnamara, K. S. Suslick, and T. J. Matula, private communication.
24. There has been some experimental evidence (unpublished) that a single sonoluminescing bubble generates chemical activity; T. Lepoint and F. Mullie-Lepoint used a Weissler reaction scheme to show the precipitation of iodide emanating from the vicinity of the bubble.

STAR IN A JAR*

W. C. MOSS, D. B. CLARKE, AND D. A. YOUNG
Lawrence Livermore National Laboratory
7000 East Ave.
Livermore, CA 94550
USA

Abstract. A sonoluminescing bubble has been modeled as a thermally conducting, partially ionized two-component plasma. The use of accurate equations-of-state, plasma physics, and radiation physics distinguishes our model from all previous models. The model provides an explanation of many features of single bubble sonoluminescence that have not been collectively accounted for in previous models, including the origin of the picosecond pulse widths and spectra. The calculated spectra for sonoluminescing nitrogen and argon bubbles suggest that a sonoluminescing air bubble probably contains only argon, in agreement with a recent theoretical analysis.

1. Introduction

In the beginning, Gaitan said

“I need a small spot of light to get my Ph. D.”

Then....

Gaitan made the light and saw that it was good.

Crum saw the light and quickly signed the thesis [1].

Puttermann saw the light...

- it was hot [2]

- it was brief [3]

...and for a while we all believed in magic [4].

But most scientists prefer not to believe in magic, even though most everyone else does. Consequently, it was natural for every scientist to explain the phenomenon as a simple example of his/her area of expertise: The Quantum Field Theorists said, “Energy is extracted from the vacuum;” The Fluid Dynamicists said, “Colliding liquid jets;” The Plasma Physicists said, “Electric discharge from tiny balls of plasma;” The Mechanical Engineers said, “Energy from acoustic resonances;” The Chemists said, “Energy from chemical reactions;” and The Shock Physicists said, “Energy from shock waves.” Amidst the controversy, the scientific community showed an unusual amount of respect and tolerance:

The Experimentalists said “The Theorists are nuts;”

The Theorists said, “Every other theorist is nuts.”

Only the Hollywood movie *Chain Reaction* claimed to have the answer, but the details were scattered across the floor of the cutting room. This left the theorists still having to explain the “Star in a Jar.”

2. Model

We have developed a new theoretical model for single bubble sonoluminescence (SBSL) that for the first time is consistent with experimental results, makes predictions about the sensitivity of SBSL to various parameters, and provides an explanation of many features of SBSL that have not been collectively accounted for in earlier models [5]. In particular, our model shows that: (i) the optical pulse width and spectra are very sensitive to the maximum bubble radius, which is controlled by the applied acoustic pressure; (ii) the emitted light is described by neither a pure Planckian, nor a pure bremsstrahlung spectrum, but a convolution of the two; (iii) the spectral flux of nitrogen SBSL is approximately 1/25 that of air, which agrees with experimental measurements [6]; (iv) the spectrum of argon SBSL is nearly identical to the measured spectrum of air SBSL, which suggests that a sonoluminescing air bubble is actually an argon bubble undergoing SL [7], and may also explain why SBSL in noble gases is more intense than in diatomic gases [6]; (v) electron conduction and the emission properties of the hot, compressed gas are the mechanisms responsible for the picosecond duration of SBSL; and (vi) that after the main flash there cannot be an “afterglow” emitted by the expanding hot bubble [8].

Our model has two basic assumptions. The first assumption is that as the bubble collapses, the gas inside is compressed and heated. This is analogous to the heat that is generated in the housing of a foot pump when it is used to fill a tire. The second assumption is that the hot gas emits light. We performed fluid dynamics simulations of the growth and collapse of a gas-filled bubble and the liquid surrounding it [5]. Our calculations show that during the collapse of the bubble, a shock wave is generated that compresses and heats the contents of the bubble [9]. More heating occurs at the center of the bubble than at its boundary because the shock wave’s strength increases as it approaches the

bubble's center. The hotter central region begins to ionize and creates a two-component partially ionized plasma of ions and electrons. The hot matter emits light by an energy cascade from the ions, to the electrons, to the photons. Although work is done on both the ions and the electrons as the bubble collapses, the mechanical energy from the shock goes only into the ions [10]. The ions lose energy by thermal conduction (ion conductivity $\sim T_i^{5/2} Z^{-4} M_i^{-1/2}$, where T_i , Z , and M_i , are the ion temperature, ion charge, and ion mass) and by collisions with the electrons. The electrons also lose energy by thermal conduction (electron conductivity $\sim T_e^{5/2} Z^{-1} M_e^{-1/2}$, where T_e , Z , and M_e , are the electron temperature, ion charge, and electron mass). Electron conduction is typically the dominant energy loss mechanism because of the mass term. It should be noted that plasma thermal conduction is a much faster process than normal atomic thermal conduction, which is proportional to $T^{1/2}$. In the final step of the cascade, the electrons lose energy to the photon field to produce the SL flash. Although the details of the electron-photon coupling are in general very complicated, the high density of the plasma ($\sim 1\text{g/cc}$) results in very short collisional times in the plasma ($\sim\text{femtoseconds}$), which greatly simplifies the calculation of the emitted light [11].

3. Results

Figure 1 shows our calculated temporal and spatial evolution of the SL flash from a collapsing argon bubble. The ambient bubble radius, R_o , is $4.5\mu\text{m}$. The maximum bubble radius, R_{\max} , is $45\mu\text{m}$. Five snapshots of the final 50ps of the collapse are shown, during which the radius decreases from 0.45 to $0.43\mu\text{m}$. Time is referenced to the instant when the shock wave reaches the center of the bubble.

At -10ps, the shock wave (solid curve) is near the center of the bubble and light begins to be emitted (lightly shaded region) just behind the shock wave. At 0ps, the shock reaches the center of the bubble. At this point, the power that is emitted in the visible spectrum is one-half its eventual peak value.

The emitting regions of the bubble are very much like those in a miniature star: Visible light from the sun appears yellow, which is indicative of a temperature of approximately 6000K. However, the center of the sun is much hotter, nearly 10^7K . This temperature can't be seen, because the light that is emitted from the deeper regions is absorbed before it reaches the surface. This deeper absorbing region is described as being "optically thick." The solid black region in the figure shows where the bubble is optically thick. Only the light emission from the "halo" (lightly shaded region) and from the surface of the optically thick region can be seen. At 15ps, the shock has reflected from the center of the bubble and is moving outward, but the gas outside the shock is still moving towards the bubble's center, compressing, and heating. Consequently, the emitting halo is slightly larger. The emitted visible optical power is at its peak value.

At 25ps, the light emitting halo is even larger, but the bubble has cooled, so that the emitted visible optical power has decreased to one-half its peak value. At 40ps, the bubble is

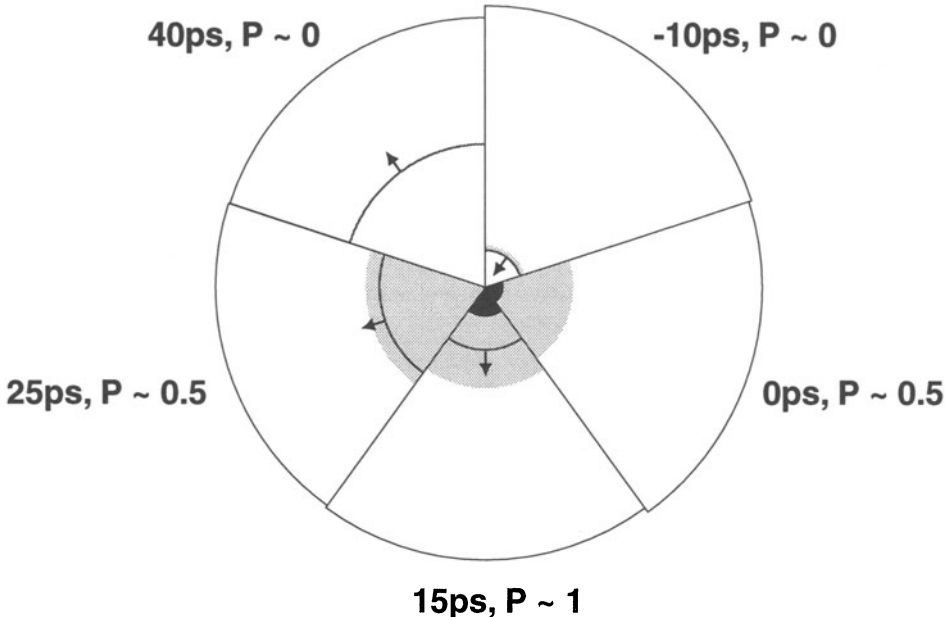


Figure 1. The final 50ps of the calculated collapse of an argon bubble. The bubble radius (outermost curve), shock wave location (inner curve), and emitting regions (optically thin [shaded], optically thick [solid]) are shown. P is the relative emitted optical power in the visible part of the spectrum.

too cool to emit light. The bubble temperature decreases due to electron conduction and the expansion and adiabatic cooling behind the outgoing shock. By comparing the times at which one-half peak power occurs, a 25ps pulse width can be deduced from the figure, which is consistent with experimentally measured values [3]. Our model predicts that there is no afterglow as the bubble expands and cools. The calculations show that the short pulse width and lack of afterglow are intimately related and are due to electron conduction, adiabatic cooling behind the divergent shock, and the strong temperature dependence of the emission properties of the plasma.

We note that the agreement of our calculated results with the experimental data arises from our use of accurate high temperature/pressure equations of state, plasma physics, and radiation physics. This additional physics is required to obtain our results and distinguishes our model from all previous models.

Figure 2 shows the wavelength dependence of the computed spectral content (femtojoules per nanometer) of argon (dashed line) and air (nitrogen) bubbles (solid and dotted lines) [$R_o = 4.5\mu\text{m}$, $R_{\max}/R_o = 10.0$, for both bubbles]. The experimental SBSL spectrum for room-temperature air [2] (solid circles) is also shown. Our calculation agrees with the observation that the measured air spectrum is ~ 25 times more intense than the measured

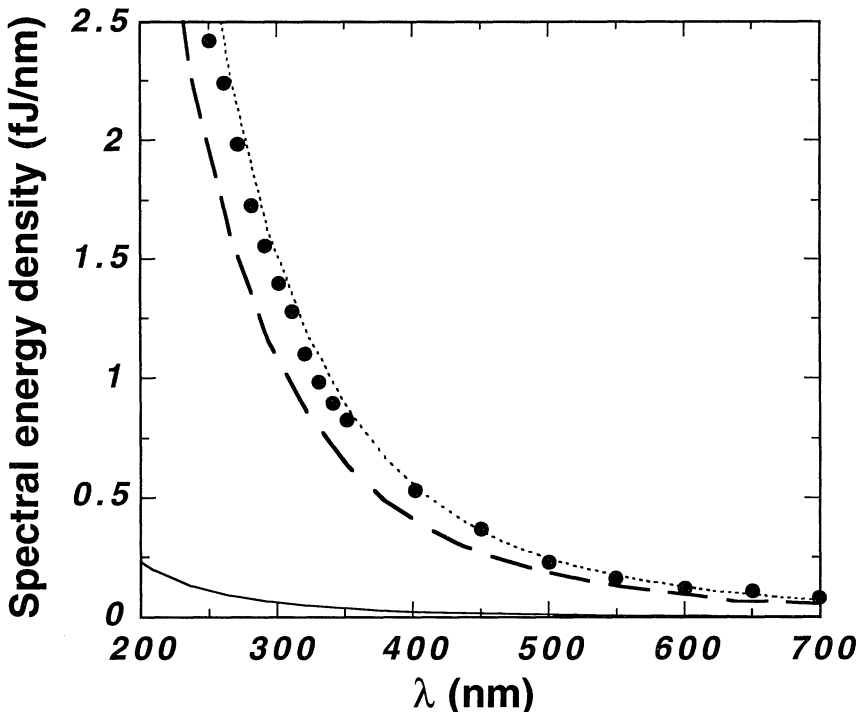


Figure 2. The wavelength dependence of the measured SBSL spectrum for air (circles) and calculated spectra for nitrogen (solid line) and argon (dashed line). The calculated spectrum of a nitrogen bubble undergoing SL is only 4% as intense as the measured air spectrum, in agreement with experimental data. The dotted line shows the calculated nitrogen spectrum multiplied by 25.

nitrogen spectrum [6]: The dotted line shows our calculated spectrum multiplied by 25.

Experimental measurements have shown that the intensity of air SBSL is affected strongly by the amount of noble gas (0.9% argon) in the air [6]. The addition of 0.9% argon has a negligible calculated effect on the optical emission and cannot account for the factor of 25 for the calculated results shown in Fig. 2. Lohse et al. [7] have suggested that chemical reactions due to the high temperatures in an air bubble undergoing SL can rectify its contents so that only the chemically inert argon remains. The calculated spectrum from the results shown in Fig. 1 is plotted (dashed line) in Fig. 2. The agreement of this argon calculation with the air data is very good.

The shock is stronger in the nitrogen than in the argon bubble, because argon's higher specific heat ratio ($5/3$ vs. $7/5$) makes it more difficult to generate a shock in argon than in nitrogen. This produces higher sound speeds in argon, for similar compressions, yet the calculated output of the argon bubble is over 20 times greater than the nitrogen bubble. Although the shock is weaker in argon than in nitrogen, the temperature is a stronger

function of compression in argon because of the larger specific heat ratio. Consequently, the argon bubble is compressed more isentropically than the nitrogen bubble and has a lower peak temperature, but a higher average temperature. This is confirmed by the calculations, which show that the light is emitted by the inner $0.18\text{ }\mu\text{m}$ of the argon bubble, compared to the inner $0.03\text{ }\mu\text{m}$ of the nitrogen bubble. The radiating volume of argon is ≈ 220 times greater than that of nitrogen, so the argon bubble is brighter. This analysis may explain why SBSL is brighter in noble gases than in diatomic gases [6]. We believe that these results provide strong support for Lohse's [7] hypothesis that a sonoluminescing air bubble contains mostly argon.

The physics of matter under SL conditions is not yet understood with high precision. Our results, based on approximate thermodynamic and transport property models, suggest that the basic strategy of hydrodynamic code simulation is valid, and that semiquantitative predictions are possible. Although it remains to be confirmed experimentally that shock waves or plasmas are present in a bubble undergoing SL, no other model of which we are aware has been able to explain such a broad array of experimental data.

4. Acknowledgments

This work was performed under the auspices of the U. S. Department of Energy by Lawrence Livermore National Laboratory under Contract No. W-7405-Eng-48.

5. References

- * This review paper contains previously published material.
- 1. D. F. Gaitan, (1990) An experimental investigation of acoustic cavitation in gaseous liquids, Ph. D. thesis, Univ. of Mississippi; Gaitan, D. F. et al. (1992) Sonoluminescence and bubble dynamics for a single, stable, cavitation bubble, *J. Acoust. Soc. Am.* **91**, 3166-3183.
- 2. Hiller, R., Putterman, S. J., and Barber, B. P. (1992) Spectrum of synchronous picosecond sonoluminescence, *Phys. Rev. Lett.* **69**, 1182-1184; The emission spectrum is consistent with that of a 2eV black body radiator.
- 3. Barber, B. P. and Putterman, S. J. (1991) Observation of synchronous picosecond sonoluminescence, *Nature* **352**, 318-320; The measured pulse width is less than 50ps.
- 4. No existing model of sonoluminescence could explain the 50ps pulse width.
- 5. Moss, W. C. et al. (1997) Calculated pulse widths and spectra of a single sonoluminescing bubble, *Science* **276**, 1398-1401.
- 6. Hiller, R. et al. (1994) Effect of noble gas doping in single-bubble sonoluminescence, *Science* **266**, 248-250.
- 7. Lohse, D. et al. (1997) Sonoluminescing air bubbles rectify argon, *Phys. Rev. Lett.* **78**, 1359-1362.
- 8. Matula, T. J. et al. (1997), unpublished data.
- 9. Jarman, P. (1960) Sonoluminescence: a discussion, *J. Acoust. Soc. Am.* **32**, 1459-1462; Moss, W. C. et al. (1994) Hydrodynamic simulations of bubble collapse and picosecond sonoluminescence, *Phys. Fluids* **6**, 2979-2985; Wu, C. C. and Roberts P. H. (1993) Shock-wave propagation in a sonoluminescing gas bubble, *Phys. Rev. Lett.* **70**, 3424-3427.
- 10. Zel'dovich, Ya. B. and Raizer, Yu. P. (1966) *Physics of Shock Waves and High-Temperature Hydrodynamic Phenomena*, Academic Press, New York, chaps. VI-VII.
- 11. Pomraning, G. C. (1973) *The Equations of Radiation Hydrodynamics*, Pergamon, New York, pp. 44-49.

THE HYDRODYNAMICAL / CHEMICAL APPROACH TO SONOLUMINESCENCE

A detailed comparison to experiment

MICHAEL P. BRENNER

*Department of Mathematics, Massachusetts Institute of
Technology Cambridge, MA 02146, USA*

AND

SASCHA HILGENFELDT AND DETLEF LOHSE

*Fachbereich Physik der Universität Marburg
Renthof 6, 35032 Marburg, Germany*

Abstract. Detailed comparison between experimental data and the recent hydrodynamical/chemical approach towards single bubble sonoluminescence (SBSL) is offered. Many of the unknowns can be resolved following this approach.

1. Introduction

The unknowns of single bubble sonoluminescence (SBSL [1, 2]) have been defined by Puterman's UCLA group in Ref. [2]. This proceedings contribution argues that many of the unknowns can be rationally resolved through a combination of classical bubble dynamics [3–13] supplemented by a consideration of chemical effects [14–16]. Through detailed comparisons between experiments and the classical bubble dynamics/chemical theory, the following problems of Ref. [2] are adequately resolved:

- What determines the radius of the SBSL bubble?
- What determines the upper and lower sound pressure thresholds above which one can observe SL?
- Why are noble gases so essential for producing stable, bright bubbles?
- Why do pure diatomic gas bubbles jitter and give such dim light?

Other questions remain open, in particular

- What exactly is the light emitting mechanism?

The goal of this proceedings contribution is to give further detailed comparisons between experimental measurements [1, 2, 17–20] and the hydrodynamic/chemical approach, in addition to the analysis in Refs. [11, 14–16].

The organization of the paper is as follows: In section 2 we give a short review of the hydrodynamic/chemical approach towards SBSL [9, 11, 15], focusing on the conditions necessary for SBSL to occur. The main part of the paper (section 3) offers a detailed comparison between theory and experiment. Section 4 presents conclusions and outlines the most important remaining open questions from our point of view.

2. The hydrodynamic/chemical approach towards SBSL

2.1. EXPERIMENTAL PARAMETERS

The important adjustable parameters in an SBSL experiment are the driving pressure amplitude P_a , the gas pressure overhead p_∞ , and the chemical composition of the dissolved gas; to change the latter, the inert gas ratio ξ of the mixture is often varied. Further experimental parameters are the temperature of the liquid, its viscosity ν_l , and the surface tension σ ; we will restrict ourselves to the values for water at 20°C. – The driving frequency ω is fixed at the resonance frequency of the Crum cell.

The ambient radius R_0 of the bubble, i.e., the bubble radius at ambient conditions of $P_0 = 1\text{ atm}$ and room temperature, is not an adjustable parameter but the system chooses R_0 dynamically. It can be measured by Mie scattering techniques [21], or by the “ringing down” technique of Holt and Gaitan [17].

2.2. BUBBLE HYDRODYNAMICS

The goal of the theory of bubble hydrodynamics is to delimit the regime of parameter space where stable sonoluminescence can occur. Since the parameter space is multi-dimensional (P_a , p_∞ , ξ , and R_0), and the dynamics involves timescales spanning ten orders of magnitude (from the timescale of the light flash (100–300ps [22] or even shorter [2, 23, 24]) to the diffusive timescale ($\sim 1\text{ s}$)), it is necessary to make approximations in modeling the hydrodynamics of sonoluminescence.

Experiments [6] have demonstrated that the *Rayleigh-Plesset* (RP) approximation for the spherical bubble radius $R(t)$ [3, 4, 13] accurately reproduces the bubble radius as a function of time in the parameter regime of sonoluminescence. The pressure $p(R, t)$ inside the bubble is assumed to have no spatial variations; the temporal variation of the pressure follows from a van der Waals polytropic law with a polytropic exponent γ . The

Rayleigh-Plesset ODE reads

$$R\ddot{R} + \frac{3}{2}\dot{R}^2 = \frac{1}{\rho_l}(p(R, t) - P(t) - P_0) + \frac{R}{\rho_l c_l} \frac{d}{dt}(p(R, t) - P(t)) - 4\nu_l \frac{\dot{R}}{R} - \frac{2\sigma}{\rho_l R} \quad (1)$$

Here, $P(t) = P_a \cos \omega t$ is the acoustic driving field (if not otherwise noted, we have used $\omega = 2\pi 26.5 \text{ kHz}$ for our calculations), and ρ_l and c_l are the density and speed of sound of water, respectively. The polytropic law not only gives the pressure in the bubble but also the temperature in this approximation. References [15, 16] follow Plesset and Prosperetti [4] and introduce a time dependent Péclet number, giving a time dependent polytropic exponent $\gamma(t)$. For all times but the bubble collapse $\gamma = 1$, i.e., isothermal bubble motion. At the bubble collapse γ reaches the adiabatic value of $5/3$ for argon and $7/5$ for nitrogen. The approximation gives temperatures as high as 10^5 K at the bubble collapse, see [16]. The actual temperature values are probably even higher thanks to gas dynamical effects (i.e. shock wave formation [25, 26]), but the general features of our results presented here are robust towards such changes in the model.

We call the approach of using a simplified model of bubble dynamics to understand sonoluminescing bubbles the *RP-SL-bubble approach* [11]. The advantage of this approach is that it is possible to explore the entire SL parameter space and compute phase diagrams. The disadvantage is that we cannot make any statement on the gas dynamics in the bubble and how exactly the light is emitted. We will demonstrate below that the predictions of the RP-SL bubble approach agree with experiments (within the limitations of experimental accuracy), and provide adequate explanations to the unknowns listed above.

2.3. CONDITIONS FOR SL

We now formulate the necessary conditions for SL within the RP-SL bubble approach. Four conditions have to be fulfilled for stable SBSL [9, 11, 15]: 1. Energy focusing, 2. Shape stability, 3. Diffusive stability, and 4. Chemical stability.

Energy focusing: The essential condition for SBSL is sufficient *energy transfer* from the fluid to the gas bubble and focusing of the energy. We take as a criterion for energy transfer and subsequent heating of the gas that the Mach number of the bubble wall (with respect to the speed of sound in the gas) has to be larger than one ($|M_{\text{gas}}| = |\dot{R}|/c_{\text{gas}} \gtrsim 1$). From RP simulation, it is easy to compute a corresponding line in the $P_a - R_0$ parameter space (dashed in Fig. 1). This criterion marks the onset of SL both within conventional shock theories [25, 26] and within the acoustic resonator theory [27].

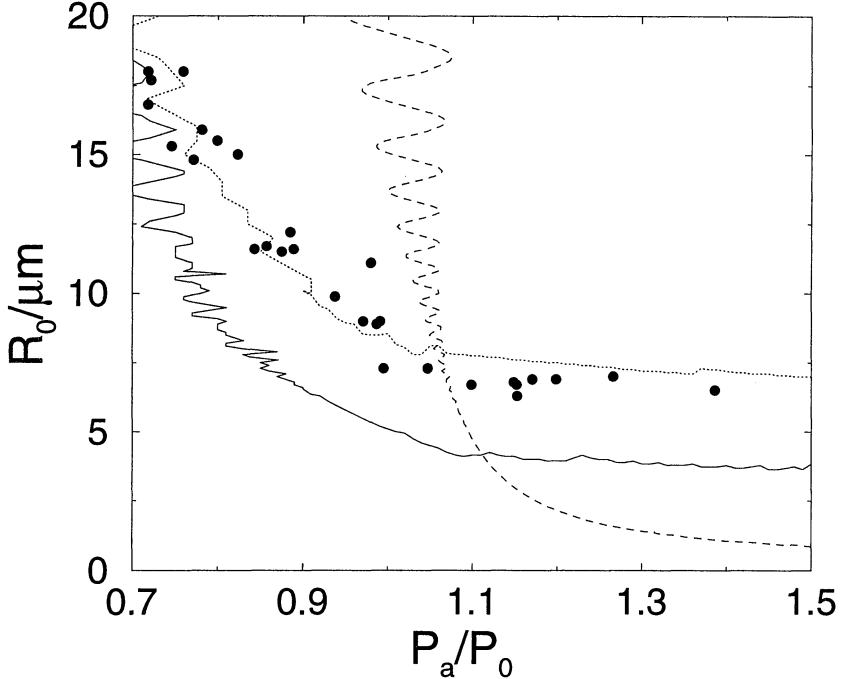


Figure 1. Stability conditions for a bubble in the $P_a - R_0$ parameter space. Bubbles above the line $|M_{gas}| = 1$ (dashed) fulfill the energy focusing condition. Bubbles below the shape instability lines (solid thick line) are stable towards non-spherical parametric surface oscillations (for the SL region, $n = 2$ is the most unstable mode). These curves are for water, $\nu_l = \nu_{water}$. The figure also contains the data for the shape instability line as measured by Holt and Gaitan [17] (circles). One can obtain more stable bubbles by changing the parameters of the equations. For illustrative purposes, we include here a calculation where we assume a larger (unphysical) viscosity, as done in Barber *et al.* [2]. The solid thin line shows the shape stability border for a viscosity $\nu_l = 4\nu_{water}$ – the $|M_{gas}| = 1$ curve hardly changes in this case. Both experiment and theory refer to a frequency $\omega/2\pi = 20.6\text{kHz}$. Not shown in the figure is the (short timescale) Rayleigh-Taylor shape instability [9, 11] which becomes important around $P_a = 1.4 - 1.5\text{atm}$ and presumably sets the upper threshold of the SL domain.

Shape stability: In order to emit light for a large number of driving cycles, the bubble should be (spherically) *shape stable* to guarantee sufficient focusing power of the collapse and to avoid bubble disruption and fragmentation. The idea of the RP approach can be extended to deal with *shape oscillations* [9, 11, 28]. In a linear approximation around the spherically symmetric solution $R(t)$ one obtains an ODE for the amplitude $a_n(t)$ of a spherical harmonic distortion of order n . To deal with nonlocal effects, we introduced a boundary layer approximation of the vorticity field around the bubble. It turns out that different types of shape stabilities exist, operating on different timescales [9, 11]. Our results – shown in Fig. 1

– quantitatively depend on the details of the approximation (e.g., the exact thickness of the boundary layer), however, the qualitative features and the rough magnitude of the results do not. Together with the energy focusing criterion, the shape stability lines define a small region in $P_a - R_0$ parameter space of potentially sonoluminescing bubbles (see Fig. 1).

Diffusive stability: *Diffusive processes* can also be understood within the RP approach to the SL bubble [7, 8, 10, 29]. At first sight this is surprising because there is no diffusive timescale in the RP equation. However, the boundary conditions from the full advection-diffusion problem are determined by the RP dynamics [30], as very nicely elaborated in the careful work of Fyrillas and Szeri [7] and Löfstedt *et al.* [8]. By separating the slow diffusive timescale from all timescales in the RP equation the diffusive equilibrium and its stability can be understood solely from the RP dynamics.

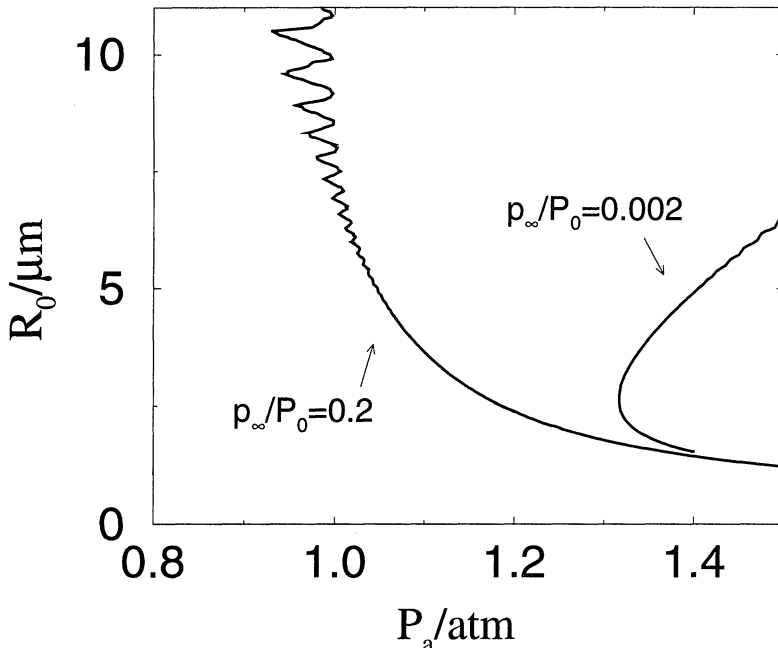


Figure 2. Diffusive equilibria for $p_\infty/P_0 = 0.20$ and $p_\infty/P_0 = 0.002$ in the $P_a - R_0$ phase space. The dissolved gas is pure argon, $p_\infty = p_\infty^{Ar}$.

The calculations for pure argon as dissolved gas were done in Ref. [11] and yield the lines in Fig. 2, which give the location of diffusive equilibria in $P_a - R_0$ parameter space. Also, the stability of the equilibria can be immediately read off from these curves: points with positive slope are stable, those with negative slope unstable. For relatively large argon pressure

p_∞^{Ar}/P_0 (e.g. 20%) the bubble behaves as follows: if the radius is below the equilibrium line, it shrinks and dissolves, whereas above the line it grows by rectified diffusion, until shape instabilities cause mass loss (shedding of microbubbles) and limit the growth. We call this state, in case light is emitted, *unstable SL*.

For very small p_∞^{Ar}/P_0 (e.g. 0.2%) the situation is entirely different. The curve of diffusive equilibria bends back, displaying a branch of positive slope and thus *stable* equilibria. If this branch intersects the region of Fig. 1 where the energy focusing condition and the shape stability condition are fulfilled, *stable SL* becomes possible. The light emitting bubbles have a defined R_0 , which does not change by diffusion. These bubbles oscillate in precisely the same way in every cycle, keeping fixed phase and intensity of light emission for *ever*. From a practical point of view, the sealing of the Crum cell (as influx of air has to be avoided) sets limitations.

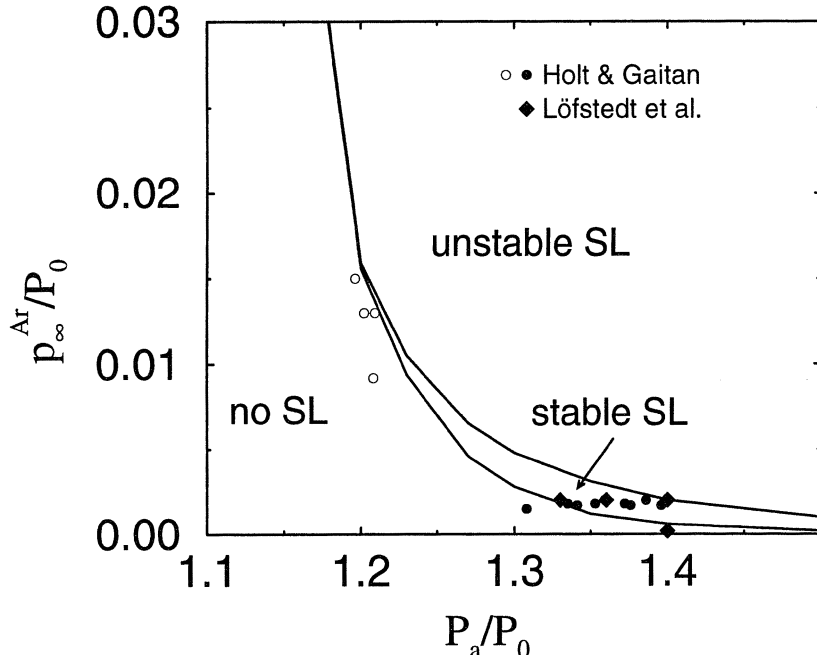


Figure 3. Phase diagram for pure argon bubbles in the p_∞^{Ar}/P_0 versus P_a/P_0 parameter space. Stable SL is only possible in a very small window of argon concentration. The experimental data points included for comparison refer to observed stable SL (filled symbols) or stable non-SL bubbles (open symbols) from Refs. [8] (diamonds) and [17] (circles) and show good agreement with the theory. Note that only those data can be included for which P_a , p_∞ and ξ are experimentally known.

From an experimental point of view the problem with phase diagrams such as Fig. 1 or 2 is that R_0 is not freely adjustable (cf. section 2.1).

Therefore, we in addition give the phase diagram [11,15] Fig. 3 in the $P_a - p_\infty^{Ar}$ phase space of the directly controllable experimental parameters, obtained through evaluation of diffusive stability curves for many overhead pressures p_∞^{Ar}/P_0 . We restrict ourselves to argon (or any other inert gas) here; the extension to diatomic gas mixtures is straightforward [14–16], as we will see in the next paragraph. For given P_a and p_∞^{Ar} we predict with Fig. 3 whether the bubble is in the diffusively unstable SL state, the diffusively stable SL state, or does not show SL at all. We stress that the theory relies only on classical formulations of bubble dynamics, and requires *no* fit parameters.

Chemical stability: The reason that *chemical instabilities* (i.e., dissociation and subsequent reactions) have to be considered [14–16] is that the high central bubble temperatures of at least several 10^4 K are more than sufficient to dissociate any molecular gas constituent, including N₂ and O₂ in the case of an air-filled bubble. The formed radicals immediately react with water vapor molecules to a variety of products, probably predominantly NO, NH, and NO₂. These substances are extremely soluble in water and are readily absorbed by the surrounding liquid, leaving only the inert gas component of air (i.e., argon) inside the bubble.

To model this mechanism within the RP-SL bubble approach, we have to assume an equation of state for the gas in the bubble and an Arrhenius type reaction law for molecular gases, as done in Refs. [15, 16]. Consider a mixture (at p_∞) of a molecular gas (say, nitrogen) and argon at a ratio of $\xi = 0.01$. As molecular gases dissociate at the high temperatures achieved in the SL bubble collapse and their reaction products dissolve in water, *only the partial argon pressure $p_\infty^{Ar} = \xi p_\infty$ is relevant for stability*. To put it in a nutshell, sonoluminescing “air” bubbles are in fact argon bubbles!

The chemical dissociation mechanism introduces new features into the $P_a - R_0$ phase diagram of Fig. 2. Consider an air bubble at a partial pressure of $p_\infty/P_0 = 20\%$. For low P_a , the (non-SL) bubble does not heat sufficiently for chemical reactions to occur. Thus, p_∞ is the relevant quantity for the diffusive stability – in this case, the bubble is diffusively unstable (curve A in Fig. 4a). For high P_a , the bubble contains only argon; thus, the relevant quantity is now the argon partial pressure $p_\infty^{Ar}/P_0 \approx 0.2\%$ – which allows for stable equilibria (curve C). Because of the topology of the diagram Fig. 4, another *stable* equilibrium line must necessarily exist in between. If it were unstable, it would mean that stronger forced bubbles are heated less, which of course cannot be the case. Indeed, such a stable equilibrium (curve B) is found in our computations. It describes bubbles for which the chemistry can only partially eliminate the reactive gases; as not all of these bubbles collapse hard enough to fulfill the energy focusing criterion, they do not, in general, emit SL light.

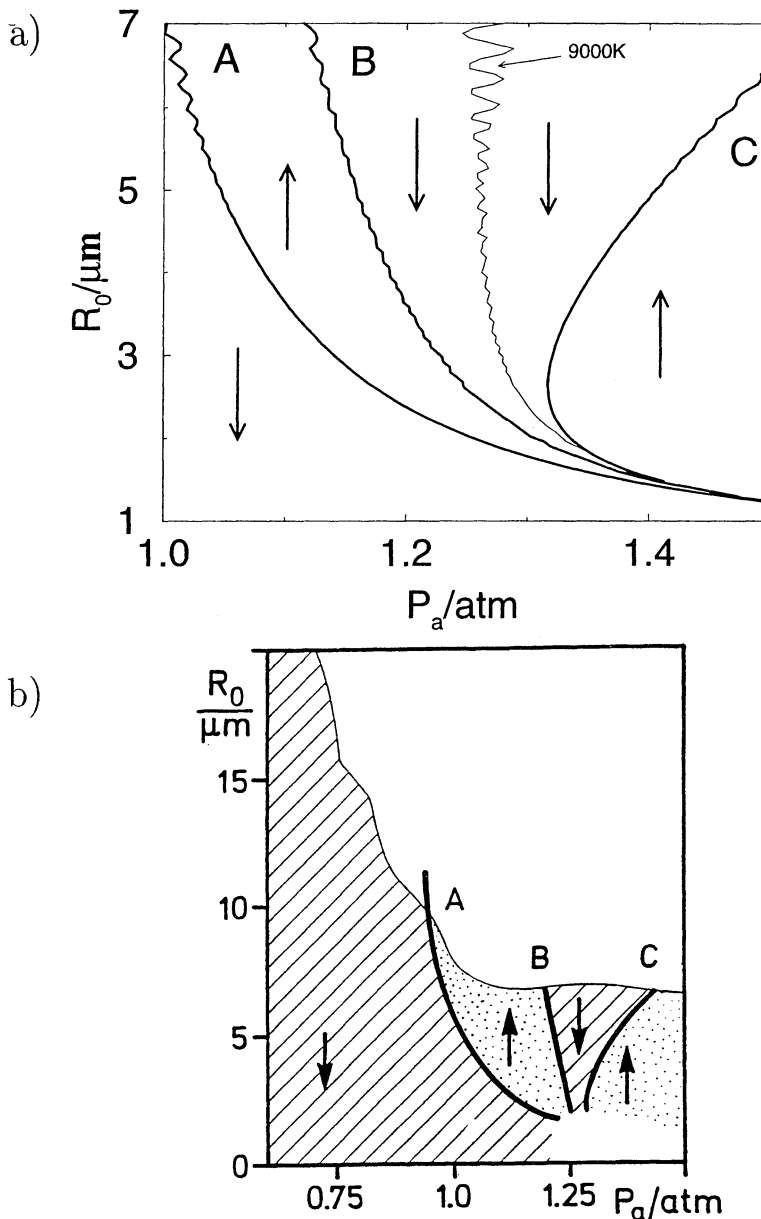


Figure 4. (a) Phase diagram for air (i.e. $\xi = 0.01$) at $p_\infty/P_0 = 0.20$ in the $P_a - R_0$ space. The arrows indicate whether the ambient radius grows or shrinks in the corresponding parameter region. Curve A denotes the expected *unstable* equilibrium for an air bubble at this high gas pressure, on curve C the bubble only contains argon. The intermediate curve B necessarily exists because of the topology of the diagram, and represents an additional stable equilibrium. The thin curve shows when the nitrogen dissociation threshold $\sim 9000K$ is reached. (b) Experimental measurement of the same phase diagram by Holt and Gaitan (adapted from figure 1 of [17] with kind permission of the authors). Bubbles in shaded areas are shape stable.

Chemical reactions play a role as a *transient* phenomenon when slowly increasing the forcing amplitude – the bubble will be “cleaned” from its molecular gases. But chemistry is also important in the *stationary* state: When the bubble is big, the pressure inside is tiny and the dissolved gas mixture (N_2 and Ar) is sucked into the bubble. On collapse, the N_2 reacts and the reaction products are thrown out of the bubble and dissolve. The bubble can be understood as a micrometer size reaction chamber for high temperature chemistry, as we suggested in Ref. [15].

3. Comparison to experiment

3.1. STABLE VS. UNSTABLE SBSL

According to our phase diagram Fig. 3 for argon as dissolved gas *stable SL* should only be possible for tiny gas pressures in the range of (for $P_a = 1.3\text{atm}$) $p_\infty^{\text{Ar}}/P_0 = 0.2 - 0.4\%$. Indeed, Barber *et al.* [2] observe stable SL at $p_\infty^{\text{Ar}} = 3\text{mmHg}$, corresponding to 0.4%.

At larger $p_\infty^{\text{Ar}} = 50\text{mmHg}$ and $p_\infty^{\text{Ar}} = 200\text{mmHg}$ (6% and 20% saturation, respectively) unstable SL is observed, again as expected from Fig. 3. This phase is characterized by an increase of the relative phase of light emission with respect to the driving pressure on the slow (diffusive) timescale $\sim 1\text{s}$, followed by a rapid breakdown and another subsequent increase. The light intensity itself behaves in the same way (cf. [2]) and the bubble is reported to be dancing or jiggling [1, 31]. This state of SL is also unstable in the sense that often all of a sudden the bubble disappears, i.e., it cannot be trapped in the acoustic field for a very long time. The same features of unstable SL can also be seen in the *acoustic* emission of the bubble [19].

In Ref. [12] we interpreted this behavior as a signature of bubble growth by rectified diffusion (see also the previous section). When growing, the bubble runs into the shape instability line of Fig. 1. Consequently, the bubble breaks up and microbubbles pinch off, leading to a recoil which makes the bubble dance. The (parameter free) theoretical calculations in Ref. [11] could produce results for the phase of light emission which resemble the experimental result in figure 27 of [2].

3.2. ONLY THE ARGON PARTIAL PRESSURE IS RELEVANT

For gas mixtures of nitrogen (or oxygen) and argon one expects the same two phases “stable SL” and “unstable SL”, but at a $(1/\xi)$ times higher total gas concentration $p_\infty = p_\infty^{\text{Ar}}/\xi$. Moreover, according to the chemical hypothesis the type of reactive gas in the mixture is irrelevant for diffusive stability in the regime of large P_a . Indeed, as reported by Barber *et al.* [2], argon-oxygen mixtures and argon-nitrogen mixtures show very similar

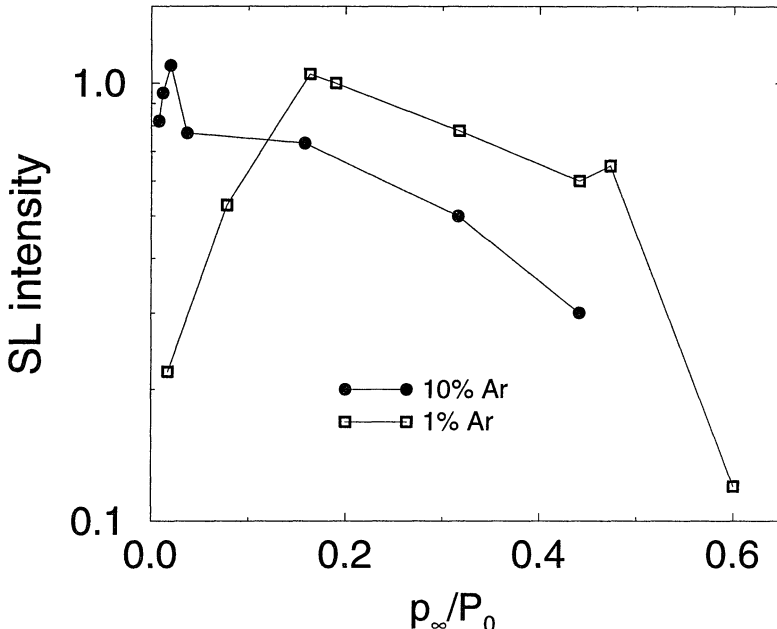


Figure 5. SL intensity (normalized to air) from a SL bubble in water as a function of the gas mixture p_{∞}/P_0 for two different argon-nitrogen gas mixtures. The data are taken from figure 23 of Barber *et al.* [2].

behavior, see figure 24 of this reference. Therefore, we put all available data for stable SL into the p_{∞}^{Ar} vs P_a phase diagram; very good agreement with our prediction is found. The stable, non-sonoluminescing bubbles of branch B in Fig. 4 are observed at parameter values in the no-SL regime, as predicted. Also for unstable SL the relevant value $p_{\infty}^{Ar} = \xi p_{\infty}$ is always in the correct domain of Fig. 3.

In Fig. 5 we show Barber *et al.*'s experimental results for the SL intensity of argon-nitrogen mixtures. The largest intensity occurs for stable SL. According to the phase diagram Fig. 3 at $P_a = 1.3\text{ atm}$ SL is stable between $p_{\infty}^{Ar}/P_0 = 0.002 - 0.004$. This corresponds to $p_{\infty}/P_0 = 0.1 - 0.2$ for a N_2/Ar mixture with 1% argon (or also for air) and to $p_{\infty}/P_0 = 0.01 - 0.02$ for a N_2/Ar mixture with 10% Ar. Indeed, these are the pressure overheads where the corresponding SL intensities peak in Fig. 5.

3.3. BUBBLE REACTION TO FORCING PRESSURE CHANGES

What happens when slowly increasing the forcing pressure P_a for fixed p_{∞}/P_0 ? The Puttemans group has done various experiments of this kind

and the results are given in the “waterfall plots” figs. 18, 21, 30, 32, 33, 42, 70 of Ref. [2]. All of these plots can be understood along the lines of the diffusive/chemical theory of Refs. [14–16]. Let us take a look at some of these results:

Pure argon: Consider e.g. the case of pure Ar dissolved at $p_\infty^{Ar}/P_0 = 0.004$, cf. [2]. According to Fig. 2, bubbles forced with $P_a < 1.2\text{atm}$ dissolve. On increasing P_a beyond 1.2atm, the bubble follows the line of stable diffusive equilibria in Fig. 2 and its ambient size increases, also leading to a larger maximal radius, see figure 42 of [2]. Finally, it hits the shape instability (cf. Fig. 1) and gets destroyed.

Inert/reactive gas mixtures: For gas mixtures, say, a 1% xenon doped nitrogen bubble at $p_\infty/P_0 = 0.20$ or an air bubble (cf. [2] for both cases), the sequence of events on increasing P_a can be read off Fig. 4. For low P_a the bubble is diffusively unstable and “dances”. At a certain pressure around $P_a \sim 1.1\text{atm}$ (see [16]) the bubble gets trapped by the stable equilibrium B and does not jiggle any more. On further increase of P_a it decreases in size R_0 along curve B until it reaches the stable equilibrium C, now increasing in ambient size again. This sequence of events was reported already by Gaitan [1] and later again and again by various experimental groups, see e.g. Ref. [2].

Hysteresis for low inert gas content: If the partial pressure of inert gas is very low, say, $p_\infty/P_0 = 0.20$ and $\xi = 0.001$ as in figure 21 of Ref. [2] or the theoretical analogue figure 13 of Ref. [16], there is no stable SL around $P_a = 1.1\text{atm} - 1.3\text{atm}$. However, stable bubbles are still possible in this range, in analogy to those on curve B of Fig. 4a. These bubbles contain a slightly enhanced argon concentration. At $P_a = 1.4\text{atm}$ the stable equilibrium curve C is reached, displaying stable SL. As reported by Löfstedt *et al.* [8] and explained in detail in Ref. [16], this sequence of events shows hysteresis: Bubbles on branch C can be reached by slowly increasing P_a , but when decreasing P_a , the bubbles on branch B cannot be reestablished, because bubbles on branch C contain pure argon.

Hysteresis at the onset of SL: Another wonderful hysteresis experiment has recently been performed by Matula and Crum [18], now for unstable SL in air bubbles. Here, the bubble is boosted from the non-SL regime to the SL regime by a sudden increase of P_a (see also [2]). The radius adjusts within less than a second through rectified diffusion, whereas it takes several seconds for the chemical reaction to clear the bubble from N₂ and O₂. Finally, only argon remains and the bright signal of stable sonoluminescing bubbles is emitted. As seen from figure 35 of Ref. [2] the SL turn on time is in the range of seconds for air, whereas it takes only several 100 cycles

for pure argon bubbles. Now Matula and Crum sweep down P_a below the SL threshold for some 2700 cycles ($\sim 0.1s$). Diffusive processes are too slow to change the contents of the bubble (argon) abruptly. Therefore, if P_a is increased again after 2700 cycles, the bubble emits light immediately, which shows very nicely that argon has accumulated before.

3.4. BUBBLE SIZE

We now come to a more quantitative comparison of bubble radii. The phase diagrams 2 and 4 predict the fixed bubble size of stable SL and with the help of Fig. 1 the range of possible bubble radii of unstable SL can also be given.

Holt and Gaitan [17] have measured the phase diagram Fig. 4b experimentally using air, and have identified both stable SL equilibria at the expected location for pure argon concentrations (curve C) and stable non-SL bubbles for smaller driving pressures (curve B). The agreement with our theory Fig. 4a is very good.

Figure 6 compares the experimental ambient radii given in [2] and the theoretical predictions following from the approach of Refs. [15, 16]. The curves show the same features. For low P_a there is unstable SL. The bubble grows from A up to the shape instability. The measured radii (circles) in this range have to be interpreted as either instantaneous or averaged values from Mie scattering data. The small discrepancies in the location of branches B and C could be a consequence of many factors, including: (a) the simplistic modeling assumptions made in our calculations (e.g. for the internal bubble temperature and for the chemical reactions) and (b) the experimental uncertainties in both P_a and R_0 ; the latter are related to the unrealistic values of the fluid parameters (σ, ν_l, γ) assumed by Barber *et al.* [2] for determining R_0 . – The theoretical estimate $|M_{\text{gas}}| = 1$ for the onset of light emission is about 0.05atm off the experimentally observed onset which is in the range of the experimental precision.

3.5. SHAPE STABILITY THRESHOLDS

In our theoretical Fig. 1 we included the experimental data measured by Holt and Gaitan (priv. comm. and Ref. [17]). The two curves show the same features, although the measured values of the upper domain of stability are slightly larger than our theoretical value. One of the reasons presumably is that there is some freedom in the boundary layer approximation done in Refs. [9, 11]. Of course, by changing details of that approximation it is possible to achieve a better quantitative description. For example, by taking a value for the liquid viscosity which is four times as large as that of water (the value Barber *et al.* take for their fits in Ref. [2]) the calculated

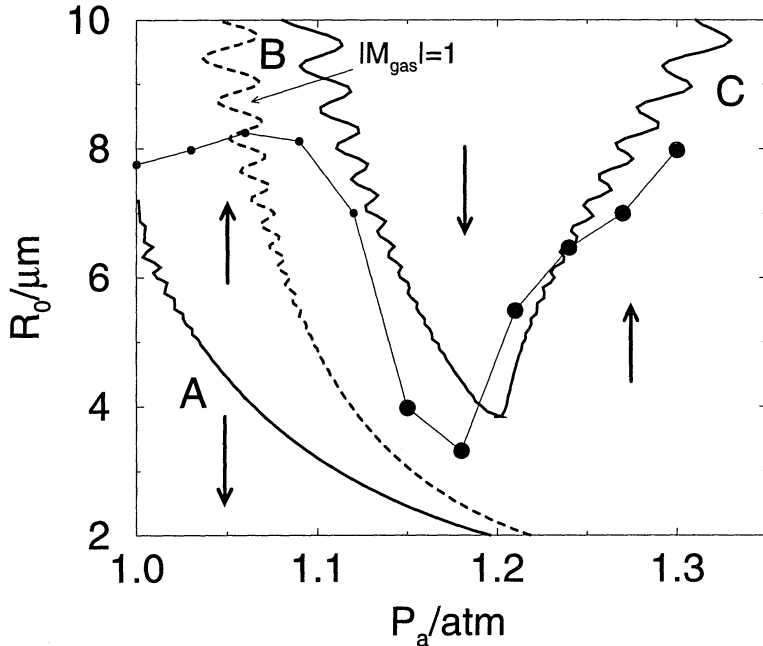


Figure 6. Circles show the ambient radii R_0 for a 150mmHg ($p_\infty/P_0 = 20\%$) bubble of 5% argon in nitrogen as they follow from a 4 parameter fit to the RP equation to Mie scattering data performed in [2] (leading to unphysical values for σ , ν_i , and γ). Light emission from the bubble is indicated by larger circles. The data are taken from figure 43 of Ref. [2]. The first few data points represent unstable bubbles. They grow by rectified diffusion up to the parametric shape instability which for clarity is not shown in this figure (but see Fig. 1). The solid lines result from our theory for the same frequency $\omega/2\pi = 23\text{kHz}$ as employed in the experiment. B and C represent stable equilibria, A an unstable equilibrium. The thick dashed line is the $|M_{\text{gas}}| = 1$ -curve corresponding to that of Fig. 1. Arrows illustrate regions of growing and shrinking bubbles.

domain of stability becomes even larger than the measured one (cf. Fig. 1). However, our main point in Refs. [9, 11] was to establish that there exists a shape instability in the relevant R_0 and P_a range, which is in fact strongly supported by Holt and Gaitan's recent data.

In Fig. 7 we show how the theory of refs. [9, 11] compares to Holt and Gaitan's measurements of bubble shape oscillations in the small forcing pressure – large ambient radius regimes. Again, the agreement is reasonably good.

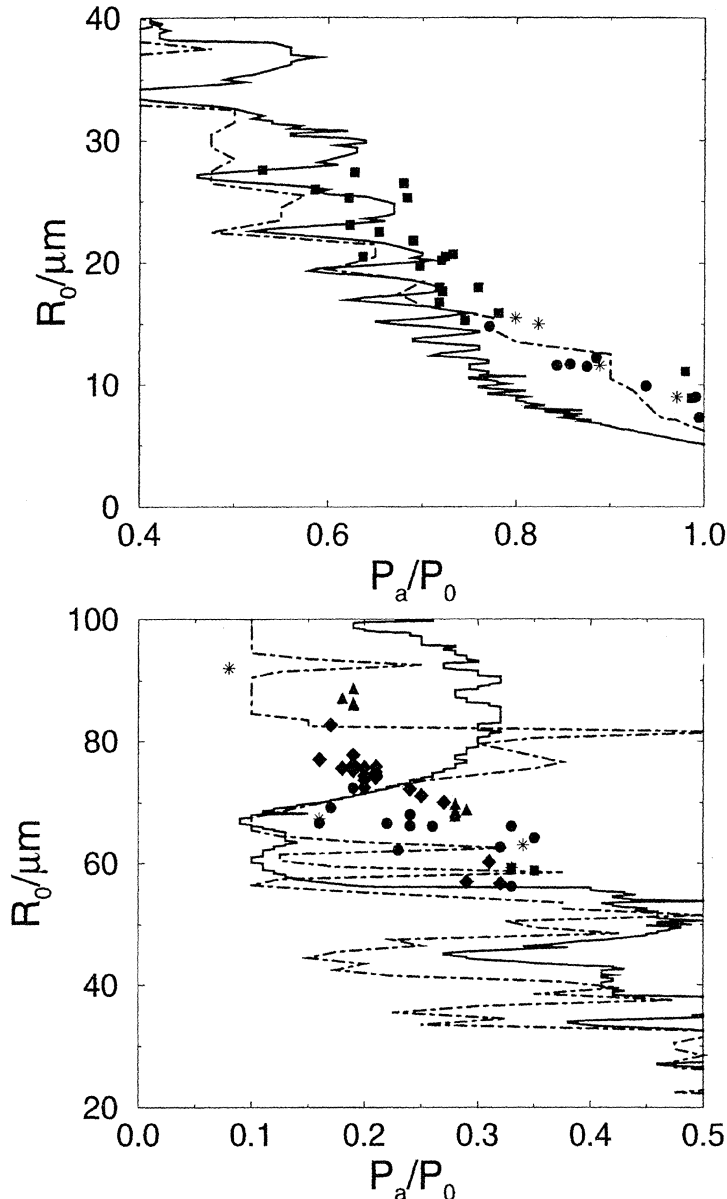


Figure 7. Onset of shape instabilities from Holt and Gaitan's experiments [priv. communication] and from the theory of refs. [9, 11] in two different non-SL regimes, $\omega/2\pi = 20.6\text{kHz}$. No data are available between these two regimes. The symbols show the measured onsets for the mode $n = 2$ (bullets), $n = 3$ (squares), $n = 4$ (diamonds), $n = 5$ (triangles), or an unknown mode (stars). The solid (dot-dashed) line shows the theoretical onset for the $n=2$ mode ($n=3$ mode). Note that the transition of the most unstable mode from $n = 3$ to $n = 2$ occurs around $P_a = 0.75\text{atm}$ both in experiment and theory.

3.6. FURTHER SUPPORT FOR THE NITROGEN DISSOCIATION HYPOTHESIS

Ejection of reaction products from the bubble: A very direct proof of the chemical activity inside the bubble is the detection of reaction products expelled from it. For air bubbles we expect NO and NO₂ to be produced which then dissolve in water to form nitric acid etc. This should result in a tiny PH decrease [15, 16], which, to our knowledge, has not yet been detected. However, in a recent wonderful experiment Lepoint-Mullie *et al.* [20] managed to detect iodine I₂ as a reaction product coming out of a single driven bubble; the surrounding fluid contained NaI and CCl₄, the dissolved gas was air.

Numerical simulations: Also Moss *et al.*'s numerical simulation [26] of shock dynamics, coupled to a light emission model, supports the nitrogen dissociation hypothesis. In the simulations nitrogen bubbles are found to glow 200 times weaker than argon bubbles, in contrast to all experimental observations, in which argon and air bubbles show roughly the same light intensity. Therefore, Moss *et al.*'s simulations suggest that a sonoluminescing air bubble contains mostly argon.

Stable SL without degassing: An immediate consequence of our theory is that stable SBSL is possible without degassing, if only the ratio of the partial argon pressure to the ambient pressure is properly adjusted. Meanwhile such experiments have been performed both by Kondic *et al.* [32] and Barber *et al.* [2]. In figure 23 of the latter paper it is reported that SL can be observed in tap water ($p_\infty/P_0 = 1$ at ambient pressure) for $P_0 = 5\text{atm}$, i.e., $p_\infty/P_0 = 0.20$ and $p_\infty^{\text{Ar}}/P_0 = 0.002$, just as required for stable SL according to our phase diagram Fig. 3.

4. Conclusions and Outlook

To summarize our findings we now explicitly answer the four questions listed in the introduction and originally posed by Putterman's group [2]:

- Rectified diffusion, together with chemical reactions, determines the size (ambient radius) of SL bubbles. An upper limit for bubble growth is set by shape instabilities.
- The *lower* limit in the forcing pressure P_a for SL to occur is given by a combination of shape stability, diffusive stability and the condition that the bubble wall velocity is supersonic (cf. Fig. 6). – Calculations (see Ref. [9, 11]) suggest that it is the (short timescale) Rayleigh-Taylor shape instability which gives the *upper* limit in P_a . However, we would like to caution that further instability mechanisms might exist in the large forcing pressure regime. One is the micro-jet formation as sug-

gested by Prosperetti [33], an effect related to the Rayleigh-Taylor instability. Another instability is caused by the Bjerknes forces becoming repulsive for large P_a . Recent calculations locate this Bjerknes threshold around $P_a \sim 1.8\text{atm}$ [34]. If the emitted acoustic radiation from the bubble is included in these calculations, this threshold may be shifted to even lower P_a .

- Noble gases are essential for producing stable, bright bubbles because all molecular gases dissociate at the high temperatures achieved during bubble collapse and their reaction products dissolve in water.
- Bubbles of pure diatomic gases jitter for the same reason. They can only exist in the unstable SL domain. If they are stable as on curve B in Fig. 4a, growth by rectified diffusion and mass loss by chemical reactions balance. In this state, the energy focusing condition is not necessarily fulfilled, i.e., there are stable, non-sonoluminescing bubbles.

Another open question that can be addressed using the above approach is the dependence of the sonoluminescence intensity on the temperature of the liquid [35, 36]: as the saturated gas concentration increases with decreasing liquid temperature, the pressure range for stable sonoluminescence becomes larger for lower temperature (see the phase diagrams presented above). This means that it is possible to force the bubble harder in cooler water, producing a greater light intensity. Moreover, the liquid viscosity increases with decreasing temperature, allowing for larger shape stable bubbles. Taking the temperature dependence of the relevant material constants of water into account, the observed variations of SBSL intensity [2] are satisfactorily explained [35].

The solution of the remaining open questions requires knowledge of the energy focusing and light emission mechanisms. Compelling experimental evidence distinguishing between various theories is still lacking. The major stumbling block in our view is the current disagreement in the literature on the width of the light pulse: Original measurements showing pulse widths lower than 50ps [2, 23] have been challenged by Gompf *et al.* [22], who measure pulse widths in the range of $100 - 300\text{ps}$. This difference is of utmost importance: Whereas the former measurements allowed for speculation on huge energy focusing up to table top fusion [37], the newer measurements do not, since, as noted by Gompf *et al.*, these longer pulse widths are comparable to the time the bubble spends in its collapsed state, which is exactly what would be expected from simple adiabatic heating of the gas. Indeed, the observed variation of the pulse width with experimental parameters p_∞/P_0 and P_a/P_0 can be rationalized simply from hydrodynamical considerations [22]. Until this experimental controversy is resolved, it is impossible to validate adiabatic heating or other theories of energy focusing (e.g. shocks [25, 26]). If Gompf *et al.*'s experimental results hold up,

it seems that the explanation for single bubble sonoluminescence will be “classical bubble dynamics with a twist” – the twist coming both from the interaction of chemistry with hydrodynamic stability, and from the nonhomologous motion of the gas within the bubble.

Acknowledgments: We would like to thank G. Holt and F. Gaitan for data exchange and for allowing us to reproduce their figures. We are grateful to them and to T. Matula for various discussions. – Support for this work by the National Science Foundation Division of International Programs, and the Deutsche Forschungsgemeinschaft (DFG) under grant SFB185-D8 is gratefully acknowledged.

References

1. Gaitan, D. F. (1990) An experimental investigation of acoustic cavitation in gaseous liquids, PhD thesis, The University of Mississippi; Gaitan, D. F., Crum, L. A., Roy, R. A., and Church, C. C. (1992), *J. Acoust. Soc. Am.* **91**, 3166.
2. Barber *et al.* (1997), *Phys. Rep.* **281**, 65.
3. Rayleigh, Lord (1917), *Philos. Mag.* **34**, 94; Plesset, M. (1949), *J. Appl. Mech.* **16**, 277; Keller, J. B. and Miksis, M. J. (1980), *J. Acoust. Soc. Am.* **68**, 628.
4. Plesset, M. and Prosperetti, A. (1977), *Ann. Rev. Fluid Mech.* **9**, 145.
5. Prosperetti, A. (1977), *Quart. Appl. Math.* **34**, 339.
6. Löfstedt, R., Barber, B. P., and Puterman, S. J. (1993), *Phys. Fluids A* **5**, 2911.
7. Fyrillas, M. M. and Szeri, A. J. (1994), *J. Fluid Mech.* **277**, 381.
8. Löfstedt, R., Weninger, K., Puterman, S. J., and Barber, B. P. (1995), *Phys. Rev. E* **51**, 4400.
9. Brenner, M., Lohse, D., and Dupont, T. (1995), *Phys. Rev. Lett.* **75**, 954.
10. Brenner, M., Lohse, D., Oxtoby, D., and Dupont, T. (1996), *Phys. Rev. Lett.* **76**, 1158.
11. Hilgenfeldt, S., Lohse, D., and Brenner, M. P. (1996), *Phys. Fluids* **8**, 2808.
12. Hilgenfeldt, S., Brenner, M. P., Grossmann, S., and Lohse, D. (1997) Analysis of Rayleigh–Plesset dynamics for sonoluminescing bubbles, submitted to *J. Fluid Mech.*
13. Brennen, C. E. (1995) *Cavitation and Bubble Dynamics*, Oxford University Press, Oxford.
14. Brenner, M. P., Hilgenfeldt, S., and Lohse, D. (1996) Why air bubbles in water glow so easily, in J. Parisi, S. C. Müller, and W. Zimmermann (eds.), *Nonlinear Physics of Complex Systems – Current Status and Future Trends*, Springer Lecture Notes in Physics, Berlin, p. 79.
15. Lohse, D., Brenner, M. P., Dupont, T., Hilgenfeldt, S., and Johnston, B. (1997), *Phys. Rev. Lett.* **78**, 1359.
16. Lohse, D. and Hilgenfeldt, S. (1997), *J. Chem. Phys.* **107**, 6986.
17. Holt, G. and Gaitan, F. (1996), *Phys. Rev. Lett.* **77**, 3791.
18. Matula, T. J. and Crum, L. A. (1997), “Evidence for gas exchange in single bubble sonoluminescence”, submitted to *Phys. Rev. Lett.*
19. Holzfuss, J., Rüggeberg, M., and Billo, A. (1997), *Fortschritte der Akustik DAGA*.
20. Lepoint-Mullie, F., Lepoint, T., and Henglein, A. (1997).
21. Barber, B. P. *et al.* (1994), *Phys. Rev. Lett.* **72**, 1380.
22. Gompf, B. *et al.* (1997), *Phys. Rev. Lett.* **79**, 1405.
23. Barber, B. P. and Puterman, S. J. (1991), *Nature (London)* **352**, 318.
24. Moran, M. J. *et al.* (1995), *Nucl. Instr. and Meth. in Phys. Res. B* **96**, 651.

25. Jarman, P. (1960), *J. Acoust. Soc. Am.* **32**, 1459; Greenspan, H. P. and Nadim, A. (1993), *Phys. Fluids A* **5**, 1065; Wu, C. C. and Roberts, P. H. (1993), *Phys. Rev. Lett.* **70**, 3424; Moss, W., Clarke, D., White, J., and Young, D. (1994), *Phys. Fluids* **6**, 2979; Kondic, L., Gersten, J. I., and Yuan, C. (1995), *Phys. Rev. E* **52**, 4976.
26. Moss, W., Clarke, D., and Young, D. (1997), *Science* **276**, 1398.
27. Brenner, M. P., Hilgenfeldt, S., Lohse, D., and Rosales, R. (1996), *Phys. Rev. Lett.* **77**, 3467.
28. Plesset, M. (1954), *J. Appl. Phys.* **25**, 96.
29. Epstein, P. and Plesset, M. (1950), *J. Chem. Phys.* **18**, 1505.
30. Eller, A. and Flynn, H. G. (1964), *J. Acoust. Soc. Am.* **37**, 493.
31. Barber, B. P., Weninger, K., Löfstedt, R., and Puttermann, S. J. (1995), *Phys. Rev. Lett.* **74**, 5276.
32. Kondic, L., Yuan, C., and Chan, C. K. (1997).
33. Prosperetti, A. (1997), *J. Acoust. Soc. Am.* **101**, 2003.
34. Akhatov, I. et al. (1997), *Phys. Rev. E* **55**, 3747; Matula, T., Cordry, S. M., Roy, R. A., and Crum, L. A. (1997), *J. Acoust. Soc. Am.* **102**, 1522.
35. Hilgenfeldt, S., Lohse, D., and Moss, W. (1997), "Temperature dependence of single bubble sonoluminescence", submitted to *Phys. Rev. Lett.*
36. Vuong, V. Q., Fyrillas, M. M., and Szeri, A. J. (1997), "The influence of liquid temperature on the sonoluminescence hot spot", submitted to *J. Acoust. Soc. Am.*
37. Moss, W., Clarke, D., White, J., and Young, D. (1995), *Phys. Lett. A* **211**, 69.

ASPHERICAL BUBBLE COLLAPSE AND SONOLUMINESCENCE

C. D. OHL, O. LINDAU AND W. LAUTERBORN

Drittes Physikalisches Institut

Universität Göttingen

Bürgerstr. 42-44, D-37073 Göttingen

Germany

1. Introduction

Laser induced bubbles make it possible to investigate cavitation bubble dynamics in detail [1], in particular during the final stages of collapse [2]. In this paper we extend our previous work by studying not only the bubble shape but also the light emission [3] during the collapse. We will address the question whether an aspherical bubble collapse boosts or lessens the light emission.

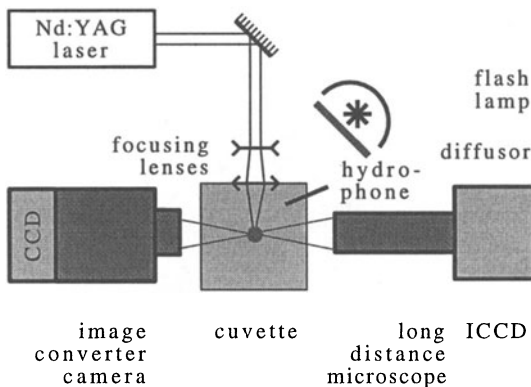


Figure 1. Experimental arrangement for studying the dynamics and the light emission of laser induced cavitation bubbles.

In contrast to experimental sonoluminescence studies (see, e.g. [4]), where a sound field drives the bubble to a large expansion, in *single cavitation bubble luminescence* (SCBL) a bubble expands through vaporization of liquid at the laser focus. The experimental arrangement is depicted in

Fig. 1. Single bubbles are produced inside a water filled cuvette at the focus of a Nd:YAG laser beam. The laser delivers pulses of 8 ns FWHM with a pulse energy of up to 20 mJ at the fundamental wavelength of 1064 nm. A two lens system is used to produce a nearly pointlike bubble nucleation site. Successive images of the bubble dynamics are taken with an image converter camera at 227.000 frames/s illuminated with a long duration photo flash. A different photographic system is used to observe the luminescence event, an intensified CCD camera (ICCD) and a long distance microscope. The ICCD with a high contrast ratio between shuttered and opened state suppresses the intense continuum light emission from the dielectric breakdown process. An optical resolution of the luminescence image better than 3 μm is achieved.

The acoustic transients at bubble generation and at bubble collapse are recorded with a hydrophone on a digital storage oscilloscope. The aspherical bubble collapse is investigated using a rigid perspex boundary of adjustable height placed below the laser focus.

2. Spherical Bubble Collapse

The technique for generation of cavitation through a laser induced dielectric breakdown allows for the creation of a bubble in a highly reproducible way [1,2]. In absence of a boundary, the bubble collapses spherically and emits a single shock wave [2]. Its dynamics can be described by Gilmore's model [5] until the final stages of collapse.

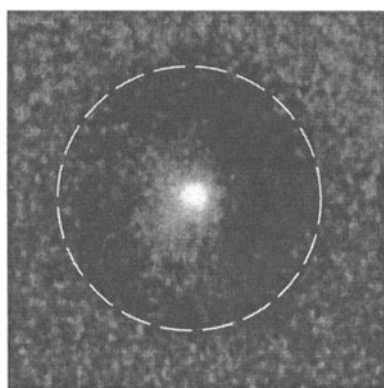


Figure 2. ICCD image with shutter open for 5 μs with an additional weak illumination from the front. The bubble appears dark on a bright background with the luminescence spot in the middle. During the gating time, the bubble wall collapses from the position marked with the dashed outline to a smaller bubble size. The rapid motion blurs the bubble outline. The size of the frame is 0.784 mm \times 0.784 mm.

Figure 2 shows an image of the luminescence which occurs during the spherical bubble collapse taken with the ICCD camera. The gating time was adjusted to $5\ \mu\text{s}$ and an attenuated flash illuminates the bubble outline. The bright SCBL spot in Fig. 2 is in the center of the bubble outline. Light emission is observed when the gating time of the ICCD covers the bubble collapse, measured simultaneously from the hydrophone signal. The maximum radius of the bubble, R_{max} , in Fig. 2 was determined through Rayleigh's formula [6] (Eq. 1) from the duration between bubble generation and bubble collapse $2T_c = 150.4\ \mu\text{s}$ to $R_{max} = 0.813\ \text{mm}$:

$$R_{max} = \left(0.915 \sqrt{\frac{\rho}{p - p_d}} \right)^{-1} T_c , \quad (1)$$

where $\rho = 998.2\ \text{kg/m}^3$ is the density of the liquid, $p = 1\ \text{bar}$ is the ambient pressure and $p_d = 0.0233\ \text{bar}$ the vapor pressure at $T = 20^\circ\ \text{C}$.

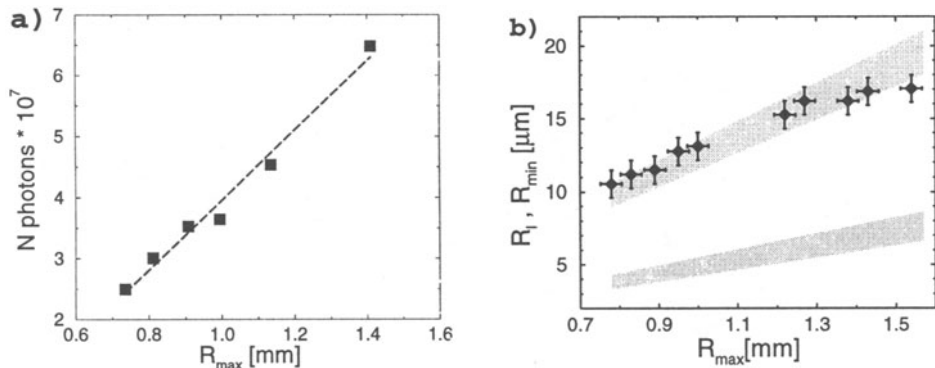


Figure 3. a) Lower bound of the number of photons emitted during the primary bubble collapse for different maximum bubble radii. b) Comparison of the measured radii of luminescence spots (filled diamonds) with minimum bubble radii according to Gilmore's model. The upper shaded area assumes a van der Waals gas, and the lower shaded area an ideal gas equation of state.

The measured lower bound for the number of photons emitted takes into account the sensitivity of the ICCD but neglects reflection losses of the imaging optics. Figure 3 a is a plot of this lower bound during primary bubble collapse for different maximum bubble sizes (filled squares). A linear regression (dashed line in Fig. 3 a) gives a slope of $57 \cdot 10^6$ photons per mm maximum radius.

Figure 3 b shows the measured radii, R_l , of the luminescence spot (dark diamonds) for different maximum bubble sizes R_{max} . This size is compared with the minimum bubble radius R_{min} calculated from Gilmore's model for different gas equations. We find good agreement with a van der Waals equation of state for the gas (upper shaded area of Fig. 3 b). This agreement is

reasonable. The light is emitted during the time of maximum compression of the bubble volume. Thus, the image of luminescence are photographs of the self illuminated bubble. The time between minimum and maximum bubble wall velocity of the bubble collapses lies in the order of 10 ns! Assuming that the time of light emission is short compared to this time scale, the measured size of the luminescence should be approximately the calculated minimum bubble size. However, R_{min} calculated using an ideal gas equation, (lower shaded area) disagrees with the observed R_l . If R_l is equated with R_{min} , the compression ratio R_{max}/R_{min} for the investigated bubble radii can be estimated to 82 ± 8 . For the same bubbles, the expansion ratio R_{max}/R_0 is 9.1 ± 7 .

3. Aspherical Bubble Collapse

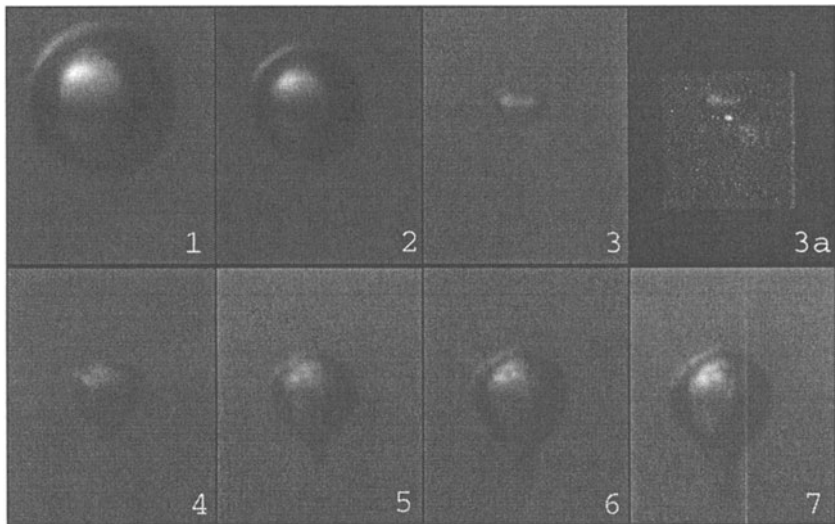


Figure 4. Frames 1–7: Bubble dynamics and light emission near a rigid boundary (not visible) placed $s=4.9$ mm below the laser focus photographed with the image converter camera. The bubble reaches a maximum radius of $R_{max} = 0.83$ mm for $\gamma = 5.9$. The frames have $4.4\mu s$ interframe time. Frame 3a: The picture of frame 3 is superimposed with a photograph of the light emission with the ICCD for a bubble with the same experimental parameters. The size of all individual frames is 1.56 mm \times 1.25 mm.

When the fluid flow in the surroundings of a bubble is disturbed, e.g. by a rigid boundary, the bubble dynamics before collapse is altered. As the bubble collapses, the bubble reduces its size, but the bubble wall nearer to the boundary is less strongly accelerated (as its flow is hindered by the boundary) than the radial flow from above. An indentation at the opposite bubble wall is formed and gives rise to an additional flow, apart from

the pure radial one, in direction towards the boundary. The bubble center accelerates during the collapse and moves towards the boundary due to momentum conservation [7]. Using the method of images for the velocity boundary conditions on the rigid boundary, this attraction can be described by the *secondary Bjerknes force* [8]. After the collapse, the bubble reexpands with a liquid flow. A *jet* flowing in direction towards the boundary forms a protrusion of the bubble wall. This is shown in Fig. 4 (frames 4–7).

The dimensionless parameter $\gamma = s/R_{max}$ helps to characterize the bubble collapse for different bubble radii, R_{max} , and distances, s , of the bubble center from the boundary. Varying the parameter γ from ∞ , (the spherical case) to a smaller value increases the influence of the boundary and thus the asphericity of the bubble collapse. Figure 4 consists of a combination of the two shared photographic devices. First, the frames 1–7 show the bubble dynamics for $\gamma = 5.9$. The bubble prior to collapse (frame 1 and 2) has a spherical shape. The bubble reaches minimum volume between frame 3 and 4 as the bubble center moves towards the boundary. The protrusion at the lower bubble wall develops on a slower time scale than the bubble collapse, which in this case is not resolved in great detail. The liquid jet pushes the protrusion, whereas the main bubble body returns to a nearly spherical shape.

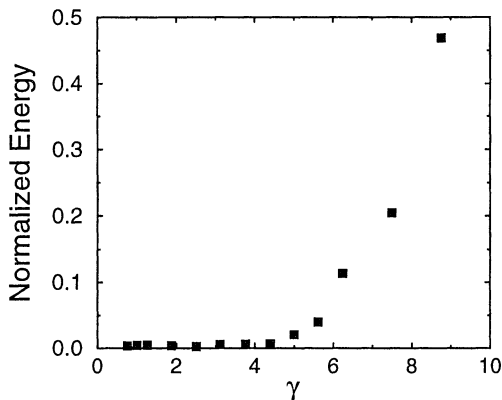


Figure 5. Light energy radiated at bubble collapse, normalized to the spherical case with different γ values but with the same maximum radius $R_{max} = 0.8$ mm.

Frame 3a of Fig. 4 is a blended image of the ICCD picture and frame 3. The cavitation luminescence is visible as the bright spot at the center of the lower bubble wall. The two imaging devices have photographed a different bubble, but the experimental parameters have not been altered. The high reproducibility of the experiment has been checked with the image

converter camera, comparing the bubble dynamics for similar hydrophone signals and an unaltered boundary position. This is a precaution needed to compare the image of the ICCD and the images of the converter camera. Blending of the two frames has been controlled in the following manner. The position of the light emission of the spherical bubble collapse was taken to determine the displacement of the luminescence in the aspherical case. With the displacement and the center of the bubble in frame one and the correct scaling of the ICCD image both images are superposed as done in frame 3a of Fig. 4. With this blending technique, we find that the light emission is located $103\ \mu m$ below the laser focus. The light emission is a single event that occurs at the final stages of the bubble collapse. If multiple emission events would occur, a line or several discrete bright spots would have been imaged as the movement of the collapsing bubble would induce spatial separation. Calculating the number of photons, in the same way as in the spherical case, gives $1.7 \cdot 10^6$ photons for $\gamma = 5.9$.

In Fig. 5 the sensitivity of the radiated energy on the γ value is shown. The points give the normalized (with respect to the spherical case) energy for a fixed R_{max} but different γ values. For $\gamma \leq 3.5$ the light output is not distinguishable from the dark signal. The integrated luminescence decreases rapidly with smaller γ values. *Thus we can conclude that cavitation luminescence draws from a highly spherical bubble collapse.*

4. Conclusion

Luminescence is observed for spherically collapsing cavitation bubbles. No luminescence is observed during the second bubble collapse. After the first collapse the bubble rebounds to a smaller maximum radius due to the energy loss, mainly from emission of a shock wave. Thus the second collapse is not strong enough to produce light emission.

The emission occurs at the geometrical center of the bubble, and as stated above, we assume the shape of the emission to be an image of the bubble scattering the light from its interior. The photon numbers per luminescence event are at least an order of magnitude greater than observed in SBSL experiments [4]. This is as reasonable, since the maximum bubble sizes for laser induced bubbles are 10 to 30 times larger compared to an SBSL experiment. Fitting measured radius-time curves up to the second bubble collapse with Gilmore's model [5] gives an approximate equilibrium bubble radius, R_0 (bubble radius under static conditions). For the bubbles investigated the ratio R_{max}/R_0 is determined to be $9.1 \pm .7$ (independent on R_{max}) and this value was used in Fig. 3 b. The onset of asphericity early at the bubble collapse strongly diminishes the light output.

Jet theories [9] also rely on a nearly spherical collapse as then the jet

velocities are higher when the jet forms. However, they are invalid for a perfectly spherical collapse, i.e. in the limit where asphericity turns to sphericity. An investigation of the interior of a collapsing bubble to determine whether a jet has formed is still beyond the current experimental capabilities. Aspherically collapsing bubbles luminesce at the bubble site of jet impact. This feature they share with shock compressed cylindrical bubbles in gels [10]. Time resolution in this experiment can not distinguish whether it is the instant of jet impact or the instant of bubble minimum when the luminescence flash is emitted. Even a framing rate of 20 million frames/s [3] would not be high enough for γ larger than 3.5. For these cases, due to the increased sphericity, jet impact and bubble minimum are separated by less than 50 ns, the framing resolution of the camera.

Laser induced cavitation bubbles may become an intrinsic tool for studies of luminescence accompanying bubble collapse. The experimental problems associated with very small size of SBSL bubbles can be overcome with laser induced bubbles in SCBL. Another significant advantage is that no sound field is necessary. Experiments with laser induced bubbles avoid the experimental difficulties with diffusion stability [11] and with the Bjerknes force threshold [12]. Further studies of luminescence from aspherical bubble collapse may elucidate the mysterious connection between SBSL and MBSL [13]. SCBL can also be expanded to MCBL (multi cavitation bubble luminescence). Two luminescence spots have been observed from two nearby cavitation bubbles, for example.

This work has been supported by the Fraunhofer Gesellschaft. We thank the company LaVision, Göttingen, for the loan of the ICCD camera and the friendly support from Ramesh Ahuja. We are especially grateful for the inspiring discussions with the members of the Cavitation and Sonoluminescence Group at the Drittes Physikalisches Institut, Göttingen. Further thanks goes to John Allen (DAAD-fellowship) for helpful suggestions.

References

1. W. Lauterborn, *Acustica* **31**, 51 (1974). W. Lauterborn, H. Bolle, *J. Fluid Mech.* **72**, 391 (1975). A. Vogel, W. Lauterborn and R. Timm, *J. Fluid Mech.* **206**, 299 (1989). B. Ward and D.C. Emmony, *J. Acoust. Soc. Am.* **88**, 434 (1990). Y. Tomita and A. Shima, *Acustica* **71**, 161 (1990). A. Philipp and W. Lauterborn, *Acustica* **83**, 223 (1997).
2. C.D. Ohl, A. Philipp, W. Lauterborn, *Ann. Physik* **4**, 26 (1995).
3. A.A. Buzukov, V.S. Teslenko, *JETP Lett.* **14**, 189 (1971). A.G. Akmanov, V.G. Ben`kovskii, P.I. Golubnichii, S.I. Maslennikov, V.G. Shemanin, *Sov. Phys. Acoust.* **19**, 417 (1974) 417.
4. L.A. Crum and T.J. Matula, *Science* **276**, 1348 (1997). W.C. Moss,

- D.B. Clarke, D.A. Young, Science **276**, 1398 (1997). B.P. Barber, R.A. Hiller, R. Löfstedt, S.J. Puttermann, K.R. Weninger, Phys. Rep. **281**, 65 (1997).
5. F.R. Gilmore, *The growth or collapse of a spherical bubble in a viscous compressible liquid*, Hydrodynamics Laboratory, California Institute of Technology, Pasadena, California, Report No. 26-4, 1952.
 6. Lord Rayleigh, Phil. Mag. **34**, 94 (1917).
 7. T.B. Benjamin and A.T. Ellis, Philos. Trans. R. Soc. Lond. A **260**, 221 (1966).
 8. V.F.K. Bjerknes, *Fields of Force* (Columbia University Press, New York 1906). T.G. Leighton, *The Acoustic Bubble* (Academic Press, London, 1994).
 9. A. Prosperetti, J. Acoust. Soc. Am. **101**, 2003 (1997). T. Lepoint, D. De Pauw, F. Lepoint-Mullie, M. Goldman, A. Goldman, J. Acoust. Soc. Am. **101**, 2012 (1997).
 10. N.K. Bourne und J.E. Field, J. Fluid. Mech. **244**, 225 (1992).
 11. S. Hilgenfeldt, D. Lohse, M.P. Brenner, Phys. Fluids **8**, 2808 (1996). I. Akhatov, N. Gumerov, C.D. Ohl, U. Parlitz, W. Lauterborn, Phys. Rev. Lett **78**, 227 (1997).
 12. R. Mettin, I. Akhatov, U. Parlitz, C.D. Ohl, W. Lauterborn, Phys. Rev. E **55**, 3747 (1997).
 13. L.A. Crum, J. Acoust. Soc. Am. **95**, 559 (1994). T.J. Matula, R.A. Roy, P.D. Mourad, W.B. McNamara III, K.S. Suslick, Phys. Rev. Lett. **75**, 2602 (1995). T.J. Matula, R.A. Roy, P.D. Mourad, J. Acoust. Soc. Am. **101**, 1994 (1997).

HOT SPOT CONDITIONS DURING MULTI-BUBBLE CAVITATION

K.S. SUSLICK, W.B. McNAMARA III, AND Y. DIDENKO

Department of Chemistry

University of Illinois at Urbana-Champaign

601 S. Goodwin Ave., Urbana, IL 61801, USA

1. Introduction

Together with the chemical effects of ultrasound, light is often emitted [1-5]. Such sonoluminescence provides an extremely useful spectroscopic probe of the conditions created during cavitation bubble collapse. Acoustic cavitation is the origin of both sonochemistry and sonoluminescence. The collapse of bubbles caused by cavitation produces intense local heating and high pressures, with very short lifetimes. As we will demonstrate in this chapter, in clouds of cavitating bubbles, these hot spots have equivalent temperatures of roughly 5000 K, pressures of about 1000 atmospheres, and heating and cooling rates above 10^{10} K/s. In single bubble cavitation, conditions may be even more extreme [6-7]. Thus, cavitation can create extraordinary physical and chemical conditions in otherwise cold liquids.

Fundamentally, chemistry is the interaction of energy and matter. Chemical reactions require energy in one form or another to proceed: chemistry stops as the temperature approaches absolute zero. Chemists have only limited control, however, over the nature of this interaction. In large part, the properties of a specific energy source determine the course of a chemical reaction. Ultrasonic irradiation differs from traditional energy sources (such as heat, light, or ionizing radiation) in duration, pressure, and energy per molecule. The immense local temperatures and pressures together with the extraordinary heating and cooling rates generated by cavitation bubble collapse mean that ultrasound provides an unusual mechanism for generating high energy chemistry. Like photochemistry, very large amounts of energy are introduced in a short period of time, but it is thermal, not electronic, excitation. As in flash pyrolysis, high thermal temperatures are reached, but the duration is very much shorter (by $>10^4$) and the temperatures are even higher (by five- to ten-fold). Similar to shock-tube chemistry or multiphoton infrared laser photolysis, cavitation heating is very short lived, but it occurs within condensed phases. Furthermore, sonochemistry has a high-pressure component, which suggests that one might be able to produce on a microscopic scale the same macroscopic conditions of high temperature-pressure "bomb" reactions or explosive shockwave synthesis in solids. Figure 1 presents an interesting comparison of the parameters that control chemical reactivity (time, pressure, and energy) for various forms of chemistry.

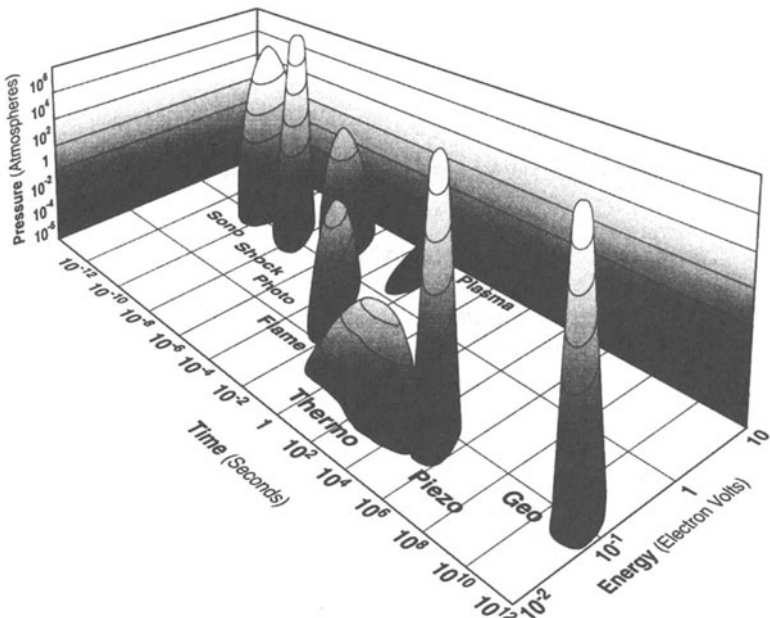


Figure 1. Chemistry: the interaction of energy and matter.

1.1 ACOUSTIC CAVITATION

Ultrasound spans the frequencies of roughly 15 kHz to 1 GHz. With sound velocities in liquids typically about 1500 m/s, acoustic wavelengths range from roughly 10 to 10^{-4} cm. These are not molecular dimensions. Consequently, no direct coupling of the acoustic field with chemical species on a molecular level can account for sonochemistry or sonoluminescence.

Instead, sonochemistry and sonoluminescence derive principally from acoustic cavitation [4], which serves as an effective means of concentrating the diffuse energy of sound. Compression of a gas generates heat. When the compression of bubbles occurs during cavitation, heating is more rapid than thermal transport, creating a short-lived, localized hot spot. There is a nearly universal consensus that this hot spot is the source of homogeneous sonochemistry. Rayleigh's early descriptions of a mathematical model for the collapse of cavities in incompressible liquids predicted enormous local temperatures and pressures [8]. Ten years later, Richards and Loomis reported the first chemical effects of ultrasound [9], and these effects have been ascribed, nearly universally, to localized hot spots created during bubble collapse [10]. Alternative

mechanisms involving electrical microdischarge have been occasionally proposed [e.g., 11-12], but remain an extreme minority viewpoint with many failings [13-14].

If the acoustic pressure amplitude of a propagating acoustic wave is relatively large (greater than ≈ 0.1 MPa), local inhomogeneities in the liquid can serve as nucleation sites for rapid inertial growth into a cavity of macroscopic dimensions, primarily filled with vapor and dissolved gases. Such a bubble is inherently unstable, and its subsequent collapse can result in an enormous concentration of energy. This violent cavitation event has been termed "transient cavitation" [10]. A normal consequence of this unstable growth and subsequent collapse is that the cavitation bubble itself is destroyed. Gas-filled remnants from the collapse, however, may serve as nuclei for continuation of the process.

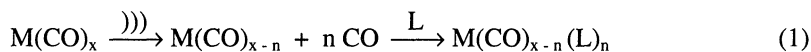
The generally accepted explanation for the origin of sonochemistry and sonoluminescence is the hot spot theory, which holds that the potential energy given the bubble as it expands to maximum size is concentrated into a heated gas core as the bubble implodes. The oscillations of a gas bubble driven by an acoustic field are generally described by the "Rayleigh-Plesset" equation or minor modifications thereof, such as the Gilmore equation [4]. The validity of these equations for computing the behavior of a single, isolated cavitating bubble has been experimentally confirmed. Various researchers have used light scattering off the bubble to measure the radius-time curve for single collapsing bubbles, simultaneously observing the optical emission from sonoluminescence (see below). The single-bubble sonoluminescent emission is seen as the sharp spike appearing at the final stages of bubble collapse. Note that the emission occurs at the point of minimum bubble size, and that the general shape of the theoretical curve is reproduced [15-17].

Single bubbles, while creating extreme conditions, simply do not contain sufficient material to be useful for driving chemical reactions in any practical amount. In multi-bubble systems ("cavitation clouds"), on the other hand, the interactions between bubbles as they collapse will lead to both substantial asymmetry and the formation of jets during collapse [4], which one may well expect to limit the collapse efficiency. Thus, the conditions created during multi-bubble cavitation, which is used of necessity for all sonochemical reactions, will be somewhat less extreme than those created during single bubble sonoluminescence.

1.2 TWO-SITE MODEL OF SONOCHEMICAL REACTIVITY

Probing the conditions present in the cavitation hot spot has proved to be a difficult problem. The transient nature of cavitation, especially in bubble clouds, precludes conventional measurement of the conditions generated during bubble collapse. Chemical reactions themselves, however, can be used to probe reaction conditions. The effective temperature realized by the collapse of clouds of cavitating bubbles can be determined by the use of competing unimolecular reactions whose rate dependencies on temperature have already been measured. This technique of "comparative-rate chemical thermometry" was used by Suslick, Hammerton, and Cline to make the first experimental determination of the effective temperature reached during cavity collapse [18]. The sonochemical ligand substitutions of volatile metal carbonyls

were used as the comparative rate probes (Eqn. 1).

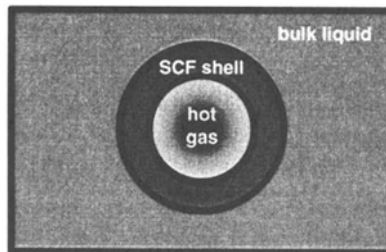


where $M = Fe, Cr, Mo, W$; L represents a substituting ligand;

and the symbol $\xrightarrow{\text{)))}$ represents ultrasonic irradiation of a solution.

These kinetic studies revealed that there are in fact *two* sonochemical reaction sites: the first (and dominant site) is the bubble's interior gas-phase while the second is an *initially* liquid phase. The latter corresponds either to the heating of a shell of liquid around the collapsing bubble or to the injection of liquid droplets into the hot spot by surface wave distortions of the collapsing bubble, as shown schematically in Figure 2.

Thermal Diffusion Shell Model



Surface Wave Droplet & Jet Model

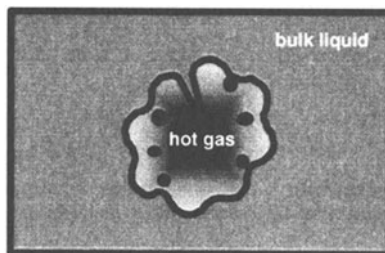


Figure 2. Two-site models of sonochemical reactions.

The effective local temperatures in both sites were determined by combining the relative sonochemical reaction rates for Eqn. 1 with the known temperature behavior of these reactions. The effective temperatures of these hot spots were measured at \approx 5200 K in the gas-phase reaction zone and \approx 1900 K in the initially liquid zone [18]. Of course, the comparative rate data represent only a composite temperature: during the collapse, the temperature within the bubble has a rapidly changing temporal and spatial profile. This two-site model has been confirmed with other reactions [19]. The study of sonoluminescence, which will now be discussed, has both confirmed and extended these temperature measurements of the cavitation hot spot.

2. Sonoluminescence as a Probe of Cavitation

2.1. TYPES OF SONOLUMINESCENCE

Sonoluminescence was first observed from water in 1934 by Frenzel and Schultes [20]. As with sonochemistry, sonoluminescence derives from acoustic cavitation. There are two classes of sonoluminescence: multiple-bubble sonoluminescence (MBSL) and single-bubble sonoluminescence (SBSL) [6, 15, 21]. Cavitation is a nucleated process, and liquids generally contain large numbers of particulates that serve as nuclei. As a consequence, the “cavitation field” generated by a propagating or standing acoustic wave typically consists of very large numbers of interacting bubbles, distributed over an extended region of the liquid. If this cavitation is sufficiently intense to produce sonoluminescence, then we call this phenomenon “multiple-bubble sonoluminescence” (MBSL).

Under the appropriate conditions, the acoustic force on a bubble can balance against its buoyancy, holding the bubble stable in the liquid by acoustic levitation. This permits examination of the dynamic characteristics of the bubble in considerable detail, from both a theoretical and an experimental perspective. Such a bubble is typically quite small compared to an acoustic wavelength (e.g., at 20 kHz, the resonance size is approximately 150 μm). It was recently discovered, for rather specialized but easily obtainable conditions, that a single, stable, oscillating gas bubble can be forced into such large amplitude pulsations that it produces sonoluminescence emissions on each (and every) acoustic cycle [22, 23]. This phenomenon is called single-bubble sonoluminescence (SBSL).

2.2. MULTIPLE-BUBBLE SONOLUMINESCENCE SPECTRA

Over the last three decades, the sonoluminescence of aqueous solutions has been studied at length, most recently and carefully by Didenko and co-workers [24, 25]. The spectrum of MBSL in water consists of a peak at 310 nm and a broad continuum throughout the visible region. The emission at 310 nm is from excited-state OH $^{\bullet}$, but the continuum is difficult to interpret. MBSL from aqueous and alcohol solutions of many metal salts has been reported and are characterized by emission from metal atom excited states [26].

More recently sonoluminescence from non-aqueous liquids has been examined. Flint and Suslick reported the first MBSL spectra of organic liquids [27]. With various hydrocarbons, the observed emission is from excited states of C₂ ($d^3\Pi_g - a^3\Pi_u$, the Swan lines), the same emission that is seen in flames. Furthermore, the ultrasonic irradiation of hydrocarbons in the presence of N₂ (or NH₃ or amines) gives emission from CN excited states, but not from N₂ excited states. Emission from N₂ excited states would have been expected if the MBSL originated from microdischarge, whereas CN emission is typically observed from thermal sources. When oxygen is present, emission from excited states of CO₂, CH[•], and OH[•] is observed, again similar to flame emission.

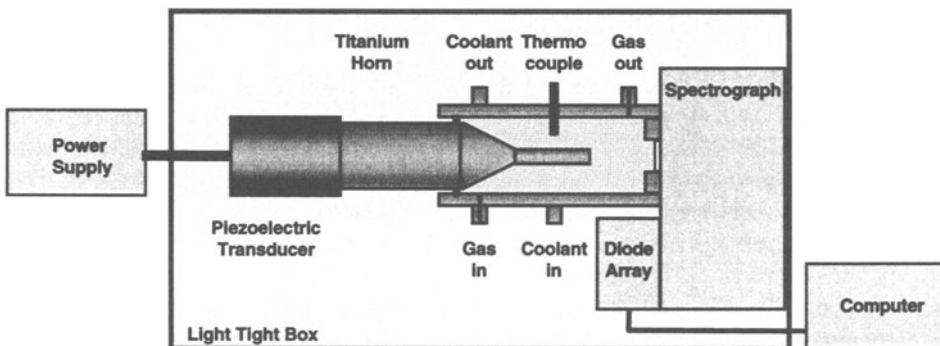


Figure 3. Block diagram of sonoluminescence spectrometer.

Most recently, we have extended our spectral analysis approach to MBSL from excited metal atom spectra. Volatile organometallics (such as Fe(CO)₅ or Cr(CO)₆), when irradiated with ultrasound in a low volatility organic liquid, emit an intense sonoluminescence that corresponds to the known atomic emission lines of the metals [28], again analogous to flame emission. Figure 3 shows a block diagram of our sonoluminescence spectrograph, which is carefully calibrated for both wavelength and radiance using standard lamps. Figure 4 shows a typical MBSL spectrum from a metal carbonyl solution. Note the intense line emission from the metal atom excited states as well as bands from excited states of the diatomics, C₂ and CH.

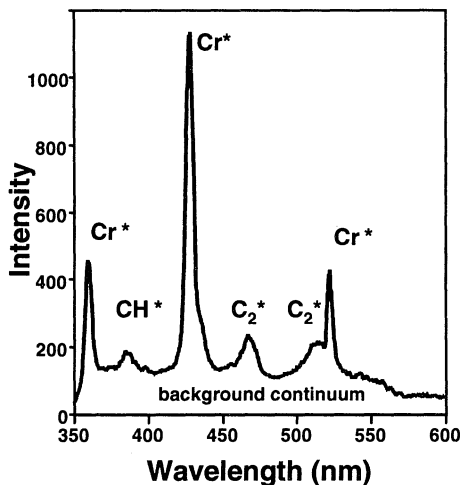


Figure 4. Typical MBSL spectrum from a metal carbonyl solution in silicone oil.

For both aqueous and non-aqueous liquids, MBSL is caused by chemical reactions of high-energy species formed during cavitation by bubble collapse. Its principal source is most probably not blackbody radiation or electrical discharge. MBSL is a form of chemiluminescence, not unlike flame emission.

2.3 SPECTROSCOPIC PROBES OF CAVITATION CONDITIONS

Determination of the conditions reached in a cavitating bubble has remained a difficult experimental problem. Spectral analysis of MBSL provides a solution. We have used two very different spectroscopic reporters to provide such information: (1) resolved molecular emission from diatomics (notably C_2) produced during cavitation and (2) atomic line emission derived from the sonolysis of volatile organometallic compounds.

Flint and Suslick first reported high-resolution MBSL spectra from silicone oil under Ar [29]. The observed emission comes from excited state C_2 and has been modeled with synthetic spectra as a function of rotational and vibrational temperatures, as shown in Figure 5. From comparison of synthetic to observed spectra for several different emission bands, the effective rotational and vibrational emission temperature is 5050 ± 150 K. The excellence of the match between the observed MBSL and the synthetic spectra provides definitive proof that the sonoluminescence event is a thermal, chemiluminescence process, although the issue of thermal equilibration in such systems is not without its complexities [30]. The agreement between this spectroscopic determination of the cavitation temperature and that made by comparative rate thermometry of sonochemical reactions [18] is surprisingly good.

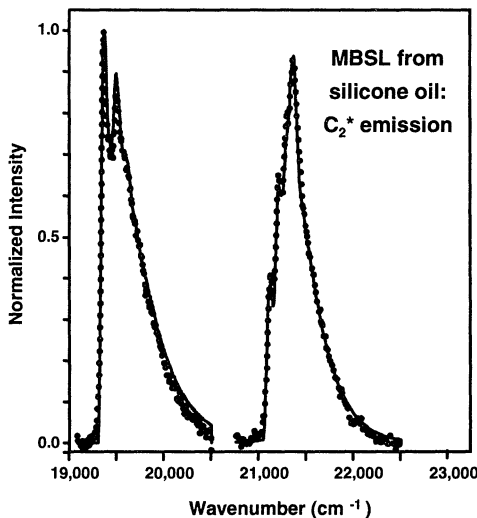


Figure 5. Excited state C_2 MBSL spectrum from silicone oil under Ar.

Emission from the $\Delta v = +1$ manifold of the $d^3\Pi_g - a^3\Pi_u$ transition (Swan band) of C_2 .

- • • • Observed MBSL spectrum from polydimethylsiloxane silicone oil under Ar at 0°C.
- Best fit synthetic spectrum for these two bands, with $T_v = T_r = 4900$ K.

We have now analyzed the relative intensities of atomic emission lines in the sonoluminescence spectra of excited state metal atoms produced by sonolysis of volatile Fe, Cr, and Mo carbonyls dissolved in silicone oil under argon. Sufficient spectral information about emissivities of many metal atom excited states are available to readily calculate emission spectra as a function of temperature. Because of this, the emission spectra of metal atoms are extensively used to monitor the surface temperature of stars. For example, the expected spectra for iron emission as a function of temperature is shown in Figure 6.

From comparison of such calculated spectra and the observed MBSL spectra from metal carbonyls, another measure of the cavitation temperature can be obtained. The effective emission temperature during cavitation under argon at 20 kHz is 4900 ± 250 K, with excellent agreement among the three systems tested (5150 ± 300 K for Fe, 4700 ± 400 K for Cr, and 4750 ± 400 K for Mo), as shown in Figures 7 through 9. Again, agreement with our prior comparative rate thermometry and the MBSL emission temperature of C_2^* excited states is excellent.

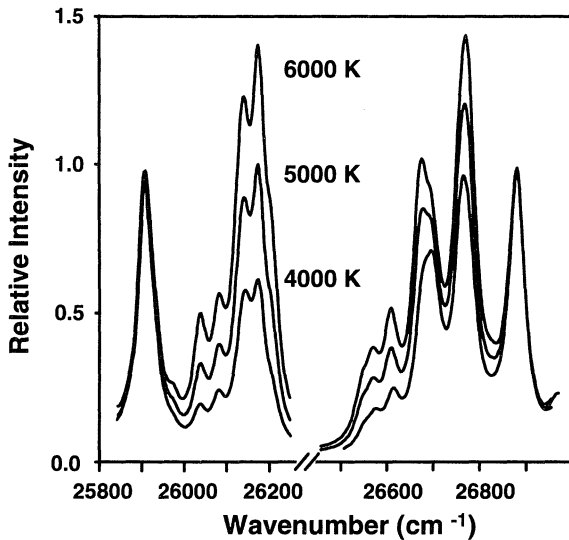


Figure 6. Calculated emission spectra of Fe atoms as a function of temperature.

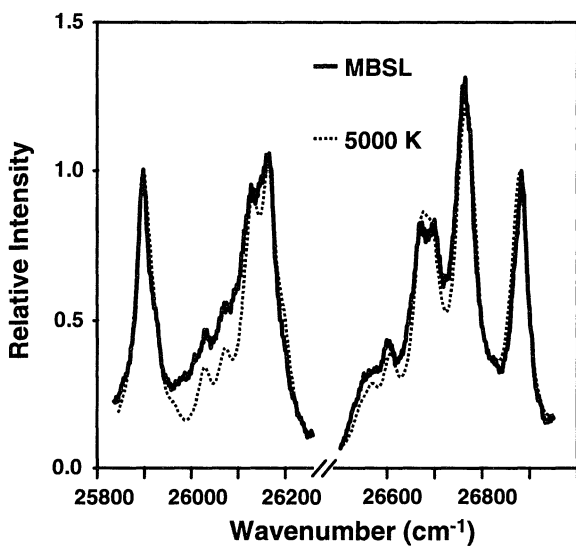


Figure 7. Sonoluminescence of excited state Fe atoms produced during sonolysis of $\text{Fe}(\text{CO})_5$ dissolved in silicone oil under Ar. Effective emission temperature is 5150 ± 300 K

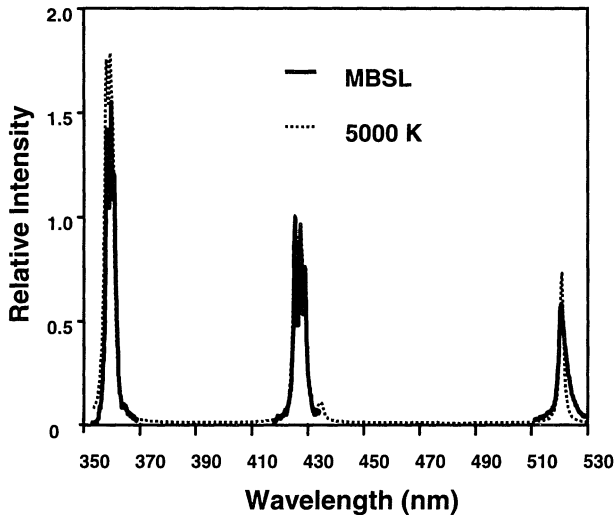


Figure 8. Sonoluminescence of excited state Cr atoms produced during sonolysis of $\text{Cr}(\text{CO})_5$ dissolved in silicone oil under Ar. Effective emission temperature is 4700 ± 400 K

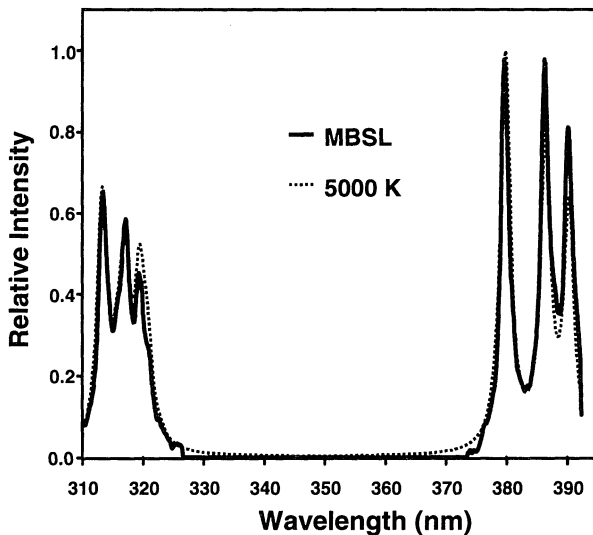


Figure 9. Sonoluminescence of excited state Mo atoms produced during sonolysis of $\text{Mo}(\text{CO})_6$ dissolved in silicone oil under Ar. Effective emission temperature is 4750 ± 400 K

We are also able to control the temperature within the cavitation bubble simply by changing the bubble contents. For example, upon addition of gaseous hydrocarbons (methane, ethylene, or propane), the observed emission temperatures from Cr atom excited states decrease dramatically, as shown in Figure 10. As polyatomic molecules are added to the bubble contents, the polytropic ratio of the gas in the bubble decreases, and so too does the expected temperature from adiabatic compression, as shown by Eqn. 2. The presence of the polyatomic gas simply provides vibrational and rotational modes that will divert much of the kinetic energy of collapse away from direct temperature increase. The effects of the addition of polyatomic gases to the observed cavitation emission temperature can be quantitatively modeled by simple adiabatic compression of a bubble during cavitation collapse. This simple model predicts pressures on the order of 10^3 Bar, which is quantitatively consistent with the linewidth broadening and small peak wavelength shifts observed in the metal atom emission.

$$T_{\max} = T_{\min} \left(\frac{R_{\max}}{R_{\min}} \right)^{3(\gamma-1)} \quad (2)$$

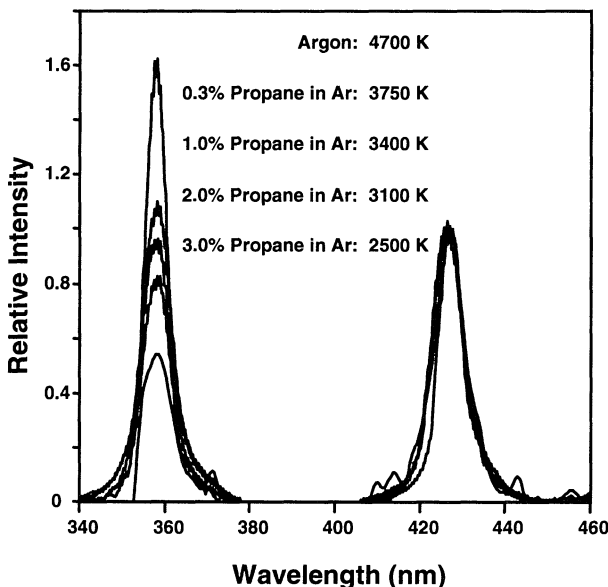


Figure 10. Control of cavitation temperature. Sonoluminescence of excited state Cr atoms produced during sonolysis of $\text{Cr}(\text{CO})_5$ dissolved in silicone oil with increasing amounts of propane in Ar.

2.4 SINGLE-BUBBLE SONOLUMINESCENCE SPECTRA

The spectra of MBSL and SBSL are dramatically different and the interpretation of SBSL spectra is much less clear. MBSL can be observed in essentially all liquids, whereas SBSL has been observed primarily in aqueous liquids. While MBSL is generally dominated by atomic and molecular emission lines (e.g. excited states of OH[•] in water and of C₂ in hydrocarbons), SBSL is an essentially featureless emission that increases with decreasing wavelength. Unusual effects on the intensity of this featureless SBSL emission are observed when the gas contents of the bubble are changed [22, 23, 31, 32]. Furthermore, the SBSL spectra show no evidence of OH emissions, and when He and Ar bubbles are considered, continue to increase in intensity even into the deep ultraviolet. For example, the MBSL spectrum of an aqueous solution of NaCl is dominated by strong bands from excited states of both OH[•] and Na; however, the SBSL spectrum of an identical solution shows no evidence of these peaks [21]. Similarly, the MBSL spectrum falls off at low wavelengths, while the SBSL spectrum continues to rise, at least for most noble gases [22, 23].

Early work on SBSL stirred intense interest due primarily to the exceptionally short duration of the sonoluminescence flash. The initial reports by Puttermann et al. placed the emission lifetimes well below 50 ps [23], but more recent studies by Gompf [33] have shown that the emission is generally longer, \approx 200 ps. The standard hydrodynamic models of adiabatic collapse of a single bubble could not have explained emission lifetimes below 50 ps, which generated a wide range of quite speculative (and often just plain silly) theories on the origin of SBSL. The consensus appears to be settling on intense adiabatic compression, with sonochemical reaction and rectification into the water of reactive gases (e.g., O₂ and N₂ from air filled bubbles) [31], and with some ionization occurring in the last stages of bubble collapse [34, 35]. There may also be a convergent shockwave within the single bubble, although this remains an open issue.

The difference between SBSL and MBSL spectra appears likely to be related to the sphericity of collapse. In SBSL, where bubble collapse is more spherical and the extent of compression greater, sufficient temperatures are reached (probably above \approx 20,000 K) to form a plasma and the primary emission becomes electron-ion or electron-atom bremsstrahlung [34,35]. In such a plasma, the temperatures will ensure dissociation of all molecules and will broaden, through Stark and pressure effects, any remaining molecular or atom emission beyond recognition [35]. The issue of a spherically convergent shockwave remains an open question. There continues the possibility of extraordinarily high energy conditions (up to and including those needed for inertial confinement fusion!) at the center of the bubble (which would be shielded from direct observation by the opacity of the surrounding plasma) [34, 36].

3. Conclusion

Sonochemistry and sonoluminescence are closely related phenomenon, both of which derive from acoustic cavitation. Bubble collapse in liquids results in an enormous concentration of energy from the conversion of the kinetic energy of liquid motion into heating of the contents of the bubble. The enormous local temperatures and pressures so created provide a unique means for fundamental studies of chemistry and physics under extreme conditions. A diverse set of applications of ultrasound to enhancing chemical reactivity has been explored, with important applications in mixed phase synthesis, materials chemistry, and biomedical uses. Many of these are discussed throughout this monograph.

4. Acknowledgments

This work was supported by the National Science Foundation and in part by .the Department of Energy.

5. References

1. Suslick, K.S., ed. (1988) *Ultrasound: Its Chemical, Physical, and Biological Effects*, VCH Publishers, New York.
2. Suslick, K.S. (1990) *Science*, **247**, 1439.
3. Mason, T.J., Lorimer, J.P. (1988) *Sonochemistry: Theory, Applications and Uses of Ultrasound in Chemistry*, Ellis Horwold, Ltd., Chichester, U.K.
4. Leighton, T.G. (1994) *The Acoustic Bubble* Academic Press, London, pp. 531-551.
5. Suslick, K.S.; Crum, L.A. (1997) "Sonochemistry and Sonoluminescence," in *Encyclopedia of Acoustics*; Crocker, M. J., ed.; Wiley-Interscience, New York, vol. 1, ch. 26, pp. 271-282.
6. Crum, L.A. (1994) *Physics Today*, **47**, 22.
7. Puttermann, S.J. (1995) *Scientific American*, **Feb. 1995**, 46.
8. Lord Rayleigh (1917) *Philos. Mag.*, **34**, 94.
9. Richards, W.T. Loomis, A.L. (1927) *J. Am. Chem. Soc.*, **49**, 3086.
10. Flynn, H.G.(1964) "Physics of Acoustic Cavitation in Liquids," in *Physical Acoustics*, ed. by W.P. Mason, Academic Press, New York, Vol IB, p. 157.
11. Margulies, M.A. (1992) *Ultrasonics* **30**, 152.
12. Lepoint, T., Mullie, F. (1994) *Ultrasonics Sonochem.*, **1**, S13.
13. Suslick, K.S.; Kemper, K.A. (1993) *Ultrasonics* **31**, 463-465.
14. Suslick, K.S.; Dokytz, S.J.; Flint, E.B. *Ultrasonics* **1990**, **28**, 280-290.
15. L.A. Crum, *J. Acoust. Soc. Am.* **95**, 559 (1994).
16. B.P. Barber and S.J. Puttermann, *Phys. Rev. Lett.* **69**, 3839 (1992).
17. Puttermann, S. J.; Weninger, K.; Barber, B.P. *Phys. Rev. Lett.* **1997**, **78**, 1799-180.
18. Suslick, K.S.; Hammerton, D.A.; Cline, Jr., R.E. (1986) *J. Am. Chem. Soc.* **108**, 5641.
19. Henglein, A. (1993) *Adv. Sonochem.*, **3**, 17.
20. Frenzel, H. Schultes, H. (1934) *Z. Phys. Chem.* **27b**, 421.
21. Matula, T.J.; Roy, R.A.; Mourad, P.D.; McNamara III W.B.; and Suslick, K.S. (1995) *Phys. Rev. Lett.* **75**, 2602.

22. Cheeke, J.D.N. (1997) *Can. J. Phys.* **75**, 77-98.
23. Barber, B. P.; Hiller, R.A.; Loefstedt, R.; Puterman, S.J.; Weninger, K.R. (1997) *Phys. Rep.* **281**, 65-143.
24. Didenko, Y.T.; Pugach, S.P. (1994) *Ultrasonics Sonochemistry* **1**, s10-s12.
25. Didenko, Y.T.; Nastich, D.N.; Pugach, S.P.; Polovinka, Y.A.; Kvochka, V.I. (1994) *Ultrasonics* **32**, 71-76
26. Flint, E.B.; Suslick, K.S. (1991) *J. Phys. Chem.* **95**, 1484.
27. Flint, E.B.; Suslick, K.S. (1989) *J. Amer. Chem. Soc.* **111**, 6987.
28. Suslick, K.S.; Flint, E.B.; Grinstaff, M.W.; Kemper, K.A. (1993) *J. Phys. Chem.*, **97**, 3098-3099.
29. Flint, E.B.; Suslick, K.S. (1991) *Science* **253**, 1397.
30. Jeffries, J.B.; Copeland, R.A.; Flint, E.B.; Suslick, K.S. (1992) *Science* **256**, 248.
31. Lohse, D.; Brenner, M.P.; Dupont, T.F.; Hilgenfeldt, S.; and Johnston, B. (1997) *Phys. Rev. Lett.*, **78**, 1359-1362.
32. Barber, P.; Hiller, R.; Arisaka, K.; Fetterman, H. and Puterman, S.J. (1992) *J. Acoust. Soc. Am.* **91**, 3061.
33. Gompf, B., Günther, R.; Nick, G.; Pecha, R.; Eisenmenger, W. (1997) *Phys. Rev. Lett.* **79**, 1405.
34. Moss, W.C.; Clarke, D.B.; Young, D.A. (1997) *Science* **276**, 1398-1401.
35. Bernstein, L.S.; Zakin, M.S.; Flint, E.B.; Suslick, K.S. (1996) *J. Phys. Chem.* **100**, 6612-6619
36. Barber, P.; Hiller, R.A.; Lofstedt, R.; Puterman, S.J.; Weninger, K.R. (1994) *Phys. Rev. Lett.*, **72**, 1380.

SOME PHYSICO-CHEMICAL ASPECTS OF SO-CALLED "HOMOGENEOUS SONOCHEMISTRY"

J. REISSE*, T. CAULIER, C. DEKERCKHEER,
Y. KEGELAERS, N. SEGEBARTH, K. BARTIK
Université Libre de Bruxelles (CP 165),
50, avenue F.D. Roosevelt, B 1050 Bruxelles, Belgium.

1. FOREWORD

This paper is essentially devoted to the discussion of some physico-chemical concepts, laws and formulae which are of interest in quantitative "homogeneous sonochemistry". Only a few examples of sonochemical reactions will be given. Those interested by specific data will find many examples in books and review articles. A non-exhaustive list of references is given in the bibliography under the heading "general bibliography".

2. INTRODUCTION

2.1. Homogeneous sonochemistry: a misleading concept

The misleading expression "homogeneous sonochemistry" is used so extensively that it is probably pointless to suggest that it be abandoned. Therefore it is important to explain what is wrong with the association of these two words which are mutually incompatible. In thermodynamics a homogeneous system is one whose properties are either the same in all parts or vary in a continuous way from point to point. In other words, it is a system in which there are no apparent discontinuities. Before sonication a liquid can be homogeneous but no sonochemistry is occurring then. However, a cavitating liquid does not fulfil this definition and therefore, on a purely logical basis, the terms "sonochemistry" and "homogeneous" are mutually incompatible. It could be argued that all chemists know what the expression means and that such rigour is not important. This would be an acceptable argument if, but only if, the expression "homogeneous sonochemistry" were not so misleading.

The reactions which are accelerated by sonication are generally radical reactions. According to Luche [1], it was necessary to formulate a rule in order to explain the puzzling fact that ionic reactions are generally insensitive to sonication. The recently reformulated Luche rule no.1 states that "reactions which are sensitive to the

sonochemical effect are those which proceed via radical or radical-ion intermediates" [2]. Since the majority of organic reactions take place through electron doublet transfer, we are faced with the unfortunate fact that only a small number of organic homogeneous reactions are sensitive to sonication. As soon as we realise that so-called "homogeneous sonochemistry" is in fact gas phase (bubble) chemistry, sometimes followed by secondary reactions taking place in the liquid, we no longer need any rules. Indeed, ionic reactions are extremely rare in the gas phase because separated ions are unstable if they are not solvated. A very simple calculation based on the Coulomb law can illustrate this point. If we take as a criteria of interaction between two chemical species **i** and **j** the fact that the interaction energy is greater than the thermal energy ($|\epsilon_{ij}| > kT$), it is easy to calculate that at 3000 K this condition is already fulfilled for a distance of 55 Å. In other words, the dissociation of a molecule into ions is a process of very low probability in the gas phase. Even chemical reactions where the activated complexes are characterised by high dipole moments are uncommon in gas phase chemistry. It is interesting to mention here that the sonoluminescence spectrum of a water solution of sodium chloride shows the typical emission lines of Na° and not of Na⁺. No rule is necessary to explain the fact that NaCl does not dissociate into Na⁺ and Cl⁻ in the gas phase.

2.2. Quantitative aspects of homogeneous sonochemistry

To complement our general comments concerning the misleading concept of "homogeneous sonochemistry", we would like to emphasise that the chemical yields of so-called "homogeneous sonoreactions" are generally very poor. On the basis of a survey of the literature, it can be concluded that a typical rate for a primary sonochemical reaction, obtained with electrical generators characterised by a power of 100-500 W, is of the order of 10^{-4} to 10^{-5} mole/minute [3]. In some rare cases the rates are higher [4]. A rate of 10^{-5} mole/minute implies that a reaction time of approximately 1.5×10^3 hours is necessary to obtain one mole of transformed product at an energy cost which is far from negligible, even if we neglect the cost of refrigeration. "Homogeneous sonochemistry" is a very inefficient kind of chemistry in terms of reaction time and energy cost. Of course, the situation could change in the future if better experimental devices become available but it will require a major technical breakthrough to obtain much better results than those that we obtain today with baths, horns or cup-horns. Some reactions classified as "homogeneous sonochemical reactions" are characterised by high yields. However, as we will see later, these reactions are in fact secondary chain reactions taking place in the liquid phase i.e. a different phase, and which are initiated, directly or indirectly, by radicals produced in the gas phase during the true (and only) sonochemical step. These secondary reactions do not seem to be affected by the pressure wave. Strictly speaking, they are not sonochemical reactions.

3. THE THREE PHASES ENCOUNTERED IN "HOMOGENEOUS SONOCHEMISTRY"

3.1. The intra-bubble gas phase

Since "true homogeneous sonochemistry" takes place in the bubbles, it is necessary to determine what the intra-bubble gas content could be. We have only very indirect information concerning the intra-bubble medium and it is not at all obvious that what is known about gas-liquid equilibrium is of any help in predicting what the state, and even the nature, of the intra-bubble medium could be. When we are working with a "pure liquid", for example water or CCl_4 under one atmosphere of argon or nitrogen, we are, strictly speaking, in the presence of a solution of a gas. The dissolved gas concentration (i.e. the gas solubility at equilibrium) is a function of temperature and pressure and can be easily measured. Before sonication, the solubility of rare gases, nitrogen and air in water or in an organic liquid is low enough for the solution to be considered as ideal. The Raoult law is therefore valid for the solvent in equilibrium with the macroscopic gas phase above the liquid.

As we will see in this paragraph, and also in a later paragraph devoted to the bubble-bulk interface, the intra-bubble gaseous content is certainly different for many reasons from the macroscopic gaseous phase above the solution. The first and most important reason is that a cavitating liquid, described as a thermodynamic system, cannot be at equilibrium (even if it can be stationary). Secondly, the local pressure and temperature inside the bubbles are time dependent. At the end of the collapse they are certainly very different from the macroscopic values. Finally, cavitation bubbles are surrounded by an interface which probably has a composition different from the bulk composition. Strictly speaking, the gas-liquid equilibrium also depends on the curvature of the interface. Indeed the vapour pressure over a concave surface is decreased with respect to the situation prevailing above a planar surface and this change increases exponentially when the radius of the concave surface decreases [5]. Nevertheless, it is safe to consider this dependence as a second order effect, at least in the case of cavitating bubbles of a few microns like those associated with a 20 kHz pressure wave. The situation could be different in the MHz range, when the bubbles are much smaller.

Sonication will lead to the degassing of the solution. After a few minutes of sonication, the gas concentration in solution decreases by a factor which can be as high as 0.6. This is the consequence of the well-known degassing effect of intense pressure waves and the associated cavitation phenomenon. On the basis of results obtained in our laboratory with CCl_4 as solvent under a pressure of 1 bar and with 20 kHz ultrasound, the stationary solubility under sonication compared to the equilibrium solubility is gas dependent: 0.6 for argon but only 0.85 for xenon [6].

During the expansion of the bubbles by rectified diffusion [7,8], it is probably safe to assume that the gas content of the bubbles obeys the equation of state of a perfect gas. This will remain true as long as the intra-bubble temperature and pressure

remain similar to the external values. During the collapse of a bubble, or for a bubble undergoing unstable cavitation, the temperature and pressure will however reach higher values. At a pressure of 150 bar, the fugacity of a gas like N₂ is very similar to the pressure of the hypothetical perfect gas, taken as a reference state [5]. This means that the volume which is occupied by one mole of nitrogen is not very different to what can be predicted by using the PV = RT equation. However, at 1000 bars the PV/RT ratio is no longer equal to 1 but to 2.070 indicating that the repulsive energies between gas phase molecules are now far from negligible [5]. This leads to the conclusion that different equations of state must be used during the collapse in order to take the gas phase imperfections into account. The virial expansion or the van der Waals equation are examples of equations of state which are able to describe the behaviour of real gases in a moderate range of pressures. In the well known virial expansion, it is important to remember that the first coefficient, B, is strongly temperature dependent and, of course, gas dependent. In the case of xenon it is - 129 cm³.mole⁻¹ at 300 K but only -21 at 600 K. For N₂, it is - 4 cm³.mole⁻¹ at 300 K but + 21 at 600 K [9]. For xenon the correction term is dominated by attraction between molecules at the two temperatures, while for nitrogen repulsion already dominates at 600 K. As soon as more extreme temperatures and pressures must be taken into account, (leading to some ionisation of the gas), more sophisticated equations of state must be used like those used by Moss et al [10].

Even if the content of the bubble is far from perfect, the state equation for the perfect gases is frequently used in an explicit or implicit way and we will illustrate this point with the well known C_p/C_v problem i.e. the ratio between the heat capacity at constant pressure and at constant volume. Anyone involved in sonochemistry will know the importance of the $\gamma = C_p/C_v$ ratio. Indeed, if the isothermal expansion of the bubble is followed by a fast adiabatic compression, the γ value determines the temperature at the end of the collapse. Even if the collapse is not strictly adiabatic and if heat exchange occurs, the γ value is still an important parameter. Gas sequences in sonoluminescence and sonochemistry are generally explained on this basis.

Here, it could be useful to discuss and analyse the underlying assumptions of the well known sequence:

$$\gamma_{\text{monoatomic}} > \gamma_{\text{diatomic}} > \gamma_{\text{polyatomic}}$$

If a system is heated at constant volume no work is done and the heat absorbed is equal to the increase in internal energy. The definition of C_v is given by equation (1):

$$C_v = \left(\frac{\partial E}{\partial T} \right)_V \quad (1)$$

However, if there is a change in volume during the heating process, the heat absorbed is different from the increase in internal energy and the difference corresponds to the work which is done (first principle of thermodynamics). The definition of C_p is given by equation (2):

$$C_p = \left(\frac{\partial E}{\partial T} \right)_P + P \left(\frac{\partial V}{\partial T} \right)_P \quad (2)$$

which is equivalent to (3):

$$C_p = \left(\frac{\partial H}{\partial T} \right)_P \quad (3)$$

From fundamental relationships of equilibrium thermodynamics [9], it is easy to derive the following relationship between C_p and C_v :

$$C_p = C_v + \left[P + \left(\frac{\partial E}{\partial V} \right)_T \right] \left(\frac{\partial V}{\partial T} \right)_P \quad (4)$$

For a perfect gas $\left(\frac{\partial E}{\partial V} \right)_T$ is equal to zero and $P \left(\frac{\partial V}{\partial T} \right)_P$ is equal to R . Therefore, in the case of a perfect gas, and only in this case:

$$C_p = C_v + R \quad (5)$$

The energy of a tridimensional translator, estimated by the classical kinetic molecular theory, is $3/2 RT$. C_v for a monoatomic perfect gas at the high T limit (which corresponds to the classical limit) is therefore simply $3/2 R$ and γ is the ratio of $5/2 R$ to $3/2 R$ (i.e. 1.66).

An estimation of γ can also be easily obtained for diatomic or polyatomic perfect gases, if the high T conditions (classical limit) are simultaneously fulfilled for the translational, rotational and vibrational degrees of freedom. Indeed, in the classical kinetic molecular theory, the contribution of each translational and rotational degree of freedom to C_v is $R/2$ and the contribution of each vibrational degree of freedom to C_v is R . γ will then be equal to 1.28 for a diatomic molecule and 1.08 for a penta-atomic molecule. γ will tend towards 1 as the number of atoms (and therefore the number of vibrational degrees of freedom) increases.

The C_v values at 300 K and 1 bar for H_2 and N_2 are respectively 21.6 and 20.8 J/mole.K [8]. It is apparent that the classical perfect gas limit ($C_v = 29.08$ J/mole.K i.e. $7/2 R$) is not reached for these diatomic molecules at 300 K. Since the gas

imperfection is negligibly small at 1 bar the difference between the actual value and the calculated value must be essentially due to the fact that the temperature is too low for the classical approximation to be applied. For H₂, due to its low inertia moment, the classical limit is not reached for the rotational degrees of freedom. For both molecules, the classical limit is not reached for the vibrational degrees of freedom.

If the classical limit is not reached, it is still possible to calculate the vibrational contribution to C_V if each vibrational mode is harmonic [5,11]. This contribution is given by equation (6):

$$C_v^{vib} = R \sum_{n=1}^{n=(3N-6)} \frac{x^2 e^x}{(e^x - 1)^2} \quad (6)$$

where

$$x = \frac{h\nu}{kT} = \frac{1.44\nu(cm^{-1})}{T(K)} \quad (7)$$

x is of course different for each of the 3N-6 modes of vibration.

C_V^{vib} varies monotonically from zero for x >> 1 to R for x = 0 (high T limit). It is interesting to observe that even at 4000 K, a vibrational mode with a wave number of 3000 cm⁻¹ (a typical CH stretching vibration) contributes to C_V^{vib} by only 7.52 J/mole.K and not by R (8.31 J/mole.K). Even at this temperature the classical limit is not reached for this vibrational mode.

Experimental values of γ are reported in table 1 for Ar, N₂ and CH₄, at various pressures and temperatures [9]. We will first of all discuss the values for Ar. At a pressure of 1 bar and a temperature of 300 K, the perfect gas approximation is clearly valid: $\gamma = 1.66$. This also indicate that the high T limit (classical limit) is already reached at this temperature. This is predictable on a theoretical basis: the translational quantum states are only narrowly separated in energy and the continuum of states approximation is valid at normal T. Nevertheless, as soon as the pressure increases, the perfect gas phase approximation is no longer valid and γ becomes higher than the perfect gas value. The increase in γ with pressure is temperature dependent.

In the case of N₂ and CH₄, γ decreases when T increases: the system evolves towards the classical limit. Nevertheless, the gas imperfection certainly plays a role at the high pressures but the evolution of γ with P is masked by the evolution of γ with T.

During the bubble oscillation and the final bubble implosion, neither P nor T are constant [7]. This means that γ itself is not constant during the bubble life-time. This introduces supplementary difficulties in the evaluation, for example, of the maximum temperature, T_{max}, or the maximum pressure, P_{max}, at the final stage of the collapse. As discussed in detail in ref. [7], T_{max} and P_{max} can be estimated on a theoretical basis. Various approaches have been suggested in the literature. They are based on the

pioneering work of Rayleigh. According to Noltingk and Neppiras, T_{\max} is proportional to $(\gamma - 1)$ [12]. This $(\gamma - 1)$ factor is based on the assumption that the collapse is strictly adiabatic. γ also plays an important role in theoretical calculations devoted to defining the instability criterion of Benjamin.

This criterion estimates the radius of a bubble with surface deformations and for which the radial collapse is no longer valid [7].

It is possible to take into account a collapse which is not strictly adiabatic by replacing the γ value by the so-called polytropic coefficient κ . When the sample is a perfect gas, κ is equal to 1 for an isothermal change of P or V ($PV = \text{constant}$) and κ is equal to γ for an adiabatic change of P or V ($PV^\gamma = \text{constant}$). κ has also been measured for a single pulsating bubble maintained in levitation [13] but is difficult to imagine a similar experimental approach for a bubble field.

TABLE 1: γ values for Ar, N₂ and CH₄ at different pressures and temperatures [9].

	1 bar	10 bar	100 bar
Ar			
300 K	1.66	1.70	1.97
380 K	1.66	1.68	1.82
N ₂			
300 K	1.40	1.42	1.56
900 K	1.35	1.35	1.36
CH ₄			
300 K	1.30	1.32	1.66
600 K	1.19	1.19	1.22

As previously discussed, even at moderate pressures with respect to the values which are probably reached at the end of the collapse, the perfect gas approximation is no longer valid. Moreover it is κ and not γ which is the relevant parameter. Nevertheless, γ values based on the perfect gas phase approximation are still frequently used in the sonochemical literature to qualitatively or semi-quantitatively explain the gas effects. Due to its wide-spread use in sonochemistry, it could be suggested that the variation of γ with pressure be preferentially used as an indicator of gas imperfection. Indeed, γ is more sensitive to gas imperfections than the RT/PV ratio (we saw previously that even at 150 bars this ratio is close to 1 for N₂).

It is important to remind here that the two conditions which must be simultaneously fulfilled for a gas to be perfect are $PV = RT$ and $\left(\frac{\partial E}{\partial V}\right)_T$ is equal to

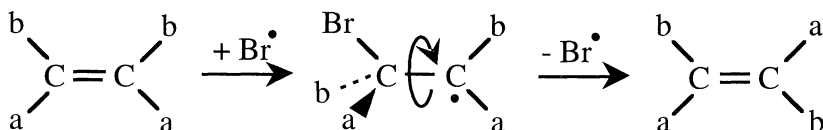
zero. For obvious reasons, the second condition plays an important role on the γ value.

To conclude this paragraph, we would like to emphasise the importance of all experimental studies devoted to a better knowledge of the pressure and temperature conditions prevailing in collapsing bubbles in a bubble field. Calculated values based on non realistic assumptions could lead to serious errors and the experimental approach must be favoured [14, 15].

3.2. The liquid phase in "homogeneous sonochemistry"

In "homogeneous sonochemistry" we are concerned with the intra-bubble gas phase but also with two other phases: the bulk of the liquid and the bubble-bulk interface. Until recently, the importance of this last domain has been frequently underestimated and we will come back to it in a later paragraph. The bulk of the liquid in sonochemistry is not different, in any way, from the bulk liquid in a reaction cell not submitted to sonication. The bulk is sometimes a pure liquid but most often it is a solution i.e. a homogeneous mixture of a solvent, one or more liquid or solid solutes and a gaseous solute which can be reactive. A priori, all gases except the monoatomic rare gases are reactive and if they reach the bubble gas phase are able to give a primary sonochemical reaction. The solvent, all liquid and even solid solutes have a non-zero vapour pressure. They can therefore also reach the bubble interior and be involved in primary sonochemical reactions. With probably few exceptions, these primary reactions lead to the formation of polyatomic radicals or atoms. These species are ejected from the collapsing bubble into the bulk through the interface. If they do not react at the interface, they are able to participate in secondary reactions, taking place in the bulk, at the bulk temperature, and involving some bulk molecules.

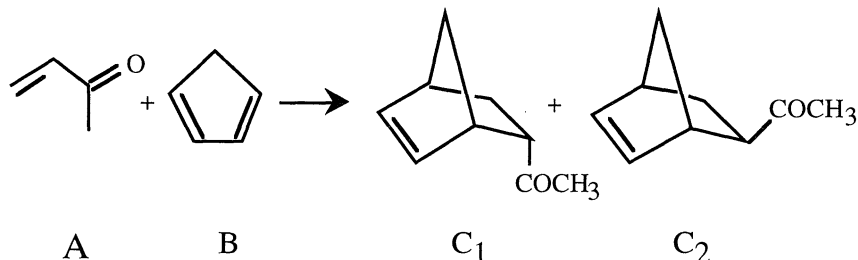
The study undertaken in our laboratory [16] on the induced sonoisomerization of 1,2-dichloroethene in the presence of a bromoalkane is a good example of what has just been described:



As in the case of the fumarate-maleate isomerization which was also studied in our laboratory [17], the primary sonochemical step is the sonocleavage of the bromoalkane. The bromine atoms, ejected into the bulk at the end of the collapse, add reversibly onto

the ethylenic solute. This reversible addition of the bromine atom to the carbon-carbon double bond allows the ethylenic compound to isomerize by rotation around the single bond of the reaction radicalar intermediate. If we start with the pure trans or the pure cis derivative, we obtain a trans-cis mixture with a composition which corresponds to an isomerization temperature of 260 ± 30 K. One bromine atom is able to isomerize approximately 8000 ethylenic molecules and the overall yield of the isomerization is satisfactory: 0.1 mole of dichloroethene isomerizes in one hour. However, the primary reaction is, as usual, a very inefficient reaction: the quantitative analysis of the bromoalkane by gas chromatography does not show any significant change in its concentration. Interestingly enough, a careful kinetical study of this reaction shows that the solvent CCl_4 plays a role. First of all, it does not act as a scavenger for the bromine atoms but, perhaps more importantly, it contributes to the formation of bromine atoms probably through a halogen exchange between RBr and Cl° . We were unable to determine if this last reaction takes place inside the bubble or in the bulk. The thermal isomerization of dichloroethylene is a well known reaction [18, 19] which takes place at a moderate rate, in the gas phase, at temperatures above 500K. Nevertheless, the direct isomerization of the dichloroethylene molecules is not observed when the ethylenic molecules are sonicated for a few hours in absence of bromoalkane. The isomerization of 1,2-dichloroethylene catalysed by a bromine atom is not a sonochemical reaction. The only sonochemical step is the initiation step i.e. the homolytic cleavage of R-Br (and probably also the homolytic cleavage of CCl_4). Because the induced isomerization itself is a chain reaction taking place in the liquid phase, the isomerization reaction takes place at a measurable rate while the true sonochemical step is so inefficient that its rate cannot be estimated.

Another example of a secondary reaction taking place in the bulk at a measurable rate was discovered during our study of the effects of sonication on the Diels-Alder reaction [20]. This important reaction in organic chemistry can be described as the addition of a dienophile (A) onto a diene (B) leading to a product (C). In some cases, C can be a mixture of two isomers (C_1 and C_2). Various mechanisms have been proposed for the Diels-Alder reaction which is characterised by a negative activation volume [21, 22]. The study of the effect of pressure waves on the reaction rate and on the C_1/C_2 ratio is therefore interesting. Several papers devoted to the effect of ultrasound on the Diels-Alder reaction have been published. Some of these papers are concerned with heterogeneous reactions while others are concerned with reactions which seem to belong to the field of "homogeneous sonochemistry" (the diene and the dieonophile are fully soluble into the solvent) [23 - 28]. The results are contradictory in some cases. We decided to study this reaction in various solvents with A=methylvinylketone, B=cyclopentadiene and where C_1 and C_2 are the endo and exo adducts:



As shown in table 2, no effect was observed on the reaction rate nor on the C₁/C₂ ratio in all solvents used, except in CHCl₃, CH₂Cl₂ and CH₂Br₂. A series of complementary experiments showed that in these halogenated solvents the only primary sonochemical step occurring is the homolytic cleavage of the halogenated solvent. This leads, through recombination reactions (taking place probably in the bulk), to the formation of HCl or HBr. These acids are able to catalyse the Diels-Alder reaction under study and lead also to a change in the C₁/C₂ ratio. This example is similar to the one described previously. The rate increase and the C₁/C₂ change is due to the catalytical effect of HX which is already the product of a non-sonochemical step. The carbon-halogen bond cleavage of solvent molecules is the only true sonochemical step taking place inside the bubble. Indeed, the same rate increase of the Diels-Alder reaction and the same C₁/C₂ variation can be obtained if a trace of gaseous HX is dissolved in the halogenated solvent before adding the reactants or, if the solvent is presonicated for one hour.

TABLE 2: Influence of US irradiation on the yield and the endo]/[exo] ratio of the Diels-Alder reaction (after 1h at 10°C) in various organic solvents [20].

solvent	Yield (%)		[endo]/[exo]	
	silent	US	silent	US
CH ₃ OH	17 ± 1	17 ± 2	11.5 ± 0.5	11.5 ± 0.5
C ₆ H ₅ CH ₃	3 ± 1	3 ± 1	5.0 ± 0.3	4.9 ± 0.3
CHCl ₃	7 ± 1	15 ± 2	7.2 ± 0.4	12.7 ± 0.5
CH ₂ Cl ₂	4 ± 1	18 ± 2	6.7 ± 0.3	15.5 ± 0.5
CH ₂ Br ₂	7 ± 1	58 ± 3	6.5 ± 0.3	19.5 ± 0.6

As already mentioned, the literature concerning the effect of sonication on the Diels-Alder reaction is contradictory. For the examples where a significant effect is observed, it would be of interest to demonstrate that this effect is not due to a catalytical effect similar to the one described above. It is also important to ensure that the authors verified that the diene and dienophile were perfectly dissolved before sonication [29, 30, 31]. Indeed, a slow dissolution rate of the reactants can be at the origin of artefacts in “homogeneous sonochemistry” since the strong agitation induced by sonication increases the dissolution rate. It is not always easy to exclude the risk of this artefact

because a simple visual inspection is usually insufficient to ensure that the dissolution is perfect. This is a supplementary problem which takes place in “homogeneous sonochemistry”: “to see or not to see” is not a safe scientific criteria of homogeneity.

3.3. The bubble-bulk interface

The domain around each collapsing or non-collapsing bubble is of prime importance in sonochemistry. Indeed between the gas phase and the bulk there is an interface but this interface, like all interfaces, is not a bidimensional mathematical boundary. A gas phase-liquid-phase transition zone, different from bulk and from the bubble gaseous phase, should be explicitly considered. Acousticians take this phase into account when they describe rectified diffusion (shell effect) [7]. This phase must also be considered in all discussions concerning the temperature and the state of matter around a collapsing bubble. According to Hoffmann et al. [32], the interface between the very hot gaseous bubble and the bulk is in a supercritical state. The dielectric constant of supercritical water is strongly reduced with respect to water and this supercritical state could explain the accumulation of hydrophobic molecules in this particular environment.

The true nature of the interface is not yet fully known. What seems certain is the fact that, at least in water, the interface is much less polar than the bulk due to the accumulation of hydrophobic molecules [33]. In a series of very convincing experiments Riesz and his co-workers have shown that the accumulation of various nitrone spin traps depends on their hydrophobicity [34].

Henglein’s work on the scavenger effect of molecules of various hydrophobicities on the production rate of H_2O_2 clearly shows that the most hydrophobic molecules, therefore those with the highest concentration at the bubble periphery, have the highest scavenger activity [3]. 2-methyl-2-propanol is more efficient than methanol even if it is known that the specific rate of reaction of the OH° with 2-methyl-2-propanol is smaller than with methanol.

von Sonntag et al. [33] have calculated the upper limit of the concentration of t-butanol in the boundary layer. With respect to the concentration in the bulk, they have estimated an enhancement factor of 17. This means that for a bulk concentration of 0.2 M, the properties of the interface are similar to those of neat 2-methyl-2-propanol.

In more recent papers, Grieser et al. [35, 36] have reported results that also show the relationship between, on the one hand, the concentration of surface active agents and on the other hand, the sonochemical formation and dissolution of various sols in aqueous solutions and sonoluminescence. In the case of linear alcohols, a correlation was observed between the chain length, the sonoluminescence signal decrease and the Gibbs surface excess of the alcohol at the air/water interface. It is interesting to observe that even ethanol, a solute which is perfectly miscible with water, accumulates at the water-air interface. The surface tension of ethanol in water is already very similar to the surface tension of pure ethanol when the mole fraction of ethanol is 0.2 [5].

Riesz et al. [37], but also Grieser et al. [38], have studied the effect of surfactants on cavitation bubble activity. The effect of the surfactants on sonoluminescence is

different for ionic and non-ionic surfactants. At low concentration, charged surfactants have an inhibiting effect on bubble clustering due to electrostatic repulsion between charged bubbles. However, as soon as the surfactant concentration increases, the electrostatic repulsion between bubbles decreases because the dielectric constant of the inter-bubble medium increases. A similar effect can be observed when NaCl is added to the solution. Nothing similar is observed with a neutral surfactant. According Greiser et al. [38] it is the effect of the surfactant on the bubble clustering and not necessarily on the bubble coalescence, as has been suggested by other authors [39, 40, 41], that is important. The situation is probably even more complex and both explanations could be simultaneously partially valid. Indeed, the role of simple electrolytes on bubble coalescence is very intriguing [38]. Depending on the electrolyte concentration, but also of its composition, bubble coalescence can be inhibited or not. The so-called transition concentration is correlated to the inverse of the Marangoni factor [42] and therefore to the dependence of the surface tension dependence on concentration. The interpretation of the phenomenon remains obscure. Even if their effect on coalescence phenomena is not fully elucidated, electrolytes will have a direct influence on the time evolution of bubbles in a bubble field and therefore on sonochemistry and sonoluminescence.

As already mentioned, Henglein et al. [3] showed that the scavenger property of added substances in water towards OH° radicals increases with the hydrophobicity of the added substance. In our laboratory we have studied the Weissler reaction [43] in presence of various chlorine radical precursors. The Weissler reaction consists essentially of the oxidation, in water, of iodide anions (I^-) into iodine (I_2) by Cl° radicals. The Cl° radicals are generated sonochemically via the cleavage of C-Cl bonds of a precursor (CCl₄). We have shown that the same result can be obtained, in a much more reproducible way, with CBr₄. In this case, the Br° radical is the oxidising agent. What is much more interesting in the context of the present discussion, is that we have also used other precursors like 1,1,1-trichloroethanol and 1,1,1-trichloroacetic acid.

As shown in Figure 1, these chlorine atom precursors act very differently. The more hydrophobic CCl₄ molecules appear to be the best precursors, not because they contain four chlorine atoms per molecule (instead of three for the two others) but because they accumulate at the bubble interface. The comparison between CBr₄ and CCl₃CH₂OH is interesting: it proves that the difference between the precursor capabilities cannot be simply explained by a vapour pressure effect. Indeed the vapour pressure at 25°C of CCl₃CH₂OH is 2.1 mmHg and of CBr₄ is 0.7 mmHg.

The accumulation at the interface leads to a concentration of chlorine atoms precursors in the gas phase which is higher than what can be calculated using the mole fraction in the solution (x_2) and the vapour pressure of the pure solute (P_2°). For example, in a water-ethanol solution, if the mole fraction of ethanol is 0.04, the partial pressure is 8.09 mm Hg at 25°C while $P_2^\circ x_2$ is equal to 2.36 mm Hg. Similar behaviours are observed in many cases [5]. This is one of the reasons why the Henry constant cannot, generally, be identified to the vapour pressure of the pure solute.

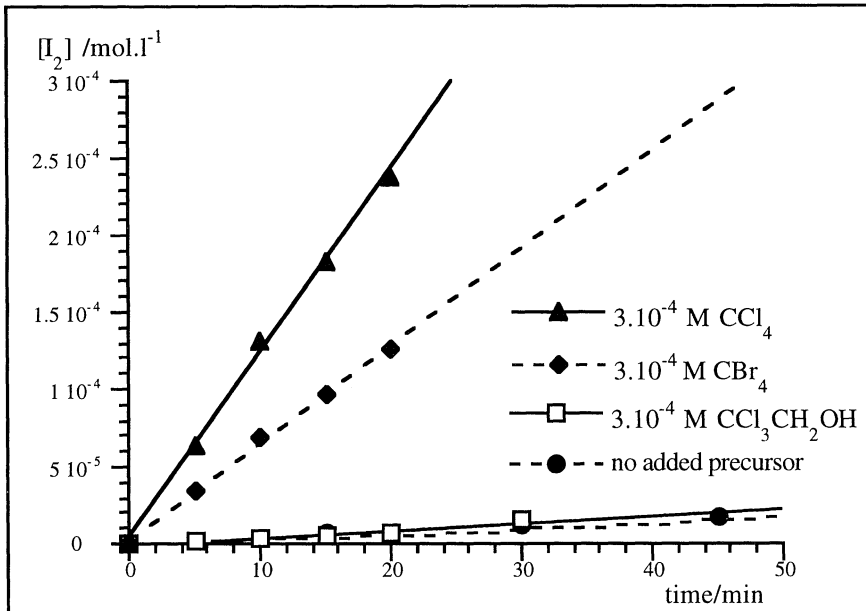


FIGURE 1: Weissler reaction with different halogen radical precursors.

Another reason why an hydrophobic solute could be present inside the bubble with an abnormally high concentration could be due to bubble wall ablation [33] or to bubble surface instabilities leading to a direct injection of small droplets or liquid clusters into the bubble. The surface instabilities of an oscillating bubble were first studied theoretically by Plesset in 1954 [44]. Other approaches were developed later [7]. The instabilities of a spherical surface depend not only on its acceleration, as in the case of the well-known Rayleigh-Taylor instabilities of a planar surface, but also on the surface velocity. The surface of a bubble in transient cavitation is characterised by very high velocities and accelerations. It is possible that micro droplets or liquid clusters coming from the surface can be injected directly into the bubble where they can remain as liquid micro droplets or vaporise. This mode of injection of matter directly inside the hot intra-bubble medium could explain the pyrolysis of non volatile solutes as observed by Henglein et al.[3, 45]. In this case too, the hydrophobicity of the solute plays a role. Of course, another explanation is also plausible: pyrolysis could occur in a warm region, at the interface between the bulk and the bubble. This last explanation which was the one suggested by Henglein himself [3] is very similar to the one suggested by Suslick et al. [14] to explain the kinetics of the sonocleavage of iron pentacarbonyl. Indeed Suslick et al. explained the presence of two different reaction zones by considering that the very hot bubble interior is surrounded by a warm shell. Nevertheless, Suslick [46] and Henglein [45], are now also considering the possibility

previously discussed i.e. a direct injection of liquid matter inside the hot bubble interior leading to intra-bubble micro-domains characterised by temperatures lower than the very hot gaseous phase but sufficient to promote pyrolysis or dissociation. It is probably impossible to make a clear choice between these two interpretations. Nevertheless, if a warm shell, whether in a supercritical state or not, surrounds the imploding bubble it would become dangerous to use the surface tension measured at room temperature to describe its properties.

In any case, the bulk-bubble interface is characterised by a composition and perhaps also other properties which are not those of the bulk: the bubble composition is not related in a simple way, or even in a known way, to the bulk composition. Recently, in a very interesting paper, Lohse et al. suggested a chemical rectification process by which an oscillating single bubble (which never truly implodes) accumulates inert gases [48]. Physical rectification processes must also be efficient, not only because the diffusion properties depend on properties of the diffusing species [49], but also because the medium directly surrounding the bubble acts as a concentrator of hydrophobic and more generally solvophobic molecules. In this context, we would observe that xenon for example, is hydrophobic [50].

4. ON THE DIFFICULTY OF MEASURING A SONOCHEMICAL EFFECT

In the previous paragraphs, we have discussed some, but certainly not all, the reasons why the interpretation of a sonochemical effect (but also of sonoluminescence) is so difficult. In this last paragraph we would like to address a problem which is of pivotal importance in sonochemistry. The problem may seem simple but it is not: How can a sonochemical effect be measured? How can we be sure that ultrasound has an effect on a reaction rate? If we call R the rate of a reaction performed in the presence of ultrasound and R_0 the rate of the same reaction in absence of ultrasound, the sonochemical effect, S.E, is simply given by equation (8)

$$\text{S.E} = \frac{R}{R_0} \quad (8)$$

Generally, in organic sonochemistry, R and R_0 are replaced by a reaction yield after a definite period of time. This procedure is only acceptable if the period of time is short. After an infinite time, the yields in the presence and in the absence of ultrasound must obviously become equal.

If ultrasound has an effect on the reaction mechanism (if chemical switching occurs) the sonochemical effect becomes qualitative and the equation is no longer valid. Such cases are rare but according to Mason and Luche [2] "this type of result shows that sonication is definitively not just another method of providing agitation to the medium but exhibits its own peculiarities, it stands to reason that it should obey some rules of its own".

The measurement of a sonochemical effect (equation 8) or the detection of a chemical switching requires the comparison of a reaction performed without US (the so-called silent reaction) and a reaction performed with US, all other parameters remaining the same. This last condition is extremely difficult to fulfil. This is the problem we would like to address. Intense pressure waves like those we use in sonochemistry agitate the medium very efficiently and agitation obviously has a direct effect on chemical rates. While this is true for homogeneous reactions it is particularly true for heterogeneous reactions. The silent reaction must therefore be performed under optimised agitation conditions in order to avoid artefacts or false sonochemistry as defined by Luche [1, 2]. Optimisation of agitation is not common practice in research laboratories while it is of prime importance in industry. In research laboratories the most widely used stirrers are magnetic stirrers characterised by a rotation rate of the order of 1000 rpm.

The basic equation of stirring relates P, the mixer power produced by a stirrer to Q, the pumping capacity (i.e. the ability of the stirrer to promote a macroscopic flow of liquid inside the reactor) and to H which is associated to the gradient of fluid velocity induced in the reactor by the stirrer. The equation is very simple:

$$P = Q \cdot H \quad (9)$$

where P is expressed J/S, Q is expressed in kg/s and H in J/kg. The gradient of velocity is directly related to shear rates and shear forces [51].

Equation (10) shows that the Q over H ratio is a function of the diameter D of the stirrer:

$$\frac{Q}{H} \approx D^{8/3} \quad (10)$$

A large-size low rotation speed stirrer like a magnetic stirrer can be described as a Q stirrer, while a small size-high rotation speed stirrer (impeller or propeller) can be described as an H stirrer. In homogeneous chemistry, a Q stirrer is satisfactory but an H stirrer is also convenient. In heterogeneous chemistry a H stirrer is better because, as previously said, it creates shear forces but also an intense hydrodynamic cavitation. Knowing the mechanical effects of ultrasound [7], it appears that a comparison between a silent reaction performed with a magnetic stirrer and a sonochemical reaction could lead to artefacts. Sonication leads to high shearing forces, intense cavitation and acoustic micro-streaming i.e. an ensemble of characteristics induced also by an H stirrer but not by a Q stirrer. H stirrers are well known devices which are much less expensive than an immersion horn ultrasonic system.

In our laboratory, we have performed a careful study of various homogeneous and heterogeneous reactions for which sonochemical effects including sonochemical switching have been observed. We compared results obtained by stirring with a magnetic stirrer to results obtained by stirring with an Ultra Turax (i.e. a H stirrer characterised by adjustable rotation rates between 8000 rpm and 24000 rpm). For

homogeneous reactions, no differences were observed between agitation with the Q stirrer or with the H stirrer. Therefore, when sonochemistry is performed and if $R/R_0 \neq 1$, it can be safely concluded that a sonochemical effect is present.

For heterogeneous reactions, in the four cases studied until now, the reaction rate measured with the H stirrer is always higher than with a Q stirrer and sometimes even higher than under sonication (sonochemical “anti-effect”). Probably even more interesting is that the qualitative chemical switching described by Ando et al. [52, 53] was observed under efficient agitation with the Ultra-Turax [54].

In the context of this general review, it is not necessary to describe in details the results that we have obtained. It is however important to insist on the absolute necessity to clearly define under which conditions the silent reaction must be performed before claiming that a sonochemical effect is observed. It can simply be an artefact associated with an incorrect measurement of R_0 . On the basis of what has been discussed in this last paragraph, this kind of artefact is probably much more frequent than suggested [2].

ACKNOWLEDGEMENTS

The authors thank EC (COST Chemistry D6 Program) for its support. Y. Kegelaers would like to thank the FRIA (Fonds pour la Formation à la Recherche dans l'Industrie et dans l'Agriculture) for financial support. N. Segebarth would like to thank the FNRS (Fonds National de la Recherche Scientifique) for financial support.

GENERAL BIBLIOGRAPHY

- Lindley, J. and Mason, T. (1986) Sonochemistry. Part 2. Synthetic Applications, *Chem. Soc. Rev.* **16**, 275-311.
- Lorimer, J.P. and Mason, T. (1987) Sonochemistry. Part 1. The Physical Aspects, *Chem. Soc. Rev.* **16**, 239-274.
- Henglein, A. (1987), Sonochemistry: historical developments and modern aspects, *Ultrasonics* **25**, 6-16.
- Suslick, K.S. (1988) Homogeneous Sonochemistry, in K.S. Suslick (Ed.) *Ultrasound, its Chemical, Physical and Biological Effects*, VCH publishers, New York, pp.123-163.
- Riesz, P. (1991) Free Radical Generation by Ultrasound in Aqueous Solutions of Volatile and Non Volatile Solutes, in T.J. Mason (ed.) *Advances in Sonochemistry* vol.2, Jai Press Ltd, London, pp. 23-64
- Henglein, A. (1993) Contribution to Various Aspects of Cavitation Chemistry, in T.J. Mason (ed.) *Advances in Sonochemistry Vol.3*, pp.17-83.
- Leighton, T.G.(1994) *The Acoustic Bubble*, Academic Press.
- Margulis, M.A. (1995) *Sonochemistry and Cavitation*, Gordon and Breach Publishers.
- Mason, T.J. and Luche, J.L. (1997) Ultrasound as a New Tool for Synthetic Chemists, in R. van Eldik and C.D. Hubbard (eds.), *Chemistry under Extreme and Non-Classical Conditions*, Wiley, New York, pp. 317-380.

REFERENCES

1. Luche, J.L. (1993) Sonochemistry from experiment to theoretical considerations, in T. Mason (ed.), *Advances in Sonochemistry*, vol.3, Jai Press Ltd, London, pp. 85-124.
2. Mason, J.J. and Luche, J.L. (1997) Ultrasound as a new tool for synthetic chemists, in R. van Eldik and C.D. Hubbard (eds), *Chemistry under Extreme and Non Classical Conditions*, Wiley, New York, pp.317-380.
3. Henglein, A. (1993) Contributions to various aspects of cavitation chemistry, in T. Mason (ed.), *Advances in Sonochemistry*, vol. 3, Jai Press Ltd, London, pp. 17-83.
4. Hart, E.J. and Henglein, A. (1986) Sonolysis of Ozone in Aqueous Solution, *J. Phys. Chem.* **90**, 3061-3062.
5. Lewis, G.N., Randall, M., Pitzer, K.S. and Brewer, L. (1961), *Thermodynamics*, Mc Graw Hill.
6. Reisse, J., Broeckaert, L., Caulier, T., Fabre, O., Maerschalk, C., Vandercammen J., Yang, D.H., Lepoint, Th. and Mullie, F. (1992) Quantitative Homogeneous Sonochemistry: Scope and Limitations, in G.J. Price (ed.), *Current Trends in Sonochemistry*, Royal Society of Chemistry, pp. 8-25.
7. Leighton, T.G.(1994) *The Acoustic Bubble*, Academic Press.
8. Crum; L.A. (1984) Rectified Diffusion, *Ultrasonics* **22**, 215-223
9. *Handbook of Chemistry and Physics* (1996), 77th Ed., CRC Press.
10. Moss, W.C., Clarke, D.B. and Young, D.A. (1997) Calculated Pulse Widths and Spectra of a Single Sonoluminescing Bubble, *Science* **276**, 1398-1401.
11. Benson, S.W. (1968) *Thermochemical Kinetics*, J. Wiley, N.Y
12. Noltingk, B.E. and Neppiras, E.A. (1950) Cavitation produced by ultrasonics, *Proc. Phys. Soc.* **B63**, 674-685.
13. Crum, L.A. (1983) The polytropic exponent of gas contained within air bubbles pulsating in a liquid, *J. Acoust. Soc. Am.* **73**, 116-120.
14. Suslick, K.S., Hammerton, D.A. and Cline, R.E. Jr. (1986) The Sonochemical Hot Sport, *J. Am. Chem. Soc.* **108**, 5641-5642.
15. Flint, E.B., Suslick, K.S. (1991) The Temperature of Cavitation, *Science* **253**, 1397-1399.
16. Caulier, T., Maeck, M. and Reisse, J. (1995) Homogeneous Sonochemistry: A Study of the Induced Isomerization of 1,2-Dichloroethene under Ultrasonic Irradiation, *J. Org. Chem.* **60**, 272-273.
17. Reisse, J., Yang, D.H., Maeck, M., Vandercammen, J. and Vander Donckt, E. (1992), Sonochemistry: a systematic study of the maleate-fumarate isomerization in the presence of alkyl bromides, *Ultrasonics* **30**, 397-401.
18. Wood, R.E. and Dickinson, R.G.(1939) The Equilibrium and Kinetics of the Thermal Isomerization of Dichloroethylene Catalysed by Iodine, *J. Am. Chem. Soc.* **61**, 3259-3269.

19. Wood, R.E. and Stevenson, D.P. (1941) The Energy of Isomerization of cis- and trans-Dichloroethylene, *J. Am. Chem. Soc.* **63**, 1650-1653.
20. Caulier, T. and Reisse, J. (1996) On Sonochemical Effects on the Diels-Alder Reaction, *J. Org. Chem.* **61**, 2547-2548.
21. Carruthers, W. (1990), *Cycloaddition in Organic Synthesis*, Pergamon Press.
22. March, J. (1992), *Advanced Organic Chemistry*, Wiley & Sons
23. Gore, J. and Bourgeois-Cury, A. (1992) Réaction de Diels-Alder en phase aqueuse de dérivés du 2,5-diméthylpyrrole, *Bull. Soc. Chim. Fr.* **129**, 490-495.
24. Buchbauer, G., Spreitzer, H. and Knobel, H. (1994) Synthesen in der Isocamphanreihe, 39. Mitt. [1]: Verbesserung der Diels-Alder Reaktion von Cyclopentadien mit Mesityloxid durch Ultraschale und eine neue Synthese von Dehydrocamphen, *Monatsch. Chem.* **125**, 421-925.
25. Javed, T., Mason, T.J., Phul, S.S., Baker, N.R. and Roberstson, A. (1995) Influence of ultrasound on the Diels-Alder cyclization reactions; synthesis of some hydroquinone derivatives and lonapalene, an anti-psoriatic agent, *Ultrasonics Sonochemistry* **2**, 3-4.
26. Nebois, P., Bouaziz, Z., Fillion, H., Moeini, L., Aurell Piquer, M.J., Luche, J.L., Riera, A., Moyano, A. and Pericàs, M.A. (1996), The Diels-Alder cycloaddition, an intriguing problem in organic sonochemistry, *Ultrasonics Sonochemistry* **3**, 7-13.
27. Low, C.M.R. (1992), Ultrasound in Synthesis: Sonochemistry s a Tool for Organic Chemistry, *Current Trends in Sonochemistry*, Royal Society of Chemistry, pp. 59-86.
28. Elguero, J., Goya, P., Paez, J.A., Cativiela, C. and Mayoral, C.(1989) Study of the influence of ultrasound and aqueous solvent on the Diels-Alder reaction: the case of cyclopentadiene and acetaidoacrylates, *Synth. Commun.* **19**, 473-476.
29. Lee, J. and Snyder, J.K. (1989), Ultrasound-Promoted Diels-Alder Reactions: Syntheses of Tanshinone IIA, Nortanshinone, and (\pm)-Tanshindiol B, *J. Am. Chem. Soc.* **111**, 1522-1524.
30. Lee, J. and Snyder, J.K. (1990) Asymmetric Syntheses of Salvia miltiorrhiza Abietanoid 0-Quinones: methyl Tanshinonate, Tanshinone IIB, Tanshindiol B and 3-Hydroxytanshinone, *J. Org. Chem.* **55**, 5008-5013.
31. Lee, J., Li, J., Oya, S. and Snyder, J.K.(1992) Asymmetric Synthesis of Tanshindiol A, *J. Org. Chem.* **57**, 5301-5312.
32. Hua, I., Höchemer, R.H. and Hoffmann, M.R. (1995) Sonolytic Hydrolysis of p-Nitrophenyl Acetate. The Role of Supercritical Water, *J. Phys. Chem.* **99**, 2335-2342.
33. von Sonntag, C., Mark, G., Tauber, A. and Schuchmann, H.P., OH Radical Formation and Dosimetry in the Sonolysis of Aqueous Solutions, in T. Mason (ed.) *Advances in Sonochemistry*, Jai Press Ltd, to be published
34. Riesz, P. (1991) Free Radical Generation by Ultrasound in Aqueous Solutions of Volatile and Non Volatile Solutes, in T.J. Mason (ed.) *Advances in Sonochemistry* vol.2, Jai Press Ltd, London, pp. 23-64

35. Grieser, F., Hobson, H., Sostaric, J. and Mulvaney, P. (1996) Sonochemical reduction processes in aqueous colloidal systems, *Ultrasonics* **34**, 547-550.
36. Sostaric, J., Mulvaney, P. and Grieser, F.J. (1995) Sonochemical Dissolution of MnO₂ Colloids, *J. Chem. Soc., Faraday Trans* **91**, 2843-2846.
37. Alegria, A.E., Lion, Y., Kondo, T. and Riesz, P. (1989) Sonolysis of Aqueous Surfactant Solutions. Probing the Interfacial Region of Cavitation Bubbles by Spin Trapping, *J. Phys. Chem.* **93**, 4908-4913.
38. Ashokkumar, J.M., Hall, R., Mulvaney, P. and Grieser, F. (1997) Sonoluminescence from aqueous alcohol and surfactant solution, *J. Phys. Chem.*, to be published.
39. Henglein, A., Ulrich, R. and Lilie, J. (1989), Luminescence and Chemical Action by Pulsed Ultrasound, *J. Am. Chem. Soc.* **111**, 1974-1979.
40. Henglein, A. and Gutierrez, M. (1993) Sonochemistry and Sonoluminescence: Effects of External Pressure, *J. Phys. Chem.* **97**, 158-162.
41. Sehgal, C. and Wang, S.Y. (1981), Threshold Intensities and Kinetics of Sonoreaction of Thymine in Aqueous Solutions at Low Ultrasonic Intensities, *J. Am. Chem. Soc.* **103**, 6606-6611.
42. Christenson, H.K. and Yaminsky, V.V (1995) Solute Effects on Bubble Coalescence, *J. Phys. Chem.* **99**, 10420-10422.
43. Bartik, K., Vandercammen, J., Eulaerts, O. and Reisse, J., unpublished results.
44. Plesset, M.S. (1954) On the Stability of Fluid Flows with Spherical Symmetry, *J. Appl. Phys.* **25**, 96-98.
45. Henglein, A. and Gutierrez, M. (1988) Sonolytic Decomposition of Poly(vinylpyrrolidone), Ethanol and Tetranitromethane in Aqueous Solution, *J. Phys. Chem.* **92**, 2978-2981.
46. Suslick, K.S., Sonochemistry, in *Kirk-Othmer Encyclopedia of Technical Technology*, 4th Edition, J. Wiley and Sons, in press.
47. Henglein, A., private communication.
48. Lohse, D, Brenner, M.P., Dupont, T.F., Hilgenfeldt, S. and Johnston, B. (1997), Sonoluminescing Air Bubbles Rectify Argon, *Phys. Rev. Letters* **78**, 1359-1362.
49. Lohse, D. and Hilgenfeldt, S. (1997), Inert gas accumulation in sonoluminescing bubbles, *J. Chem. Phys.* **107**, 6986-6997.
50. Olofsson, G., Oshodj, A.A., Qvarnström, E. and Wadsö (1984), Calorimetric measurements on slightly solute gases in water. Enthalpies of solution of helium, neon, argon, krypton, xenon, methane, ethane, propane, n-butane, and oxygen at 2.88.15, 298.15 and 308.15 K, *J. Chem. Thermodynamics* **16**, 1041-1052.
51. Oldshue, J.Y. and D.B. Todd (1981) Mixing and Blending, in Kirk-Othmer (ed.), *Encyclopedia of Chemical Technology*, J. Wiley and Sons, Inc., pp. 604-637.
52. Ando, T., Sumi, S., Kawate, T. and Hanfusa, T. (1984) Sonochemical Switching of Reaction Pathways in Solid-liquid two-phase Reactions, *J. Chem. Soc. Chem. Commun.*, 439-440.

53. Ando, T. and Kimura, T. (1991), Ultrasonic Organic Synthesis Involving Non-metal Solids, in T.J.Mason (ed.), *Advances in Sonochemistry*, Jai Press Ltd, London, pp. 211-251.
54. Kegelaers, Y., Vandercammen, J. and Reisse, J. (1997) Heterogeneous Sonochemistry: a Comparison between Sonication and Mechanical Agitation, submitted for publication.

DETECTION OF PRIMARY FREE RADICAL SPECIES IN AQUEOUS SONOCHEMISTRY BY EPR SPECTROSCOPY

VLADIMÍR MIŠÍK and PETER RIESZ

*Radiation Biology Branch, National Cancer Institute, NIH
Bethesda, Maryland 20892-1002, U.S.A.*

Abstract. In this paper we discuss the identification of the primary free radical species produced by sonolysis of noble gas-saturated aqueous solutions (i.e. $\cdot\text{H}$, $\cdot\text{OH}$, $\text{O}_2\cdot^-$) and in N_2 -containing aqueous solutions (i.e. $\cdot\text{H}$, $\cdot\text{OH}$, $\text{O}_2\cdot^-$, and $\cdot\text{NO}$) predominantly by means of electron paramagnetic resonance (EPR) spectroscopy with spin trapping. The EPR experiments which show that no detectable level of hydrated electrons is formed in the sonolysis of water at neutral pH are summarized.

1. Introduction

Sonochemistry and cavitation. Several books and review articles are available in the area of sonochemistry [1-3]. Chemical effects of ultrasound in liquids are due to acoustic cavitation, a term which refers to the growth by rectified diffusion, and inertial collapse of cavitation microbubbles, which are gas and vapor filled cavities driven by the acoustic pressure changes. High temperatures (several thousands Kelvin) and pressures (hundreds of atmospheres) are produced during the collapse of the cavitation bubbles [1]. Thus, these cavitation bubbles are the sonochemical micro-reactors in which the solvent vapor undergoes pyrolysis. The effective temperatures generated during the collapse, and thus the sonochemical radical yields, can be modified by many physico-chemical parameters of the liquid and dissolved gas. One of the most crucial parameters is the ratio of the specific heats at constant pressure and constant volume, $\gamma = C_p/C_v$, of the gas and vapor inside the cavity; decreasing γ from 1.67 (monoatomic gases, such as argon), to 1.4 (diatomic gases, such as N_2 , O_2), to 1.3 (triatomic molecules, such as N_2O), and to less than 1.3 (molecules with more than 3 atoms), dramatically lowers the final temperature inside the collapsing bubble [3].

Sonochemical reactions can occur in three different regions. The

first region is the interior of collapsing gas bubbles in which extreme temperatures and pressures exist. Under these conditions the solvent vapor inside the bubble undergoes pyrolysis reactions. The second region is the interface between the collapsing bubble and the bulk solvent, where high temperature and pressure gradients exist. The relative efficiencies of non-volatile solutes to decompose thermally in this region depend on their hydrophobicity, which determines their ability to accumulate at the gas-liquid interface, and also on the activation energies of bond scission [2,3]. Alternatively, pyrolysis of non-volatile solutes may be due to the splashing of liquid into the hot gaseous interior of the bubbles, due to the asymmetry of the bubble collapse which is a result of microjet or surface wave action. In the third region, the bulk of the solution at ambient temperature, free radicals formed in the hot regions, which have not recombined, disproportionated, or have not been scavenged in the interfacial region, can react to yield products similar to those found in aqueous radiation chemistry. Thus many aspects of sonochemistry can be understood in terms of a combination of combustion chemistry and radiation chemistry.

EPR spin trapping. The method of choice for a conclusive analysis of free radical formation is the spin trapping technique with EPR (electron paramagnetic resonance) spectroscopic detection. In this technique the short-lived reactive radical is stabilized by addition to the double bond of a diamagnetic molecule (the spin trap) to form a relatively long-lived covalent paramagnetic adduct (the spin adduct) which is EPR observable. The EPR spectra of the spin adducts usually allow the identification and quantification of the spin trapped radicals. The structures of nitrone spin traps suitable for use in sonochemical studies of water-derived radical intermediates and the mechanism of formation of paramagnetic adducts are shown in Figure 1.

2. Experimental

In most experiments samples (1.7 ml) containing the spin trap were fixed in the center of the Bransonic 1200 50 kHz sonication bath (temperature of the coupling water 20°C) in Pyrex test-tube and bubbled with argon or other gas before and during exposure to ultrasound. For comparison, sonolysis of 1.7 ml of aqueous argon-bubbled ferrous sulphate Fricke dosimeter solution [4] for 5 minutes in this experimental set-up gave an absorbance of 0.536 ± 0.050 at 302 nm in a 1 cm cell.

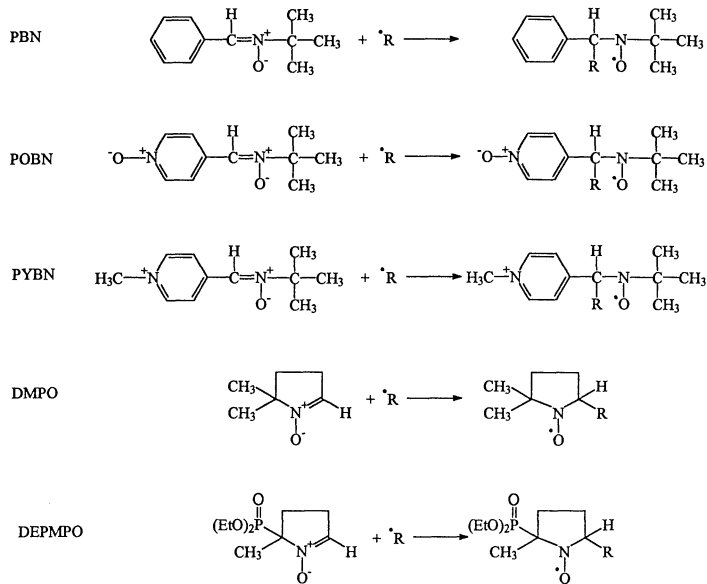


Figure 1. Nitronate spin traps suitable for identification of primary water-derived free radicals in aqueous sonochemical studies. The mechanism of the addition of a radical ($\cdot R$) to the double bond of the spin traps to form stable nitroxide radicals is shown.

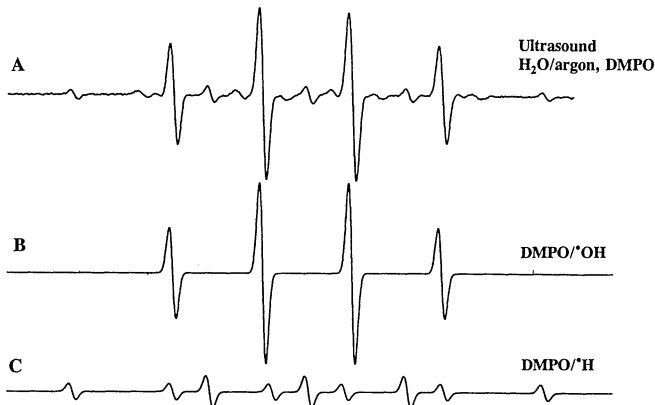


Figure 2. Overlapping EPR spectra of $\cdot OH$ and $\cdot H$ adducts of DMPO obtained after 3 minute exposure of argon-saturated water to 50 kHz ultrasound in the presence of 25 mM DMPO (A). Computer-simulated spectra of the two components of spectrum A are shown in B and C.

3. Results and Discussion.

3.1. SONOLYSIS OF WATER UNDER NOBLE GAS ATMOSPHERE

3.1.1. Hydrogen atoms and hydroxyl radicals

Formation of $\cdot\text{H}$ and $\cdot\text{OH}$,

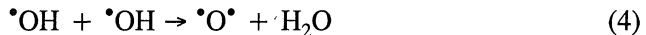


which are the primary free radical intermediates produced by pyrolysis of water molecules in the hot cavitation region, was demonstrated originally using the spin trap DMPO (a representative EPR spectrum of $\cdot\text{H}$ and $\cdot\text{OH}$ adducts of DMPO is shown in Figure 2), and the validity of this assignment was confirmed employing $\cdot\text{OH}$ radical scavengers and using isotopically substituted water (D_2O and H_2O^{17}) [5-7]. Other nitroxyl spin traps, such as PBN, POBN, and PYBN (see Figure 1) were also used [6, 8], the latter being particularly suitable for measurement of $\cdot\text{H}$ atoms, while DMPO is the spin trap of choice for $\cdot\text{OH}$ radicals. DMPO and POBN spin traps were employed to demonstrate that microsecond ultrasonic pulses can produce $\cdot\text{OH}$ radicals and $\cdot\text{H}$ atoms through acoustic cavitation in water [9], thus providing an experimental confirmation of Flynn's theoretical predictions [10].

Hydroxyl radicals and hydrogen atoms undergo mutual reactions either directly in the gas phase or in the surrounding liquid to produce the typical molecular products of aqueous sonolysis H_2 and H_2O_2 [2]:



Alternatively, disproportionation of hydroxyl radicals at high temperature yields oxygen atoms [11]:



Formation of oxygen atoms has never been directly shown in aqueous sonolysis but their existence is confirmed by O_2 formation during sonolysis of oxygen-free aqueous solutions [2].

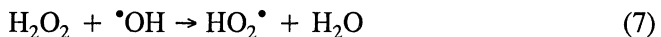
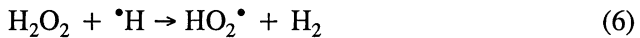
3.1.2. Superoxide radical

Formation of superoxide radical ($\text{O}_2^\bullet/\text{HO}_2^\bullet$) was established originally during sonolysis of oxygen-saturated aqueous solutions using the SOD-inhibitable cytochrome c reduction [12]. Demonstration of superoxide formation using the

same method has recently been extended to oxygen-free argon-saturated solutions [13] and the following pathways were proposed for its formation:



(where O_2 in the absence of dissolved oxygen is formed via recombination of oxygen atoms formed by reaction 4)



So far, superoxide eludes EPR spin trapping identification due to its low rate of addition to DMPO ($\sim 30 \text{ M}^{-1} \text{ s}^{-1}$) and the high instability of the resulting adducts. A new phosphorus-substituted spin trap, DEPMPO (see Figure 1), may offer some improvement in this respect due to the higher stability of DEPMPO-superoxide adducts.

3.1.3. Hydrated electrons

The formation of hydrated electrons in neutral aqueous ultrasound-exposed solutions has been postulated previously [14] and arguments were presented in favor and against their existence (see e.g. [15] for a list of related references). The issue of the existence of these species as principal sonochemical intermediates was addressed recently using a sensitive method for detecting the presence of hydrated electrons in argon-saturated water exposed to ultrasound [15].

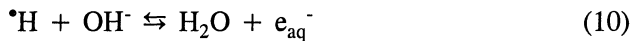
Nitronate spin traps are particularly suitable for detection of hydrated electrons. The spin trap POBN has been shown to react with e_{aq}^- with a rate constant of $3.1 \times 10^{10} \text{ M}^{-1} \text{ s}^{-1}$ [16]:



Hence, the EPR detectable adduct of e_{aq}^- at neutral pH is $\text{POBN}/\cdot\text{H}$, identical to the $\text{POBN}/\cdot\text{H}$ adduct formed by a direct reaction of POBN with $\cdot\text{H}$:



The formation of hydrated electrons from $\cdot\text{H}$ atoms in alkaline solutions is well known [17]:



and the pK_a value of this equilibrium is 9.8. Using the formation of metallic thallium from Tl^+ , Guttiérrez et al. [18] have demonstrated the formation of hydrated electrons in the sonolysis of aqueous solutions at $pH \geq 12.7$. To avoid a significant contribution of this pathway in the formation of hydrated electrons, the current spin trapping experiments were performed at neutral pH.

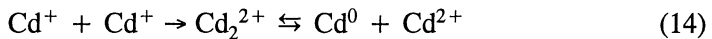
Cadmium (Cd^{2+}) is one of the most efficient scavengers of hydrated electrons [19]:



and has also been used to study the yield of dry electrons, which are the precursors of e_{aq}^- , by pulse radiolysis [20]. If Cd^+ were formed in our system it would be recycled back to Cd^{2+} [21]:



or react with another Cd^+ to yield Cd^{2+} and metallic cadmium [21]:

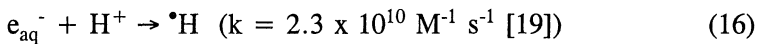


At suitably selected concentrations of Cd^{2+} and POBN, the reaction:



can be completely suppressed, while the yield of the reaction of $\cdot H$ with POBN will not be changed, because the relative rates of Cd^{2+} and POBN with e_{aq}^- are approximately equal, while POBN reacts $\geq 10^4$ times faster with $\cdot H$ than Cd^{2+} ($k_{POBN + H} = 3 \times 10^9 \text{ M}^{-1} \text{ s}^{-1}$ [22], $k_{POBN + e_{aq}^-} = 3.1 \times 10^{10} \text{ M}^{-1} \text{ s}^{-1}$ [16], $k_{Cd^{2+} + e_{aq}^-} = 5.4 \times 10^{10} \text{ M}^{-1} \text{ s}^{-1}$ [19], $k_{Cd^{2+} + H} < 3 \times 10^5 \text{ M}^{-1} \text{ s}^{-1}$ [19]).

The reaction:



could not contribute significantly at neutral pH due to the high rates and high concentrations of the competing processes for e_{aq}^- removal (reactions of e_{aq}^- with POBN and with Cd^{2+}).

Figure 3 shows the EPR spectra obtained by sonolysis of argon-saturated solutions of H_2O and D_2O , containing 2 mM POBN. The comparison of the experimental spectra (Figure 3A and B) with the computer simulated

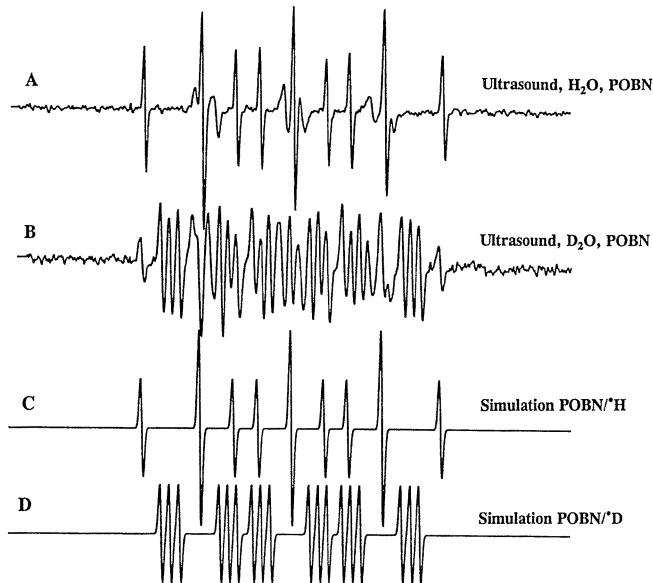


Figure 3. EPR spectra of spin adducts produced by 50 kHz sonolysis of neutral argon-saturated H₂O (A), D₂O (B), in the presence of 2 mM POBN. Computer simulations of POBN/*H (C) and POBN/*D (D).

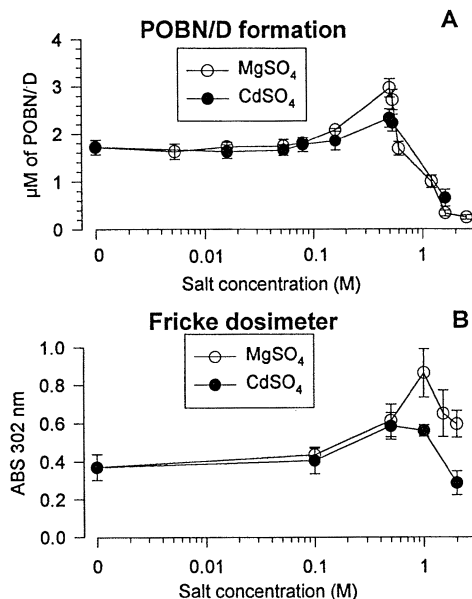


Figure 4. Effect of CdSO₄ (closed symbols) and MgSO₄ (open symbols) concentration on the yield of POBN/*D adducts (A) and on the ferric yield in argon-saturated Fricke dosimeter solution (B) in argon-saturated aqueous solutions exposed to 50 kHz ultrasound.

spectra of POBN/ $^{\bullet}\text{H}$ and POBN/ $^{\bullet}\text{D}$ adducts (Figure 3C and D) reveals that the dominant adducts in H_2O and D_2O were POBN/ $^{\bullet}\text{H}$ and POBN/ $^{\bullet}\text{D}$ respectively. However, small yields of POBN/ $^{\bullet}\text{H}$ adducts were detected in D_2O solutions (Figure 3B). This artifactual production of $^{\bullet}\text{H}$ atoms by pyrolysis of the spin trap has been described previously [8, 23] and was the reason for performing all experiments in D_2O , where the measured POBN/ $^{\bullet}\text{D}$ yields originate entirely from the sonolysis of D_2O and can easily be separated from the artifactual POBN/ $^{\bullet}\text{H}$ signal.

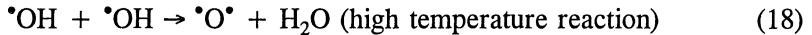
The effect of CdSO_4 and MgSO_4 (MgSO_4 was used as a control, since it does not react with e_{aq}^- or $^{\bullet}\text{H}$ ($^{\bullet}\text{D}$) at an appreciable rate, but mimics the potential effect of ionic strength on the reaction rates) on the sonochemical yields of $^{\bullet}\text{D}$ adducts of POBN is shown in Figure 4. If hydrated electrons were formed by sonolysis, a decrease of POBN/ $^{\bullet}\text{D}$ yield with increasing concentration of Cd^{2+} would be expected. However, the yields of POBN/ $^{\bullet}\text{D}$ were unaltered up to approximately 0.1 M Cd^{2+} (Figure 4A) and a similar trend was also observed for Mg^{2+} which served as an ionic strength control (Figure 4B). At 0.1 M Cd^{2+} 98.8% of e_{aq}^- would be scavenged by Cd^{2+} in the presence of 2 mM POBN. Hence, allowing for a 10% error margin in our measurements, the e_{aq}^- yield cannot exceed $\sim 10\%$ of the total $^{\bullet}\text{H}$ yield, i.e. less than 0.036 μM $e_{\text{aq}}^-/\text{min}$ would be produced in our system.

Thus, our data show that no detectable yield of hydrated electrons (or less than the detection limit of approximately 0.04 $\mu\text{M}/\text{min}$) is formed in neutral argon-saturated aqueous solutions exposed to 50 kHz ultrasound, thus arguing against the importance of this species as the reactive intermediate in the sonochemistry of neutral aqueous solutions. It would be of interest to ascertain the validity of the present conclusions for the repetitive collapse of a single oscillating sonoluminescent bubble.

3.2. SONOLYSIS OF WATER IN THE PRESENCE OF DISSOLVED N_2

3.2.1. Nitric oxide

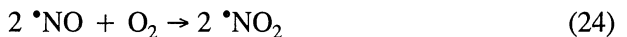
As discussed above, the primary species produced by pyrolysis of water molecules in noble-saturated aqueous solutions exposed to ultrasound are $^{\bullet}\text{H}$ atoms and $^{\bullet}\text{OH}$ radicals, and H_2 , O_2 , H_2O_2 and O_2^- are formed in subsequent reactions. In addition to these species, production of NO_2^- and NO_3^- was demonstrated in N_2 -containing aqueous solutions exposed to ultrasound [24-26]. Hart *et al.* [27] postulated that the following reactions are involved in the formation of nitrite and nitrate by ultrasound in aqueous solutions containing argon and nitrogen:



They suggested that NO_2^- and NO_3^- are formed by subsequent oxidation of $\cdot\text{NO}$ by $\cdot\text{O}^\bullet$ and $\cdot\text{OH}$ [27]. Although a likely intermediate in the "hot" gas phase of cavitation bubbles, the formation of $\cdot\text{NO}$ has never before been directly demonstrated and the feasibility of its diffusion outside the cavitation bubble and hence its ability to exert biological effects in ultrasound-exposed systems has never been considered.

Recently we have demonstrated formation of nitric oxide in aqueous nitrogen-containing solutions exposed to 50 kHz ultrasound [28] using EPR detection of $\cdot\text{NO}$ by trapping with sodium N-methyl-D-glucamine dithiocarbamate iron(II) complex (Figure 5), and by measuring the conversion of the nitronyl nitroxide, 2-(4-carboxyphenyl)-4,4,5,5-tetramethylimidazoline-3-oxide-1-oxy, to the imino nitroxide, 2-(4-carboxyphenyl)-4,4,5,5-tetramethylimidazoline-1-oxy (Figure 5).

The formation of nitric oxide by ultrasound was independent of the pH of the sonicated water throughout the measured range (pH 3-8.5). The rate of $\cdot\text{NO}$ production by ultrasound in air-saturated water was $\sim 0.5 \mu\text{M}/\text{minute}$. The presence of dissolved oxygen was not essential for production of $\cdot\text{NO}$: the highest yields of $\cdot\text{NO}$ ($\sim 1.2 \mu\text{M} \cdot\text{NO}/\text{minute}$) were found under an atmosphere of 40% N_2 and 60% argon (Figure 6). The formation of $\cdot\text{NO}$ by ultrasound in aqueous solutions can be understood in terms of combustion chemistry-type reactions occurring inside the "hot" collapsing cavitation bubbles. The formation of nitrite and nitrate which are known sonochemical products in N_2 -containing solutions can be rationalized in terms of chemistry of nitric oxide:



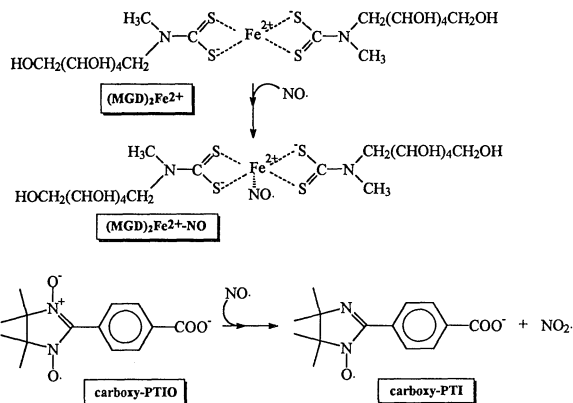


Figure 5. Structures of $(\text{MGD})_2\text{Fe}^{2+}$ complex and carboxy-PTIO and their reactions with $\cdot\text{NO}$ to give EPR detectable products.

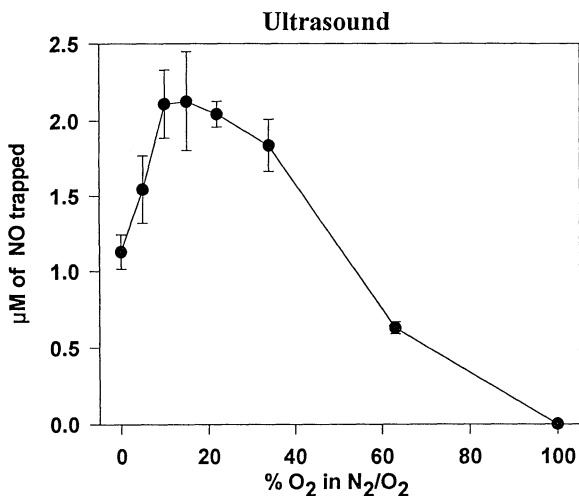
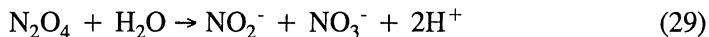
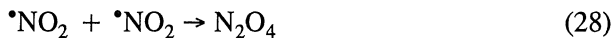
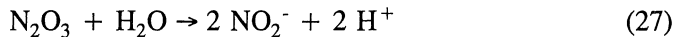


Figure 6. Measurement of $\cdot\text{NO}$ ($(\text{MGD})_2\text{Fe}^{2+}\text{-NO}$ formation) after 5 minutes of ultrasound in aqueous solutions saturated with different mixtures of O_2 and N_2 . All samples contained 1 mM $(\text{MGD})_2\text{Fe}^{2+}$.



Conclusions. In this paper the formation of free radical intermediates by sonolysis of aqueous solutions and their detection, primarily by EPR spectroscopy, are discussed. Interplay between these primary radical intermediates, which include $\cdot\text{H}$, $\cdot\text{OH}$, O_2^- , and $\cdot\text{NO}$ (this species can sonochemically be produced only in N_2 -containing solutions), and their subsequent reactions in the sonicated solutions determine the aqueous sonochemistry and possibly play a role in the sonoluminescent emissions in a multibubble field. Formation of nitric oxide and other oxides of nitrogen are also likely pathways of "argon rectification" which was proposed to be the process of N_2 and O_2 "burning-out" from the interior of a single oscillating bubble with only argon at its partial pressure remaining inside at the onset of sonoluminescence [29, 30].

4. References

1. Suslick, K.K. (1988) *Ultrasound, its Chemical, Physical and Biological Effects*, VCH Publishers, New York.
2. Henglein, A. (1987) Sonochemistry: historical developments and modern aspects, *Ultrasonics* **25**, 1-64.
3. Riesz, P. and Kondo, T. (1993) Free radical formation induced by ultrasound and its biological implications, *Free Radical Biol. Med.* **13**, 247-270.
4. Spinks, J.W.T. and Woods, R.J. (1976) *An Introduction to Radiation Chemistry*, 3rd edition, John Wiley and Sons, New York.
5. Makino, K., Mossoba, M.M. and Riesz, P. (1982) Chemical effects of ultrasound on aqueous solutions. Evidence for $\cdot\text{OH}$ and $\cdot\text{H}$ by spin trapping, *J. Am. Chem. Soc.* **104**, 3537-3539.
6. Makino, K., Mossoba, M.M. and Riesz, P. (1983) Chemical effects of ultrasound on aqueous solutions. Formation of hydroxyl radicals and hydrogen atoms, *J. Phys. Chem.* **87**, 1369-1377.
7. Kondo, T., Krishna, M.C. and Riesz, P. (1988) Effect of non-volatile scavengers of hydroxyl radicals on thymine radical formation induced by gamma rays and ultrasound, *Int. J. Radiat. Biol.* **53**, 891-899.
8. Mišík, V., Miyoshi, N. and Riesz, P. (1995) An EPR spin trapping study of the sonolysis of $\text{H}_2\text{O}/\text{D}_2\text{O}$ mixtures - probing the temperatures of cavitation regions, *J. Phys. Chem.* **99**, 3605-3611.
9. Riesz, P., Berdahl, D. and Christman, C.L. (1985) Free radical generation by ultrasound in aqueous and nonaqueous solutions, *Environmental Health Perspectives* **64**, 233-252.
10. Flynn, H.G. (1982) Generation of transient cavities in liquids by microsecond pulses of ultrasound, *J. Acoust. Soc. Amer.* **72**, 1926-1932.
11. Warnatz, J. (1984) Rate coefficients in the C/H/O system, in W.C. Gardiner, Jr.

- (ed.), *Combustion Chemistry*, Springer-Verlag, New York, pp.197-360.
12. Lippitt, B., McCord, J.M. and Fridovich, I. (1972) The sonochemical reduction of cytochrome c and its inhibition by superoxide dismutase, *J. Biol. Chem.* **247**, 4688-4690.
 13. Kondo, T., Mišík, V. and Riesz, P. (1996) Sonochemistry of cytochrome c. Evidence for superoxide formation by ultrasound in argon-saturated aqueous solution, *Ultrasonics Sonochemistry* **3**, S193-S199.
 14. Margulis, M.A. (1995) *Sonochemistry and Cavitation*, Gordon and Breach Publishers, Luxembourg.
 15. Mišík, V. and Riesz, P. (1997) Effect of Cd²⁺ on the [·]H-atom yield in the sonolysis of water. Evidence against the formation of hydrated electrons, *J. Phys. Chem.* **101**, 1441-1444.
 16. Faraggi, M., Carmichael, A. and Riesz, P. (1984) OH radical formation by photolysis of aqueous porphyrin solutions. A spin trapping and ESR study. *Int. J. Radiat. Biol.* **46**, 703-713.
 17. Hart, E.J. and Anbar, M. (1970) *The Hydrated Electron*, John Wiley and Sons, New York.
 18. Gutiérrez, M., Henglein, A. and Dohrmann, J.K. (1987) H atom reactions in the sonolysis of aqueous solutions, *J. Phys. Chem.* **91**, 6687-6690.
 19. Buxton, G.V., Greenstock, C.L., Helman, W.P. and Ross, A.B. (1988) Critical review of the rate constants for reactions of hydrated electrons, hydrogen atoms and hydroxyl radicals ([·]OH/[·]O⁻) in aqueous solutions, *J. Phys. Chem. Ref. Data* **17**, 513-886.
 20. Jonah, C.D., Matheson, M.S., Miller, J.R. and Hart, E.J. (1976) Yield and decay of the hydrated electron from 100 ps to 3 ns, *J. Phys. Chem.* **80**, 1267-1270.
 21. Kelm, M., Lilie, J. and Henglein, A. (1975) Pulse radiolytic investigations of the reduction of cadmium (II) ions, *J. Chem. Soc. Faraday Transact. I* **71**, 1132-1142.
 22. Finkelstein, E., Rosen, G.M. and Rauckman, E.J. (1980) Spin trapping of superoxide and hydroxyl radical: practical aspects. *Arch. Biochem. Biophys.* **200**, 1-16.
 23. Kondo, T. and Riesz, P. (1989) Hydrogen atom formation by ultrasound in D₂O solutions of nitrone spin traps, *Free Radical Res. Comms.* **7**, 11-18.
 24. Beuthe, H. (1933) Über den Einfluss der Ultraschallwellen auf chemische Prozesse, *Z. physikal. Chem. A* **163**, 161-171.
 25. Virtanen, A.I. and Ellfolk, N. (1950) Nitrogen fixation in an ultrasonic field, *J. Am. Chem. Soc.* **72**, 1046-1047.
 26. Henglein, A. and Gutiérrez, M. (1986) Chemical reactions by pulsed ultrasound: memory effects in the formation of NO₃⁻ and NO₂⁻ in aerated water, *Int. J. Radiat. Biol.* **50**, 527-533.
 27. Hart, E.J., Fischer, Ch.-H. and Henglein, A. (1986) Isotopic exchange in the sonolysis of aqueous solutions containing ^{14,14}N₂ and ^{15,15}N₂, *J. Phys. Chem.* **90**, 5989-5991.
 28. Mišík, V. and Riesz, P. (1996) Nitric oxide formation by ultrasound in aqueous solutions: An EPR spin trapping study, *J. Phys. Chem.* **100**, 17986-17994.
 29. Lohse, D., Brenner, M.P., Dupont, T.F., Hilgenfeldt, S. and Johnson, B. (1997) Sonoluminescing bubbles rectify argon, *Phys. Rev. Lett.* **78**, 1359-1362.
 30. Moss, W.C., Clarke, D.B. and Young, D.A. (1997) Calculated pulse width and spectra of a single sonoluminescent bubble, *Science* **276**, 1398-1401.

ACOUSTIC DOSIMETRY FOR SONOCHEMISTRY

SAMEER I. MADANSHETTY

Mechanical Engineering Department
Kansas State University
Manhattan KS 66506-5106

1. Introduction

If it is reported that a certain aqueous chemical reaction occurs at, say, 70°C, it is relatively straightforward to replicate reproducibly that aqueous chemical reaction in any other laboratory. If, however, it is reported that the same reaction occurred twice as fast at 70°C when it was also sonicated for 20 minutes in an ultrasonic cleaning bath, it would be quite difficult to duplicate this reaction occurrence. While, similar temperature environments can be easily achieved, similar acoustic environments can be ensured only with elaborate deliberations. The intensive property, temperature, is bulk independent and is easily monitored and maintained; uniform temperatures are easy to thermostat. The acoustic field on the other hand can be complex, context determined and needs careful specification before replication can be attempted. In discussing ultrasonic dosimetry here, we will attempt to provide pointers for specifying and implementing sound fields meaningfully.

A primary intent of dosimetry is to provide measures to quantify causes that the magnitude of effects might be predictable and containable. Ideally, one would like to know the safe levels of causation before deleterious effects ensue. Accordingly working in radioactive environments the radiation dose is measured, and in diagnostic ultrasound the total acoustic exposure during a treatment might be relevant. Operationally, in certain contexts dosimetry might translate into proper calibration of conditions so that desired performance is achievable. Thus, in acoustic applications it would be useful to calibrate the acoustic fields relevantly—typically, beam profiles and relative response for non-destructive applications, and additionally, absolute intensity measurements for diagnostic applications. In the case of sonochemistry the issue of dosimetry is complicated by the fact that acoustics mediates sonochemistry via cavitation and, at fine details, ensuring uniformly consistent cavitation levels is a daunting task yet unaccomplished. Useful cavitation for sonochemistry remains a chance dominated process relying on the (nucleational) characteristics of the reaction host.

A practical approach to dosimetry, then, requires that we calibrate and maintain a required sound field. Ensuring a required sound field reduces the uncertainty in the chain of events only to the nucleational properties of the reaction host. Further to ensure an end results uniformity, operationally one would observe certain well characterized chemical (sonochemical) reactions that might be the measures of sonochemical performance, and indirectly, therefore, the end measures of relevant physical conditions ensuring intended sonochemistry.

In the following we will review: cavitation in the context of sonochemistry, comparison of equipment used to implement aqueous sonochemistry, effects of physical variables that influence cavitation and hence sonochemistry, and calibration of acoustic fields. We will only briefly allude to dosimetry reactions because these will be discussed in detail in another session.

2. Cavitation in the context of sonochemistry

Most of sonochemistry is influenced by cavitation, and acoustic cavitation is a complex phenomenon very sensitively affected by its context environment. While acoustic cavitation is fairly well understood, sonoluminescing cavitation is still an open research question.

Ordinarily, sound is a weak mechanical perturbation propagated in an otherwise quiescent medium. Low energy density in a sound wave is not high enough to produce chemical reactions. Cavitation concentrates acoustic energy and creates within the liquid bulk transient points of enormous energy density which have the potential to affect chemical reactions. Relatively large stable bubbles merely oscillate in response to the sound field and are not responsible for the chemical effects of ultrasound. Small bubbles that grow to more than two times their equilibrium size within a few acoustic cycles implode violently creating momentary points of enormous energy density within the liquid. Such transient cavitation is responsible for observed sonochemical effects. The details of nucleation and bubble growth have not concerned sonochemistry routinely, and the energetics of bubble implosion are being explored in detail only recently.

A pulsating bubble is a site of intense mechanical and thermodynamic activity. There are three physical regions which can influence chemistry. First, within the imploding bubble intense pressures and temperatures are possible. Also the vaporous-gaseous cavity contents can have significantly different concentrations compared to those of the surrounding host. Second, the liquid host within the vicinity of the bubble, a liquid shell around the bubble, experiences the shock waves from imploding bubble. Extremely high shear gradients are possible here due to acoustic streaming close to the bubble wall. Third, the interface region at the bubble wall is often the site of ionic electrification and surface activity. The activities in the various regions are, of course, more or less pronounced depending on the intensity of bubble implosion. A region of bubble cloud then becomes a chemical reactor of uncommonly rich processes, providing uncommonly intense gradients of many physical quantities. It features enhanced diffusive transport, high shear rates, electrically active surfaces, in addition to increased pressures and temperatures with enormously high heating and cooling rates. In current implementations such cloud bursts are often sporadic, random and affect only small regions. One of the design goals for sonochemical engineers is to articulate and control such small scale "cloud reactors", multiply them to pervade globally, filling the entire reaction vessel, and regulate the intensity, so that a consistently performing standard test cell is available for sonochemistry studies.

3. Comparison of equipment used to implement aqueous sonochemistry

In current practice sonochemistry research primarily uses any of the four devices or their modifications: 1. ultrasonic sound baths or cleaners, 2. cup-horn reactor, 3. immersion

probe flow cell and 4. minisonic homogenizer or whistle reactor. Ultrasonic cleaners or baths are a general purpose laboratory equipment used variously for cleaning, agitating and degassing. Typically, it is a substantial stainless tank filled with water, with base mounted acoustic drivers operated nominally at a fixed frequency between 20 kHz and 40 kHz. This device operates in continuous mode setting up standing wave field in the tank and in any reaction container immersed in the tank. Here the acoustic field is weak, maximum pressure effects being felt at the pressure antinodes whose location is determined by and is sensitive to the insonified liquid geometry. The modal pattern varies significantly with the liquid levels and only slightly with frequency drift and bath temperature. The cleaners offer a low level cavitation activity and are useful mostly for heterogeneous sonochemistry. Typical acoustic intensities are between 0.1 to 1 Watt/cm². Because of the nonspecific insonification offered in an ultrasonic tank, a specialized modification of it, the cup horn reactor is more useful. Even though it suffers from the same sensitivity to liquid level and the wetted shape of the vessel as an ultrasonic cleaner, it uniformizes and intensifies insonification by limiting the liquid volume. It is also more amenable to closer temperature regulation.

Instead of driving the container and setting up ultrasonic field in the liquid bulk, an adaptation of the cell disrupter involves an ultrasonic horn directly immersed in the reaction liquid. The advantage is that high intensity ultrasound, typically upwards of several hundred watts per square centimeter can be brought to bear on the liquid in the immediate vicinity of the probe tip. This arrangement is often favored for homogeneous sonochemistry investigations which need high intensities. In the flow cell modification liquid is continuously flown under the probe.

In a whistle reactor cavitation occurs as the fluid flows over a vibrating reed/blade, thus limiting the insonification time available per unit volume. Most effects observed arise not so much from cavitation, but from increased interfacial area. This device is useful in bringing about emulsification of liquids, and as such not much used in sonochemistry research. Before we discuss dosimetry for reproducibility, we will briefly review the physical parameters that affect cavitation.

4. Effect of physical variables on cavitation and hence sonochemical performance

Based on the information in [6, 10] here we briefly discuss how cavitation and hence sonochemical reactivity is affected by acoustic conditions and environment.

1. Frequency: It is popularly argued that sonochemical effects are independent of frequency over a wide range, from 10 Hz to over 1 MHz. The argument is based on the premise that sound field doesn't affect chemistry at molecular species level. Sound merely brings about cavitation, and even though cavitation bubbles, depending on their size, might be variously affected by the sound field, sonochemical effects remain unaffected by frequency. At higher frequencies it is difficult to bring about cavitation and one is often advised to stick to lower frequencies associated with the cleaning baths or ultrasonic horns, typically 20 kHz.

It is, however, reported by Broeckaert *et al* [2] that for the same power measured by calorimetry the Weissler reaction occurred faster at 1.1 MHz than at 20 kHz.

2. Pressure: Cavitation is nucleated mostly by imperfectly wetted crevice like features present on the container walls or liquid borne particulates. Imposing a static pressure on the reaction liquid drives the liquid meniscus at a crevice to its root and eventually the

liquid might perfectly wet the crevice feature thus preempting cavitation. If cavitation does occur then the violence of cavitation implosion is more energetic in the presence of bias static pressure. Intense implosions will enhance sonochemical activity. Owing to these opposing effects the observed results in the literature vary greatly.

3. Temperature: Vapor pressure of a liquid increases with increase in temperature, consequently the implosive collapse of a cavitation bubble is cushioned, leading to reduced sonochemical performance.

4. Power Input: For a given acoustic source the power input directly correlates to the acoustic output. Hence observed cavitation and sonochemical effects should increase with increased power input. Despite being easy to measure, power input, however, is a misleading parameter for dosimetry purposes. Transducer systems vary greatly in their transduction efficiencies and mere specification of the power inputs does not ensure repeatable performance. Additionally, variation in the insonified enclosure geometries also lead to non repeatable performance.

There are several other variables that influence cavitation but information concerning them is needed only for very detailed experiments in cavitation: surface tension, viscosity and vapor pressure of the liquid and dissolved gas content, particulate content of the reaction host, etc.

5. Calibration of acoustic fields

An ultrasonic cleaner is operated in continuous mode and it sets up standing wave field within the liquid bulk. Standing wave fields can be quite complex and the detailed mapping of pressure nodes and antinodes tedious and not quite useful. It would be adequate to probe the field in the region where a sample is to be held by dipping a needle hydrophone in a sample of distilled water. Weissler *et al.* [11] have probed a typical ultrasonic cleaner in terms of cavitation activity as determined by monitoring amount of chlorine liberated during a 10 second insonification of a 20 ml sample of saturated solution of carbon tetrachloride in distilled water. Thermocouple probes have been used for investigating ultrasonic fields in cleaning baths (Martin *et al.* [7]) which correlate well with a qualitative check offered by the cavitation perforations on an aluminum foil (Pugin [9]). At high frequencies, cup-horns can be readily calibrated using calorimetry.

Ultrasonic horns generate acoustic intensities much higher than the cleaners, typically by one to two orders of magnitude. When operated in pulse mode horns do not generate any appreciable standing wave fields. Most of the acoustic energy is coupled to the liquid in the immediate vicinity of the horn tip, often manifested by a cavitation cloud at the discharge of the horn, sonochemical effects are predominant near the tip. Horns also produce much stronger acoustic streaming, compared to ultrasonic cleaners, which assists in stirring the reaction vessel contents. Because of these factors and the fact that ultrasonic horns appear to be well standardized, for a given make and type of horn, performance can be reliably quoted in terms of the power input. Horn output can be reliably calibrated by calorimetry if the horn tip is uneroded, horn has not become detuned, and preferably if the horn is used in pulse mode. (The intent is to ensure that only the acoustic energy is converted into heat during calorimetric calibration.)

The ultrasonic horns operate at low tens of kilohertz frequencies. Should one decide to use higher frequencies (e.g. 1 MHz) for generating cavitation then it would be advisable to use focused transducers (spherical segment elements). If such transducers are operated in pulse mode (tone bursts at low duty cycles) they will generate fairly uniform cavitation

in the focal volume. Pulse mode obviates standing wave fields and essentially provides a progressive wave field. The sonochemical reaction sample cuvette could be located at the transducer focus for controlled acoustic exposure.

Focused fields can be very well calibrated and many ingenious techniques have been developed for measuring acoustic power which are described in Preston [8]. Acoustic power can be measured either through calorimetric techniques or any of the various radiation force balances. The calorimetric approach relies on absorbing all the acoustic energy as converted thermal energy and then measuring the consequent temperature rise. Kossoff [4] describes one of the earliest applications of the radiation force balance technique for measuring ultrasonic power outputs using both absorbing targets and reflecting targets. Absorbing targets tend to heat up and therefore require elaborate and delicate schemes for buoyancy compensation. Major problems with reflection-based methods are that standing waves are set up, when using continuous wave mode, and streaming flows are generated if the acoustic frequency is high. One might avoid these problems by using short duty factors to preclude standing waves, and use a thin acoustically transparent mylar screen to arrest streaming motion. Because it is easy to implement reflection type radiation force balance we will describe it in detail.

A radiation force balance is essentially a "bifilar suspension" which maintains a 45° orientation as it pendulates (see figure 1). It is suspended by four thin fishing lines of equal lengths from a roof oriented to the horizontal level also at 45°. The suspension perimeter is congruent with the perimeter of anchoring points on the target: the target is always parallel to the roof. The target is rectangular with a 3.2 mm deep rectangular cavity milled in 6.4 mm thick plexiglass. The dimensions of the rectangle are such that it projects a square area while intercepting the beam. A stainless-steel shim stock 12 μm thick is used to seal the air window in the target. When the target intercepts the beam being calibrated, the shim stock provides an interface which is essentially acoustically transparent while its air backing provides a fully reflecting surface. The suspension length is typically 40 cm, while the largest deflections encountered are, typically, less than 1 cm. To counter buoyancy due to the trapped air suitable lead weights are centrally attached to the target so that it sinks stably, and tensions the suspension lines uniformly. Heavier ballast enables one to measure higher acoustic powers. The time constant for the typical target is large compared with the time between the pulses, this provides a representative mean deflection response to radiation force.

The operational relation between the acoustic power, W , of a source and the radiation force, F , it exerts on a perfectly absorbing (or reflecting) target (placed in a host medium characterized by sound speed, c) is given by (Leighton [5]):

$$F = W / c . \quad (1)$$

It is assumed here that the target fully intercepts the beam. The target is in equilibrium under the action of three forces: the radiation force, the tension T in the suspending wires and the net weight of the target in water (corrected for buoyancy) mg . The horizontal component of the radiation force F is balanced by the horizontal component of the string tension T , while the vertical component of T balances $mg - F$. If the target deflection is d , and the suspension length is l then the radiation force in the direction of target displacement is given by

$$F = \frac{mgd}{l + d} . \quad (2)$$

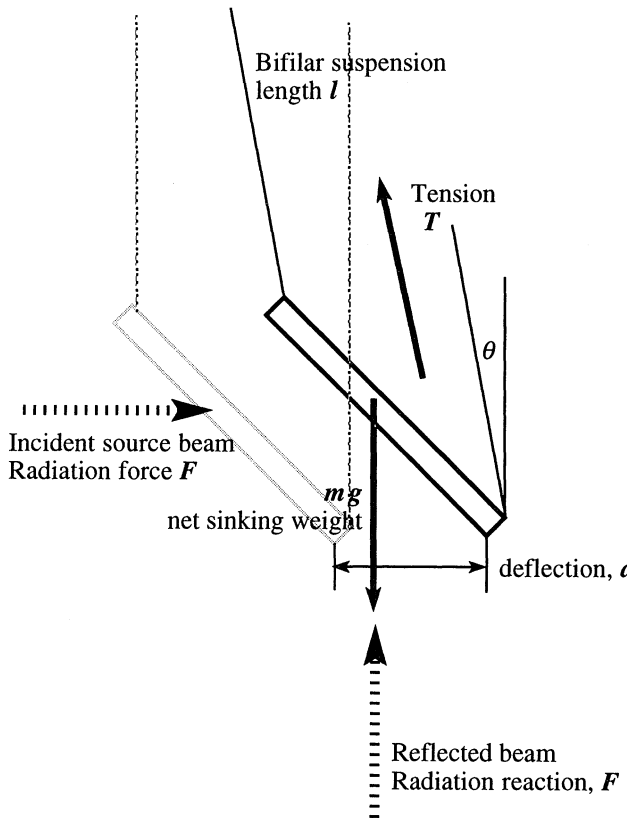


FIGURE 1 RADIATION FORCE BALANCE

For equilibrium:

$$T \sin \theta = F, \text{ and}$$

$$T \cos \theta = mg - F.$$

Therefore,

$$F = \frac{mg \tan \theta}{1 + \tan \theta}$$

or

$$F = \frac{mgd}{l + d}, \text{ where}$$

$$\tan \theta = \frac{d}{l}$$

for $d \ll l$

Thus measuring the target deflection, d , enables one to compute, F , from (2) and hence, using (1) determine the acoustic power of the source if it is operated at 100% duty cycle. The location of focus can be determined by holding a piece of xerographed inked square and observing the deinked spot at various locations along the transducer axis. Also one is guided by the fact that the focus of a spherical segment transducer is at the center of the corresponding sphere.

Of course if one has access to a calibrated reference transducer like the GEC-Marconi bilaminar PVDF membrane hydrophone, the task of calibrating acoustic fields is relatively easy: the pre-calibrated reference transducer directly gives the pressure amplitude generated at various locations in the transducer field to be calibrated. Often a calibrated needle hydrophone is more convenient to use, and the method of radiation force target described above can be used to calibrate inexpensively needle hydrophones for routine use (details in [3]).

6. Dosimetry reactions

A standardized dosimetry reaction would ensure that the acoustic cavitation conditions necessary for the dosimetry reaction have been met and any sonochemistry investigations carried out under these conditions would yield reproducible results. We will mention here only two dosimetry reactions and refer the reader to Suslick [10] and Ley *et al.* [6] for a chemistry perspective on dosimetry. For homogeneous sonochemistry a commonly used dosimetry reaction is the Weissler reaction, which involves oxidation of I^- by an oxidant generated by the sonication of water saturated with CCl_4 . By monitoring the rate of iodine liberation one would infer the presence and adequacy of cavitation necessary for sonochemistry. For heterogeneous reactions a chemical dosimeter proposed by Pugin [9], the reaction between 1-bromopentane and lithium yielding n-pentyl-lithium, might be useful. Here a Lithium wire provides the heterogeneity in the otherwise homogeneous aqueous reaction host. It can be positioned at any location within the reaction host where dosimetric data is needed.

7. Summary

In studying any cavitation dependent phenomenon, it is useful to remind ourselves of the three golden rules according to Apfel [1]: know thy sound field; know thy liquid; and know when something happens. As mentioned earlier acoustics influences sonochemistry via cavitation. Therefore for replicable sonochemistry performance the first two golden rules must be followed. For a well defined reaction host one will have to carefully specify the acoustic field. Merely stating the power input of a sonicating device like an ultrasonic cleaner and the duration of insonification are not adequate to replicate the acoustic conditions. Ideally one would like to specify the frequency, the mode of insonification, and the acoustic intensity distribution, spatial and temporal, in the reaction volume. Or, on a lighter note, specify the temperature as probed by a suitable thermistor (Martin *et al.* [7]).

8. References

1. Apfel R. E. (1981) "Acoustic Cavitation," in Methods of Experimental Physics, **19** pp. 355-411 (Academic Press, New York).
2. Broeckaert, L., Caulier, T., Fabre, O., Maerschalk, C., Reisse, J., Vandercammen, J., Yang, D., Lepoint, Th. and Mullie, F. (1992) Qualitative Homogeneous Sonochemistry: Scope and Limitations, in *Current Trends in Sonochemistry*, Ed. Price G. J., Royal society of Chemistry, pp. 9-25.
3. Kapodistrias, G., Madanshetty S. (1995) Measuring Peak Pressures Amplitudes in High Intensity Focused Fields, ASME paper 95-WA/NCA-19.
4. Kossoff G. (1965) Balance Technique for the Measurement of Very Low Ultrasonic Power Outputs, *J. Acoust. Soc. Am.*, **38**(5), 880-881.
5. Leighton T. G. 1994 *The Acoustic Bubble*, Academic Press London. pp. 21-22.
6. Ley, S., Low, C. (1989) *Ultrasound in Synthesis*, Springer Verlag New York.
7. Martin, C., Law, A. (1980) The use of thermistor probes to measure energy distribution in ultrasonic fields, *Ultrasonics*, **18**, pp. 127-133.
8. Preston, R. (ed.) (1991) *Output Measurements for Medical Ultrasound*, Springer-Verlag, New York.
9. Pugin, B. (1987) Qualitative characterization of ultrasound reactors for heterogeneous sonochemistry, *Ultrasonics*, **25**, pp. 49-55.
10. Suslick, K. S. (1988) "Ultrasound: Its Chemical, Physical and Biological Effects" VCH Publishers (Ed. Suslick).
11. Weissler, A. and Hine, E. (1962) Variation of Cavitation Intensity in an Ultrasonic Generator, *J. Acoust. Soc. Am.* **34** pp. 130-131.

LABORATORY EQUIPMENT AND USAGE CONSIDERATIONS

T.J.MASON

*School of Natural and Environmental Sciences
Coventry University
Coventry CV1 5FB
U.K.*

1. Introduction

An increasing number of chemists are turning to power ultrasound as an alternative energy source for the enhancement of reactivity. However, before plunging headlong into this technology, it is useful to obtain a little guidance as to the type of equipment available and its suitability for a particular chemical application. This article will identify the instruments currently available and discuss the advantages and disadvantages of each as laboratory tools for sonochemistry. Some consideration will also be given to scale-up equipment for industrial purposes.

2. The generation of power ultrasound

The essential device in the generation of power ultrasound for sonochemistry is the transducer of which there are three main types: liquid driven, piezoelectric and magnetostrictive.

2.1 LIQUID-DRIVEN TRANSDUCERS

The principle of operation of these devices has been described elsewhere in this volume¹. Such devices are particularly useful in applications where homogenisation and efficient mixing are important. This type of transducer has not been used extensively in sonochemistry.

2.2 MAGNETOSTRICTIVE TRANSDUCERS

These are electromechanical devices which use magnetostriction, an effect found in some ferromagnetic materials e.g. nickel or an alloy. Such materials reduce in

size when placed in a magnetic field and return to normal dimensions when the field is removed. This type of transducer is normally constructed using laminated metal as the core of a solenoid. Repeated rapid switching on and off of the current generates the mechanical vibrations required. In practise the magnetostrictive laminate is used in the form of a closed loop to improve electrical efficiency (Figure 1).

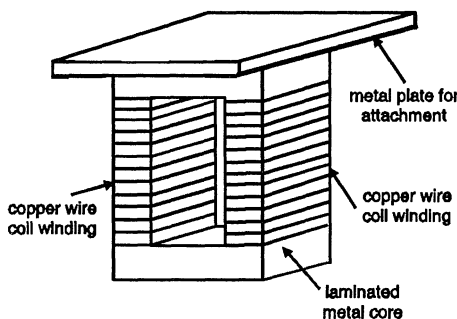


Figure 1: Schematic Diagram of a Magnetostrictive Transducer

There are two major disadvantages of this type of transducer. Firstly the upper limit to the frequency range is only 100kHz and secondly the original systems have an electrical efficiency of about 60% with the majority of the loss due to heating. As a result of the second of these problems all magnetostrictive transducers subject to extended use should be cooled. The major advantages are that they are of an extremely robust and durable construction and provide very large driving forces.

2.3 PIEZOELECTRIC TRANSDUCERS

Currently the most common method employed for the generation and detection of ultrasound utilises the piezoelectric properties of certain materials. Originally exploited using specially cut crystals of quartz the piezoelectric effect relates to the instantaneous generation of an electric charge between opposite faces of a material when a sudden pressure is applied across them. The polarity of charge can be reversed when sudden tension is applied. Piezoelectric transducers use the inverse of this effect *i.e.* if an electrical potential difference is applied across such faces the material will respond by either expanding or contracting depending on the polarity of the applied charges. Thus alternating the charge at 20kHz or above leads to fluctuations in dimensions and the generation of ultrasonic vibrations.

Quartz is a rather brittle material and so other piezoelectric materials

have been employed in transducer construction. The three which are commonly used in transducers are barium titanate (BaTiO_3), lead metaniobate (PbNb_2O_6) and the mixed crystal lead zirconate titanate. Such materials cannot be obtained as large single crystals and so, instead, they are ground with binders, sintered at above 1000°C to form a ceramic and then polarised. This process allows for the production of a wide range of shapes since the method is essentially that used in potteries but the piezoceramic element commonly used in cleaners and for probe systems is produced in the form of a disk with a central hole. These piezoelectric elements are clamped between metal blocks which serve both to protect the delicate crystalline material and to prevent it from overheating by acting as a heat sink. Usually two elements are combined so that their overall mechanical motion is additive (Figure 2).

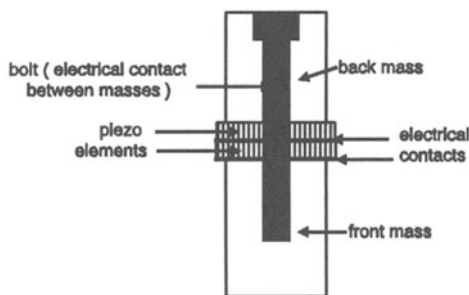


Figure 2: Schematic Diagram of a Piezoelectric Sandwich Transducer

In common with magnetostrictive type, for optimum performance the piezoelectric transducer must be constructed to correspond to a resonant size for the frequency used. For this reason for each frequency required a specific transducer size must be constructed.

3. Apparatus available for sonochemistry

There are essentially three methods for the introduction of ultrasound into a reacting system (Table 1) and of those listed only the first two have received any extensive use in the chemical laboratory. Applications of radial ultrasound will be considered later in this chapter. The majority of these systems rely upon the piezoelectric transducer as a source of power ultrasound and all three suffer from the disadvantage that optimum performance is obtained at a fixed frequency which depends upon the particular transducer employed. For most commercial probe systems this frequency is 20kHz and for baths around 40kHz.

TABLE 1 Methods of Introducing Ultrasound into a Reaction

-
- Immerse reactor in a tank of sonicated liquid
(e.g. flask dipped into a cleaning bath)
- Immerse an ultrasonic source directly into the reaction medium
(e.g. probe placed in a reaction vessel)
- Use a reactor constructed with ultrasonically vibrating walls
(e.g. a tube operating through radial vibrations)
-

3.1 THE ULTRASONIC CLEANING BATH

The ultrasonic cleaning bath is by far the most widely available and cheapest source of ultrasonic irradiation for the chemical laboratory. Although it is possible to use the bath itself as a reaction vessel this is seldom done because of the problems involved with chemical attack of the bath walls and with the containment of any evolved vapours and gases. Normal usage therefore involves the immersion of standard glass reaction vessels into the bath (Figure 3). This is important since conventional apparatus can be transferred directly into the bath and so an inert atmosphere or a static pressure can be readily achieved and maintained throughout a sonochemical reaction.

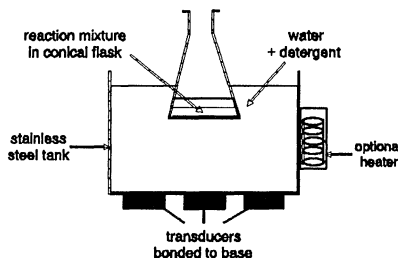


Figure 3: The Ultrasonic Cleaning Bath for Sonochemistry

It is important to establish the optimum position for the reaction vessel in the bath both vertically (due to the discrete wavelength of sound in water) and horizontally (in terms of the position of the vessel with respect to the transducers on the base). The simplest method of establishing this point is to locate the vessel such that maximum disturbance is observed on the surface of the liquid contained in that vessel. Once this position is found a template can be used to ensure future reactions are carried out in the same region of the bath. Naturally, in order to attain reproducible results, the same glass vessel should be used each time since differences in the thickness of the glass bases of vessels will affect

ultrasonic power transfer into the reacting system.

The amount of energy which reaches the reaction is low - normally between 1 and 5 Wcm⁻². This is so low that, for heterogeneous systems, it is almost always necessary to mechanically agitate the reaction mixture during sonication. A further complication in trying to reproduce work reported in the literature is that all baths operate at frequencies and powers dependent upon the transducers used and with bath geometries peculiar to the particular manufacturer.

Water (containing a little surfactant) is normally used as the coupling medium in the bath and this will limit the upper temperatures of operation to a maximum of just below 100°C. Factory fitted thermostatic control in baths is normally available for temperatures above that reached under its normal working conditions (generally about 40°C). Below this temperature a cooling system (cooling coil or circulating bath liquid) is required although this can interfere with the clear passage of ultrasound through the bath. It is important to record the temperature inside the reaction vessel since this will always be a few degrees above that of the bath itself due to localised ultrasonic heating.

3.2 THE ULTRASONIC PROBE

In order to increase the amount of ultrasonic power available to a reaction it is desirable to introduce the energy directly into the system rather than rely on its transfer through the water of a tank and the reaction vessel walls. The simplest method of achieving this is to introduce the ultrasonically vibrating tip of a sonic probe into the reaction itself (Figure 4). The part of the probe system which conducts and amplifies the vibrational energy from the transducer into the reaction is the acoustic horn.

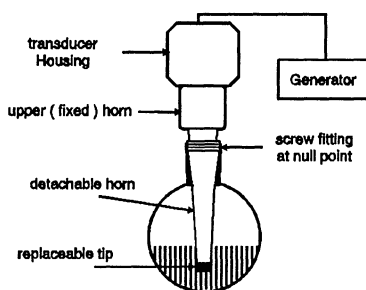


Figure 4: The Ultrasonic Probe System for Sonochemistry

The probe system has several major advantages over a bath including control of ultrasonic power delivered to the reaction. Maximum powers of

several hundred Wcm^{-2} can be easily achieved (depending on the size of the unit). One side benefit of such high powers is that ultrasonic streaming from the tip of the probe is often sufficiently powerful to provide bulk mixing without the need for additional stirring. Most modern units have a pulse facility allowing the operator to sonicate reactions repeatedly for fractions of a second. This gives adequate time for bulk cooling between sonic pulses.

Although so much extra power is available using the probe system it is more expensive than the bath and it is significantly less convenient in use especially in terms of the glassware required. Special seals will be needed if the horn is to be used in any reactions which involve reflux, inert atmospheres or the use of pressures above (or below) ambient. The cavitation which is the source of chemical activation is also the source of a common problem with probe systems - tip erosion - which occurs despite the fact that most probes are fabricated of titanium alloy which is very hard. There are two unwanted side effects associated with erosion (a) metal particles may erode from the tip and can contaminate the reaction mixture and (b) the physical shortening of the horn causes a loss of efficiency (eventually it will become too short to be tuned to the ultrasonic frequency used). The latter problem is avoided by the use of screw-on tips for the probe in the form of studs, this eliminates the need for a costly replacement of the whole horn.

3.3 PRACTICAL USAGE OF AN ULTRASONIC BATH

The use of an ultrasonic bath for homogeneous and heterogeneous reactions generally involves immersing a glass reaction vessel into the bath liquid². In these situations not only must the vessel be placed in the region of maximum activity (*vide supra*) but also the vessel shape must be considered.

As a model for a homogeneous reaction the sonication of water containing 4% potassium iodide in the presence of 1% carbon tetrachloride was chosen. Cavitation in this mixture produces four species, HO^\cdot radicals and H_2O_2 from the water together with Cl^\cdot and chlorine from the CCl_4 each of which is capable of oxidising iodide ion from the KI to iodine. The reaction was monitored by periodically withdrawing an aliquot and measuring any increase in the liberation of iodine by increases in its uv / vis absorption at 351nm. The results obtained at 30°C (Figure 5a) illustrate the great importance of both the source of ultrasound and the type of reaction vessel chosen for sonochemical studies.

A reaction volume of 50cm³ was placed in each of three different glass vessels, two conical flasks (250cm³ and 100cm³) and a 100cm³ round bottomed flask. When immersed in a cleaning bath the best sonochemical effect was obtained using the 250cm³ followed by the 100cm³ conical flask with the poorest

result in the 100cm^3 round bottomed flask. Both conical vessels present the preferred configuration for transfer of energy from the bath to the reaction media i.e. a flat glass base at right angles to the propagating sound wave. The results suggest that the greater base area of the 250cm^3 flask allows more power input to the system - and hence a more effective sonochemical reaction. The use of a 100cm^3 round bottomed flask gives an inferior result compared with both of these confirming that reflection and deflection of the sound waves as they impinge upon the rounded bottom surface of the vessel detracts from efficient power transfer into the reaction.

The heterogeneous "reaction" chosen was the reduction in particle size of commercial potassium carbonate (1g) by sonication in dimethylformamide (50cm^3). Results show two features of particle size reduction using a bath (Figure 5b). Firstly from the results obtained using a 100cm^3 conical vessel, optimum results are achieved using mechanical stirring. This is because, without stirring, the solid material settles to the base of the vessel and impedes efficient transfer of the acoustic energy. Secondly, with stirring, the trend in results for particle size reduction in differently shaped vessels is the same as that found in the homogeneous reaction above.

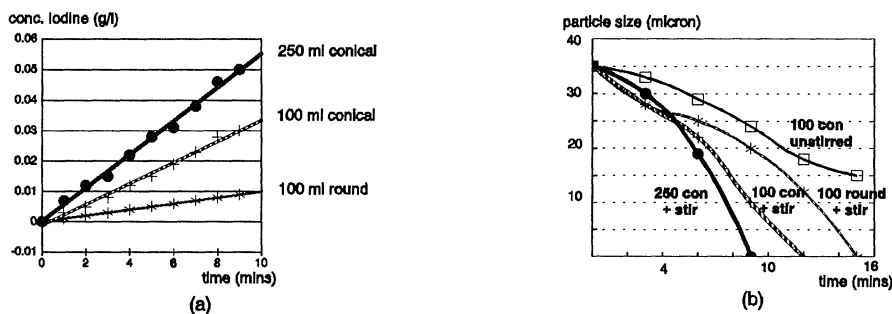


Figure 5: Effect of Vessel Shape on a Sonochemical Reaction
 (a) Oxidation of iodide ion (b) Particle size reduction of K_2CO_3

3.4 PRACTICAL USAGE OF AN ULTRASONIC PROBE

A probe system has the potential for providing variable power and a far greater energy input into a reaction than a bath system. In addition it is possible to find different probe systems which can operate at different individual frequencies (each probe system is tuned to a particular frequency). For these reasons it is more difficult to quantify the performance of a probe system and indeed any system providing controllable power or different frequency input. One approach

is to use the concept of sonochemical yield³ where:

Sonochemical Yield = "measured effect" / "sonic power entering the system"

The "measured effect" is the amount of product generated in a fixed time (e.g. the amount of I₂ liberated from 4% KI containing 1% CCl₄ in 5 minutes). The "sonic power" is the energy entering the reactor and is not the same as the electrical power consumed. This can be assessed by calorimetry by monitoring the initial temperature rise of system when the ultrasonic irradiation is first switched on taking care to use the same proportions of reagents as were used in observing the measured effect. Ultrasonic power units are quoted either as the total energy entering the system in Watts or the energy emitted at the surface of an ultrasonic device in Wcm⁻² or the energy dissipated into the bulk medium (in Wcm⁻³).

3.4.1 Variation in tip size

The ultrasonic generator provides energy to the transducer and the vibrational energy is conducted to the reacting medium by the horn. Most commercial probe systems have a selection of horns available typically with different sized tips. For the same generator input the sonochemical effect through such horns depends upon the tip size⁴. A typical sonicator system (20kHz) was used to irradiate a 27.5cm³ volume of the KI solution described in 3.3 above using the same generator setting but with different horns attached of tip diameters 1.2, 0.6 and 0.3 cm. The results show that for a fixed volume the most efficient result (iodine yield / power in Watts) is obtained using the horn with the largest tip diameter (Table 2). This is explained in terms of the improvement in energy transfer through a larger face of the irradiating source.

TABLE 2: Effect of horn tip size on sonochemical yield

Tip Diameter	1.2	0.6	0.3
Power (W)	27.8	18.0	10.1
Iodine (mole.dm ⁻³ × 10 ⁵)	101.5	48.2	5.4
Sonochemical Yield	3.65	2.68	0.53

3.4.2 Variation in power

Any increase in ultrasonic power entering the reaction should be associated with an increase in cavitation effect within the system and this, in turn, with a greater sonochemical effect. This statement is only true if the amount of energy delivered to the system is not excessive. Many examples exist of situations where above a certain energy input the sonochemical effect is reduced and a very good example of this is shown in Figure 6⁵. The initial response of iodine yield appears to be proportional to power but this effect is reduced beyond 40W and

drops dramatically above 100W. The explanation for this lies in the production of a large number of cavitation bubbles which act as a "cushion" to dampen the efficiency of energy transmission into the reaction medium. As more and more such bubbles are produced they act as a barrier to energy transmission into the system and the sonochemical effects are substantially reduced.

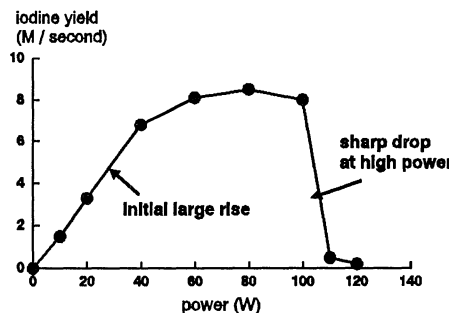


Figure 6: Effect of Increasing Power on a Sonochemical Reaction

If the power input is maintained below the point of excessive production of cavitation bubbles then a good relationship can be found between power and effect. To this end some experiments were performed to monitor the production of OH· radicals under cavitation using the reaction of OH· with terephthalic acid anion (TA) to produce fluorescent hydroxyterephthalate ions (HTA)^{7,8}.

In this study⁷ the following terms were used:

Fluorescence Intensity (F) is the direct reading of fluorescence as recorded on a Perkin Elmer Luminescence Spectrometer LS 50 instrument adjusted by subtraction of the small "zero" reading obtained after the ultrasonic irradiation is switched on and the system attains temperature equilibration. There are no units for fluorescence intensity (F).

Ultrasound Dosage (D) in parallel with other radiation dosages is the ultrasonic power entering the liquid system (Watts) as recorded by calorimetry multiplied by the time of exposure in seconds. The units of Dosage (D) are Watt.seconds i.e. Joules.

Fluorescence Yield is the fluorescence intensity produced per unit ultrasound dosage (F/D) and has units of Joules⁻¹.

The fluorescence yield obtained after 1 hour of sonication using an Undatim Sonoreactor (Belgium) operating at 20kHz and four different powers was calculated (Table 3). The results indicate that the fluorescence yield at all four settings remains effectively the same i.e. the yield of OH· radicals is directly proportional to power input.

TABLE 3: The effects of Ultrasonic Power on OH Radical Production using Terephthalic Acid as a Dosimeter^{a,b}.

Power	F (Fluorescence)	Yield (F/D) ^c
50.4	106.3	5.86
54.6	113.1	5.75
61.1	125.2	5.69
64.8	137.1	5.88

(a) 50 cm³; sonication time 60 minutes; T = 30°C

(b) Concentration of TA = 2 x 10⁻³ mol.dm⁻³

(c) Fluorescence Yield x 10⁻⁴ J⁻¹, mean of two runs reproducibility ± 2%

3.4.3 Variation in frequency

Until a few years ago it was believed that sonochemical reactions were unaffected by changes in irradiation frequency. This arose from the idea that once the cavitation threshold was exceeded the ensuing cavitation collapse would provide the same effects whatever the frequency. In an important paper on this topic the effectiveness of 20 and 514kHz irradiation was compared in the oxidation of aqueous KI to iodine and the generation of hydrogen peroxide in water at the same input power⁸. The rate of production of iodine in oxygen saturated KI (10⁻²M) was some six times and peroxide formation 12 times faster at the higher frequency. This result is ascribed to the fate of the OH· radical formed by the breakdown of water on cavitation bubble collapse. The OH· can be destroyed by reactions in the bubble or can migrate into the bulk and produce peroxide. At the higher frequency a shorter bubble lifetime allows more of the OH· to escape from the bubble. We have also some evidence for this frequency effect in work involving OH· detection by fluorescence using the terephthalate dosimeter⁷. The results of fluorescence intensity measurements at three different frequencies are shown in Table 4. It can be seen that after 60 minutes irradiation the 40kHz probe gives the best result in terms of fluorescence intensity. However, this does not take into account the ultrasonic power used. When the power is taken into account the fluorescence yields increase with the frequency from 20kHz to 40kHz and 60kHz (Table 4) in a ratio of approximately 1:2:4. This indicates that, within the narrow range of frequencies chosen in this part of the study, 60kHz is the best frequency for the formation of OH· radicals.

TABLE 4: Effects of Ultrasonic Power on ·OH Radical Production with a Probe using Terephthalic Acid as a Dosimeter^{a,b}.

Frequency	Power	F (Fluorescence)	Yield (F/D °)
20	50.4	106.3	5.86
40	26.0	131.7	14.07
60	11.0	103.4	26.15

(a) 50 cm³; sonication time 60 minutes; T = 30°C

(b) Concentration of TA = 2×10^{-3} mol.dm⁻³

(c) Fluorescence Yield $\times 10^{-4}$ J⁻¹, mean of two runs reproducibility $\pm 2\%$

3.5 FLOW REACTORS

This type of system provides the greatest hope for general usage of ultrasound in the chemical industry. While the bath system may well prove adequate for low power treatment of small to medium scale batch processing it cannot accommodate high power sonication of large volumes which would be required for industrial applications. The alternative is to use a high intensity source to treat small volumes of a reaction as part of a flow system with the treated material either being recycled to a reservoir or passing on to further processing applications. For this purpose probe systems will certainly provide the power required but by their very nature will suffer from erosion of the horn tip and, in the long term, this could prove expensive in terms of "down-time" for repair and replacement. An alternative solution to the problem of large scale flow processing is the use of radially transmitted vibrations into a flowing liquid either from the walls of the containing pipe or from a tubular insert placed within the pipe itself. Such systems are capable of handling high flow rates and viscous materials.

3.5.1 Flow reactors with vibrating walls.

Ultrasound can be introduced into a reaction flowing through a tube via transducers attached to the outside of the tube walls. In such cases the cross-sectional geometries have a significant effect on the power transmission. A cylindrical resonating pipe will provide a focus of ultrasonic energy in the centre of the tube as will a hexagonal pipe. Thus relatively low power at the perimeter inner surface will give high energy in the centre, this reduces erosion problems at the emitting surface. An alternative pentagonal cross-section provides non-focused ultrasound with a reasonably even power distribution throughout. In all cases the length of such a pipe must be accurately designed so that a null point exists at each end and it can then be retro-fitted to existing pipework.

The Sodeva Sonitube (France) (Figure 7a) is a radially emitting hollow tube of cylindrical cross-section which uses a transducer horn system coupled directly to an annular collar which then drives the cylindrical resonator. The collar is screw fitted to take one or two stainless steel pipes accurately machined so that the remote end is a null point and may be further coupled to other pipework. The maximum resonance power then operates on any liquid flowing inside at half-wavelength distances along the tube.

The Nearfield Acoustic Processor (NAP) (Lewis Corporation, U.S.A.) provides an alternative design for a flow reactor (Figure 7b). This device consists of two sonicated metal plates between which the reagents flow. The plates are driven at different frequencies (16 and 20kHz) giving an intensity in the liquid between the plates greater than the sum of single plate intensities. This processor is driven by magnetostrictive transducers, is very robust and can cope with large throughput.

3.5.2 Flow reactors constructed using inserts

This approach to sonication involves the introduction of a radial resonator into the central axis of a tube containing the flowing liquid. The insert then generates ultrasound along its length, at half wave distances, offering both direct sonication and also sonication as a result of reflected ultrasound from the inside walls of the containing tube.

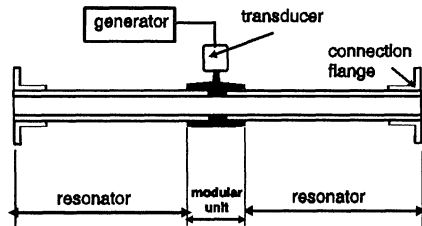
The Telsonic Tubular Resonator (Switzerland) (Figure 8c) consists of a hollow, gas filled, steel tube sealed at one end and driven at the other by a standard piezoelectric transducer. This device looks like a conventional probe system but is significantly different in that the sealed end is at a null point and the ultrasound is emitted radially at half wavelength distances along its length.

The essential element of the Martin Walter Push-Pull system (Germany) (Figure 8d) is a solid cylinder of titanium cut to a multiple of half wavelengths with opposing piezoelectric transducers attached to each end. The transducers are electrically connected through a central hole in the cylinder and, when operating the bar responds to the push-pull mode to give a "concertina" effect down its length. Unlike the hollow tube system, this device uses the acoustically more efficient titanium as the radiator and, being essentially a solid bar, it offers extended operational lifetime since erosion by cavitation will not change the resonant length of the resonating bar.

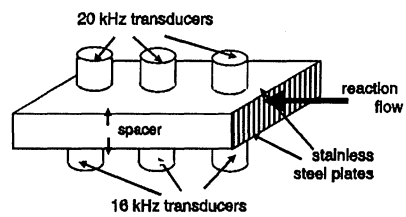
4. Conclusion

Over the last few years a greater appreciation of the underlying principles of power ultrasound by chemists has led to more efficient laboratory experiments and the development of a wide range of equipment. It is to be hoped that

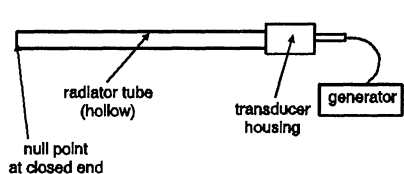
laboratory workers who are now entering this field will learn from the practical experience of those who have been studying sonochemistry for some years and avoid the errors involving the incorrect use of equipment which have been a problem in the past.



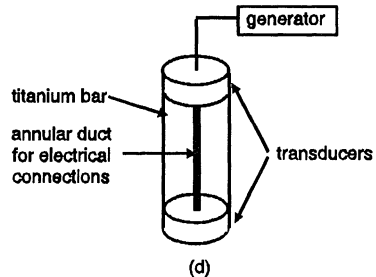
(a)



(b)



(c)



(d)

Figure 7: Different Configurations for Flow Reactors (a) Sodeva Sonitube (b) Nearfield Acoustic Processor (c) Telsonic Tubular Resonator (d) Martin Walter Push-Pull system.

5. References

1. Mason T.J. (1998) Industrial Applications of Sonochemistry and Power Ultrasonics, *in this volume*.
2. Mason T.J., Lorimer J.P., Cuesta F. and Paniwnyk L. (1989) *Ultrasonics International 89, Conference Proceedings*, Butterworths, 1253-1256.
3. Mason T.J. and Berlan J. (1992) *Ultrasonics in Industrial Processes: The Problems of Scale-up*, Current Trends in Sonochemistry, 148-157 ed Price G., Royal Society of Chemistry, Cambridge.
4. Paniwnyk L. (1994) Ph.D. thesis, Coventry University.
5. Henglein A. (1992) *Contributions to Various Aspects of Cavitation Chemistry, Advances in Sonochemistry 3*, ed Mason T.J., JAI Press, London.
6. Mason T.J. (1998) Introduction to Organic Chemistry, *in this volume*.
7. Mason T.J., Lorimer J.P., Bates D.M. and Zhao Y. (1994) *Ultrasonics Sonochemistry*, **1**, S91-S96.
8. Petrier C., Jeunet A., Luche J-L. and Reverdy G. (1992) *J.Amer.Chem.Soc.* **114**, 3148-3150.

HIGH POWER ULTRASONIC TRANSDUCERS

JUAN. A. GALLEGOS-JUÁREZ

Institute of Acoustics, CSIC

Serrano, 144, 28006 Madrid, Spain

1. Introduction

The use of high-intensity ultrasound in processing is generally based on the application of nonlinear effects produced by finite amplitude pressure variations. The most important effects produced by high-intensity ultrasonic waves are: heat, cavitation, agitation, acoustic streaming, interface instabilities and friction, diffusion and mechanical rupture. These effects are used to enhance a wide range of processes, such as machining, welding, metal forming and powder densification in solids; cleaning, emulsification, atomisation of liquids, acceleration of chemical reactions, degassing, defoaming, drying, aerosol agglomeration, etc., in fluids. A certain number of these processes have already been introduced in industry, but many of them still remain at a laboratory stage and have not been commercially developed. This is probably because of the problems related to the development of adequate ultrasonic power generation technology. The main points to be considered in the ultrasonic transducers for large scale applications are power capacity, efficiency, vibration amplitude, and volume to be treated.

Transducers for processing are narrow-band transducers working at frequencies within the range of 10 to 100 kHz, power capabilities of a hundred watts to several kilowatts and large vibration amplitudes.

This paper reviews the main present types of high power ultrasonic transducers and discusses their characteristics and performance.

2. Transducer materials

At present, most ultrasonic transducers are of the piezoelectric type. Therefore, we will mainly focus our attention on this kind of transducers. Nevertheless, it is interesting to point out recent developments of new and promising magnetostrictive materials (rare earth compounds), which show a great potential for high-power transducers.[1]

Transducers are typically composite devices in which the core is a piezoelectric (or magnetostrictive) element, which changes dimensions in response to an electric (or magnetic) field. Other passive components complement the transducer structure to improve energy transfer. These components are generally made of metallic alloys.

This section will describe the basic characteristics of active and passive materials used for high-power transducers, with special emphasis on piezoelectric ceramics.

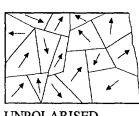
2.1 PIEZOELECTRIC CERAMICS

In modern transducers, the piezoelectric materials generally used are piezoelectric ceramics. It can be shown that piezoceramics offer the highest electromechanical conversion and efficiency, and have, in general terms, the most favourable properties for high-power ultrasonic transducers.

Piezoelectric ceramics are materials constituting a conglomerate of ferroelectric crystallites which are randomly oriented. They generally originate from a solid-state reaction of several oxides followed by high-temperature firing. After firing, a ceramic is isotropic and non-piezoelectric because of the random orientation and structure of the domains (regions within each crystallite in which the electric dipoles have common orientation) (Figure 1.a). The ceramic material may be made piezoelectric by a poling treatment consisting of applying a high electric field in a chosen direction to switch the polar axes of the crystallites to those directions, allowed by symmetry, which are nearest to that of the electric field (Figure 1.b). After removal of the poling field, the dipoles cannot easily return to their original positions, and the ceramic will now have a permanent polarisation, and will respond linearly to applied electric fields or mechanical pressures as long as their magnitude is kept well below that needed to switch the polar axis. Therefore a poling treatment is indispensable for these materials, although it is evident that it is not possible to achieve perfect dipole alignment with the field, as in single crystals. The measured polarisation value can be good indicator of the alignment.

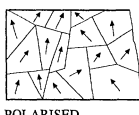
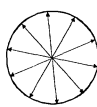
Figure 1

DOMAIN VECTORS



UNPOLARISED

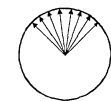
(a)



POLARISED

(b)

Domain alignment by applying a poling treatment



In piezoelectric materials the elastic and electrical properties are coupled; mechanical and electrical parameters must therefore be involved in constituent relations. Usually, stress T and strain S from one side, and electric field E and dielectric displacement D from the other, are considered.

For a piezoelectric medium, the interaction between electrical and mechanical variables can be described by linear relations of the form

$$\begin{aligned} D &= dT + \epsilon^T E \\ S &= s^E T + dE \end{aligned}$$

where ϵ and s are the permittivity and compliance of the medium, respectively and d the piezoelectric constant. The first equation describes the direct and the second the converse piezoelectric effect. The superscripts denote the quantity kept constant under boundary conditions.

An important parameter to be considered in piezoelectric materials is the electromechanical coupling factor (k). This factor may be defined as the square root of the ratio of energy available in electrical (mechanical) form under ideal conditions to the

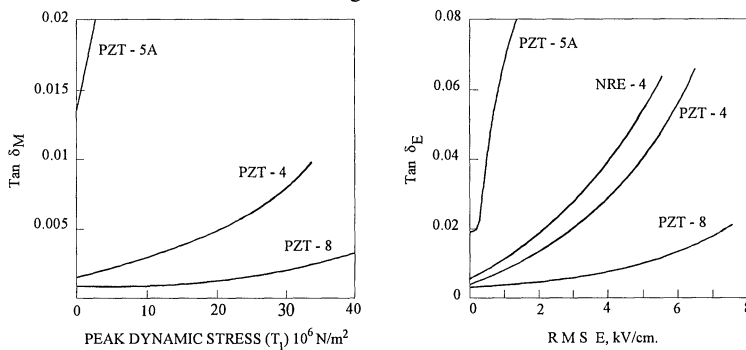
total energy stored from a mechanical (electrical) source. Although the electromechanical coupling coefficient provides a measure of the ability of the piezoelectric material to change energy from one form to another, it must not be thought of as a measure of transducer efficiency. In fact, this parameter does not take into account the losses in the system, and, in principle, the energy which is not converted remains in the initial form and can be recovered. The efficiency is the ratio of the useful power output to the power input.

The electrical properties and dimensions of a piezoelectric transducer are dependent on the dielectric, piezoelectric and elastic constants of the material.

Mechanical and dielectric quality factors, Q_m and Q_E , account for losses and determine efficiency and bandwidth. In general, in ceramic materials dielectric losses are not very relevant. In practical transducers, the mechanical quality factor is generally a determinant parameter.

For transducer applications it is important that the characteristic constants of the material should remain stable with respect to time, temperature, mechanical stress and electric field. In addition, the limits of usefulness of the material (strain saturation, fatigue, limiting temperature, etc) may serve to establish its power capability. Piezoelectric ceramics present the widest variety in their elastic, electric and piezoelectric constants. In addition, the ceramic materials can be formed into a large variety of shapes and sizes and the polar axis can be directed according to the geometry and the vibration mode.

Figure 2



Dielectric and mechanical losses for several piezoelectric ceramics

At present the most suitable and popular ceramic materials are lead zirconate titanates(PZT) of which various commercial versions are manufactured in different countries. There are also commercial compositions based on barium titanate, lead metaniobate and sodium niobate. The leading position of the lead zirconate titanates is due to their strong piezoelectric effect and high Curie point, together with the wide range of properties they offer simply by making small changes in composition. The PZT-4 and PZT-8 compositions are particularly adapted for high-power transducers [2]. The latter has remarkably low dielectric and elastic losses at high drive levels (Fig. 2).

Table 1 lists the principal characteristics and applications of the most useful types of lead zirconates titanates. It can be observed from the table that different types, corresponding to different compositions, are prominent with respect to different characteristics.

Table 1 Principal characteristics and applications of piezoelectric ceramics

Material	Characteristics	Applications
Lead zirconate titanates		
PZT-4	High coupling, high permittivity, good high signal properties	Sonar and macrosonics
PZT-5A	High coupling, very high permittivity, high compliance.	Transducers for NDT and diagnostics, hydrophones
PZT-6B	Very high mechanical Q value, good stability	Electric wave filters
PZT-7A	Low permittivity	Ultrasonic delay lines
PZT-8	Very good high-signal properties	Power ultrasonic transducers
Niobates $\text{Pb}(\text{NBO}_3)_2$	Low permittivity, very low mechanical Q value	Ultrasonic NDT and diagnostics
$\text{NaK}(\text{NbO}_3)_2$	Low compliance (high wave velocity)	Delay lines
Barium titanate	Low Curie point	Ultrasonic transducers

2.1.2. Power limitations of piezoelectric ceramics

Power limitations of piezoelectric ceramics are due to mechanical and dielectric losses and they can be characterized by using the equivalent circuit.

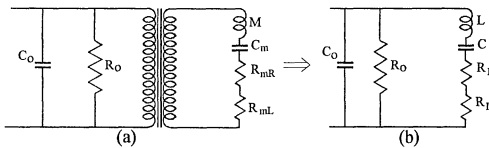
A resonant piezoelectric transducer can be described by the well known circuit of Fig. 3, where C_0 and R_0 are respectively the capacitance and the electrical resistance of the piezoelectric element. Both components appear in parallel with a series branch that includes the converted mechanical impedances. These impedances consist of an inductance M due to the mass of the transducer, a capacitance C_m due to the compliance of the transducer, a radiation resistance R_{mR} and a resistance R_{mL} due to the mechanical losses in the transducer. The mechanical branch of Fig. 3a transforms into electrical components in Fig. 3b by the transformer ratio. The effect of internal losses can be analyzed by means of R_0 (dielectric losses) and R_L (mechanical losses). In fact it can be easily seen that by using the circuit of Fig 3a the radiated power can be expressed by

$$P_R = \frac{\eta \omega U_m}{Q_m}$$

where η is the electroacoustic efficiency, ω the angular frequency, Q_m the mechanical quality factor and U_m the elastic energy stored in the transducer. From the circuit of Fig. 3b we can find for the radiated power

$$P_R = \eta \omega \frac{k^2}{1-k^2} Q_m U_e$$

Figure 3



Equivalent circuit of a resonant piezoelectric transducer

The mechanical limit, which may correspond to the nonelastic behaviour of materials, is more important with high-Q transducers while the electrical limit is with low-Q. The electrical limit mainly refers to depolarisation of the ceramics under high electric fields. A comparison of the dissipated power for several piezoelectric ceramics (Table 2) shows the advantages of PZT-8 material [2].

Table 2: Dissipated power in W/cm^3 for piezoceramic transducers with $P=25\text{W/cm}^3$ at 10kHz

Material	Electrical dissipated power (W/cm^3)		Mechanical dissipated power (W/cm^3)	
	Q=3	Q=30	Q=3	Q=30
PZT-8	0.10	0.01	0.09	3.0
PZT-4	0.20	0.01	0.23	9.9
PZT-5	1.35		3.75	

The overheating due to internal mechanical losses in the piezoelectric ceramics represents a thermal limit. It can produce, if it is excessive, a decrease in their electromechanical properties or even a depolarisation.

2.2 PIEZOMAGNETIC MATERIALS

The magnetostrictive effect occurs in ferromagnetic materials such as metallic alloys of nickel and cobalt, iron-chromium-vanadium, etc. and in certain ceramic called ferrites of general formula $(\text{MO})(\text{Fe}_2\text{O}_3)$ (M being a bivalent atom). As is well known when a rod or bar of these materials is subjected to a magnetic field it experiences a change in length. Conversely, a mechanical stress applied to a rod or bar causes a change in intensity of magnetisation. The magnetostrictive effect is analogous to the electrostrictive effect: whether there is an increase or decrease in length depends entirely on the nature of the material and this is independent of the direction of the field. When an alternating magnetic field is applied along the direction of the axis of a rod of ferromagnetic material, the rod oscillates at twice the frequency of the applied field. Therefore, the waveform of the strain is a rectified sine curve. A purely sinusoidal waveform is obtained if the rod is polarized by applying at the same time a direct magnetic field of sufficiently high-intensity.

Alternative fields will set up eddy currents in the magnetic materials causing losses which are very dependent of frequency. Magnetostrictive transducers are essentially low frequency devices. They have been used at ultrasonic frequencies (20-50 kHz) but eddy currents of considerable magnitude are induced in the core materials. During the 70's,

where k is the electromechanical coupling factor and U_e the electric energy stored in the transducer [3].

From the previous expression it is clear that the radiated power can be limited by the maximum mechanical or electrical energy stored in the transducer.

there was a shift of interest from magnetostrictive to piezoelectric materials, probably due to the good performance of the new piezoelectric ceramic. In recent years new magnetostrictive materials, based on the heavy rare earth, have been developed and they have shown to possess a giant magnetostrictive effect [1]. In particular the alloy of Terbium, Dysprosium and Iron ($Tb_{0.3} - Dy_{0.7} Fe_{1.9}$) which is known as Terfenol , can reach strains greater than 1000 parts per million. At the present time, the commercial availability of this material has increased the possibilities of magnetostriction in power sonic and ultrasonic transducers design.

2.3 COMPARISON OF PIEZOCERAMIC AND PIEZOMAGNETIC MATERIALS.

It is clear that the wide use of piezoceramics is due to their outstanding electromechanical properties. The presently used piezoceramic materials have higher electromechanical coupling factors than any of the magnetostrictive materials (with the possible exception of the new rare earth materials). [4,5] (see Table 3). It means that the power capacity of the piezoceramics is higher too and this is a primary value for high-power transducers. The dielectric losses in the ceramics are lower than the magnetic losses in most magnetostrictive materials and the mechanical losses are also very low in the piezoceramics (mechanical quality factors greater than 1000).

Table 3: Comparison of piezoelectric and magnetostrictive materials

	Piezoelectric ceramic	Cobalt Nickel	Terfenol
Coupling factor	0.7	0.5	0.7
Saturation strain (ppm)	200	35	1000
Young's modulus (Gpa)	74	190	26
Density (g/m ³)	7.5	8.9	9

Another important feature of the piezoceramics is their ability to be formed with a great variety of shapes and the ease with which they can be permanently polarised.

Piezoceramic and piezomagnetic materials have some common limitations that can be overcome for high-power applications. One of these limitations is their low tensile strength. This problem can be surmounted by prestressing to a level of compressive stress in such a way that the ceramic is always working in compression for the whole vibration cycle.

Another problem with piezoceramics is the change of their properties with time (ageing). This is mainly due to the slow decrease of the remnant polarisation as the material tends to return toward its unpolarised state. That suppose the appearance of a certain degree of nonlinear behaviour with the consequence of an increase in dielectric losses.

2.4 METALLIC COMPONENTS

As already mentioned, transducers are composite devices composed of active piezoelectric materials and other passive materials. In high-power transducers, the

passive materials are generally metals. The metal choice affects the transducer power capacity and efficiency. Titanium alloys, specially Ti-6Al-4V, are the best for high-power. Other useful metals are duraluminium, aluminium bronze, naval brass and tool steel. Table 4 shows some properties of materials used in macrosonic transducers.

Table 4: Properties of materials used in macrosonic transducers

Material	Young's modulus (10^{11}N/m^2)	Density (10^3kg/m^3)	Velocity of sound (m/s)	Fatigue strength (10^7N/m^2)	Maximum strain (10^{-3})
Titanium alloy (Ti-6Al-4V)	1.06	4.42	4900	72	6.80
Duraluminium	0.74	2.80	5130	19	2.57
Aluminium bronze	1.43	8.50	4070	37	2.59
Naval brass	0.89	8.45	3240	15	1.69
Tool steel	2.20	7.80	5200	55	2.52

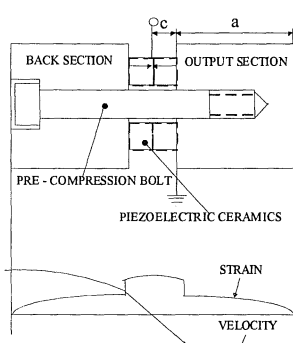
An experimental investigation about the real behaviour of metals subjected to high intensity ultrasound [6] showed that under dynamic conditions the titanium alloy (Ti-6Al-4V) offers limiting strains one order of magnitude higher than the duraluminium.

3. The sandwich transducer

The most characteristic piezoelectric transducer for high-power applications is the well-known sandwich transducer, which is reminiscent of the Langevin transducer [7]. When ceramics for narrow-band low-frequency applications were first used, the transducers consisted of simple piezoceramic blocks. However, this plain arrangement did no prove to be very useful, especially for high power applications, due to the low tensile strength of the ceramic and to the physical dimensions of the single-piece needed for such a low

frequency. Because of these difficulties, Langevin's design was re-investigated and adapted to the new circumstances. The sandwich transducer is a half-wave resonant length-expander structure, which, in its simple version, consists of a disc, or of paired discs, of piezoelectric ceramics sandwiched between two identical metal blocks (Figure 4). When used in pairs, the piezoelectric ceramics are polarised in opposite directions and separated by an electrode connected to the high-voltage lead. The electrode is therefore located at a node. Coupling between the piezoelectric elements at the metal end-sections and increase to the tensile strength are

Figure 4



Structure of prestressed sandwich transducer

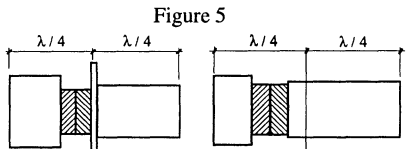
achieved by mechanically prestressing the assembly in the axial direction by means of a bolt [8].

The calculation of the dimensions of the sandwich transducer, can be made by using the expression [9]

$$\tan \frac{\omega c}{v_c} \tan \frac{\omega a}{v_l} = \frac{\rho_c v_c A_c}{\rho_l v_l A_l} \quad (1)$$

where c and a are the piezoelectric ceramic and the natal section thickness, ρ_c and A_c are the density and the sectional area of the ceramics, ρ_l and A_l the density and sectional area of the metal pieces, v_c and v_l the extensional sound velocities in the ceramic and in the metal pieces, and ω the angular resonance frequency of the whole sandwich transducer. After choosing the materials, the resonance frequency and two of the three

geometrical quantities, the previous equation can be used to fix the unknown dimension.

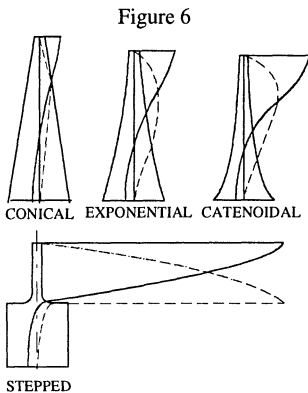


Asymmetric sandwich transducers

In practice, the sandwich construction does not generally follow the symmetrical structure just described. In most applications the output and back sections are made of metals of different density in order to increase the vibration amplitude on the radiating face and to improve matching to the load.

Other cases require the node, which is the supporting point, to be in one of the metallic sections. The result in all these cases is an asymmetric sandwich structure as schematically shown in Fig. 5. The output section is a cylindrical $\lambda/4$ piece and the other $\lambda/4$ section, including the piezoelectric ceramics, is designed by applying equation (1).

4. Transducers for applications in solids

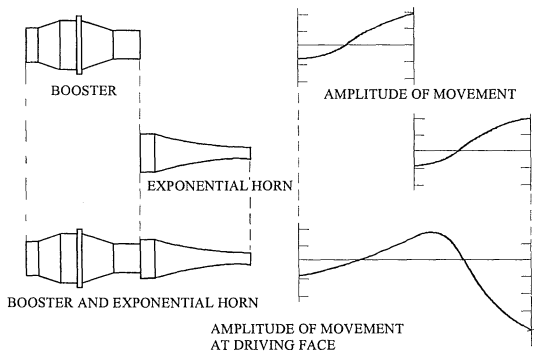


Basic horn shapes and amplification effect

High-intensity applications of sonic and ultrasonic energy in solids such as machining, welding, metal forming, etc. are based on mechanical effects as a result of particle motion. In these processing applications, the sandwich transducer is also used, but it also includes a metallic transmission line of special shape, which produces a displacement amplification at the working end. These transmission lines are formed by half wavelength resonant elements, called mechanical amplifiers or horns, which are generally stepped, conical, exponential or catenoidal (Fig. 6). The horn must be designed to resonate at the same frequency as the transducer which is to drive it. A schematic drawing of a typical processing transducer with one exponential horn is shown in Fig. 7.

A successful application of these transducers depends on obtaining the correct amplitude of movement at the horn tip. Amplitude depends on shape and dimensions. It can be difficult to design a horn having the correct shape and required gain. In such cases more than one horn section is used in order to obtain some amplification stages (Fig. 8). The intermediate horns, which are inserted between the transducer and the work horn are sometimes called booster horns. In general practice, the horns used in industry are those which can be easily and rapidly designed, constructed and modified. That means horns with cylindrical or conical straight sections. Of all designs, the most popular and probably the most efficient one is the stepped horn which, in its simple form, consists of two quarter wavelength cylinders of different diameter (Fig. 6). In the stepped horn, the amplification factor is equal to the ratio of the areas of the larger and smaller cross-section, which, for a given ratio of end diameters, is the greatest possible magnification to be obtained with a single horn [10]

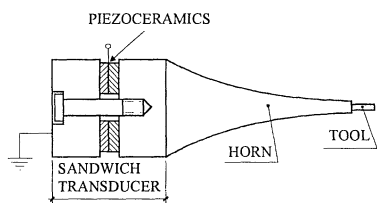
Figure 8



Effect of intermediate booster horns on movement amplitude

wavelength, in order to obtain a pure extensional mode of vibration. Nevertheless, most applications require wide horns or horns of large cross-sections. In these cases, one of the main problems is to obtain a uniform amplitude distribution on the radiating face avoiding radial or lateral vibration modes. For this purpose, large horns are constructed with slots running parallel to the direction of longitudinal motion (Fig. 9). This way, the large horn, can be considered as an array of narrow horns in which the apparent cross-sectional dimension of each element is less than a quarter of a wavelength. The slots are also useful for heat dissipation. Large horns may be of different geometrical shapes and the procedure for designing must take into account that the bridging section joining the elements is an additional mass which presents a mechanical impedance to the longitudinal element

Figure 7

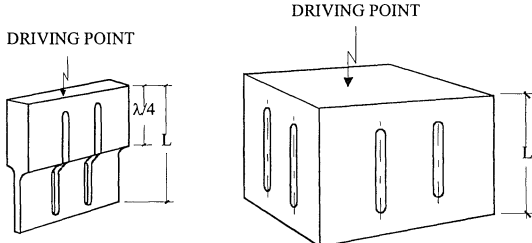


Schematic structure of a typical ultrasonic processing transducer

In the horns described in Fig. 6, the cross-sectional dimensions were assumed to be smaller than one-quarter or one-third of the

quarter wavelength, in order to obtain a pure extensional mode of vibration. Nevertheless, most applications require wide horns or horns of large cross-sections. In these cases, one of the main problems is to obtain a uniform amplitude distribution on the radiating face avoiding radial or lateral vibration modes. For this purpose, large horns are constructed with slots running parallel to the direction of longitudinal motion (Fig. 9). This way, the large horn, can be considered as an array of narrow horns in which the apparent cross-sectional dimension of each element is less than a quarter of a wavelength. The slots are also useful for heat dissipation. Large horns may be of different geometrical shapes and the procedure for designing must take into account that the bridging section joining the elements is an additional mass which presents a mechanical impedance to the longitudinal element

Figure 9

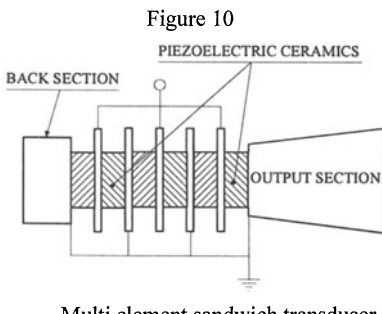


Horns of large cross-section

of the horn [11]. Recently some methods for modal vibration control of large horns have been proposed [12].

5. Transducers for applications in fluids

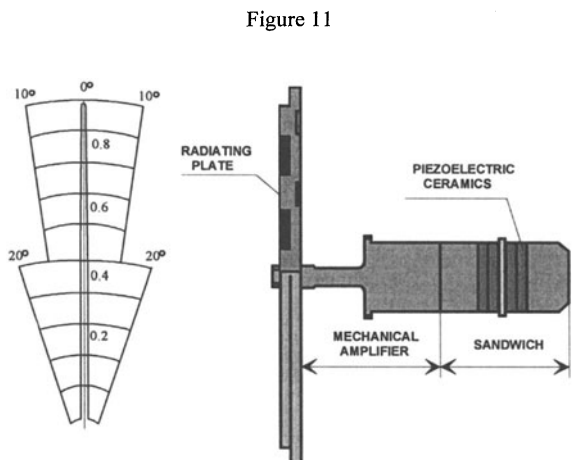
The sandwich transducer, as described above, is employed directly for applications in liquids, such as ultrasonic cleaners and reactors. The use of single or multi-element sandwiches is widespread. Multi-element sandwiches incorporate an even number of piezoceramic discs (Fig. 10). In addition, the work-face area can be increased by tapering the output section. This can be useful in the matching of the transducer to its load. Most high-power ultrasonic devices are designed on the basis of different kinds of multi-element sandwich transducers and they are constructed very often in arrays of a number of elements in order to cover a large working area and to obtain the desired total power.



Multi element sandwich transducer

directional or focused beams for industrial applications, high-power capacity and extensive radiating area would be required in the transducers. The existing high-power commercial transducers have many limitations to cover all the above-mentioned requirements. The development of a new type of stepped-plate transducer, in which these prerequisites have been attained, opens up new possibilities. The new transducer consists essentially of an extensive circular flexural vibrating plate of stepped shape driven at its center by a piezoelectrically activated

A new concept for the generation of ultrasonic energy in fluids has been introduced in recent years by means of the so-called stepped-plate transducer [13, 14]. Generation of ultrasonic energy in fluids presents problems related to the low specific acoustic impedance and high absorption of the medium. Therefore, in order to obtain an efficient ultrasonic transmission and to produce high pressure levels, it is necessary to achieve good impedance matching between the transducer and the fluid, large amplitudes of vibration and highly energy concentration. In addition, for large-scale



Stepped-plate transducer and directivity diagram

vibrator (Fig.11). The vibrator, formed by a sandwich transducer and a solid horn, is similar to the one used for applications in solids. The extensive surface of the plate increases the radiation resistance and offers the vibrating system good impedance matching with the medium. The special shape of the plate permits, despite its flexural vibration, a piston-like radiation to be obtained. As is well known, a flat-plate radiator vibrating in its flexural modes shows a poor directivity, due to phase cancellation. Nevertheless, if the surface elements vibrating in counterphase on both sides of the nodal circles are alternately shifted along the acoustic axis, half a wavelength of the radiated sound, the radiation produced will be in phase across the whole beam. Following this procedure, it is possible, with adequate modifications of the plate surface, to obtain any acoustic field configuration. Focused radiators have also been constructed [15]. Stepped-plates vibrating up to seven nodal circles and diameters up to 70 cm have been designed and constructed. In the latest version of this transducer, efficiencies of around 80%, beam width (at 3 dB) of 1.5 degrees and power, capacities of 1 kW have been attained for the frequency range 10-40 kHz. Presently a new model with one-meter diameter plate, for a power capacity of about 2-3 kW is under development.

These new transducers have to be driven by a special electronic system producing a signal lying permanently within their very narrow resonance frequency band [16].

The stepped-plate transducers have been widely tested in power applications in gases and in the interphases gas-liquid, gas-solid. Their application in liquids is a current objective.

Conclusion

As a conclusion, it is to be noted that high power ultrasonics refers to a very wide range of processes, the majority of which are still far from being successfully applied at the industrial level. To increase applications of these processes, an essential point is the development of powerful and efficient transducers to couple and distribute the acoustic energy in the medium to be treated.

References

1. Clark, A.E. (1988), "Highly magnetostrictive rare earth compounds for high power acoustic projectos" in *Power Sonic and Ultrasonic Transducers design*, B. Hamonic and J.N. Decarpigny, Springer-Verlag Berlin Heidelberg, 41-99.
2. Berlincourt D, (1971), "Piezoelectric crystals and ceramics", *Ultrasonic Transducer Materials*, (Edited by O. E. Mattiat), Plenum Press, New York, 63-124
3. Woolet R.S, (1968) "Power limitations of sonic transducers", *IEEE trans. on Sonics and Ultrasonics*, SU-15, 218-228.
4. Oswin J.R. and Maskery A., (1987) Proc. Institute of Acoustics Vo 9, part 2, 23-30

5. Sewell J.M. and Kuhn P.M (1988) *Power Sonic and Ultrasonic Transducers Design*, B. Hamonic and J.N. Decarpigny, Springer-Verlag Berlin Heidelberg, pp 134-142.
6. Campos-Pozuelo C, Gallego-Juárez J.A., (1996) "Limiting strain of metals subjected to high intensity ultrasound", *Acustica united with Acta Acustica* , Vo. 82, nº6, 1996, pp. 823-828.
7. Langevin P, French patents nº 502913 (29.5.1920), nº 505703 (5.8.1920), nº 575435 (30.7.1924).
8. Van Randeraat S, Stterington R.E. (1974) *Piezoceramic ceramics* , 2nd edition, Mullard Ltd., London.
9. Neppiras E.A., (1973) "The prestressed piezoelectric sandwich transducer", *Ultrasonics International Conference Proceedings*, pp 295-302.
10. Neppiras E.A. (1960), "Very high energy ultrasonics", *British Journal of Applied Physics*, 11, pp 143-150.
11. Ensminger D, (1988) *Ultrasonics* 2nd Edition, Marcel Dekker Inc. , New York.
12. Adachi K. and Uhea S., (1990) "Modal vibration control of large ultrasonic tools with the use of wave-trapped horns", *J. Acoust. Soc. Am.* 87, pp. 208-214.
13. Gallego Juárez J. A., Rodriguez-Corral G., Gaete-Garretón L., (1978) "An ultrasonic transducer for high power applications in gases", *Ultrasonics* 16, 6, 267-271.
14. Gallego-Juárez J.A. (1988) "High power ultrasonic transducers for use in gases and interphases" in *Power Sonic and Ultrasonic Transducers Design*, B. Hamonic and J.N. Decarpigny, Springer-Verlag Berlin Heidelberg, pp.175-184
15. Rodriguez-Corral G., San Emeterio J.L. and Gallego-Juárez J.A. (1987) "Focused high-power ultrasonic transducer with stepped-plate radiator for industrial application in gases", *Ultrasonics International Proceedings* pp. 794-799.
16. Gallego Juárez J. A., Rodriguez-Corral G., San Emeterio Prieto J.L., Montoya Vitini F., "Electroacoustic unit for generating high sonic and ultrasonic intensities in gases and interphases", U.S. Patent 5,299,175, 29 March 1994.

ELEMENTS OF ORGANIC CHEMISTRY OF INTEREST TO SONOCHEMISTS

T.J.MASON

School of Natural and Environmental Sciences

Coventry University

Coventry CV1 5FB

U.K.

1. Introduction

Within chemistry there are three main divisions: physical, inorganic and organic. Of these the least accessible to physicists and mathematicians is organic chemistry since this branch, whilst being entirely self consistent and logical to this author, is the least numerate of the three and for that reason appears to rely on few of the normal "physical" laws of science. Generally the organic chemist is primarily concerned with chemical reactivity and synthesis rather than thermodynamics and kinetics.

In broad terms organic chemistry involves reactions in the liquid phase, seldom in the gas phase and so the majority of sonochemical reactions in this field will be in the solution phase. We will therefore find that the majority of organic reactions which are influenced by ultrasound will be those which take place outside the bubble.

There are a vast number of chemical reactions which the organic chemist needs to know in order to pursue his calling. Fortunately however, in order to gain an appreciation of the possible effects of ultrasound in organic chemistry only a few basic reactions need be considered. The subject is further simplified by the need to consider the chemistry of the compounds of one main element carbon.

When the reactions of carbon compounds are cross referenced with those which appear to be influenced by ultrasound some generalisations can be made. These were first proposed by Luche some years ago and have served since then as a rough guide for sonochemists (Table 1)¹. Within these it is worth noting that there is a differentiation between the two main effects of cavitation namely chemical (generally involving radical species) and mechanical (providing powerful mixing, mass transfer and surface activation).

2. The Chemistry of Carbon Compounds

Amongst the features which make carbon so special as the building block element in organic chemistry are:

- It is unique amongst the elements in that it can form chains of C atoms all strongly (covalently) linked together as in polymers such as polythene
- It can form strong (covalent) links with a whole range of non-metallic and even some metallic elements
- The carbon chains can form rings of carbon atoms from three to tens in size (sometimes these rings include other atoms e.g. N and O)
- The arrangement of electrons in the ground state of the carbon atom is $(1s)^2(2s)^2(2p)^2$. In organic compounds carbon always has a valency 4 i.e. there are 4 electrons available for bonding to other elements. When the carbon atom does not have the equivalent of four bonds attached the species formed are reactive intermediates e.g. free radicals.

TABLE 1. Reaction which can be affected by ultrasound

Reaction type	Effect of sonication
Homogeneous	positive chemical effect if at least one step involves radical or radical ion species
Heterogeneous <i>(polar or ionic)</i>	influenced mainly through the mechanical effects of cavitation
Heterogeneous <i>(radical or radical ion)</i>	positive chemical effect on both types

3. Structure and Reactivity of "Saturated" Carbon Compounds

Carbon electrons in the $(1s)^2$ level are too low lying (close to the nucleus) to be involved in bonding. When the remaining four electrons are used to form four separate covalent (single) bonds as with hydrogen atoms in methane CH_4 so-called saturated compounds are formed. Here the electrons in the second shell $(2s)^1(2p_x)^1(2p_y)^1(2p_z)^1$ combine to produce 4 sp^3 orbitals with a *tetrahedral* arrangement of the 4 covalent bonds often referred to as sigma (σ) bonds. This gives the minimum interaction through the maximum separation of H atoms. The same bonding occurs in saturated carbon-carbon linkages of alkanes e.g. ethane ($\text{CH}_3\text{-CH}_3$) and the end groups can rotate around the axis of such bonds. The C-C single bond length is 1.54\AA ($1\text{\AA} = 10^{-10}$ metre).

In a symmetrical compound such as ethane the electron distribution in the C-C bond will be totally symmetrical however in a covalent bond between carbon and any other element the distribution will be unsymmetrical i.e. the bond will

be polarised this is termed the *Inductive Effect*. Thus in a C-Cl bond the greater electronegativity of Cl drags electrons away from the C atom to give unequal covalent bond with the C having a slightly positive charge ($\delta+$) and the Cl slightly negative ($\delta-$). In simple terms, using the abbreviated Periodic Table shown below, elements to right give C ($\delta+$) and elements to the left give C ($\delta-$) except for C-H which is considered to give zero charge on the C atom. Thus $\text{H}_3\text{C}^{(0)} - {}^{(0)}\text{CH}_3$; $\text{H}_3\text{C}^{(\delta+)} - {}^{(\delta-)}\text{Cl}$ and $\text{H}_3\text{C}^{(\delta-)} - {}^{(\delta+)}\text{Li}$.

Table 2a. Abbreviated Periodic Table of the Elements

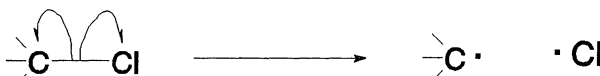
H							
He	Li	Be	B	Ca	N	O	F
Ne	Na	Mg	Al	Sn	P	S	Cl
			K				Br
							I

In order for saturated compounds to react bond breakage must occur. The two processes leading to bond fission are *Heterolytic Fission* which generates ions and *Homolytic Fission* which leads to radicals. These processes are represented below:



HETEROLYTIC FISSION

both electrons go to one atom resulting in the formation of a very reactive carbon cation and a chloride ion



HOMOLYTIC FISSION

one electron goes to each atom resulting in the formation of two free radical species

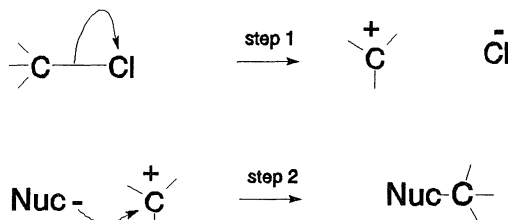
Note that in these formalised representations of reaction mechanisms a double headed arrow represents movement of both electrons together while a single headed arrow represents only a single electron movement.

4. Classification of Reagents

<i>Electrophile</i>	a species deficient in electrons which seeks electron rich centres e.g. groups with +ve charge H^+ , NO_2^+ , Br^+
	or Lewis acids, electron pair acceptors BF_3 , AlCl_3 , FeBr_3
<i>Nucleophile</i>	a species rich in electrons seeking electron deficient centres e.g. groups with -ve charge OH^- , Cl^- , Br^- or Lewis bases, electron pair donors :NH_3 , H_2O^- ; alcohols

5. Sonochemical Reactions Involving Covalent Bonds

5.1 NUCLEOPHILIC DISPLACEMENT REACTIONS



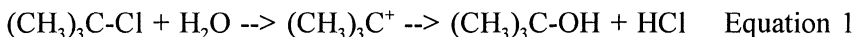
TWO STEP reaction via the formation of high energy carbocation



ONE STEP reaction which avoids the generation of a carbocation

In general these reactions involve the breaking of covalent bonds and the mechanism depends upon whether the high energy carbocation intermediate species which would be produced by direct heterolytic fission of the bond has any transient stability. In this case a two step reaction occurs where the first produced carbocation is rapidly attacked by any nucleophile present. When the carbocation is highly unstable another reaction route is possible via direct displacement of the leaving group by the nucleophile avoiding the formation of a discreet carbocation. These are but two extreme situations which might exist during nucleophilic displacement and for any individual system the true

mechanism may well be considered to be leaning towards one of these extremes rather than actually following one process specifically. Whichever process is followed any assistance by cavitation is more likely to be outside the bubble (mechanical) rather than inside. Nevertheless there are some remarkable effects observed in this domain. Consider for example the homogeneous hydrolysis reaction of tert-butyl chloride in aqueous ethanol (Equation 1)².



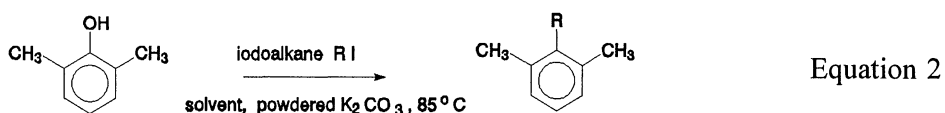
In 40% aqueous ethanol a comparison of results at two different temperatures reveal that sonication has more effect at the lower temperature. This would fit with the idea that cavitation collapse would be more energetic at lower temperatures. In fact this increased effectiveness of sonication at the lower temperature leads to the other remarkable finding that under sonication it is possible to achieve an increase in reaction rate with a drop in temperature - a result which appears to be completely against "classical" thermodynamics but explicable through sonochemistry.

Table 2b. Hydrolysis of tert-Butyl Chloride
in 40% (w/w) Ethanol/Water

	Rate Constant $\times 10^5$	25°C	10°C
k_{ult}		11.4	17.2
k_{non}		6.8	0.86
ratio		1.7	20.0

Where k_{non} = conventional "silent" rate constant and k_{ult} = rate constant in presence of ultrasound (20 kHz)

In some cases the assistance provided by sonication to a nucleophilic displacement reaction can be seen to be mainly mechanical in origin. Such is the case with the alkylation of the phenol below (Equation 2) where the neighbouring methyl groups hinder the O atom which is to be alkylated³.



Under normal stirred conditions the phenol in contact with powdered solid base (K_2CO_3) produces the phenoxide anion ($C_6H_5O^-$) which then acts as a

nucleophile in the displacement of iodine from the iodoalkane. The reaction is slow and after several hours effectively comes to a stop. This is almost certainly due to an inactivation of the powdered base through a coating of salts and can be remedied by the use of ultrasound which provides efficient continuous surface cleaning.

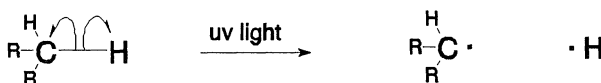
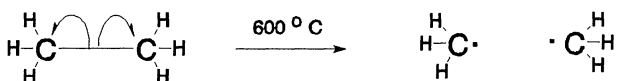
TABLE 3. Yield of Alkylated Phenol after 1.5 hours at 65°C

iodoalkane (R-I)	Yield % (stir, 1.5h)	Yield % (stir + sonicate)
iodomethane	45% (60% after 4h)	90%
1-iodopropane	33% (45% after 4h)	95%

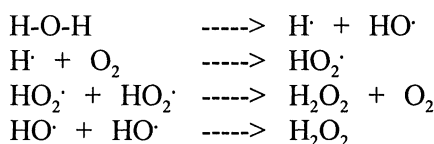
Solvent = N-methylpyrrolidinone, 20 kHz probe system

5.2 RADICAL REACTIONS - HETEROLYTIC FISSION

In classical organic chemistry covalent bonds can be broken to form radicals using heat or light. Heterolytic fission can also be achieved through sonochemistry and such reactions are typified by the sonochemical degradation of hydrocarbons. Reactions of this type which involve radical species are the ones which are most prone to ultrasonic enhancement.

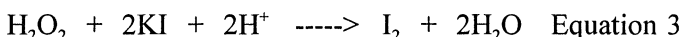


The sonochemical reaction most frequently quoted for radical production is the sonolysis of water in the cavitation bubble a simplified scheme for which is shown below. The initial homolytic fission of the H-O bond is followed by a whole series of other radical reactions.



Here the water molecule initially fragments to H· and HO· radicals under the extreme conditions experienced in the cavitation bubble. A whole range of reactions can take place subsequently one of which is the production of H₂O₂ hydrogen peroxide a common oxidant. It is the decomposition of water from which are derived the most frequently used forms of chemical dosimetry for sonochemistry. These are (a) the oxidation of iodide ion to iodine and (b) methods based on the trapping of the free radical species HO· as they emerge from the bubble. The latter will be dealt with later in this chapter.

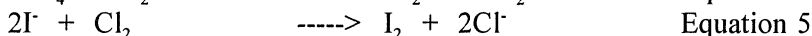
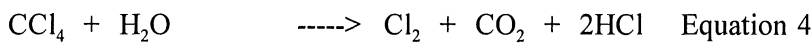
Iodine dosimetry is based upon the oxidation of iodide ion by the hydrogen peroxide generated by sonolysis of water (Equation 3).



The iodine liberated can then be analyzed quantitatively either:

- by direct spectroscopic observation of the solution through the intensity of the iodine absorption band at (350 nm) or
- by titration of the iodine liberated with a standard solution of sodium thiosulphate using starch as an indicator.

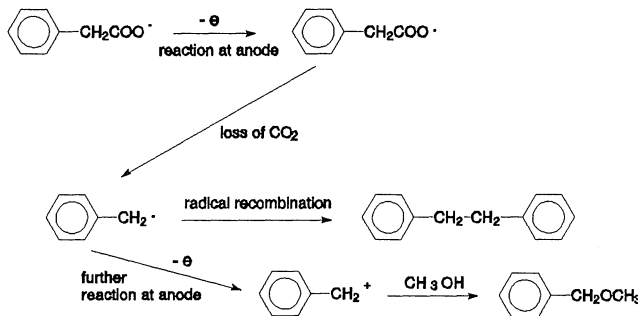
The yield of iodine is usually quite small when the reaction is carried out using pure aqueous potassium iodide solution. In order to increase the iodine yield i.e. the sensitivity of the reaction a saturated aqueous solution of carbon tetrachloride is sometimes used in place of water as the solvent (Weissler's solution). When this solution is sonicated the normal oxidation process occurs together with the generation of chlorine from the heterolytic breakdown of CCl₄ in the bubble (Equation 4). The chlorine itself then acts as an oxidising agent for iodide ion (Equation 5).



5.2.1 The Generation of Radicals and Cations via Electrochemistry

Another method of generating reactive species is via electrochemistry whereby the transfer, or removal, of electrons generates reactive intermediates at the electrode surface. A good example of such a process is the electrolysis of a carboxylic acid anion (RCOO⁻) which loses one electron to the positively charged electrode to which it is attracted (this is a single electron process). The carboxylate radical which results loses CO₂ and is thus converted into a hydrocarbon radical (R·). Once formed the radical readily recombines with another to generate a dimeric species (R-R), this is the Kolbe reaction. Alternatively the radical, while still close to the anode surface, will give up

another electron to form a carbocation (this is a two electron process) which can then be attacked by any nucleophile solvent present e.g. methanol to give an ether ($\text{R}-\text{OMe}$). Consider the case of the Kolbe electrolysis of phenylethanoic acid anion⁴.



Under normal conditions this electrolysis does not occur due to the formation of a layer of non-conducting material which builds up on the electrode surface. Classically this problem is solved by the addition of pyridine to the reaction medium which dissolves the coating. Both single electron (dimer) and two electron (ether) products are generated. For this reaction it is interesting to note that applying ultrasound has the same effect as pyridine in that the continuous surface cleaning engendered by cavitation near the surface prevents the build-up of the non-conducting layer and allows the reaction to proceed without the need for the potentially harmful pyridine additive (Table 4). The other benefit of using ultrasound is the marked drop in voltage (from 6.6V to 7.9V) required to maintain the steady current of 200 mA representing an overall energy saving in the process.

TABLE 4. Kolbe Electrolysis of Phenylethanoic Acid

Product	Yield % with pyridine (silent)	Yield % no pyridine (sonicated)
Ph-CH ₂ -CH ₂ -Ph single electron process	59.8	52.7
Ph-CH ₂ -OCH ₃ two electron process	21.1	32.3

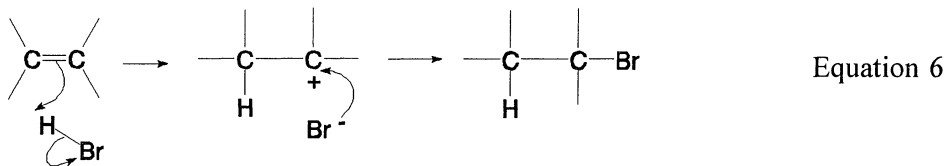
Pt electrodes, 100 mA/cm², 7.9V silent, 6.6V with 38kHz (bath)

6. Structure and Reactivity of "Unsaturated" Compounds - Alkenes

6.1 IONIC ADDITION

When the four electrons of carbon in the second shell are used to form an unsaturated "double bond" linkage, as is the case for ethene ($\text{H}_2\text{C}=\text{CH}_2$), three covalent bonds are formed at each carbon using an sp^2 combination of orbitals (one 2s and two 2p electrons). The maximum separation for these bonds is produced with an angle of 120° . Each carbon has one of its 2p electrons spare so these overlap to form what is termed a π bond. The resulting bonding between the carbons consisting of a σ and a π bond is stronger and shorter (1.35 Å) than a simple covalent bond. The π clouds of electrons above and below plane prevent rotation and make it a rigid structure.

The reactions of carbon-carbon double bonds differ from those of single bonds in that being electron rich they are open to attack by electrophilic species (positively charged ions or free radicals) giving addition reactions. In the case of the addition of the polarised HBr to an alkene the H^{8+} end of the molecule adds first to produce a carbocation which is highly reactive and readily attacked by the remaining Br^- anion. The product is a saturated bromoalkane (Equation 6).

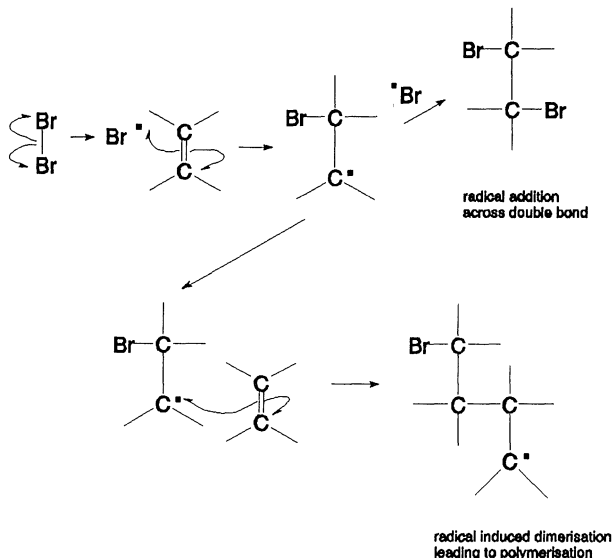


When the compound adding to the alkene is already ionised (e.g. H^+ and I^- from hydroiodic acid) the mechanism is very similar except that a discrete H^+ adds first to give the carbocation which is then attacked by I^- .

6.2 RADICAL ADDITION

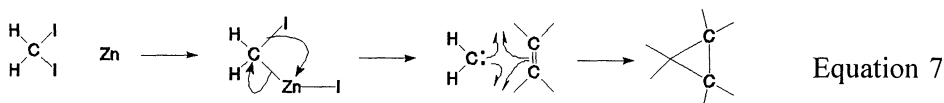
In the case of the addition of a radical species to the double bond the initial product is itself a carbon free radical. Thus the homolytic fission of Br_2 generates a carbon radical which then undergoes a radical recombination reaction with a further Br to give a dibromide. An alternative possibility for the carbon radical is that it can undergo a series of successive additions of alkene molecules to generate a polymer although the recombination of the larger carbon radical with an alkene is less likely than bromine recombination. Radical polymerisation is however a valuable means of generating polymers when the radical species is in such low concentration that the carbon radical formed initially has a greater

chance of combining with another alkene rather than another radical (see below).



6.3 CARBENE ADDITION

There is another radical type species which can be added to a double bond. This species is essentially a neutral carbon atom which has only two covalent bonds attached and therefore two electrons "free" rather than the single electron of a radical. The two electrons are capable of forming two separate covalent bonds with a double bond - the result of which is a three membered carbon ring (cyclopropane). A number of ways exist to make these highly reactive transient intermediates one of the most common of which uses a metal to remove halogens from a halocarbon. Thus zinc reacts with CH₂I₂ by essentially pulling off an iodine atom to generate the carbene :CH₂ in what is known as a Simmons-Smith reaction (Equation 7).



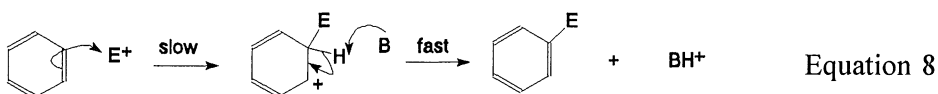
This is another example of a reaction which is significantly assisted by ultrasound. The generation of the carbene type intermediate depends on the reaction between the organic compound and the metal surface. Conventional methods of increasing the reactivity of the metal involve careful cleaning with

solvent and/or reduction of the metal to a smaller particle size giving greater surface area. If powdered zinc is used however it can become too reactive and the reaction could "run away". Using ultrasound zinc can be used in the form of solid lumps because the surface effects of cavitation permit rapid and immediate reaction at the surface (through continuous cleaning and activation). Without ultrasound the reaction at the large surface slows considerably and so the overall reaction rate can be controlled through switching the ultrasound on and off.

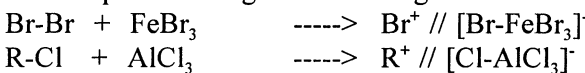
7. Structure and Reactivity of "Unsaturated" Compounds - Aromatics

When double bonds are arranged alternately with single covalent bonds an extra degree of stability is introduced to the system which is due to resonance energy. The most significant example of this is benzene which is some 150 kJmol⁻¹ more stable than the calculated energy based on the presence of three isolated double bonds in the molecule. Compounds which contain one or more benzene rings are collectively known as aromatics.

The extra stability of benzene is revealed when its reactivity is compared with that of alkenes. It is much more difficult to hydrogenate even though it is electron rich, it does not easily react with electrophiles unless they themselves are very reactive. An important reaction for aromatics is the replacement of hydrogen by another group through substitution by an active electrophile E⁺ (Equation 8).

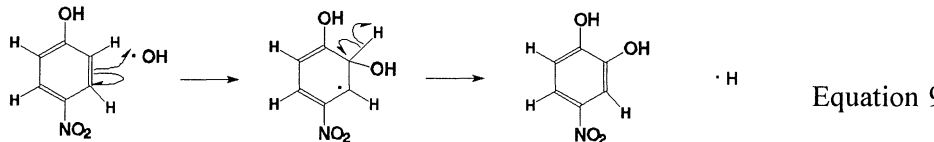


An example of this is provided by alkylation where a catalyst of the Lewis Acid type which pulls a halogen atom and generates a cation thus:

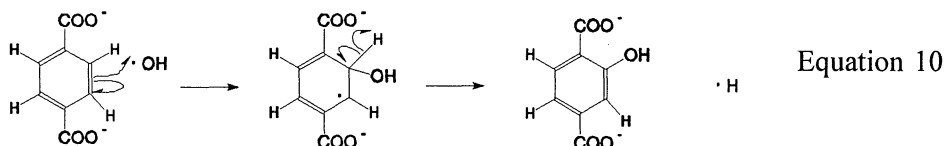


The overall substitution is termed a Friedel Craft alkylation and is typical of a range of substitutions where electrophile activation is required.

Free radicals can also react with aromatic systems and this type of reaction has been used as a method of dosimetry in sonochemistry. If an aqueous solution of 4-nitrophenol is sonicated then cavitation collapse in the water generates hydroxy radicals which, when they enter the bulk solution can react with the aromatic compound to form a hydroxylated compound (Equation 9).



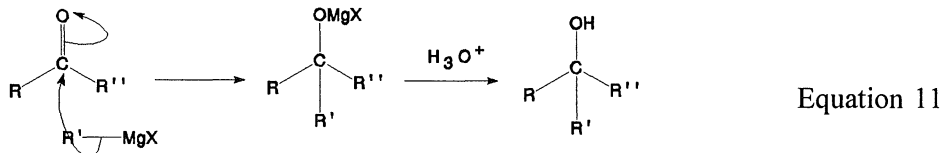
Aqueous 4-nitrophenol has a ultraviolet maximum at 401 nm and the hydroxylated product at 512 nm. It is therefore possible to quantify the number of hydroxy radicals formed during sonication by observing the amount of product formed. Another dosimeter which operates on the principal of trapping the hydroxy radicals liberated is aqueous terephthalate anion. This yields hydroxyterephthalate, a fluorescent material (Equation 10).



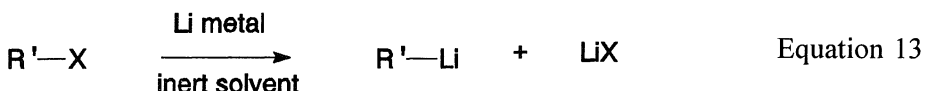
The fluorescence generated by the product is measured at 425 nm using an excitation wavelength of 315 nm. The method is extremely sensitive and has been used as a method of estimating the cavitation threshold using medical ultrasonic instrumentation.

8. Structure and Reactivity of "Unsaturated" Compounds - the carbon-oxygen double bond.

The C=O bond, like the C=C bond is electron rich with clouds of π -electrons. Unlike the C=C bond however it is permanently polarised with a small positive charge on the carbon atom and small negative charge on the oxygen. This makes the C=O (carbonyl) group subject to attack by nucleophiles including the addition of organometallic compounds which is particularly important in synthesis.



Typical amongst such syntheses is the preparation of alcohols from the addition of an organomagnesium (Grignard) reagent. Essentially this involves the attack of $R'MgX$ (R' =alkyl group) on a carbonyl compounds $RCOR''$ ($R''=H$ or alkyl group) followed by quenching with acid (Equation 11).



The formation of organometallic reagents from organic halides has been of great interest (Equation 12) especially those factors which influence initiation. A long-standing problem associated with Grignard reagent synthesis is that in order to facilitate reaction between the organic halide and the metal in an ether solvent all of the reagents must be dry and the surface of the magnesium must be clean and oxide free. Such conditions are difficult to achieve and so many methods of initiating the reaction have been developed most of which rely on adding activating chemicals to the reaction mixture. Magnesium activation is rather easy by sonication, even in damp solvents.

Organolithiums can be obtained in good yields from primary alkyl bromides although secondary and tertiary alkyl bromides require longer reaction times (Equation 13). For a large number of organometallic syntheses there is an induction period which can make these reactions somewhat hazardous when performed on an industrial scale. Sonication usually reduces the induction period or even completely suppresses it.

9. Conclusions

Although organic chemistry is both a broad and deep subject there are a few types of reaction which are particularly susceptible to sonochemical effects. Within this short chapter it is hoped that the non-specialist reader will be able to appreciate at least some of these facets of organic chemistry.

References

1. Mason, T.J. and Luche, J-L., Ultrasound as a new tool for synthetic chemists, *Chemistry under Extreme or Non-classical Conditions*, ed R.van Eldick and C.D.Hubbard, John Wiley, New York, 1997, 317.
2. Mason T.J. Lorimer, J.P. and Mistry, B.P., *Tetrahedron*, 41, 5201 (1985)
3. Mason, T.J., *Practical Sonochemistry, A users guide to applications in chemistry and chemical engineering*, Ellis Horwood Publishers, Chichester, 1991.
4. Walton, D.J. and Phull, S.S., Sonoelectrochemistry, *Advances in Sonochemistry*, ed. T.J.Mason, JAI Press, London, 1996, 4, 205.

SINGLE BUBBLE SONOCHEMISTRY

T. LEPOINT¹, F. LEPOINT-MULLIE¹, A. HENGLEIN²

1. Institut Meurice-CERIA, 1, Avenue E. Gryzon, 1070 Brussels,
Belgium.

2. Hahn-Meitner Institut, 14109 Berlin, Germany

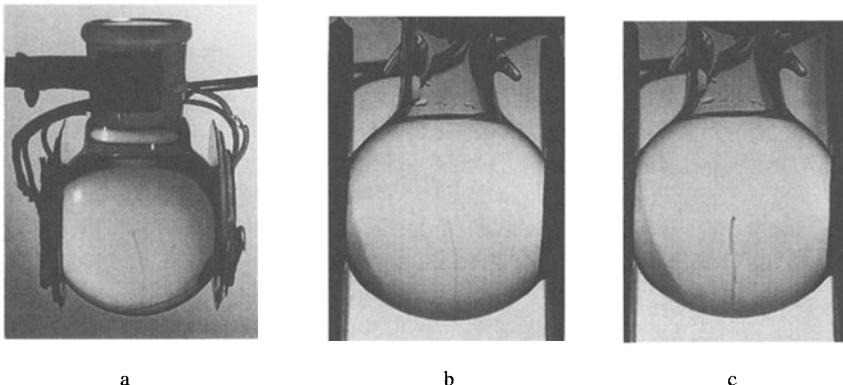
1. Introduction

Until recently, SL has often been studied in the case of inertial (transient) cavitation [1,2] although a correlation 'SL/bubble dynamics' has been difficult and relatively inaccurate. These drawbacks -associated with multi-bubble fields- are due to the fact that, under these conditions, bubbles of different sizes are loosely coupled and their growth and collapse are somewhat random. Most interesting are the recent findings on single bubbles maintained in levitation in a resonant acoustic set-up [3] -an acoustic energy concentration factor equal to ~11 orders of magnitude [4], the shortness of the SL flash [4,5] (< 50ps), the clock-like emission [4], the appearance of the flash within 500 ps near maximum collapse, the sensitivity to noble gases [6] and the non-sphericity of the bubble at the time of emission [7]. This considerable progress in the knowledge of SL is due to the fact that single bubbles constitute very controllable systems [8]. Up to now, the sonochemical activity of cavitating media [9,10,11] has only been described in the case of multi-bubble clouds (stable [12] and inertial cavitation; aqueous and organic [13,14] solutions). We report here that single bubbles in levitation are also chemically active. A dosimetry is reported in the case of Weissler's system. The interest to use chemical species as tracers for the investigations of liquid flow around single bubbles will be reported with more details elsewhere.

2. Visual observations

We describe two experiments in which a single air bubble is driven (Undatim Ultrasonics generator) in a solution of Weissler's reagent [15], *i.e.* the direct visualisation of chemical activity and the dosimetry of iodine produced by such a levitating bubble. Concerning visualisation, we used a 175 ml spherical flask driven at 24.1 kHz onto which two PZT transducers were glued laterally and face to face (cell diameter: 64 mm) and partially degassed solutions which were prepared as follows: 200 ml of 1 M NaI and 10 ml of an aqueous solution of starch (4g/L) to which 20 ml of a saturated aqueous solution of CCl₄ (kept under vacuum) was added. An air bubble was introduced by means of a glass capillary. Bubble behaviour previously reported by Gaitan et al. [3] was observed, *i.e.* for increasing acoustic stress (i) the position of the bubble at the centre of the cell, (ii) the dancing motion of the bubble (the "to-and-fro" motion around the equilibrium position without any apparent emission of small bubbles from the parent bubble - observation via a Leica MS5 stereomicroscope), (iii) the formation of a "shuttlecock" structure (a levitating cluster of small bubbles moving around the

parent bubble), (iv) the apparent stabilization of the bubble and, finally, the sonoluminescent emission.



Photograph 1. *a*, General view of the 24.1 kHz resonant cell (the case of the dancing bubble in levitation; acoustic pressure: ~ 1.3 atm; space between the two lateral PZT transducers: 57 mm; volume of solution: 175 ml). The filament originating from the center of the cell indicates the complexation reaction between starch and I_2 produced through the oxydation of I^- anions by $Cl(\cdot)$ radicals arising from the intracavity decomposition of CCl_4 (Weissler system [15]). *b*, Pattern associated with a dancing bubble at 43.1 kHz (space between PZT transducers: 36 mm). *c*, Idem than in *b* but with the shuttlecock structure (remark the broader filament). The distance between the thread extremities is from 1 to 2 cm. No sonoluminescence was detected for *a*, *b* and *c* (dancing or shuttlecock bubbles; sensitivity of the PMT: 3×10^{-11} lm for a signal-on-noise = 10).

In photograph 1a we report the situation associated with a frequency of 24.1 kHz and a low acoustic pressure (P_{ac} estimated to 1.3 ± 0.1 atm; Brüel and Kjaer 8103 hydrophone, diameter: 10 mm, length: 30 mm, frequency range: 0.1 to 100 kHz, sensitivity: $26.9 \mu V/Pa$). This corresponds to a dancing bubble (before the formation of a "shuttlecock" structure). Such an entity is able to dance for several hours, during which its translation motion does not exceed a few hundreds μm . In our case we did not detect any sonoluminescence (Hamamatsu R446 photomultiplier tube; voltage 1 kV (anode sensitivity = 400 A/lm; dark current = 0.3 nA/lm at 100 A/lm); the estimated sensitivity: 3×10^{-11} lm for a signal-on-noise = 10). However a chemical reaction did occur. In fact, a single weak blue thread was seen that originated at the bubble, so indicating that I_2 had been formed by the oxidation of I^- and that the I_2 then complexed with starch. This filament formed in a direction that was likely to change during the experiment (i.e. upwards or downwards). The origin of this change in direction remains elusive though visual observations lead us to suspect that dusts trapped at the bubble surface (secondary Bjerknes force) could play a role. The time taken for the formation of the thread over a few centimeters was about one minute.

The production of I_2 may be attributed to the oxidation of I^- by the $Cl(\cdot)$ atoms released by the bubble (decomposition of CCl_4). A strong chemical activity occurred under "shuttlecock" regime ($P_{ac} \sim 1.7$ atm). When the acoustic pressure was increased still further the bubble stabilised and the blue thread tended to become much less intense than under shuttlecock conditions. However it should be noted

that a chemical activity was maintained in this regime for which a single bubble is stable for hours and (as pointed out by other authors [3,8]) no sonoluminescence could be detected. At still higher intensities, strong SL appeared, with the number of photons per burst (N) in the UV-visible range being about 1.3×10^4 ($T = 20 \pm 1$ °C; mean value of the integrated electric charge measured through a 50Ω resistance for one burst (Q): 1.9×10^{-11} C; total surface of irradiation (S in m^2): $4\pi (95 \times 10^{-3})^2$; PMT gain (g): 6×10^7 ; first dynode efficiency (E_d): 0.9; q = electron charge; cathode efficiency (E_c): 0.1; surface of PMT window(s_w): $1.92 \times 10^{-4} m^2$; $N = (Q.S)/(g E_d q E_c s_w)$). The blue thread could be detected by means of the naked eye, but with less intensity than under shuttlecock regime. This qualitative observation tends to suggest that optimum sonochemical activity is not coincident with maximum sonoluminescence. Moreover as emphasized above, in the stable non-sonoluminescing regime (the so-called "bouncing" regime [8]) there was a weak chemical activity. Unfortunately, at the present time, we have not succeeded in determining the amount of iodine produced by such a stable non-luminescing bubble. We therefore decided to focus on the chemical characterisation of the sonoluminescent and shuttlecock bubbles.

3. Dosimetry.

In order to perform the comparative dosimetry of iodine (shuttlecock vs SL regime) we used a 30 ml spherical flask (43.1 kHz; cell diameter: 36 mm; same configuration than in the case of the 24.1 kHz reactor). The solutions were analyzed by a Perkin Elmer Lambda 2 UV-visible spectrophotometer. Firstly, for solutions prepared as described above we obtained the results plotted in Figure 1 (curves (a): shuttlecock regime; (b) SBSL, $N = (4 \pm 2) \times 10^3$ in the visible range for $T = 21 \pm 1$ °C; (c) reference). The advantage of this procedure involving starch was the visual control in the chemical activity of the bubble (see photographs 1b and c).

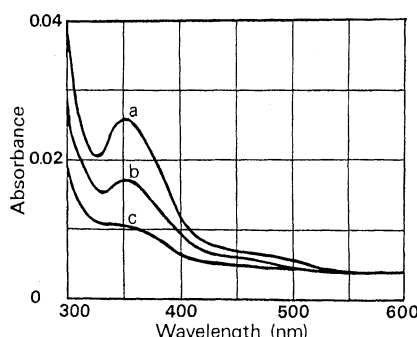


Figure 1. Comparison of the absorption spectra after 2 hours of insonation in presence of starch (see text for the procedure of preparation): (a) shuttlecock regime, (b) sonoluminescent regime (number of photons measured in the visible range: $(4 \pm 2) \times 10^3$); (c) reference solution, i.e. insonation without bubble.

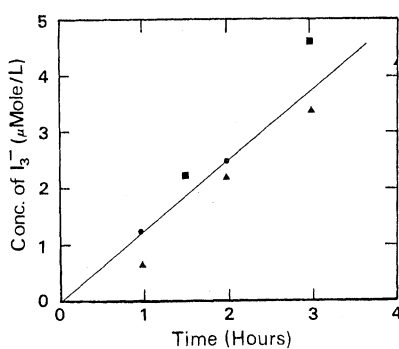


Figure 2. Kinetics associated with a shuttlecock structure pulsating in a 1M NaI solution saturated with CCl_4 . Dosimetry was carried out on the absorption band of I_3^- at $\lambda = 350$ nm ($\epsilon = 25,000 M^{-1}cm^{-1}$).

In the case of the shuttlecock regime, assuming no side-reactions and using appropriate calibration curve (absorbance read at 350 nm) we deduced that the number of Cl atoms released in the solution per acoustic cycle (N_{Cl}) was $\sim 10^8$ and that, under SL conditions $N_{\text{Cl}} \sim 4 \times 10^7$.

Secondly, we analysed the chemical activity of a shuttlecock structure pulsating in a starch-free solution prepared with 200 ml of 1 M NaI solution partially degassed, and to which 5 ml of CCl₄ were added (vigorous manual agitation during 3 min; filtration and sonification). The amount of I₃⁻ was determined from the absorption band at $\lambda = 350$ nm ($\epsilon = 25,000 \text{ M}^{-1} \text{ cm}^{-1}$). Under these conditions no stable bubble could form. From Figure 2, it can be deduced that the maximum number of Cl (-) released in the solutions is $\sim 3 \times 10^8$ over an acoustic cycle. The fact that, in the absence of CCl₄ we did not detect any measurable amounts of iodine implies that CCl₄ was involved in the rate determining step through the intracavity cleavage of the C-Cl bond [15] (energy of dissociation of C-Cl in CCl₄ = 292.6 kJ/mole ~ 3 eV). The substitution of the volatile (vapour pressure $p_v = 100 \text{ mm Hg}$ at $T = 23^\circ\text{C}$) and hydrophobic CCl₄ solute by a hydrophilic chlorinated compound, i.e. chloral hydrate which is freely soluble in water ($p_v = 10 \text{ mm Hg}$ at $T = 20^\circ\text{C}$; with a concentration $-5 \times 10^{-3} \text{ M}$ corresponding to the saturation concentration of CCl₄ in water) also fails to produce detectable amounts of iodine. This observation emphasizes the importance of the hydrophobic and volatile character that a chlorinated compound must have in order to participate efficiently in the Weissler reaction.

Both the facts were unexpected that (i) sonochemistry may occur for acoustic pressures lower than those required to trigger off SL (in particular, in the case of a stable non-sonoluminescent bubble, even if the chemical activity was weak) and (ii) dosimetry reveals that chemical activity of non-luminescent shuttlecock bubbles is greater than for luminescing cavities. Indeed, in the past, Flynn [16] developed the argument according to which the relatively good parallelism observed experimentally between the sonochemical and sonoluminescent activities was indicative of a common origin for multi-bubble SC and SL. Our observations suggests that this argument cannot be transposed to the case of a single bubble, i.e. the conditions giving rise to SC and SL are different either in nature or in intensity.

4. Flows around a levitating bubble: preliminary results.

The appearance of a blue thread instead of a halo in the immediate vicinity of either a shuttlecock structure or a single sonoluminescing bubble may arise from several scenarios, i.e. (i) global streaming due to thermal gradients caused by external factors and/or the loss of energy from the sound wave, the heat flow between rarefaction and the compression in the sound wave (entropy increase), (ii) acoustic streaming due to the absorption of the acoustic wave by the medium. In this latter case, the momentum absorbed from the acoustic field manifests itself as a flow of the liquid in the direction of the sound field. The two other possibilities are related to the presence of a bubble, i.e. (iii) microstreaming arising from the frictional forces between a boundary (an obstacle such as a levitating bubble) and the medium carrying the vibrations [17], and (iv) the formation of one [18-20] (or more [21]) inward jets.

In the absence of a levitating bubble, we carefully released a small amount a red organic water-soluble dye -i.e. fuchsin- near the center of the 24.1 kHz cell by means of a flat-tip syringe in order to check possibilities (1) and (2). The syringe was very

slowly introduced to, and removed from, the solutions. The velocity with which a fuchsin spot fell under the influence of gravity ($180 \pm 20 \mu\text{ms}^{-1}$; $110 \pm 40 \mu\text{ms}^{-1}$, respectively) in the cell depended only little on whether the ultrasonic field was on or off. On the other hand, the presence of a shuttlecock or a stable bubble systematically induced the repulsion of the dye in the form of an at least 5 mm streak. Though released very near either the bubble or the shuttlecock structure, the dye was excluded from a radius of at least $\sim 2\text{-}3$ mm. These experimental observations led us to conclude that possibilities (iii) and/or (iv) played a major role in our experimental conditions.

Concerning the dancing and shuttlecock bubbles, a possibility for the development of a streak of colour arising from chemical reactions could be either microstreaming near the bubble interface or the formation of an inward jet which could expel the chemically active species in a preferential direction; both mechanisms could also be involved. The appearance of surface oscillations (previously reported by Gaitan et al. [3]) under dancing and shuttlecock regimes is likely to be associated with microstreaming of regime III and/or IV according to the Elder's nomenclature [22] and, consequently, the preferential orientation of chemical species. Concerning the stable (sonoluminescing or non-sonoluminescing) bubbles, the formation of an inward jet as suggested by Longuet-Higgins and Oguz [18], Longuet-Higgins [19] or Prosperetti [20] is likely (see also Benjamin and Ellis [23], and Lauterborn [24]).

5. Conclusion.

In conclusion, we wish to emphasize here that (i) a stable non-luminescing bubble is chemically active, (ii) the intensity regimes of strong chemical activity and the strong sonoluminescence of a single bubble are clearly separated from each other, (iii) the sonochemical activity of a single levitating bubble may be quantified, (iv) sonochemistry may provide information on the dynamics of levitating bubbles as well as of the neighbouring fluid. Our observations should be important for the interpretation of chemical and luminescent effects of acoustic cavitation. For example, the present investigations indicate implicitly that the experimental determinations of the extreme intracavity conditions based on SL spectral distributions (intracavity temperature(s), pressure(s), electronic densities, etc.) should not be transposed or extrapolated to sonochemical studies. It is noteworthy that single bubble sonochemistry is highly controllable. Consequently levitating bubbles under their different regimes of chemical activity will offer a unique probe for the study of a possible correlation "SC/SL/bubble dynamics" since the dimension and shape of levitating cavities may be connected with reaction kinetics and spectral emission distributions. A careful analysis of the flows of liquids around a bubble with chemical species as tracers - is the subject of another paper [25].

Acknowledgments

F. Lepoint-Mullie and T. Lepoint are very indebted to Prof. M. S. Longuet-Higgins for very fruitful discussions and acknowledge Mrs. N. Voglet for assistance with the analytical measurements, Mr. F. Hendrickx for the photographs and the Fonds National de la Recherche Scientifique for financial support.

They are also very indebted to Prof. L.A. Crum for his great confidence.

References.

1. Walton, A.J. and Reynolds, G.T. (1984) Sonoluminescence, *Adv. Phys.* **33**, 595-660.
2. Verrall, R.E. and Sehgal, C. (1988) Sonoluminescence, in K.S. Suslick (ed.), *Sonochemistry: Its Chemical, Physical and Biological Effects*, VCH publishers, New York, pp. 227-286.
3. Gaitan, D.F., Crum, L.A., Church, C.C. and Roy, R.A. (1992) Sonoluminescence and bubble dynamics for a single stable, cavitation bubble, *J. Acoust. Soc. Am.* **91**, 3166-3183.
4. Barber, B. P. and Putterman, S.J. (1991) Observation of synchronous picosecond sonoluminescence, *Nature* **352**, 318-320.
5. Barber, B.P., Hiller, R., Arasika, K., Fetterman, H. and Putterman, S.J. (1992) Resolving the picosecond characteristics of synchronous sonoluminescence, *J. Acoust. Soc. Am.* **91**, 3061-3063.
6. Hiller, R., Weninger, K., Putterman, S.J. and Barber, B. P. (1994) Effect of noble gas doping in single-bubble sonoluminescence, *Science* **266**, 248-250.
7. Weninger, K., Putterman, S.J. and Barber, B. P. (1996) Angular correlations in sonoluminescence: Diagnostic for the sphericity of a collapsing bubble, *Phys. Rev. E* **54**, 2205-2208.
8. Barber, B.P., Hiller, R.A., Löfstedt, R., Putterman, S.J., Weninger, K.R. (1997) Defining the unknowns of sonoluminescence, *Phys. Rep.* **281**, 65-143.
9. Suslick, K. S. (1988) Homogeneous sonochemistry, in K.S. Suslick (ed.), *Ultrasound: Its Chemical, Physical and Biological Effects*, VCH, New York, pp. 123-163.
10. Henglein, A. (1993) Contributions to Various Aspects of Cavitation Chemistry, in T.J. Mason (ed.), *Advances in Sonochemistry*, JAI Press, London, Vol. 3, pp17-83.
11. Leighton, T. G. (1994) *The Acoustic Bubble*, Academic Press, London, pp. 464-495.
12. Henglein, A. (1954) Chemische Wirkungen von kontinuierlichen und implusmodulierten hörbaren Schallwellen, *Z. Naturforsch.* **10B**, 20-26.
13. Schulz, R. and Henglein, A. (1953) Über den Nachweis von freien Radikalen, die unter dem Einfluß von Ultraschallwellen gebildet werden, mit Hilfe von Radikal-Kettenpolymerisation und Diphenyl-pikryl-hydrazyl, *Z. Naturforsch.* **B8**, 160-161.
14. Suslick, K.S., Gawienowski, J.J., Schubert, P.F. and Wang, H.H. (1983) Alkane sonochemistry, *J. Phys. Chem.* **87**, 2299-2301.
15. Weissler, A., Cooper, H. W. and Snyder, S.J. (1950) Chemical effect of ultrasonic waves: Oxidation of potassium iodide solution by carbon tetrachloride, *J. Am. Chem. Soc.* **72**, 1769-1775.
16. Flynn, H.G. (1964) Physics of acoustic cavitation in liquids, in W.P. Mason (ed.), *Physical Acoustics*, Academic Press, New York, Vol. 1, Part B, pp. 57-172.
17. Kolb, J. and Nyborg, W. (1956) Small-scale acoustic streaming in liquids, *J. Acoust. Soc. Am.* **28**, 1237-1242.
18. Longuet-Higgins, M.S. and Oguz, A. (1995) Critical microjet in collapsing cavities, *J. Fluid Mech.* **290**, 183-201.
19. Longuet-Higgins, M.S. (1996) Shedding of vortex ring by collapsing cavities, with application to single-bubble sonoluminescence, *J. Acoust. Soc. Am.*, **100**, 2678 (This reference is the abstract of a lecture presented at the 132th. meeting of the Acoustical Society of America, Honolulu, Hawaii, 2-6 December 1996; manuscript submitted).
20. Prosperetti, A. (1997) A new mechanism for sonoluminescence, *J. Acoust. Soc. Am.*, **101**, 2003-2007.
21. Lepoint, T., De Pauw, D., Lepoint-Mullie, F., Goldman, M. and Goldman, A. (1997) Sonoluminescence: an alternative "electrohydrodynamic" hypothesis, *J. Acoust. Soc. Am.*, **101**, 2013-2030.
22. Elder, S.A. (1959) Cavitation microstreaming, *J. Acoust. Soc. Am.* **31**, 54-64.
23. Benjamin, T.B. & Ellis, A.T. (1966) The collapse of cavitation bubbles and the pressures thereby produced against solid boundaries, *Phil. Trans. R. Soc. Lond.* **A260**, 221-240.
24. Lauterborn, W. (1974) General and Basic Aspects of Cavitation, in L. Bjorno (ed.), *Finite-Amplitude Wave Effects in Fluids*, IPC Sci. Technol. Press, Guilford, pp. 195-202.
25. T. Verraes, F. Lépoint-Mullie, T. Lepoint, iExperimental study of the liquid flow near a single sonoluminescent bubble, submitted

APPLICATIONS OF SONOCHEMISTRY TO MATERIALS SYNTHESIS

K.S. SUSLICK, M.M. FANG, T. HYEON, M.M. MDLELENI

Department of Chemistry

University of Illinois at Urbana-Champaign

601 S. Goodwin Ave., Urbana, IL 61801, USA

1. Introduction

One of the most important recent applications of sonochemistry has been to the synthesis and modification of inorganic materials [1-5]. In liquids irradiated with high intensity ultrasound, acoustic cavitation drives bubble collapse producing intense local heating, high pressures, and very short lifetimes; these transient, localized hot spots drive high energy chemical reactions [5-11]. As described in detail elsewhere in this monograph, these hot spots have temperatures of roughly 5000°C, pressures of about 1000 atmospheres, and heating and cooling rates above 10^{10} K/s. Thus, cavitation serves as a means of concentrating the diffuse energy of sound into a unique set of conditions to produce unusual materials from dissolved (and generally volatile) solution precursors.

Ultrasonic cavitation in liquid-solid systems produces related phenomena. Cavity collapse near an extended solid surface becomes non-spherical, drives high-speed jets of liquid into the surface, and creates shockwave damage to the surface [11]. This process can produce newly exposed, highly heated surfaces and is responsible for the erosion/corrosion problems associated with hydrodynamic cavitation [12]. Furthermore, during ultrasonic irradiation of liquid-powder slurries, cavitation and the shockwaves it creates can accelerate solid particles to high velocities [13, 14]. As discussed later, the interparticle collisions that result are capable of inducing striking changes in surface morphology, composition, and reactivity [1-5, 14].

There is a wide range of chemical and physical consequences that high intensity can induce, as shown schematically in Figure 1. The chemical effects of ultrasound fall into three areas: homogeneous sonochemistry of liquids, heterogeneous sonochemistry of liquid-liquid or liquid-solid systems, and sonocatalysis (which overlaps the first two). Applications of ultrasound to materials chemistry are found in all of these areas. Chemical reactions are not generally seen in the ultrasonic irradiation of solids or solid-gas systems.

To demonstrate the utility of sonochemistry in materials synthesis, we will examine a range of applications discovered at the University of Illinois. Specifically, we will describe the sonochemical synthesis and heterogeneous catalytic studies of nanostructured amorphous iron and alloys, nanostructured Fe on silica, nanocolloids of Fe, and nanostructured Mo₂C and MoS₂. In addition, we will summarize earlier studies on the effects of high intensity ultrasound on slurries of inorganic solids.

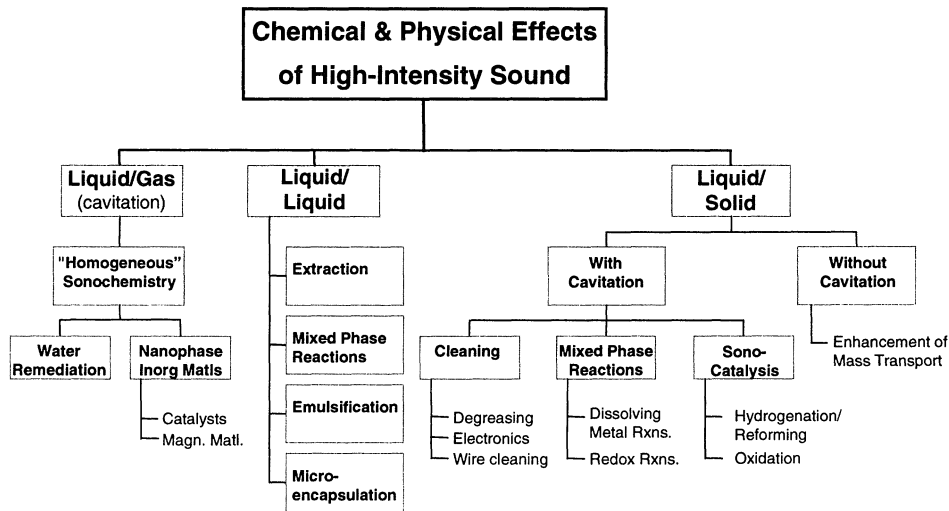


Figure 1. Classification of the chemical and physical effects of ultrasound.

2. Synthesis of Nanostructured Inorganic Materials

Solids made from nanometer sized components often exhibit properties distinct from those of the bulk, in part because clusters that small have electronic structures that have a high density of states, but not yet continuous bands [15-17]. Such nanostructured materials have been a matter of intense current interest, and several preparative methods have been developed for their synthesis. Nanostructured material syntheses include both gas phase techniques (e.g., molten metal evaporation, flash vacuum thermal and laser pyrolysis decomposition of volatile organometallics), liquid phase methods (e.g., reduction of metal halides with various strong reductants, colloid techniques with controlled nucleation), and mixed phase approaches (e.g., synthesis of conventional heterogeneous catalysts on oxide supports, metal atom vapor deposition into cryogenic liquids, explosive shock synthesis). To this range of techniques, over the past ten years we have added the sonochemical reactions of volatile organometallics as a general approach to the synthesis of nanophase materials, as shown in Figure 2.

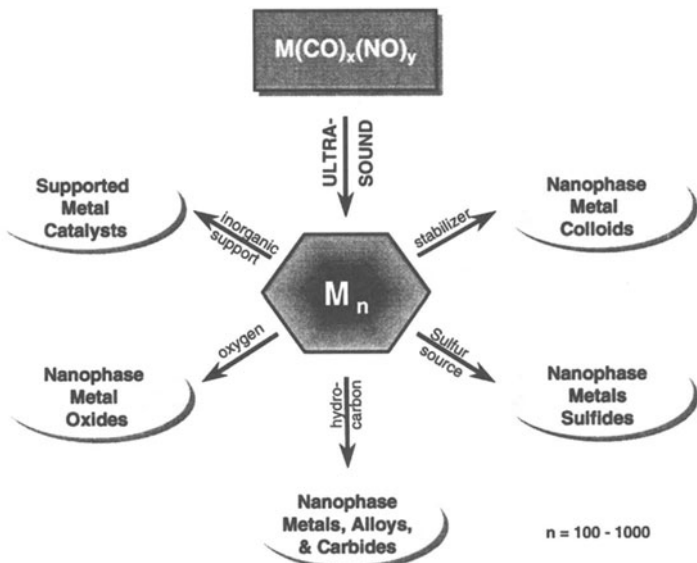


Figure 2. Sonochemical synthesis of nanostructured materials.

Using these extreme conditions, we have produced a variety of nanostructured and often amorphous metals, alloys, and carbides and examined their catalytic activity [1-4, 18-33]. Volatile organometallic compounds decompose inside a collapsing bubble, and the resulting metal atoms agglomerate to form nanostructured materials. Our sonochemical synthesis of nanostructured materials is also extremely versatile: various forms of nanophase materials can be generated simply by changing the reaction medium (Figure 2). When precursors are sonicated in high boiling alkanes, nanostructured metal powders are formed. If sonication occurs in the presence of a bulky or polymeric surface ligand, stable nanophase metal colloids are created. Sonication of the precursor in the presence of an inorganic support (silica or alumina) provides an alternative means of trapping the nanometer clusters. These nanoparticles trapped upon these supports produce active supported heterogeneous catalysts.

2.1. EXPERIMENTAL CONSIDERATIONS

High-intensity ultrasonic probes [50 to 500 W/cm²] of the type used for biological cell disruption are the most reliable and effective source for laboratory-scale sonochemistry. A typical apparatus that permits easy control over ambient temperature and atmosphere is shown in Fig. 3. Lower acoustic intensities can often be used in liquid-solid heterogeneous systems, because of the reduced liquid tensile strength at the liquid-solid interface. For such reactions, a common ultrasonic cleaning bath will therefore often suffice. The low intensity available in these devices [≈ 1 W/cm²], however, can prove

limiting. In addition, the standing wave patterns in ultrasonic cleaners require accurate positioning of the reaction vessel. On the other hand, ultrasonic cleaning baths are easily accessible, relatively inexpensive, and useable on moderately large scale. Finally, for larger scale irradiations, flow reactors with high ultrasonic intensities are commercially available in modular units of as much as 20 kW [34, 35].

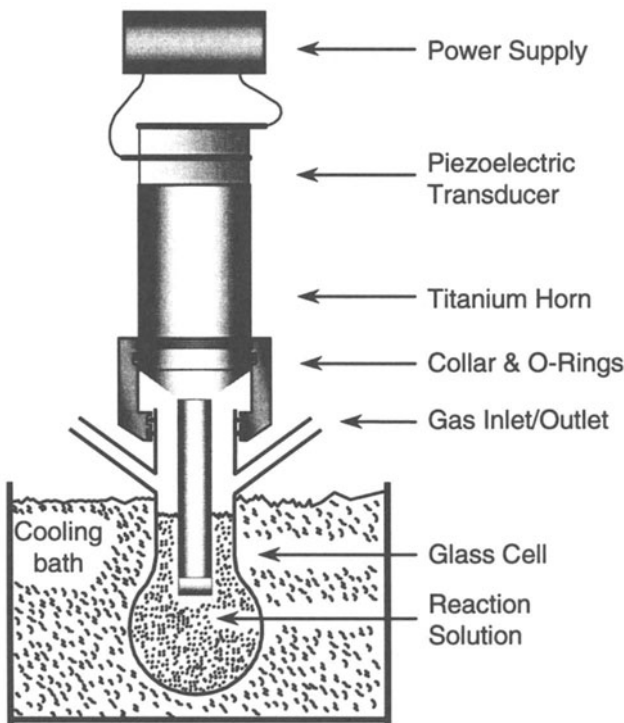


Figure 3. A typical sonochemical apparatus with direct immersion ultrasonic horn. Ultrasound can be easily introduced into a chemical reaction with good control of temperature and ambient atmosphere. The usual piezoelectric ceramic is PZT, a lead zirconate titanate ceramic. Similar designs for sealed stainless steel cells can operate at pressures above 10 bar.

Sonochemical decomposition rates for volatile organometallic compounds depend on a variety of experimental parameters such as vapor pressure of precursors, solvent vapor pressure, and ambient gas. In order to achieve high sonochemical yields, the precursors should be highly volatile since the primary sonochemical reaction site is the vapor inside the cavitating bubbles [36]. So that decomposition takes place only during cavitation, thermal stability is also important. In addition, the solvent vapor pressure should be low at the sonication temperature, because significant solvent vapor inside the bubble reduces the bubble collapse efficiency.

2.2. AMORPHOUS METALS

The ultrasonic irradiation of solutions containing volatile transition metal carbonyls (e.g., $\text{Fe}(\text{CO})_5$, $\text{Ni}(\text{CO})_4$, $\text{Co}(\text{CO})_3\text{NO}$) produces highly porous aggregates of nanometer-sized clusters of amorphous metals [18-21]. For example, sonication of 1 M iron pentacarbonyl in decane at 0 °C under argon flowing yielded a dull black powder. Elemental analysis of the powder, after heating at 100 °C under vacuum to remove residual solvent, showed it to be >96 % iron by weight, with trace amounts of carbon (<3%) and oxygen (1%, by difference), presumably from the decomposition of alkane solvent or carbon monoxide during ultrasonic irradiation. Scanning electron micrographs (SEM) revealed that the powder is an agglomerate of 20 nm particles (Figure 4). Transmission electron micrographs (TEM) further indicated that these 20 nm particles consist of smaller 4~6 nm particles.

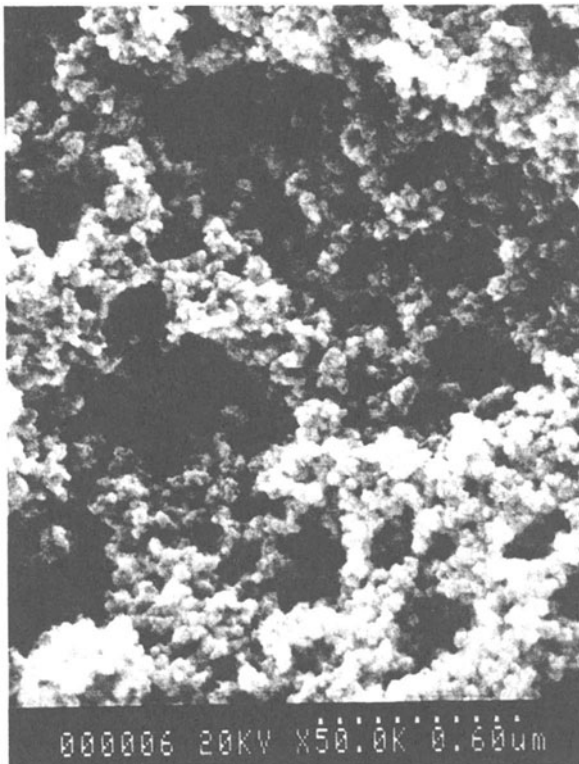


Figure 4. Amorphous iron prepared by the sonochemical decomposition of $\text{Fe}(\text{CO})_5$ [18].

The amorphous nature of the iron powder was confirmed by several different techniques, including SEM, differential scanning calorimetry (DSC), electron microdiffraction, X-ray powder diffraction, and neutron diffraction. Initial X-ray powder diffraction showed no diffraction peak; after heat treatment under helium at 350

$^{\circ}\text{C}$ the diffraction lines characteristic of bcc iron metal are observed. Electron microdiffraction revealed a diffuse ring pattern, characteristic of amorphous materials. DSC also shows one exothermic irreversible disorder-order transition temperature at 308 $^{\circ}\text{C}$. The amorphous metal formation appears to result from the extremely high cooling rate during acoustic cavitation.

There had been a long-standing controversy concerning the magnetic properties of amorphous iron, which had not been previously available without substantial amount of added alloying elements (e.g., boron). Magnetic studies of the sonochemically prepared amorphous iron showed that amorphous iron is a very soft ferromagnetic with a saturation magnetization of ≈ 173 EMU/g and a Curie temperature in excess of 580K. The effective magnetic moment is $1.7 \mu_{\text{B}}$ with an effective exchange constant of only $\approx 30\%$ of crystalline Fe [20]. The neutron diffraction data [21] confirmed these measurements and was consistent with a random packing model, as in many thin amorphous metal films. The magnetic properties fall close to those of liquid iron.

2.3. NANOSTRUCTURED ALLOYS

Sonochemical techniques can also be used to prepare nanostructured alloys. We chose Fe/Co alloys as a demonstration case because $\text{Fe}(\text{CO})_5$ and $\text{Co}(\text{CO})_3(\text{NO})$ were readily available as precursors that are thermally stable at the modest bulk solution temperatures necessary for high volatility. The composition of the Fe-Co alloys can be controlled simply by changing the ratio of solution concentrations of the precursors; alloy compositions ranging from pure Fe to pure Co are readily obtained [23-25].

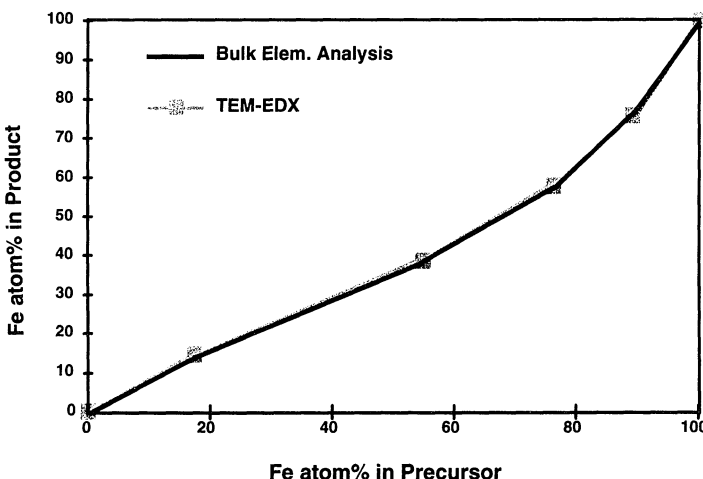


Figure 5. Bulk and nanometer Energy Dispersive X-ray (EDX) analysis of Fe/Co alloys prepared sonochemically from $\text{Fe}(\text{CO})_5$ and $\text{Co}(\text{CO})_3\text{NO}$ [23].

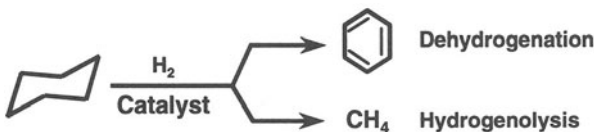
The solid-solution nature of the alloys was confirmed by Energy Dispersive X-ray (EDX) measurements. Analyses made on various nanometer spots showed that the alloys were homogeneous on a nanometer scale and were consistent with bulk elemental analysis (Figure 5). The Fe, Co, and Fe-Co alloys produced by ultrasound are initially amorphous, as determined by XRD and electron-beam microdiffraction. After heat treatment under H₂ gas flow at 400°C for 2 hours, all samples underwent crystallization. The XRD results show no peaks attributable to iron/cobalt oxide, iron/cobalt carbide or other iron/cobalt impurity phases. Pure Fe crystallizes to cubic (bcc) structure, and pure Co crystallizes to cubic (fcc) and hexagonal (hcp) mixed structures. All the alloys that we have tested so far crystallize in the bcc structure. This result is consistent with the known Fe-Co equilibrium phase diagram that strongly favors the bcc structure. Elemental analysis results show that nearly pure metal and alloys are produced after H₂ treatment. SEM at high magnification indicates that these materials are porous aggregates of small clusters of 10-20 nm particles. Surface electronic structures and surface compositions of the sonochemically prepared Fe-Co alloys were also examined by using x-ray photoelectron spectroscopy (XPS). The XPS measurements have been performed on heat-treated samples before catalytic reactions. The electronic structures of the surfaces of these samples appear to be the same as the pure metals. The surface compositions of the alloys demonstrate a slight enrichment of Fe over Co. Similar trends towards an iron-enriched surface have been reported by other researchers with other preparations using coprecipitation methods [37].

Heterogeneous catalysts containing two metals often show unusual activity or selectivity for a wide range of industrially important reactions [38-40]. For this reason, we made catalytic studies of the sonochemically prepared Fe-Co alloys for hydrocarbon dehydrogenation and hydrogenolysis reactions. In general, dehydrogenation of hydrocarbons is the important and desirable reaction, and hydrogenolysis (to methane generally) is a wasteful side-reaction. Unfortunately, most metals (with the notable exception of Pt and other noble metals) are much too active as hydrogenolysis catalysts to be commercially useful. The suppression of hydrocarbon cracking during dehydrogenation remains an important challenge for non-platinum catalysts.

All catalysts were treated under H₂ gas flow at 400°C for 2 hours before the catalytic studies. While this does not alter the size of the clusters that make up the nanostructure of these materials significantly, it does cause their crystallization. H₂ treatment is necessary, however, to provide a reproducible catalytic surface. Two kinds of products were formed during the cyclohexane reaction: benzene from the dehydrogenation reaction and aliphatic hydrocarbons (mostly methane) from the hydrogenolysis. The catalytic selectivity (in terms of the percentage of benzene among all the reaction products) as a function of temperature is shown in Figure 6.

The catalytic properties of the sonochemically prepared Fe, Co and Fe-Co alloys in the cyclohexane reaction exhibit interesting trends. First, they are all active catalysts for cyclohexane conversion: pure Co has the highest activity (albeit primarily for hydrogenolysis), pure Fe has the lowest activity, and Fe-Co alloys are intermediate. Second, Fe-Co alloys generate much more dehydrogenation product (benzene) than pure Fe or Co. Third, the 1:1 Fe/Co alloy has both much higher dehydrogenation activities and selectivities at all reaction temperatures (250°C to 300°C) than the other

alloys or pure metals. In the best cases, the selectivity for dehydrogenation approaches 100%. We believe that the increase in selectivity comes from a selective poisoning of the sites responsible for hydrogenolysis. Fe/Co alloys prepared conventionally with very high purity do *not* show high selectivity for dehydrogenation *unless* they are pre-treated with methane or carbon monoxide at high temperatures in order to deposit a small amount of surface carbon. The sonochemical preparations inevitably produce catalysts with small amounts of surface carbon and hence with high dehydrogenation selectivity.



	Hydrogenolysis	Dehydrogenation
Product	Methane	Benzene
Surface structure	Sensitive	Insensitive
Active site	Ensemble of metal atoms	Single metal atoms
Active catalyst	Ru, Os, most metals	Pt

Figure 6. Catalytic dehydrogenation versus hydrogenolysis.

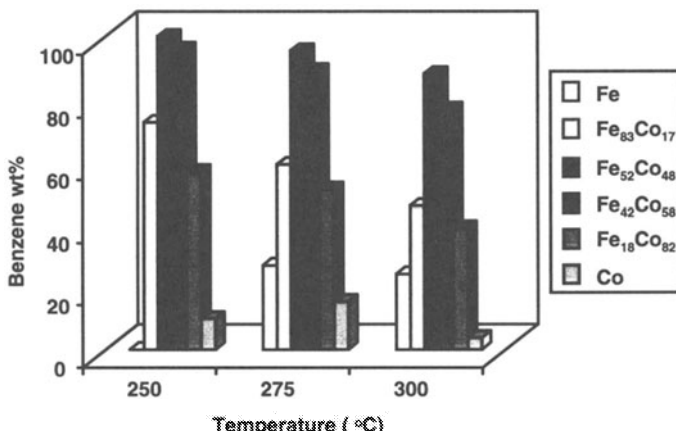


Figure 7. Selectivity for cyclohexane dehydrogenation (to benzene) over hydrogenolysis (to methane) by sonochemically prepared Fe/Co alloys [23].

2.4. NANOSTRUCTURED SUPPORTED “EGGSHELL” CATALYSTS

Most heterogeneous metal catalysts are supported, i.e., the metal is deposited on a high surface area solid, such as silica or alumina. In general, these materials are made by taking simple metal salts (usually the nitrates), soaking aqueous solutions of them into the porous support, and calcining under hydrogen at high temperatures to produce small metal particles throughout the support. Often, the metal particles are not very uniform and are dispersed throughout the ill-defined pore structure of the support. The creation of “eggshell” catalysts where uniform-sized nanoparticles of metals are deposited on the outer surface of supports has potential advantages for catalyst preparation [40].

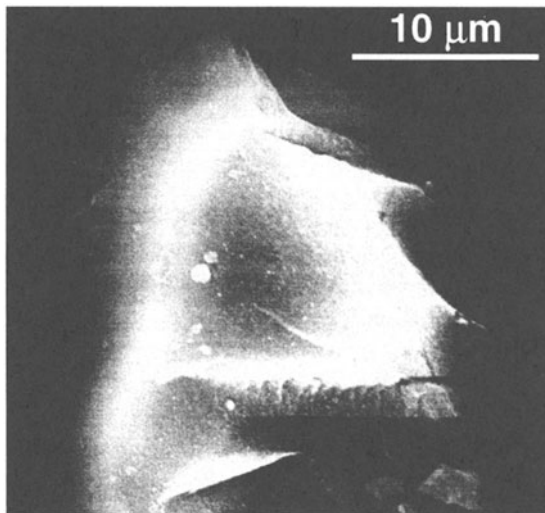
Ultrasonic irradiation of decane solutions of iron pentacarbonyl, $\text{Fe}(\text{CO})_5$, in the presence of silica gel produces a silica-supported amorphous nanostructured iron in which the iron particles are all on the outer surface of the silica [23, 28]. The iron particles are formed during cavitation events and then deposited on the silica suspended in solution. The iron loading on the SiO_2 can be easily varied by changing the initial concentration of the $\text{Fe}(\text{CO})_5$ solution. Elemental analysis reveals Fe, Si, O and a trace amount of carbon (<1%) to be present.

The amorphous nature of these supported iron particles as initially deposited has been confirmed by several different techniques, including DSC, XRD, and electron-beam microdiffraction. DSC shows one irreversible exothermic transition at 335°C corresponding to a disorder-order transition (i.e., crystallization) of the amorphous iron. X-ray powder diffraction shows no diffraction peaks from the initial products. After heat treatment under He at 400°C for 4 hours (sufficient to induce crystallization), the lines characteristic of α -Fe metal are observed, and no peaks can be attributed to iron oxide, iron carbide or other iron-based phases. Electron microdiffraction by transmission electron microscopy (TEM) confirms these observations.

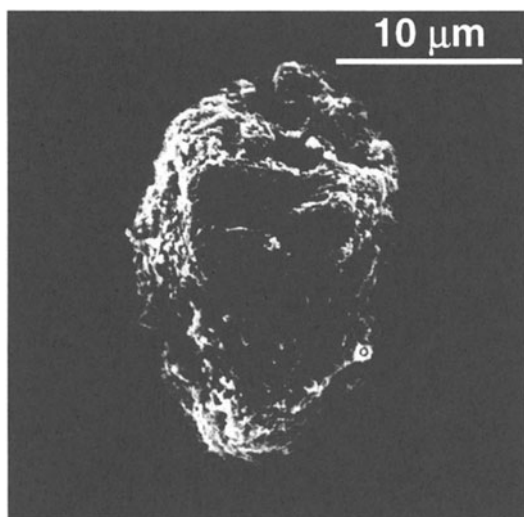
The TEM showed that the iron particles produced by sonolysis of $\text{Fe}(\text{CO})_5$ were highly dispersed on the SiO_2 surface. The iron particles range in size from 3 to 8 nm; CO chemisorption measurement data at -78°C on our samples gives an average iron particle size of 7 nm. The particles are on the surface of the silica only, which gives a very different surface morphology to the silica compared to a conventionally prepared catalyst (Figure 8).

The catalytic activity of the silica supported nanostructured iron was probed in the commercially important Fischer-Tropsch synthesis reaction (i.e., hydrogenation of CO). Under our conditions, the major reaction products for both catalysts are short-chain C₁ to C₄ hydrocarbons and CO₂. The catalytic activity of the sonochemically produced iron on silica catalyst is an order of magnitude higher than the conventional supported iron at similar loadings and dispersions. Moreover, the silica-supported nanostructured iron catalyst exhibits high activity at low temperatures (<250°C), where the conventional catalyst has no activity. The dramatic difference in activity between the two samples below 300°C may be due to the amorphous nature of iron and the inherently highly-defected surface formed during sonolysis of $\text{Fe}(\text{CO})_5$ when the amorphous state of iron is preserved. At higher temperatures, the activity decreases, which may be due to iron crystallization, surface annealing, or catalyst deactivation

from surface carbon deposition.



Conventionally Prepared Catalyst



Sonochemically Prepared "Eggshell" Catalyst

Figure 8. Scanning electron micrographs of conventionally and sonochemically prepared iron catalysts supported on silica.

2.5. NANOCOLLOIDS

The existence of aggregates of nanometer clusters in our sonochemically prepared materials suggests the possibility of trapping these particles before they aggregate. Colloids of ferromagnetic materials are of special interest due to their many important technological applications as ferrofluids [41, 42]. Such magnetic fluids find uses in information storage media, magnetic refrigeration, audio reproduction, and magnetic sealing. Commercial magnetic fluids are generally produced by exhaustive grinding of magnetite (Fe_3O_4) in ball or vibratory mills for several weeks in the presence of surfactants, which produces a very broad particle size distribution [41, 42]. We have developed a new method for the preparation of stable ferromagnetic colloids of iron using high intensity ultrasound to sonochemically decompose volatile organometallic compounds [31]. These colloids have narrow size distributions centered at a few nanometers and are found superparamagnetic.

Sonochemical decomposition of iron pentacarbonyl in the presence of stabilizers such as polyvinylpyrrolidone or oleic acid produced a colloid of nanometer sized iron particles [31]. Transmission electron micrographs show that the iron particles have a relatively narrow range in size from 3 to 8 nm for polyvinylpyrrolidone, while oleic acid gives an even more uniform distribution at 8 nm (Figure 9). Electron microdiffraction revealed that the particles are amorphous on the nanometer scale as formed and that after *in situ* electron beam heating these particles crystallize to bcc iron.

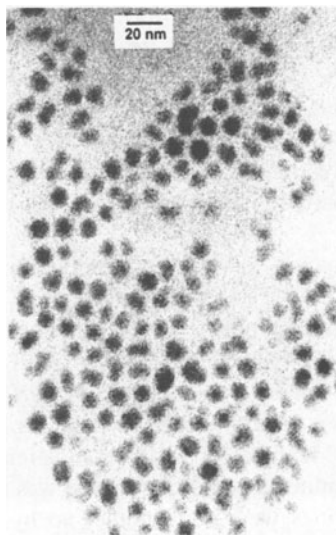


Figure 9. Transmission electron micrograph of sonochemically-prepared iron colloid stabilized by oleic acid [31].

Magnetic studies indicate that these colloidal iron particles are superparamagnetic with a saturation magnetization of a respectable 101 emu/g (Fe) at 290K. High saturation magnetization is desirable for magnetic fluid application and is highly sensitive to the method of preparation. Bulk amorphous Fe saturates at 156 emu/g (Fe) [20, 21, 30]. For a comparison, the saturation magnetization of a commercial magnetite-based magnetic fluid is 123 emu/g (Fe) (Ferrofluids Corp., Cat. #APG-047)

2.6. NANOSTRUCTURED MOLYBDENUM CARBIDE

Molybdenum and tungsten carbides have been explored as heterogeneous catalysts because of the similarity in activity that these carbides share with platinum group metals [43-45]. For catalytic applications, high surface-area materials are generally needed, but the refractory nature of these carbides makes this very difficult. Boudart and Völpe prepared carbides of molybdenum and tungsten with high surface areas by a complex temperature programmed carburization of the corresponding nitrides. We have developed a simple sonochemical synthesis of nanoparticle molybdenum carbide from the ultrasonic irradiation of molybdenum hexacarbonyl [25-29].

Sonochemical decomposition of molybdenum hexacarbonyl in hexadecane produced a black powder. After heat treatment at 450°C under He flow for 12 hours, peaks in the XRD were observed at d spacing values of 2.39 Å, 1.49 Å, and 1.27 Å, which match very well with face centered cubic (fcc) molybdenum carbide, Mo₂C. The formation of molybdenum carbide can be explained by the disproportionation of carbon monoxide on the active metal surface to form carbon and carbon dioxide. Small amounts of residual oxygen were removed by treating the solid with 1:1 CH₄/H₂ mixture at 300 to 500 °C for 48 h. The elemental analysis results showed that the sample had a stoichiometry of Mo₂C_{1.02} with less than 0.09 wt. % oxygen (by difference) and <0.02 wt. % hydrogen. The XRD was essentially unchanged by carburization. SEM showed that the surface is extremely porous. TEM revealed that the material is a porous aggregate of 3 nm diameter particles (Figure 10); BET gas adsorption showed a surface area of 130 m²/g.

Again, the dehydrogenation versus hydrogenolysis of cyclohexane served as our standard reaction using a flow catalytic microreactor. To compare the catalytic properties, commercial ultrafine powders of platinum and ruthenium (Aldrich Chemicals Co., 0.27 - 0.47 µm diameter) were also used under identical conditions, after heating at 400°C for 3 h under H₂ flow to remove surface contaminants. Figure 11 shows the catalytic activity as a function of temperature for the Mo₂C sample pretreated under CH₄/H₂ at 500 °C for 48 hours compared to commercial ultrafine Pt powder.

At all reaction temperatures examined, benzene was the only product formed for both samples and their activities were comparable: no hydrogenolysis products were detected. In contrast, only hydrogenolysis, mostly to methane, occurred with commercial ruthenium powder. The analogy has often been made that Mo₂C is similar to Ru whereas W₂C behaves like Pt [46]. These results demonstrate, however, that for dehydrogenation of alkanes, sonochemically prepared nanostructured molybdenum carbide has selectivity similar to Pt rather than to Ru.

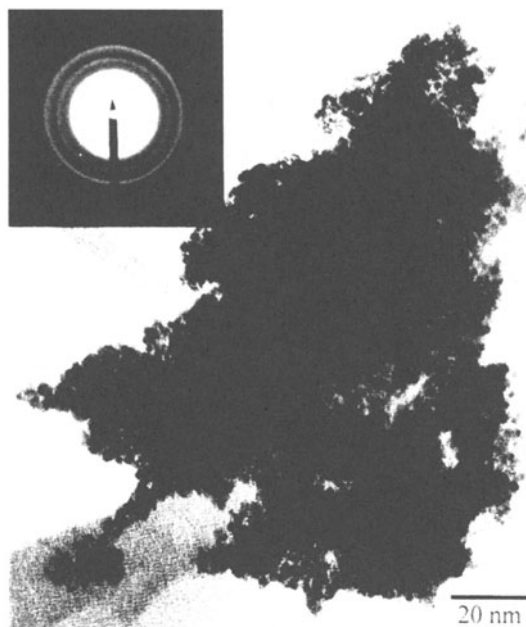


Figure 10. TEM and electron microdiffraction of sonochemically prepared Mo_2C .

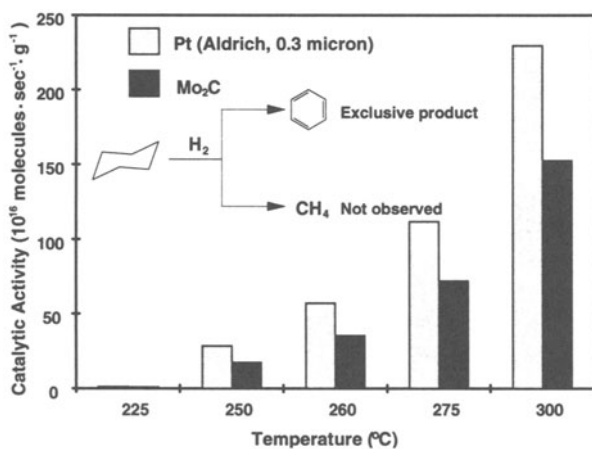


Figure 11. Catalytic activity of sonochemically prepared Mo_2C compared to Pt [27].

2.7. NANOSTRUCTURED MOLYBDENUM SULFIDE

Very recently, we have reported the sonochemical synthesis of nanostructured molybdenum sulfide. MoS_2 is best known as the standard automotive lubricant; its lubricant properties are due to its layered structure. Planes of molybdenum atoms are sandwiched on both faces by planes of sulfur atoms tightly bonded to the Mo. Interactions between the sulfur planes are weak, thus producing lubrication properties similar to graphite. Of greater interest here, however, MoS_2 is also the predominant hydrodesulfurization catalyst heavily used by the petroleum industry to remove sulfur from fossil fuels before combustion [39].

We prepared an unusual morphology of MoS_2 by the irradiation of solutions of molybdenum hexacarbonyl and sulfur in 1,2,3,5-tetramethylbenzene with high intensity ultrasound [33]. The MoS_2 was amorphous as initially prepared, but subsequently crystallized upon heating at 450°C for 10 h under an atmosphere of flowing He. EDX analysis performed on these particles gave a S/Mo atomic ratio of 2.06, identical within experimental error to bulk chemical analysis. The morphologies of the sonochemical and conventional MoS_2 , however, are dramatically different, as shown in Figure 12. Conventional MoS_2 shows a plate-like morphology typical for such layered materials. The sonochemical MoS_2 exists as a porous agglomeration of clusters of spherical particles with an average diameter of 15 nm.

Despite the morphological difference between the sonochemical and conventional MoS_2 , TEM images (Figure 13) of these sulfides both show lattice fringes with interlayer spacings of 0.62 ± 0.01 nm, the same as conventional MoS_2 [47]. The sonochemically prepared MoS_2 , however, shows much greater edge and defect content, as the layers must bend, break or otherwise distort to fit outer surface of the 15 nm particle size (Fig. 13).

It is well established that the activity of MoS_2 is localized at the edges and not on the flat basal planes [39, 48]. Unfortunately, the nature of this layered material causes the basal planes to dominate the total surface area under most synthetic conditions. Given the inherently higher edge concentrations in nanostructured materials, the catalytic properties of our sonochemically prepared MoS_2 become especially interesting. To this end, the catalytic activity and selectivity for thiophene HDS by sonochemically prepared MoS_2 was examined in a single-pass microreactor [33]. Conventional MoS_2 , sonochemical Mo_2C , commercial ReS_2 (Gallard-Schlesinger Ind., Carle Place, NY), and RuS_2 (Gallard-Schlesinger) were also investigated under the same conditions for comparison. For conventionally prepared sulfides, ReS_2 and RuS_2 are inherently more reactive than MoS_2 [48], but are too expensive to be generally used. Given the difference in edge versus basal surface activity, catalytic activity does not correlate with total surface area and therefore comparisons must be made on a catalyst mass basis.

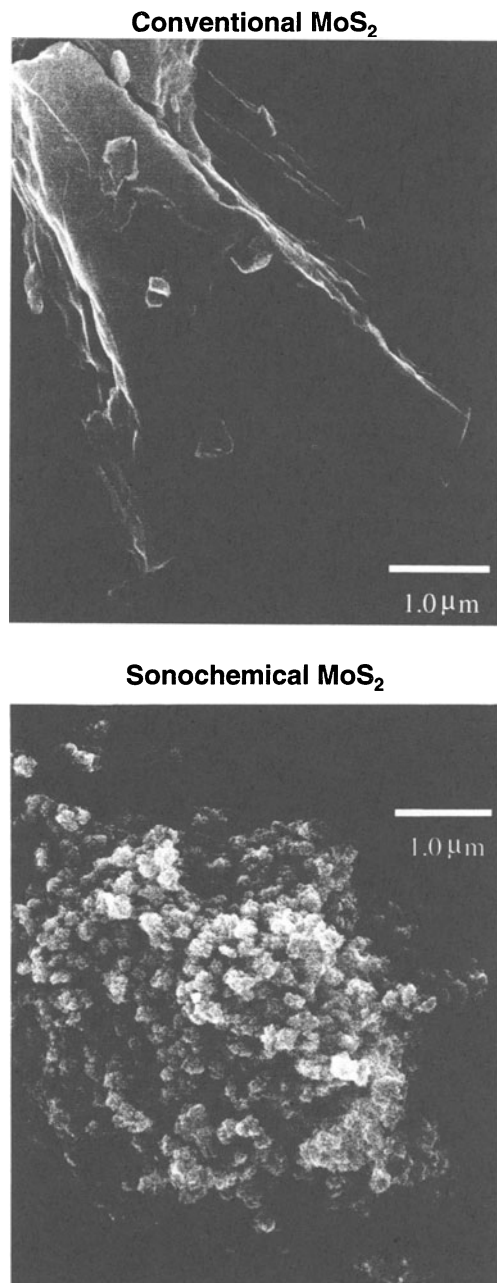


Figure 12. Morphology of conventional and sonochemically prepared MoS₂ [33].

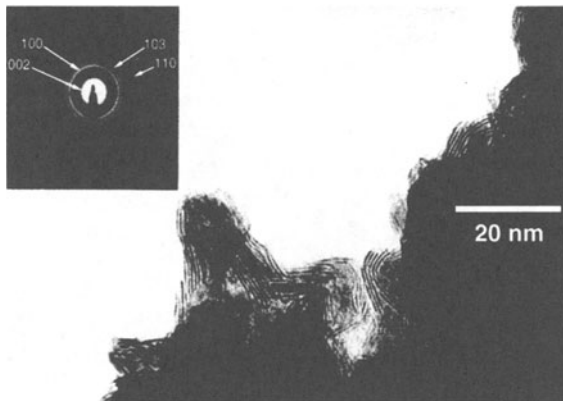


Figure 13. TEM of sonochemically prepared MoS₂. Basal planes are seen as dark fringes with interlayer spacings of 0.62 ± 0.01 nm, the same as conventional MoS₂ [33].

The observed turnover frequencies as a function of temperature for these catalysts are shown in Figure 14. The principal products detected by GC were the C₄ hydrocarbons: butadiene, 1-butene, *trans*-2-butene, *cis*-2-butene, and butane. No partially hydrogenated thiophenes were detected, and lighter (C₁-C₃) hydrocarbons accounted for less than 1% of the reaction products. The observed HDS activity order is MoS₂ (sonochemical) > RuS₂ (conventional) > ReS₂ (conventional) ~ Mo₂C (sonochemical¹¹) > MoS₂ (conventional). The sonochemically prepared MoS₂ catalyzes the hydrodesulfurization (HDS) of thiophene with activities roughly five-fold better than conventional MoS₂ and comparable to those observed with RuS₂, one of the best commercial catalysts.

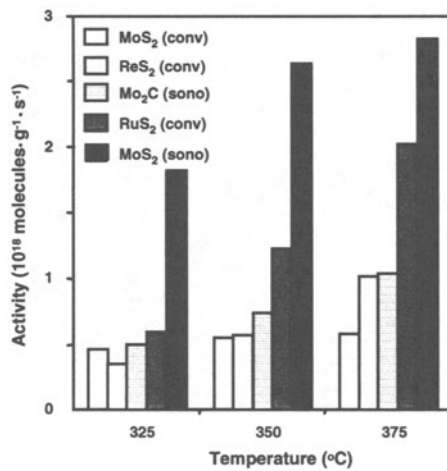


Figure 14. Catalytic activity for hydrodesulfurization of thiophene by various catalysts [33].

The product selectivities, expressed as percent of total C₄ hydrocarbons, observed at 375 °C were also examined. All the catalyst studied show high selectivity for butenes with the exception of the sonochemical MoS₂, which is selective to butane. The accepted mechanism for thiophene HDS involves initial hydrogenolysis of the C-S bonds to give butadiene, followed by rapid hydrogenation to 1-butene, which is subsequently hydrogenated to butane or isomerized to a thermodynamic mixture of *cis*- and *trans*-2-butenes [39]. It is not surprising to see increased butane production from the sonochemical MoS₂, given its higher HDS activity.

There remains much to explore in the sonochemical synthesis of inorganic materials, and this technique has only begun to be exploited. The use of ultrasound in the synthesis of metal oxides, for example, has some promise as well [49-50].

3. Sonochemical Synthesis Of Biomaterials

Another important application of sonochemistry to materials chemistry has been the preparation of biomaterials, most notably protein microspheres [51-57]. While the chemical effect of ultrasound on aqueous solutions have been studied for many years, the development of aqueous sonochemistry for biomaterials synthesis is very recent, particularly in the area of microencapsulation. It is beyond the scope of this chapter to review this area thoroughly, but a brief synopsis and bibliography will be provided.

Using high intensity ultrasound and simple protein solutions, a remarkably easy method to make both air-filled microbubbles and nonaqueous liquid-filled microcapsules has been developed. Figure 15 shows an electron micrograph of sonochemically prepared microspheres. These microspheres are stable for months, and being slightly smaller than erythrocytes, can be intravenously injected to pass unimpeded through the circulatory system.

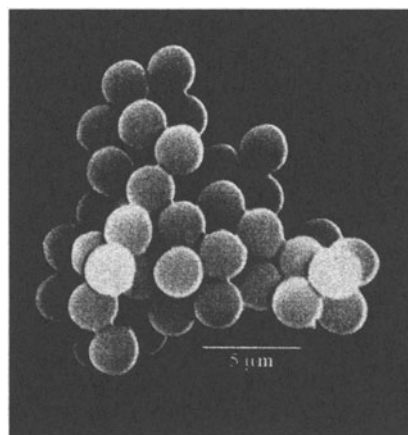


Figure 15. Scanning electron micrograph of sonochemically prepared protein microspheres from bovine serum albumin [6].

The mechanism responsible for microsphere formation is a combination of *two* acoustic phenomena: emulsification and cavitation. Ultrasonic emulsification creates the microscopic dispersion of the protein solution necessary to form the proteinaceous microspheres. Alone, however, emulsification is insufficient to produce long-lived microspheres. The long life of these microspheres comes from a sonochemical cross-linking of the protein shell. Chemical reactions requiring O₂ are critical in forming the microspheres. It has been known for some time that the primary products from the sonolysis of water are H₂ and H₂O₂ coming from the sonolysis of water yielding H[·] and OH[·]; in the presence of O₂, the latter produces HO₂ [58]. Based on chemical trapping experiments, we established that the proteinaceous microspheres are held together by disulfide bonds between protein cysteine residues and that superoxide is the crosslinking agent, as shown schematically in Figure 16. The crosslinked shell of the microspheres is only about ten protein molecules thick, as shown in Figure 17.

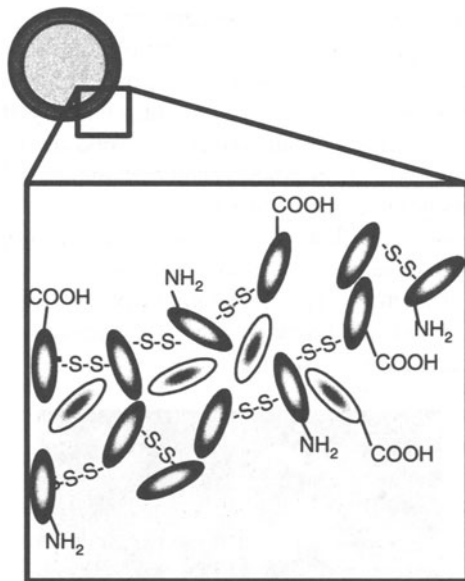


Figure 16. Schematic of the disulfide crosslinking that holds the protein microspheres together.

These protein microspheres, have a wide range of biomedical applications, including their use as echo contrast agents for sonography [59], magnetic resonance imaging contrast enhancement [54, 56, 57], oxygen or drug delivery [55], among others. An extensive patent literature now exists in this area [60-71].



Figure 17. Transmission electron micrograph of protein-stained microtome section from sonochemically prepared protein microspheres [55].

4. Sonochemical Modification of Inorganic Materials

The use of ultrasound to accelerate chemical reactions in liquid-solid heterogeneous systems has become increasingly widespread. The sonochemical enhancement the reactivity of reactive metals as stoichiometric reagents has become an especially routine synthetic technique for many heterogeneous organic and organometallic reactions [4, 6, 9-10, 72-75], particularly those involving reactive metals, such as Mg, Li or Zn. Rate enhancements of more than tenfold are common, yields are often substantially improved, and byproducts avoided. This development originated from the early work of Renaud and the more recent breakthroughs of Luche. The effects are quite general and apply to reactive inorganic salts and to main group reagents as well. Less work has been done with unreactive metals (e.g., Ni, V, Nb, Mo, W), but results here are promising as well [76, 77].

The physical phenomena primarily responsible for such enhancements include improvement of mass transport from turbulent mixing and acoustic streaming, the generation of surface damage at liquid-solid interfaces by shock waves and microjets, the generation of high-velocity interparticle collisions in slurries, and the fragmentation of friable solids to increase surface area. We will focus our attention here on the last three of these.

In examining heterogeneous sonochemistry for either stoichiometric and catalytic reactions, one must adopt techniques not often employed by synthetic

chemists. It is important to use both chemical kinetic and surface characterization techniques. The following protocol has proved quite successful in such investigations: (1) monitor the kinetics of the chemical reactivity of the solids, both during sonication and following irradiation of the solid in the absence of substrate, (2) determine effects of irradiation on surface morphology and size distributions of powders and solids by electron microscopy, and (3) measure surface composition depth profiles and composition by Auger electron spectroscopy (AES), EDX, and XPS. The power of this three-pronged approach has been proved in studies of the sonochemistry of transition metal powders [14, 76-80].

4.1. SURFACE CAVITATION

Cavitation near extended liquid-solid interfaces is very different from cavitation in pure liquids [11, 12]. There are general physical mechanisms responsible for the effects of cavitation near surfaces: microjet impact and shockwave damage. Whenever a cavitation bubble is produced near a boundary, the asymmetry of the liquid particle motion during cavity collapse often induces a deformation in the cavity (as shown schematically in Figure 18). The potential energy of the expanded bubble is converted into kinetic energy of a liquid jet that extends through the bubble's interior and penetrates the opposite bubble wall. Because most of the available energy is transferred to the accelerating jet, rather than the bubble wall itself, this jet can reach velocities of hundreds of meters per second. Because of the induced asymmetry, the jet often impacts the local boundary and can deposit enormous energy densities at the site of impact. Such energy concentration can result in severe damage to the boundary surface.

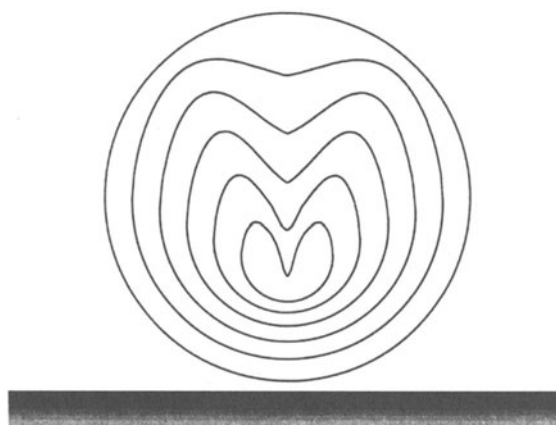


Figure 18. Formation of a liquid microjet during bubble collapse near an extended surface.

The second mechanism of cavitation-induced surface damage invokes shockwaves created by cavity collapse in the liquid [11]. The impingement of microjets and shockwaves on the surface creates the localized erosion responsible for ultrasonic cleaning and many of the sonochemical effects on heterogeneous reactions. The erosion of metals by cavitation can generate newly exposed, highly heated surfaces and even eject metal from the surface. The importance of this process to corrosion and erosion phenomena of metals and machinery has been thoroughly reviewed elsewhere [12].

4.2. INTERPARTICLE COLLISIONS

Distortions of bubble collapse depend on a surface several times larger than the resonance bubble size. Thus, for ultrasonic frequencies of ≈ 20 kHz, damage associated with microjet formation cannot occur for solid particles smaller than ≈ 200 μm . This takes on a special importance for sonochemistry, since fine powders are generally preferred for use as solid reagents or catalysts.

In liquid-solid slurries, cavitation still occurs, however, and the bubble collapse will still launch shock waves out into the liquid. When these shock waves pass over particles in close proximity to one another, high-velocity interparticle collisions can result. If the collision is at a direct angle, metal particles can be driven together at sufficiently high speeds to induce effective melting at the point of collision [13, 14], as seen in Figures 19 and 20. From the volume of the melted region of impact, the amount of energy generated during collision was determined. From this, a lower estimate of the velocity of impact was several hundred m/s, or roughly one half the speed of sound!

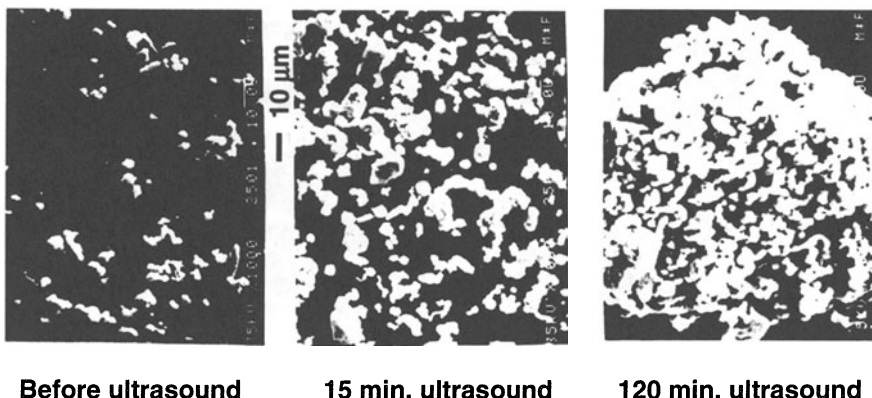


Figure 19. The effect of ultrasonic irradiation on aggregation of Ni powder as a slurry in decane [76].

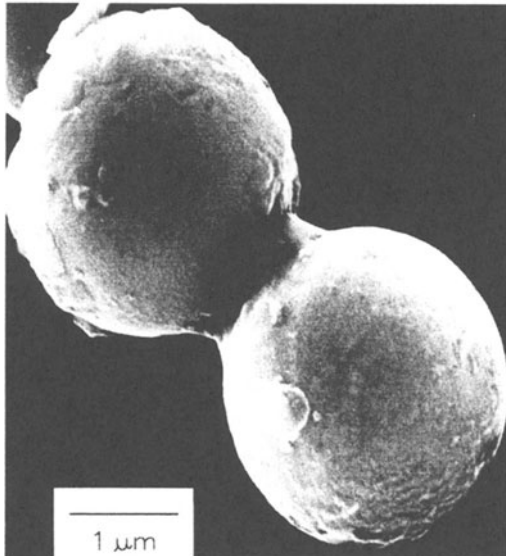


Figure 20. Scanning electron micrograph of Zn powder after ultrasonic irradiation as a slurry in decane [13].

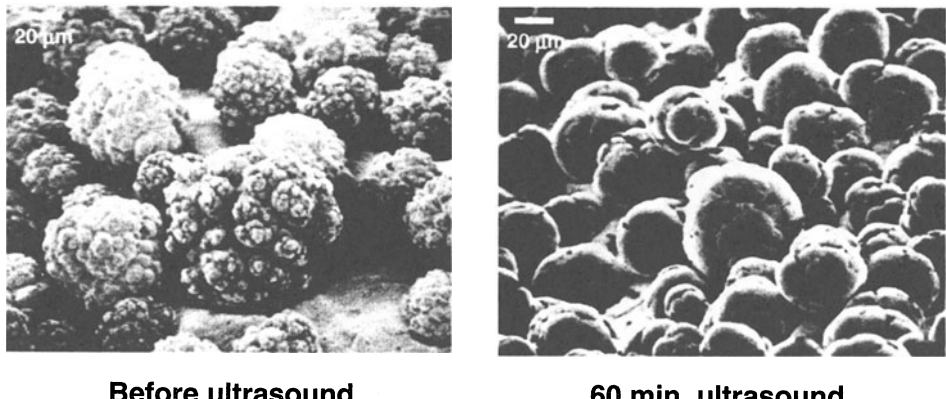


Figure 21. The effect of ultrasonic irradiation on the surface morphology of Ni powder. High-velocity interparticle collisions caused by ultrasonic irradiation of slurries is responsible for these effects [80].

If the particles collide at a glancing angle, a mechanical removal of surface material results with a macroscopic smoothing (and at the atomic level, a microscopic roughening) of the surface (as shown in Figure 21), in analogy to lapidary ball milling. Especially for reactive metals that form oxide, nitride or carbonaceous coatings, the consequences to the reactivity of metal particles can be quite substantial [3, 4, 14, 76-80]. Surface composition studies with depth profiling by Auger electron spectroscopy and by sputtered neutral mass spectrometry reveal that ultrasonic irradiation effectively removes surface oxide and other contaminating coatings [14, 76-80]. An example of such an analysis is shown in Figure 22. The removal of such passivating coatings can dramatically improve chemical reaction rates. The reactivity of clean metal surfaces also appears to be responsible for the greater tendency for heterogeneous sonochemical reactions to involve single electron transfer [81] rather than acid-base chemistry, which generally arises from surface sites of the oxide coatings.

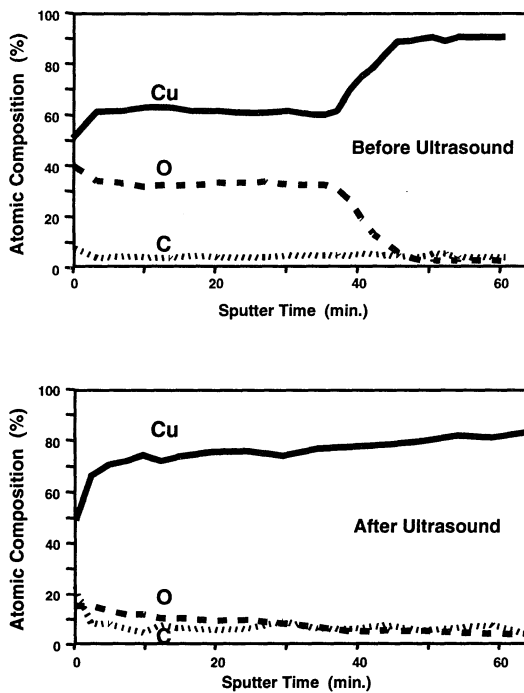


Figure 22. The effect of ultrasonic irradiation of Cu powder slurries on the surface composition. 50 min. sputter time is roughly 1 μm depth [78].

In order to probe the conditions created during interparticle collisions in slurries irradiated with ultrasound, a series of transition metal powders were examined (Figure 23). Using the irradiation of Cr, Mo, and W powders in decane at 20 kHz and 50 W/cm², one observes agglomeration and what appears to be localized melting for the first two metals, but not the third [13]; the melting points of these metals are 1857° for Cr, 2617° for Mo, and 3410°C for W. If one compiles a table of the effects of ultrasonic irradiation of slurries of different metal powders (Figure 24), one discovers that there is a break point in aggregation and surface deformations that occurs as the metal melting points increase. It appears that the effective transient temperature reached at the point of impact during interparticle collisions is roughly 3000°C. This effective local temperature has no direct connection with the temperatures inside the cavitating bubble, but they are another demonstration of the extreme conditions which ultrasound can create in an otherwise cold liquid.

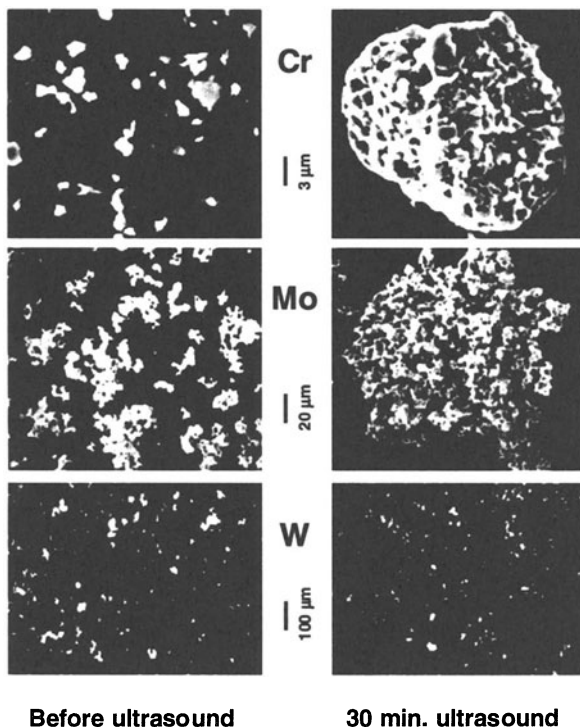


Figure 23. Scanning electron micrograph of Cr, Mo, and W powder after ultrasonic irradiation of decane slurries under Ar. The melting points of these metals are 1857°, 2617°, and 3410°C, respectively [13].

METAL	MELTING POINT	AGGLOMERATION	SURFACE MORPHOLOGY
Sn	505 K	++	++
Zn	693 K	++	++
Cu	1358 K	++	++
Ni	1726 K	++	++
Cr	2130 K	++	+
Mo	2890 K	+	-
W	3680 K	-	-

20 kHz, 50 W/cm², 293 K, 10 µm powder, in decane under Ar.

Figure 24. The effects of ultrasonic irradiation on slurries of metal powders [14].

For brittle solids, interparticle collisions can also induce fragmentation. This can substantially increase the available surface area of the powders and thus enhance liquid-solid reaction rates. An example of this effect is found in the application of ultrasound to the process of molecular intercalation into layered inorganic solids [82, 83]. The adsorption of organic or inorganic compounds between the atomic sheets of layered solids permits the systematic change of optical, electronic, and catalytic properties. Such materials have many technological applications (for example, lithium batteries, hydrodesulfurization catalysts, and solid lubricants). The kinetics of intercalation, however, are generally extremely slow, and syntheses usually require high temperatures and very long reaction times. High-intensity ultrasound dramatically increases the rates of intercalation (by as much as 200-fold) of a wide range of compounds (including amines, metallocenes, and metal sulfur clusters) into various layered inorganic solids (such as ZrS₂, V₂O₅, TaS₂, MoS₂, and MoO₃). SEM of the layered solids coupled to chemical kinetics studies demonstrated that the origin of the observed rate enhancements comes from particle fragmentation (which dramatically increases surface areas), and to a lesser extent from surface damage. The activation of heterogeneous reagents, especially non-metals, often arises from this effect. The effects of ultrasound on silica, for example, can substantially alter reactivity patterns [75].

4.3. EFFECTS OF ULTRASOUND ON HETEROGENEOUS CATALYSIS

Catalytic reactions are of enormous importance in both laboratory and industrial applications. Heterogeneous catalysts often require rare and expensive metals. The use of ultrasound offers some hope of activating less reactive, but also less costly, metals. Such effects can occur in three distinct stages: (1) during the formation of supported catalysts, (2) activation of preformed catalysts, or (3) enhancement of catalytic behavior during a catalytic reaction. Some early investigations of the effects of ultrasound on

heterogeneous catalysis can be found in the Soviet literature [3, 84]. In this early work, increases in turnover rates were usually observed upon ultrasonic irradiation, but were rarely more than tenfold. In the cases of modest rate increases, it appears likely that the cause is increased effective surface area; this is especially important in the case of catalysts supported on brittle solids (e.g., noble metals supported on carbon).

More impressive effects, however, have been reported [3], especially for hydrogenations and hydrosilations with Ni or Raney Ni powder. For example, as shown in Figure 25, the hydrogenation of alkenes by Ni powder is enormously enhanced by ultrasonic irradiation [76, 80]. This is not due to fragmentation of the solid: the surface area did not change significantly even after lengthy irradiation. There is, however, a very interesting effect on the surface morphology (Figures 19 and 21). Ultrasonic irradiation smoothes, at a macroscopic scale, the initially crystalline surface and causes agglomeration of small particles. Both effects are due to interparticle collisions caused by cavitation-induced shockwaves. AES revealed that there is a striking decrease in the thickness of the oxide coat after ultrasonic irradiation. It is the removal of this passivating layer that is responsible for the $>10^5$ -fold increase observed in catalytic activity.

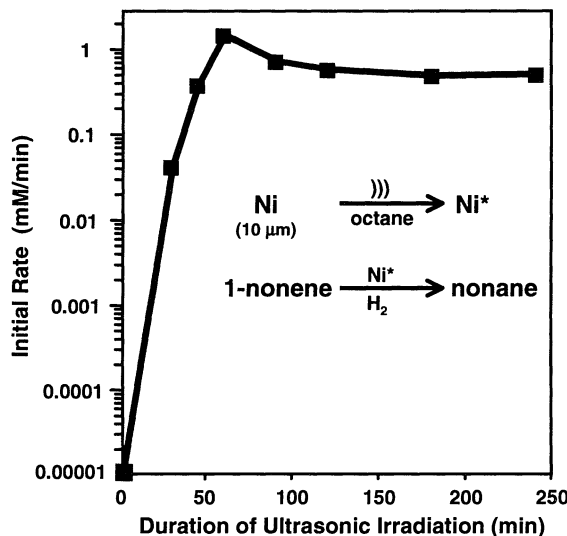


Figure 25. Effect of ultrasonic irradiation of Ni slurries in octane on its activity as a hydrogenation catalyst [3].

5. Conclusion

A diverse set of applications of ultrasound to enhancing chemical reactivity has been explored, with important applications in mixed phase synthesis, materials chemistry, and biomedical uses. Bubble collapse in liquids results in an enormous concentration of energy from the conversion of the kinetic energy of liquid motion into heating of the contents of the bubble. The enormous local temperatures and pressures so created provide a unique means for fundamental studies of chemistry and physics under extreme conditions. For example, the sonochemical decomposition of volatile organometallic precursors in high boiling solvents produces nanostructured materials in various forms with high catalytic activities. Nanostructured metals, alloys, carbides and sulfides, nanometer colloids, and nanostructured supported catalysts can all be prepared by this general route. Cavitation can also have dramatic effects on the reactivities of both extended solid surfaces and on fine powders. Microjet and shock wave impact (on large surfaces) and interparticle collisions (with powders) have substantial effects on the chemical composition and physical morphology of solids that can dramatically enhance chemical reactivity.

6. Acknowledgments

This work was supported by the National Science Foundation. We would like to acknowledge the work of earlier members of the group at Illinois: the microsphere work discussed was primarily that of M.W. Grinstaff, M. Wong, and K.J. Kolbeck; the studies of the effects of ultrasound on slurries was primarily that of D.J. Casadonte and S.J. Doktycz; and early catalytic studies were by A.A. Cichowlas. We also thank M. Marshall, P. Mochel, V. Petrova, and the UIUC Center for Microanalysis of Materials, which is supported by the Department of Energy, for their assistance in surface characterizations.

7. References

1. Suslick, K.S. (1995) *MRS Bulletin* **20**, 29.
2. Suslick, K.S. (1993) Ultrasound: Applications to Materials Chemistry, in *Encyclopedia of Materials Science and Engineering*; Cahn, R.W., ed.; Pergamon Press, Oxford; 3rd Suppl., pp. 2093-2098.
3. Suslick, K.S. (1997) Sonocatalysis, in *Handbook of Heterogeneous Catalysis*; Ertl, G.; Knozinger, H.; Weitkamp, J.; eds.; Wiley-VCH, Weinheim; vol. 3, ch. 8.6, pp. 1350-57.
4. Suslick, K.S. (1994) Sonochemistry of Transition Metal Compounds, in *Encyclopedia of Inorganic Chemistry*; King, R.B., ed.; J. Wiley & Sons, New York, vol. 7, pp. 3890-3905.
5. Suslick, K.S.; Crum, L.A. (1997) Sonochemistry and Sonoluminescence, in *Encyclopedia of Acoustics*; Crocker, M.J., ed.; Wiley-Interscience, New York, vol. 1, ch. 26, pp. 271-282.
6. Suslick, K.S. (1998) Sonochemistry, in *Kirk-Othmer Encyclopedia of Chemical Technology*; 4th Ed. J. Wiley & Sons, New York, vol. 26, 517-541.
7. Flint, E.B.; Suslick, K.S. (1991) *Science* **253**, 1397.
8. Suslick, K.S. (1990) *Science*, **247**, 1439.
9. Suslick, K.S., ed. (1988) *Ultrasound: Its Chemical, Physical, and Biological Effects*, VCH Publishers, New York.
10. Mason, T.J., Lorimer, J.P. (1988) *Sonochemistry: Theory, Applications and Uses of Ultrasound in Chemistry*, Ellis Horwood, Ltd., Chichester, U.K.
11. Leighton, T.G. (1994) *The Acoustic Bubble* Academic Press, London, pp. 531-551.
12. Preece, C.M., Hansson, I.L. 1981 *Adv. Mech. Phys. Surf.* **1**, 199.
13. Doktycz, S.J., Suslick, K.S. (1990) *Science* **247**, 1067.
14. Suslick, K.S., Doktycz, S.J. (1990) The Effects of Ultrasound on Solids in *Advances in Sonochemistry*, Mason, T.J., ed., JAI Press, New York, pp. 197-230.
15. Weller, H. (1993) *Adv. Mater.* **5**, 88.
16. Moser, W.R., ed. (1996) *Advanced Catalysts and Nanostructured Materials*; Academic Press: New York.
17. Gleiter, H. (1992) *Adv. Mater.* **4**, 474.
18. K.S. Suslick, S.B. Choe, A.A. Cichowlas, M.W. Grinstaff (1991) *Nature* **353**, 414.
19. Grinstaff, M.W.; Cichowlas, A.A.; Choe, S.B.; Suslick, K.S., (1992) *Ultrasonics* **30**, 168.
20. Grinstaff, M.W.; Salamon, M.B.; Suslick, K.S. (1993) *Phys. Rev. B* **48**, 269.
21. Bellissent, R.; Galli, G.; Grinstaff, M.W.; Migliardo, P.; Suslick, K.S. (1993) *Phys. Rev. B* **48**, 15797-15800.
22. Suslick, K.S.; Hyeon, T.; Fang, M.; Cichowlas, A.A. (1994) *Molecularly Designed Nanostructured Materials*, MRS Symp. Proc., v. 351. Gonsalves, K.E.; Chow, G.M.; Xiao, T.O.; Cammarata, R.C., eds. Materials Research Society, Pittsburgh,, pp. 201-206.
23. Suslick, K.S.; Fang, M.; Hyeon, T.; Cichowlas, A.A. (1994) *Molecularly Designed Nanostructured Materials*, MRS Symp. Proc., v. 351. Gonsalves, K.E.; Chow, G.M.; Xiao, T.O.; Cammarata, R.C., eds. Materials Research Society, Pittsburgh, pp. 443-448.
24. Bellissent, R.; Galli, G.; Hyeon, T.; Magazu, S.; Majolino, D.; Migliardo, P.; Suslick, K.S. (1995) *Phys. Scripta* **T57**, 79-83.
25. Hyeon, T.; Fang, M.; Cichowlas, A.A.; Suslick, K.S. (1995) *Matl. Sci. Eng. A*, **204**, 186-192.
26. Suslick, K.S.; Hyeon, T.; Fang, M.; Ries, J.T.; Cichowlas, A.A. (1996) *Materials Science Forum* (Transtec Publ., N.Y.), **225-227**, 903-912 .
27. Hyeon, T.; Fang, M.; Suslick, K.S. (1996) *J. Am. Chem. Soc.* **118**, 5492-5493.
28. Suslick, K.S.; Hyeon, T.; Fang, M.; Cichowlas, A.A. (1996) Sonochemical Preparation of Nanostructured Catalysts, *Advanced Catalysts and Nanostructured Materials*; Moser, W.R., ed. Academic Press, New York, pp. 197-211.
29. Suslick, K.S.; Hyeon, T.; Fang, M. (1996) *Chem. Materials* **8**, 2172-2179.
30. Bellissent, R.; Galli, G.; Hyeon, T.; Migliardo, P.; Parette, P.; Suslick, K.S. (1996) *J. Noncryst. Solids*, **205-207**, 656-659.
31. Suslick, K.S.; Fang, M.; Hyeon, T. (1996) *J. Am. Chem. Soc.*, **118**, 11960-11961.
32. Long, G.J.; Hautot, D.; Pankhurst, Q.A.; Vandormael, D.; Grandjean, F.; Gaspard, J.P.; Briois V.; Hyeon, T.; Suslick, K.S. (1998) *Phys. Rev. B*, in press.
33. Mdleleni, M.M.; Hyeon, T.; Suslick, K.S. (1998) *J. Am. Chem. Soc.*, **120**, 6189-90.

34. Hunicke, R.L. (1990) *Ultrasonics* **28**, 291.
35. Mason, T.J.; Cordemans, E.D. (1996) *Chem. Eng. Res. Des.* **74**, 511.
36. Suslick, K.S.; Cline, Jr., R.E.; Hammerton, D. A. (1986) *J. Amer. Chem. Soc.* **106**, 5641.
37. Nishizawa, T.; Ishida, K. (1984) *Bull. Alloy Phase Diagrams* **5**, 250.
38. Sinfelt, J.H. (1983) *Bimetallic Catalysts: Discoveries, Concepts, and Applications*, J. Wiley & Sons, New York, pp. 18-31.
39. Gates, B.C. (1992) *Catalytic Chemistry*; John Wiley & Sons, New York; pp. 387-392.
40. Klabunde, K.J.; Li, Y.-X. (1993) *Selectivity in Catalysis*; Davis, M.E., Suib, S.L., Eds.; American Chemical Society, Washington, D.C., pp. 88-108 and references therein.
41. Fertman, V.E. (1990) *Magnetic Fluids Guidebook: Properties and Applications*; Hemisphere Publishing Co., New York.
42. Berkovsky, B.M.; Medvedev, V.F.; Krakov, M.S. (1993) *Magnetic Fluids: Engineering Applications*; Oxford University Press, Oxford.
43. Ranhotra, G.S.; Haddix, G.W.; Bell, A.T.; Reimer, J.A. (1987) *J. Catal.* **108**, 40.
44. Lee, J.S.; Oyama, S.T.; Boudart, M. (1990) *J. Catal.*, **125**, 157.
45. Ledoux, M.J.; Pham-Huu, C.; Guille, J.; Dunlop, H. (1992) *J. Catal.* **134**, 383.
46. Volpe, L.; Boudart, M. (1985) *J. Solid State Chem.* **59**, 332.
47. Inamura, K.; Prins, R. (1994) *J. Catal.* **147**, 515.
48. Pecoraro, T.A.; Chianelli, R.R. (1981) *J. Catal.* **67**, 430.
49. Cao, X.; Prozorov, R.; Koltypin, Y.; Kataby, G.; Felner, I.; Gedanken, A. (1997) *J. Mater. Res.* **12**, 402.
50. Shafi, K.V.P.M.; Gedanken, A.; Goldfarb, R.B.; Felner, I. (1997) *J. Appl. Phys.* **81**, 6901.
51. Suslick, K.S.; Grinstaff, M.W. (1990) *J. Am. Chem. Soc.* **112**, 7807.
52. Suslick, K.S.; Grinstaff, M.W. (1992) Proteinaceous Microspheres, *Macromolecular Assemblies*; Stroeve, P.; Balazs, A.C., eds.; Am. Chem. Soc., Washington, D.C.; pp. 218-226.
53. Suslick, K.S.; Grinstaff, M.W.; Kolbeck, K.J.; Wong, M. (1994) *Ultrasonics Sonochem.* **1**, S65-S68.
54. Liu, K.J.; Grinstaff, M.W.; Jiang, J.; Suslick, K.S.; Swartz, H.M.; Wang, W. (1994) *Biophys. J.*, **67**, 896-901.
55. Wong, M.; Suslick, K.S. (1995) Sonochemically Produced Hemoglobin Microbubbles, *Hollow and Solid Spheres and Microspheres*; MRS Symp. Proc. v. 372; Wilcox, D.L.; Berg, M.; Bernat, T.; Kellerman, D.; Corchran, J.K., eds. Matl. Res. Soc., Pittsburgh, pp 89-94.
56. Eckburg, J.J.; Chato, J.C.; Liu, K.J.; Grinstaff, M.W.; Swartz, H.M.; Suslick, K.S.; Auteri, F. P. (1996), *J. Biomech. Eng.* **118**, 193-200.
57. Webb, A.G.; Wong, M.; Kolbeck, K.J.; Magin, R. L.; Wilmes, L. J.; Suslick, K.S. (1996) *J. Mag. Res. Imaging*, **6**, 675-683.
58. Riesz, P.; Berdahl, D.; Christman, C.L. (1985) *Environ. Health Perspect.*, **64**, 233.
59. Keller, M.W.; Feinstein, S.B. in *Echocardiography in Coronary Artery Disease* Kerber, R. E. ed: Future, New York, 1988.
60. Desai, N.P.; Soon-Shiong, P.; Sandford, P.A.; Grinstaff, M.W.; Suslick, K.S. (1994) Magnetic Resonance Imaging with Fluorocarbons Encapsulated in a Cross-linked Polymeric Shell, *U.S. Patent 5,362,478*; Nov. 8, 1994.
61. Desai, N.P.; Soon-Shiong, P.; Sandford, P.A.; Grinstaff, M.W.; Suslick, K.S.; (1995) Methods for *In Vivo* Delivery of Substantially Water Insoluble Pharmacologically Active Agents and Compositions Useful Therefor, *U.S. Patent 5,439,686*; Aug. 8, 1995.
62. Grinstaff, M.W.; Soon-Shiong, P.; Wong, M.; Sandford, P.A.; Suslick, K.S.; Desai, N.P. (1996) Composition Useful for *In Vivo* Delivery of Biologics and Methods Employing Same, *U.S. Patent 5,498,421*; Mar. 12, 1996.
63. Grinstaff, M.W.; Desai, N.P.; Suslick, K.S.; Soon-Shiong, P.; Sandford, P.A.; Merideth, N.R. (1996) Method for the Preparation of Fluorocarbon-Containing Polymeric Shells for Medical Imaging, *U.S. Patent 5,505,932*; Apr. 9, 1996.
64. Grinstaff, M.W.; Desai, N.P.; Suslick, K.S.; Soon-Shiong, P.; Sandford, P.A.; Merideth, N.R. (1996) Non-Fluorinated Polymeric Shells for Medical Imaging, *U.S. Patent 5,508,021*; Apr. 16, 1996.
65. Grinstaff, M.W.; Desai, N.P.; Suslick, K.S.; Soon-Shiong, P.; Sandford, P.A.; Merideth, N.R. (1996) Polymeric Shells for Medical Imaging Prepared from Synthetic Polymers, and Methods for the Use Thereof, *U.S. Patent 5,512,268*; Apr. 30, 1996.

66. Desai, N.P.; Soon-Shiong, P.; Sandford, P.A.; Grinstaff, M.W.; Suslick, K.S. (1996) Methods for *In Vivo* Delivery of Substantially Water Insoluble Pharmacologically Active Agents and Compositions for the Use Thereof *U.S. Patent 5,560,933*; Oct. 1, 1996.
67. Grinstaff, M.W.; Soon-Shiong, P.; Wong, M.; Sandford, P.A.; Suslick, K.S.; Desai, N.P. (1997) Methods for the Preparation of Blood Substitutes for *In Vivo* Delivery, *U.S. Patent 5,635,207*; June 3, 1997.
68. Grinstaff, M.W.; Soon-Shiong, P.; Wong, M.; Sandford, P.A.; Suslick, K.S.; Desai, N.P. (1997) Methods For The Preparation Of Nucleic Acids For In Vivo Delivery, *U.S. Patent 5,639,473*; June 17, 1997.
69. Grinstaff, M.W.; Soon-Shiong, P.; Wong, M.; Sandford, P.A.; Suslick, K.S.; Desai, N.P. (1997) Methods For In Vivo Delivery Of Nutriceuticals And Compositions Useful Therefor, *U.S. Patent 5,650,156*; July 22, 1997.
70. Grinstaff, M.W.; Soon-Shiong, P.; Wong, M.; Sandford, P.A.; Suslick, K.S.; Desai, N.P. (1997) Methods for the Preparation of Pharmaceutically Active Agents for *In Vivo* Delivery, *U.S. Patent 5,665,382*; Sept. 9, 1997.
71. Grinstaff, M.W.; Soon-Shiong, P.; Wong, M.; Sandford, P.A.; Suslick, K.S.; Desai, N.P. (1997) Methods for the Preparation of Immunostimulating Agents for *In Vivo* Delivery, *U.S. Patent 5,665,383*; Sept. 9, 1997.
72. Luche, J.-L. (1996) *Comptes Rendus Series IIB* **323**, 203 and 337
73. Pestman, J.M., Engberts, J.B.F.N., de Jong, F. (1994) *Recl. Trav. Chim. Pays-Bas*, **113**, 533.
74. Suslick, K.S. (1986) Synthetic Applications of Ultrasound, *Modern Synthetic Methods* **4**, 1-60.
75. Ando, T. Kimura, T. (1991) *Adv. Sonochem.*, **2**, 211.
76. Suslick, K.S., Casadonte, D.J. (1987) *J. Am. Chem. Soc.* **109**, 3459.
77. Suslick, K.S.; Johnson, R.E. (1984) *J. Am. Chem. Soc.* **106**, 6856-6858
78. Suslick, K.S., Doktycz, S.J. (1989) *Chem. Matls.* **1**, 6.
79. Suslick, K.S., Doktycz, S.J. (1989) *J. Am. Chem. Soc.* **111**, 2342.
80. Suslick, K.S.; Casadonte, D.J.; Doktycz, S.J. (1989) *Solid State Ionics*. **32/33**, 444-452.
81. Luche, J.-L. (1994) *Ultrasonics Sonochem.*, **1**, S111.
82. Chatakondu, K., Green, M.L.H., Thompson, M.E., Suslick, K.S. (1987) *J. Chem. Soc., Chem. Comm.* **1987**, 900.
83. Suslick, K.S.; Casadonte, D.J.; Green, M.L.H.; Thompson, M.E. (1987) *Ultrasonics* **25**, 56-59
84. Mal'tsev, A.N. (1976) *Zh. Fiz. Khim.* **50**, 1641.

POLYMER SONOCHEMISTRY: CONTROLLING THE STRUCTURE AND PROPERTIES OF MACROMOLECULES

GARETH J. PRICE
*School of Chemistry,
University of Bath,
Claverton Down,
BATH, BA2 7AY, U.K.*

1 Introduction

Since the pioneering work in the 1970's and 1980's by Boudjouk, Suslick, Luche and others on Grignard, Barbier, organolithium and similar reactions, the use of ultrasound to accelerate, control and improve the yield of chemical reactions has become commonplace. It is therefore surprising that there is relatively little activity in polymer sonochemistry, particularly when realising that the application to polymer systems considerably predates other chemical applications and originates from the 1920's and 1930's when the reduction in the viscosity of solutions of natural polymers such as agar, starch and gelatine on sonication was noted by several workers [1-3]. Interest in polymer sonochemistry has steadily increased over the past few years [4] and this paper will pick out some of the main themes of this work and attempt to predict some of the emerging areas which will become important in the future.

1.1 POLYMERS AND WHY WE SHOULD STUDY THEM

Life in the 1990's is inconceivable without polymers. Virtually every aspect of life involves their use in various forms such as packaging, coatings, construction materials, adhesives, textiles and even foodstuffs. It is estimated [5] that in 1994, 34 million tonnes of the five most common plastics - polyethylene, polypropylene, polystyrene, polyvinyl chloride, PVC, and poly(ethylene terephthalate) (polyester) - were produced in the United States alone. Other well known polymer systems include the polyamides or nylons, textile fibres such as acrylics, engineering thermoplastics such as polycarbonates, poly(ether ketone)s as well as polyurethanes and a number of others. More recently, conducting polymers, other photo- and electro-active materials as well as inorganic systems such as the silicones have risen in importance. Polymers are produced in a wide variety of chemical reactions [6] involving a range of intermediates. The use of ultrasound in many of these has been investigated and will be described in the following sections.

The distinguishing factor between polymers and low molar mass species is that they consist of a large number of repeat units organised in a chain. This means that polymer molecules are much bigger and heavier. In most cases, the properties usually associated with polymers are displayed when the chains contain around 30 - 50 units although some high strength materials can contain 100000 or more giving molar masses in the millions.

The statistical nature of polymerization reactions leads to a particular sample containing a distribution of chains with varying lengths so that only an average chain length or molecular weight can be measured. This property plays a major and fundamental role in determining the material properties and is perhaps the most important characteristic of the polymer. Molecular weights can be measured by a number of methods but one of the most useful since it also shows the breadth of the distribution, is Gel Permeation Chromatography, GPC [7]. This is a form of liquid chromatography which utilises a porous solid to separate the polymer chains according to their size to give a chromatogram of the form shown in Figure 1. Since the size of the chain directly depends on its molecular weight, comparison of the chromatogram with those from standards with known molecular weight allows calculation of the various molecular weights.

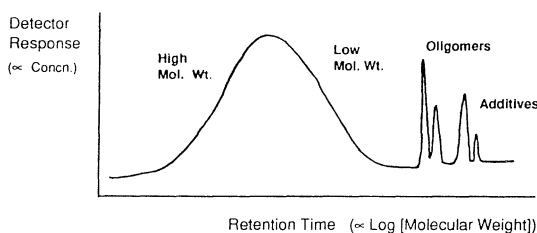


FIGURE 1. Schematic Gel Permeation Chromatogram showing the distribution of molecular weights.

1.2 ULTRASOUND, CAVITATION AND SONOCHEMISTRY

The origin of cavitation and resulting production of chemically active species has been described elsewhere in this book. For the purposes of this paper, it will be sufficient simply to consider a cavitation bubble as a chemical system consisting of three “zones” as shown schematically in Figure 2. While acknowledging that collapse will not be spherically symmetrical and the precise origin of the effects remains an item for discussion, it is certain that highly reactive, dissociated and vibrationally excited species such as free radicals can be formed in the centre of the bubble. These can diffuse out into the bulk for subsequent reaction. The interfacial region around the bubbles has very large temperature, pressure and electric field gradients and also very large shear gradients caused by rapid movement of solvent molecules. This last factor has a special importance in polymer sonochemistry as will be described in the following section.

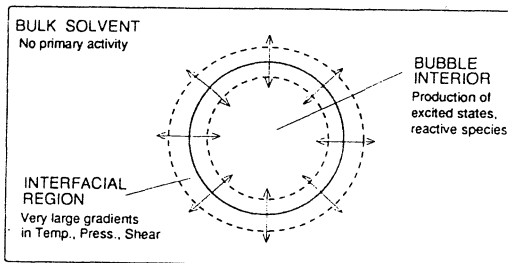


FIGURE 2. Schematic representation of bubble motion during cavitation

1.3 ULTRASOUND AND POLYMERS

So, what are the possible benefits for polymer chemists in using ultrasound? Firstly, any process which results in radical production can be used as a method of initiation for the radical polymerization of vinyl monomers. A range of other reactions such as ring opening can also be promoted by excited species. A number of polymers are produced by heterogeneous reactions and increases in yield and rate might be expected under sonication. Among the most common uses of ultrasound in synthesis has been in organometallic procedures such as Grignard or organolithium reactions, [8 - 10] a range of which have recently been used to synthesize novel polymers. Finally, very large shear gradients can be set up around cavitation bubbles and polymers often undergo modification under these conditions. Hence, there are a range of sonochemical effects for the polymer chemist to exploit. This paper will deal only with those aspects of sonochemistry that are appropriate for the preparation of polymeric materials, either by synthesis from low molecular weight monomers or by modification of pre-existing polymers. Polymer sonochemistry is a particularly rich area since, as will be seen, the opportunity exists to utilise all of the various effects caused by ultrasound and a survey of these applications will be given. Polymerizations occurring by a variety of mechanisms will be discussed and the advantages offered by ultrasound to each will be indicated.

2 Ultrasound and Polymer Processing

Two distinct areas of application for power ultrasound can be identified. Irradiation with ultrasound can cause solely physical changes such as rapid stirring and mixing or heating which can be induced by acoustic streaming. Cavitation is not always necessary for these effects but they almost always occur in a cavitating system. Examples include the formation of emulsions and melting plastics in welding systems. These can be referred as sonoprocessing. In contrast, insonation in other applications can result in chemical changes, almost invariably as a result of cavitation, and this will be described in the remainder of this paper.

Among the former category in polymer systems are the dispersal of fillers and other components into base polymers such as in the formulation of paints [11], the encapsulation of inorganic particles with polymers [12], modification of particle size in polymer powders [13] and, perhaps the major application in the polymer industry, the welding and cutting of thermoplastics [14]. These have been reviewed recently [4].

3 Ultrasonic Degradation Of Polymers In Solution

As noted above, the cleavage of polymer chains in solution on exposure to ultrasound has been known for a considerable time. The degradation is now understood with sufficient detail to make it commercially applicable in a number of areas [15, 16]. It should be stressed that in this regard, 'degradation' is taken simply to mean an irreversible lowering of the molecular weight due to chain breakage rather than any adverse chemical changes. It appears to be a universal effect and it is important to understand it as it will also occur during synthetic procedures.

3.1 CHARACTERISTICS OF ULTRASONIC DEGRADATION

The basic effects [17] of irradiating a polymer solution with power ultrasound are shown in Figure 3 using polystyrene in toluene as an example.

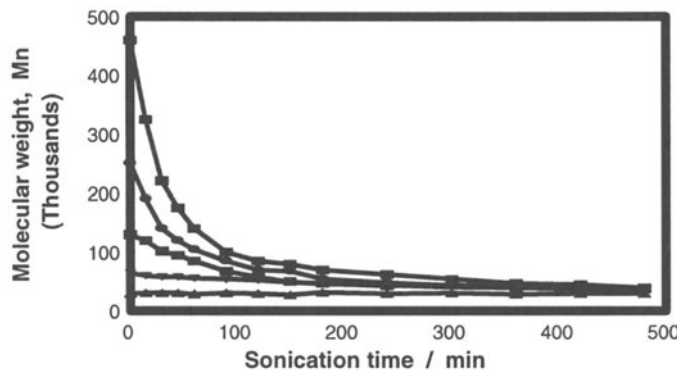


FIGURE 3 Ultrasonic degradation of 1% solutions of narrow polydispersity polystyrenes in toluene.

The degradation proceeds more rapidly at higher molecular weights and approaches a limiting value, M_{lim} , below which no further degradation takes place, in this case ~ 30000 . Polymers with this, or lower values, are unaffected by ultrasound under these conditions. These effects appear to be universal in that they have been seen for a wide range of organic polymers in organic solvents [15, 16], for inorganic polymers such as poly(organosiloxanes) and polyorganosilanes [18] and for aqueous systems such as polyethylene oxide [19], cellulose [20], polypeptides, proteins [21] and DNA [22].

This common behaviour suggests that a physical process is taking place that is more dependent on the size of the macromolecule in solution than on its chemical nature.

Most studies have shown that the degradation is relatively insensitive to the nature of the polymer. Schoon and Rieber [23] found little difference in M_{lim} for polystyrene, polyisobutylene, polychloroprene, polybutadiene, poly(dimethyl siloxane), poly(vinyl acetate) or natural rubber sonicated under the same conditions. Evidence that sonochemical degradation can occur at "weak spots" in the chain was provided by Encina et al. [24] who found that the degradation of poly(vinyl pyrrolidone) was speeded up tenfold when the polymer was prepared with a small number of peroxide linkages in the backbone. They suggested that chain cleavage occurred 5000 times faster at O–O bonds than at C–C. However, it is clear that for this effect to be noticed, there must be a substantial difference in the relative bond energies.

A large number of studies have been performed to characterise the rate of degradation in order to develop quantitative models of the process. These have led to a number of equations being proposed to describe the degradation [15, 16]. The degradation can be characterised in two ways; the limiting value of the molecular weight reached after long sonication times, M_{lim} , and also in terms of the rate constant for the degradation, k . To be able to predict behaviour under a wide range of conditions, the effect of varying all possible experimental conditions on the degradation must be understood. This has been documented in detail, but for present purposes, it is sufficient to summarise the main trends of the results. In summary, the degradation proceeds faster and to lower molecular weights at lower temperatures, in more dilute solutions and in solvents with low volatility as would be expected from the effect of these parameters on cavitation. Other factors which have been quantified are the ultrasound intensity and the nature of dissolved gases. Hence, by suitable manipulation of the experimental conditions, we can exert a great deal of control over the process, exploitation of which allows the modification of existing polymers into new materials.

While there is still some debate about the precise origins of the degradation, it has been shown that under conditions which suppress cavitation, no degradation occurs. The mechanism can briefly be best described as the polymer chain being caught in the rapid flow of solvent molecules caused by the collapse of cavitation bubbles and the shock waves generated after the implosion of the bubbles. The chains are thus subjected to extremely large shear forces resulting in the stretching of the chain and, if the force is sufficiently large breakage of a bond in the chain. There is no evidence that the extreme conditions of temperature found in cavitation bubbles contributes to the degradation. Even after very long sonication times for polystyrene dissolved in a number of solvents, none of the major product of thermal degradation, styrene monomer, was detected [25]. The degradation kinetics were also different from those of the thermal process. There are some results which indicate that other processes can take place as a result of radicals generated by sonolysis of the solvent but this is generally at a much lower level than the chain breakage. Additionally, thermal degradation produces cleavage at random points along the chain while ultrasonic degradation is much more specific. A number of workers have shown that cleavage

occurs preferentially near the middle of the chain [26]. The most persuasive evidence for this comes from the work of Van der Hoff *et al.* [27] who investigated the degradation of polystyrene in THF. They found that the degradation could be best expressed as the product of two probabilities, one accounting for the chain length dependence and the other for the position along the chain where breakage occurred. The best fit to the data was given when the breakage was distributed in a Gaussian manner within ~ 15% of the centre of the chain. Their work clearly showed that neither a random nor a model where breakage occurred exclusively at the chain centre fitted the experimental results as well as one derived from the gaussian distribution.

This "centre cleavage" model is also consistent with the stretching and breakage mechanism outlined above. Degradation of polymer solutions in shear fields formed by extensional flow in narrow capillaries [28], in other flow systems [29] as well as in high shear stirrers [30] also results in preferential breakage at the chain centres. Indeed, a detailed comparison of the chain breakage due to ultrasound and extensional flows was published recently [31].

Since we have realistic rate models for the degradation as well as being able to model the changes in molecular weight distribution with time and the variation with changes in the experimental conditions, there is a good deal of control over the process.

3.2 APPLICATIONS OF ULTRASONIC DEGRADATION.

Since the rate of degradation is molecular weight dependent, longer chains are removed from the sample and the polydispersity of the polymer is changed.

At its most straightforward level, the degradation can be used as an additional processing parameter to control the molecular weight distribution. For example, Figure 4 shows GPC chromatograms of a polymer solution undergoing sonication [25]. The degradation of the higher molecular weight species narrows the distribution markedly and it is noticeable that, after 24 hr sonication, no material with molecular weight > 10000 remains. A potential application would be to have a sonochemical step as the final processing stage during manufacture so as to "fine-tune" the polydispersity and molecular weight distribution to give the desired material properties of the polymer. There are several examples where this has been applied to commercial processes on at least pilot-plant scale.

The degradation process will operate whenever dissolved polymers are subjected to sonication, including during their synthesis. Indeed, often the degradation is significant at sound intensities below those needed to form significant amounts of radicals.

In all the carbon backbone polymers studied to date, the primary product of the degradation is a radical species arising from homolytic bond breakage along the chain. The evidence for macromolecular radicals arises from radical trapping [32] with 2,2 α -diphenyl-1-picryl hydrazyl, DPPH, from subsequent chemical reactions and, more

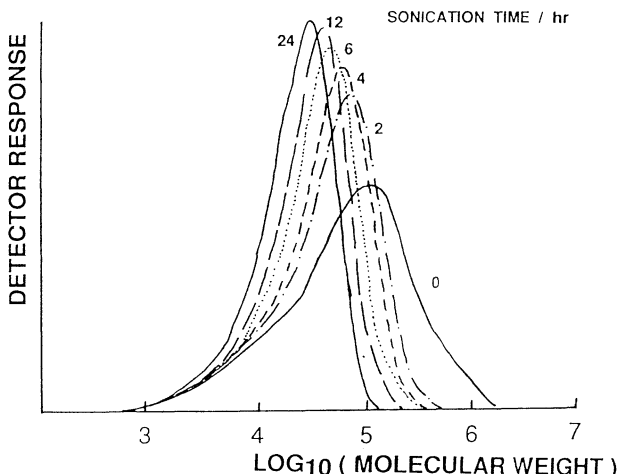


FIGURE 4 GPC chromatograms of a polyalkane sonicated in toluene.
(The values indicate the sonication time in hours)

recently, from the use of electron spin resonance spectroscopy [33] to investigate the radicals produced on sonication. A second application of the degradation utilises these macromolecular radicals as initiating species in the preparation of copolymers and end-capped materials. A number of workers have sonicated mixtures of two polymers dissolved in a common solvent, cross reaction between the two types of radicals forming a block copolymer. However, the drawback here arises from the difficulty in recovering the products by selective precipitation and also in controlling their structure. The approach which we have adopted in Bath [25] is to sonicate a polymer dissolved in a solution containing the second monomer such as polystyrene and methyl methacrylate as shown in Figure 5.

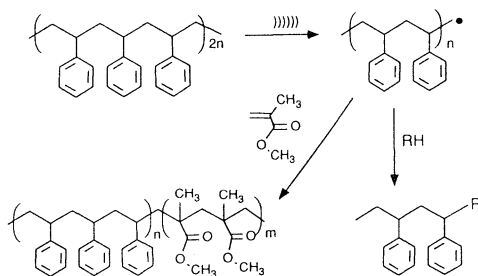


FIGURE 5 Sonochemical production of end-capped polymers and block copolymers.

Using the results of degradation studies, the structure and block length of the first polymer can be controlled quite precisely. By changing the concentration of monomer in solution the block size of the second polymer can also be varied, allowing a large degree of control over the resulting material structure. A related approach is to sonicate the polymer in the presence of a species labile to radical attack where "end

capped" polymers are formed. We have used this to prepare, for example, polystyrenes and poly(alkanes) bearing fluorescent groups.

4 Sonochemical Synthesis Of Vinyl Polymers

With an appreciation of the basic effects of ultrasound in polymer systems, we can now proceed to a discussion of its applications in polymer synthesis. Vinyl monomers (a monomer is one unit of a polymer) are those such as styrene, vinyl chloride, acrylonitrile and (meth)acrylates which have a C=C double bond activated by one or more polar or aromatic groups. Polymers derived from these monomers are in very widespread use for a range of applications. Their polymerization depends on the addition of some functionality such as a radical or an ion across the active double bond.

4.1 SONOCHEMICALLY INITIATION BY RADICAL GENERATION

The most common method for vinyl polymerization is that initiated by free radicals [34], either by simple thermal decomposition of the monomer or by the addition of a labile initiator such as an organic peroxide or azo compound. A major problem with this reaction, caused by the high reactivity of the radical centre, is controlling the structure of the resulting polymer. As already noted, sonication can produce high concentrations of radicals as a result of cavitation. Hence, application to vinyl monomers would provide an alternative method of initiation with the possibility of a great deal of control over the process.

Water is particularly susceptible to cavitation [32] and the generated H• and OH• radicals were used by Lindstrom and Lamm [35] and Henglein [36] to prepare poly(acrylonitrile) in aqueous solution as long ago as the 1950's. Radicals can also be produced as a result of cavitation in virtually all organic liquids [37]. It was a widely held opinion that polymerization could not take place in organic systems. For example, El'Piner [38] stated that "...polymerization of monomers in an ultrasonic field does not occur if these are thoroughly dried and do not contain substances in the polymerized state." Several other workers also suggested that no reaction would take place unless it was carried out with an initiator or was "seeded" with preformed polymer which would degrade to yield the initiating radicals. However, this was shown to be wrong and a number of workers have since studied radical polymerization [4] both of single monomers and their mixtures.

Most sonochemical polymerizations described here have used high intensities of ultrasound but polymers can be produced using the lower powers available from a cleaning bath. Orszulik [39] showed that while polymerization did not occur in the absence of an initiator, the decomposition of AIBN could be greatly accelerated in a laboratory bath and that moderately high yields of a range of acrylic polymers and copolymers were produced after 17 hr sonication.

One of the most studied systems has been methyl methacrylate, MMA, the precursor for Perspex or Plexiglass. A series of papers describing a detailed study of the mechanism of polymerization using sonochemically generated radicals has been

published by Kruus and co-workers [40, 41]. Early work showed that under some conditions pyrolysis of the monomer occurred inside cavitation bubbles causing the formation of significant amounts of insoluble chars in addition to linear polymers. However, they also showed that, as long as the monomers were properly purified and deoxygenated, soluble high molecular weight polymers of methyl methacrylate and styrene could be produced. It was found that reasonable rates of conversion could be achieved over a range of temperatures but, significantly, the reaction stopped when the ultrasound was switched off.

Taken from our work at Bath, [42] Figure 6(a) shows some of the features of sonochemical polymerization. High molecular weight polymer is formed at very early stages of the reaction but falls at longer times. This is not the same plot as found with conventionally initiated radical polymerization and the main reason for this is that the degradation process discussed in the previous section occurs in parallel with the polymerization once sufficiently long chains are formed. As shown in Figure 6(b), a conversion of $\sim 2 - 3 \text{ \% hr}^{-1}$ was achieved with MMA at 25 °C. However, above a particular conversion, cavitation in the solution essentially stopped and no further conversion to polymer occurred. This is probably due to the increased viscosity of the solution restricting movement of the solvent molecules and suppressing cavitation, hence preventing formation of radicals.

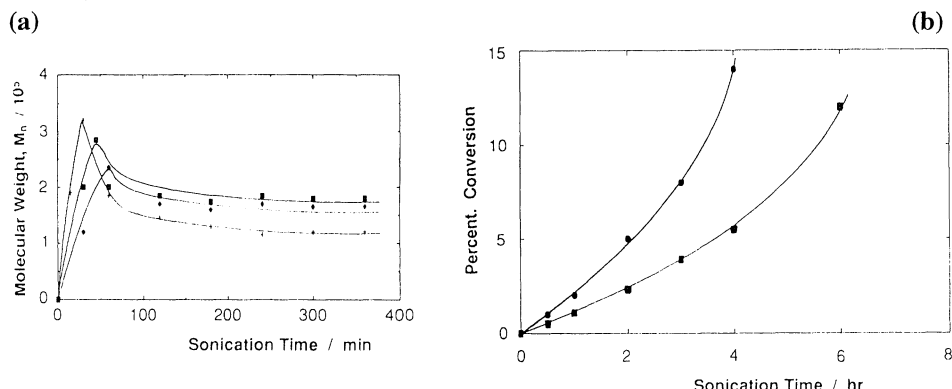


FIGURE 6 (a) Variation in molecular weight during sonochemical polymerization at 25 °C. (+ styrene; ■ methyl methacrylate; ◆ n-butyl methacrylate); (b) Ultrasonic polymerization of methyl methacrylate at 25 °C. (■ bulk MMA; ● MMA + 0.1% AIBN)

Initiation of the reaction occurs as a result of the formation of radicals, either by breakdown of the monomer or by the decomposition of an added initiator. The growth of the polymer chain by addition of monomer to its reactive end occurs to propagate the reaction before chain growth is terminated by the radicals reacting together. Detailed kinetic studies on these processes have only recently been carried out but progress has been towards a quantitative model.

Initiation can take place by two routes. Pure monomers could produce radicals through decomposition or ultrasound could accelerate the decomposition of added initiators. Both of these mechanisms have been studied recently.

The rate of initiation during the sonochemical polymerization of N-vinyl carbazole has been studied by Lorimer *et al.* [43] by monitoring the decomposition of the added initiator. The rate of initiator breakdown increased with rising ultrasound intensity, reached a maximum value and fell at high intensities to a rate lower than that in the absence of ultrasound. The same workers also showed that a sonochemical acceleration of ~40% in the rate of radical production occurred in solutions of potassium persulphate [44] an initiator for aqueous systems.

In our work with MMA, we used a radical trapping [42] using an excess concentration of DPPH. To avoid reactions with growing polymer chains, a model solvent was used. A liquid was needed that behaved in an identical manner to MMA when sonicated *i.e.* had closely matched physical properties. That most closely matching MMA is methyl butyrate so that the application of ultrasound to these two "cavitationally similar" liquids would be expected to produce similar numbers of radicals on sonication. By this method we were able to measure the rate constants for radical production under a range of conditions. Some indicative results are shown in Table 1.

TABLE 1 Rate Constants for DPPH radical trapping in methyl butyrate. (From Reference 42)

System	Temperature (°C)	Rate Constant / s ⁻¹ Ultrasound	Rate Constant / s ⁻¹ Conventional
Methyl butyrate	-10	6.3 x 10 ⁻⁵	
Methyl butyrate	25	2.2 x 10 ⁻⁵	~ 1 x 10 ⁻¹⁵
Methyl butyrate	60	1.0 x 10 ⁻⁵	
Methyl butyrate + 0.1% AIBN	25	9.1 x 10 ⁻⁵	~2 x 10 ⁻⁸
Methyl butyrate + 0.1% AIBN	70		3.1 x 10 ⁻⁵

The rate constant for purely thermal production of radicals, estimated by extrapolation from higher temperatures is negligible compared to the sonochemical reaction. The sonochemical rates are also much higher than the corresponding values for the thermal decomposition of AIBN in MMA. The results show that simply by using ultrasound alone, we can achieve at 25 °C similar rates of initiation as are usually found in thermally initiated polymerizations. To further compare with more conventional experiments, a solution of 0.1 wt% AIBN in MeOBu was sonicated. This is some three orders of magnitude higher than that expected for AIBN at this temperature so that the sonication process is clearly able to accelerate the decomposition of AIBN in solution as well as producing radicals directly by decomposition of the solvent.

Control of the sonochemical reaction demands an understanding of the effect of conditions on the process. The effect of changing the temperature is shown in Table 1 and indicates that the rate of radical production is faster at lower temperatures, as often noted in sonochemical systems. The other parameter of importance is the ultrasound

intensity, I_{us} and it was found that below an intensity of approximately $12 - 13 \text{ W cm}^{-2}$ there was no production of radicals, this presumably corresponding to the cavitation threshold in this system. Above this minimum value, there was a linear dependence of the rate of DPPH consumption on intensity up to a maximum value after which the rate dropped. Thus, by suitable manipulation of the conditions such as temperature and intensity, we can predict and control the rate of initiation.

Detailed studies of the kinetics of the other parts of the reaction have been undertaken [40, 42]. For example, the rate was found to be proportional to the monomer concentration, $[M]$, and to depend on the square root of I_{us} . The final molecular weight varied inversely with $[M]$ and scaled as $I_{us}^{-1/2}$. These are totally in accord with assuming that initiation is dependent on the intensity as described above. In contrast to the initiation, higher temperatures led to an increase in the rate of polymerization. The termination steps, being bimolecular radical reactions do not depend strongly on temperature. Hence, the main effect will be on the propagation. Addition of radicals to the growing chain is controlled by diffusion and thus would be expected to increase with temperature.

From the kinetic results, it can be concluded that the ultrasound has relatively little effect (perhaps a two or three fold acceleration) on the propagation or termination reactions and is insignificant compared with the acceleration of the initiation. This conclusion is also supported by the small amount of published work on copolymerization where two or more different monomers can be incorporated into the same polymer chain. If ultrasound were affecting the propagation, differences in the sequences of the two monomers along the chain would be expected. No significant differences were found by Miyata and Nakashio [45] for styrene-acrylonitrile copolymerizations or by Price *et al.* [46] for mixtures of styrene with methyl or butyl methacrylates.

The final factor which has been investigated for these systems is the stereochemical arrangement of the monomer units along the chain. In polymer chemistry, this is described by the tacticity of the polymer. Chains which have all of the substituents arranged on the same side of the chain are referred to as isotactic while those which have an alternating arrangement are syndiotactic. This is shown for the case of PMMA in Figure 7. Polymers with a random arrangement are termed atactic or heterotactic, the tacticity in PMMA being readily determined using NMR spectroscopy.

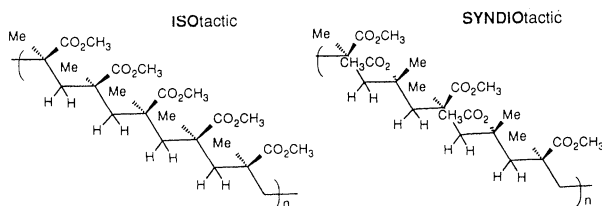


FIGURE 7 Stereochemical arrangement of substituents in PMMA.

Analysis of sonochemically prepared PMMA samples showed that they contained a greater proportion of syndiotactic sequences along the chain than when using more conventional methods of initiation. Steric hindrance between the bulky ester groups makes syndiotactic addition thermodynamically more favourable, although the energy difference is small. As the temperature is lowered, the propagation rate is slowed and there is more chance of the favoured addition taking place. This is solely a consequence of the accelerated initiation at low temperatures made possible by using ultrasound.

By analogy with the usual treatment of radical polymerization kinetics, a mechanism was proposed for the sonochemical polymerization. Essentially, the rate of initiation is proportional to the number of cavitation sites available which depends in turn on the ultrasound intensity. Using this mechanism, equations can be derived to describe the time dependence of the rate of polymerization, the molecular weight and the conversion to polymer [40, 42] which are in good agreement with the experimental observations.

There are still problems to be overcome before more widespread acceptance of this method, the main one being the relatively low final conversions achieved thus far, but there is now a good understanding of the kinetics of the polymerization.

4.2 POLYMERIZATION BY IONIC MECHANISMS

One method which has been adopted to overcome the deficiencies of radical polymerization, particularly to control the molecular weight, is to initiate the reaction using ionic species. Cationic initiators such as a number of Lewis acids can be used although anionic mechanisms utilising for example organolithium species are perhaps more common. These reactions yield polymers with very narrow molecular weight distributions and polydispersities as low as 1.03. However, they require the use of very pure reagents and dry, oxygen-free conditions.

It is the general understanding [9] that sonication is most effective in single electron transfer reactions and in mechanisms involving radicals. Indeed, there are a number of reports from the synthesis of low molar mass compounds where ionic mechanisms are completely suppressed in favour of radical processes. Thus, there has been only a small amount of work in this area. Schultz *et al.* [47] described how sonication had little effect on the anionic polymerization (addition of styrene to an ion pair at the end of a growing chain) but allowed the initiators (such as butyl lithiums) to be prepared at faster rates than under conventional conditions. Additionally, the need for dry conditions was removed as successful initiators were prepared in undried solvents.

4.3 SUSPENSION AND EMULSION POLYMERIZATIONS

An alternative route by which vinyl monomers can be polymerized is where they are dispersed as an emulsion and/or suspension [48] usually in an aqueous system. In addition to water and the monomer(s), a number of other components such as

stabilizers, dispersants and initiators are usually added. The efficient mixing and dispersion of liquids using ultrasound is a common commercial process, for example in the food industry. The large degree of motion induced by acoustic streaming provides this efficient mixing while the very high shear forces around cavitation bubbles act to break up droplets of liquid and maintain a small and even distribution of droplet sizes.

There are various aspects of these polymerizations where ultrasound could be beneficial to this type of polymerization. The dispersion could be formed and maintained during polymerization by using ultrasound. Also, the production of radicals in the aqueous phase could be used as a method of initiation. There is thus scope for the reduction or elimination of some of the additives such as emulsifiers and initiators used in the polymerization. Also, since the polymer is in a dispersed phase, the viscosity does not increase to the same extent as in bulk polymerizations so that the suppression of cavitation will not be as much of a problem.

Ultrasound was first applied to this type of reaction in 1950 and it was found that sonication increased the dispersion of styrene and other components and also significantly accelerated the rate of polymerization. Hatake *et al.* [50] also studied the suspension polymerization of styrene and found that ultrasound prevented the droplets from agglomerating or sticking to the walls of the container, so giving a more even range of particles. At the intensities used, little effect on the kinetics of the polymerization or on the molecular weight was seen but the particle size could be influenced by varying the ultrasonic frequency. More recently, Lorimer and co-workers have also compared the emulsion polymerization of styrene carried out in the presence and absence of ultrasound from a high intensity horn [44].

The decomposition of potassium persulphate initiator in aqueous solution was accelerated under ultrasound and that this, together with the production of more stable emulsions, increased the rate of polymerization as well as eliminating the induction period. An additional effect was that lower amounts of emulsifier (sodium dodecyl sulphate) were needed to maintain the reaction but that lower molecular weights were obtained than in the conventional reaction.

In the most recent example of this type, Grieser and co-workers [51] have used a horn system to produce latexes of polystyrene, poly(butyl acrylate) and poly(vinyl acetate) with low amounts of or even no surfactant and smaller particle sizes than in conventional processes. The rates of reaction were also accelerated but, significantly, this depended on the vapour pressure of the monomer. In the case of vinyl acetate, which has a high vapour pressure, the polymerization was relatively slow. This was attributed to monomer vapour entering the cavitation bubbles (primarily in the aqueous phase) and so reducing the intensity of cavitation collapse and hence the number of radicals formed. In contrast to the bulk or solution polymerizations described above, conversions close to 100 % were routinely achieved.

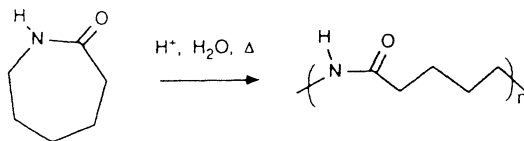
5 Sonochemical Polymerization of Non-Vinyl Monomers

While vinyl polymers are an important class of materials, there are a wide variety of other monomers which are polymerized by other mechanisms.

Articles such as tubes and tyres are made from rubber (natural or synthetic) which is lightly crosslinked. The crosslinking joins all the chains together so that while the article retains elasticity, the chains cannot be separated to flow or dissolve. Crosslinking is often carried out by heating with sulphur, a process known as vulcanization. This is very energy intensive since rubber is a poor conductor of heat so that long times and high temperatures must be utilised. In the sonochemical process [52], use is made of the fact that the heat is generated inside the article due to attenuation so that it is relatively rapid and less degradation of the rubber occurs. In some cases, both the treatment time and the energy requirements were lowered by up to a half. The same ultrasonic heating method can be applied to other systems such as epoxy resins [53]. In a neat application [54] of sonochemical technology, the opposite effect is used where a combination of heat, pressure and ultrasound can be used to break the crosslinks so that uncrosslinked material can be recovered. The most obvious practical application here is in the recycling of waste rubbers.

5.1 RING OPENING POLYMERIZATIONS

A number of commercially important polymers are produced by a ring opening mechanism of a cyclic monomer [94]. A range of polyesters can be produced from cyclic lactones but probably the most commercially significant in terms of amount of polymer manufactured is the reaction of ϵ -caprolactam to give Nylon-6.



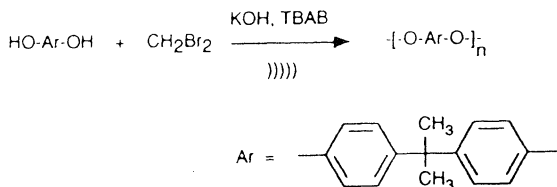
Nylon-6 is conventionally produced in a two stage process. The initial ring opening is catalysed by a small amount of water and this is followed by polymerization to high molecular weight under vacuum. The effect of ultrasound has been studied by Ragagni *et al.* [55] in Milan. Their work showed that ultrasound enhanced the ring opening phase allowing a single step polymerization without the need to add water to start the reaction. High molecular weight materials with narrower distributions were formed in shorter reaction times than when using the conventional process. Also, sonication allowed the polymerization to be run at lower temperatures than under conventional conditions.

Other work in this area has involved the polymerization of cyclic siloxanes to give the commercially very important silicone resins, [17], and the ring opening of small polycarbonate rings to form a short chain 'pre-polymer'. This was easier to process than the final, high molecular weight material but could be readily converted into a useful material. In both cases, the use of ultrasound considerably accelerated the reaction, largely attributed to better dispersion of the heterogeneous catalysts through the system.

5.2 CONDENSATION POLYMERIZATIONS

Given the large number of industrially important polymers and plastics such as polyesters, polyurethanes and nylons prepared *via* condensation reactions, there have been surprisingly few reports of the application of ultrasound in this area.

Amongst the very few other published studies of condensation processes is the work of Long who, in a wide-ranging patent [56] described various reactors which incorporated ultrasonically vibrating walls. These could be used for the precise control of both when and where polymerization took place for several polyurethane systems and was especially useful for producing foams. Watanabe *et al.* [57] applied ultrasound from a cleaning bath to the preparation of aromatic polyformals from, for example, bisphenol-A and methylene bromide. This is a two phase system using solid potassium hydroxide and normally requires the use of a phase transfer catalyst such as TBAB (tetrabutyl ammonium bromide) to promote the surface mediated reaction.



The sonicated reactions gave considerably higher yields of polymers with much higher molecular weights) than those in the absence of ultrasound.

5.3 MISCELLANEOUS EXAMPLES

5.3.1 *Electrochemically promoted polymerizations*

The combination of electrochemistry with ultrasound has produced considerable recent interest [58]. Beneficial effects arise from cleaning and regeneration of the electrode surface as well as enhanced mass transport and prevention of ion depletion from the diffusion layer at the electrodes.

Several types of polymer including polypyrroles, polythiophenes and polyanilines (which are becoming important as conductive coating materials) as well as the more usual vinyl monomers can be prepared by electrochemical methods. In a preliminary study of the electrosynthesis of copolymers containing isoprene and α -methyl styrene, Topare and co-workers [59] reported that higher yields were produced under sonication and that the reactivity ratios (or the preference for a monomer to react with a different monomer rather than itself) of both components were raised from those in the conventional reaction. The differences were attributed to the ultrasonic cleaning action allowing the continual renewal of fresh electrode surface and preventing the irreversible adsorption of impurities and fouling of the electrode. These workers have also applied ultrasound to the electroinitiated polymerization of butadiene sulphone [60]. The polymer obtained had the same structure as that from radically initiated bulk or solution polymerization but the rate of polymerization was much faster under

sonication, an effect again attributed to enhanced mass transfer effects near the electrode.

A related example involved the deposition of polypyrrole onto microporous membranes to form conducting films [61]. Sonication allowed better impregnation and a more even film to form giving enhanced material properties such as electromagnetic shielding.

5.3.2 Ziegler-Natta Polymerizations

The discovery of Ziegler - Natta catalysts in the late 1940's revolutionised polymer science in providing a method to polymerise monomers such as ethylene and propylene which are not susceptible to radical reactions. This process and more modern variants are now exploited commercially on a massive scale [62] for the production of polyolefins. Although polyolefins can be produced by other methods, the control over stereochemistry allowed by the catalyst means that this is favoured method for the production of iso- and syndiotactic polyolefins. However, molecular weight control is difficult due to the complexity of the reaction system.

The catalysts usually involve a mixed metal species prepared by reacting, for example, a trialkyl aluminium with titanium tri- or tetrachloride yielding, in the most simple view, a complex with a vacant coordination site onto which the alkene is attached. A repeated alkene insertion reaction then results in polymer formation as shown in Figure 8(a). Ultrasound was first applied to coordination polymerization as long ago as 1957 by Mertes [63] who patented a sonochemical procedure which yielded more uniform polyethylenes resulting from better dispersion of the catalyst and prevention of catalyst deactivation. In our work at Bath, we have made a preliminary study of the effect of ultrasound on the heterogeneous, Ziegler-Natta polymerization of styrene [64] using a $\text{TiCl}_4/\text{Al}(\text{C}_2\text{H}_5)_3$ catalyst.

Simply preparing the catalyst using ultrasound and allowing the polymerization to proceed under 'silent' conditions yielded polymers with identical properties to those without any sonication. However, maintaining the sonication throughout the polymerization increased the rate of reaction with no change in tacticity suggesting that ultrasound has no significant effect on the catalyst structure but it does change the nature of the reaction as shown by the GPC chromatograms shown in Figure 8(b). Differences in molecular weight caused by sonication are obvious. The reasons for the increased yields and rates of reaction are probably related to sonication causing very efficient mixing and faster mass transfer of monomer to the reactive site on the surface of the catalyst. There may possibly also be a reduction in the catalyst particle size with consequent increase in active area of the catalyst.

5.3.3 Grignard coupling of polyphenylenes

Polyphenylenes consist of linked aromatic rings and attracted considerable attention some years ago as prototypes for conducting materials and are now being used as the basis of light emitting materials. However, the available synthetic methods are complex and the polymers are difficult to process due to their very high melting points and very low solubilities. A number of the original synthetic methods are of the type to which

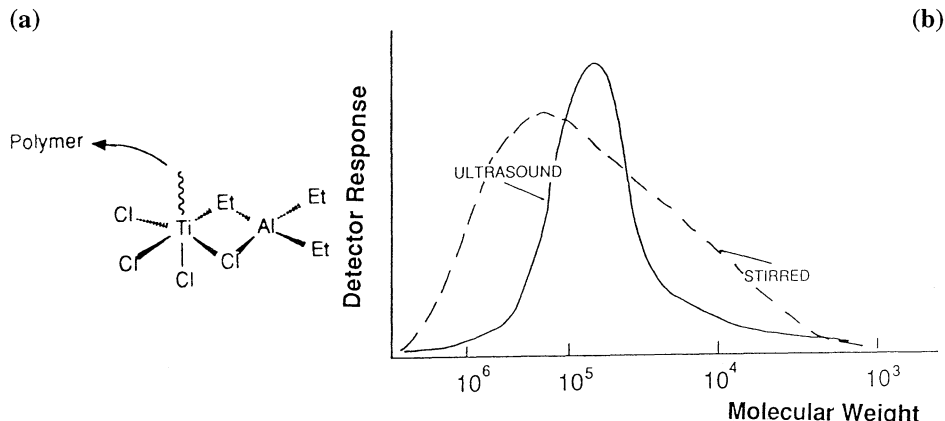
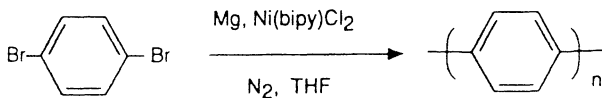


FIGURE 8 Sonochemical polymerization of styrene using a Ziegler-Natta catalyst. (a) Schematic structure of the catalyst; (b) molecular weight distributions of polymers produced at 30 °C. A. Stirred; B. Ultrasound.

ultrasound has been successfully applied in low molar mass organic synthesis so that we felt it was worthwhile to explore some of these methods.

A number of routes were tried [65] but the best results were obtained using methods based on coupling reactions of dihaloaromatics. In the absence of ultrasound, these often give low yields and sometimes react only as far as the dimer or trimer. One of the more successful schemes is due to Rehann *et al.* using a Nickel catalysed Grignard type reaction [66]



Ultrasound was applied to this scheme under various conditions and some results, which show a clear ultrasonic acceleration, are given in Table 2

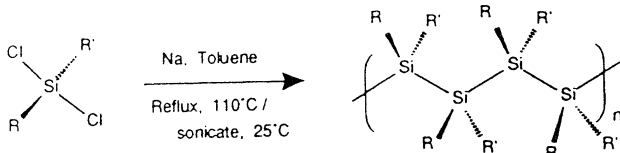
TABLE 2 Effect of ultrasound on Grignard coupling of dibromobenzene.

Conditions	Ultrasound	Polymer Yield / %
Reflux, 2 hr	No	20
Reflux, 5 hr	No	35
20 °C, 24 hr	No	40
60 °C, 2 hr	Bath	48
20 °C, 2 hr	Horn	33
60 °C, 2 hr	Horn	45

In each case, sonication gives better yields than the equivalent 'silent' conditions as well as allowing the reaction to proceed at lower temperatures.

5.3.4 Wurtz coupling of poly(organosilanes)

These polymers have a backbone of silicon atoms substituted with a variety of organic groups and are currently attracting considerable interest due to their range of potential applications [67, 68] as photoactive and photoconductive materials including photoresists and photoinitiators and also as precursors to ceramics. The usual synthetic method is a Wurtz type coupling of dichlorodorganosilanes using molten sodium in refluxing toluene. However, the reactions are irreproducible, the yields are rather low and the polymers often have a very wide, usually bi- or tri-modal, molecular weight distribution.



To achieve commercial use, polymers with a controlled structure and preferably monomodal distribution are needed. A synthesis under more environmentally acceptable conditions is also desirable.

The possibility of applying ultrasound to this type of reaction comes from the use in the early 1980's by Han and Boudjouk of lithium to couple organochlorosilanes to give R_3SiSiR_3 [69]. The work has been extended by using R_2SiCl_2 to give the polymeric materials. While polymers with a range of substituents have been prepared, most work has been done with poly(methyl phenyl silane) as it yields soluble, easily characterizable polymers.

The first reports of ultrasound being applied to the synthesis of this poly(organosilane) were by Matyjaszewski and co-workers [70]. Their extensive studies [71] produced materials with monomodal molecular weight distributions albeit in rather low yield (11-15%), using ultrasound at 60°C in toluene. Conversely, Miller *et al.* [72] reported somewhat conflicting results in that the sonication method did not yield polymers with a monomodal distribution unless diglyme or 15-crown-5 were added to the solvent. In the absence of such additives, bimodal distributions were obtained in which the higher molecular weight fraction (~ 146000) comprised about 65% of the polymer, the remainder being of relatively low molecular weight (~ 9700).

We have studied a number of silanes under a range of conditions [73, 74] and all give higher yields and faster reactions under ultrasound. However, of most significance are the changes in the molecular weights and distributions of the polymers. The use of ultrasound from a horn allowed the preparation of a polymer with a monomodal, though broad, molecular weight distribution. Figure 9 shows the molecular weight distributions resulting from four polymerizations performed under identical conditions except that the intensity was varied. Higher intensities clearly lead to narrower distributions and less low molar mass material.

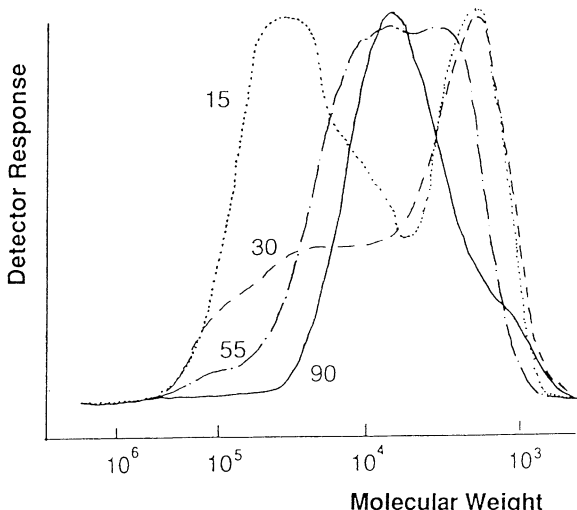


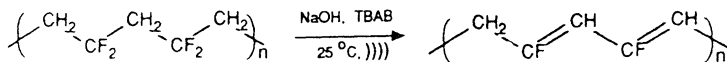
FIGURE 9 Effect of ultrasound intensity on GPC chromatograms of sonochemically prepared poly(methyl phenyl silane). (From Reference 73) Values indicate the ultrasound intensity in W cm^{-2} .

Many sonochemical reactions have been interpreted in terms of preferential promotion of radical and single electron transfer processes over those involving ionic intermediates. However, there is no firm evidence of radical intermediates in this polymerization and the explanation of the effects probably lies in the physical rather than chemical effects of sonication. Sonochemical acceleration of heterogeneous reactions is usually attributed to increased mass transfer and the continual sweeping of the surface leading to a greater number and faster regeneration of reactive sites. This would, in this case, give a more homogeneous chain growth and hence a narrower distribution of chain lengths. In addition, as described earlier, high molecular weight material formed early in the reaction will be degraded by the ultrasound, a process known to be more efficient at high intensity. However, this is not the complete story as Margulis [75] has suggested that this is, in fact, an oscillating reaction with the system varying with time between linear polymer and cyclic oligomers with 4 - 7 Si units. A modification of the sonochemical synthesis of linear polymers was used by Bianconi and co-workers [76] which involved sonochemical activation of Na / K alloy in the preparation of polysilynes, $(\text{RSi})_n$. Again, the use of ultrasound removed the very high molecular weight fractions and hence allowed the synthesis of polymers with molecular weights in the range 10000 - 100000 and monomodal distributions.

6 Sonochemical modification of polymer surfaces

The cleaning action of ultrasound to remove surface contaminants is one of the most well established sonochemical processes. This takes advantage of the asymmetric collapse of a cavitation bubble near a surface which "jets" streams of liquid against the

surface. One of the earliest reports of similar effects in polymer systems was by Urban and Salazar-Rojas [45] in which HF was removed from the surface of poly(vinylidene difluoride), PVF₂, to give a surface consisting of conjugated C=C double bonds.



PVF₂ is a piezoelectric material but is an insulator whereas a conjugated surface would confer conductive properties. A more conventional approach would be to reflux powdered polymer in a solution of a strong base such as sodium hydroxide together with a phase transfer catalyst *e.g.* tetrabutyl ammonium bromide, TBAB, to enhance wetting of the surface. Little reaction was found in the absence of TBAB but the use of ultrasound accelerated the dehydrofluorination, particularly at low temperatures. However, the maximum thickness of the surface layer was thinner when ultrasound was used, which was attributed to ultrasonic erosion of the modified surface.

In addition to conferring conductivity, the unsaturation gives sites which can be further modified by subsequent chemical reaction. Examples [78] of this have been seen by the grafting of silicon and germanium centred phthalocyanines (Pc) onto the surface of PVF₂. Lithium was used with (Pc)SiCl₂ or its germanium analogue for the reaction which was shown to anchor the (Pc) to the surface via a Si—C or Ge—C bond.

In our work at Bath [13], we have used a similar approach to modify the surface of PVC, an inexpensive, commodity polymer. If the surface could be functionalised it would be an inexpensive method of producing materials with the properties of more expensive polymers. We have shown that it is possible to graft a number of compounds including metal ions, dyes and hydrophilic monomers. In this way, we can change the chemical nature of the surface so that it has greater functionality than the base polymer. A more difficult example is polyethylene, PE, which has a very unreactive surface which needs to be activated by *e.g.* chromic acid or other strong oxidising agents prior to adhesion or printing. Using ultrasound, we were able to rapidly modify the character of PE [79] using milder, more environmentally friendly oxidising agents such as potassium persulphate or hydrogen peroxide. The water contact angle, a measure of the surface hydrophilicity, could be changed from ~100° to < 60° using mild reagents as shown in Table 3.

TABLE 3. Water contact angles for sonochemically treated polyethylene surfaces

Reagent	Contact angle / °	
	Sonochem.	Stirred
Water	94	97
30% H ₂ O ₂	90	95
H ₂ O ₂ / Maleic acid	85	96
K ₂ S ₂ O ₈ , 1 hr	89	96
K ₂ S ₂ O ₈ , 5 hr	81	96
K ₂ S ₂ O ₈ , 24 hr	59	96

Spectroscopic analysis indicated that a thin layer of polar groups had been formed on the surface. In practical terms, this would mean that inks, surface coatings *etc.* would adhere much more strongly than to the original material. The polar groups also give sites where further chemistry can be performed so that, for instance, other polymers can be grafted onto the surface to increase its compatibility with hydrophilic environments.

7 Conclusions and Future Prospects

To date, there has been a relatively small amount of work related to sonochemical polymerization. However the benefits offered to the polymer chemist in a range of reaction types warrant further studies in the area.

Perhaps the major factor which has made industrial acceptance of sonochemistry slow, is that it is regarded by many as a small-scale, laboratory technique. However, in addition to laboratory apparatus, equipment for operating at much larger, commercially realistic, scales is being developed [80, 81] and should there be sufficient value in sonochemical polymerizations, the equipment exists to exploit the effects on at least pilot-plant and possibly low-volume production scale.

Perhaps the most obvious application would be in an "add-on" to existing processes where the ultrasonic degradation can be utilised to control the final molecular weight of polymers. When any polymerization processes in solution is subject to sonication, the degradation will always occur concurrently with chain growth processes. However, it seems unlikely that a sonochemical process will replace current methodology unless it allows significant improvement of material properties or saving in production or energy costs. Thus, sonochemical manufacture of polystyrene, polyethylene and similar materials on a large industrial scale seems improbable. However, ultrasound has the possibility in a number of areas of producing polymers with no initiators or emulsifiers being needed. There are areas such as biomedical materials and food uses where the presence of additives and impurities is undesirable but where the added value of the products would support the (at present) extra costs of introducing sonochemical technology.

As far as the author is aware, there have been no examples to date of commercial processes for ultrasonically producing vinyl polymers. Indeed, the possibility of using the methodology may be very limited. While there are situations where low temperature, site-specific initiation can be useful, this can often be achieved photochemically, particularly in thin films. It seems unlikely that sonochemically initiated polymerization will be used on a large scale, but there may be small-scale, specialised cases where the absence of initiator fragments may be useful.

In similar fashion, it is difficult to envisage high tonnage production of polyolefins by Ziegler polymerization under ultrasound but there may well be some cases where relatively small amounts of high value materials needing specific molecular weight distributions are required where sonochemistry can play a part.

Perhaps the most promising (and so-far least studied) examples are those which can be classified as 'organometallic' polymerizations. These, and other heterogeneous

reactions can be used in the production of a range of highly functionalised materials. These are low-volume, high-value products and it is in this general area where ultrasound may have a major role in the near future.

8 References

1. E.W. Flosdorf and L.A. Chambers (1933) *J. Amer. Chem. Soc.* **55**, 3051
2. A.S. Szalay (1933) *Phys. Chem. A.* **164**, 234
3. A.S. Gyorgi (1933) *Nature* **131**, 278
4. G.J. Price (1996) "Applications of high intensity ultrasound in polymer chemistry" in *Chemistry under extreme or non-classical conditions* R. van Eldik and C.C. Hubbard (Eds.) J. Wiley & Sons, New York
5. M.S. Reisch (1995) *Chem. Eng. News* May 22, p30
6. F.W. Billmeyer (1984) *Textbook of Polymer Science* J. Wiley & Sons, 3rd Ed., New York
7. B.J. Hunt and S.R. Holding (1989) *Size Exclusion Chromatography* Blackie, London
8. S.V. Ley and C.R. Low (1989) *Ultrasound in Chemistry* Springer Verlag, London
9. J.L. Luche (1992) in *Current Trends in Sonochemistry* G.J. Price (Ed.), R.S.C. Special Publication 116, R.S.C., Cambridge, p 34
10. P. Boudjouk (1990) in *Ultrasound: Its chemical, physical and biological effects*, K.S. Suslick (Ed.) V.C.H. Publishers, New York, p165.
11. J.O. Stoffer and M. Fahim (1991) *J. Coating Technol.* **63**, 61
12. J.P. Lorimer, T.J. Mason, D. Kershaw, I. Livsey and R. Templeton-Knight (1991) *Coll. Polym. Sci.* **29**, 392
13. G.J. Price and A.A. Clifton (1996) *Polymer* **37**, 3971
14. F. Rawson (1994) *Brit. Plastics and Rubber* May, p22
15. A.M. Basedow and K. Ebert (1977) *Adv. Polym. Sci.* **22**, 83
16. G.J. Price (1990) *Advances in Sonochemistry* **1** 231
17. G.J. Price and P.F. Smith (1993) *Eur. Polym. J.* **29**, 419
18. G.J. Price, E.N. Wallace and A.M. Patel (1995) in *Silicon containing polymers* R.G. Jones (Ed) Royal Society of Chemistry, Cambridge, p 147
19. S. Koda, H. Mori, K. Matsumoto and H. Nomura (1994) *Polymer* **35**, 30
20. T. Sato and D.E. Nalepa (1977) *J. Coating Technol.* **49**, 45
21. J.H. Bradbury and J. O'Shea (1973) *Aust. J. Biol. Sci.* **26**, 583
22. P.F. Davison and D. Freifelder (1962) *2*, 235
23. T.G. Schoon and T. Rieber (1972) *Agnew. Makromol. Chem.* **23**, 43
24. M.V. Encina, E. Lissi, M. Sarasusa, L. Gargallo and D. Radic (1980) *J. Polym. Sci. Polym. Lett.* **18**, 757
25. G.J. Price et al. Unpublished results - manuscripts in preparation.
26. B.M.E. Van der Hoff and P.A.R. Glynn (1974) *J. Macromol. Sci. Macromol. Chem.* **A8**, 429
27. B.M.E. Van der Hoff and C.E. Gall (1977) *J. Macromol. Sci.* **A11**, 1739
28. A.J. Muller, J.A. Odell and A. Keller (1990) *Macromolecules* **23**, 3090
29. T.Q. Nguyen H.H. Kausch (1992) *Adv. Polym. Sci.* **100**, 73
30. O. Watanabe, M. Tabata, T. Kuedo, J. Sohma and T. Ogiwara (1985) *Prog. Polym. Phys. Japan* **28**, 285
31. T.Q. Nguyen, Q.Z. Liang and H.H. Kausch (1997) *Polymer* **38**, 3783
32. P. Riesz (1992) *Advances in Sonochemistry* **2**, 23
33. M. Tabata, T. Miyawaza, J. Sohma and O. Kobayashi (1980) *Chem. Phys. Lett.* **73**, 178
34. J.C. Bevington (1989) in *Comprehensive Polymer Science* Vol. 3 Ch. 6 J.C. Bevington and G. Allen, (Eds.) Pergamon Press, Oxford
35. O. Lindstrom and O. Lamm (1951) *J. Phys. Colloid Chem.* **55** 1139
36. A. Henglein (1954) *Makromol. Chem.* **14** 15
37. K.S. Suslick (1990) *Ultrasound: Its chemical, physical and biological effects*, V.C.H. Publishers, New York, Ch. 4.
38. I.E. El'Piner (1964) *Ultrasound: Physical, chemical and biological effects* Consultants Bureau, New York

39. S.T. Orszulik (1993) *Polymer* **34**, 1320
 40. P. Kruus and T.J. Patraboy (1985) *J. Phys. Chem.* **89**, 3379
 41. P. Kruus (1991) *Advances in Sonochemistry* **2**, 1
 42. G.J. Price, D.J. Norris and P.J. West (1992) *Macromolecules* **25**, 6447
 43. J.P. Lorimer, T.J. Mason and D. Kershaw (1991) *J. Chem. Soc. Chem. Commun.* 1217
 44. J.P. Lorimer, T.J. Mason, K. Fiddy, D. Kershaw, T. Groves and D. Dodgson (1989) *Ultrasonics International Conference Proceedings* 1283
 45. T. Miyata and F. Nakashio (1975) *J. Chem. Eng. Japan* **8**, 469
 46. G.J. Price, M.R. Daw, N.J. Newcombe and P.F. Smith (1990) *Br. Polym. J.* **23**, 63
 47. D.N. Schultz, J.A. Sissano and C.A. Costello (1994) *Polym. Prepr.* **35**, 514
 48. D.R. Bassett and A.E. Hamielec (1981) *Emulsion polymers and emulsion polymerization* A.C.S. *Symposium Series* **165**, A.C.S., Washington
 49. A.S. Ostroski and R.B. Stanbaugh (1950) *J. Appl. Phys.* **21**, 478
 50. Y. Hatate, A. Ikari, K. Kondo and F. Nakashio (1985) *Chem. Eng. Commun.* **34** 325
 51. G. Cooper, F. Greiser and S. Biggs (1994) *J. Coll. Interface Sci.* **184** 52
 52. N. Senapati and D. Mangaraj U.S. Patent 45489771 (1985)
 53. T.K. Salensa and N.K. Babbar (1971) *Ultrasonics* **13**, 21
 54. A.I. Isayev, S.P. Yushanov and J. Chen. (1996) *J. Appl. Polym. Sci.* **59**, 803; 815
 55. V. Ragaini Italian Patent Appl. 20478-A/90; R. Carli, C.L. Bianchi, P. Gariboldi and V. Ragaini (1993) *Proc. 3rd Europ. Sonochem. Soc.*, Coimbra, Portugal
 56. G.B. Long (1967) United States Patent 3346472
 57. S. Watanabe, I. Matsubara, M. Kakimoto, and Y. Imai (1993) *Polym. J.* **25**, 989
 58. R.G. Compton, J.C. Eklund, S.D. Page, G.H.W. Sanders and J. Booth (1994) *J. Phys. Chem.* **98**, 12410
 59. L. Toppare, S. Eren and U. Akbulut (1987) *Polymer Commun.* **28**, 36
 60. S.P. Aybar, B. Hacioglu and U. Akbulut and L. Toppare (1991) *J. Polym. Sci. Polym. Chem.* **29**, 1971
 61. P. Kathirgamanathan, A.M. Souter and D. Baulch (1994) *J. Appl. Electrochem.* **24**, 283
 62. P.J.T. Tait (1989) in *Comprehensive Polymer Science* Vol. 4, Ch. 1, p. 1, Bevington, J.C. and Allen, G. (Eds.) Pergamon Press, Oxford
 63. T.S. Mertes (1960) United States Patent 2899414
 64. G.J. Price and A.M. Patel (1992) *Polymer Commun.* **33**, 4435
 65. G.J. Price (1992) in *Current Trends in Sonochemistry* G.J. Price (Ed.), R.S.C. Special Publication 116, R.S.C., Cambridge p 87.
 66. M. Rehann, A. Schluter and W.J. Feast (1988) *Synthesis* 386
 67. R.D. Miller and J. Michl (1989) *Chem. Rev.* **89**, 1359
 68. R. West (1986) *J. Organometal. Chem.* **300**, 327
 69. B.H. Han and P. Boudjouk (1981) *Tetrahedron Lett.* **22**, 3813
 70. H.K. Kim and K. Matyjaszewski (1989) *J. Amer. Chem. Soc.* **110**, 3321
 71. H.K. Kim, H. Uchida and K. Matyjaszewski (1995) *Macromolecules* **28**, 59
 72. R.D. Miller, D. Thompson, R. Sooriyakumaran and G.N. Fickes (1991) *J. Polym. Sci. Polym. Chem.* **29**, 813
 73. G.J. Price (1992) *J. Chem. Soc. Chem. Commun.* 1209
 74. G.J. Price and A.M. Patel (1997) *Eur. Polym. J.* **33**, 599
 75. M.A. Margulis (1993) *Sonochemistry* Gordon and Breach, London
 76. T.W. Weidman, P.A. Bianconi and E.W. Kwock (1990) *Ultrasonics* **28**, 310
 77. M.W. Urban and E.M. Salazar-Rojas 1988) *Macromolecules* **21**, 372
 78. B.J. Exsted and M.W. Urban (1994) *Polymer* **35**, 5560
 79. G.J. Price, F. Keen and A.A. Clifton (1996) *Macromolecules* **29**, 5664
 80. P. Martin (1992) in *Current Trends in Sonochemistry* G.J. Price (Ed.), R.S.C. Special Publication 116, R.S.C., Cambridge p 158
 81. J. Berlan and T.J. Mason (1992) *Ultrasonics* **30**, 203

SONOCHEMISTRY AND SONOLUMINESCENCE IN COLLOIDAL SYSTEMS

FRANZ GRIESER, MUTHUPANDIAN ASHOKKUMAR and JOE Z. SOSTARIC

Advanced Mineral Products Research Centre, School of Chemistry,
University of Melbourne, Parkville, 3052. Australia

1. Introduction

The use of ultrasound to disperse and to coagulate colloidal material is a common practice among the colloid science community. Nevertheless, it is rarely recognised that the action of ultrasound on a colloidal dispersion can lead to the chemical dissolution of the colloidal material. There are only a few reports in the literature examining ultrasonically induced

TABLE 1. Examples of sonochemical dissolution and formation of colloids

Colloid	Dissolved (D)/ Formed(F)	Reference	
Ag	D	Prakash and Ghosh ('59)	[1]
Au	F	Baigent and Müller ('79)	[2]
Ag, Au, MnO ₂ , Tl	F	Gutiérrez and Henglein ('87)	[3]
Au	F	Au Yeung et al. ('93)	[4]
MnO ₂	F	Sostaric et al. ('94)	[5]
CdS	F	Hobson et al. ('94)	[6]
Polystyrene latex	F	Biggs and Grieser ('95)	[7]
MoSi	F	Trentler et al. ('95)	[8]
MnO ₂ , CdS	D	Sostaric et al. ('95)/('97)	[9, 10]
Fe	F	Suslick et al. ('96)	[11]
Polybutyl acrylate latex	F	Cooper et al. ('96)	[12]
Co, Mo ₂ C, Fe-Co alloy	F	Suslick et al. ('96)	[13]
Au	F	Nagata et al. ('96)	[14]
Ag, Pd, Au, Pt, Rh	F	Okitsu et al. ('96)	[15]
Ni	F	Koltypin et al. ('96)	[16]
Pt, Pd, Au, ZnS, CuS, PbS.	F	Caruso ('97)	[17]
Ni	F	Ramesh et al. ('97)	[18]

colloid dissolution [1, 9, 10]. The earliest work was reported in 1959, dealing with the dissolution of colloidal Ag [1]. More recently we have examined the dissolution of colloidal MnO₂ [9] and CdS [10]. The formation of colloids by the application of ultrasound has received slightly more attention although even here there is a surprisingly small number of reports. The studies to date show that the particles generated are generally in the nanometer size range which makes them of interest for applications as catalysts and in the preparation of "advanced materials".

In Table 1 is a list of the colloidal material that has been prepared or dissolved using ultrasound at various frequencies in the range of 20 kHz to 1 MHz. An examination of the work listed in this Table does not seem to indicate that the ultrasound frequency affects the size of the particle formed. There is evidence, however, that the concentration and additive type has a significant affect.

This review sets out to describe some of the reactions responsible for colloid dissolution and formation. It also describes how surface active solutes can be used to enhance the formation/dissolution rates of the colloids. Our use of sonoluminescence (SL) to aid in understanding the role of the surface active additives in sonicated solutions is presented to provide a greater dimension in explaining reactions that occur under extreme, and heterogeneous reaction conditions.

2. Dissolution of Colloidal MnO₂

The effect of sonicating a colloidal aqueous solution of MnO₂ is shown in Figure 1. Under the conditions of the experiment the MnO₂ colloids were of the order of 10 nm diameter

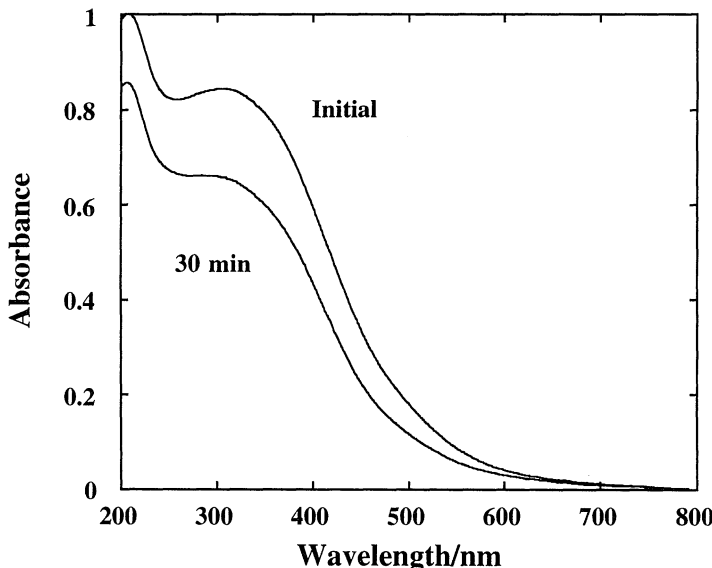


Figure 1. Absorption spectra of colloidal MnO₂ (1.3×10^{-4} M) before and following 30 minutes of sonication. The solution contained Ludox HS30 (silica stabilizer; 0.2%) at a pH of 4.5 and was saturated with N₂ gas. f=20 kHz; I=14 W/cm²

and at a particle concentration of about 3 nM [9]. The figure shows that the absorbance band due to MnO_2 decreases following sonication. The addition of aliphatic alcohols enhanced the rate of dissolution and also the amount dissolved for a given time of sonication. Figure 2 shows that the extent of dissolution is highly dependent on the alkyl chain length of the alcohol at low alcohol concentrations, but a common plateau value is reached at higher alcohol levels.

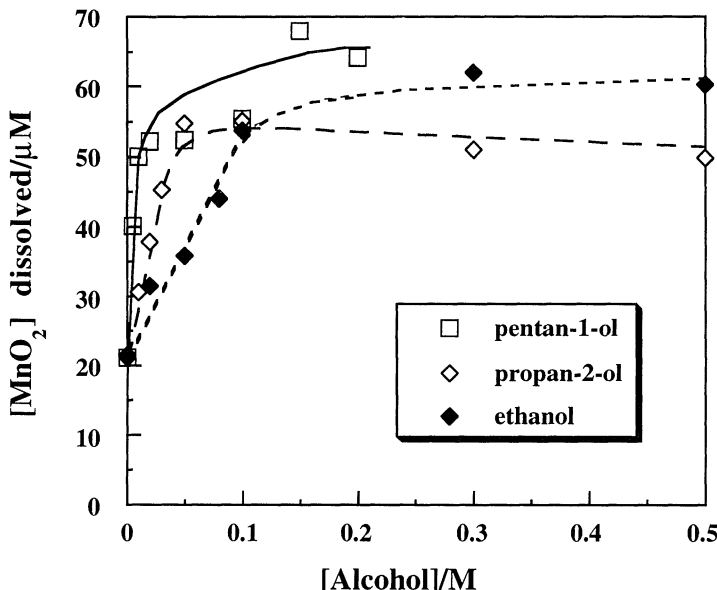
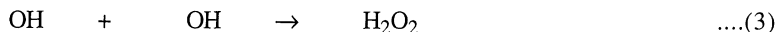
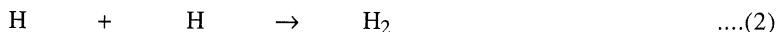


Figure 2. The effect of bulk alcohol concentration and type on the change in concentration of an MnO_2 sol sonicated under N_2 gas for a total time of 30 minutes. $f=20$ kHz; Ludox HS30 (0.2%); $\text{pH}=4.5$; $I=14$ W/cm².

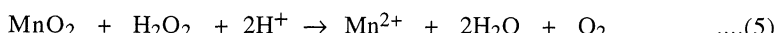
To understand the results of Figure 2 the likely chemical reactions occurring in solution need to be considered. On sonication of water the reactions



are known to occur [19, 20], and with MnO_2 present the additional steps,



and

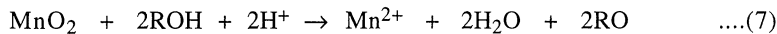


can be expected to take place [21].

In the presence of aliphatic alcohols, known H and OH radical scavengers, the reactions,

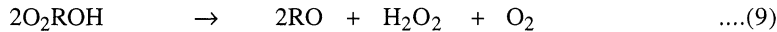


and



can occur [22].

Since oxygen will be present in trace amounts the following additional reactions are likely to take part [23],



Although the specific steps involved in the dissolution of the MnO_2 are reasonably accounted for by the above reactions they do not explain the observed trend seen with the different alcohols. It is known that the reaction of OH (or H) with alcohols does not increase linearly with alkyl chain length [24]. It can also be expected that the reaction of the various alcohol radicals (all strong one electron reductants) produced in reaction (6), with colloidal MnO_2 would be close to the diffusion controlled limit. Hence, there should be no systematic dependence of reaction (7) on the chain length of the alcohol.

The trends observed do, however, follow the order of the hydrophobicity of the different aliphatic alcohols and this raises the possibility that an interfacial process is involved in the reaction of the alcohols. This interpretation of the results is not dissimilar to that of Henglein and Kormann [25], Alegria et al. [26] and Seghal et al. [27] who have also noted that their sonochemical results are consistent with the accumulation of solute at the bubble/water interface.

To take interfacial solute adsorption into account the following model can be constructed, and is depicted in Figure 3. What this figure illustrates is the collapse of a bubble in the presence of aliphatic alcohol molecules. The primary radicals that are generated through the adiabatic heating of the gas contained in the bubble, as discussed earlier, may be scavenged by the alcohol that has equilibrated with the gas/water interface. At a given concentration in the bulk, the more hydrophobic the alcohol, the more it will accumulate at the gas/water interface [28]. The secondary radicals thus produced either diffuse away or are convectively mixed with the bulk solution when the bubble explodes following its collapse.

If quasi-equilibrium conditions prevail around the bubbles during sonication, the accumulation of alcohol at the interface should be suitably described by the Gibbs surface excess function, Γ_i [28]. The surface excess of the alcohol then determines the efficiency of interfacial radical scavenging, and not the bulk alcohol concentration. The conditions for quasi-equilibrium are probably met because the time scale for a microbubble to grow to its cavity collapse size under the influence of an ultrasonic wave oscillating at a frequency of 20 kHz is a few hundred microseconds [29], which would be sufficient time for the bulk alcohol to equilibrate with the bubble interface [30].

The surface excess of alcohol, Γ_{RHOH} , can be calculated from the variation of the air-water surface tension ($d\gamma$) with the natural log of the bulk alcohol concentration (C_{RHOH}) using the Gibbs-Duhem equation [28],

$$\Gamma_{\text{RHOH}} = - (1 / kT) d\gamma / d \ln C_{\text{RHOH}} \quad \dots(11)$$

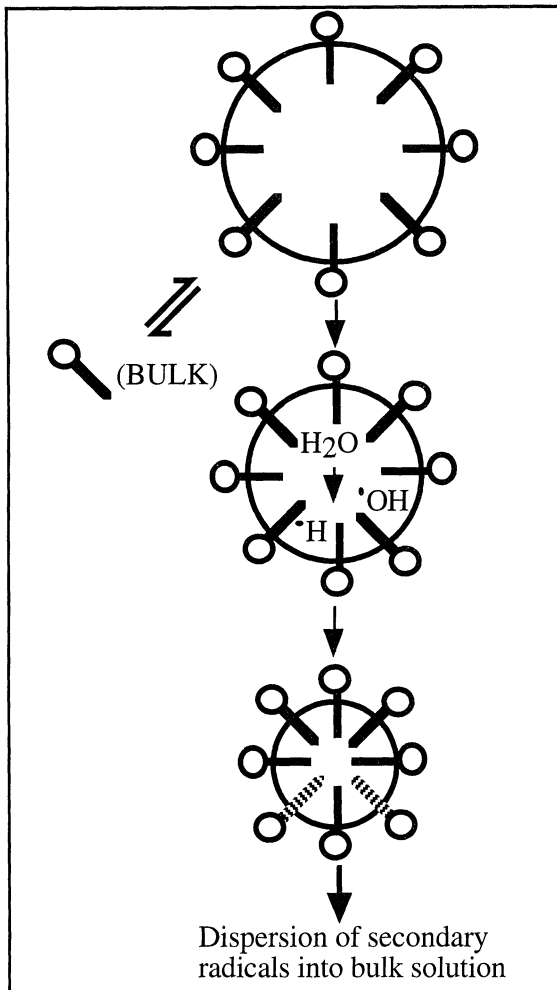


Figure 3. A representation of the events occurring during the collapse of a bubble in a sound field in the presence of surface active additives. The surface active molecules accumulate at the bubble interface and may react with the 1° radicals produced on bubble collapse. The 2° radicals produced (the shaded molecules) can then be dispersed into the solution when the bubble explodes after collapse.

Using surface tension data available in the literature a plot of the extent of colloid dissolution as a function of the surface excess of each alcohol can be constructed. The results are presented in Figure 4. This figure shows that within experimental error, the

reduction of colloidal MnO_2 is dependent only on the surface excess of the alcohol, and not on the alcohol type. This is an important result because it links a quantitative thermodynamic parameter of a solute to its sonochemical reactivity.

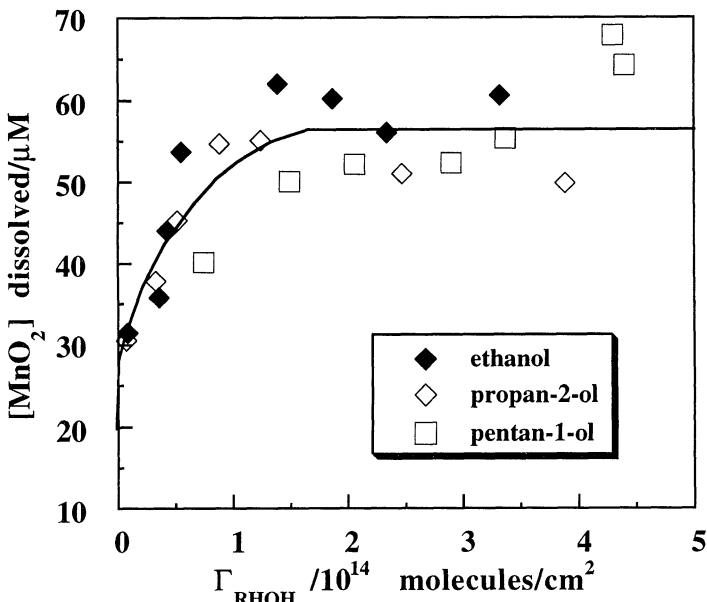
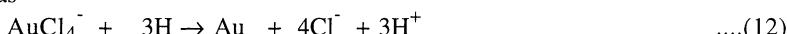


Figure 4. The effect of the surface excess of various alcohols, Γ_{RHOH} on the concentration of MnO_2 dissolved following 30 minutes of sonication ($f=20$ kHz), under N_2 gas. $\text{pH}=4.5$; Ludox HS30=0.2%; $I=14$ W/cm².

In the frame work of the above model the plateau obtained in Figures 2 and 4 simply represents the maximum number of primary radicals scavenged from the collapse of the bubble, and therefore the maximum amount of MnO_2 dissolved. It should be remembered however, that reactions 1 and 6 are not the only pathways for producing reducing radicals. Riesz [31] and Henglein and coworkers [32] have also shown that pyrolysis of the alcohols occurs in solution. To be consistent with the proposed model the pyrolysis products would have to stem from the alcohol molecules adsorbed at the bubble-water interface prior to collapse of the bubble. This conclusion will be expanded upon in a later section.

3. Formation of Colloidal Gold

The sonication of aqueous solutions containing AuCl_4^- readily leads to the formation of colloidal gold. This can be spectroscopically seen by the formation of the Au plasmon band, which has an absorption maximum at 532 nm. In the insert of Figure 5 is shown the reduction of AuCl_4^- and the concomitant formation of colloidal gold. The actual mechanism for the reduction of AuCl_4^- is not yet known but a stoichiometric reaction step can be written as



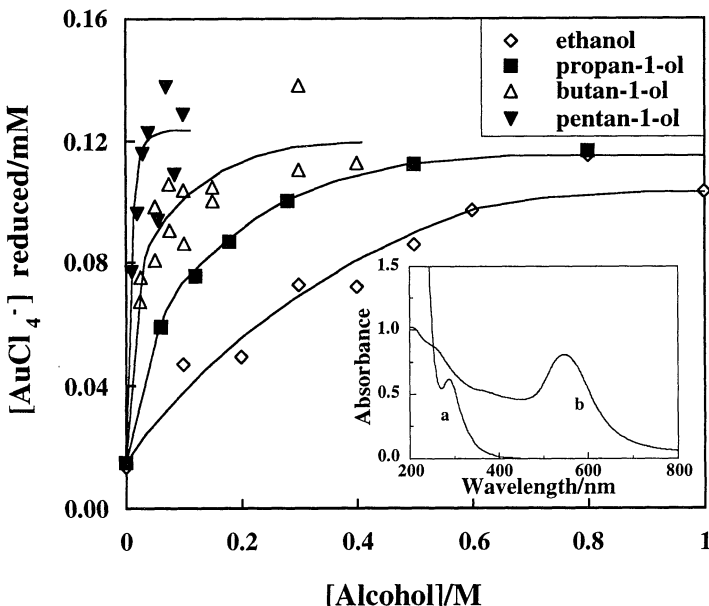
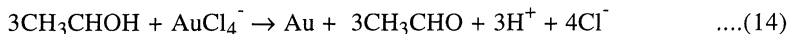


Figure 5. The effect of bulk alcohol concentration and type on the amount of AuCl_4^- reduced during 2.5 minutes of sonication under argon gas. $\text{pH}=3.3$; $f=20 \text{ kHz}$; $I=10 \text{ W/cm}^2$; $[\text{AuCl}_4^-]_0=2\times 10^{-4} \text{ M}$. The insert shows the absorption spectra of AuCl_4^- in the presence of propan-1-ol (0.1 M) a) before and b) following 10 minutes of sonication under the same conditions.

In the presence of an alcohol, e.g., ethanol, the additional steps



can be proposed. It is important to state that reaction (12) although plausible is not established, and reaction (15) is a simplification of the growth mechanism for the formation of colloidal gold.

Figure 5 shows the effect that different alcohols have on the reduction of AuCl_4^- . As with the MnO_2 case the reduction can be compared to the surface excess of the alcohol rather than the bulk solution concentration. This is done in Figure 6 which shows a very good correlation with the interfacial concentration of the alcohol, further supporting the role of interfacially adsorbed species in directing the sonochemical reaction yields.

This was examined further by using the surfactants sodium dodecyl sulfate (SDS) and octa-ethyleneglycol mono n-dodecyl ether (C_{10}E_8), rather than alcohol, as radical scavengers. Figures 7 and 8 show the extent of reduction of AuCl_4^- as a function of $[\text{C}_{10}\text{E}_8]$ and $[\text{SDS}]$ respectively. The breaks in the extent of reduction with surfactant concentration seen at 1 mM and 8 mM match the experimental critical micelle concentration (cmc) of the C_{10}E_8 and SDS, respectively [28].

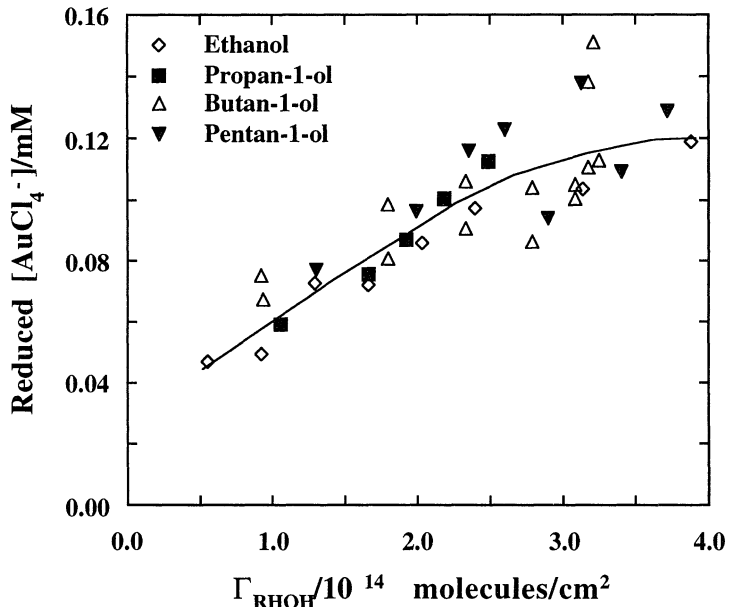


Figure 6. The effect of the surface excess of various alcohols on the reduction of AuCl_4^- during 2.5 minutes of sonication under argon gas. $\text{pH}=3.3$; $f=20\text{kHz}$; $I=10\text{ W/cm}^2$; $[\text{AuCl}_4^-]_i=2\times 10^{-4}\text{ M}$.

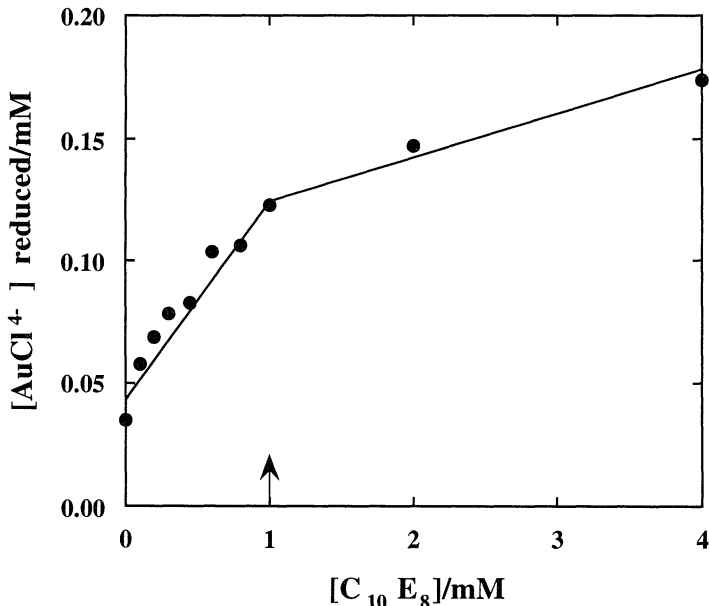


Figure 7. The effect of $[\text{C}_{10}\text{E}_8]$ on the reduction of aqueous AuCl_4^- solutions ($2\times 10^{-4}\text{ M}$) following 7.5 minutes of sonication under argon gas. $\text{pH}=4.5$. $f=20\text{ kHz}$; $I=10\text{ W/cm}^2$.

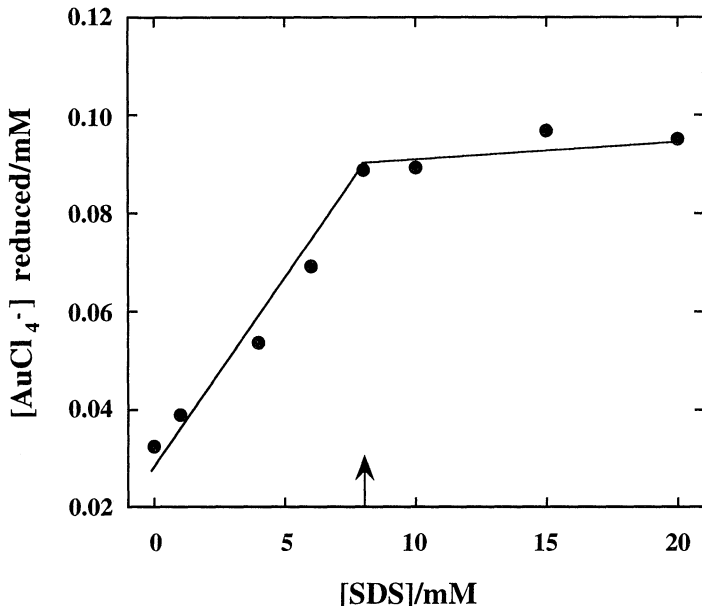


Figure 8. The effect of [SDS] on the reduction of aqueous AuCl_4^- solutions (2×10^{-4} M) following 7.5 minutes of sonication under argon gas, pH=4.5, $f=20$ kHz; $I=10$ W/cm².

At concentrations above the cmc the free monomer concentration remains virtually constant with increasing surfactant concentration and so too does the amount of surfactant adsorbed at air-water interface [28]. As the interfacial concentration is constant above the cmc the number of primary radicals that can be scavenged is fixed though the total surfactant concentration in solution increases.

4. The Role of Surface Active Solutes in Sonoluminescence

The creation of a dispersion of bubbles in an aqueous solution by ultrasound means that interbubble interactions will occur and that these interactions will be dependent on the type and amount of solute species adsorbed at the bubble water interface [33]. The effect of aliphatic alcohols and surfactants on the SL intensity generated from pulsed 500 kHz ultrasound in aqueous solutions is detailed in the next two sections.

4.1 SL IN AQUEOUS ALCOHOL SOLUTIONS

The SL intensity obtained from a train of 4 ms ultrasound pulses, with increasing concentration of methanol, is seen in Figure 9. SL spectra obtained are also shown in this figure.

The extent of SL quenching with an increasing concentration of alcohol increases with an increase in the hydrocarbon chain length of the alcohol, as can be seen in Figure 10. The trends seen are very similar to the behaviour observed for the dissolution of colloidal MnO_2 and for the reduction of AuCl_4^- and suggests that the SL quenching is,

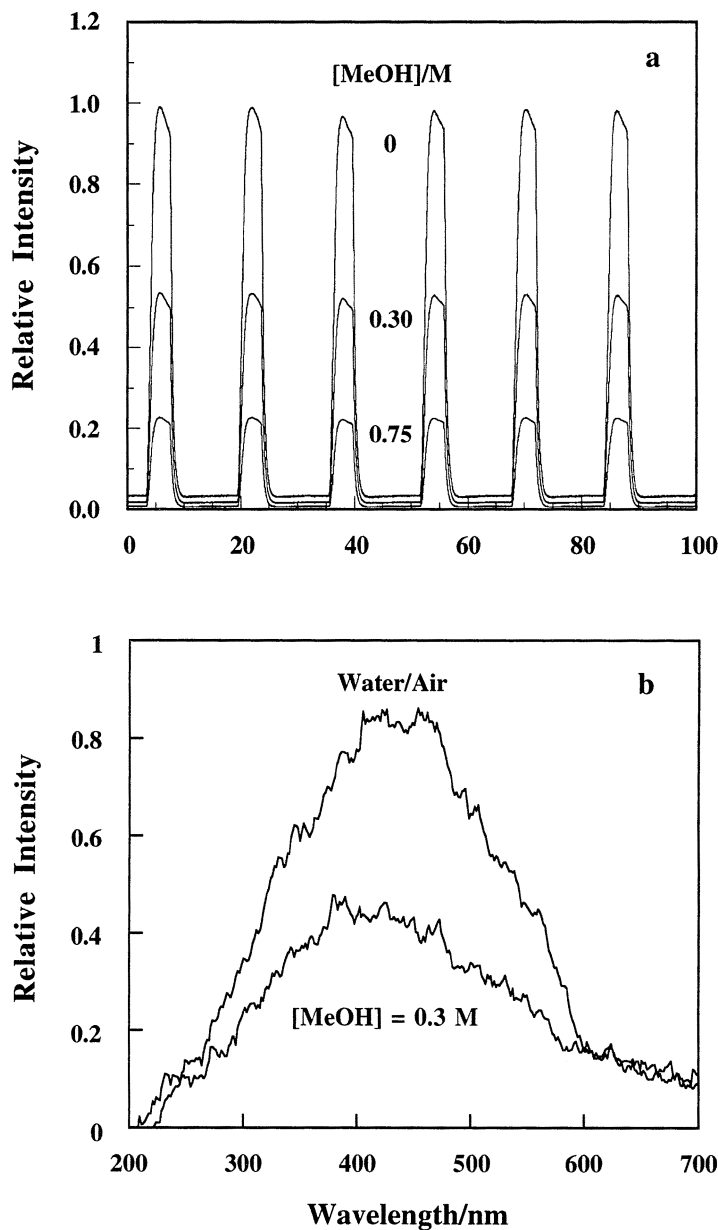


Figure 9. a)The effect of methanol concentration on the total SL intensity obtained from water at specific times of sonication ($f=500$ KHz) in air.
 b) the SL spectrum obtained from water during sonication ($f=500$ KHz) in air and in the presence and absence of methanol (0.3 M).

similarly, related to the amount of alcohol at the bubble/water interface. This postulate is borne out in Figure 11 which shows that the extent of SL quenching increases with the surface excess of the alcohol.

Since the source of SL is within the bubble a possible explanation for how the alcohol quenches the signal is depicted in Figure 12. As the bubble collapses some of the alcohol molecules adsorbed at the bubble-solution interface are expelled from the interface as well as evaporated into the core. The alcohol molecules in the core of the bubble either prevent the formation of the precursor species that produce SL or quench the species that emit light. More evidence to support this suggestion is given in the next section.

4.2 SL IN AQUEOUS SURFACTANT SOLUTIONS

The pulsed sonication of air saturated aqueous solutions containing non volatile surfactants does not lead to SL quenching as seen for the case of alcohol solutions. In contrast, the behaviour observed is quite dependent on the concentration and on the type of head group possessed by the surfactant. In the case of SDS an anionic head group surfactant, the SL intensity at first increases above the signal seen in water alone, reaches a maximum at about 2 mM, then decreases back to the water signal level. The behaviour is shown in Figure 13.

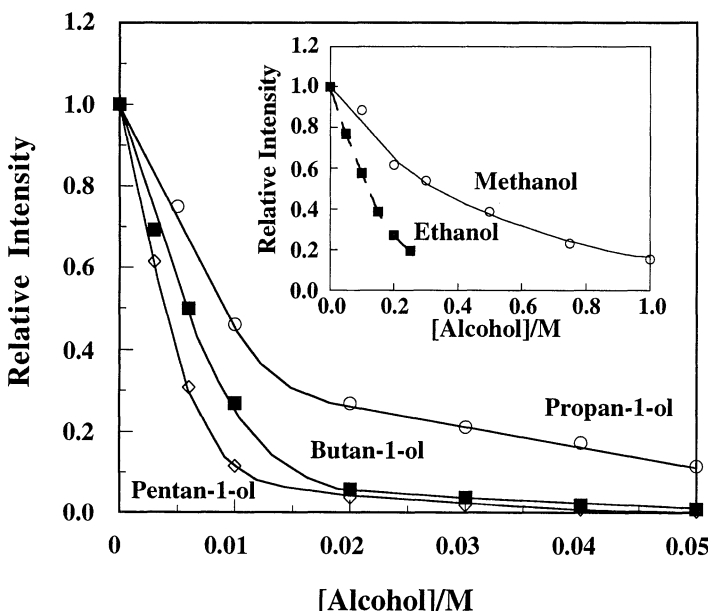


Figure 10. Effect of alcohol concentration and type on the quenching of the SL spectral intensity obtained from water sonicated at 500 kHz. The insert shows that a much larger amount of alcohol is required to totally quench the spectrum for smaller chain length ethyl and methyl alcohol solutions.

If, however, 0.1 M NaCl is present in solution the signal intensity remains constant with the addition of SDS in the concentration range shown above [33]. The possibility that surfactant micelles play a role in the behaviour seen in Figure 13 can be excluded. The

critical micelle concentration for SDS is 8 mM [28], well above the concentration at which the maximum effect is seen. Also, the same profile seen in Figure 14 was observed for the cationic surfactant dodecytrimethyl ammonium chloride (DTAC) which has a cmc of 20 mM [28]. In addition, if the zwitterionic surfactant, N-dodecyl-N, N-dimethyl-3-ammonio-1-propanesulfonate (DAPS), cmc of 2 mM [28] or the decyl derivative which has a cmc of 40 mM, were added to water there was no change in the signal relative to water.

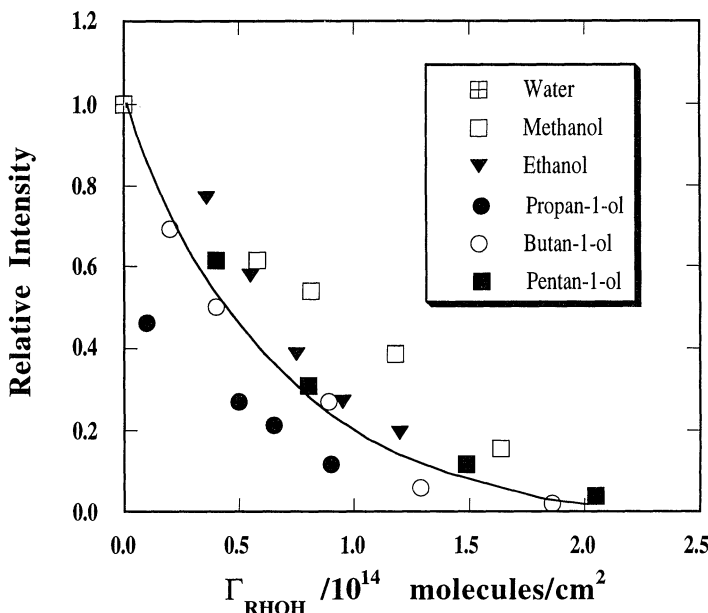


Figure 11. The effect of the surface excess of alcohol, Γ_{RHOH} on the quenching of SL obtained from water sonicated at 500 kHz in air.

Before attempting to explain the behaviour described above it is instructive to consider certain aspects associated with the sonication of surfactant solutions. As bubbles are created and grown in a pulsed ultrasound field, surfactant molecules will adsorb at the bubble/water interface. For the case with charged surfactants the bubbles will acquire a surface charge and an associated diffuse charge layer. The electrostatic field around the bubble surface will act to repel the bubbles from each other thereby inhibiting bubble clustering. Addition of an electrolyte, such as NaCl, will screen the electrostatic field around a bubble surface [28] and allow bubble clustering to occur. Clustering of bubbles will occur naturally because the sum of the van der Waals forces between two similar materials in a fluid are attractive [34]. In a sound field bubble clustering will also be driven by the longer range hydrodynamic Bjerknes forces but at short separation distances van der Waals forces will dominate [34]. A pictorial representation of all this is given in Figure 14. It has been suggested that bubbles within a cluster are shielded from the sound field applied to the solution and as a consequence do not undergo collapse [35]. However bubbles that are more uniformly dispersed will experience a more uniform sound field and more bubbles will undergo collapse, hence a larger SL signal in this situation.

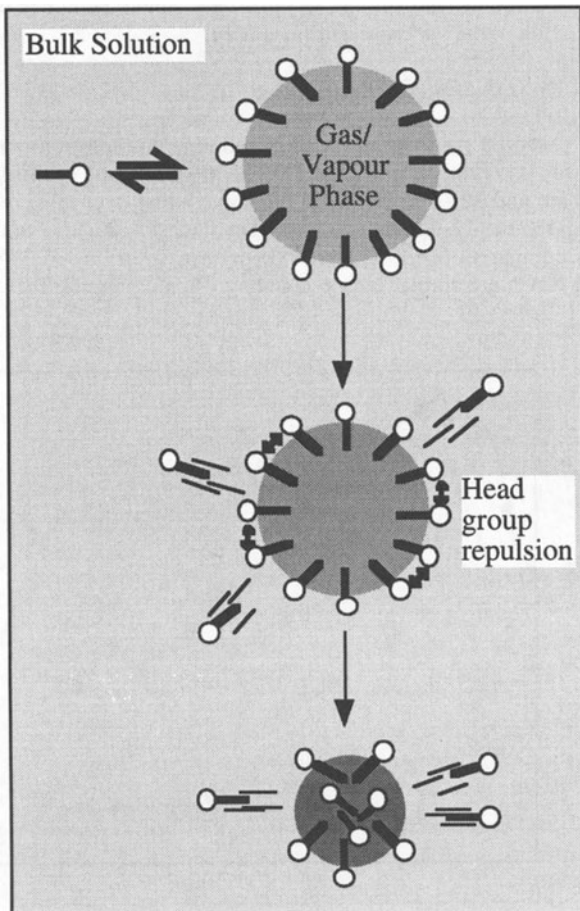


Figure 12. Diagrammatic representation of a possible scenario leading to the quenching of SL from water by alcohol molecules.

Based on this model the results of Figure 13 can be rationalised. The rise in the SL signal, reaching a maximum at about 2 mM SDS, is due to a decrease in the extent of bubble clustering, brought about by an increase in the amount of SDS that is adsorbed at the bubble surface, and hence an increase in negative surface charge. It should be noted that at about 2 mM of SDS, under equilibrium conditions, the air/water interface is about 90% saturated. The decrease in the SL signal above 2 mM is due to the rise in the total electrolyte level in solution which acts to screen the repulsion between bubbles which leads to more bubble clustering and therefore fewer bubble collapses. Evidence to support this interpretation comes from the results of the addition of NaCl where, as stated earlier, it was found that the SL signal obtained in SDS solutions was the same as that in pure water. Further, with DAPS solutions, which has a net zero charged head group and therefore no interbubble electrostatic repulsion, the same signal intensity was obtained as found in pure water. It is also known that the equilibrium surface excess for all the surfactants over the

concentration ranges examined are similar, so the effects cannot be due to differences in the interfacial concentration of the various surfactants used.

4.3 SL SPECTRA IN SDS SOLUTIONS

The SL spectrum observed from an argon saturated aqueous solution containing SDS (2 mM) and NaCl (10 mM) is shown in Figure 15. The main features of this spectrum are the band between 300 nm and 325 nm, the broad band extending over most of the wavelength range recorded, and the band centred at 595 nm. The latter band is due to the sodium atom emission [36]. In comparison, the spectra taken from solutions of DAPS and DTAC containing 10 mM NaCl, are similar but do not show Na atom emission.

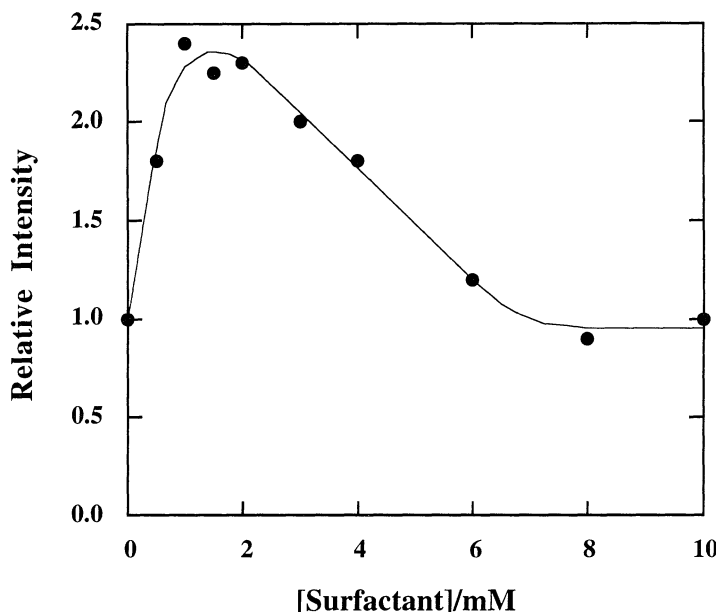


Figure 13. Effect of SDS on the SL intensity from water sonicated at a frequency of 500 kHz under air.

The results strongly support the earlier interpretation of the existence of an interfacial charge layer around bubbles produced when solutions containing charged surfactant are sonicated. With SDS adsorbed at the bubble-solution interface the negative charge density at the bubble surface will attract Na^+ counterions and therefore the surface concentration of Na^+ ions will be far greater than that in bulk solution. An estimate of the Na^+ surface concentration can be made if it is assumed that the electrostatic surface potential of the SDS loaded bubble is comparable to SDS micelles [37] and emulsions [38]. Under the conditions used the surface potential (ψ) for the latter system is ≈ -120 mV. Hence, using the Boltzmann relationship,

$$[\text{Na}^+]_{\text{surface}} = [\text{Na}^+]_{\text{bulk}} \cdot \exp(-e\psi/kT) \quad \dots(16)$$

a value of 1 M for the surface concentration of Na^+ is calculated. Interestingly, this concentration is of the order that is required to obtain a comparable Na emission intensity in NaCl solutions.

The mechanism for producing the Na atom emission is not known. Two possibilities exist: (i) Na is produced at the bubble surface in the hot shell [39] that is formed around the bubble following compression; (ii) small amounts of interfacial liquid is "injected" into the bubble core during the likely asymmetric collapse of the bubble. At present we do not have any evidence to discriminate between these two possibilities.

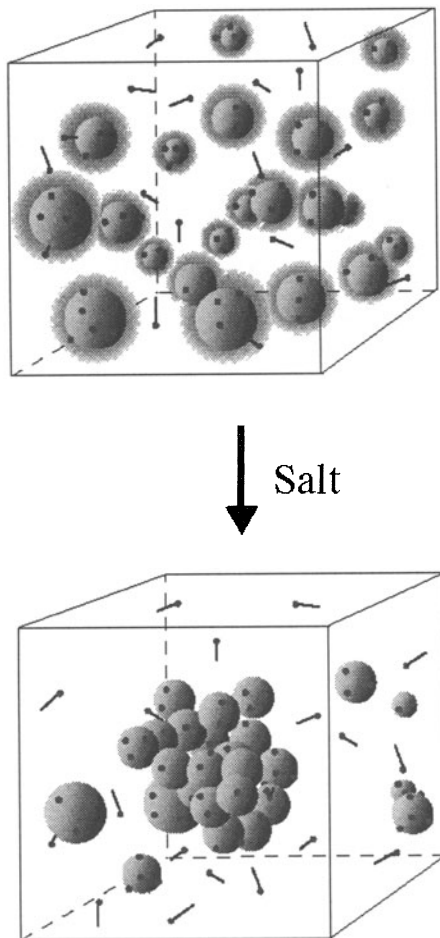


Figure 14. Diagrammatic representation of the bubble clustering phenomenon which may lead to the decrease in SL intensity from aqueous, ionic surfactant solutions in the presence of salt. The top part of the diagram represents the bubble distribution in the presence of SDS and the lower half shows the bubble clustering that occurs on the addition of salt.

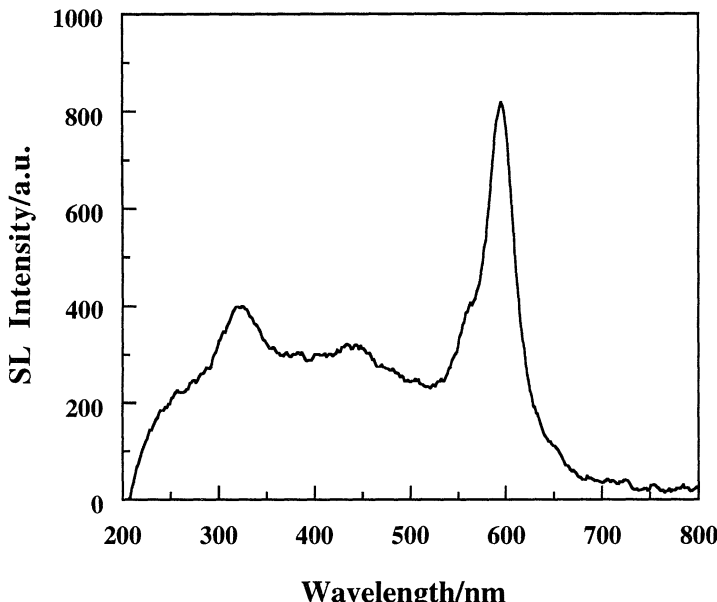


Figure 15. The SL spectrum obtained from an aqueous solution of SDS (2 mM) and NaCl (10 mM) sonicated at 358 kHz under argon gas. $T = 16.9 \pm 0.3^\circ\text{C}$.

Summary

The results presented show that surface active solutes, such as aliphatic alcohols and surfactants have a marked effect on the sonochemical reactions leading to colloid formation and dissolution. The major parameter that characterizes the surface active effect is the Gibbs surface excess. This represents the 2 dimensional concentration of the surface active solute at the bubble-solution interface.

For the case of SL from aqueous solution, surface active solutes also affect the emission yield. The behaviour recorded indicates that both interbubble and intrabubble effects are responsible for the observations. Details of the actual processes for SL quenching remain vague because the source of the emission is still undefined.

Overall, the results highlight the importance of solutes adsorbed at the bubble-solution interface in the expression of both sonochemical and sonoluminescence events.

References

- 1 Prakash, S., Ghosh, A. (1959) *J. Colloid Sci.*, **14**, 338.
- 2 Baigent, C. L., Müller, G. (1980) *Experientia*, **36**, 472.
- 3 Gutiérrez, M., Henglein, A. (1987) *J. Phys. Chem.*, **91**, 6687.
- 4 Au Yeung, S., Hobson, R., Biggs, S. and Grieser, F. (1993) *J. Chem. Soc., Chem. Commun.*, 378.
- 5 Grieser, F. (1996) Sonochemistry in colloidal systems, in P.V. Kamat and D. Meisel (eds.) *Semiconductor Nanoclusters: Studies in Surface Science and Catalysis*, Elsevier Science B.V., Vol. 103, 66.

- 6 Hobson, R. A., Mulvaney, P., and Grieser, F. (1994) *J. Chem. Soc., Chem. Commun.*, 823.
- 7 Biggs, S. and Grieser, F. (1995) *Macromolecules*, **28**, 4877.
- 8 Trentler, T. J., Suryanarayanan, R., Sastry, S. M. L. and Buhro, W. E. (1995) *Mater. Sci. Eng.*, **A204**, 193.
- 9 Sostaric, J. Z., Mulvaney, P. and Grieser, F. (1995) *J. Chem. Soc. Faraday Trans.*, **91**, 2843.
- 10 Sostaric, J. Z., Caruso-Hobson, R., Mulvaney, P. and Grieser, F. (1997) *J. Chem. Soc., Faraday Trans.*, **93**, 1791.
- 11 Suslick, K. S., Fang, M. and Hyeon, T. (1996) *J. Am. Chem. Soc.*, **118**, 11960.
- 12 Cooper, G., Grieser, F. and Biggs, S. (1996) *J. Colloid Interface Sci.*, **184**, 52.
- 13 Suslick, K. S., Hyeon, T., Fang, M., Ries, J. T. and Cichowlas, A. A. (1996) *Materials Science Forum*, **225-227**, 903.
- 14 Nagata, Y., Mizukoshi, Y., Okitsu, K. and Maeda, Y. (1996) *Rad. Res.*, **146**, 333.
- 15 Okitsu, K., Mizukoshi, Y., Bandow, H., Maeda, Y., Yamamoto, T. and Nagata, Y. (1996) *Ultrasonics Sonochemistry*, **3**, 249.
- 16 Koltypin, Y., Katahi, G., Cao, X., Prozorov, R., and Gedanken, A. (1996) *Journal of Non-Crystalline Solids*, **201**, 159.
- 17 Caruso, R.A. (1997) Ph.D. Thesis: "Colloidal Particle Formation using Sonochemistry", University of Melbourne.
- 18 Ramesh, S., Koltypin, Y., Prozorov, R. and Gedanken, A. (1997) *Chem. Mater.*, **9**, 546.
- 19 Suslick, K. S. (1988) *Ultrasound: It's chemical, physical and biological effects*, VCH Publishers Inc., New York.
- 20 Mason, T. J. (1990) *Sonochemistry: The uses of ultrasound in chemistry*, Royal Society of Chemistry, Cambridge.
- 21 Mulvaney, P., Cooper, R., Grieser, F. and Meisel, D. (1990) *J. Phys. Chem.*, **94**, 8339.
- 22 Mulvaney, P., Denison, L., Grieser, F., Cooper, R., Sanders, J.V. and Meisel, D. (1988) *J. Colloid Interface Sci.*, **121**, 70.
- 23 Spinks J.W.T. and Woods R.J. (1990) *An Introduction to Radiation Chemistry*, 3rd ed., Wiley Interscience, New York.
- 24 (a) Anbar, M., Farahatiaziz and Ross, A. B. (1975) *Selected Specific Rates of Reactions of Transients from Water in Aqueous Solution. II*, U.S. Department of Commerce, National Bureau of Standards;
 (b) Farahatiaziz, Ross, A. B. (1977) *Selected Specific Rates of Reactions of Transients from Water in Aqueous Solution. II*, U.S. Department of Commerce, National Bureau of Standards.
- 25 Henglein, A. and Kormann, C. (1985) *Int. J. Radiat. Biol.*, **48**, 251.
- 26 Alegria, A.E., Lion, Y., Kondo, T. and Riesz, P. (1989) *J. Phys. Chem.*, **93**, 4908.
- 27 Sehgal, C., Sutherland, R.G., and Verrall, R.E. (1980) *J. Phys. Chem.*, **84**, 2920.
- 28 Rosen, M.J. (1989) *Surfactants and Interfacial Phenomena*, J. Wiley and Sons, N.Y.
- 29 Suslick, K. S. (1989) *Scientific American*, 80.
- 30 Frenkel, J. (1940) *Russ. J. Phys. Chem.*, **14**, 305.
- 31 Riesz, (1991) Free radical generation by ultrasound in aqueous solutions of volatile and non-volatile solutes, in T.J. Mason (ed.) *Advances in Sonochemistry*, JAI Press Limited, Connecticut, Vol.2, 23-64.
- 32 Henglein, (1993) Contributions to various aspects of cavitation chemistry, in T.J. Mason (ed.) *Advances in Sonochemistry*, JAI Press Limited, Connecticut, Vol. 3, 17-83.

- 33 Ashokkumar, M., Hall, R., Mulvaney, P. and Grieser, F. (1997) *J. Phys. Chem.*, in press.
- 34 Israelachvili, J. (1992) *Intermolecular and Surface Forces*, Academic Press.
- 35 Leighton, T.G. (1994) The Acoustic bubble, Academic Press Limited, London, 521.
- 36 Flint E.B. and Suslick, K.S. (1991) *J. Phys. Chem.*, **95**, 1484-1488.
- 37 Hartland, G., Grieser, F. and White, L.R. (1986) *J. Chem. Soc. Faraday Trans. I*, **83**, 591.
- 38 Anderson, P.J. (1959) *Trans. Faraday Soc.*, **55**, 1421-1429.
- 39 Suslick, K., Hammerton, D. and Cline Jr., R. (1986) *J. Am. Chem. Soc.*, **108**, 5641.

SONOCHEMICAL ENVIRONMENTAL REMEDIATION

T.J.MASON

*School of Natural and Environmental Sciences
Coventry University
Coventry CV1 5FB
U.K.*

Introduction

At the time of writing this is one of the most rapidly expanding areas of research in sonochemistry with the majority of investigations focusing on the harnessing of cavitation effects for the destruction of chemical pollutants. The field is, of course, much broader than this and in this brief review we will explore several aspects in addition to chemical decontamination (Table 1).

Table 1: The uses of power ultrasound
in environmental remediation

biological decontamination
chemical decontamination
acoustic deliquoring
ultrasonic dispersion

1. Biological remediation.

There are essentially three main areas of interest in this domain; surface disinfection, potable water purification and food sterilisation.

1.1 SURFACE DECONTAMINATION

The use of power ultrasound for surface cleaning, is a long-established and efficient technology. Ultrasound is particularly effective in this type of decontamination because the cleaning action is induced by cavitation collapse on and near surfaces which will dislodge bacteria adhering to them. The particular advantage of ultrasonic cleaning in this context is that it can reach crevices that are not easily reached by conventional cleaning methods. Objects for cleaning can range from large crates used for food packaging and

transportation to delicate surgical implements such as endoscopes. One recent example of surface cleaning in food technology is the use of a combination of a bactericide and ultrasound to decontaminate chicken eggs in hatcheries¹. In hatcheries the eggs are normally laid within the nest and relatively clear of contamination but a number are laid (or dislodged to) outside of the nest (some 10%) and generally have contaminated surfaces. These dirty eggs are removed from the hatchery because egg shells are porous and the contamination can penetrate to the inside and kill the developing embryo. The result of this is that these eggs "explode" after about 10 days due to the build-up of gas inside due to decomposition.

Ultrasonically assisted cleaning has proved to be more efficient than the currently used spraying or gassing techniques for the decontamination of "clean" eggs but, more significantly, ultrasonic decontamination of the "dirty" eggs is so good that they can also be used in the hatchery.

1.2 DISINFECTION OF LIQUIDS

Power ultrasound is known to disrupt biological cell walls and thereby destroy bacteria however for complete disinfection of water very high acoustic intensities are required. Conventional methods of disinfection involve the use of a bactericide e.g. chlorine or ozone in the water industry. Despite the fact that chlorine has proved to be successful in combating a range of water borne diseases there are problems associated with using it, these include:

- Micro-organisms (especially bacteria) are capable of producing strains that are tolerant to normal chlorine treatment levels. This can be overcome by increasing the chlorine dose, however, this can lead to the generation of unpleasant flavours and odours due to the formation of chlorophenols and other halocarbons through reaction with chemical contaminants in the water.
- Certain species of micro-organisms produce colonies and spores which agglomerate in spherical or large clusters. Chlorination of such clusters may destroy micro-organisms on the surface leaving the innermost organisms intact.
- Fine particles such as clays are normally removed by flocculation using chemicals such as aluminium sulphate. The flocs can entrap bacteria and spores and although the vast majority of floc particles are removed during processing it is possible that one or two may pass through the system and the bacteria protected by the floc material may well be unaffected by further disinfection.

Current trends are towards the reduction in use of chlorine as a disinfectant either by replacement with other biocides or by a reduction in the concentration required for treatment. Low power ultrasound offers the latter

possibility since is capable of enhancing the effects of chemical biocides. The effect is thought to be due in part to the break-up and dispersion of bacterial clumps and flocs which renders the individual bacteria more susceptible to chemical attack. In addition cavitation induced damage to bacterial cell walls will allow easier penetration of the biocide.

The results of a study of the combined effect of low power ultrasound and chlorination on the bacterial population of raw stream water is shown in Table 2. Neither chlorination alone nor sonication alone was able to completely destroy the bacteria present. It is significant however that extending the time of chlorination or sonication from 5 minutes to 20 minutes seems to double the biocidal effect of the individual techniques. When sonication is combined with chlorination however the biocidal action is significantly improved. These results suggest that ultrasound could be used in conjunction with chemical treatments to achieve a reduction in the quantity of bactericide required for water treatment².

Table 2: The effect of ultrasound and chlorination on bacterial growth

treatment	% bacteria kill after 5 minutes	% bacteria kill after 20 minutes
no treatment	0	0
chlorine 1 ppm	43	86
ultrasound alone	19	49
ultrasound + chlorine	86	100

Conditions: 1:10 dilution of raw stream water, using ultrasonic bath (power input to system = 0.6 W cm^{-2}), $T = 20^\circ\text{C}$.

The traditional method of sterilising foodstuffs is thermal and some efforts have been made to improve such treatment with the concurrent use of ultrasonic irradiation. This process has been named thermosonication and has been shown to be effective against a range of biopollutants e.g. *Bacillus subtilis* spores³. This treatment provides a substantial reduction in treatment time using a small scale reactor operating at 20kHz and 150W. It can be envisaged that process times and/or temperatures could be reduced to achieve the same lethality values. A modified treatment process for food sterilisation involving a combination of heat and sonication under pressure has also been reported⁴. This methodology was found to decrease the heat resistance of *Staphylococcus aureus* by 63% and *Bacillus subtilis* by 43% as compared to heat treatment alone. Under pressure the boiling point is raised and lethality of the microbes above boiling point is maintained with values 5 to 30 times greater than those achieved with heat treatment alone. Spores appeared to be most resistant and yeasts the most susceptible to this type of treatment.

2. Chemical Remediation

2.1 DECONTAMINATION OF WATER

Ultrasonic irradiation of aqueous solutions results in the formation of free radicals due to the homogeneous sonolysis of water, if the pollutants enter the bubble they may also suffer decomposition. A study of sonochemical treatment of chlorinated hydrocarbons in water demonstrated the homogeneous destruction of CH_2Cl_2 , CCl_4 , MeCCl_3 , and ClCH=CCl_2 in solution at concentrations of 100-1000 ppm by volume⁵. The method appears to be potentially quite powerful for the purification of contaminated water. In a separate study when saturated aqueous solutions of CH_2Cl_4 (110 ppm) and MeCCl_3 (1300 ppm) were sonicated for 20 minutes some 75% of the contaminant was degraded⁶.

The sonochemical removal of chlorinated aromatic compounds from water is attracting considerable attention. The degradation of the aromatic species is generally initiated by an attack on the aromatic ring by HO^- radicals generated through the sonochemical break-down of water itself. Using phenol as a model substrate it has been shown that degradation takes place *via* sequential oxidation and the intermediate formation of hydroquinone and catechol⁷. The final products of the process using ultrasound at 541kHz are low molecular weight carboxylic acids. The process for the degradation of phenol (100mg $^{-1}$) requires long reaction times of from 1 to three hours depending on the entrained gas used.

Table 3: Sonophotochemical dechlorination of aqueous pentachlorophenol

conditions	Cl^- yield (50 mins)	Cl^- yield (120 mins)
uv	40%	no change
uv/ultrasound	60%	100%

Pentachlorophenol ($2.4 \times 10^{-4}\text{M}$) in water containing 0.2% TiO_2

There are a few reports on the combined application of ultrasound and ultraviolet light for the destruction of chemical pollutants. A great potential exists for synergistic improvements in technology *e.g.* the removal of 1,1,1-trichloroethane from aqueous solutions using the combined application of ultrasound and light is more efficient than the application of either technique individually⁸. In the presence of an aqueous suspension of TiO_2 powder, uv irradiation causes the breakdown of polychlorobiphenyls (PCB's). Using pentachlorophenol as a model substrate in the presence of 0.2% TiO_2 , uv irradiation induces dechlorination but only to a limit of 40% completion probably due to surface contamination of the powder⁹. When ultrasound is used in conjunction with the photolysis the dechlorination is dramatically improved

(Table 3). This improvement can be ascribed largely to the mechanical effects of cavitation involving surface cleaning and increased mass transport to the powder surface.

The advantages of using ultrasound in conjunction with electrochemistry have been referred to elsewhere¹⁰. This combination has been particularly beneficial in the destruction of phenols by electrochemical oxidation. Ultrasound (25kHz, 10^4 W/m²) when applied to a solution containing phenol (100gl⁻¹) and NaCl (2gl⁻¹) achieves better than 80% oxidation to maleic acid¹¹. In the absence of ultrasound only 50% decomposition was obtained under the same conditions. In a more recent study an almost complete sonochemical destruction of phenol in saline solution at pH6 was obtained at a current density of 170 Am⁻² in 10 minutes¹². The reaction was shown to proceed via intermediate chlorinated phenols.

A long-time environmental problem has been the removal of colour from the effluent streams of textile factories since the presence of residual dyes is rather obvious even at low dilutions. There are several conventional approaches to the solution of this problem including absorption onto activated charcoal, flocculation, chemical oxidation, ozonolysis and irradiation with uv light. Sonication can be added to any of these and the combination of ultrasound with ozonolysis seems particularly efficient¹³. We have investigated the sonoelectrochemical destruction of dyes and in particular the destruction of Sandolan Yellow. The process entails the electrolysis of aqueous NaCl solution which involves the liberation of chlorine at the anode and hydroxide ion at the cathode. The overall cell reaction is:



The improvement using ultrasound in conjunction with electrolysis is evident (Figure 1). Electrolysis was carried out in an open beaker immersed in an ultrasonic bath (38kHz, 1.1 Wcm⁻²) at 75mA using 1.5 mg l⁻¹ dye in 0.1 M NaCl solution. The results are normalised to an initial dye concentration of 100% at zero time.

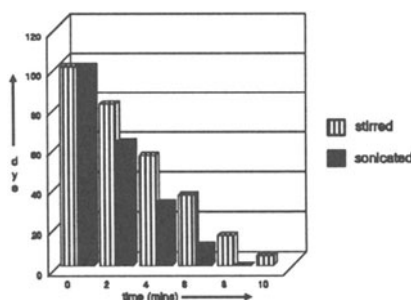


Figure 1 Sonoelectrochemical removal of Sandolan Yellow in saline solution

2.2 DECONTAMINATION OF SOIL

Power ultrasound can be used for the rehabilitation of polluted industrial sites through the removal of chemical and biological contamination from soil. Conventional soil washing processes are based on the principle that many pollutants adsorb onto the fine fractions of soil such as silt, clay and humic matter which tend to be attached to coarser sand and gravel particles which make up the majority of the soil content. Therefore the primary aim in soil washing is to separate these fine components from the bulk soil. Isolation of the fine materials will result in a "concentrated" volume of polluted soil which may be treated or disposed of, and a large volume of residual soil which requires relatively little treatment and can be returned to the site as back fill. A comparison has been made of the efficiencies of conventional and ultrasonically assisted pollutant extraction procedures using model soil samples (granular pieces of brick) which had been deliberately contaminated with copper oxide at 51 ppm¹⁴. Analysis of the brick particles after 30 minutes sonication on a Vibrating Tray¹⁵ revealed an average reduction in copper content to 31 ppm, a reduction of about 40%. Using a conventional mechanically shaken tray for the same time period the residual contamination was 48 ppm representing a reduction of only 6% (Table 4).

Table 4: Ultrasonic washing of brick particles

Washing with mechanical shaking			
residual brick = 746.5g 48 ppm	< 20 mesh = 2.9g 310 ppm	fines = 0.63g 3200 ppm	water = 12.6 l 0.22 ppm
Reduction in copper contamination in treated brick = 6%			
Washing with Vibrating Tray			
residual brick = 744.7g 31 ppm	< 20 mesh = 3.4g 96 ppm	fines = 1.89g 4700 ppm	water = 13.5 l 0.49 ppm
Reduction in copper contamination in treated brick = 40%			

Initial mass of brick 750g, copper contamination 51.4 ppm

3. Acoustic Deliquoring

The subject of acoustic filtration has been covered elsewhere¹⁰. Within this section the particular advantages of combining ultrasound alone with

filtration (acoustic filtration) and in conjunction with an electric field (electroacoustic filtration) were discussed. The former technique is currently being successfully applied to a specific environmental separation problem - the removal of fine particulate and cellular material from the white water outflow of paper mills. This is a particularly difficult filtration process since the filters readily clog under conventional filtration conditions. Acoustic filtration appears to offer an extremely good means of separation when applied to the type of membranes used in filter cartridges¹⁵.

4. Ultrasonic Dispersion

On offshore oil drilling rigs an environmental problem exists related to the disposal of drilling cuttings. This material is particulate and must be cleaned of oil thoroughly before being dumped at sea. Cleaning technologies exist for the first phase of this process but when the clean material is dumped it sinks to the sea bed and accumulates around the platform legs presenting a problem to sea life and eventually rig maintenance. An ultrasonic device has been built which is suitable for use on an oil rig and provides a flow treatment for the drilling mud which substantially reduces particle size and, as a result, the cleaned mud disperses across the sea bed and does not accumulate around the legs¹⁷.

References

1. Slapp P., Production Line Cleaning, Diss, U.K. British Patent 95 00587 2.
2. Phull,S.S., Newman,A.P., Lorimer,J.P., Pollet,B. and Mason, T.J. (1997) *Ultrasonics Sonochemistry*, **4**, 157.
3. Ordonez J.A., Sanz B., Burgos J. and Garcia M.L. (1989) *Journal of Applied Bacteriology*, **67**, 619.
4. Effect of Heat and Ultrasound on Microorganisms and enzymes, Sala F.J., Burgos J., Condon S., Lopez P. and Raso J. (1995) *New Methods of Food Preparation*, ed G.W.Gould, Blackie (London).
5. Cheung, H.M., Bhatnagar, A. and Jansen, G. (1991) *Environ. Sci.Techol.*, **25**, 1510.
6. Nagata, Y., Kurosaki, Y., Nakagawa, M. and Maeda, Y. (1993) *Chem.Express*, **8**, 657.
7. Berlan, J., Trabelsi, F., Delmas, H., Wilhelm, A-M. and Petrignani, J.F. (1994) *Ultrasonics Sonochemistry*, **1**, S97.
8. Toy, M.S., Carter, M.K. and Passell, T.O. (1990) *Environmental Technology*, **11**, 837.
9. Information produced by the Stanford Research Institute, 333 Ravenswood Ave., Menlo Park, CA, U.S.A.
10. See chapter on "Industrial Applications of Sonochemistry and Power Ultrasonics" by T.J.Mason in this volume.
11. Mizera, J. (1992) *Chem. Abs.*, **99**, 127904x, (Polish).
12. Berlan, J., presented at Industrial Sonochemistry Symposium, ENSIGC, Toulouse, France, 1994.
13. See chapter on "Cavitation Environmental Remediation" by J.R.Russell in this volume.
14. Newman, A.P., Lorimer, J.P., Mason, T.J. and Hutt, K.R. (1997) *Ultrasonics Sonochemistry*, **4**, 153.
15. Vibrating Tray™ is a product of Lewis Corporation, 102 Willenbrock Road, Oxford, Connecticut 06478-1033, U.S.A.
16. Information provided by VTT Energy, Dewatering Research Group, PO Box 1603, FIN-40101 Jyväskylä, Finland.
17. Information provided by Sonic Process Technologies Ltd., P.O. Box 82, Astley, Shrewsbury SY4 4WP, U.K.

CAVITATIONAL ENVIRONMENTAL REMEDIATION

JOHN P. RUSSELL

ARC Sonics Inc.

P.O. Box 24

Suite 722 - 601 West Broadway

Vancouver, British Columbia

Canada V5Z 4C2

ARC Sonics Inc. (ARC) has developed, patented, and successfully demonstrated a new acoustic energy technology for use in ultra-fine grinding, sonochemistry, or remediation of contaminated soils, sludges and liquids. The technology generates low-frequency sonic energy at high power levels - up to 75 kW with plans for up to 250 kW. In operation it creates extreme vibration and cavitation. This paper describes the technology and summarizes an extensive series of tests which demonstrate the capacity of the equipment.

1. Resonant Beam Configuration

The heart of the ARC system is the cylindrical steel beam, supported at its nodal points and driven into resonant oscillation by a series of electromagnets, to which is attached the reaction chambers.

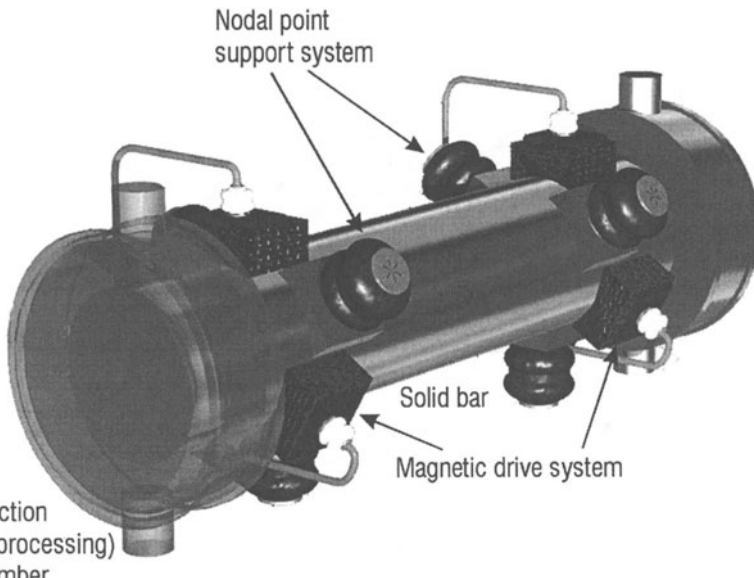


Figure 1 depicts the equipment and its configuration.

Figure 2 shows the electromagnetic drive. The magnets are placed at 120 degrees symmetrically about each end of the resonant beam. The power used is industrial three phase; the frequency is modified to match the frequency of the resonant beam. It is this resonant feature that allows the beam to be driven into large amplitudes of oscillation with minimal power. In this configuration, the rotating magnetic force vector produced by the three drive units causes a nutational, or clover-leaf shaped, vibration. The result is a highly efficient method of converting electrical energy into a fluid-coupled field of intense sonic power.

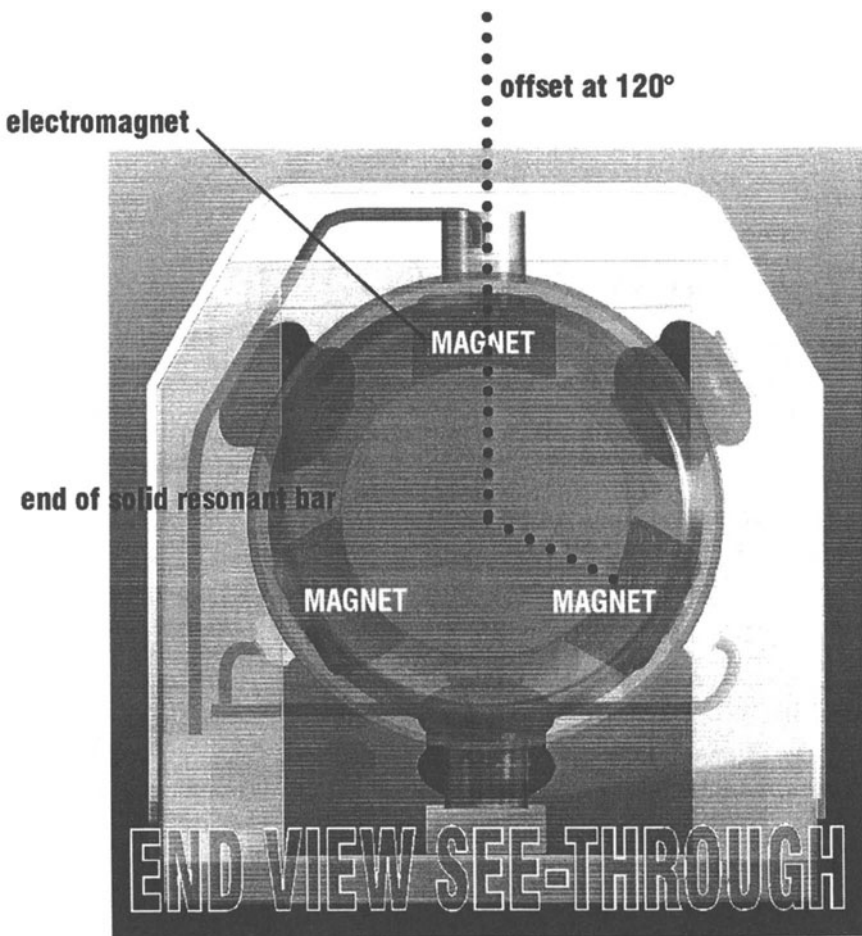


Figure 2 The Magnetic Drive Configuration

Reaction chambers (2) of up to 35 litres (each) are attached to each end of the vibrating beam. Fluid or slurry is continuously flowed through the reaction chambers where it is subjected to very high amplitudes of vibration. The resulting shock loading has been calculated as up to 600 g¹. Cavitation results.

2. Three Operating Machines

2.1 THE 5 kW UNIT

To date, three systems have been built and tested. The smallest, a 5 kWatt unit, has a vertical bar driven from the top. It is like a very large ultrasonic probe with a 3 foot (90 cm) rod available for insertion into the target material. This unit is very good for mixing liquids, degassing, gas/liquid saturation, and driving sonochemical reactions. When a clear acrylic tank is used, the results can be clearly seen: as the beam is driven at low power, donut shaped rings begin to appear at the anti-nodal planes; as the power level is increased, these zones broaden to take in the whole volume.

2.2 THE 20 kW UNIT

The 20 kW machine is designed horizontally with reaction chamber at both ends. It is presently being used for extensive batch testing and limited continuous testing for a variety of industrial clients.

2.3 THE 75 kW UNIT

The 75 kW unit is also horizontal in design. The steel beam of the 75 kWatt machine is 14 inches (35.5cm) in diameter, 14 feet (4.27 meters) long and weights about 6000 pounds (2.7 tonnes). This machine was tested over a 6 month period at a mine mill where it was used to grind gold-bearing ore - throughput was approximately 100 tonnes per 24 hour day. This unit has operated for close to ten thousand hours, processing minerals, decontaminating various soils, and conducting tests for clients. It has proved to be highly reliable.

These machines oscillate at various resonant frequencies. The 75 kW unit operates at 104 Hz ,the 20 kW unit at 460 Hz and the 5 kWatt at 330 Hz . The vibrational amplitudes variety from 8 millimeters to 1 millimeters respectively. The units weigh 13.5 tonnes, 3 tonnes and 1 tonne.

3. Generation Of Cavitation

ARC has not measured the characteristics of the cavitation generated by its technology. Project test results indicate that cavitation does occur. Much of our understanding of cavitation stems from the information on ultrasound.² The literature and proceedings of conferences indicates that collapsing bubbles in the cavitation “swarm” achieve temperatures of up to 5000° Kelvin and pressures of 1000 atmospheres.³ There could be as many as one 1,000,000 cavitation events per second per cc of liquid⁴. Cavitation is known to cause pyrolytic reactions, chemical changes, and even light radiation (sonoluminescence) from the zone of cavitation. ARC Sonics technology does not induce as many cavitation events as ultrasound due to its lower frequency.

The use of the cavitational phenomena in industry has been restricted in the past because it has not been possible to create this phenomena at an industrial scale level. ARC Sonic has proven the capacity to reliably generate high acoustic power in large volumes of material, suitable for industrial applications.

4. Sonic Destruction of Organic Substances

Since 1992, extensive tests have been conducted in the area of destruction of organic bases contaminants. Results have shown the reduction of contaminant levels in liquids and contaminated soil. This work was financed by ARC, and the DESRT program⁵: the final report is entitled "Integration of Enhanced Oxidation and Sonic Mixing for Treatment of Contaminated Soil"⁶.

The report documents the destruction of pentachlorophenol (PCP) in water solution, from over 100 ppm to less than 1 ppm in about 3 minutes using ozone at 116 mg per minute. With concentrations of 1000 ppm of PCP, destruction of 99.99% was achieved in 12 minutes. Other organic and organochloride materials were treated with similar results. (These results have since been improved on.) In other similar projects, the positive results have been extended to sequestering of metal contaminants and destruction of dye in a water solution.

5. Theoretical Basis for Advanced Oxidation

Experimental and theoretical modeling of the sonic destruction process has been carried out by Huang⁷ and Kang⁸, leading to very plausible predictions of the reaction rate kinetics and contaminant destruction curves, not unlike those achieved by ARC. The use of advanced oxidation processes (AOP) are well documented in dealing with solid and groundwater contamination.⁹

6. Conclusions

In environmental applications, sonic treatment of soil is effective in creating near perfect slurries and in liberating encapsulated chemical or metallic contaminants. The use of ozone and intense sonic energy effectively destroys organic and chlorinated organic substances. Contaminant metals can be captured after a pretreatment using sonic disruption. The ARC soil remediation system, operating on a full industrial scale of up to 100 tonnes per day, is expected to offer a cost-effective method of cleaning up contaminated soil or groundwater on-site.

The technology will also be of interest in industry for its physical and cavitation effects, where it will answer the need for scale up of cavitation and in sonochemistry .

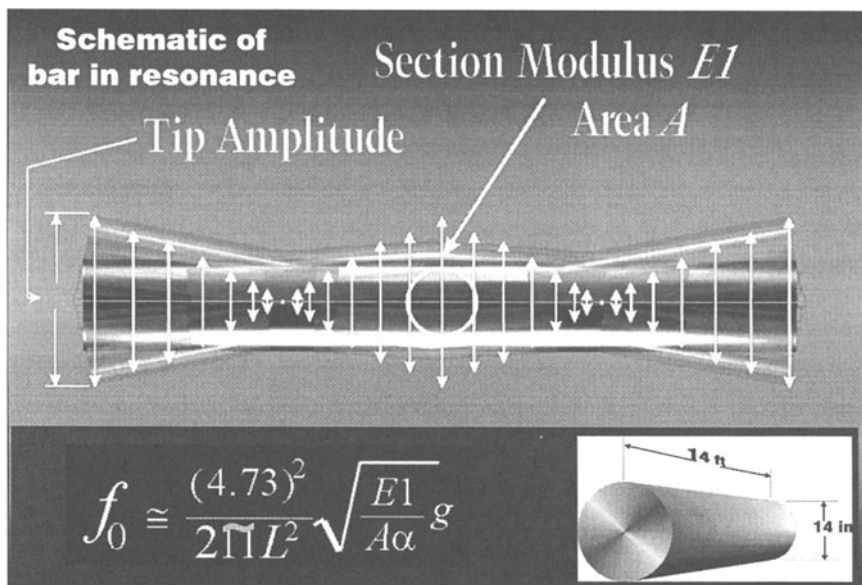
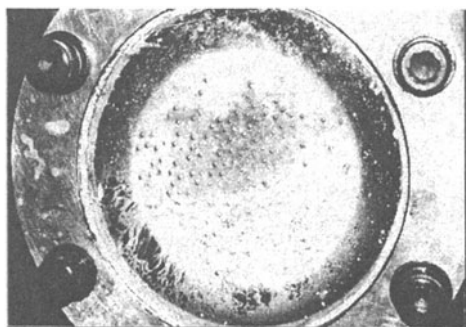
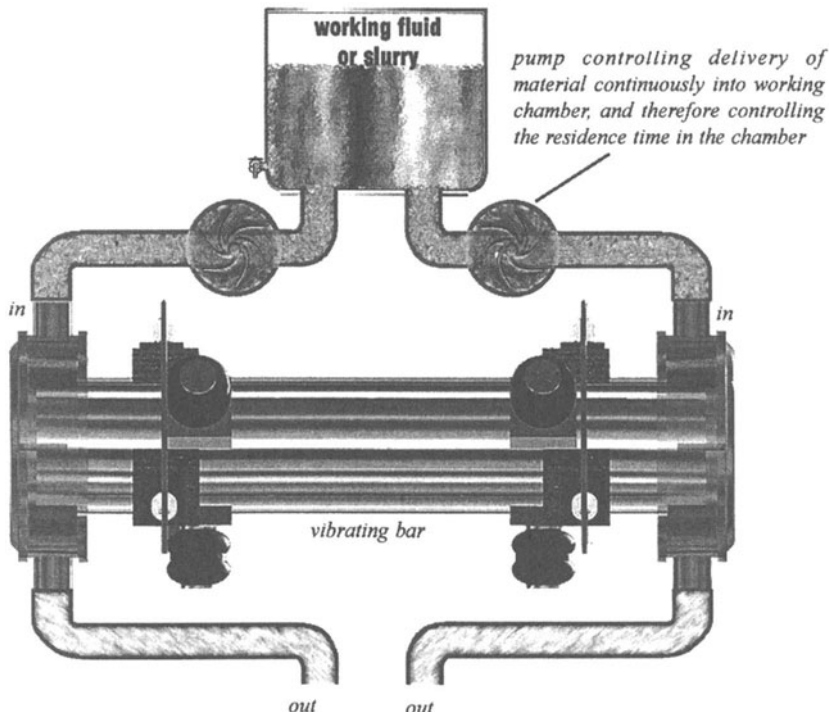
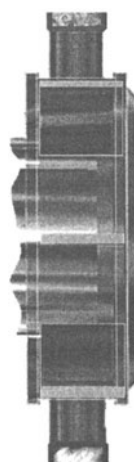


Figure 3 Beam Deflection Diagram: 75 kW Bar



end view of working chamber showing attachment bolts



side view cutaway showing internal baffles to control flow

Figure 4 System flow diagram

7. References

- ¹ gravity
- ² Suslick, K. and Doktycz, S.(Feb. 1990) Sounding Out New Chemistry, *New Scientist* **3**, 50-53.
- Suslick, K. (Feb. 1989) The Chemical Effects of Ultrasound, , *Scientific American*, pp. 80-86.
- ³ Suslick, K. (August 18 - 29, 1997), notes from a talk given, NATO Advanced Study Institute on Sonochemistry and Sonoluminescence.
- ⁴ ibid
- ⁵ Development and Demonstration of Site Remediation Technology Program, sponsored by Environment Canada, and the British Columbia Environment Ministry.
- ⁶ Warren, D. and Russell, J.P. (July, 1995) Integration of Enhanced Oxidation and Sonic Mixing for Treatment of Contaminated Soil - Final Report, DESRT Program.
- ⁷ Huang, C.P. and Huang, Y.C. (October 26 - 29, 1996) Degradation of 1, 4 Dioxane and 2 - Methyl - 1, 3 Dioxolane in Aqueous Solutions by Ultrasound, *3rd International Conference on Advanced Oxidation Technologies*, Cincinnati, Ohio.
- ⁸ Kang, J.W. and Lee, K.H. (October 26 - 29, 1996) The Kinetics of Sonochemical Process for the Destruction of Aliphatic and Aromatic Hydrocarbons, *3rd International Conference on Advanced Oxidation Technologies*, Cincinnati, Ohio,
- ⁹ Keller, L. (1994) Guide for the Use of Advanced Oxidation Processes for the Mitigation of Chemical Spills, guidelines submitted to the ASTM.

INDUSTRIAL APPLICATIONS OF SONOCHEMISTRY AND POWER ULTRASONICS

T.J.MASON

School of Natural and Environmental Sciences

Coventry University

Coventry CV1 5FB

U.K.

1. Introduction

It has been recognised for many years that power ultrasound has great potential for uses in a wide variety of processes in the chemical and allied industries. Some of these applications have been known for many years^{1,2,3} while others are undergoing a renaissance and developing into new and exciting possibilities as in the use of power ultrasound in therapeutic medicine (Table 1).

TABLE 1. Some industrial uses of ultrasound

Field	Application
Plastic welding	Fabrication of thermoplastic articles
Cleaning	Cleaning in aqueous media of engineering items, medical instruments and jewellery
Cutting	Accurate cutting of all forms of material from ceramics to food products
Processing	Pigments and solid dispersion in liquid media, crystallisation, filtration
Sonochemistry	Electrochemistry, environmental protection, catalysis, benign synthesis

2. Plastic Welding

A large proportion of ultrasonic equipment currently in industry is involved in welding or rivetting plastic mouldings for the consumer market⁴. The equipment generally operates at around 20 kHz. A shaped tool or horn transmits (and

amplifies) the vibrating motion to a shaped die pressing together the two pieces of material to be welded. The vibrational amplitude is typically 50-100 microns.

Ultrasonic welding is generally used for the more rigid amorphous types of thermoplastic. It is particularly important that the vibrational energy is primarily transmitted to the joint rather than be absorbed by the body of the material producing heat. This is because any warming of the bulk material can lead to a release of internal moulding stresses and produce distortion. Thermoplastics have two properties which make them particularly suited to ultrasonic welding (a) low thermal conductivity and (b) melting or softening temperatures of between 100 and 200°C. As soon as the ultrasonic power is switched off the substrate or bulk material becomes a heat-sink, giving rapid cooling of the welded joint. When the more traditional conductive heating is used for welding however the thermal gradient has to be reversed before cooling occurs, leading to long heating/cooling process cycles. Another major advantage of the use of ultrasound is the high joint strength of the weld, reaching 90-98% of the material strength. Indeed test samples usually break in the body of the material and not at the weld itself.

3. Cleaning

Ultrasonic cleaning is now such a well established general technology that laboratories without access to an ultrasonic cleaning bath are in a minority. Although the laboratory ultrasonic cleaning bath is familiar, the industrial applications of such cleaning are perhaps less well known. Ultrasonic cleaning can be either delicately applied for the cleaning of microcomponents under clean room conditions or used for very large items such as engine blocks in factories.

4. Cutting

Ultrasonic cutting has been available to industry since the early 1950's specifically for accurate profile cutting of brittle materials such as ceramics and glass, it has been extensively used in the aerospace industry since the 1970's for glass and carbon fibre composites. In recent years ultrasonic cutting has been introduced into the food processing industry where it would appear to have far wider application than the laser and water (oil) jet cutting technologies introduced in the 1980's⁵.

Ultrasonic cutting uses a knife type blade attached through a shaft to an ultrasonic source. Essentially the shaft with its blade behaves as an ultrasonic horn driven normally at 20kHz and with a generator similar to that of a welder operating at around 2kW. The cutting action is a combination of the pressure applied to the sharp cutting edge surface and the mechanical longitudinal vibration of the blade. Typically the tip movement will be in the range 50 to 100 microns peak to peak. Several advantages arise from this technology:

- The ultrasonic vibration of 20kHz applies an intermittent force to the material to be cut and generates a crack (cut) at the tip, controlling its propagation or growth thereby minimising the stress on the bulk material.
- The repeated application of the cutting tip to the product applies a local fatiguing effect which reduces significantly the overall force required to break the bonds of the bulk material.
- In conventional cutting the blade has to compress the bulk material to allow a gap the width of the blade to pass through and this applies a tensile rupturing force at the crack tip. With ultrasonic cutting the whole blade moves or vibrates continuously as it stretches and contracts. This very high frequency movement effectively reduces the co-efficient of friction to a very low level, enabling the blade to slide more easily through the bulk material.

5. Atomization

The conventional method of producing an atomised spray from a liquid is to force it at high velocity through a small aperture. (A typical domestic examples being a spray mist bottle for perfume). The disadvantage in the design of conventional equipment is that the requirement for a high liquid velocity and a small orifice restricts its usage to low viscosity liquids and these atomizers are often subject to blockage at the orifice.

Figure 1 shows a schematic gas driven atomiser. The system comprises of an air or gas jet which is forced into an orifice where it expands and produces a shock wave. The result is an intense field of sonic energy focused between the nozzle body and the resonator gap. When liquid is introduced into this region it is vigorously sheared into droplets by the acoustic field. Air by-passing the resonator carries the atomised droplets downstream in a fine soft plume shaped spray. The droplets produced are small and have a low forward velocity. Atomised water sprays have many uses including dust suppression in industry

and humidifiers for horticultural use under glass⁶.

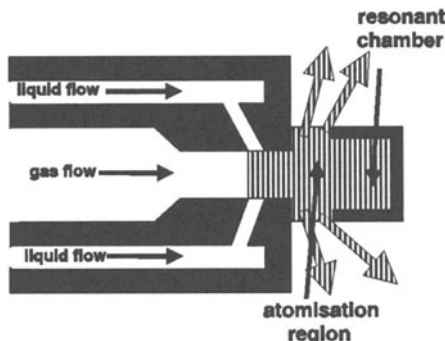


Figure 1: Schematic Atomisation Nozzle (gas driven)

There are several different types of ultrasonic atomizer based on a sonic horn in which the liquid is pumped through a central tube and emerges at the vibrating tip⁷. Although this construction is usually restricted to fairly low viscosity material the ultrasonic vibration itself does help to reduce the shear viscosity of the liquid. When using sonic atomization, it is the tip motion which causes atomization and not the velocity of ejection through the orifice. Since the "nozzle" is under constant agitation there is less risk of blockage with this design.

In the coating industry, apart from the obvious advantages of being able to use higher viscosity material with no jet blockage sonic spraying has another great advantage over conventional methodology. Normal jet atomization ejects particles at high velocity and some of these would collide with a surface with such high energy that "bounce-back" might occur, particularly if there was no strong adhesion between the ejected spray and the surface. Although electrostatic methods have been employed in conventional spraying in order to reduce "bounce-back", sonic atomization does not produce high particle velocity and so impact adhesion is much less of a problem. The particle size of sonically atomised sprays can be accurately controlled by either the ultrasonic power or the frequency of tool vibration such that greater control of coating is possible. Ultrasonic atomization has also been used to produce finely particulate sprays from such materials as molten glass and metal.

Ultrasonic sprays produced via horns are also finding use in spray drying installations where there are clear advantages in producing minimal particle velocity with a controlled particle size through a non-clogging nozzle⁸.

6. Mixing and Homogenisation

There are a large number of industrial processes which employ power ultrasound as a means of mixing material. These are summarised in Table 2. Although the ultrasound can be supplied through bath or horn systems there is another method of achieving the mixing via mechanical means. The device used for this purpose is often called the liquid whistle and it was developed many years ago for liquid processing particularly for homogenisation. As the name suggests it operates on the whistle principle in that ultrasonic vibrations are generated via the flow of a liquid. Process material is forced at high velocity by the homogeniser pump through a special orifice from which it emerges as a jet which impacts upon a steel blade (Figure 2). There are two ways in which cavitation mixing can occur at this point. Firstly through the Venturi effect as the liquid rapidly expands into a larger volume on exiting the orifice and secondly via the blade which is caused to vibrate by the process material flowing over it. The relationship between orifice and blade is critically controlled to optimise blade activity. The required operating pressure and throughput is determined by the use of different sized orifices or jets and the velocity can be changed to achieve the necessary particle size or degree of dispersion^{6,9}. With no moving parts, other than a pump, the system is rugged and durable.

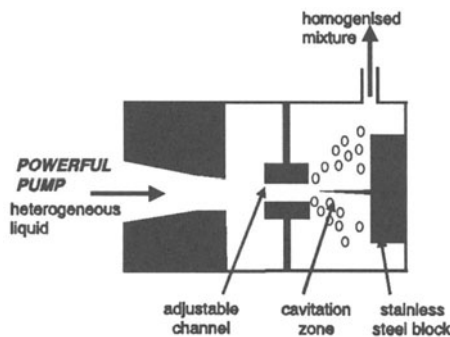


Figure 2: Liquid Whistle

6.1 APPLICATIONS IN THE FOOD INDUSTRY

A typical emulsion base for soups, sauces or gravies would consist of water + milk powder + edible oil and fat together with flour or starch as thickening agent. These materials are premixed together and, after passing through the homogeniser, produce a fine particle size emulsion with a smooth texture.

Ketchup is processed in a similar way to produce a smooth product with increased viscosity and improved taste as a result of the complete dispersion of any clumps of tomato pulp.

Often the rate determining step of a particular process involves an energy interchange through a liquid-solid interface. In the food industry one such process is the extraction of components from vegetable material. One example of ultrasonic assistance is in the manufacture of vanilla extract where extraction time from the bean has been cut from 48 hours to one hour⁹.

6.2 APPLICATIONS IN TEXTILES

Problems over the quality of dyeing in fabrics can arise from two sources. The first is that agglomerates of non-dispersed dye can lead to intense specks of colour visible in the end product and the second is a change of the shade during a batch as the mechanical mixing of the dye particles by the printing rollers change their dispersion. By passing the mixture through the homogeniser before use these problems can be overcome.

Homogenisation also finds use in the preparation of oil/water based spin finish emulsions. The traditional method involves the production of a large vat of product using conventional mixing but this is a lengthy process. The whistle style system can be used to generate the emulsion on "demand" over a wide range of water/oil combinations.

6.3 THE BLENDING OF POLYMERS

A main application in this area is the dispersion of clay or special silica thickening agents into polyester resin in order to produce the required thixotropic characteristics. It is important to achieve a very high standard of dispersion in order to make the most effective use of the material and to prevent settling out. Typically a premix might consist of 60% resin, 39% styrene and 1% thickening agent. A similar application in this field is the dispersion of tinting pigments which are mixed with polyester resin, thickening agent and solvent to produce the coloured gel coating seen on most fibreglass parts.

6.4 THE FORMULATION OF COSMETICS

In the manufacture of skin cream it is often necessary to combine a hot melted wax phase with an ambient water phase. A whistle (the Dual Feed Autosonic

device⁹) was designed to generate the emulsion in such a short time that the wax phase is prevented from solidifying due to quenching. This manufacturing approach resulted in approximately 20% less wax consumption than conventional batch techniques and reduced energy costs because it was not necessary to heat the water phase. In addition, the production rate was approximately doubled.

TABLE 2. Industrial Applications of Ultrasonic Mixing

Food	Textiles	Others
Soups and Sauces	Dispersed dyestuffs	Blending polymers
Ketchup	Thread lubricants	Cosmetic formulation
Salad Creams	Printing thickeners	Precipitation
Mayonnaise	Starch sizing solutions	
Fruit Juices		

7. Precipitation and Crystallisation

In normal crystallization techniques (e.g. in penicillin production), a solution containing materials to be crystallized is super-saturated either by cooling or by evaporation and then seeded. Because seeding may be initiated non-uniformly, resultant crystal growth proceeds at different rates at different nuclei sites, and resulting crystals may show a very broad and uneven crystal size distribution. Power ultrasound has proved to be extremely useful in crystallisation processes. It serves a number of roles in the initiation of seeding and subsequent crystal formation and growth. It also has a property which is particularly beneficial in processing application namely that the cleaning action of the cavitation effectively stops the encrustation of crystals on cooling elements and thereby ensures continuous efficient heat transfer. It is of considerable practical importance to be able to control the point at which crystallisation occurs in any large scale production process. Often crystallisation can occur in an uncontrolled manner simply due to a slight drop in temperature or pressure. On the other hand to control the initiation of crystallisation is often difficult since problems may occur due to incorrect external factors such as temperature and pressure settings. Sonication is thought to enhance both the nucleation rate and rate of crystal growth in a saturated or supercooled medium by producing fresh and/or more nucleation sites in the medium. This may be due to cavitation bubbles acting as nuclei for crystal growth or by the disruption of seeds/nuclei already present within the medium thus increasing the number of nuclei present in the solution/melt.

There are a number of examples of the use of ultrasound in crystallisation in the chemical field. Insonation of gels formed from sodium aluminate and

sodium silicate leads to increases in the nucleation and crystallisation rates for the formation of zeolites by up to 6-fold and 3-fold respectively at 85°C¹⁰. The zeolite formed in the ultrasonic field shows reduced particle size and a narrower size distribution compared with those produced by conventional methodology. The reduction in particle size was shown not to be caused by fracture of the zeolite particles by the effect of cavitation and is thought to be due to an increase in the number of crystallisation nuclei and their dispersion by the acoustic field. The rate of nucleation was shown to increase with increasing irradiation intensity and this was accompanied by a reduction in particle size.

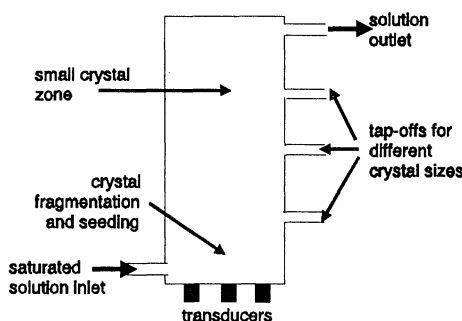


Figure 3: Large Scale Ultrasonic Crystallisation Vat

The scale-up of ultrasonically assisted crystallisation was achieved successfully some years ago in the production of a crystalline drug¹¹. The ultrasound was introduced through an array of horns at the base of the crystallisation tower and served two purposes. Firstly the saturated liquid was ultrasonically seeded as it entered the base of the tower and these small seed crystals rose with the liquid flow and continued to grow until they were large enough to start to sink under the influence of gravity. These larger crystals were fragmented by cavitation as they sank downwards moving closer to the ultrasonic sources. The fragments produced were small enough to rise once again in the flow and provide large numbers of particles which themselves could act as seeds for further nucleation.

One very important area related to crystallisation in the food industry is the formation of ice crystals during the freezing of water. The quality of "fresh" thawed foods preserved through freezing can be somewhat disappointing in terms of texture. This is particularly true of soft fruits such as strawberries. The problem arises because the small ice crystals which are formed initially inside of the cellular material of the food continue to grow. As these crystals increase in

size they break some of the cell walls leading to a partial destruction of the structure of the material. There is a considerable "dwell time" between the initiation of crystallisation (usually at about -3°C) and complete freezing at which point the temperature of the whole item can fall. Under the influence of ultrasound a much more rapid and even seeding occurs and this leads to a much shorter dwell time¹². In addition, since there are a greater number of seeds the final size of the ice crystals is smaller and cell damage is reduced.

8. Degassing

One of the easiest operations which can be performed using ultrasound is degassing since gas bubbles themselves or gas dissolved in a supersaturated solution is readily drawn into the forming cavitation bubbles in an ultrasonic field. Further diffusion into the bubbles during later acoustic cycles expand it to the point at which it floats to the surface and is vented to the atmosphere. Small gas bubbles in a liquid can act as seeds for cavitation and thereby make the process easier to perform but gas filled cavitation bubbles do not collapse readily and so do not produce efficient cavitation effects. For this reason in industrial cleaning it is necessary to degas the cleaning liquid before use. Ultrasonic cleaning baths can now be equipped with a pulsed ultrasound degassing cycle preparatory to use. The cycle involves the use of intermittent power for degassing since during the "off" periods the trapped degassed bubbles rise to the surface. Without this any standing waves in the system will trap the bubbles and their accumulation in the fluid will cause inefficiency of the energy propagation and also heat build-up in the medium.

Particularly important potential applications of ultrasonic degassing have been found in glass making where the removal of gas bubbles from the melt is essential for high quality production.

9. Power Ultrasound in Metallurgy

Traditionally there has always been a use for ultrasound in the cleaning of metal surfaces as a pretreatment for further finishing or as an end in itself. More recently, ultrasound has been adopted for the conditioning, cleaning and etching of metallic foils, which are used industrially for the production of high-specific-surface electrolytic capacitors¹³. Fuji has used ultrasound to produce its so-called multigrain lithographic plates¹⁴.

Power ultrasound has been used for many years in metal casting in the Former Soviet Union^{15,16}. For such processing the major advantages in ultrasonically assisted casting come from the physical effects of melt degassing and enhanced crystallisation during solidification. The latter leads to grain refinement in the casting of light alloys and hence improved mechanical properties. An additional benefit comes from the increased fluidity engendered by ultrasound in the melt which allows more efficient filling of the mould.

10. Ultrasound in Electrochemistry

There are several aspects of ultrasound which recommend its use in conjunction with electrochemistry a topic now known as sonoelectrochemistry¹⁷.

- Degassing limits gas bubble accumulation at the electrode.
- Surface cavitation disturbs the diffusion layer and stops the depletion of electroactive species.
- Ultrasonic agitation gives improved transport of ions across the double layer.
- Cavitation continuously cleans and activates the electrode surfaces.

These effects combine to provide enhanced yield and improved electrical efficiency¹⁷. This has been found to be particularly significant in metal plating where the use of ultrasound has been shown to improve adhesion, hardness, brightness and deposition rate¹⁸. Such benefits have been established and refined over the last 30 years or so but it was back in the 1950's that several papers were produced which first indicated the real potential of sonically assisted electroplating¹. Sonication has also been found to increase the deposition rate and to negate the fall in plating current which occurs normally due to polarisation.

11. Acoustically Assisted Filtration

The requirement to remove suspensions of solids from liquids is common to many industries. This separation can be either for the production of solids-free liquid or to isolate the solid from its mother liquors. Conventionally membranes of various sorts have been employed for these processes ranging from the simple filter pad through semi-permeable osmotic type membranes to those which are

used on a size-exclusion principle for the purification of polymeric materials. Unfortunately the conventional methodologies often lead to "clogged" filters and, as a consequence, there will always be the need to either replace filters or stop the operation and clean them on a regular basis. The application of ultrasound enables the filtration system to operate more efficiently and for much longer periods without maintenance through two specific effects. Firstly sonication will cause agglomeration of fine particles and secondly will supply sufficient vibrational energy to the system to keep the particles partly suspended and therefore leave more free "channels" for solvent elution. This so-called acoustic filtration has been studied for many years and in many systems achieving, for example, an 18 fold increase in filtration rate of motor oil through a sandstone filter¹⁹ and improved performance of membranes in the cleaning of white water from paper pulp factories²⁰.

There have been a number of developments in acoustic filtration and separation processes²¹. One such is the application of an electrical potential across the slurry mixture while acoustic filtration is performed²². The filter itself is made the cathode while the anode, on the top of the slurry, functions as a source of attraction for the predominantly negatively charged particulate material. An example of its application can be found in the dewatering of coal slurry (50% moisture content). Conventional filtration reduces the moisture to 40%, using ultrasound this was improved to 25% and using electro-acoustic filtration further improved to 15%. The potential for this process is clearly enormous when applied to a continuous belt drying process in say the deliquoring of such extremes as sewage sludge or fruit pulps.

The use of ultrasound has also enabled the development of a new efficient method of separating particulate matter from a liquid without the need for a filter membrane. The basis of such processes is that when a standing wave is set up in a liquid medium any particulate contaminant in the fluid will collect rapidly in regions corresponding to half wavelength distances (nodal points) on the axis of the ultrasonic beam²³. If the standing waves are set up vertically using transducers of equivalent frequency arranged on either side of a small vertical vessel (say a test tube) then particulate material will migrate and gather at the nodes and will be held static in those positions when the vessel is removed in a vertical direction from the ultrasonic field. The net result is that particles are physically collected at the bottom of the vessel as the base reaches them. This device is known as the "Wavecomb"²⁴.

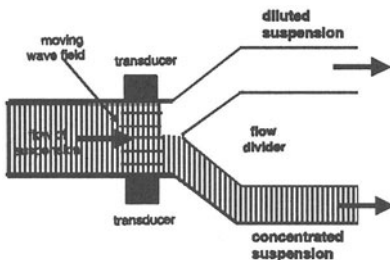


Figure 4: Separation of Particles in an Acoustic Field

If there is a phase difference between the signals from the two transducers a drifting wave may be established. This effect is the key to a separation process in which the standing waves traverse through the medium carrying the particles trapped at half-wavelength distances. The particles are thus swept towards one of the two transducers. If this sweep is applied to a flow system and the stream beyond the ultrasonic field is divided (Figure 4). A concentration of particulate matter will be produced in one of the two outflows.

12. Conclusion

In the last years ultrasonic engineering has advanced in keeping with the increased interest in chemical and processing applications. At the time of writing there are several commercially available devices which could either be used directly or fairly easily adapted. This is not to say that the problems of large-scale application of power ultrasound are solved - far from it. The devices now available "do the job" but it is almost certain that they could be improved by optimisation of the energy input, the correct choice of reactor geometry and maybe even the correct choice of frequency or frequency tracking as the reaction or process proceeds towards its final state.

References

1. Brown, B. and J.E.Goodman, J.E. (1965) *High Intensity Ultrasonics*, ILLiffe Books Ltd, London.
2. El'Piner, I.E. (1964) *Ultrasound, Physical, Chemical and Biological Effects*, Consultants Bureau, New York.
3. Frederick, J.R. (1965) *Ultrasonic Engineering*, John Wiley. London
4. Rawson, F.F., (1987) *Phys.Bull.*, 38, 255.
5. Rawson, F.F. (1997) An introduction to ultrasonic food cutting, *Ultrasound in Food Processing*, 193, ed Povey, M.J.W. and Mason T.J., Thomson Science, London.
6. Donovan J., Ultrasonics, 85 Riverside Park, Otley, LS21 2RW, U.K.
7. Morgan A (1993) *Ultrasonic Atomisation*, Advances in Sonochemistry, **3**, 145-164, ed. Mason T.J., JAI Press, London.
8. Sodeva, Bat Modul - BP 299, Savoie Technolac, 73375 Le Bourget du Lac Cedex, France.
9. Sonic Corp., One Research Drive, Stratford, CT 06497, U.S.A.
10. Lindley J. Lorimer J.P. Maan R. Mason T.J. and Roberts C.W. (1989) *Ultrasonics International '89, Conference Proceedings*, 1264, Butterworths, Guildford.
11. Midler M., (1970) *U.S. PATENT* 3,510,266.
12. Acton, E, and Morris, G.J. (1992) W.O. 99/20420.
13. Matsushita Electric Industrial Ltd. (1993) EP 0189595 A2.
14. Fuji Photo Film Ltd. (1993) US 5213666.
15. Abramov O. (1991) *The Action of Ultrasound on Solidifying Metals*, Advances in Sonochemistry, **2**, 135-187, ed. Mason T.J., JAI Press, London.
16. Eskin G. (1996) *Degassing, Filtration and Grain Refinement Processes of Light alloys in an acoustic field*, Advances in Sonochemistry, **4**, 101-160, ed. Mason T.J., JAI Press, London.
17. Mason, T.J., Lorimer, J.P. and Walton, D.J., (1990). *Ultrasonics* 28, 333.
18. Walker, M.R. (1993). *Ultrasonic agitation in metal finishing*, Advances in Sonochemistry, **3**, 125-144, ed. Mason T.J., JAI Press, London.
19. Fairbanks H.V. and Chen W.I. (1971) *Chem.Eng.Symp.Series.* 67, 108.
20. Sabri, N., Tuori T. and Huotari, H., (1997) *Ultrasonically Enhanced Membrane Filtration of Waste Waters from the Pulp and Paper Industries*, Special publication, VTT Energy, PO Box 1603, FIN-40101, Jyvaskyla, Finland.
21. Tarleton E.S. and Wakeman R.J., (1997) *Ultrasonically Assisted Separation Processes*, Ultrasound in Food Processing, ed M.J.W.Povey, M.J.W. and Mason T.J., 193, Thomson Science, London.

22. Senapati N., (1991). *Ultrasound in Chemical Processing*, Advances in Sonochemistry, **2**, 187-210, ed. Mason T.J., JAI Press, London.
23. Schramm C.J., (1991) *The manipulation of particles in an acoustic field*, Advances in Sonochemistry, **2**, 293-323, ed. Mason T.J., JAI Press, London.
24. British Technology Group, 101 Newington Causeway, London SE1 6BU, U.K.

SUBJECT INDEX

γ	187
acoustic cavitation	25, 97, 156, 192
acoustic deliquoring	368
acoustic dosimetry	237
acoustic emission	152, 173
acoustic emission lines	196
acoustic filtration	369, 387
acoustic levitation	7, 55
acoustic radiation	9
acoustic radiation forces	16, 147
acoustic spectrum	10
acoustic streaming	6, 288
acoustical streaming	124
acrylic polymers	328
adiabatic behavior	1, 49, 136, 180, 202
amorphous metals	295, 296
anionic polymerization	332
applications of ultrasonic degradation	326
asymmetric collapse	113, 183
bends	2
bifurcations	9
Bjerknes force	28, 56, 104, 139, 146, 148, 180, 189
Blake mechanism	7
bubble	
clustering	144, 356, 359
dynamics	5, 9, 32
evolution	5
field	139
formation	2
growth	7
implosion	130, 210
interactions	11
nucleation	3
phenomena	94
shielding	35
translation	14
buoyancy	147
calibration	240
calorimetry	240
cavitation	
bubbles	99
hot spot	193
inception	6
microstreaming	25, 28, 33
nucleation	2, 7, 25, 26
threshold	331

chaos	9
chaotic dynamics	67
chaotic bubble oscillations	67, 100
charged surfactants	356
chemical remediation	366
chemical stability	171
coexisting attractors	65
collapse microjets	25, 34
collapsing bubble	90
colloidal formation	346, 360
comparative rate thermometry	198
compression ratio	186
condensation polymerizations	335
continuity equation	40, 41
crevice model	26
critical scattering angle	78
cyclic cavitation	16
cylindrical resonator	141
degradation of shear fields	326
diagnostic ultrasound	7
dielectric breakdown	184
diffusion stability	169, 189
diffraction	74
dispersal of fillers	324
drag force	141
eggshell catalysts	299
electrochemically promoted polymerizations	335
electrochemistry	335
electromechanical coupling factor	260
electron conduction	161, 162
emulsion polymerizations	332
emulsions	323
encapsulation of inorganic particles	324
energy focusing	167
enhanced mass transport	335
expansion ratio	186
extinction threshold	145
filaments	98, 140
fluid jetting	6
food sterilisation	363
forward scattering	80
fractoluminescence	58
free radicals	22, 225, 235, 322
gassy cavitation	28, 32
gel permeation chromatography	322
giant resonance	63
Gilmore model	46, 63, 184
Grignard type reaction	337
harmonic oscillations	132

harmonic resonances	64
harmonics	13
heat pumping	136
heat transfer	134
heat transfer phenomena	127
heterogeneous catalysts	293, 297, 315
heterogeneous reactions	219
heterogeneous sonochemistry	291
homolytic bond breakage	326
heterolytic fission	273
high speed holographic cinematography	99
homobaricity	134
homogeneous nucleation	26
homogeneous reactions	219
homogeneous sonochemistry	205
homolytic fission	273
hydrated electrons	229, 232
hydrodynamic cavitation	4
hydrodynamic code	164
hydrophobicity	348
hypothermia	19
iodine dosimetry	277
ionic addition	279
incompressible flow	87
induced mass force	141
inertial cavitation	29
inertial forces	7
interparticle collisions	311
isothermal behavior	49
isothermal expansion	208
Keller-Miksis model	141
Laplace pressure	32
large shear gradients	322
laser induced bubbles	183
lateral oscillations	124
levitation	146, 147
light scattering	73
light spectra	22
liquid compressibility	128
liquid jet	25, 90, 187, 189
luminescence threshold	145
Luminol®	20
magnetostrictive effect	263
magnetostrictive transducer	246
materials synthesis	291
mechanical index	30
microgravity	149
microstreaming	25, 288
Mie theory	73

modification of particle size	324
modification of polymer surfaces	339
modification polymers	325
molar masses	322
molecular weight	336
multi-bubble sonoluminescence	97, 139, 155, 195
nanocolloids	301
nanoparticles	293
nanophase materials	292
nanostructured alloys	296
nanostructured materials	304
nanostructured metal powders	293
nitrogen spectrum	163
nonharmonic oscillations	127
nonlinear bubble dynamics	9, 63, 65
nonlinear oscillator	63
nonsphericity	81
nucleation	2, 6
numerical simulations	179
optical emission	163
optical extinction	75
optical trapping	81
organometallic compounds	301
oscillating reaction	339
period doubling	67, 100
piezoelectric ceramics	260
piezoelectric transducers	246
piezomagnetic materials	263
plasma	161
plastics in welding	323
polymer processing	323
polymerization by ionic mechanism	332
polymers	321
polyphenylenes	336
polysilynes	339
polytropic approximation	49, 166
polyurethane	335
poly (vinylidene difluoride)	340
potassium persulphate initiator	333
power ultrasound	245, 256
pressure antinode	141
primary bjerknes force	141
protein microspheres	308
pulse duration	155
pulse enhancement	35
pyrolysis	217, 350
radical addition	279
radiation force balance	241
radiation forces	6

radiation pressure	75
radical oscillations	117, 118
radical scavengers	228
radical trapping	330
rate of initiation	325, 326, 330
Rayleigh-Plesset equation	27, 43, 44, 45, 127, 128, 166
Rayleigh-Taylor instability	12, 53, 179
rectified diffusion	16, 28, 31, 173, 179
recycling of waste rubbers	334
reduction in the viscosity	321
resonance curves	65
resonance frequency	9, 27, 28, 133, 166
resonance radius	15, 27
response curves	63, 64, 67
ring opening polymerizations	334
rotational flow	123
sandwich transducer	265
secondary bjerknes force	141
shape oscillations	82, 168, 175
shock waves	6, 11, 100, 160
shuttlecock structure	286
silicone resins	334
single-bubble sonochemistry	285
single-bubble sonoluminescence	29, 73, 145, 160, 165, 189, 195
single cavitation bubble luminescence	183
sonic destruction	374
sonochemical polymerization	341
sonochemistry	21, 22, 191, 192, 225
sonocleavage	217
sonoluminescence	20, 21, 29, 48, 133, 145, 156, 183, 192
sonolysis	228
sonophysics	25
spherical bubble	63, 166
spherical bubble collapse	184
spherical symmetry	12
spin trap	228
stability regions	149, 168
stable cavitation	28
stable sonoluminescence	166
stepped-plate transducer	268
streaming	20, 98, 106, 139
structure formation	139
subharmonics	13, 64
superheat limit	2
superoxide radical	228
surface active solutes	353
surface cavitation	310
surface decontamination	363
surface disinfection	363

surface instability	12
surface tension	67, 69
surface waves	12
surfactant	83
surfactant micelles	355
syndiotactic polyolefins	336
tensile strength	6, 7
thermal effects	6, 9, 161
tribonucleation	26
ultraharmonics	13
ultrasonic atomizer	380
ultrasonic cleaning	248, 378
ultrasonic crystallisation	384
ultrasonic cutting	378
ultrasonic degradation of polymers	324
ultrasonic dispersion	369
ultrasonic transducers	259
ultrasound degassing	385
ultrasound dosage	253
ultrasubharmonic resonances	64
Van der Waals	185
velocity potential	111
viscous losses	9
volume pulsations	9
vulcanization	334
Weissler reaction	239
Wurtz coupling	338
Ziegler-Natta polymerizations	336

CONTRIBUTORS

I.Sh. Akhatov •
Ufa (Bashkortostan)
Branch of Russian Academy of Sciences
K. Marx Str. 6
Ufa, 450000
Russia

R.E. Apfel
PO Box 208286
Yale University
New Haven, CT 06520-8286
USA

M. Ashokkumar
Advanced Mineral Products Research Centre
School of Chemistry
University of Melbourne
Parkville 3052
Australia

K. Bartik
Université Libre de Bruxelles (CP 165)
50, avenue F.D. Roosevelt
B 1050 Bruxelles
Belgium

J.R. Blake
School of Mathematics and Statistics
University of Birmingham
Edgbaston, Birmingham, B15 2TT
United Kingdom

M.P. Brenner
Department of Mathematics
Massachusetts Institute of Technology
Cambridge, MA 02146
USA

T. Caulier
Université Libre de Bruxelles (CP 165)
50, avenue F.D. Roosevelt
B 1050 Bruxelles
Belgium

D.B. Clarke
PO Box 808, 7000 East Avenue
Lawrence Livermore National Laboratory
Livermore, CA 94550
USA

L.A. Crum
1013 NE 40th Street
Applied Physics Laboratory
University of Washington
Seattle, WA 98105-6698
USA

C. Dekerckheer
Université Libre de Bruxelles (CP 165)
50, avenue F.D. Roosevelt
B 1050 Bruxelles
Belgium

Y. Didenko
601 S. Goodwin Avenue
Department of Chemistry
University of Illinois at Urbana-Champaign
Urbana, IL 61801
USA

M.M. Fang
601 S. Goodwin Avenue
Department of Chemistry
University of Illinois at Urbana-Champaign
Urbana, IL 61801
USA

J.A. Gallego-Juárez
Institute of Acoustics, CSIC
Serrano, 144
28006, Madrid
Spain

F. Grieser
Advanced Mineral Products Research Centre
School of Chemistry
University of Melbourne
Parkville 3052
Australia

A. Henglein
Hahn-Meitner Institut
14109 Berlin
Germany

S. Hilgenfeldt
Fachbereich Physik der Universität Marburg
Renthof 6
35032 Marburg
Germany

T. Hyeon
601 S. Goodwin Avenue
Department of Chemistry
University of Illinois at Urbana-Champaign
Urbana, IL 61801
USA

G.S. Keen
School of Mathematics and Statistics
University of Birmingham
Edgbaston, Birmingham, B15 2TT
United Kingdom

Y. Kegelaers
Université Libre de Bruxelles (CP 165)
50, avenue F.D. Roosevelt
B 1050 Bruxelles
Belgium

R.T. Lahey
Rensselaer Polytechnic Institute
Troy, NY 12180-3590
USA

W. Lauterborn
Drittes Physikalisches Institut
Bürgerstr. 42-44
D-37073 Göttingen
Germany

T. Lepoint
Institut Meurice – CERIA
1, Avenue E. Gryzon
1070 Brussels
Belgium

F. Lepoint-Mullie
Institut Meurice – CERIA
1, Avenue E. Gryzon
1070 Brussels
Belgium

O. Lindau
Drittes Physikalisches Institut
Bürgerstr. 42-44
D-37073 Göttingen
Germany

D. Lohse
Fachbereich Physik der Universität Marburg
Renthof 6
35032 Marburg
Germany

M. Longuet-Higgins
Institute for Nonlinear Science
University of California, San Diego
La Jolla, CA 92093-0402
USA

S. Madanshetty
Mechanical and Nuclear Engineering Department
Kansas State University
Manhattan, KS 66506-5106
USA

P.L. Marston
Department of Physics
Washington State University
Pullman, WA 99164-2814
USA

T.J. Mason
School of Natural and Environmental Sciences
Coventry University
Coventry CV1 5FB
United Kingdom

T.J. Matula
1013 NE 40th Street
Applied Physics Laboratory
University of Washington
Seattle, WA 98105-6698
USA

W.B. McNamara III
601 S. Goodwin Avenue
Department of Chemistry
University of Illinois at Urbana-Champaign
Urbana, IL 61801
USA

M.M. Mdeleleni
601 S. Goodwin Avenue
Department of Chemistry
University of Illinois at Urbana-Champaign
Urbana, IL 61801
USA

R. Mettin
Drittes Physikalisches Institut
Bürgerstr. 42-44
D-37073 Göttingen
Germany

V. Misík
Radiation Biology Branch
National Cancer Institute, NIH
Bethesda, MD 20892-1002
USA

W.C. Moss
PO Box 808, 7000 East Avenue
Lawrence Livermore National Laboratory
Livermore, CA 94550
USA

R.I. Nigmatulin
Ufa (Bashkortostan)
Branch of Russian Academy of Sciences
K. Marx Str. 6
Ufa, 450000
Russia

C.D. Ohl
Drittes Physikalisches Institut
Bürgerstr. 42-44
D-37073 Göttingen
Germany

G.J. Price
School of Chemistry
University of Bath
Claverton Down
Bath BA2 7AY
United Kingdom

A. Prosperetti
Department of Mechanical Engineering
The Johns Hopkins University
Baltimore, MD 21218
USA

J. Reisse
Université Libre de Bruxelles (CP 165)
50, avenue F.D. Roosevelt
B 1050 Bruxelles
Belgium

P. Riesz
Building 10, Room B3-B69
National Cancer Institute, NIH
Bethesda, MD 20892-1002
USA

R.A. Roy
Boston University
Department of Aerospace and
Mechanical Engineering
110 Cummington St.
Boston, MA 02215
USA

J.P. Russell
ARC Sonics Inc.
PO Box 24
Ste. 722-601 W. Broadway
Vancouver, BC V5Z 4C2
Canada

N. Segebarth
Université Libre de Bruxelles (CP 165)
50, avenue F.D. Roosevelt
B 1050 Bruxelles
Belgium

J.Z. Sostaric
Advanced Mineral Products Research Centre
School of Chemistry
University of Melbourne
Parkville 3052
Australia

K.S. Suslick
601 S. Goodwin Avenue
Department of Chemistry
University of Illinois at Urbana-Champaign
Urbana, IL 61801
USA

Y. Tomita
Hakodate College
Hokkaido University of Education
Hakodate
Japan

R.P. Tong
School of Mathematics and Statistics
University of Birmingham
Edgbaston, Birmingham, B15 2TT
United Kingdom

N.K. Vakhitova
Ufa (Bashkortostan)
Branch of Russian Academy of Sciences
K. Marx Str. 6
Ufa, 450000
Russia

D.A. Young
PO Box 808, 7000 East Avenue
Lawrence Livermore National Laboratory
Livermore, CA 94550
USA

REPORT DOCUMENTATION PAGE			<i>Form Approved OPM No. 0704-0188</i>
<p>Public reporting burden for this collection of information is estimated to average 1 hour per response, including the time for reviewing instructions, searching existing data sources, gathering and maintaining the data needed, and reviewing the collection of information. Send comments regarding this burden estimate or any other aspect of this collection of information, including suggestions for reducing this burden, to Washington Headquarters Services, Directorate for Information Operations and Reports, 1215 Jefferson Davis Highway, Suite 1204, Arlington, VA 22202-4302, and to the Office of Information and Regulatory Affairs, Office of Management and Budget, Washington, DC 20503.</p>			
1. AGENCY USE ONLY (Leave blank)	2. REPORT DATE	3. REPORT TYPE AND DATES COVERED	
	1 October 1998	Conference Proceedings	
4. TITLE AND SUBTITLE	5. FUNDING NUMBERS		
Sonochemistry and Sonoluminescence	N00014-97-1-0149		
6. AUTHOR(S) Lawrence A. Crum Timothy J. Mason	Jacques Reisse Kenneth S. Suslick	8. PERFORMING ORGANIZATION REPORT NUMBER	
7. PERFORMING ORGANIZATION NAME(S) AND ADDRESS(ES) Applied Physics Laboratory University of Washington 1013 NE 40th Street Seattle, WA 98105-6698	10. SPONSORING / MONITORING AGENCY REPORT NUMBER		
9. SPONSORING / MONITORING AGENCY NAME(S) AND ADDRESS(ES) Office of Naval Research, ONR 331 800 N. Quincy Street Arlington, VA 22217-5660			
11. SUPPLEMENTARY NOTES			
12a. DISTRIBUTION / AVAILABILITY STATEMENT Approved for public release. Distribution unlimited.		12b. DISTRIBUTION CODE	
13. ABSTRACT (Maximum 200 words) This book contains 29 tutorial lectures and research articles on the topics of sonoluminescence and sonochemistry. These lectures and articles resulted from a NATO-sponsored Advanced Study Institute held in Leavenworth, Washington, USA in August of 1997. Because this volume contains tutorial lectures as well as detailed research articles, it can serve both as an introduction, as well as a comprehensive and detailed overview of these two interesting and topical subjects.			
14. SUBJECT TERMS sonoluminescence, sonochemistry, acoustic cavitation, bubble implosion, light emission		15. NUMBER OF PAGES 396	16. PRICE CODE
17. SECURITY CLASSIFICATION OF REPORT unclassified	18. SECURITY CLASSIFICATION OF THIS PAGE unclassified	19. SECURITY CLASSIFICATION OF ABSTRACT unclassified	20. LIMITATION OF ABSTRACT SAR